University of Huddersfield Repository

Hamilton, Ian

The Development of Microwave Thermal Analysis (MWTA)and its application to the study of Carbons and other materials

Original Citation

Hamilton, Ian (2009) The Development of Microwave Thermal Analysis (MWTA)and its application to the study of Carbons and other materials. Doctoral thesis, University of Huddersfield.

This version is available at http://eprints.hud.ac.uk/8748/

The Development of Microwave Thermal Analysis (MWTA) and its application to the study of Carbons and other materials

Ian E. Hamilton M.Chem.(Hons)

A thesis submitted to the University of Huddersfield in partial fulfilment of the requirements for the degree of Doctor of Philosophy.

Department of Chemical and Biological Sciences
The University of Huddersfield

December 2009

Contents

Acknowledgments

Abstract

This research involves the development of a totally new approach to thermal analysis in which microwave energy is used not only to heat the sample but also to detect thermally induced transformations via the effects of changes in its dielectric properties. Use of these properties, rather than the more usual mass or enthalpy changes of conventional thermal analysis, provide a unique insight into thermal processes.

Microwave thermal analysis (MWTA) is a technique for studying the efficiency of the conversion of microwave to thermal energy by measuring the microwave power-temperature relationship for different materials. Power/temperature verses time profiles in some cases give an indication of physical and chemical changes occurring in the sample, via changes in the dielectric constant.

An instrument for performing microwave thermal analysis (MWTA) has been designed, constructed and applied to an extensive range of chemical systems exhibiting a variety of physicochemical transformations, including melting, decomposition and solid-solid phase changes. MWTA has been shown to provide both qualitative and quantitative information with sample masses ranging from the analytical (1 to 20 mg) to semi-preparative (0.5 to 5.0 g) scales. It has been demonstrated that MWTA can be used in conjunction with complementary techniques such as differential thermal analysis (DTA) and X-ray powder diffraction (XRD) to provide additional data. MWTA has the potential to be extended to incorporate some of the latest developments in thermal analysis, including methods involving temperature modulation and evolved gas analysis.

MWTA has the potential to have applications in the design of industrial processes by providing detailed information on the effect of microwave radiation on both physical (e.g. phase changes) and chemical processes.

Glossary of terms

RAE	The research assessment exercise
MWTA	Microwave thermal analysis
MWDTA	Microwave differential thermal analysis
MWTA (MWDTA)	Microwave thermal analysis performed in the HPB cell, allowing any material to be tested whilst still controlling on the sample
TA	Thermal analysis
DSC	Differential scanning calorimetry
DTA	Differential thermal analysis
TGA	Thermogravimetric analysis
ΔT	Change in temperature
T_s	Sample temperature
T_r	Reference temperature
T_m	Fusion temperature
T_g	Glass transition temperature
ΔH	Change in enthalpy
Q	Heat transfer
Cp	heat Capacity (J/g °C)
dT/dt	Heating rate (°C/min)
GHz	Giga hertz
MHz	Mega hertz
$\varepsilon_s\ \varepsilon_\infty$	Dielectric constants
ε^*	Complex dielectric constant
ω	Angular frequency
ε'	Permittivity
ε''_{eff}	Effective loss factor
σ	Electrical conductivity
ε_0	Permittivity of free space ($8.8542 \times 10^{-12}\,C^2\,N^{-1}\,m^{-2}$)
α	Attenuation factor
Dp	Penetration depth
λ	Wavelength
λ_c	Cut off wavelength
λ_0	Wavelength in free space

λ_g	Wavelength in a waveguide
Z	Impedance
Ω	Electrical resistance
μ	Relative permeability
MCRC	Materials and catalysis research centre – University of Huddersfield, School of applied sciences
XRD	X-Ray powder diffraction
SEM	Scanning electron microscopy
Hot zone	The area within the waveguide where the highest likelihood of coupling can be obtained.
Hot spots	Where the applied field is stronger at a point causing a localised area to heat more than the rest of the sample (an undesirable effect).
MWDTA-GEA	Microwave differential thermal analysis with gas evolution analysis
Evanescent	Last for only a short time, then disappearing quickly and being forgotten
j	When no real number can be used in a equation that squares into a negative real number, an imaginary number can be used and given the symbol j (in travelling wave theory), by treating j as an unknown while rearranging the equation, j^2 can be said to be equal to -1.
Cavity	A volume enclosed by a conducting wall used to house microwave energy.
HPB cell	Hamilton-Parkes-Barnes cell
Anisotropic	Possesses different properties in one direction compared to another
Birefringent	A macroscopic property of anisotropic materials which causes an incident ray of polarized light to produce two patterns, due to differences in refractive indices and long range molecular orientational order
Polymorphism	Crystalline compounds which appear in different solid forms, while retaining identical vapours and liquids.
(o.s)	Onset temperature
(pk)	Peak temperature
Antioxidant	A molecule capable of slowing or preventing oxidation of other molecules
PID hunting	As the control system tries to return to the set-point it may continually overshot (or undershoot) the value resulting in oscillation or hunting around the set-point value.

PID overshoot	On going through a transition the PID controller responds to the change in error signal, if the PID controller can respond strongly to the change it can cause it to exceed the set point, resulting in an increase in the sample temperature
PCM	Phase change material
ADC	The Analogue-to-digital controller, converts analogue signals to digital signals which are capable of being read by the instrument operating system.
ISA	Industry Standard Architecture, an 8 bit system used in personal computers to connect peripheral cards to the motherboard.
Q	Quality factor (general, isolated empty, isolated with dielectric, loaded, external, effective, dielectric workload)
IUPAC	International Union of Pure and Applied Chemistry
Atactic	No regular pattern of orientation of the repeat units
Syndiotactic	Regular pattern in the orientation of the repeat unit
Isotactic	Repeat units all possess the same orientation
SD	Standard deviation
Permittivity	Describes how an electric field affects and is effected by a dielectric material. It is determined by the ability of a material to polarize and respond to the applied field.
Attenuation	On passing electromagnetic energy through a medium, part of the energy is absorbed and converted to a different form
Permeability	The degree of magnetisation of a material that responds to an applied magnetic field
Reactance	The imaginary part of electrical impedance, a measure of opposition to an alternating current. Reactance arises from the presence of inductance and capacitance within a circuit
E	Electrical field strength
η_0	Intrinsic impedance of free space ($\sqrt{(\mu_0/\varepsilon_0)}$)
M/S	Mass spectrometry
m/z	Mass unit
rms	Root mean squared
Hysteresis	The lag of a response to a change in a system
RCHPB	Removable crucible Hamilton-Parkes-Barnes cell

List of Equations, Figures, Graphs, Tables and Charts

Graphs

Tables

Introduction

In this section the field of thermal analysis is introduced and the advantages of developing microwave thermal analysis are detailed. The theory behind microwave heating is discussed along with the instrumentation used throughout this research.

Chapter 1

Introduction and previous work

The first few chapters provide a detailed overview of thermal analysis and microwave heating, followed by the introduction of the microwave thermal analysis equipment and the reasons for developing the technique.

Currently one of the main areas of research within the materials group at the University of Huddersfield has been to create novel thermal methods for analysing and processing materials whilst using microwave heating. Microwave Thermal Analysis (MWTA) is a totally new thermal analysis technique that has the potential to provide data of considerable interest to chemical and pharmaceutical companies, which use microwave heating for manufacture or processing. By monitoring how a material behaves when subjected to microwave radiation, MWTA could indicate which systems would be most amenable to microwave processing and possibly aid the design of a process plant.

1.1 Thermal analysis (TA)

1.1.1 Thermally induced processes

1.1.1.1 Enthalpy

The change in internal energy (U) is a result of the sum of the work done on (w), and heat supplied (q) to a system.

$$\Delta U = dw + dq$$

Equation 1: Definition for the change in internal heat

Most TA experiments are performed at atmospheric pressure, therefore changes in the heat supplied is of greater significance under experimental conditions.

When energy is supplied as heat (and the system is at a constant pressure) it can be said to be equal to the thermodynamic property, enthalpy.

The enthalpy (H) of a system is defined as:

$$H = U + pV$$

Equation 2: Definition of enthalpy

Where: p = pressure

                V = volume

Accordingly, a change in the enthalpy of a system is equal to the energy supplied, providing that it is heated at constant pressure and no additional work is performed by the system.

$$\Delta H = q_p$$

Equation 3: Relationship between enthalpy and supplied heat energy

Where: q_p = The energy supplied by heat (at constant pressure)

Therefore, if heat energy is increased in a system (e.g. during an exothermic transition) then the enthalpy will increase positively and vice versa.

1.1.1.2 Heat capacity

The slope of a tangent to a plot of temperature against internal energy (U) equates to the heat capacity (C_p when at constant pressure) at that temperature. Heat capacity can be used to relate changes in temperature to changes in enthalpy (assuming that C_p remains constant over the temperature range of interest).

$$\Delta H = C_p \Delta T$$

Equation 4: Relationship between enthaply and a measurable change in temperature

As the enthalpy of a system is said to be equal to the supplied heat the equation can be written as:

$$\Delta H = q_p = C_p \Delta T$$

Equation 5: Combination of Equation 3 and Equation 4

Most systems when heated (at a constant pressure) expand, therefore work is done on the surrounding and some energy is lost.

A smaller temperature rise of a system compared to a reference during dynamic heating (in the absence of a transition) can indicate a larger C_p in that system, the result of which is that in differential TA methods the sample temperature will lag further behind the reference as the heat capacity differences between the two cause a drift in the calculated baseline.

1.1.1.3 Examples of thermally induced processes

Enthalpy or heat changes result from phase changes such as fusion, boiling, sublimation, vaporisation and dehydration reactions, dissociation or decomposition reactions, glass transition temperatures, specific heat capacity, oxidations, reductions, polymorphs, destruction of crystalline lattice structures and chemical reactions.
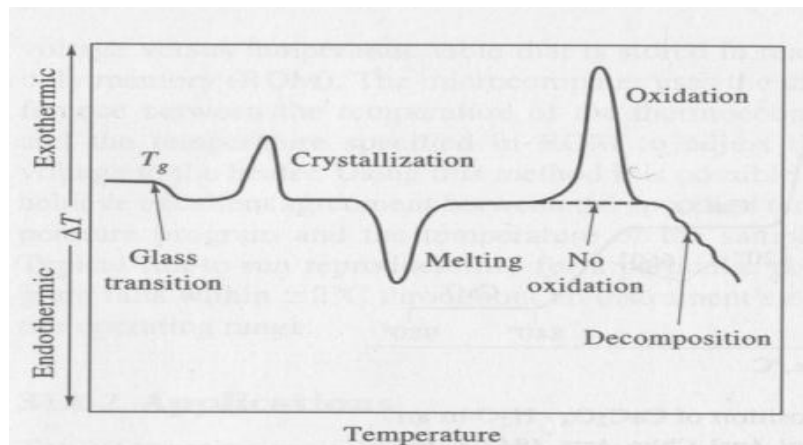
Figure 1: Typical DTA/DSC trace [1]

Typical DTA reference materials include alumina, silicon carbide or glass beads and are selected for their thermal stability and inertness.

The general definition of thermal analysis (TA) is a group of techniques in which a physical property of a sample is measured as a function of temperature, while the sample is subjected to a set temperature program. This method of analysis can be used for both quality control and as a research tool in industry; for information on products such as polymers, pharmaceuticals, clays, minerals, metals and alloys.

TA has a diverse range of applications [2] including :-

- Identification,
- Characterisation,
- Quantification,
- Substance quantities,
- Purity tests,
- Obtaining fundamental thermodynamic and reaction kinetics data.

The most commonly used TA techniques are Differential Thermal Analysis (DTA), Differential Scanning Calorimetry (DSC), and Thermogravimetric Analysis (TGA) [1].

1.2 Thermal analysis instrumentation

1.2.1. Differential thermal analysis (DTA)
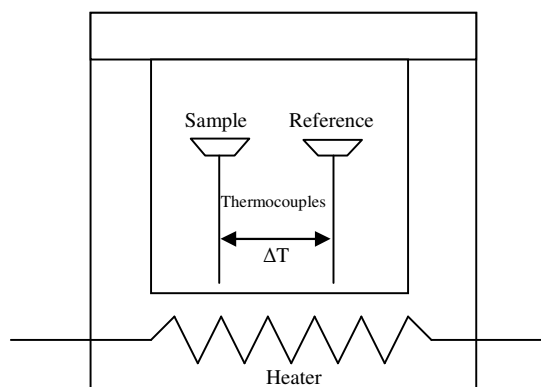
Figure 2: Schematic of a typical DTA instrument

DTA is used to characterise materials by raising the temperature at a linear rate while heating a reference at the same rate. The difference in temperature or heat flow between the sample and reference pans is plotted as a function of temperature or time. By heating both the sample and reference in the same furnace, any thermal changes that occur in the sample will result in more or less heat required by the sample to maintain linear heating, and any resulting exothermic or endothermic processes will be represented by a peak on the trace of ΔT or ΔH verses temperature or time.

When using DTA techniques the sample temperature is continuously compared with a reference temperature. Experimentally, this is achieved using a furnace which contains a sample holder which holds two identical and symmetrical areas for sample placement. These areas contain identical thermocouples (or another appropriate temperature measuring device). The sample is placed in one holder, and a thermally inert substance (usually α-alumina, silicon carbide, glass beads or an empty pan) is placed in the other, then both holders are heated at a uniform rate, and the difference in temperature between the two (ΔT) is recorded as a function of time or temperature.

1.2.1.1 History of DTA

In 1899 W.C. Roberts-Austen introduced the concept of modern differential thermal analysis [3]. Previous to his work, samples were tested with a thermocouple in the sample, while the furnace temperature was monitored and deviations from linearity between the two were recorded as transitions.

The Roberts-Austen instrument included a reference within a close thermal environment to the sample, which ensured the temperature difference ($\Delta T = T_s - T_r$) between the sample and reference was very small. The advantage of the arrangement meant that as the sample went through a transition, its rate of cooling/heating slowed, whereas the reference rate remained constant, resulting in a larger value of ΔT. After the transition the sample temperature gradually returned to the reference temperature, returning ΔT to near zero again. As ΔT was always near zero, regardless of the sample temperature, the sensitivity of the technique was greatly improved.
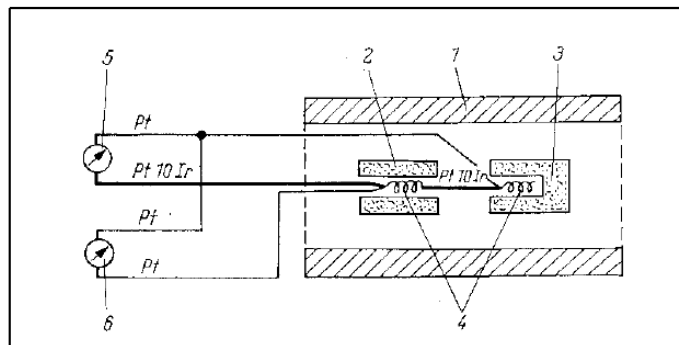
DTA design
1-ceramic tube; 2- reference sample; 3-sample; 4-thermocouples; 5-galvanometer indicating sample temperature; 6- galvanometer indicating temperature difference

Figure 3: Roberts-Austen's DTA design [3]

Early DTA suffered from poor repeatability until 1939 where Norton *et al.* [4] empirically decided to use the peak area of the curve rather than the peak height to make quantitative measurements; it was later found that the peak area was in fact proportional to the heat (Q) in the sample.

The next major advance in the development of differential methods was in 1955 by Boersma *et al.* [5]. At the time both the reference and the sample temperature were measured using a single thermocouple, therefore the sample was used to both produce heat and develop a differential signal.

Boersma's new sample holder was designed to separate these two functions by heating both the sample and reference on a piece of thermally conductive material, on which the differential temperature could be measured (assuming each pan and thermocouple were identical). This meant the sample and reference temperature were not equal to the pan temperature due to the low thermal conductivity of the sample compared to that of a metal pan. Instead there was an average temperature measurement of both the sample (and reference) and pan combined, that was not impeded by the thermal conductivity of the sample itself.

The advantage of this design allowed the peak area to now be solely dependent on the production/absorption of heat originating from the transition. Another advantage became evident as sample sizes could now become much smaller. When large samples were used the thermal gradient that existed due to the rate of heat conduction compared to the heating rate, gave rise to peak broadening. With the new sample cell design there was no longer a need for the thermocouple to be completely covered by the sample in order for a good thermal contact to exist. As long as the thermal contact between the pan and the measurement material was good then it could be assumed all other factors stayed constant or in equilibrium with the surroundings so the measurements obtained were reduced in errors caused by the samples thermal mass and duel temperature readings from a signal source.
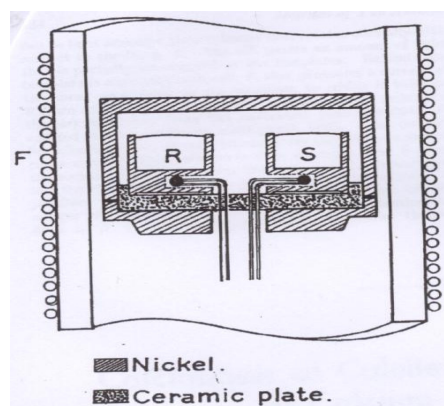
Figure 4: Example of Boersma sample chamber design. S, sample; R, reference material; F, furnace [5]

Several years later a technique that was a combination of all the previous advances in DTA was created and named Differential Scanning Calorimetry or DSC [1].

1.2.2 Differential scanning calorimetry (DSC)
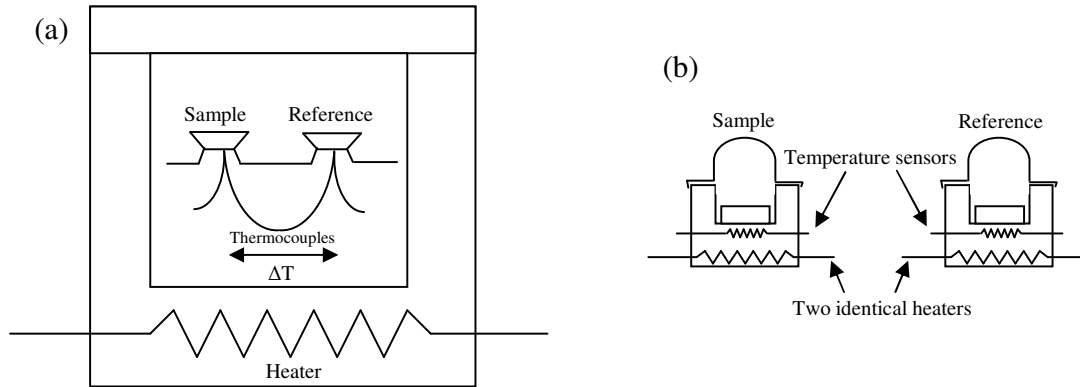
Figure 5: Schematic diagrams of the two DSC types (a) Heat flux DSC (b) Power-compensation DSC

Differential Scanning Calorimetry (DSC) is now the most widely used form of thermal analysis. It works in a similar way to DTA, except that it is a calorimetric method and so differences in energy are recorded not temperature.

There are two popular types of DSC instruments, power compensated DSC [Figure 5 (b)] and the heat flux DSC [Figure 5 (a)]. In the former method the sample and reference are heated separately so that there temperatures are kept equal and the difference in energy needed to maintain these temperatures are recorded. In the latter the changes in heat flow are measured as the sample and reference temperatures are increased linearly in one furnace. In some cases there is a thermal contact between the sample and reference to ensure that neither of the two temperatures can deviate too far away from each other.

1.2.3 Thermogravimetric analysis (TGA)

(a)

(b)
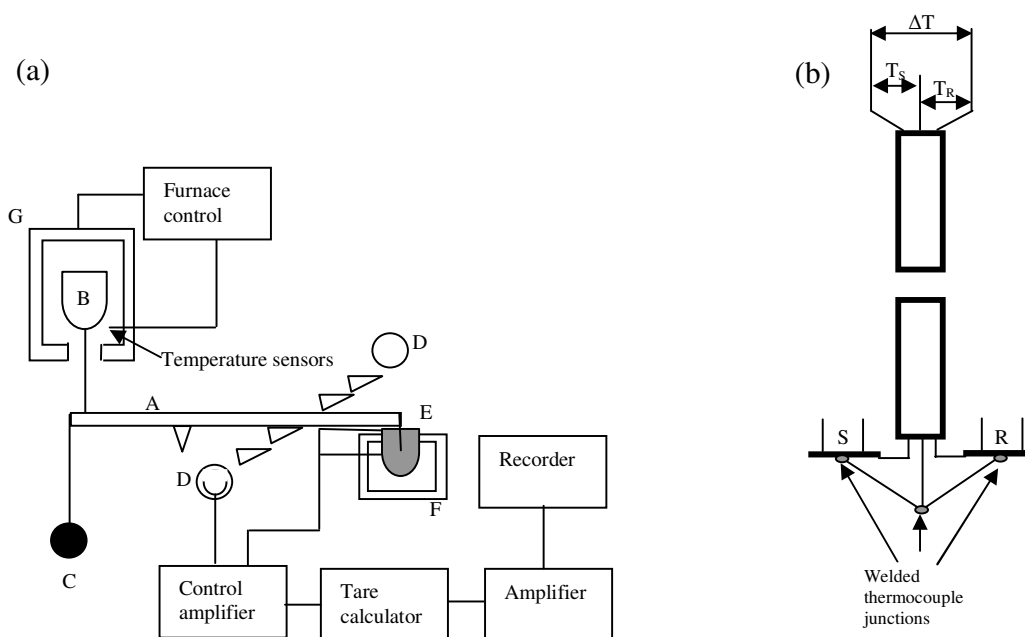
Figure 6: Schematic diagram of (a) Thermal balance: A – beam, B – sample, C – counter balance, D – lamp and photodiode, E – coil, F – magnet, G – furnace (b) SDTGA head mounted on a thermal balance beam

TGA involves determining changes in mass as a function of temperature. It is commonly used to research degradation temperatures, absorbed content of materials, levels of inorganic and organic parts contained in a material and analyse solvent residues. It employs a sensitive electronic balance from which the sample is suspended in a furnace controlled by a temperature programmer.

All current conventional thermal analysis instruments utilise electrical furnaces for heating where the heat passes from the furnace wall to the surface of, and then through the sample by conduction. This process produces temperature gradients within the sample that reduce the resolution of the data produced by the TA technique being used to study it.

1.3 History of microwaves

The use of microwave heating as an industrial application was originally considered around 1948 [6]. The magnetron was invented during the Second World War for military radar but its possible civil applications were quickly realised. Using microwaves for the preparation of food is attributed to Percy LeBaron Spencer from the Raytheon Corporation, who by chance discovered that when walking past a radar mast a chocolate bar melted in his pocket. Upon further investigation it was found that microwaves could induce heating in many foodstuffs more rapidly than via a conventional furnace. The transformation from military to civil applications was not an easy transition as the appropriate equipment was unavailable and (perhaps more importantly) there was no data on dielectric properties of materials to be considered for microwave heating.

Von Hippel [7] led a group at the Massachusetts institute of technology (M.I.T.) in the late forties/early fifties working solely on obtaining reliable data on material dielectric properties. Their work on organic and inorganic materials in the region of $100 < f < 10^{10}$ Hz is now the basis for radio and microwave heating techniques [6].

Wavelength (m)
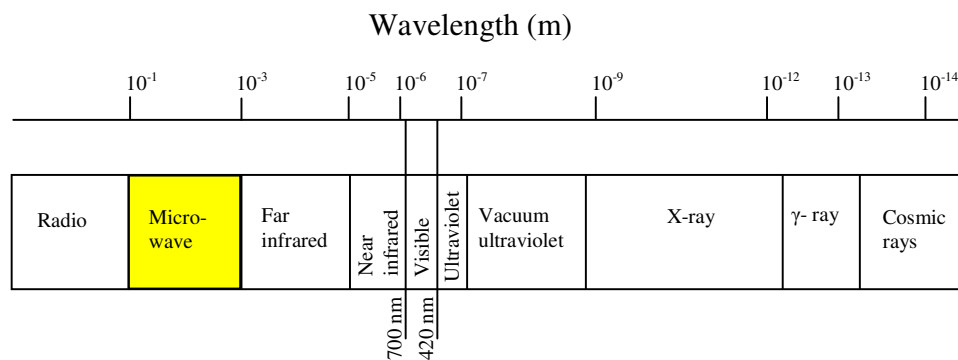
Figure 7: Diagram of the electromagnetic spectrum

Microwaves and radiowaves are both forms of non-ionizing electromagnetic energy. Ionizing radiation has a very high frequency making it of high energy and able to penetrate most objects. Non-ionizing radiation, such as microwaves, have a much lower frequency and as such reduced energy, making them less damaging to biological tissue. Microwaves are defined as the region of the electromagnetic spectrum with wavelengths of between 0.01 and 1 m, corresponding to frequencies of between 0.3 and 30 GHz. Microwave frequencies correspond to those that cause molecular rotation and microwave

absorption spectroscopy has been used for the analysis of gas phase molecules. However, in solids and liquids microwaves can induce heating as will be explained in detail in Chapter 2.

To stop interference with radio signals (and other forms of telecommunications) the wavelength at which microwaves can be used for scientific and industrial uses is regulated. In most countries, the allowed frequency is 2.450 (+/- 0.050) GHz although other frequencies have been allocated (Table 1 shows the allocated frequencies for industrial, medical and scientific uses worldwide). If heating needs to be done outside the allocated band, an effective shield (Faraday cage) must be used to enclose the source to prevent radiation leakage.

Frequency (GHz)	Tolerance (+/-)	Area permitted
0.434	0.2%	Austria, Netherlands, Portugal, Germany, Switzerland
0.896	**10MHz**	**United Kingdom**
0.915	13MHz	North and South America
2.375	50MHz	Albania, Bulgaria, CIS, Hungary, Romania, Czech /Slovak Republics,
2.450	**50MHz**	**World-wide, except where 2.375 is used**
3.390	0.6%	Netherlands
5.800	**5MHz**	**World-wide**
6.780	0.6%	Netherlands
24.150	**25MHz**	**World-wide**
40.680	**25MHz**	**United Kingdom**

Table 1: Permitted Frequencies for Industrial, Medical and Scientific uses

In October 1954 the first microwave oven was patented. For the following 20 years advances and new applications followed.

To begin with, microwave heating was used mainly by the DuPont company for industrial applications such as drying, where the company built large microwave drying plants for the removal of water from nylon in the 1950s and 1960s [8]. Recently, the use of microwaves has become more widespread and

covers processes such as ceramic sintering, polymer curing and the drying of wet analytical samples [8].

Currently, microwaves have found applications in organic synthesis following the work of microwave-assisted organic synthesis (MAOS) described by Gedye *et al*. [9, 10]. Since his investigations the area has become of great interest to synthetic chemists and has led to the publication of over 2000 papers on the subject.

Microwave heating has many advantages including:

- Increased heating speed which improves efficiency,
- Ease of operation (can be turned off and on instantaneously),
- Better thermal efficiency compared to conductive heating,
- Improved product quality.

1.3.1 Previous thermal analysis with microwaves

Although the use of microwaves has broadened vastly since the discovery of its heating capabilities, its use in thermal analysis is not widely mentioned, other than the work of Karmazsin *et al*. [11-13] which led to the work of Barnes, Parkes and Bond [14-17] and the later related work of Nesbitt *et al*. [18].

The Karmazsin *et al*. [11-13] instrument was based around a single-mode cavity operating in a TE10 (H10) mode (see 2.6.1 Modes of propagation, page 54). It demonstrated that larger samples (loads) could be heated with greatly reduced thermal gradients than exhibited with conventional furnaces. Interestingly, the instrument also highlighted differences to conventional methods, for instance the reversal of the observed peak when water in different forms was evolved in dehydration experiments. Vaporised water does not couple to microwaves, whereas liquid water is known to be a strongly absorbing material. Therefore water in the liquid state resulted in a sharp increase in the sample temperature, while in the vapour state the transition was illustrated as a fall in sample temperature, making the two different states very easily distinguishable (see 7.6.1 Copper sulphate pentahydrate, page 251 for an example from this research).

The machine also possessed a DTA function which proved problematic, owing to the differences in tan δ between the sample and reference (a similar problem which was overcome in the current research in Chapter 7, and Section 5.3 Development of a microwave differential cell page 196, 128 respectively). Karmazsin also suggested heating the waveguide as a possible solution for reducing the reverse thermal gradients exhibited by microwave experiments, a problem which has been investigated in this research during the development of new sample cells (see 5.1 Development of new sample cells, page 118).

A prototype microwave thermal analysis apparatus (MWTA) was constructed in the Materials and Catalysis Research Centre (MCRC), University of Huddersfield by Parkes *et al.* [15-17]. This instrument also utilised a single-mode cavity to set up a standing wave to focus the electric field of the microwave radiation onto the sample while using either the sample temperature or the applied microwave power as a means of detecting thermally induced transitions such as melting or decomposition.

The potential of the instrument for thermal analysis was demonstrated in a series of DTA experiments on a range of materials [14]. Microwave energy can produce more uniform heating than conventional methods involving furnaces which rely on conduction. In the context of thermal analysis this suggests that MWTA has the potential to give enhanced resolution.

Recently, a modified form of MWTA has been developed at the MCRC called Microwave Dielectric Thermal Analysis (MDTA) [19] which incorporates a network analyser to allow direct measurement of the dielectric properties of a material heated using microwaves.

The development of microwave thermal analysis was shown to have the potential to provide a further insight into the properties of materials during microwave heating, and will be discussed further in Chapter 6 and Chapter 7.

1.3.2 Microwave Thermal analysis (MWTA)

The instrument built at the University of Huddersfield further developed the initial work of Karmazsin *et al.* and is described in the following sections.

1.3.2.1 MWTA

Microwave thermal analysis has the potential to investigate the interactions of matter with electromagnetic radiation at microwave frequencies. It provides both heating and informative data resulting from changes in dipolar polarization, and electrical conductance using changes in the applied power.

With the advances detailed in this thesis MWTA is capable not only to monitor the changes mentioned earlier but also to provide data comparative to conventional thermal techniques such as DSC and DTA.

1.3.2.2 MWDTA

The application of differential methods (as detailed in previous sections) provides an increase in the sensitivity of the instrument in detecting small enthalpy changes. It is likely that most of these types of transitions are coupled with dielectric changes. Where this is not the case, without the development of this method as detailed in this thesis, the range of samples that could be investigated would be limited to those that exhibit dielectric discontinuities. The addition of the MWDTA method allows conventional thermal analysis to be performed using microwaves with the added advantage of increased sensitivity at points where changes in dielectric properties are not evident.

1.3.2.3 The need for MWTA

Typically, transitions which are observed by TA are in the order of a few degrees whereas a transition observed via MWTA can be within the order of 10's or 100's of degrees when using similar masses to methods such as DSC, making a transition very evident. The advantage of this increase in sensitivity allows transitions such as dehydrations very easy to determine. Water couples strongly to microwave radiation and when it is lost the power required for the instrument to reach the set point changes significantly. This is therefore a very useful method for the identification of water in pharmaceutical samples for example.

Aside from the conventional uses for microwave thermal analysis, in the growing area of microwave heating, MWTA has the potential to give much needed information on how materials interact with

microwaves and are heated which could determine whether a process is suitable for microwave treatment or if other factors (such as thermal runaway) would make it undesirable.

Microwave thermal analysis is also very efficient as nearly all the energy used during an experiment is used to heat the sample and not the furnace walls, or dead spaces.

Chapter 2

Theory

Microwaves can be described as a propagation phenomenon that requires no material support and involves an electric and a magnetic field component, each of which is a function of time [20].

Even though they are grouped in the same category as other electromagnetic waves such as X-rays and gamma rays they are not ionising as they do not posses enough energy.

The MWTA technique is based on how materials interact with microwaves. The extent of this interaction creates both the heating and the analytical signal for a sample during an experiment.

This chapter describes a fairly non mathematical basis of the production and application of microwaves and their interaction with matter. The advantages and disadvantages of the propagation of microwaves through a waveguide and the appropriate calculations are also discussed.

The theory of microwave heating

2.1 Microwaves

A schematic diagram of a microwave is shown below. As with all electromagnetic waves the electrical (E) and magnetic (H) components are at 90° to each other with both components in phase.
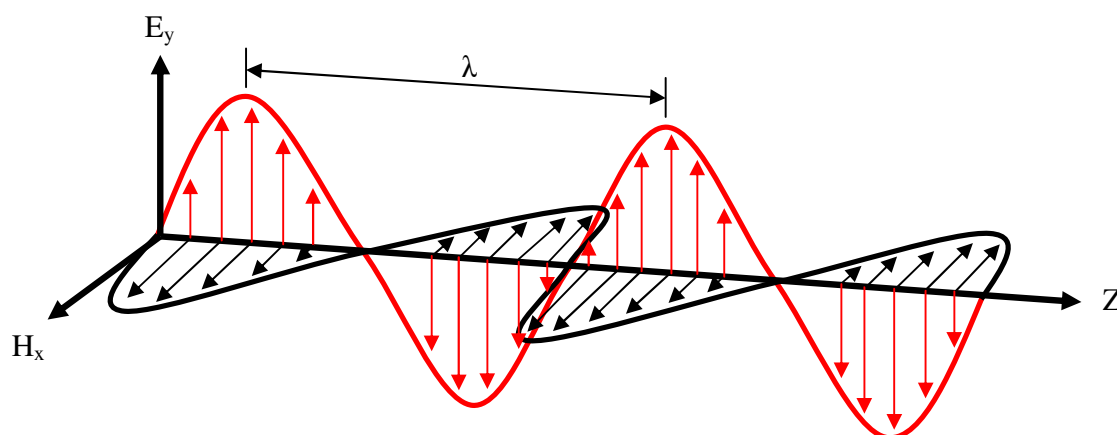
Figure 8: Diagram of the propagation of an electromagnetic wave, E_y, the electrical component in the y axis, H_x, the magnetic component in the x axis, Z, direction of propagation, λ the wavelength.

2.2 Electrical properties of dielectric materials
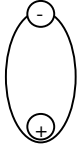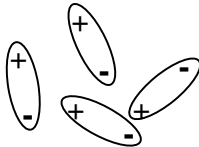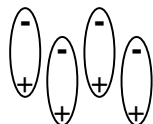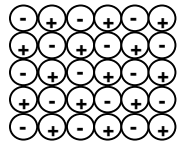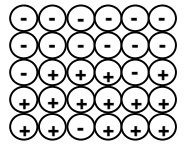
A dielectric material is a material in which polarisation can occur in an applied electric field.

Dielectrics differ from conductors, as their charges are bound, i.e. held in place by atomic or molecular forces, and are unable to move macroscopic distances unlike the charges in conductive materials.

The extent to which these materials interact with microwaves is dependent on several factors within the material:

- Polarisation,
- Permittivity,
- Electrical properties of materials,
- Permeability.

2.2.1 Polarisation

Mechanism	No applied field	Applied field
Electronic polarisation		
Dipolar polarisation		
Interfacial polarisation (Maxwell-Wagner polarisation		

Figure 9: Illustrations of mechanisms for electrical polarisation

In the presence of an applied electric field the induced charges in the dielectric material will tend to realign. In the case of electronic polarisation the electrons shift from their position near the nuclei to one which can track the field more easily. When a permanent dipole is present the dipole again realigns with respect to the applied field resulting in dipolar polarisation. An alternative form of polarisation arises from the accumulation of charge at the interfaces in heterogeneous materials, causing an induced dipole in the bulk of the material (interfacial polarisation).

2.2.2 Permittivity

The complex dielectric constant of a material, ε^*, is given by

$$\varepsilon^* = \varepsilon' - j\,\varepsilon''_{eff}$$

Equation 6: Complex dielectric constant

Where: ε' is the real permittivity (a dielectric constant)

ε''_{eff} is effective the dielectric loss factor

$j = \sqrt{-1}$,

ε' is a measure of the material's ability to be polarised by the applied electrical field, whereas the imaginary part of the complex permittivity, ε'', is related to the efficiency in which the electromagnetic energy is converted into heat. The effective dielectric loss factor, ε''_{eff}, is made up of the dielectric loss (from polarisation) and the conductive (Ohmic) loss:

$$\varepsilon''_{eff} = \varepsilon'' + \frac{\sigma}{\omega \varepsilon_0}$$

Equation 7: Effective loss factor equation

Where: σ is the electrical conductivity of the material.

ω is the angular frequency of the radiation ($\omega = 2\pi f$, where f is the microwave frequency)

ε_0 is the permittivity of free space

ε'' is the loss factor

The ratio of the loss factor and the real permittivity is equal to tan δ (the tangent of the angle δ), the phase lag between the applied electrical field and the resultant polarisation:

$$\tan \delta = \frac{\varepsilon_{eff}^{"}}{\varepsilon^{'}}$$

Equation 8: Equation for the calculation of tan δ

Tan δ is a good indication of how efficiently the material converts the applied waves into heat, as the greater the phase angle (see 2.4 Heating via dipolar polarisation, page 42) the greater the losses from the material. It is worth noting that tan δ is not a linear function as it is greatly affected by both temperature and frequency.

The power dissipated per unit volume of a material subjected to a microwave field is given as:

$$P = \omega.\varepsilon_0.\varepsilon'.\tan\delta.E_{rms}^2 = 2.\pi.f.\varepsilon_0.\varepsilon_{eff}^{"}.E_{rms}^2$$

Equation 9: Equation for power dissipated per unit volume

Where : E_{rms} is the root mean square of electrical field strength in the material (V/m)

From this equation it can be seen that the greater the value of tan δ the more power is dissipated in the material and the greater the extent of heating.

2.2.3 Electrical properties of materials

As microwave heating is in no small part electrical heating, the electrical properties of a material have a major effect on the extent it heats. Electrical conductivity and resistivity can be crucial factors their relationship to each other can be shown using the following simple equation:

$$\rho = \frac{1}{\sigma} = \frac{1}{\omega\varepsilon^{"}}$$

Equation 10: Relationship between resistivity, electrical conductivity and dielectric properties

Where: ρ is resistivity

2.2.4 Permeability

This thesis mainly concentrates on the heating resulting from the electrical component of the wave, although when materials are heated using microwaves it is not clear if the magnetic component of the wave also plays a significant part. The complex permeability (μ^*) of material is given by:

$$\mu^* = (\mu' - j\mu'')$$

Equation 11: Complex permeability equation

Where: μ^* is the complex permeability

μ' is the real permeability

μ'' is the magnetic loss resulting from relaxation and resonance

Permeability losses of dielectric materials do not have the same trends as other magnetic properties, such as hysteresis, and are associated with electron spin resonance. In practice in non-magnetic materials the permeability can be said to be equal to 1 and so is negligible.

2.3 Microwave heating

Microwave heating arises from a number of factors relating from the dielectric properties of the material being heated. When a material is subjected to an applied electric field, the total polarisation (α_t) is calculated from the sum of four components: electronic polarisability (α_e), atomic polarisability (α_a), dipolar or re-orientation (α_d) and interfacial polarisation (α_i). The latter is sometimes referred to as the Maxwell-Wagner effect. The total polarisation equation is:

$$\alpha_t = \alpha_e + \alpha_a + \alpha_d + \alpha_i$$

Equation 12: Total polarisation equation

In the microwave frequency range, the electronic polarisability and atomic polarisability can follow the alternating electric field component of the electromagnetic energy without the generation of heat. The most important term is α_d, which is the result of polar molecules or permanent dipoles in a material attempting to re-orientate in an alternating electric field.

The role of the Maxwell-Wagner polarisation is dependent on a range of complex factors relating to the heterogeneity of solid surfaces at the microscopic level. It generally only has a small contribution to heating although it is involved in the build up of charge between particles which can produce localised plasmas with some materials.

The two main causes of microwave heating of solids and liquids (gases are not heated by microwave energy at atmospheric pressure) are as follows:

- Dipolar polarisation
- Ohmic heating

2.4 Heating via dipolar polarisation

The microwave frequency which is applied to the material affects the extent of heating, which can be calculated using the Debye equation.

$$\varepsilon^* = \varepsilon' - j\varepsilon_d'' = \varepsilon_\infty + \frac{\varepsilon_s - \varepsilon_\infty}{1 + j\omega\tau}$$

$$\therefore \varepsilon'' = \frac{(\varepsilon_s - \varepsilon_\infty)\omega\tau}{(1 + \omega^2\tau^2)}$$

Equation 13: Debye equation

Where: ε_s and ε_∞ are dielectric constants under direct current and high frequencies respectively

τ is the relaxation time of the system which controls the build-up and decay of polarisation

ε''_d is the relative dipolar loss factor

j is an imaginary number ($\sqrt{-1}$)

ω is the angular frequency of microwaves ($\omega = 2\pi f$ where f is the microwave frequency)

The Debye equation can be interpreted as the effect frequencies have on the dielectric.

At a low frequency, there is enough time for the dipoles in the material to follow the applied field easily. The material at this point stores most of the applied energy and, although some is lost in collisions, the overall heating effect is low. If the frequency is too high the dipoles do not have sufficient time to respond and so do not rotate, resulting in no motion and hence no energy transfer or heating.

However, at microwave frequencies the electric field alternates slowly enough for the dipoles to attempt to track the electric field but too quickly for the rotating dipoles to keep up. The phase difference (tan δ) between the orientation of the field and the dipole causes energy to be lost from random collisions between dipolar molecules, an effect termed 'molecular friction' [6, 7] and it is this which produces heating under these conditions.

2.4.1 Heating via Ohmic heating (conduction losses)

Dipolar polarisation is the primary cause of heating in polar liquids and solvents but in the case of solids, conduction effects can be more important. Here, polar particles are drawn back and forth through a semi-conducting material by the high strength of the alternating electric field, giving rise to a process known as 'Ohmic heating' [8] or dielectric hysteresis, a process seen in resistors when a current is passed.

2.4.2 Thermal runaway

One drawback arises from the fact that the terms ε' and ε''_{eff} (and hence tan δ) are dependent both on the material and, crucially, the temperature. For some materials, their ability to couple with microwave energy can increase sharply with temperature, potentially leading to undesirable 'thermal runaway' effects. MWTA is ideally suited to investigate this phenomenon.

A large number of solids have low dielectric losses, and these losses increase with temperature. As the temperature increases tan δ rapidly increases and the temperature then rises exponentially. The temperature can only be stabilized if heat can be removed at a rate that equals the rise, or by limiting the microwave power.

2.4.2.1 Behaviour of ε''_{eff} with temperature

The effective loss factor or ε''_{eff} is of great importance in the context of microwave heating, and is believed to be the main contributing factor to the responses seen in quantitative MWDTA experiments. As shown in the microwave heating equation (see Equation 14) changes in ε''_{eff} directly affect the rise in temperature observed, therefore how ε''_{eff} is affected by temperature cannot be ignored.

In conventional thermal methods the enthalpy of a system controls the area of the peak, moreover the system returns to equilibrium with little change to the baseline. Where the baseline is altered it is an effect of heat capacity. In a microwave run where the sample has dielectric changes the standard response is an alteration in baseline which does not return to the pre-transition value, as ε''_{eff} has changed and therefore so has tan δ. The return to the baseline seen in conventional methods is due to the heat required by the sample being provided by conduction from the surroundings. If microwave heating was the same as conventional heating then ΔT would be quickly equilibrated by the rate of heat loss due to the colder surroundings, but as this is not the case when larger samples are used it is believed that, strong changes in tan δ and sample masses during heating are the main cause of the non-linear results seen in Chapter 8.

2.4.2.2 Microwave induced heating rates

The equation below shows how changes of ε''_{eff} directly affect the rate of heating.

$$\frac{(T - T_0)}{t} = \frac{0.556 \times 10^{-10} \cdot \varepsilon''_{eff} \cdot f \cdot E_{rms}^2}{\rho \cdot Cp}$$

Equation 14: The combination microwave heating equation

Where: $$\rho = \frac{M}{V}$$

$$E = E_{max} \cdot e^{-\alpha z} e^{j(\omega t - \beta z)}$$

Where: α is the attenuation factor

β is the phase factor

Altering the mass and volume of a sample (and hence the density and heat capacity) will have a direct effect on the heating rate. It is documented that the value of ε''_{eff} changes exponentially as the temperature rises [6] in many cases, resulting in the rate of ΔT changing exponentially and giving rise to thermal runaway.

2.4.3 Heating of poorly coupling materials.

A number of materials do not heat by any of the mechanisms discussed previously and therefore require an auxiliary medium in order to raise their temperature when only using microwaves as the heating source.

The medium most commonly used in these cases is called a susceptor and is a material which is able to absorb electromagnetic radiation and convert it to heat resulting in the surrounding area heating via conduction. Commonly, the required amount of susceptor is mixed with the material of interest creating countless heating sources or 'intimate furnaces' which heat the material from several points within and around its volume.

The advantage of this arrangement is, although the sample is heating via conduction, (as in a conventional method) the material and heating sources are touching therefore nearly eliminating thermal mass. In addition to this, the applied power or heating rate required to heat a material can be altered by either adding or removing susceptible material. The main disadvantage of this technique occurs if the material is not thoroughly mixed or the percentage of susceptor is too high. As a result, localised hot spots can occur leading to thermal runaway, and/or inaccurate temperature measurements.

2.4.4 Diluents

A diluent is used to reduce the concentration of an active ingredient. For use in thermal analysis the diluent needs to be chemically and thermally inert and for use in microwave thermal analysis (MWTA), it must also be unable to couple to microwave energy.

2.4.5 Susceptor/diluent mixes

In previous works [14, 15, 17] the use of sample and susceptor mixes have been discussed. The advantage of this type of sample preparation is the sample is always close to a controlled heating source (intimate heating/micro furnaces), therefore aiding in removing the problem of thermal mass. From an analytical point of view the analyte has now changed, with the possibility of giving rise to depression or elevation of transition temperatures in certain cases. The mixing of a sample with a diluent to increase volume and reduce the magnitude of the reaction is not an uncommon analytical technique and diluent mixtures of a sample can be found in many other instrumental sample preparations (Atomic absorption, Ion coupled plasma, High performance liquid chromatography). In the case of MWTA it may be unavoidable to run a sample without it being a diluent mixture, as the transitions can be too strong to control by any other method.

2.5 Propagation of microwaves in a waveguide

In order to perform effective heating under microwave radiation the wave needs to be directly interacting with the material (load). To increase the likelihood of these interactions a suitable housing (cavity) needs to be installed around the load.

2.5.1 Multi-mode cavities

The medium which houses the microwaves during heating is called a cavity. There are two widely used cavities, single mode and the more commonly used multi-mode. The latter is often seen in homes within a domestic microwave oven. It works by launching microwaves along a short waveguide into the path of a mode stirrer which reflects waves to all sides of the cavity. The waves then reflect randomly off the walls onto the object to be heated. As the cavity is classed as over sized due to it being much wider than a half a wavelength, the wave is subjected to evanescent decay. In order to increase the chances of the entire object interacting with the wave, the object is usually rotated.

Multi-mode cavities in domestic microwave ovens usually have simple power controls based on pulse-width modulation, which have on/off cycles of the order of seconds. The erratic interaction of the wave

and sample together with the time between switching cycles does not allow the power to be adjusted accurately or rapidly enough for thermal analysis.
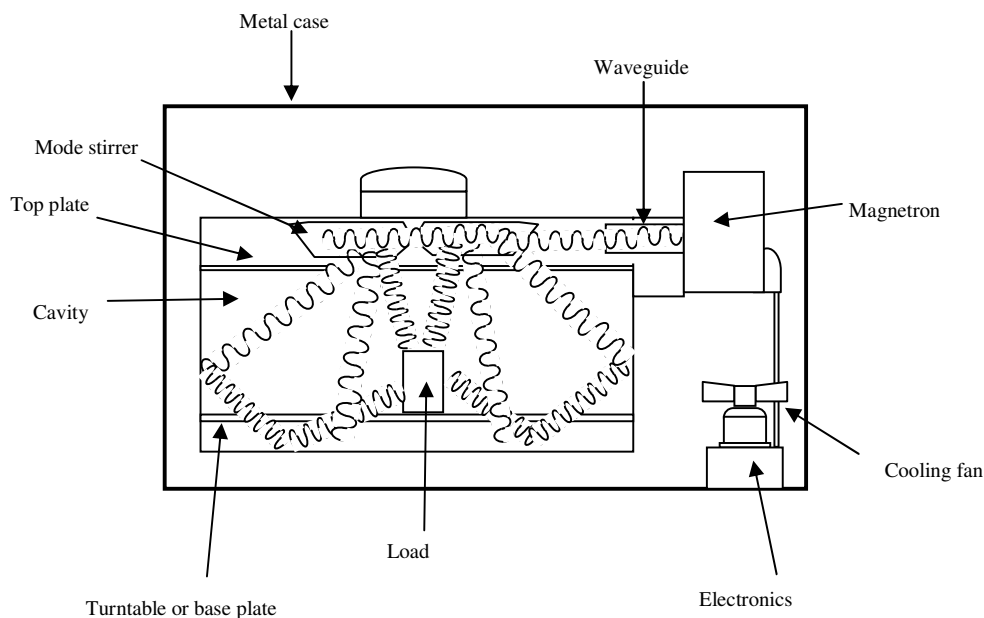
Figure 10: Cross section of a multi-mode cavity

2.5.2 Single mode cavities

A single mode cavity forces a dominant wave form to propagate, resulting in set points of minima and maxima being formed which can easily be determined by wavelengths. The advantage of this is that it allows an object always to be placed in a position of the propagating wave's maximum therefore allowing it to constantly interact with the wave. This approach is more suited for MWTA as it allows variables arising from the position of the sample in the cavity to be greatly reduced. The commonest form of the single mode cavity is the waveguide.

2.5.3 Transmission lines and waveguides

Traditionally when electrical energy was needed to be transferred, a two-wire transmission line was used. The nature of electromagnetic waves means that two-wire transmission is not suitable for transmitting microwave energy. Coaxial lines are better suited to this transfer as the field is completely confined by conductors. Waveguides can be thought of as being large coaxial lines without a conductor running through the centre. A waveguide can be a number of shapes including rectangular, circular, and elliptical and made out of a conductive material. Waveguides are normally constructed of copper, brass, silver, aluminium or any metals which have low bulk resistivity.

Waveguides are the most effective way of transferring electromagnetic energy and have many advantages. For example, due to the larger surface area in a waveguide the copper losses (I^2R) are greatly reduced. In a coaxial cable the surface area of the outer conductor within the cable is relatively large, but the inner cable (which carries the microwave energy) surface area is small in comparison. This inner cable is able to transfer the energy by restricting the current to a very small layer on the surface of the conductor by a process known as the 'skin effect'.
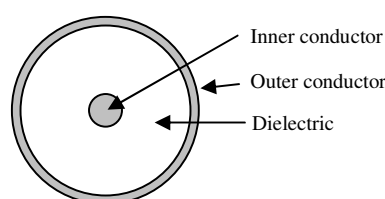
Figure 11: Illustration of a cross sectional view of a coaxial cable

The extremes of any electromagnetic wave transfer medium are a perfect conductor and a perfect dielectric. The conductivity (σ) of a perfect conductor is infinite [6], which is impossible in practice as the conduction current (J) could never be infinite.

$$I = \frac{V}{R}$$

Equation 15: Ohm's Law

$$J = \sigma \times E$$

Equation 16: Continuum form of Ohm's law [20]

Where: I   = Current

V = Voltage

R = Resistance

J = Current density (current per unit area)

σ = Conductivity

E = Electric field

The opposite case is also unlikely as if E (the electric field part of the wave) is zero it suggests that the magnetic part (H) and the fully formed wave current (J) would also be zero. In this state the wave cannot propagate as a fully formed wave and therefore any current could only exist in the form of a surface current, J_s (skin effect), it is this affect that makes the transmission of microwave through coaxial lines possible.

In a good (to perfect) conductor penetration depth (D_p) is less than 1 µm which suggests the wave, as mentioned earlier, is confined to the surface layer of the conductor or material.

In the other extreme, a perfect dielectric would have conductivity and dielectric losses both equalling zero so all the energy would be stored in the walls of the conductor (or material) via dielectric polarisation. Real dielectrics have a small conductivity which indicates that they possess a small amount of movement of charge (J).

The amount of dielectric loss can be represented by the dielectric conductivity (σ_d):

$$\sigma_d = \omega \varepsilon^{''} = \omega \varepsilon^{'} \tan \delta$$

Equation 17: Dielectric conductivity equation

Dielectric losses can occur in coaxial lines during transmission due to the insulation between the lines interacting with the propagating wave causing dielectric loss, which in-turn creates heat. This problem is greatly reduced in waveguides as the dielectric medium is air, which has a much lower dielectric loss than normal insulation materials.

There are disadvantages to using waveguides; one of the most problematic is their physical size. For example, a waveguide to be used at 1 MHz would be around 500 feet wide [6].

Three cases that can occur due to the waveguide dimensions and are detailed below:

1. The wavelength in free space ($\lambda_0 = 12.2$ cm at 2.45 GHz) is less than twice the width of the chosen waveguide (cut-off wavelength, λ_c,).

   $\lambda_0 < \lambda_c$

The wave will propagate without attenuation in the waveguide (except for the resistive losses in the wall) [6, 7].

2. When $\lambda_0 = \lambda_c$, the wavelength in the waveguide (λ_g) would become infinite, which in-turn causes propagation only to occur across the cross section of the waveguide.
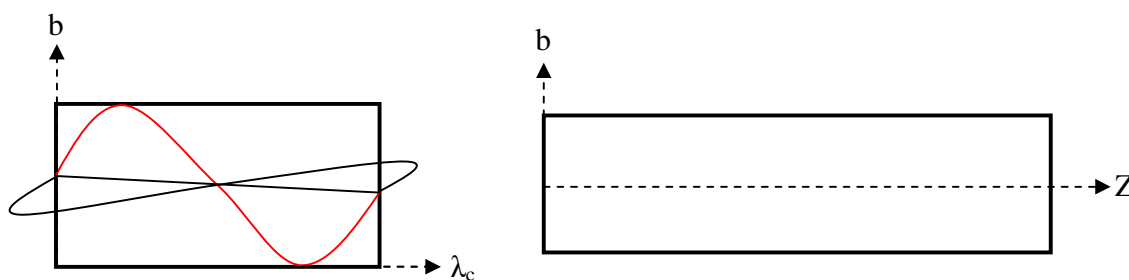
Figure 12: Cross-sections of an incorrectly sized cavity (Z is the direction down the waveguide)

3. When $\lambda_0 > \lambda_c$, the wave is said to be evanescent and is subjected to rapid decay close to the source.
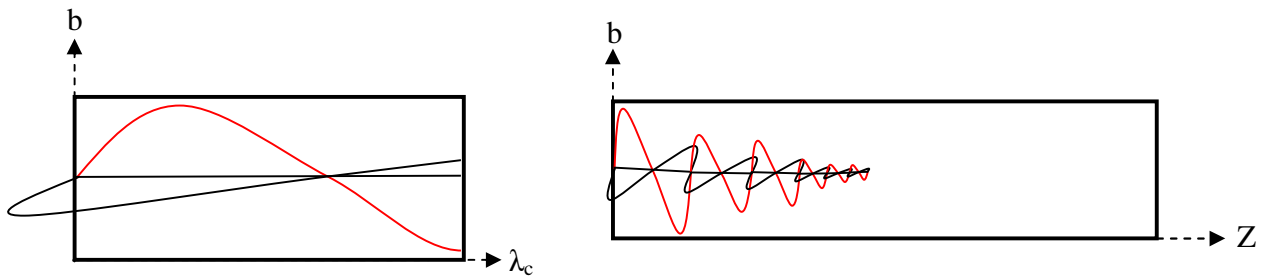
Figure 13: Cross-section of an oversized cavity (Z is the direction down the waveguide)

2.5.4 Microwave penetration depth

The power penetration depth, D_p, is defined as the distance from the surface of a material at which the power diminishes to 1/e (=37%) of the surface power [21].

If zero reflected energy is assumed, then the power penetration depth equation can be rearranged and calculated for a homogeneous material by the equation:

$$D_p = \frac{1}{\omega \left\{ 2\mu_0 \mu' \varepsilon_0 \varepsilon' \left[\sqrt{1 + (\varepsilon''/\varepsilon')^2} - 1 \right] \right\}^{\frac{1}{2}}}$$

Equation 18: Penetration depth equation for a homogeneous material [6]

Where μ_0 is $4\pi \times 10^{-7}$ Hm^{-1}, the permeability of free space

        μ' is the relative permeability of the medium (which is 1 for non-magnetic materials)

In reality the materials are rarely homogeneous therefore the penetration depth of a real conductor is defined by:

$$D_p = \frac{1}{2\alpha} = \sqrt{\frac{2}{\omega\mu\sigma}}$$

Where: α = attenuation factor

$$\alpha = \omega\left(\frac{\mu_0\mu'\varepsilon'\varepsilon_0}{2}\right)^{\frac{1}{2}}\left[\left(1+\left(\varepsilon''_{eff}/\varepsilon'\right)^2\right)^{\frac{1}{2}}-1\right]^{-\frac{1}{2}} Np/m$$

Equation 19: Penetration depth equation [6]

Microwave penetration also decreases with frequency [6]. Typically for a 2.45 GHz microwave the penetration depth is around 2 cm.

2.6 Properties of waveguides

The MWTA instrument uses a WR340 waveguide which is a standard size to allow for a dominant TE$_{10}$ mode (see 2.6.1 Modes of propagation, page 54) to be set up at 2.45 GHz.

Waveguide Flange

	WR340
A	138
B	95
C	119
D	76,2
E	34
F	90,42
G	47,24

All in (mm)

Internal Waveguide Size

	WR340
A	86
B	43

All in (mm)
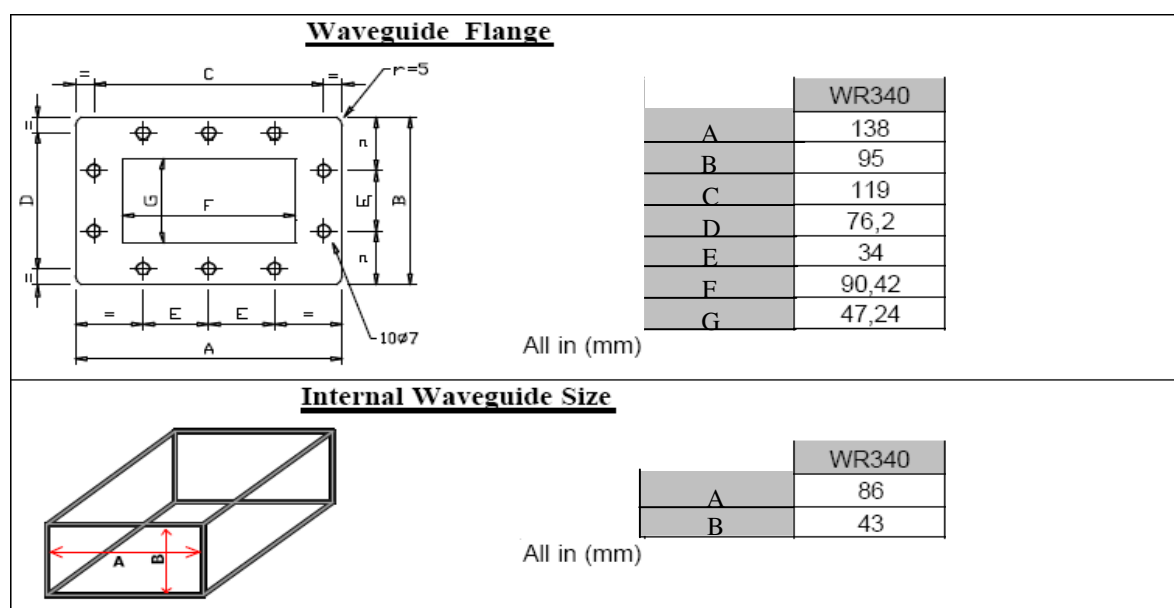
Figure 14: Dimensions of a WR340 waveguide [22]

Due to the size of the waveguide, the cut-off wavelength (λ_c = 2a = 17.2 cm) is greater than that of the wave in free space (λ_0 = 12.2 cm), resulting in propagation with no attenuation as in case 1, discussed earlier (see 2.5.3 Transmission lines and waveguides, page 48).

By enclosing the wave in a waveguide, the wavelength at a set frequency is dramatically altered. The extent of the variation can be calculated using the following equation.

$$\lambda_g = \frac{\lambda_0 \lambda_c}{\sqrt{\lambda_c^2 - \lambda_0^2}}$$

Equation 20: Wavelength in waveguide where the cut-off wavelength is greater than the wavelength in free space [20]

Where: λ_c = 2a

a = horizontal internal measurement of the waveguide (8.6 cm for WR340 waveguide).

If this calculation is applied to a WR340 waveguide then the wavelength within the waveguide (λ_g) can be calculated to be:

$$\lambda_g = \frac{\lambda_0 \lambda_c}{\sqrt{\lambda_c^2 - \lambda_0^2}} \Rightarrow \frac{12.2cm \times 17.26cm}{\sqrt{17.26^2 - 12.2^2}} \Rightarrow \frac{210.572}{12.21}$$

$$\lambda_g = 17.24cm$$

Equation 21: Calculated wavelength in WR340 waveguide

The correct wavelength of the applied wave when enclosed by a waveguide is an important calculation to be made as it allows the positions of minima and maxima to be allocated within the guide. Without this calculation these positions could be missed by ± 1.3 cm and the load therefore not correctly sited at a wave maximum, causing errors in tuning. These types of instrumental calculation allow set-up to be made (involving, sample position and device tuning) easier and crucially more accurate.

2.6.1 Modes of propagation

The fundamental mode of propagation is defined as having the shortest cut-off wavelength.

The designation TE (transverse electric) is given to waves where the electrical component of the wave is parallel to the "b" axis of the waveguide. TM modes also exist where it is the magnetic component which is parallel. Several modes of propagation can come under the designation TE therefore subscripts are given to give the full description of the dominant mode. The first subscript describes the number of half waves across the "a" axis. The width of a WR340 waveguide is equal to half a wavelength; therefore it has the first subscript "1". The second subscript describes the number of half waves across the "b" axis. As there will be no electrical component in the "b" axis (in a WR340 waveguide) the subscript "0" is given. Therefore the full name of the fundamental mode of operation where λ_c is equal to 2a is TE_{10}.
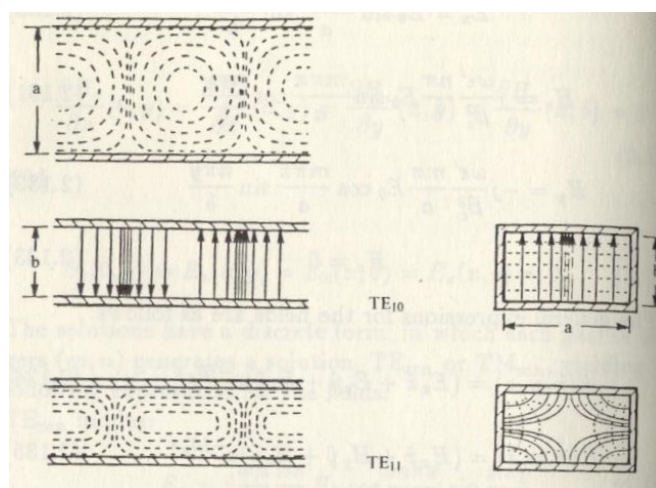
Figure 15: Diagrams of electrical field distribution for different modes of propagation [20]

The diagram also shows the case of a TE_{11} mode of propagation where there is a half wave in the b axis of the waveguide, this is the common mode of propagation in circular waveguides.
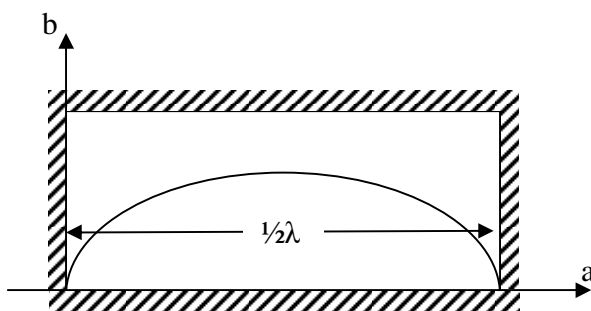
Figure 16: Variation of the electric field inside a WR340 wave guide operating in a dominant TE$_{10}$ mode

The diagram above shows the variation in the electronic field across the waveguide, it can be seen that in TE$_{10}$ mode the maximum of the E field is at the centre of the waveguide.

2.7 Stationary waves in waveguides

Propagation of waves along a waveguide is most efficient when the reflected waves are negligible. When a metal plate closes the end of a waveguide a reflected wave is set-up which superimposes itself on the incident wave, resulting in a standing wave. Under these circumstances the minima and maxima alternate at quarter wavelengths, and are subjected to constructive interference increasing the magnitude of the E field.

As the load is an impedance, it will absorb energy so the reflected wave will be of lower energy than the incident wave. The stationary pattern shifts along the waveguide depending on the capacitive or inductive effect of the load, hence changing the position of maximum and minimum (moving the load out of a position of the initial tuning), therefore impedance matching devices such as an iris, have to be installed in order to correct these changes.

2.8 Microwave power meter

Figure 17: Picture of the microwave power meter

The power meter is a 130 mm section of WR340 waveguide with two directional diodes 43 mm apart (approximately one quarter of a 2.5 GHz wavelength in a WR340 waveguide). The diodes are sufficiently within the waveguide to act as antennae and produce a half-wave rectified voltage proportional to the intensity of the E-field at their location. The forward power diode is located so that it is at an E-field maximum, while the reflected power diode is located at a node where, normally, the E-field is zero as shown in Figure 18.
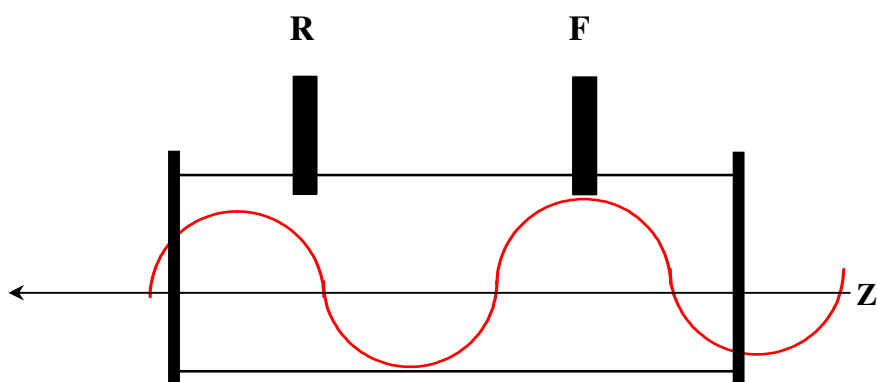
Figure 18: Diagram of cross section (across the z axis) of the power meter with the reflected probe (R) over a node and the forward probe (F) over the maximum of the applied wave.

In a perfect resonance cavity (i.e. one with no load or losses to the waveguide) the only signal would come from the forward power diode with a value equating to the applied power. However, with a

coupling load within the system there would be an out of phase component caused by refraction and reflection, therefore the value of the E-field at the position of the reflected power diode would become non-zero.
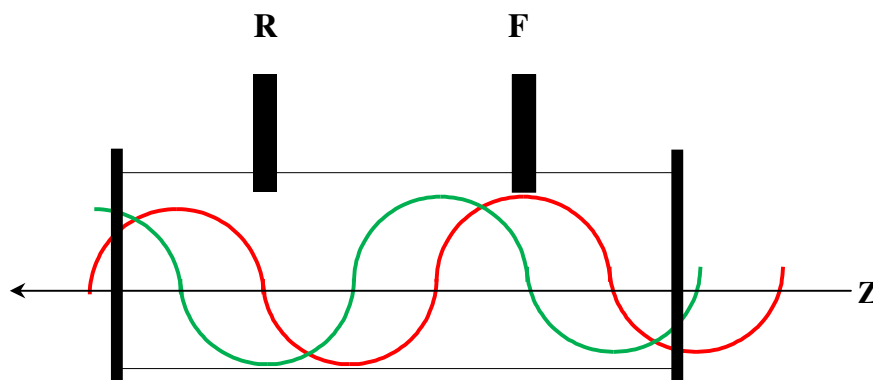
Figure 19: Diagram of cross section (across the z axis) of the power meter when the reflected wave (green line) returns out of phase.

During this research, the power meter was installed (see 4.5 Installation of a microwave power meter into the MWTA, page 112) and calibrated but time did not allow for it to be used extensively.

Chapter 3

Instrumentation

This chapter describes the instrumentation used in this project. The first part focuses on the MWTA instrument and the theoretical operation of its components. The influence these components have on MWTA experiments is discussed in Chapter 4.

The second part of this chapter gives an overview of other instrumentation used including X-Ray powder diffraction, Scanning electron microscopy, modulated differential scanning calorimetry and thermal analysis coupled with evolved gas analysis.

Microwave thermal analysis

3.1 Description of the MWTA instrument

The instrument is composed of seven modules, which are shown below.
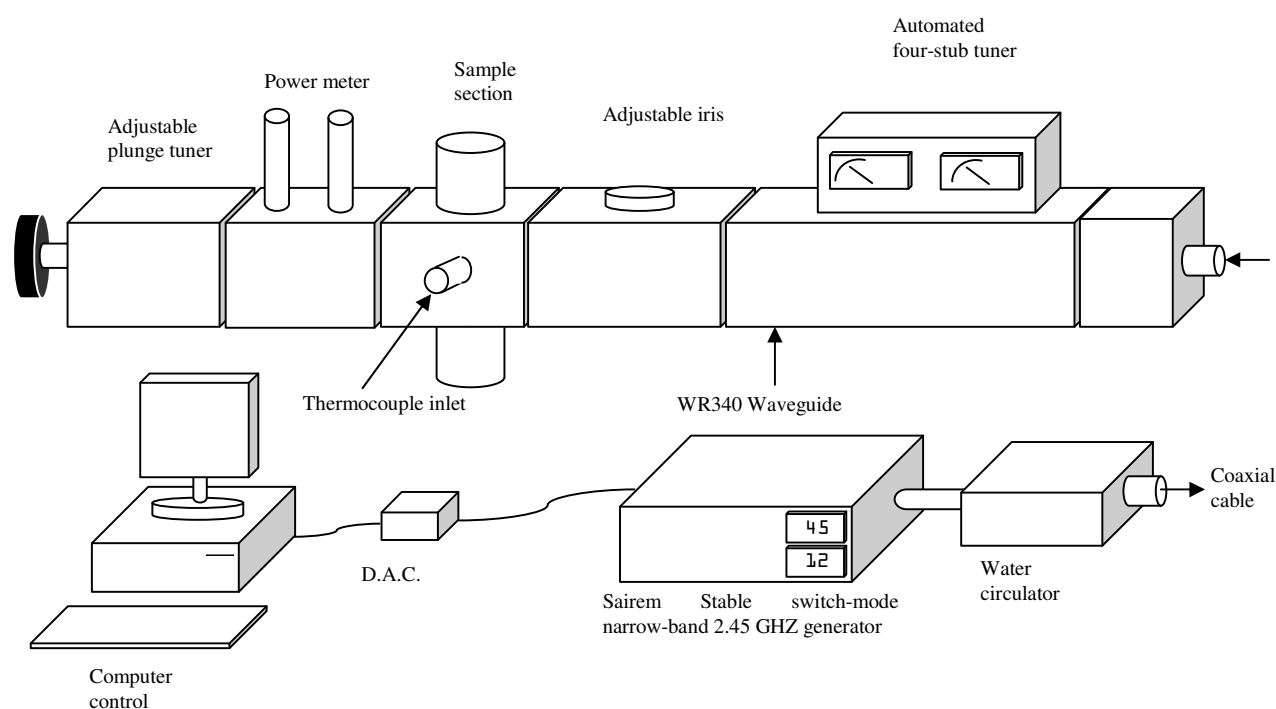
Figure 20: Illustration of the MWTA equipment.

3.2 MWTA Instrument components

3.2.1 RF Generator

MWTA utilises a very stable switch-mode narrow-band 2.45 GHz generator manufactured by Sairem. The generator can be controlled manually, by a potentiometer or, as in this case, by a 0-10 V analogue signal controlled by an analogue-to-digital converter linked to a computer by a D.A.C serial interface [14, 16].

3.2.1.1 Magnetron Operation
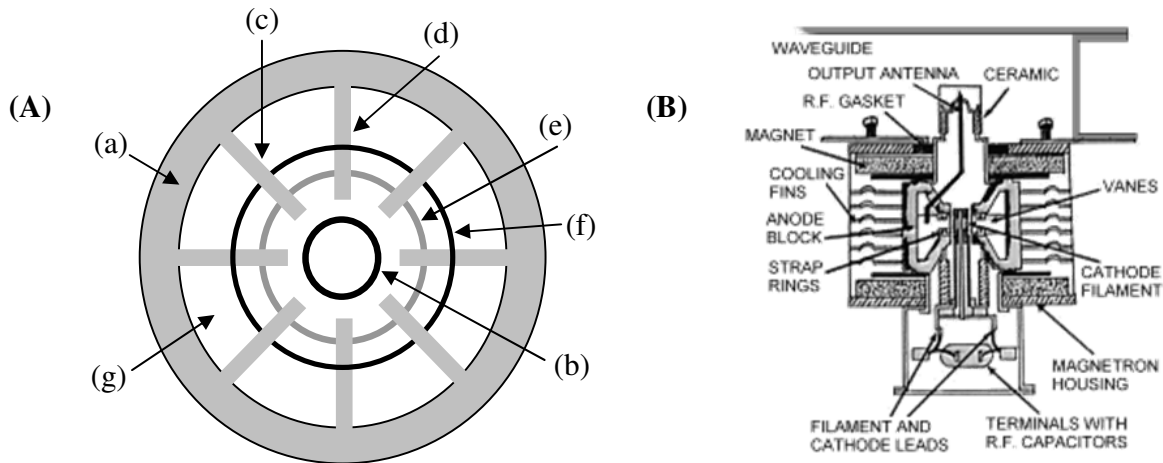
Figure 21: (A) Top view of the magnetron tube (B) Cross sectional view of a typical magnetron

A Schematic diagram of a magnetron is shown in Figure 21. It consists of a magnet surrounding the (a) anode, (b) cathode filament, (c) vane (odd), (d) vane (even), (e) strap (connecting even vanes), (f) strap (connecting odd vanes) and (g) a resonant cavity.

The anode has vanes which face the cathode, which are approximately ¼ λ_g deep allowing resonance at microwave frequencies. The charges on the tips of adjacent vanes are opposite polarities. Electrons emitted from the cathode are rapidly attracted to the anode due to the high positive voltage supplied to the anode relative to the cathode. The magnetic field which is placed perpendicular to the electrons path causes them to travel in a circular path around the cathode.

As the electrons sweep past the cavities opening they induce high-frequency microwaves in the cavity, which in turn causes the electrons to group together in an electron cloud. As the cavities are closely coupled together, microwave power can be removed to a waveguide or coaxial line by a coupling loop in a single cavity.

With a fixed magnet magnetron the current flow is controlled solely by altering the voltage to the anode.

3.2.2 Sample section
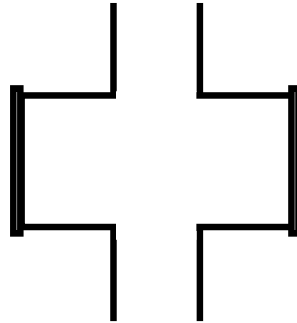
Figure 22: Cross section of the sample section of the MWTA instrument

Originally the material to be tested was placed in a suitable sample cell, and inserted through the large chokes (diameter 50 mm) directly into the waveguide. The sizes of the large chokes are designed to prevent microwave leakage (see 2.5 Propagation of microwaves, page 46).

3.2.3 Four stub tuner
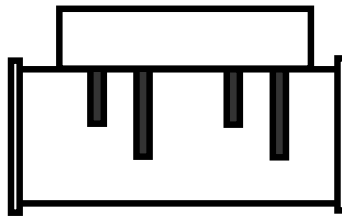
Figure 23: Cross section of the MWTA 4 stub tuner

Total efficiency can only be achieved in a single mode cavity if the output from the generator equals the input of the load (for dielectric heating). As this is an unlikely situation, some of the applied power will be reflected back from the sample section.

Stub tuners are used for load matching and to provide the maximum power transfer between the source and the load. Stub tuners are impedance transformers and they are normally made up of one or more short-circuited, length adjustable tubes (stubs) which are at right angles to the source. The amount the stub moves into and out of the cavity is determined by a computerised version of the Smith chart.

The Smith chart is a graphical aid to help in solving problems in transition lines and matching circuits. The chart is plotted in the plane of the complex reflection coefficient and is normally scaled in normalised impedance. Around its circumference the chart is scaled in wavelengths and degrees, the wavelength scales is used to represent the distance from the generator to the load whereas the degree scale indicated the angle of the reflection coefficient at that point.

The Sairem automated four-stub tuner consists of 4 hollow cylindrical rods. Their positions are constantly altered by using stepper motors to account for changes in the dielectric properties of the sample as it is heated. It is also possible to manually adjust the stubs, allowing them to be fixed in a set position. To indicate the position of a pair of stubs, the tuner supplies an optional analogue voltage signal, although this signal does not possess sufficient resolution to be able to be used as analytical measurement.
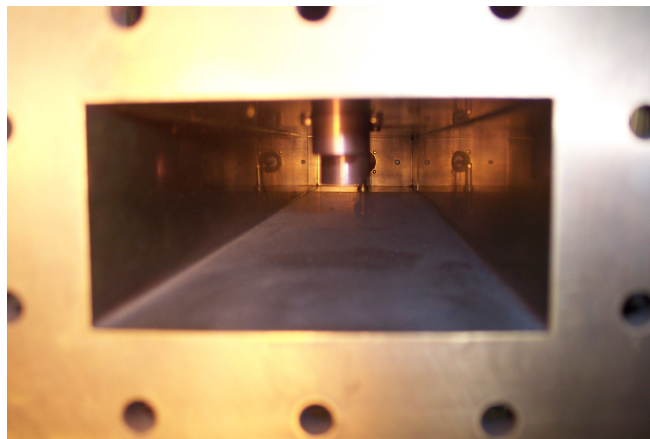
Figure 24: Image of the internal cavity of the four-stub tuner

3.2.3.1 4-stub tuner theory

It was determined that the 4-stub tuner acts as a semi reflecting device. In the forward direction the maximum of the wave is deflected off the undersides of the stubs.

Figure 25: Fundamental diagram of the forward wave passing through the 4-stub tuner

When the returning wave comes back to the 4 stub tuner it can return in a number of ways, for example, if the returning wave node is at the front face of the first stub, then the stubs can stay at the 0, 0 positions and the wave will be reflected.
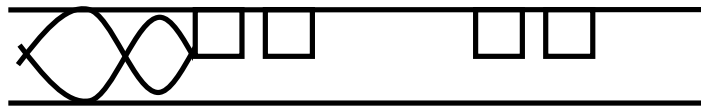
Figure 26: Fundamental diagram of the returning wave reflecting off the first set of stubs

If we say that the previous example is 90 ° out of phase then if the returning wave is 0 ° or 180 ° out of phase the node will now reflect off the next set of stubs, as the faces of the stubs are approximately ¼λ apart, but in order for this to be achieved the first set of stubs would have to be moved out of the way so as not to cause any type of interference.

Figure 27: Fundamental diagram of the returning wave reflecting off the second set of stubs

A problem does occur when the wave is 121 °-179 ° out of phase. At these angles the stubs are in the perfect position for the wave to bounce back up the waveguide towards the launch and have no reflection effect, therefore with the stubs in any position the returning wave will still reflect off the underside of the stubs back to the source, creating destructive or constructive interference of the incidence wave.
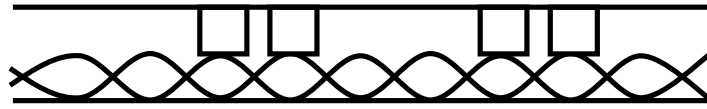
Figure 28: Fundamental diagram of the returning wave when 121 º – 179 º out of phase

In general, by moving each set of stubs, a point of reflection can be obtained and the wave sent back to the sample in most cases.
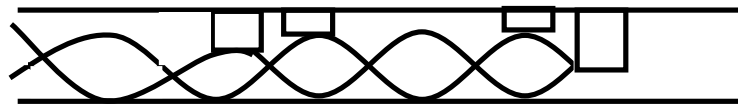
Figure 29: Fundamental diagram of possible stubs positions during operation

In reality the wavelength is much longer than the diagrams shown above and so there are certain positions where the stubs would move to achieve reflection. Also, the reflected wave will not always come back in the same phase (as it is passing through the sample more than once) and so would be subjected to refractions/deformation again, but generally a standing wave can always be achieved with active tuning.

3.2.4 Adjustable short
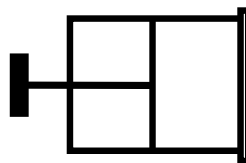
Figure 30: Cross section of the MWTA adjustable short

The adjustable short is used to reflect power when it is positioned at a node, thus creating a resonance cavity. When the plunger moves in and out of the resonance position the reflected power decreases and impedance increases. As the short moves far enough away from the point of resonance ($\frac{1}{4}\lambda$) another node is reached and the reflected power can increase [6].

3.2.5 Iris (Aperture)
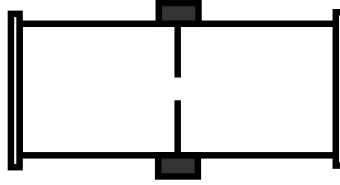
Figure 31: Cross section of the MWTA adjustable iris

The iris is made from a thin copper sheet. The aperture can be made any shape, but for matching the resistance to the E-field there needs to be a reduction or expansion of the iris horizontally across the waveguide.

The adjustable iris has a travelling range of 60 mm, and the closest it can be physically located to the sample is at a distance of 70 mm.

3.2.5.1 Iris theory

The iris can be explained by thinking of it as a capacitative and inductive device. It acts like a capacitor (for E field) building up charge until the current satisfies (equals) the load resistance (R_L) then in effect creates a path of lower resistance. For example, a very small aperture would be a very large capacitor therefore the applied power that is transmitted by the iris would have no resistance and would have a greater heating effect. However, a larger proportion of the wave's E-field would be used to charge the capacitor, meaning less current would reach the load.

An iris can either cause an inductive or capacitative effect depending on the dimensions. This is termed reactance in electronics. Reactance induces a phase shift in the applied wave (in the case of waveguides). The applied E field can be impeded by the returning waves, reflections and other impedances. It is inevitable that the returning wave will be some degree out of phase with the incident wave at a point along the length of the instrument. By placing an iris at a set point along the waveguide the impedance to the propagating wave can be reduced by shifting the phase between the opposing waves to a point closer to an in-phase position. If a purely capacitive iris is put in place then the

maximum will move to a point further away in the direction of propagation and an inductive iris will have the opposite effect.

By having a moveable iris (as in MWTA) the iris can be moved to a point where the greatest mismatch is present and as such the greatest effect. In reality the iris is cut to a shape so that both inductive and capacitive properties are present. By positioning the iris at a point of a node of the propagating wave, the wave can be shunted with the least destructive interference, and the greatest effect on the mismatch.

Capacitive iris
(Asymmetrical)

Capacitive iris
(Symmetrical)

Inductive iris
(Asymmetrical)

Inductive iris
(Symmetrical)
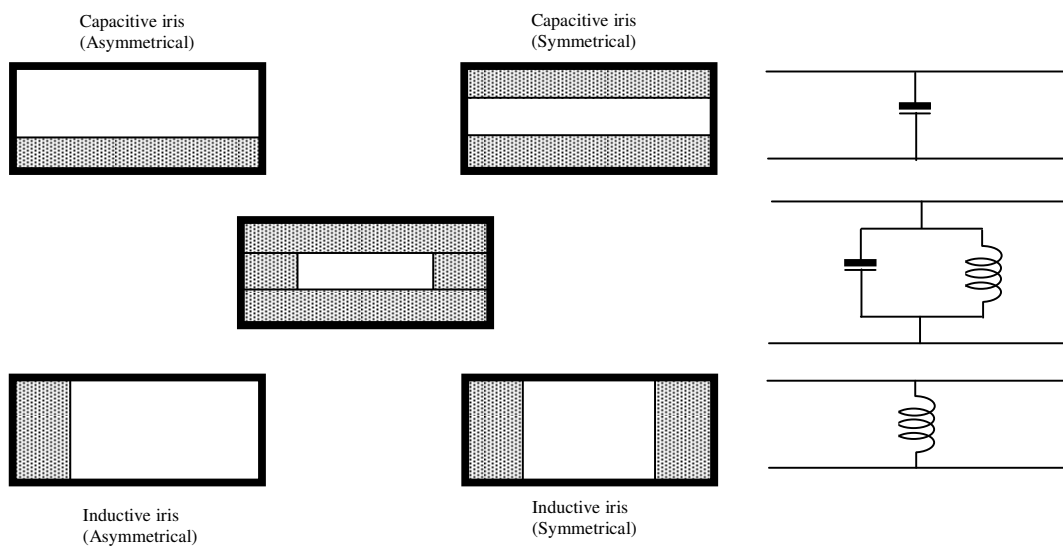
Figure 32: Diagrams of effect different iris orientations have on the capacitive and inductive properties of the MWTA

3.2.6 Dummy load

As power passes from the generator to the waveguide, to prevent damage to the magnetron by reflected waves, it must first pass though the water-cooled circulator or "dummy load" via a coaxial cable. The unit also has a crystal diode that provides a basic measurement of the reflected power, which is fed back to the generator and in turn used to the control computer through the RS232C interface.

3.2.7 Temperature measurement

Temperature measurements are obtained by using 0.5 mm diameter ungrounded stainless steel sheathed type K (chrome alumel) thermocouples (Omega). Other devices such as optical pyrometers, gas

thermometers, IR thermometers and IR fibre-optic probes have been reported in literature to also be suitable [14-17]. The disadvantages such as expense, limited temperature range or only making surface temperature measurements made them undesirable for MWTA [14]. Thermocouples are inexpensive and have a very large operating range (0 – 1000 °C). They also have the added advantage of possessing a very quick response time (<0.6 s).

The thermocouple itself is inserted into the waveguide via one of the thermocouple inlets on the side of the sample section. This arrangement allows for direct temperature measurement. As discussed in Karmazsin *et al.* [11, 12, 13,] microwave leakage can be reduced by locating the thermocouple perpendicular to the electric field. On measurement of the radiation transmitted outside of the cavity by thermocouple, it was found to be < 4 mV/cm^3 and therefore negligible.

3.2.7.1 Thermocouple inlet

Thermocouple placement is an important factor in any thermal analysis instrument. In microwave thermal analysis there is the added problem of the metal thermocouples causing cavity perturbation, in effect disrupting the instrument tuning and efficiency as mentioned in 3.2.7 Temperature measurement, see above. In order to keep the thermocouple at 90 ° to the wave and eliminate leakage [12, 13, 23], guides were installed in the waveguide which consisted of a copper reducing fitting surround by a copper tube.
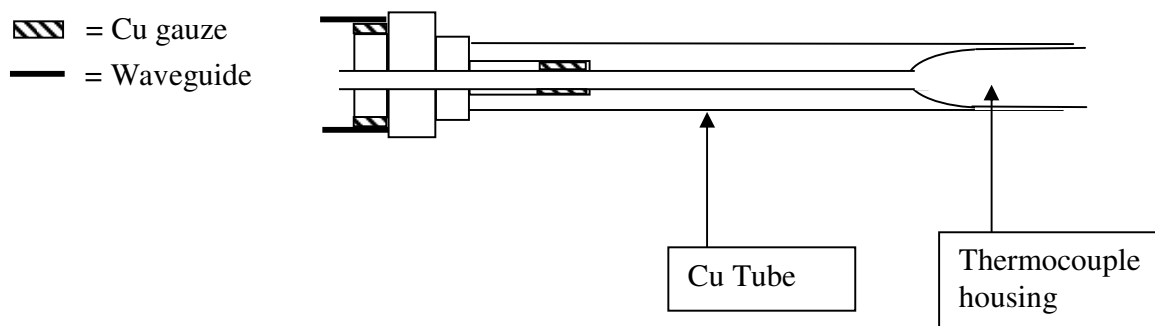
Figure 33: Original thermocouple housing

The thermocouple wire is enclosed in a borosilicate housing which at its widest end has a width of 9 mm. The internal diameter of the copper tube was 10 mm therefore there was some movement in the enclosure, thus increasing the risk of microwave leakage. The redesigned enclosure still utilised the copper tube, but it was now directly inserted into the waveguide. Inside the tube a polyethylene mould was inserted and held in place with a set of guide screws. This advancement ensures movement is kept to a minimum.
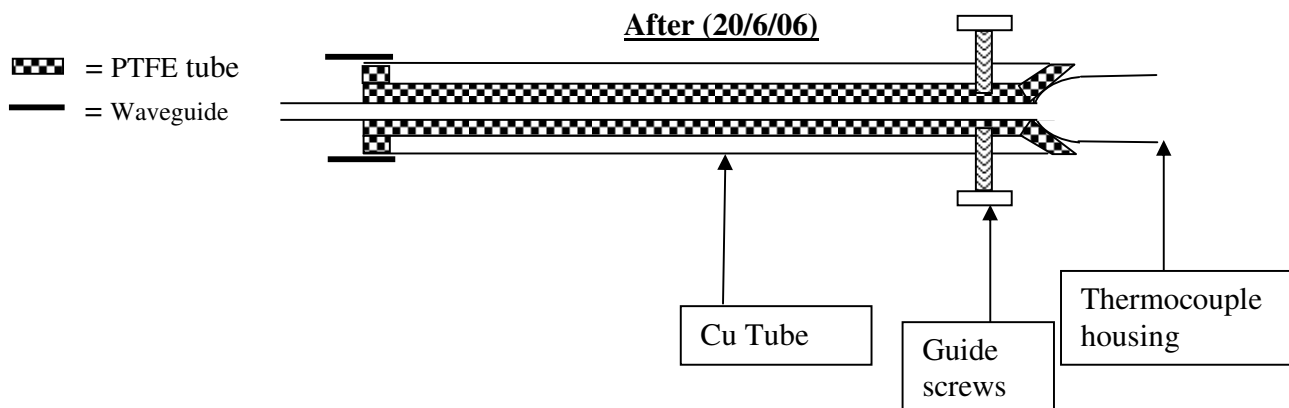
Figure 34: Revised thermocouple enclosure

With the new arrangement radiation transmitted outside of the cavity by the thermocouple was reduced from around 4 mV/cm^3 to 0 mV/cm^3.

3.2.8 Computer software and control
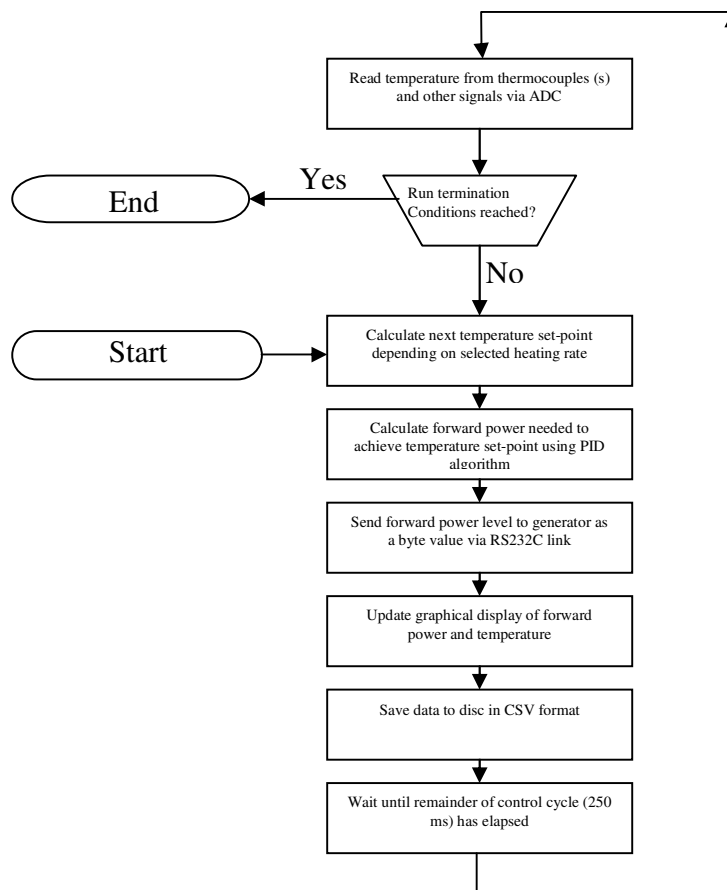
Figure 35: Flow diagram of the MWTA operating system

The heating cycle and data acquisition is controlled by software written using Visual Basic (Microsoft Visual Basic 4.0). The operating system is a 133 MHz PC (Dan Technology). The software is designed to control the forward power applied from the generator, while also displaying real-time power and temperature traces. Data is stored separately on the hard disk in a comma separated variable format (.CSV) to allow for post-experimental analysis in a spreadsheet such as Origin or Excel.

3.2.8.1 Analogue-to-digital converter (ADC)

The voltage signal produced by the thermocouple(s) are read by an 8-channel, 16-bit ADC (Strawberry Tree, DynaRes-8-Ultra). The dynamic ranging and cold junction features allow temperature measurement to be directly read from the thermocouple(s). Connections are made from the instrument to the control computer via a screw terminal box linked via the ADC card to the computer using an ISA slot.

3.2.8.2 Timing cycle

The software is designed to use a basic timing cycle of 250 ms the control cycling and data saving can be set as multiples of these cycles. A typical example would be the forward power control updating every cycle, while additions to the saved data and real-time display being only every four cycles.

3.2.9 Modes of operation

The MWTA is capable of several modes of operation, which are detailed below.

3.2.9.1 Constant power MWTA

An applied power level between 0 and 300 W is fixed and the sample is monitored as a function of time and temperature. The advantage of this mode is the responses observed from the sample are not complicated by control changes. This mode can only be used with samples that interact with microwave radiation.

3.2.9.2 Constant power MWTA (MWDTA)

Essentially the same as Constant power MWTA, though in this method the HPB-Cell allows any sample to be heated even if it is not microwave susceptible. (The HPB cell is detailed in Chapter 5)

3.2.9.3 Linear heating MWTA

The applied power is altered in order to maintain a linear pre-set heating rate of sample. The software allows for a number of heating/cooling ramps with isothermal periods in one experiment.

Heating rates can be difficult to maintain as unlike conventional TA methods, when using microwaves the sample is heated and controlled directly. The situation is complicated more by the possibility of the material rapidly coupling more strongly with the microwave field [14].

3.2.9.4 Linear heating MWDTA

The method is essentially the same as linear heating MWTA, but using the HPB cell. The advantage of this mode is the heating rate is controlled on a thermally inert susceptor, allowing for easier and more stable control. This method allowed repeatable differential signals to be obtained.

3.2.9.5 Linear Power MWDTA

Linear power MWDTA is a very useful method made possible by the HPB cell. The mode involves the microwave power being ramped at a preset rate (e.g. 1 % min^{-1} or 3 W min^{-1}) while the sample temperature and DTA signal are monitored. As with linear heating the software allows for a number of power ramps with iso-power periods in one experiment.

Examples of the advantages of this method are:
- The heating rate can be controlled by the choice of susceptor, and also the experiment is not complicated by control factors.
- Transitions that might normally by missed in other modes, for example the liquid to vapour phase change of free water, becomes more pronounced due to the higher levels of applied power.

3.2.10 PID control algorithm for linear heating

For linear heating experiments the MWTA software uses a feedback loop between the microwave power and the sample (or reference) temperature. This feedback loop contains an implementation [14-17] of a simple PID algorithm which is commonly used in many control applications. The PID algorithm takes its name from the three main terms it incorporates; Proportional, Integral and Derivative. The algorithm takes as an input the difference (called the 'error') between the measured temperature and the desired temperature (called the 'set-point'). Its output is dependent on the weighting given to each of the three terms and consists of either a positive or negative value which is used to adjust the output from the microwave generator.

The effect of each of the three terms can be considered independently:

3.2.10.1 The Proportional term

The proportional term is the simplest. It produces a value directly dependent on the magnitude of the error.

$$Output = P \times e$$

Equation 22: Equation for the proportional term in the MWTA PID algorithm

Where: P is the proportional weighting factor

e is the error

Generally, the proportional term is the predominant control component of the algorithm. However, on its own, there is a tendency to produce a steady-state condition where there is constant offset between the set-point and the temperature.

The behaviour of the algorithm with proportional only control is shown schematically below. The blue dots show the temperature set-point increasing with time for linear heating. The red dots show what the measured temperature would typically be with a constant offset between the two. In the MWTA

software the time between each measurement and each adjustment of the microwave power (i.e. the space between the dots) is approximately 0.25 s.
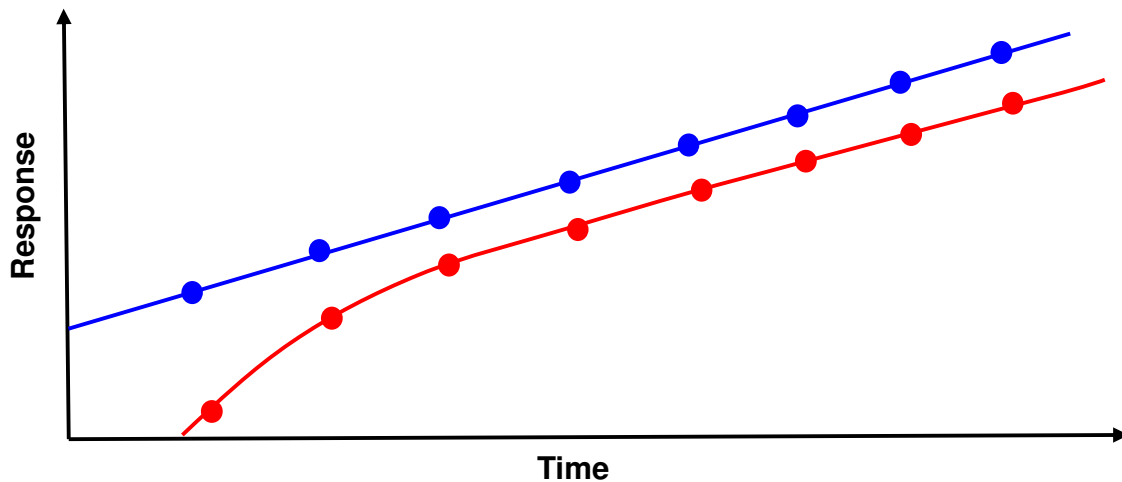
Figure 36: Illustration of how the proportional term alters the sample temperature (red line) to try and reach the set point values (blue line) over time.

3.2.10.2 The Integral term

The integral term produces a value dependent on the sum of the error over a set time period (the integral window).

$$Output = I \sum_{n=IW}^{n=1} e_n$$

Equation 23: Equation for the integral term in the MWTA PID algorithm

Where: I is the integral weighting factor

e is the error

IW is the integral window

Correctly weighted it removes the offset produced by the proportional term. However, the value produced by the integral term can become very large especially if the difference between the set-point and measured temperature is initially large. This can cause an 'overshoot' where the measured temperature exceeds the set-point (possibly followed by a, smaller, 'undershoot') before complete control is achieved.   The behaviour of the algorithm with proportional and integral terms is shown schematically overleaf.
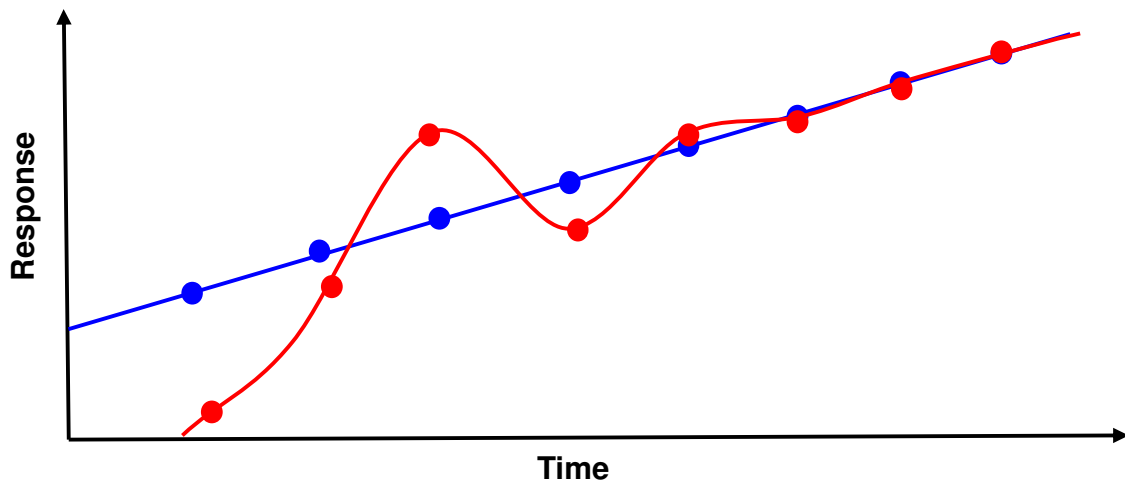
Figure 37: Illustration of how the integral term alters the sample temperature (red line) to try and reduce the offset from the set point (blue line) created by the proportional term over time.

3.2.10.3 The Derivative term

The derivative term produces an output dependent on the rate of change in the error value over a set time period (the derivative window). It acts as a 'slowing' factor that can reduce any overshoot produced by the integral term although often at the expense of more time being taken for the measured temperature to reach the set-point.

$$Output = D \times \sum_{n=DW}^{n=1} (e_n - e_{n-1})$$

Equation 24: Equation for the derivative term in the MWTA PID algorithm

Where: I is the derivative weighting factor

e is the error

DW is the derivative window

The behaviour of the algorithm with proportional, integral and derivative terms is shown schematically below.
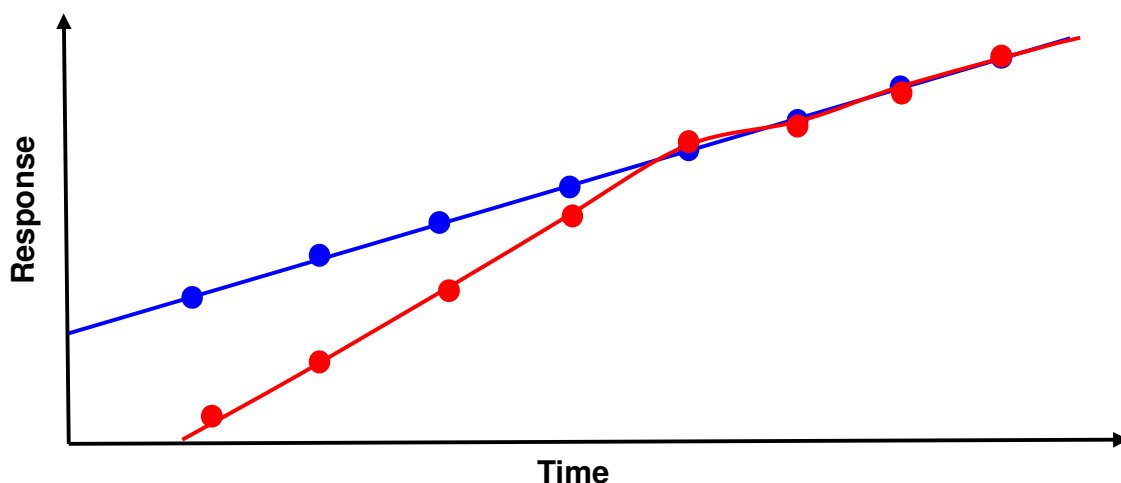
Figure 38: Illustration of how the combined terms alter the sample temperature (red line) to try and reduce the offset and overshoot from the set point (blue line) over time.

Although even simple PID algorithms can produce excellent results the three weighting terms need to be tuned very carefully to match the response of the system being controlled. Incorrect tuning can produce poor tracking of the set-point or oscillations.

For a system such as an electric furnace, the system response (i.e. the relationship between the power applied and the furnace temperature) will not change greatly over a wide temperature range as many factors (the mass of the furnace, the resistance of the windings, etc.) will remain constant. It is therefore possible to tune the PID parameters to get good control. Furthermore, the PID parameters will not need to be change irrespective of what material is heated in the furnace.

With MWTA, the situation is more complicated as the sample itself is the furnace. The relationship between microwave power and temperature will not only vary from sample to sample but also within a sample if it undergoes any changing affecting tan δ. In addition, PID algorithms are generally not good at responding to rapid changes (as might occur when a sample melts leading to a large increase in tan δ, see Chapter 6, page 172). This makes good linear heating difficult to achieve.

Tuning the PID parameters for every sample was impracticable. However, it was found that for certain cell types, particularly those with a significant inert thermal mass (see Chapter 7, page 196) a single set of parameters could successfully be used with a range of samples although loss of control could still occur. When using differential cells (Figure 60, page 131) and linear heating, generally the best results

were obtained when control was on the inert reference while the sample temperature was just monitored.

3.3 X-Ray diffraction (XRD)

3.3.1 Overview of XRD

Since 1912 when Von Laue discovered X-Ray diffraction (XRD) it has been used to find a great deal of important information for both scientific research and industry [25]. Its application to the further understanding of the physical properties of metals, polymers, and other solids, is the basis of most of what is known about the spacing and arrangement of atoms in their crystals. Recently XRD has been used to explain the structure of complex natural structures in compounds such as vitamins, steroids, and antibiotics. XRD is the only analytical method that can provide both qualitative and quantitative information about compounds present in a solid sample. Other methods are only capable of identifying the percentage of ions in the sample [25].

As with other forms of electromagnetic radiation, the sample interacts with the E-field of the electromagnetic wave, these interactions result in the scattering of the incident rays. When X-rays are scatted by a crystalline material, the ordered nature of the crystal gives rise to both constructive and destructive interference. Because the spacing between the scatting centres is of the same order of magnitude as the wavelength of an X-ray, it results in diffraction.

3.3.2 Bragg's Law

Upon an incident X-ray striking a crystal surface at an angle theta (θ), some of it is scatted by surface atoms. The unaffected portion then penetrates through to the next layer of atoms where, again some of them are scatted and the remainder continue to penetrate to the next level of atoms. This pattern of scattering and penetration continues until the maximum distance that X-rays can penetrate that material is reached.
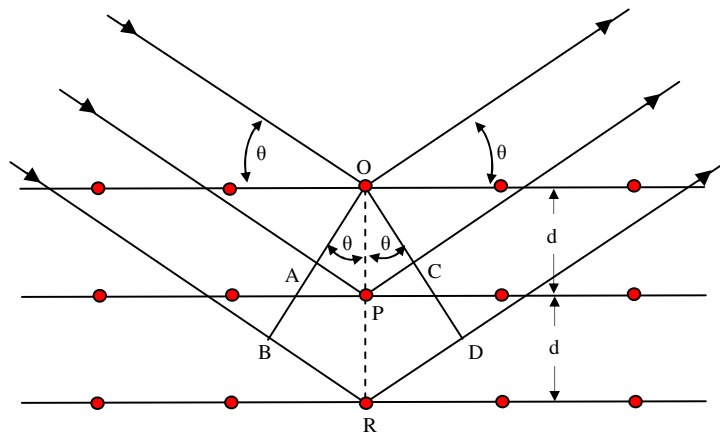
Figure 39: Diffraction of X-rays by a crystal with a high degree of order

XRD requires:

- The layers of atoms to be spaced, roughly, the same distance as the wavelength of the incident radiation.
- A high degree of order in the distributional spacing of the scattering centres leading to a high degree of regularity within the crystal.

In 1912 W.L. Bragg treated crystal diffraction of X-rays as in Figure 39. In this case a narrow beam of X-rays strikes the crystal as explained before. If diffraction occurs at the atomic centres O, P, and R the distance can be said to be:

$$AP + PC = n\lambda$$

Where: n is the integer

The crystal will appear to reflect the X-ray, and the reflected wave will be in phase at point *OCD*, as:

$$AP = PC = d \ \sin \ \theta$$

Where: *d* is the inter-planar distance of atomic centres

Meaning the conditions for constructive interference of a beam of angle θ can be written as

$$n\lambda = 2d \ \sin \ \theta$$

Equation 25: Bragg equation

It should be noted that reflection only occurs from crystals if the angle of incidence satisfies the equation:

$$\sin\ \theta = \frac{n\lambda}{2d}$$

Any other angle of incidence will result in destructive interference.

3.3.3 Production of X-rays

In analytical work the most common source of X-rays is the X-ray tube.

Cooling
water
In

Out

Ground

Beryllium
window

Copper
Target
(anode)

Cu K-α
X-Rays

Tungsten
Filament
(cathode)

Focusing cup

Vacuum tube

High
Voltage

Filament
Heating
circuit
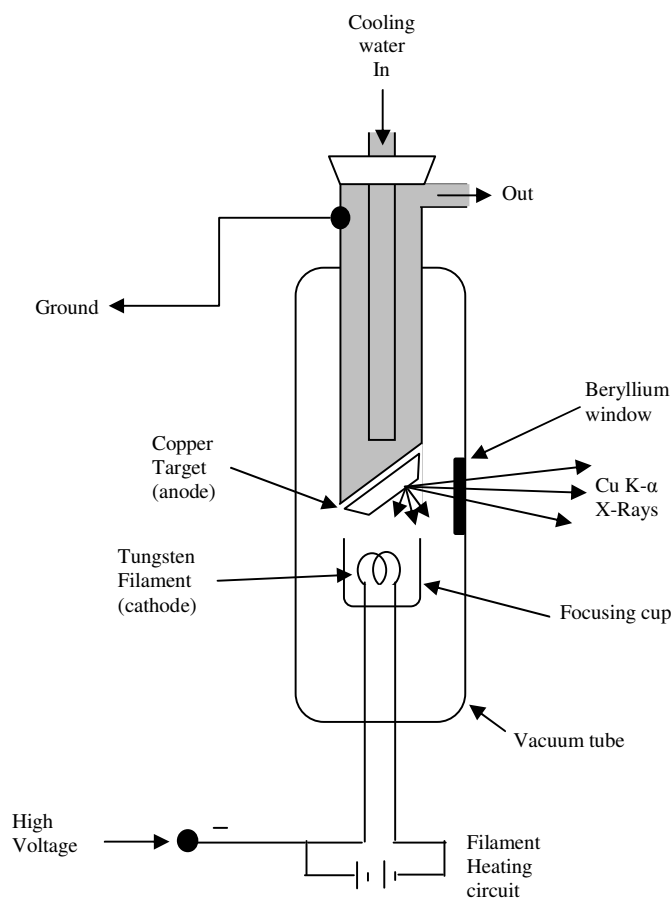
Figure 40: Schematic of an X-Ray tube

An X-ray source consists of usually a vacuum tube inside which is a tungsten filament cathode and an over sized anode. The anode (usually made of copper) consists of a metal targeting plate on the surface or embedded in the metal. Heating of the filament and acceleration of electrons are controlled by two different circuits. Electron bombardment is a very inefficient process, as less than 1 % of the electrons electrical power is converted to radiation; the remainder is dissipated as heat. The off shoot of this inefficiency is that a water cooler is required to cool the anode.

The instrument used throughout this project was a Bruker AXS D8 X-ray spectrometer. It employed a copper anode which emits an average wavelength of 1.5418 Å (Cu K–α-1 and K-α-2, although the K-α-2 signal is removed by the software post-run).

To enhance the resolution of the signal, various slits can be used. The slits are located before and after the sample, and are used to limit the area which is irradiated.

The diffraction pattern is plotted against the diffraction angle 2θ.
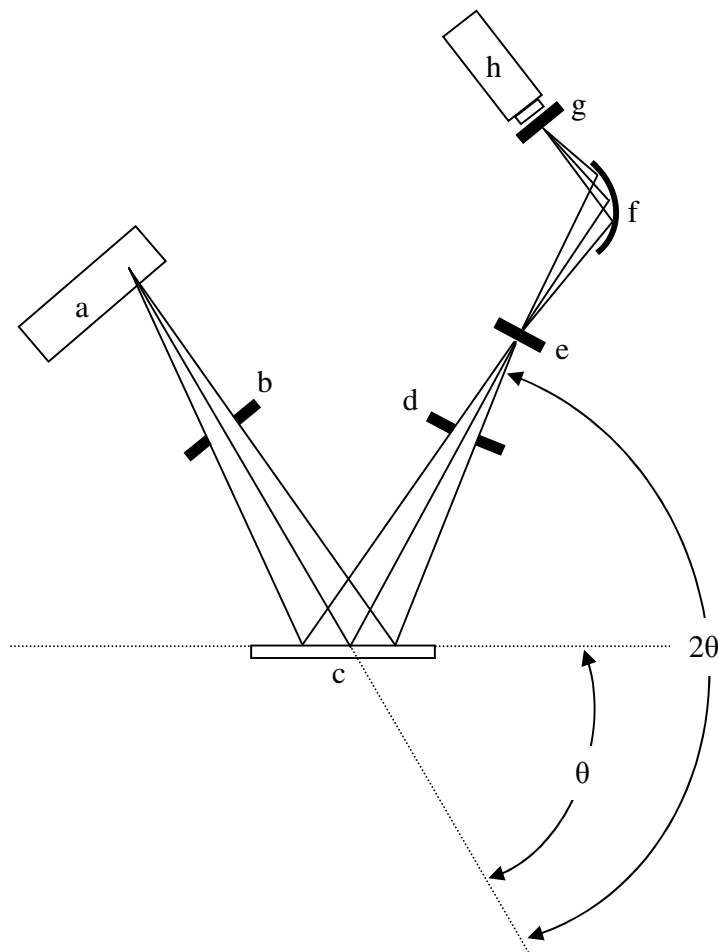
Figure 41: Beam path of a Bragg-Brentano diffractometer

a) X-ray tube

b) Divergence slit

c) Rotating sample disk

d) Anti-scattering slit

e) Monochromator slit

f) Monochromator

g) Detector slit

h) Detector

3.4 Scanning electron microscopy (SEM)

In most scientific disciplines details of the physical structure of the surfaces of a solid is of great importance. Classically this was done by optical microscopy, but optical microscopes are limited to the wavelength of light due to refraction. The SEM technique can be used to give information about the surface at much higher resolutions. To obtain an image the instrument utilises a raster pattern, in which the electron beam is:

1. Swept over the surface in a straight line (along the x axis of the object),
2. Returned to the starting point,
3. Re-positioned along the y axis by a standard increment.

Steps one to three are repeated until the area of interest has been covered. The signal that is produced by scanning is collected above the sample (in the z axis) and stored in the computer to be later turned into an image.

During the scanning process several types of signals are produced by the interaction of the object and beam of energetic electrons; these include backscattered and secondary. Backscattered and secondary electrons are the basis of SEM [25].

3.4.1 SEM Instrumentation
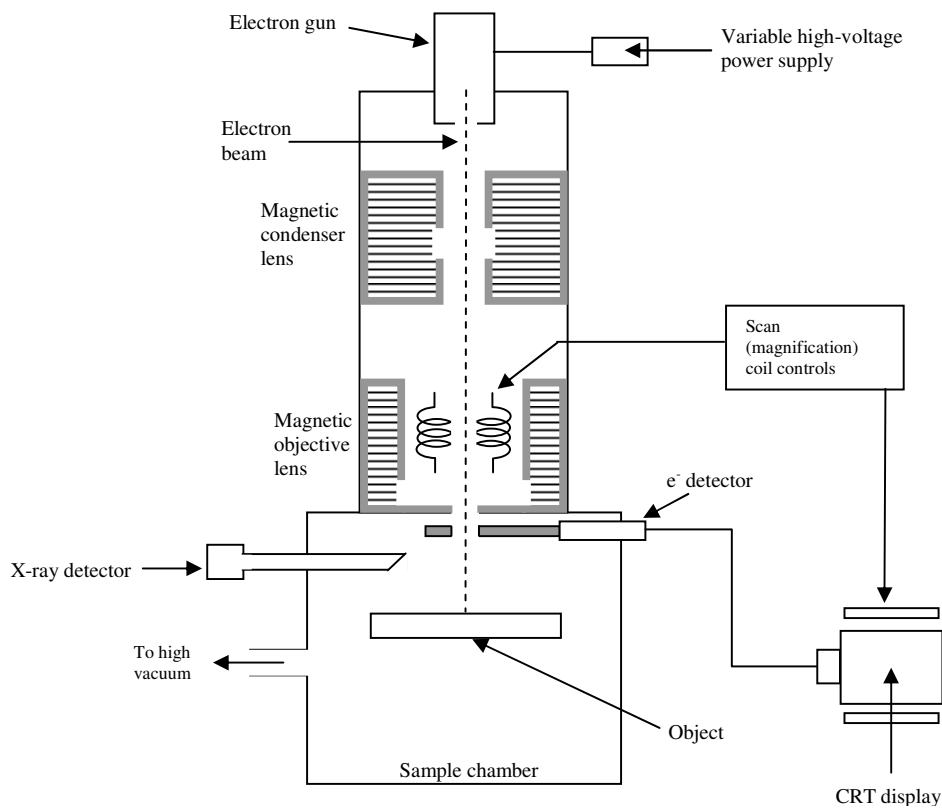
Figure 42: Schematic of an SEM

3.4.1.1 Electron optics

The magnetic condenser and objective lens are used to reduce the image to a spot (typically 5 to 200 nm). The condenser's primary job is to ensure the beam reaches the objective lens which is responsible for the area of the electron beam on the surface of the object.

Scanning is achieved using the two pairs of electromagnetic coils. One pair deflects the beam along the x axis of the sample, whereas the other pair deflects the beam along the y axis. By varying the current to these magnets (x coils) as a function of time, the beam can be swept across the object in a straight line. Once the line scan is completed, the beam returns to its starting point by reducing the current to the x coils, current is supplied to the other set of coils (y coils) causing the beam to be deflected slightly along the y axis and current is then returned to the x coils.

82

As this scanning pattern is the same method used to create an image on a cathode ray tube (CRT) display, the signal produced at a point and the corresponding point on the CRT display have a one-to-one correlation.

The achievable magnification in SEM is given by the equation:

$$M = W/w$$

Equation 26: Calculation for the obtainable magnification in SEM

Where: W   is the width of the CRT display

                 w   is the width of a single line across the sample

As W is a fixed value, magnification is achieved by decreasing w.

3.4.2 Interaction of electron beams with solids

When solids interact with an electron beam there are a variety of responses which can occur. For SEM, two modes are more relevant than the others; scattering and secondary electron production.

3.4.2.1 Scattering

Scattering of electrons can be either elastic or inelastic. In an inelastic collision some or all of the energy is transferred to the object from the electron, the energetically excited object then emits secondary electrons, X-rays and on occasions longer wavelength photons.

Elastic scattering occurs when electrons collide with the object, changing its direction but its speed is virtually unaffected, resulting in the kinetic energy remaining nearly constant. The electron can deflect off the object at any angle from 0 to 180 °.

3.4.2.2 Secondary electron production

Secondary electrons are produced from the electron beam interacting with weakly bound electrons in an object. The interaction results in electrons being force out of their conducting band. Secondary electrons are produced from a depth of between 50 to 500 Å it is possible to prevent them from reaching the detector by simply applying a small negative charge to the housing of the transducer.

3.5 Modulated Differential Scanning Calorimetry

Modulated DSC (MDSC) is used to study the same changes in materials properties as conventional DSC [28]. The advantage of MDSC is it provides additional information about the material which is being tested (which would require several repeat experiments using conventional methods) in a single experiment.

One of the advantages of this method is it can give the operator an increased knowledge of the sample in its native state. As transition temperatures can overlap, in a conventional set up to resolve two events the material would have to be heated above the transition temperature then cooled and re-heated (applying a known thermal history), there are many disadvantages to this kind of experiment :

- The sample is no longer in its native state on the second heating.
- If several events occur very close to each other, there is the undesirable possibility that the first transition could run into the onset of the adjacent transitions reducing the quantitative accuracy of the experiment.

Other capabilities of MDSC include:

- Direct Cp measurement.
- Improved resolution of closely occurring and overlapping transitions.
- Increased sensitivity for subtle transitions.
- Separation of reversing and non-reversing transitions.

Although these advanced features are of great advantage in the field of material testing many of these features are beyond the scope of this thesis due to the time restraints in this research.

In MDSC a rapid heating rate oscillation is applied to the regular linear heating ramp. The total heat flow signal information is converted by a Fourier transform deconvolution process into a reversing and non-reversing heat flow signal.

As with all TA, heating rates play a large part in the information obtained in an experiment. Faster heating rates reduce experimental time and increase sensitivity but reduce resolution as the events can become overlapped. Slower heating rates increase resolution and extend experimental time but reduce sensitivity as the events appear broader.

As sensitivity for most reversible transitions is dependent on the maximum instantaneous heating rate, by using large modulation amplitude and a relativity slow underlying heating rate, both instrumental sensitivity and resolution can be conserved while maintaining a reasonable experimental time. Non reversing transitions tend to occur at absolute temperatures and as such do not lose sensitivity, although slower heating rates are more desirable in order to improve resolution of consecutive transitions.

3.6 Thermal Analysis coupled with evolved gas analysis

Although thermal analysis is a very powerful material characterisation technique, it is limited by the fact that neither TGA nor DSC can provide direct chemical information on evolved species produced on heating [26]. TA techniques used on unknown materials are generally non-specific, and do not respond to particular chemical species. Instead they give an indication of a type of undefined thermally induced event. The addition of evolved gas analysis could possibly be one of the most powerful developments in TA [27]. By combining the energy changes and/or mass losses in a material, with a form of gas-phase analyser, provides details on the material which would be previous inaccessible.

EGA has utilised almost every type of gas detector. They can either be specific or general detectors. Specific detectors include hygrometers, non-dispersive infrared cells, paramagnetic oxygen detectors, chemiluminescence sensors, fuel cell-based devices, etc. These detectors tend to be used for quantitative analysis [28].

Systems based on multi-gas detectors such as quadrupole mass spectrometry (MS) and Fourier-transform infrared spectrometry (FTIR) are usually favoured. Although FTIR is a general detector it is

not able to respond to non-polar molecules, therefore gases such as oxygen and nitrogen are not detected. Mass spectrometry is the quickest most versatile means of monitoring all constant gases.

3.6.1 EGA Instrumentation

The conventional EGA instrument used during this research consists of a program controllable furnace, which contains a closed sample chamber connected to a high vacuum MS source. To aid flow to the MS a range of inert and oxidising carrier gases can be used.

Gas detection was performed by a bench top Hiden HPR20 quadrupole mass spectrometer.

Experimental

Chapter 4

Optimisation and development

This chapter details the effects and optimisation of the various components of the MWTA instrument and the modifications and improvements made to increase its reliability and scope. This chapter also discusses the implications of using thermal insulation around the sample cell and the impact of different diluents and susceptors.

The absence of a dedicated data analysis program meant that experimental results were plotted from raw data in Microsoft excel. The resultant graphs for constant power MWTA experiments in the following chapter are presented in a standard format shown below.
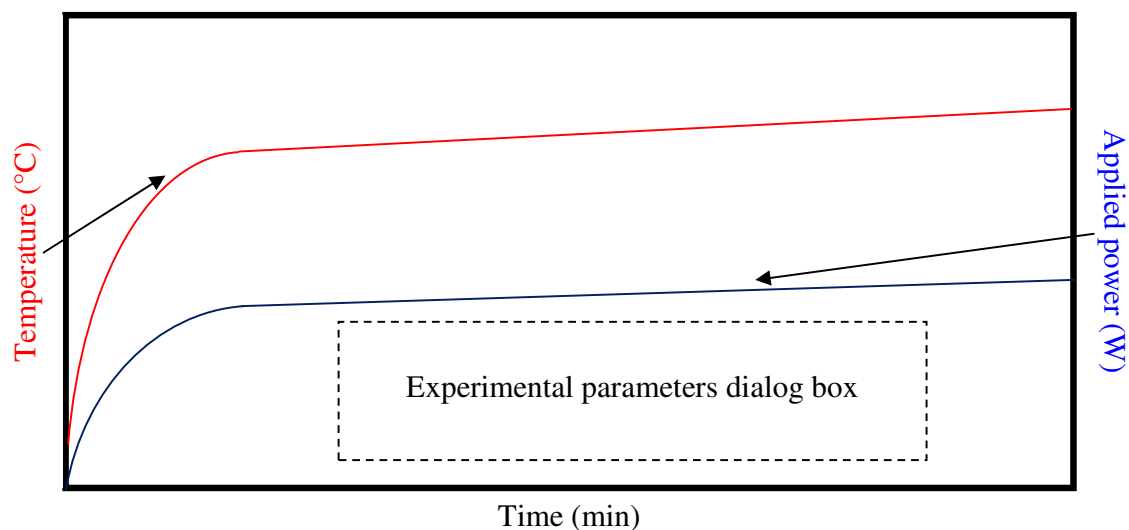
4.1 Initial familiarisation with MWTA using carbons

To gain familiarisation with the hardware components of the instrument as it existed at the start of the project and the associated control software, a series of experiments was performed on a range of activated carbons.

4.1.1 Activated carbons

Activated carbons have a long history of use as adsorbents and find applications in many areas from household water filters through to oxygen filters in hospitals and gas masks. Activated carbons are produced from precursor materials such as coal, wood, oil residues and nut shells.

The precursor is carbonised in an inert atmosphere before being activated either chemically (at temperatures typically below 200 °C) or physically using a weakly oxidising atmosphere and temperatures around 800-1000 °C. This activation stage creates the porosity and high surface area needed for adsorption. Previous workers have noted that many carbons, but not all, act as susceptors and are readily heated with microwave energy [29]. This has suggested that microwave heating may be an effective means of regenerating spent activated carbon filters [30]. MWTA is ideal for studying the reactivation of spent activated carbons in particular, solid state transitions and oxidation reactions in general.

4.1.2 Experimental and results

A range of commercial activated carbons were supplied by Dr. E. Dawson of the MCRC (University of Huddersfield). These are listed in Table 2, page 91 which shows their precursor and how they were activated.

All the experiments used 500 mg samples in a 'bulb' cell (see Chapter 5, page 117) under an atmosphere of flowing helium and were subjected to a range of constant powers (15 W, 30 W and 45 W) with the temperature of each carbon recorded after 5 and 10 minutes. The results from these experiments are summarised in Table 3 and it is apparent that there is a considerable variation in the extent to which different carbons heated.

It was also noted that certain carbons were more efficiently heated on the second and subsequent runs and it was decided to investigate this effect further using carbons 5E, 6E (which were poorly coupling) and 3E, 7E (which were strongly coupling). In each pair, one carbon had been activated chemically and the other physically. The carbons were heated under helium to 800 °C in a conventional furnace and held isothermally for 2 hours to provide a high temperature processing stage. After cooling, they were heated in the MWTA as detailed above. Table 4 compares the temperature reached in the MWTA for the carbons used as received and subjected to the pre-heating treatment. It can be seen that the susceptibility of carbon 3E was reduced by pre-heating in contrast to the other carbons where it increased (significantly in the case of carbons 5E and 6E).

Sample name	Precursor	Activation process
1E	Peat	Steam activated, treated to promote adsorption of specific gases/vapours
2E	Wood	Steam activated, treated to promote adsorption of specific gases/vapours
3E	Coal	Steam activated, treated to promote adsorption of specific gases/vapours
4E	Coal	Steam activated, treated to promote adsorption of specific gases/vapours
5E	Wood	Phosphoric Acid-Chemical Activation
6E	Wood	Phosphoric Acid-Chemical Activation
7E	Peat	Steam activated, treated to promote adsorption of specific gases/vapours
8E	Wood	Phosphoric Acid-Chemical Activation
9E	Olive Stone	Phosphoric Acid-Chemical Activation
10E	Olive Stone	Phosphoric Acid-Chemical Activation
ASC2T	Bituminous coal	Steam activated, treated to promote adsorption of specific gases/vapours
BR1	Coconut shell	Steam activated, treated to promote adsorption of specific gases/vapours
KR1	Coconut shell	Steam activated, treated to promote adsorption of specific gases/vapours
BPL	Bituminous coal	Steam activated, treated to promote adsorption of specific gases/vapours
209M	Bituminous coal	Steam activated, treated to promote adsorption of specific gases/vapours
URC	Bituminous coal	Steam activated, treated to promote adsorption of specific gases/vapours
ASZMT	Bituminous coal	Steam activated, treated to promote adsorption of specific gases/vapours
AMMONO	Bituminous coal	Steam activated, treated to promote adsorption of specific gases/vapours
ABEKR1	Coconut shell	Steam activated, treated to promote adsorption of specific gases/vapours
AR1	Coconut shell	Steam activated, treated to promote adsorption of specific gases/vapours

Table 2: List of industrial activated carbons supplied by Dr E. Dawson

Carbon	Applied power (15 W)		Applied power (30 W)		Applied power (45 W)	
	5 minutes	10 minutes	5 minutes	10 minutes	5 minutes	10 minutes
	Temperature (°C)	Temperature (°C)	Temperature (°C)	Temperature (°C)	Temperature (°C)	Temperature (°C)
1E	173	178	522	527	670	690
2E	151	151	441	456	671	712
3E	226	236	556	569	802	803
4E	79	85	358	373	550	563
5E	39	40	71	74	104	106
6E	37	38	74	78	130	275
7E	172	138	452	461	664	677
8E	62	65	143	149	229	240
9E	43	48	208	328	558	555
10E	57	66	467	473	566	567
ABEKR1	141	156	487	500	736	746
AR1	143	159	510	523	754	762
ASZMT	170	191	488	505	706	745
ASC-ZT	173	190	465	473	640	641
AMMONOSORB	120	127	488	505	689	681
KR1	154	180	442	456	728	714
BR1	129	414	540	533	728	722
BPL	135	145	460	471	804	802
URC	170	318	463	484	673	662
209M	99	109	449	500	800	776
209M REHEATED	-	-	552	557	-	-
= Known to have been activated at high temperatures				- = measurement not taken		

Table 3: Maximum temperatures reached by activated carbon in respect to time and applied power

Carbon Name	Applied Power (15 W)		Applied Power (30 W)		Applied Power (45 W)	
	5 minutes	10 minutes	5 minutes	10 minutes	5 minutes	10 minutes
	Temperature (°C)	Temperature (°C)	Temperature (°C)	Temperature (°C)	Temperature (°C)	Temperature (°C)
3E	226	236	556	569	802	803
3E	185	187	433	430	608	598
Δ°C	**-41**	**-49**	**-123**	**-139**	**-194**	**-205**
5E	39	40	71	74	104	106
5E	165	168	475	481	686	736
Δ°C	**126**	**128**	**404**	**407**	**582**	**630**
6E	37	38	74	78	130	275
6E	159	161	418	418	699	620
Δ°C	**122**	**123**	**344**	**340**	**569**	**345**
7E	172	138	452	461	664	677
7E	204	207	523	528	694	709
Δ°C	**32**	**69**	**71**	**67**	**30**	**32**
	Max. temperature reached before pre-heating					

Table 4: Table showing the difference in maximum temperature between the pre-heated samples and as received.

Overlay of 5E results

Heating Rate (℃/min)	Sample dependant
Final Temp (℃)	Sample dependant
Percentage of active sample	100%
4 stub tuning status	Auto
Sample weight (mg)	1000
Iris position (mm)	138
Iris (mm)	43 x 22.5
Tuning position (mm)	105
Comments	Pipette type MWTA cell

— 5E 15 % power (45 W)

— 5E 15 % power after heating in a conventional furnace (45 W)
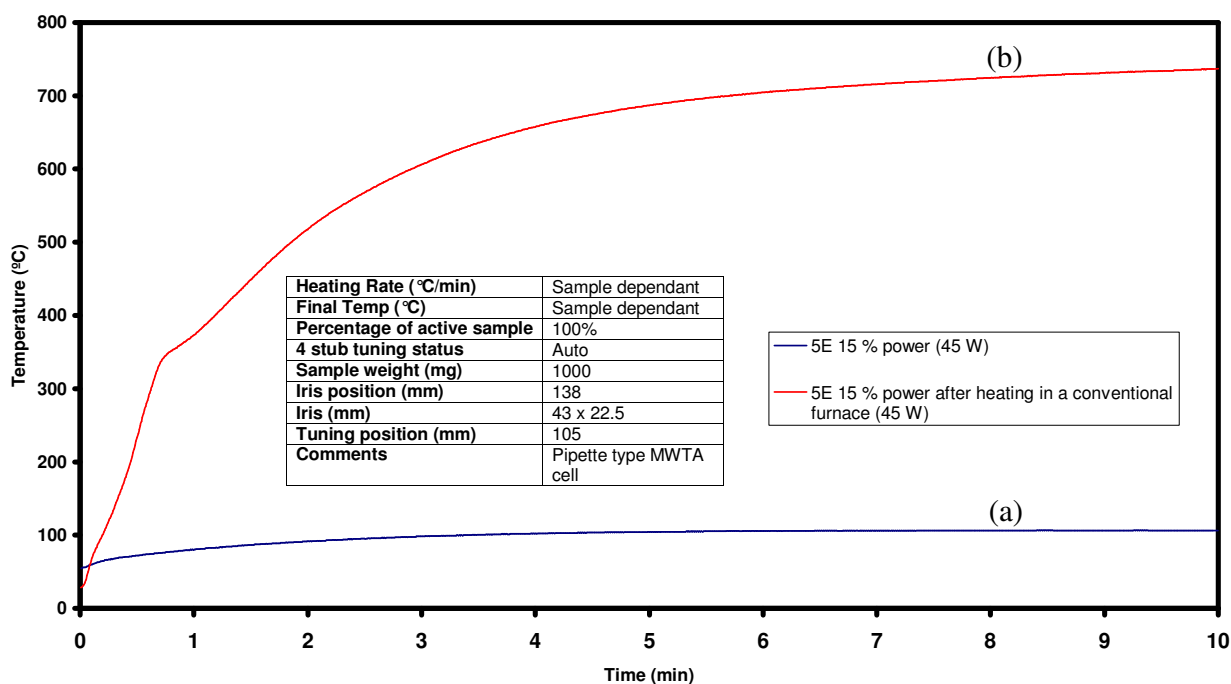
Graph 1: The variation of temperature with time for carbon 5E (a) as received and (b) after heating in a conventional furnace to 800 ºC under He.

Graph 1 shows the overlay of temperature profiles for carbon 5E (no pre-heating and conventional pre-heating) produced by a constant power of 45 W which emphasises the great increase in susceptibility obtained for this sample. The profiles are typical of what is observed for constant power experiments for samples that do not undergo thermally induced processes with temperatures levelling off over the duration of the experiment as the effects of microwave heating and heat loss reach equilibrium. The generally featureless nature of the profiles is indicative of a lack of physical or chemical changes in the material.

Dielectric measurements of the carbons at room temperature were recorded by the network analyser, to ascertain if the correlation between high tan δ values and heating held true in the MWTA. In addition to the heating results dielectric measurements of the increased coupling pre-heated carbons 5E and 6E were also performed to determine the changes in tan δ (see Table 5, page 95).

		Samples as received, ground/sieved < 125 m									
	Freq/GHz	N1E	N2E	N3E	N4E	N5E	N6E	N7E	N8E	N9E	N10E
e'_r	2.45	11.19	11.31	16.51	10.78	2.75	2.69	21.35	5.73	3.15	3.21
e''		5.53	17.41	24.12	2.40	0.17	0.13	48.82	0.43	0.30	0.37
tan δ		0.49	1.54	1.46	0.22	0.06	0.05	2.29	0.08	0.10	0.12
s/Sm^{-1}		0.75	2.36	3.27	0.33	0.02	0.02	6.61	0.06	0.04	0.05
		ASC2T	BR1	KR1	BPL	209M	URC	ASZMT	AMMONO	ABEKR1	AR1
e'_r	2.45	19.16	11.37	18.45	17.92	18.46	13.62	11.69	15.95	24.48	11.78
e''		20.76	2.28	14.98	52.92	24.68	4.45	2.69	5.46	28.94	3.49
tan δ		1.08	0.20	0.81	2.95	1.34	0.33	0.23	0.34	1.18	0.30
s/Sm^{-1}		2.81	0.31	2.03	7.17	3.34	0.60	0.36	0.74	3.92	0.47
		Preheated to 800 °C									
		5E	6E								
e'_r	2.45	15.67	14.73								
e''		25.94	24.46								
tan δ		1.66	1.66								
s/Sm^{-1}		3.52	3.31								

Table 5: Summary of dielectric measurements made on activated carbons performed at room temperature.

It can be seen from Table 3 and Table 5 that there was a close correlation between the value of tan δ and the maximum temperature, with high values of tan δ resulting in higher temperature values being obtained, there was also a substantial increase in the recorded values of tan δ (27.7 fold increase) for the carbons 5E and 6E after they had been pre-heated.

The cause of this increase in susceptibility in carbons after heating was outside the scope of the project but may be due to an increase in short-range order which may enhance the Ohmic heating by increasing the length or number of conductive pathways. However, the effect must be relatively small as XRD of the samples shows no peaks, suggesting that the samples remain amorphous or the particle size was too small (See Graph 2, page 96) to be recorded by the technique.
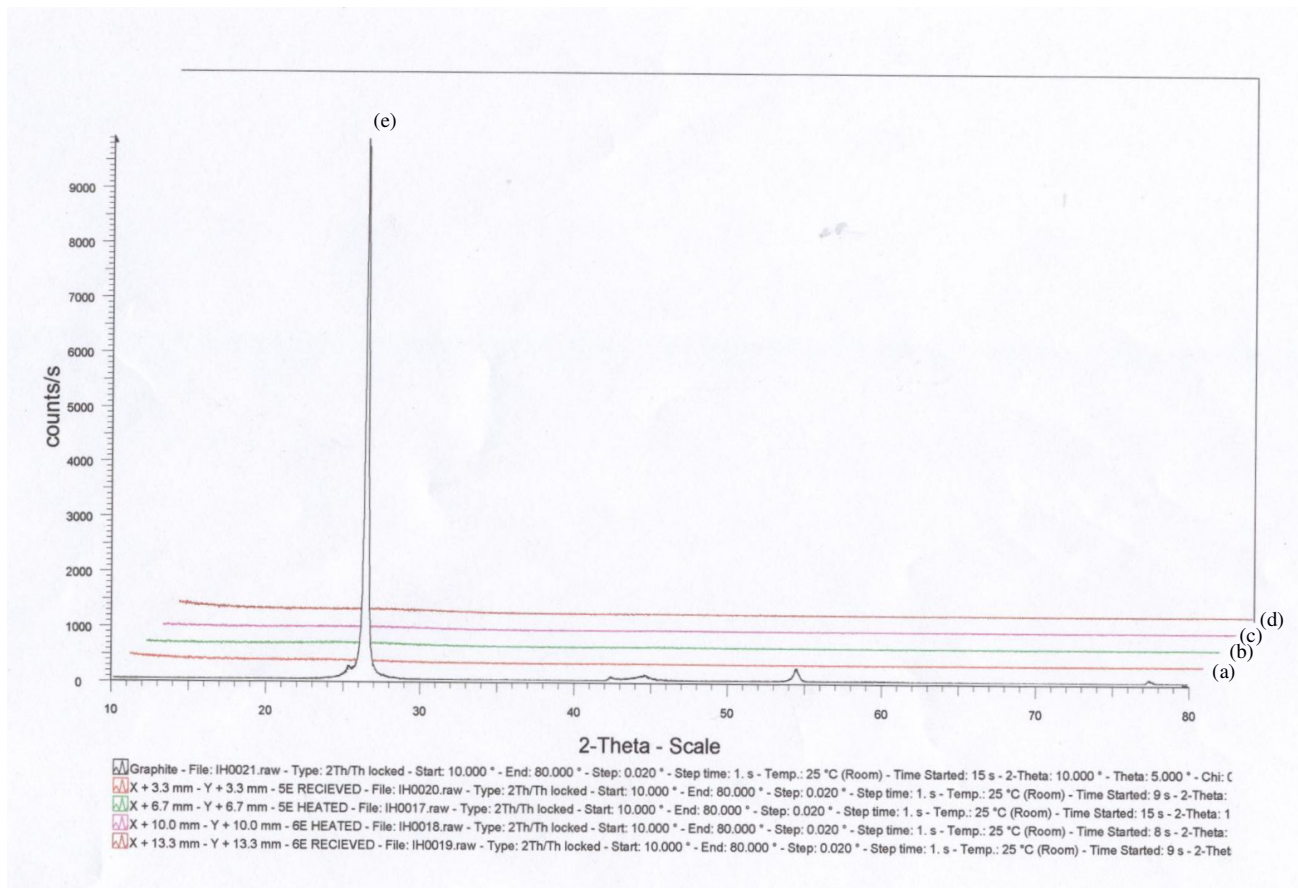
Graph 2: Overlay of the diffraction pattern of the carbons, as received 5E (a) and 6E (d) and the post- heating 5E (b) and 6E (c) compared to Graphite (e).

4.2 Experiments to investigate the effect of susceptors and diluents.

The choice of a suitable susceptor is governed by the process which it is chosen for. In the case of MWTA the susceptor is required to transfer heat to a non-microwave absorbent material, while also being chemically and thermally inert over a wide temperature range; two such materials are discussed in the following sections.

4.2.1 Susceptor 1: Silicon carbide

Silicon carbide is usually made from reacting silica sand and carbon at high temperatures (1600-2500 ºC). Pure SiC is a clear, pale yellow or green crystalline material, but as purity decreases the colour becomes darker. The alpha-SiC is the most common and has a hexagonal crystal structure. The beta

form is formed at lower temperatures and has a face-centred cubic crystal structure. There is also a rhombohedral form which is not very common. SiC strongly couples with microwave radiation, it is highly chemically inert and also possesses high thermal conductivity. With a melting point of around 2700 ºC, it is a reasonable choice for a susceptor.

Two types of SiC were obtained from Sigma-Aldrich, a 200-450 mesh, and a -400 mesh. The -400 mesh is black in appearance indicating that it is doped. The catalogue also states that the crystal structure is hexagonal in the -400 mesh. The 200-450 mesh has black-green coloured crystals indicating the sample is closer to the appearance of the pure material. The crystalline shape is not quoted so it is assumed that it may be a mixture of the possible forms.

XRD analysis of the 200-450 and -400 mesh samples of SiC showed considerable differences in crystalline structure as expected, with noticeable differences at 35° and 57° 2-Theta, in the 200-450 mesh (see Graph 4).

SiC Blue/black - File: IH0022.raw - Type: 2Th/Th locked - Start: 10.000 ° - End: 80.000 ° - Step: 0.020 ° - Step time: 1. s - Temp.: 25 °C (Room) - Time Started: 15 s - 2-Theta: 10.000 ° - Theta: 5.000 ° - Chi: 0.00 ° - Operations: Import
SiC Green - File: IH0023.raw - Type: 2Th/Th locked - Start: 10.000 ° - End: 80.000 ° - Step: 0.020 ° - Step time: 1. s - Temp.: 25 °C (Room) - Time Started: 9 s - 2-Theta: 10.000 ° - Theta: 5.000 ° - Chi: 0.00 ° - Phi: 0 Operations: Import
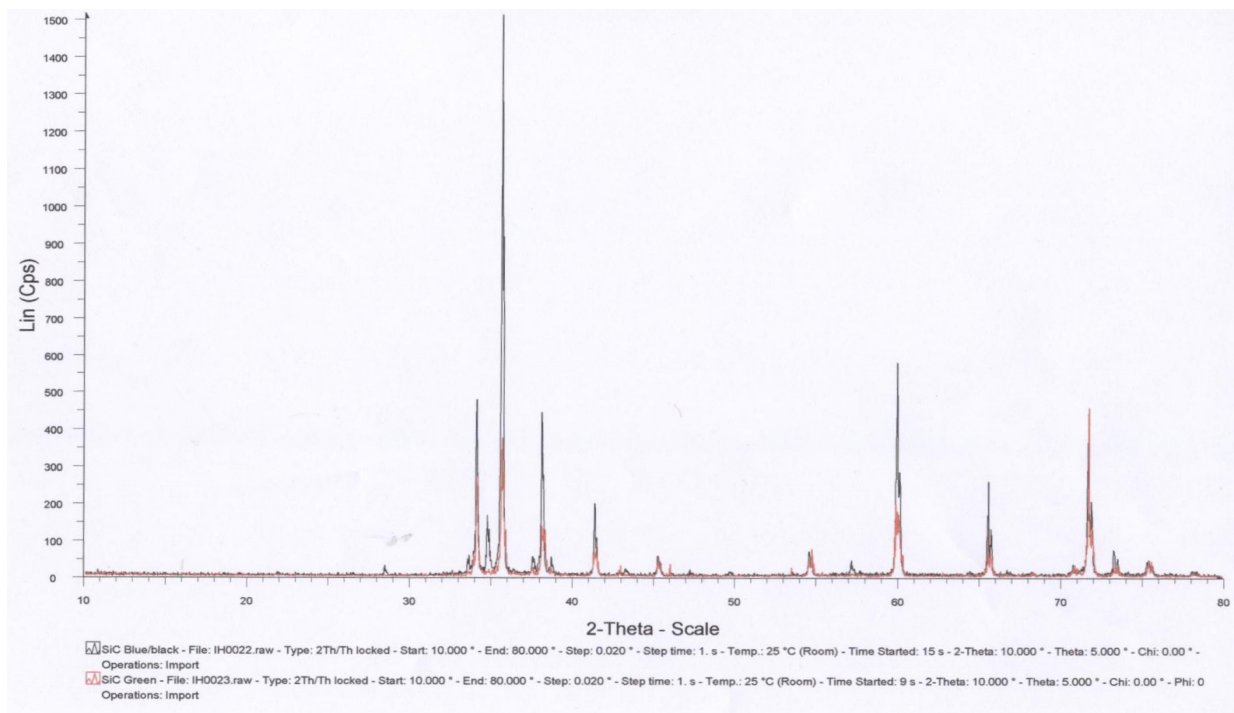
Graph 3: Overlay of the -400 mesh (black line) and the 250-450 mesh (red line) SiC samples

The -400 mesh had the addition of a different crystal form present, confirmed by the overlay of the samples and the software library which closely matched the additional peaks to the beta form of SiC.
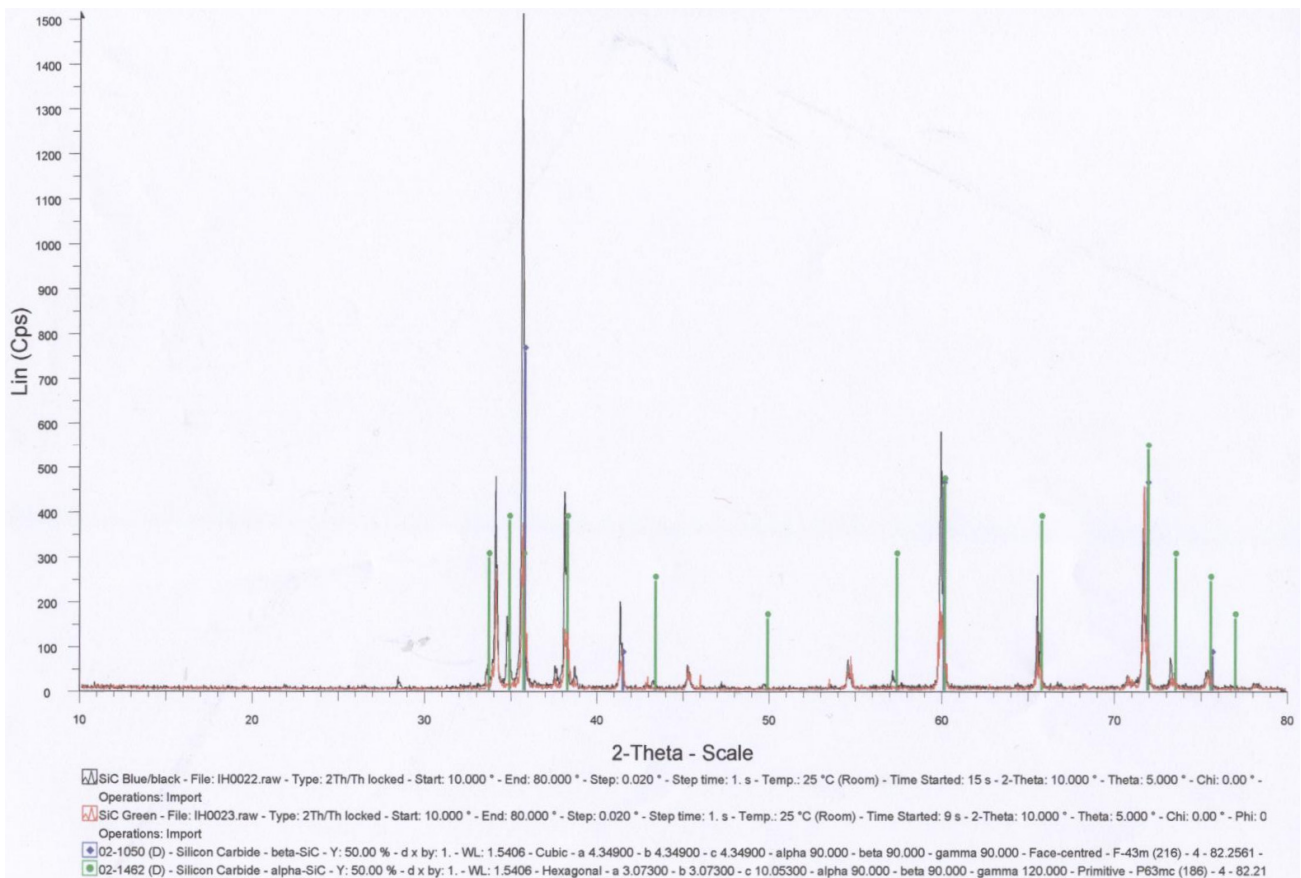
Graph 4: Overlay of the -400 mesh (black line) and the 250-450 mesh (red line) SiC samples compared to the software library

The relative difference of the two SiC samples to couple with microwave energy was tested by subjecting two equal mass samples to a microwave power of 30 % (90 W) for 15 minutes. The temperature profile for these experiments is shown in the following graph.

100% SiC constant power 30% SYS5

Heating Rate (°C/min)	N/A
Final Temp (°C)	N/A
Percentage of active sample	100%
4 stub tuning status	Auto
Sample weight (mg)	1000
Iris position (mm)	138
Iris (mm)	25 x 15
System	5
Tuning position (mm)	124
Comments	Gas chamber in place
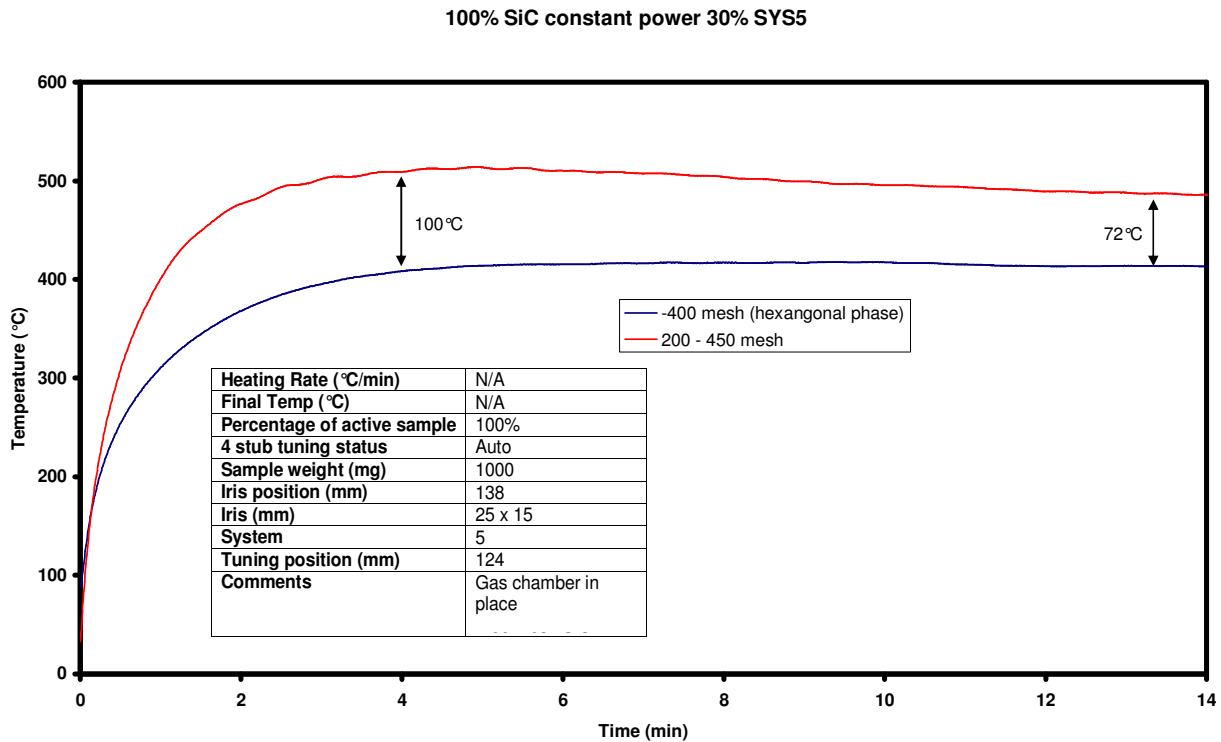
Graph 5: Maximum temperature reached by different grades of SiC at 90 W, constant power

The graph shows that the maximum temperature reached by the -400 mesh SiC was 400 °C while the 200-450 mesh form reached 500 °C. This indicates the importance of even small changes in crystal structure and particle size on the extent a material couples with microwave energy.

4.2.2 Susceptor 2: Copper (II) oxide

Copper (II) oxide has a greater dielectric loss then SiC and therefore also has the potential to be a susceptor. However, experiments showed that it was thermally unstable above 550 °C when thermal runaway would often occur; possibly as a result of a partial breakdown of the Cu(II)O to Cu(I)O.

The MWTA results clearly showed above 560°C there was a sharp increase in the dielectric loss of the copper oxide, possibly due to a reduction, further oxidation or another thermally induced event.

Lin Power MWDTA baseline 100% Alumina IH0624B

Power Rate (%/min)	0.5
Final power (W)	60
Percentage of active sample	100%
4 stub tuning status	Auto
Sample weight (mg)	N/A
Iris position (mm)	138
Iris (mm)	28 x 15
Reference material	CuO
Principle T/C	Reference
Tuning position (mm)	124
Comments	Silica wool base Copper oxide ref.
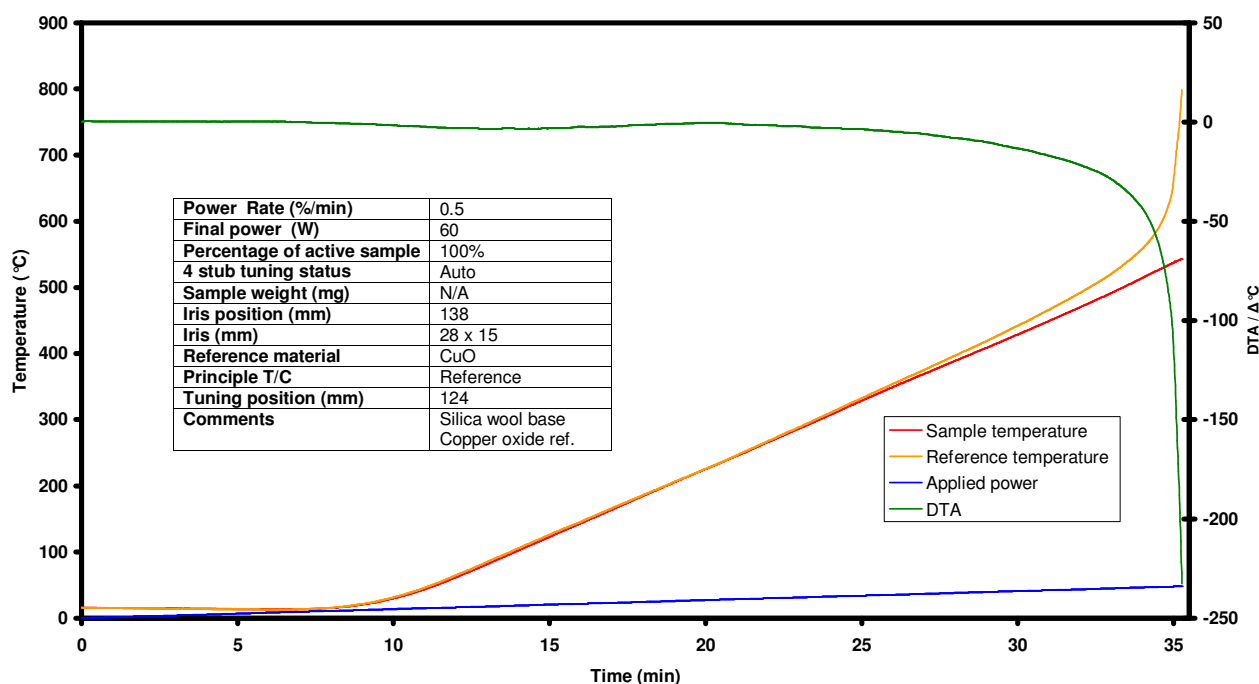
Graph 6: MWDTA of a 100 % Alumina sample using Copper oxide as a susceptor

This transition means that it was not a suitable susceptor for use as a standard full range (ambient-1000 °C) reference material, although it could be used for samples that only need to be heated close to (but not exceeding) 300 °C under low power to reduce the risk of thermal runaway.

4.2.3 Diluents

α-Alumina (Al_2O_3) is transparent to microwave radiation, and is highly chemically inert, it possess a high melting pointing (around 2000 ºC) making it an a ideal diluent for MWTA and well suited for thermal analysis.

The 'microwave transparent' nature of α-alumina can be seen in Graph 7 showing an attempted linear heating experiment on a 600 mg sample. Even though the power reached the instrument maximum of 300 W, the temperature of the alumina rose by less than 0.5 ºC.

MWTA 100% Alumina IH0474

Heating Rate (°C/min)	10
Final Temp (°C)	400
Percentage of active sample	100
4 stub tuning status	Auto
Sample weight (mg)	600
Iris position (mm)	138
Iris (mm)	28 x 15
Cell	MWTA
mixture material	N/A
Principle T/C	N/A
Tuning position (mm)	125.5
Comments	Argon 80 ml/min 100% Alumina
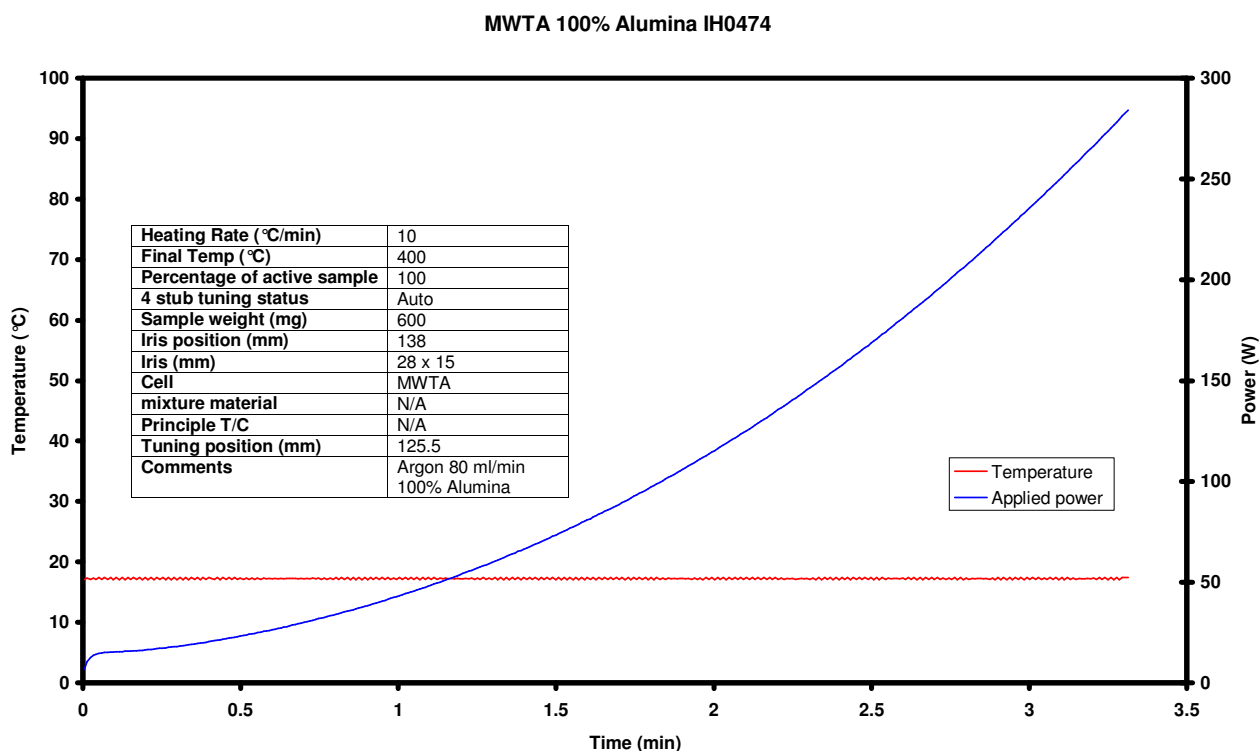
Graph 7: Graph to show the extent to which 100% alumina heats in MWTA experiments

4.2.4 Investigation of susceptor/diluent mixes

Mixtures of susceptors and diluents in different ratios would be expected to produce samples whose extent of heating with microwave energy could be adjusted to suit particular applications. To investigate this possibility a range of α-alumina/SiC mixtures were prepared (0, 1, 10, 20, 40, 50, 60, 80 and 100 % by mass). 600 mg samples of each mixture were then heated at a linear rate of 10 °C/min to 400 °C and the forward power profiles recorded. The results of these experiments are shown in Table 6.

Silicon carbide content in susceptor diluent mix (%)	Applied power require for the sample to reach 400 ºC (W)
0	300 +
1	59.96
10	58.68
20	56.08
40	52.13
50	45.71
60	48.02
80	46.58
100	58.46

Table 6: Required applied power to reach 400 ºC at a dynamic rate of 10 ºC/min for a range of SiC: Alumina mixtures.

The results showed with the mixture containing no susceptor, the power rose quickly to its maximum level as the sample did not heat at all. The addition of even 1 % (by weight) of the SiC susceptor allowed the sample to be successfully heated to 400 ºC with less than 60 W of microwave power. Generally, increasing the percentage of SiC susceptor reduced the power required to achieve the set temperature. One exception was the 80 % mixture which required less power than the 100 % SiC to reach the final temperature. This result is due to the differences in thermal properties between a mixture of two substances with different thermal conductivities and the pure material, leading to the thermal insulation properties of alumina reducing the heat loss from the SiC/Al$_2$O$_3$ mixture and therefore requiring less applied power to compensate for the loss. The loss of heating from interfacial polarisation may also mean a pure sample requires more applied power to heat to the set point.

4.2.5 Insulation

A form of thermal insulation was tested for the MWTA cells (see Chapter 5, Figure 57 (g), page 124) initially. In this case an insulation mat was wrapped around the inside of the cell.

(a)   (b)

━━━ = Ashing mat
━━━ = Large volume removable cell
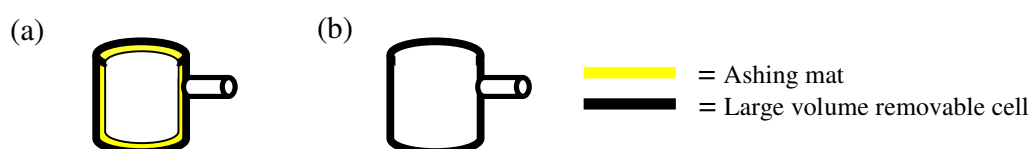
Figure 43: Cross section of (a) the position of the "Ashing" mat in the cell (b) the cell without insulation

Wrapping the outside would involve using adhesive which could couple to microwaves, or burn off at elevated temperatures giving rise to phantom transitions. The inclusive insulation reduced the sample size which was thought would reduce the possibility of thermal runaway. An insulation material called "Ashing mat" was used.

Upon testing with rubidium nitrate the thermal trace exhibited phantom transitions followed by instrumental ringing after the transitions, until it reached 230 °C where it caused thermal runaway, which was not normally observed in rubidium nitrate at that temperature.

When a sample of Ashing mat was subjected to the same heating program in the DSC it was found that at around 200 °C a relatively large exothermic event was observed which was not seen on subsequent heating, attributed to the possible decomposition of a coating on the insulation mat surface. This could give a large dielectric change caused by the coating going from a solid film to a liquid film and subsequently igniting.

4.3 Calibration of MWTA temperatures

In any form of thermal analysis accurate temperature measurement is critical and thus calibration of the temperature measurement device is essential. Temperature calibration in thermal analysis is typically based on the melting of metallic standards such as indium, lead and tin.

However, in MWTA the interaction of microwaves with metal means they cannot be reliably used. In addition, the thermocouples used in the MWTA instrument are metal sheathed and, although thin and at 90 ° to the E-field of the microwaves, may themselves still interact sufficiently to give unreliable temperature measurement.

In order to calibrate the MWTA, five commonly used non-metallic thermal analysis standards were subjected to dynamic heating (10 ºC/min) to past their transition temperatures (melting or solid-solid phase change) recorded and plotted against the corresponding literature temperatures [31-35] as shown in Graph 8 and tabulated in Table 7, page 104.

With the exception of sodium chloride and barium carbonate, the measured and literature temperatures

are within 2 ℃ of the literature values confirming the reliability of the temperature measurement and the absence of interaction between the thermocouples and the microwave radiation.
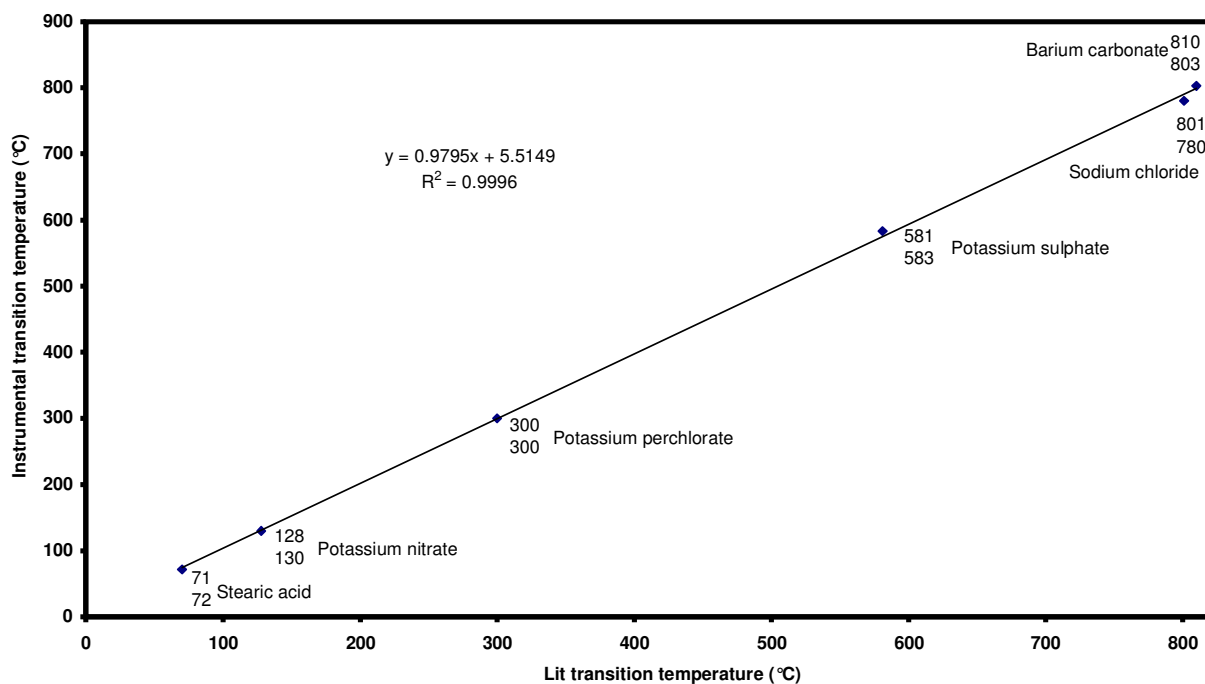
Graph 8: Thermocouple calibration within a microwave field

Material	Literature temperature (°C)	Measured temperature (°C)	Transition
Stearic acid	71	72	Fusion
Potassium nitrate	128	130	Solid phase change
Potassium perchlorate	300	300	Solid phase change
Potassium sulphate	581	583	Solid phase change
Sodium chloride	801	780	Fusion
Barium carbonate	810	803	Fusion

Table 7: Comparison of literature transition temperatures with those measured in the MWTA for a range of standards.

104

4.4 Optimisation of tuning components in the MWTA instrument

The MWTA instrument contains several components critical in the tuning of the instrument, i.e. maximising the power focussed on the sample. A comprehensive investigation was carried out on the different components and their optimal arrangement.

4.4.1 Investigation into the effect of iris size and position

The iris consists of a thin sheet of copper with a rectangular aperture, the size of which can have a dramatic effect on the extent to which a sample heats. A range of irises with different sized apertures were prepared and evaluated by monitoring the maximum steady temperature obtained by a 2536 mg sample of SiC for various constant powers at different distances from the sample (see Table 8, page 106).

The results showed a clear trend where decreasing the dimensions of the aperture produced an increase in the maximum temperature that could be obtained. With no iris present, heating was minimal. Although the smallest iris sizes produced the best heating it was found that this was at the expense of stability.

The 23 x 17 and 23 x 12 irises gave rise to increased levels of reflected power and controlled heating was often lost during an experiment, particularly if the sample underwent a large change in tan δ. It was found that for most applications the 28 x 15 iris gave the best balance between heating and stability.

All values in table measured in °C	Iris position in mm from sample section flange							
	0		100		130		138	
Iris size (mm)	30% power	60% power	30% power	60% power	30% power	60% power	30% power	60% power
No iris	65	90	N/A	N/A	N/A	N/A	N/A	N/A
36 x 18	55	83	N/A	N/A	N/A	N/A	N/A	N/A
34 x 17	62	98	N/A	N/A	N/A	N/A	N/A	N/A
32 x 16	58	102	N/A	N/A	N/A	N/A	N/A	N/A
30 x 15	59	110	N/A	N/A	N/A	N/A	N/A	N/A
(sample section, adjustable short, variable iris, and launch)								
No iris	N/A	N/A	68	93	71	93	70	93
43 x 22.5	N/A	N/A	105	158	124	172	230	712
29 x 22	N/A	N/A	172	255	209	275	235	432
28 x 15	N/A	N/A	104	110	148	248	252	537
25 x 15	N/A	N/A	112	180	138	225	225	850+
23 x 17	N/A	N/A	112	225	190	450	196	360
23 x 12	N/A	N/A	*	*	160	370	232	698
Complete system [sample section, adjustable short, variable iris, 4 stub tuner (manual), and launch]								
25 x 15	N/A	N/A	128	200	362	850+	440	850+
29 x 22	N/A	N/A	140	200	409	850+	427	850+

* = could not be tuned, N/A = not possible to obtain the required distance from the flange using iris plate

Complete system extra waveguide in place to increase distance to sample							
		Iris position in mm from sample section flange					
		230		260		268	
Iris size (mm)		30% power	60% power	30% power	60% power	30% power	60% power
25 x 15		150	220	*	*	72	93

Table 8: Summary of effects of iris size, and distance on the average maximum temperature reached for a sample of SiC at two constant powers

After the optimum iris size was determined, experiments were performed to determine if the effect of the iris would be altered by greatly increasing the distance between the iris and the sample. This was achieved by the insertion or removal of a section of waveguide between the iris and the sample section and recording the maximum temperature reached by a 2536 mg sample of SiC heated with a constant

power of 15 %. The results are shown in the following graph. It can be seen that after a set distance (around one wavelength) the effect of the iris diminishes. Unfortunately due to the design of the MWTA the critical distance could not be accurately ascertained.

Graph to show how heating is effected by the distance between the sample and the iris at 15% constant power
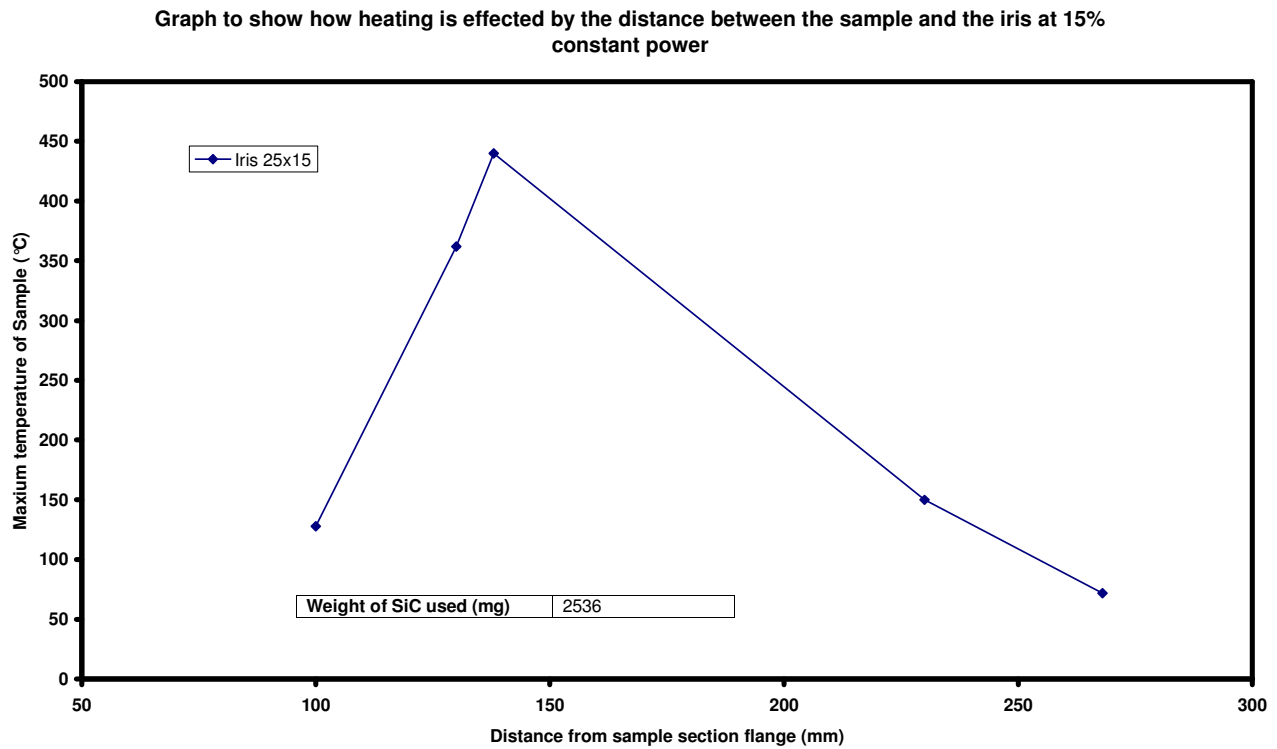
Graph 9: Result of distance on effectiveness of the iris

4.4.1.1 Discovery of the size of the 'hot zone'

Altering the iris dimensions has an impact on the size of the 'hot zone', the volume where the power density is greatest. As microwave heating is a volumetric process only in parts of the sample section where there is mass can heating take place. If the sample is outside the hot zone then it will not heat efficiently or even at all. In order to develop the instrument there needs to be a balance between the size of the hot zone (which limits the physical size of the sample cell) and the power density. Fax paper is thermally sensitive and blackens on the application of heat. As such, it is ideal for investigating hot zones within microwave cavities.

For this experiment 49 mm x 140 mm strips of Fax paper were cut (the width measurement allowed the paper to fix exactly across the inside of the sample section choke). The paper was wetted with

deionised water to ensure strong coupling. The paper was then located in the maximum of the E-field in the cavity, and a constant power applied for 10 s. The experiment was repeated several times to obtain an average size for the hot zone, and then the iris and paper changed and the procedure repeated.

Ambient temperature

Lower temperature rise (indicating weaker coupling)

High temperature rise (indicating strong coupling)

Post experimental result - darker zone deemed as the maximum working 'hot zone'
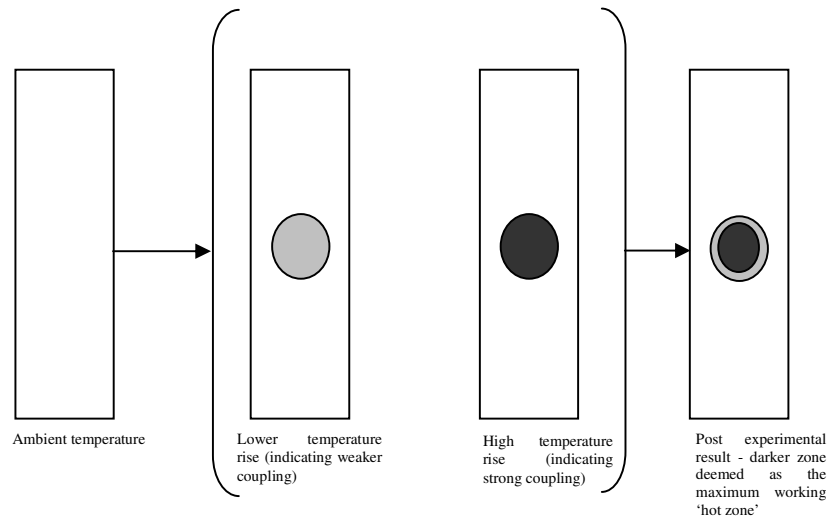
Figure 44: Illustration of the hot zone experiment

The result indicated that the size of the 'hot zone' was proportional to the iris size, i.e. the smaller the iris the smaller the hot zone. Visual observation of the extent of darkening of the thermal paper suggested that, the power density increased as the hot zone decreased. Moving the positioning of the iris along the Z-axis of the instrument also affected the size of the hot zone as shown in Table 9.

Iris size (mm)	Distance from flange	Hot zone size (cm)
43 x 22.5	100 mm	2.5 x 3.5
25 x 15	100 mm	2 x 2
25 x 15	138 mm	4 x 3.5

Table 9: Summary of the effect of iris to sample distance on the size of the hot zone

Overall, the series of experiments showed the size of the 'hot zone' in equivalent iris positions was directly dependent on the dimensions of the iris aperture, but that the 'hot zone' could be nearly doubled by moving the iris 138 mm away from the sample. The 138 mm position can be calculated to be 1¼ wavelengths from the sample which is ideal, (assuming the maximum of the electromagnetic wave is at the sample and the node is at the iris aperture)

$$\lambda_g = 17.24\, cm^3 \Rightarrow 172.4\, mm$$

$$\left(\frac{1}{4}\lambda_g\right) = 43.1\, mm$$

At the 138 mm postion :

Distance to sample from iris $= 218\, mm$

$$\therefore \; {}^{218}\!/_{43.1} = 1\frac{1}{4}\lambda_g$$

At the 100 mm postion :

Distance to sample from iris $= 177.5\; mm$

$$\therefore \; {}^{177.5}\!/_{43.1} = 1\,\lambda_g$$

(indicating the sample would be near a node)

Equation 27: Calculation of full waves to the load dependent on iris position
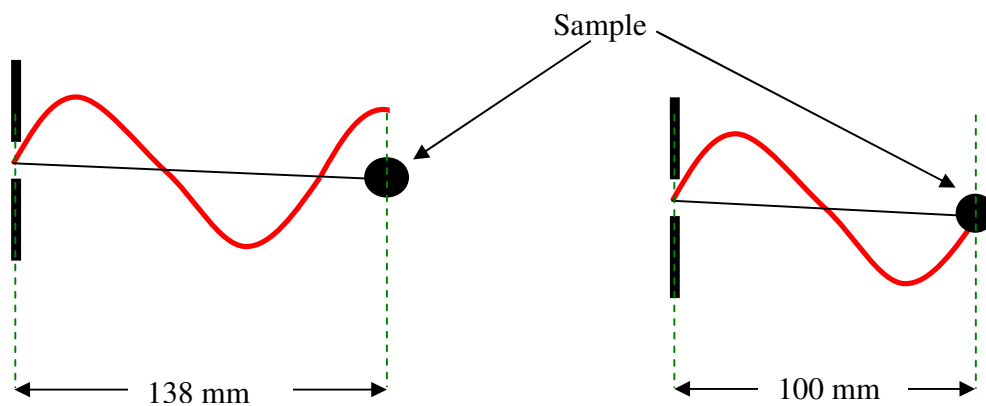
Figure 45: position of the wave in relation to the sample at different iris positions

The above figure indicates that the wave is more likely to pass the sample at a maximum if the iris is placed at the 138 mm position. When the iris was in the 100 mm position, Equation 27 indicated that the wave was passing the sample at a node, resulting in there being reduced interaction (some interaction will still remain due the width of the sample) with the applied wave and therefore diminished heating. Positioning the iris in the wrong place also increases the possibility of causing more interference to the applied wave and resulting in some of the applied power inadvertently being lost in heating the iris, in reflections or subjected to destructive interference.

= Dominant wave

= Secondary wave

= Resultant wave of lower
power caused by
destructive interference
wave
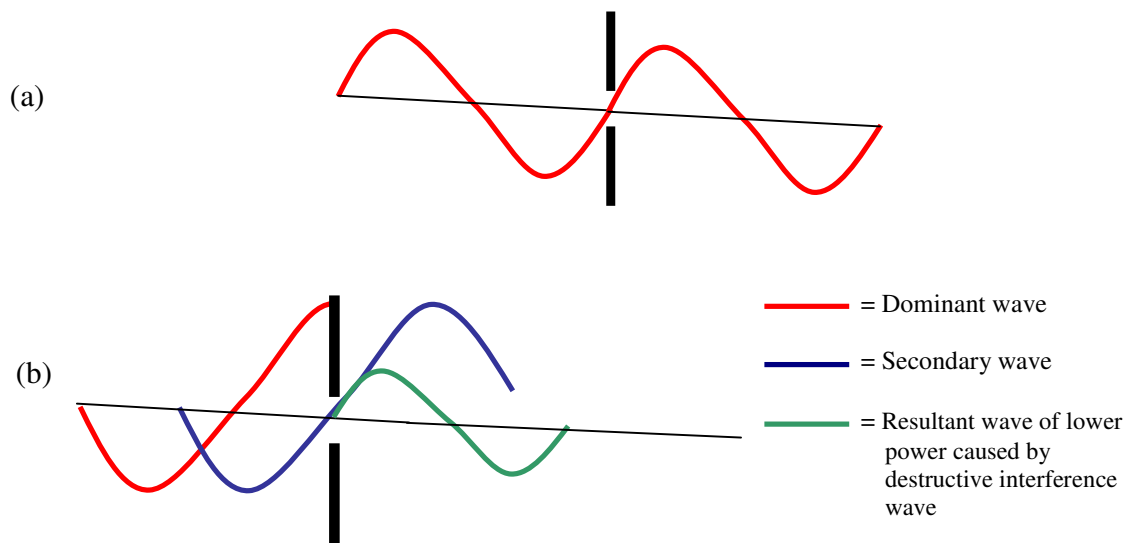
Figure 46: Illustration of (a) Iris positioned over a node (b) positioned over a maximum.

4.4.2 The 4-stub tuner

The 4-stub tuner is an active tuning device used to minimise the amount of power returning to the magnetron (and increase power transfer to the sample) by providing points of reflection within the waveguide. The stubs can be either fixed manually or be allowed to reposition themselves automatically to minimise reflected power. In the automatic setting the tuner uses diodes and servo motors attached to the stubs to move them into and out of the cavity in order to combat changes in tan δ when the sample goes through a transition.

Unfortunately, the speed and inaccuracy of the response results in the instrument 'hunting' for the best possible position during a change in tan δ and in many cases preventing linear heating to be obtained. In the manual mode the stubs can be locked in place, once a suitable tuning position has been found. Therefore changes in dielectric losses from the sample do not alter the stub positions and this makes tuning over the dynamic range of the instrument easier to control.

Its usefulness was investigated experimentally by monitoring how the maximum temperature obtained from a sample at a set power changed with and without the tuner in place. The results showed that with the 4-stub tuner in place (and in manual mode) more effective heating could be achieved. This could be due to the reduction of reflected power that the tuner provides. Examples of the effects of having the 4-stub tuner in place can be found in the lower portion of Table 8, page 106 and Graph 10.

SiC constant power 30% (90W) Variable iris 25x15 (tuning at 91mm, iris 138mm from flange (bulb cell)
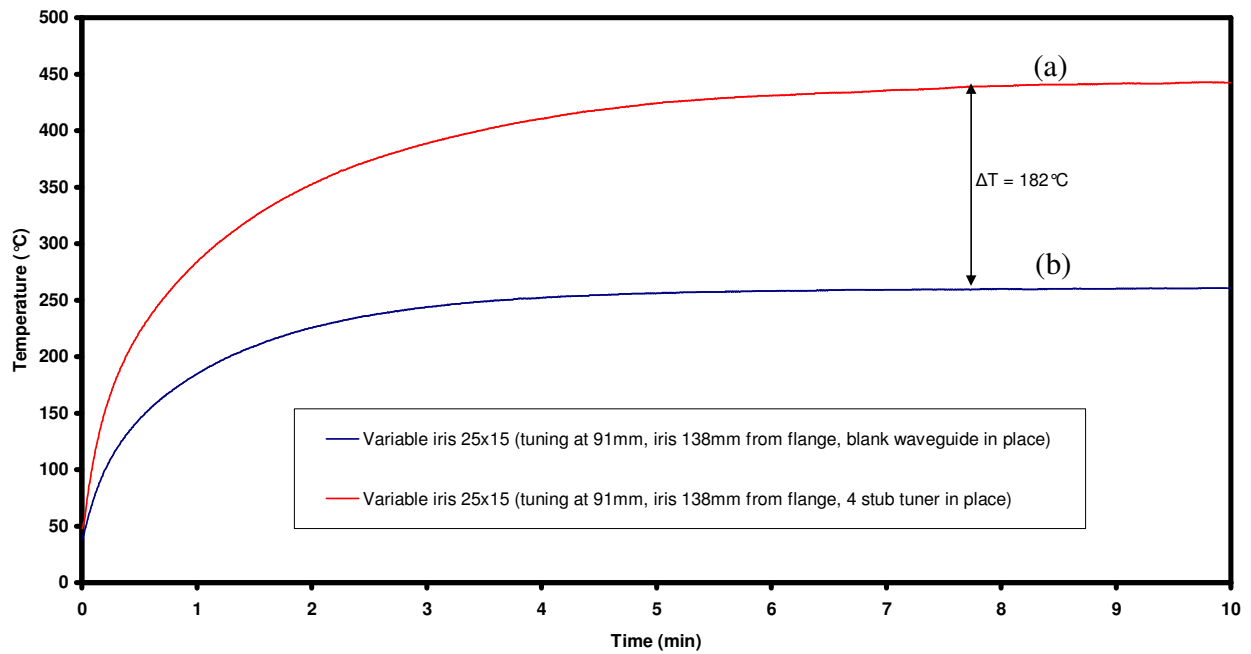
Graph 10: Effect of active tuning on the maximum temperature achieved by SiC at 90 W constant power. (a) system with 4 stub tuner in place (b) with an equidistant section of waveguide in place of 4 stub tuner.

4.4.3 The adjustable short

This is the simplest of the tuning devices and consists of a movable 'wall' at the end of the waveguide. Experiments performed with the adjustable short confirmed that, generally, optimum heating was obtained when the short was positioned so as to allow a 'standing wave' to be set-up within the waveguide, with a maximum in the electric field component of the microwave situated at the sample.

If the sample undergoes a significant change in tan δ on heating then it can 'deform' the wave in a manner analogous to refraction with light and require the adjustable short to be repositioned to maintain tuning. However, if the sample is relatively small (which is not always the case with MWTA) then this effect can generally be disregarded.
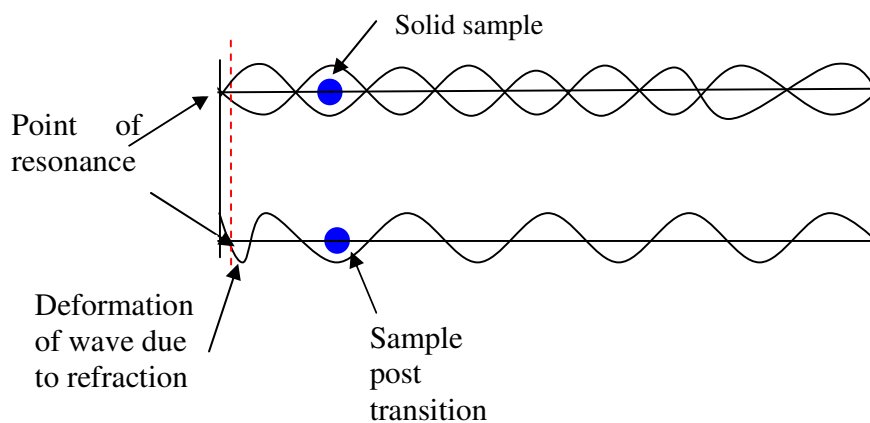
Figure 47: Fundamental illustration of how the sample state can affect the applied wave

In general, the sample size in MWDTA is too small to have a large effect. In MWTA the sample is of sufficient size for this effect to be noticeable, although the additional heating arising from dipolar polarisation tends to swamp out the change in tuning.

4.5 Installation of a microwave power meter into the MWTA

As the MWTA system comprises of modular waveguide components there are three possible locations between the launch section and the adjustable plunge tuner where the power meter could be located. In order to evaluate its optimum location within the system, in terms of the least impact on heating efficiency, a series of experiments was performed with the power meter in various positions labelled

SYS3 to SYS5 and are shown schematically in Figure 50 to Figure 52 (SYS1 was the original configuration with no power meter installed. The SYS2 arrangement was used for Table 8, page 106, and was found to be unsuited for microwave heating).
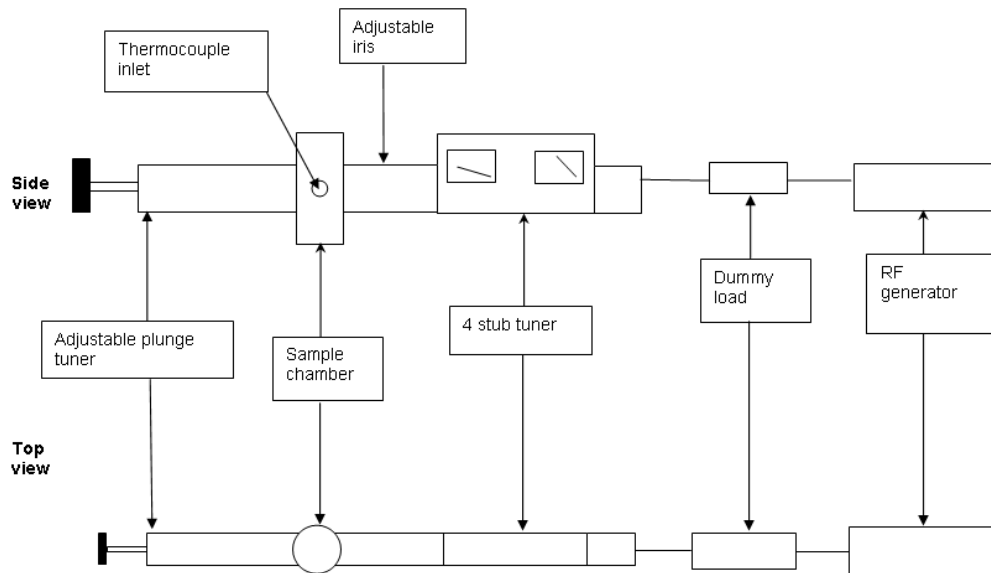
Figure 48: SYS1 – Original system set up (no power meter in place)
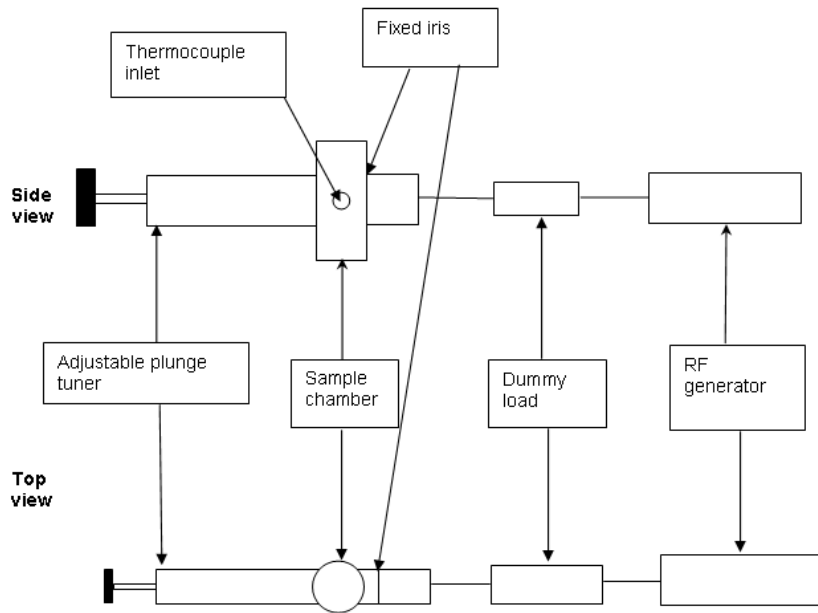
Figure 49: SYS2 – Simplest arrangement of the MWTA
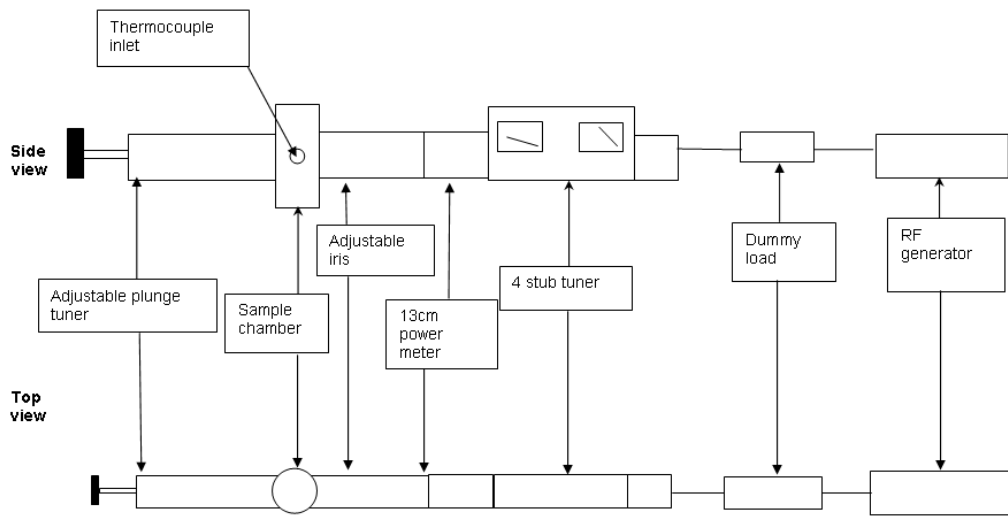
Figure 50: SYS3-Power meter placed after the 4-stub tuner
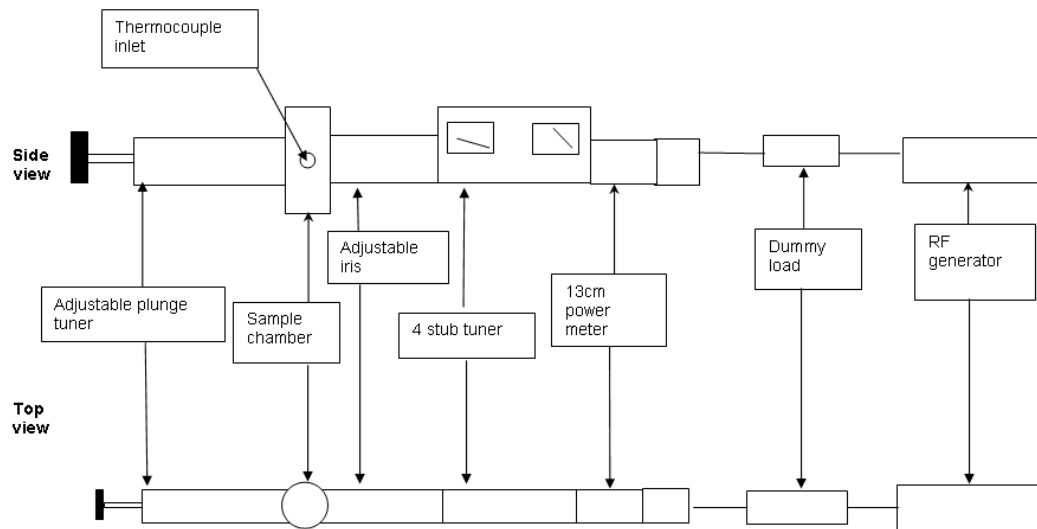
Figure 51: SYS4 – Power meter placed after the launch section
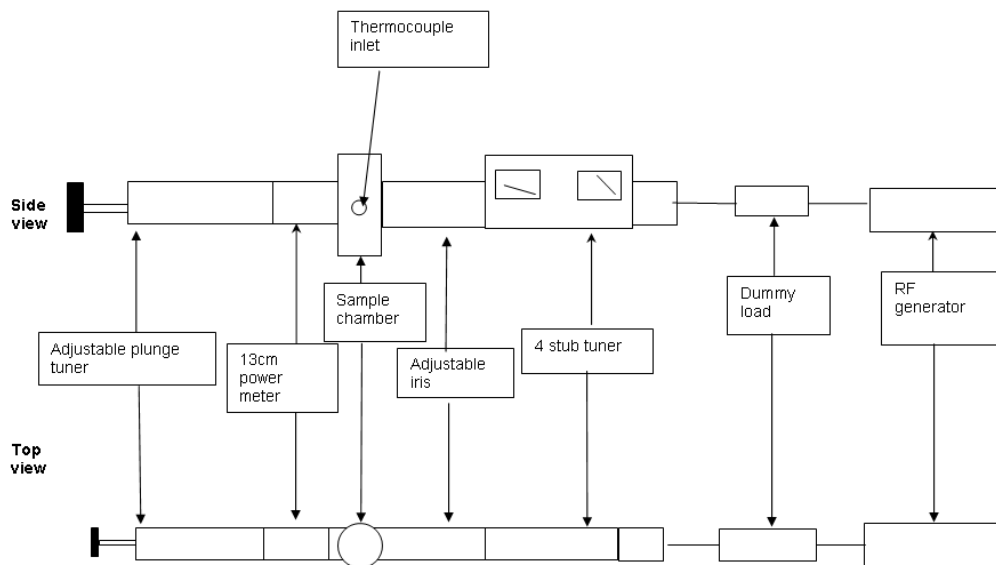
Figure 52: SYS5 – Power meter placed after the sample section

With the power meter in each position, a 1000 mg sample of SiC was subjected to a constant power of 90 W for 10 minutes and the maximum temperature recorded. Each experiment was repeated 5 times and the temperature averaged. The results are given in Table 10 below.

	SYS 1	SYS 3	SYS 4	SYS 5
Average temperature (ºC)	605	190	552	584
σ_{n-1}	27.6	14.8	2.8	9.9

Table 10: Maximum temperature reached by SiC at 30% power (in ºC)

The results indicated that inclusion of the power meter in any position resulted in some loss of power and hence a reduction in sample temperature and the original configuration showed a large standard deviation for the recorded results. Overall, the SYS5 configuration had the least impact on heating efficiency and this was used in all subsequent work. The SYS4 configuration showed promising results with a low standard deviation but proved to increase instability to an extent that made reliable tuning difficult.

4.6 Summary of optimisation and development

The effect of the various waveguide tuning components of the MWTA system were investigated and optimised to allow maximum heating efficiency with the least loss in tuning stability. The instrumental arrangement was also changed to include a forward and reflective power meter, to allow additional theoretical information to be obtained during the analysis of samples. The work with SiC also emphasised the large impact on tan δ that the presence of impurities and/or small structural differences could have. Information about the percentage of diluent/susceptors mixtures was also gathered.

The chapter also included the importance of active tuning to allow the instrument to run at its optimum efficiency and the effect pre-treatment of a sample can have on its ability to couple and therefore its tan δ (as in the activated carbon samples). Experiments to show the optimal working set-up for the MWTA were also investigated which yielded interesting results on the dimensions of the hot zone and the iris. Importantly, information was obtained from the temperature calibration of the instrument and the effect of conventional insulation methods was also obtained.

Chapter 5

Sample cell design

This chapter details the development and validation of various types of sample cells, and how these improved the results obtained by the instrument and increased its versatility.

The second half of this chapter details the design of the sample chamber and how the ability to work under inert gases was obtained and tested.

Once again the absence of a dedicated data analysis program meant that experimental results were plotted from raw data in Microsoft Excel. The resultant graphs for microwave differential thermal analysis (MWDTA) experiments in the following chapters are presented in a standard format shown below.
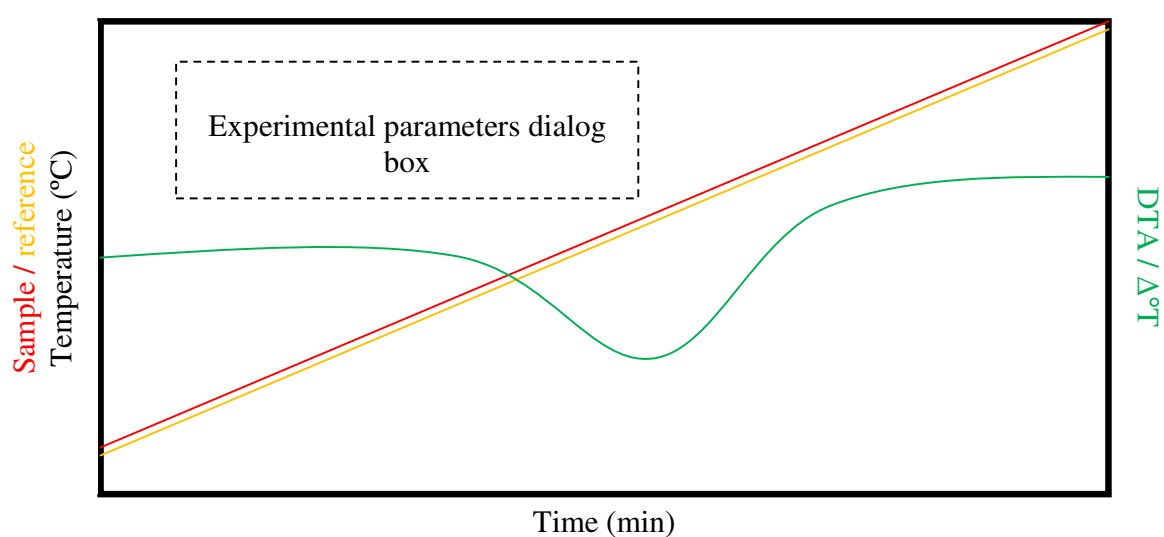
5.1 Development of new sample cells

5.1.1 Previous cells

Previous work on the MWTA instrument [14-17, 19], used a wide range of sample cells ranging from alumina cells coated with graphite, to silica glass gas flow cells. An overview of some of the cell designs are shown below.
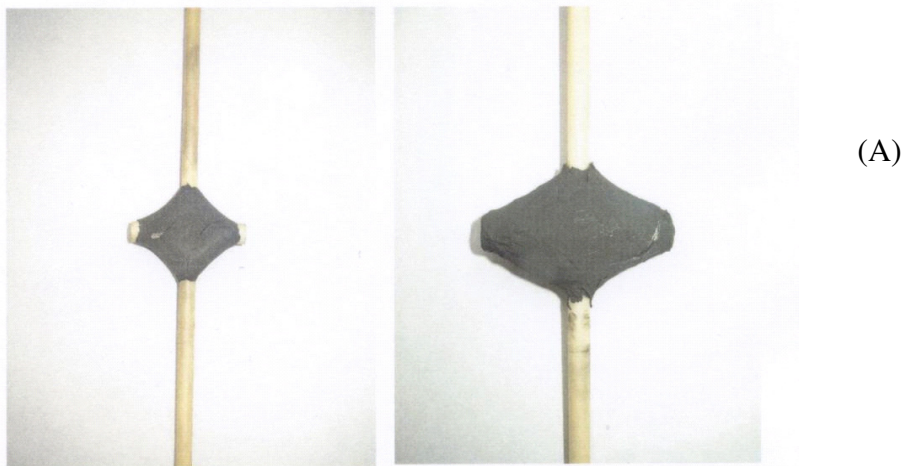
Graphite cells

a)   Appearance of fissures in non-reinforced graphite cells
b)   Carbon fibre reinforced graphite cell

(A)
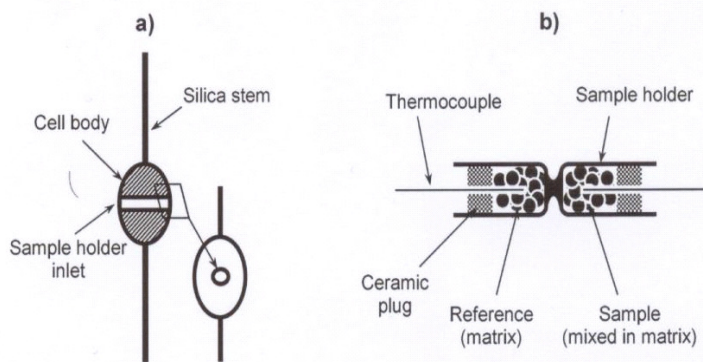
Schematic diagram of an alumino-silicate/SiC MWDTA cell

a) Silica cell with alumino-silicate/SiC body
b) Two-chambered sample/reference holder

(B)

Figure 53: Overview of previous cell designs (A) Heat assisted type (B) DTA-Type [36]
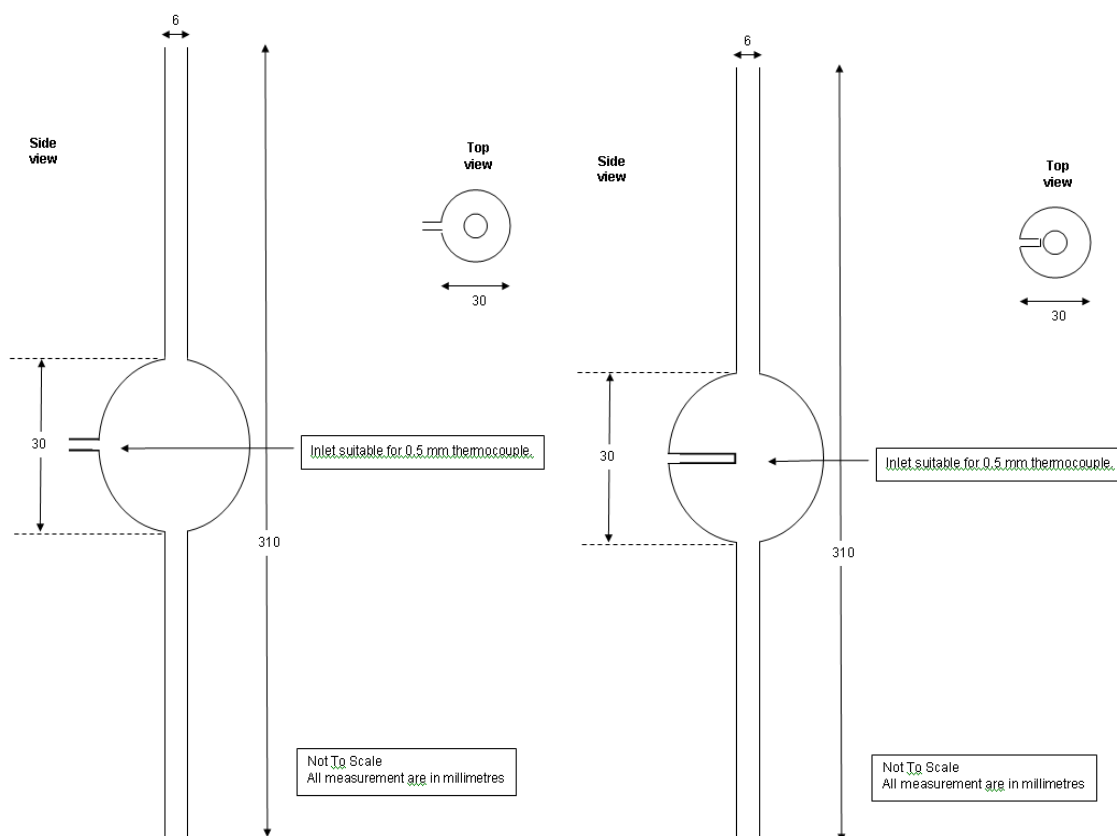
Figure 54: MWTA cells used prior to the current project.

The original cells were mainly of the 'heat assisted' type where the body of the cell contained susceptor materials which assisted in the heating of the sample through conduction (see Figure 53, page 118). However, these cells often had relatively large thermal masses and were mainly constructed of alumina ceramics which, although stable to high temperatures and chemically inert, have a low thermal conductivity (18 W m^{-1} K^{-1}) resulting in a significant temperature lag between the body of the cell and the sample. The cells were also prone to cracking with prolonged use because of the different thermal expansions of the component materials used in the design.

Other cells originally used were of a simple quartz glass 'bulb' design. Smaller volume cells required that the sample be mixed with a susceptor to heat, while large volume cells could be used with pure samples but masses in excess of 1000 mg were typically required. The main disadvantage of the bulb cell was it could only be used with a coupling material as there was no other source of heat available once inside the cavity. Regardless of this, the cell performed well although due to its size and volume there was some dispute in literature as to whether the sample was only heating through conduction from dielectric loss from sample cell walls [18]. An important aim in the project was therefore to design cells that would be more flexible, allowing the use of smaller sample masses and permitting more advanced thermal analysis techniques such as DTA and evolved gas analysis.

119

5.1.2 Sample cell material investigation

Silica glass is well-matched for use in MWTA experiments due to its chemical inertness, high temperature resistance and negligible interaction with microwaves. Fused silica is a difficult material to manufacture into specific designs due to the high temperature required to mould it. Therefore, cells designed from this material are expensive. Other glass types were investigated in order to determine if a cheaper alternative could be used with similar beneficial properties. Borosilicate (Pyrex) is known to have very good chemical resistance although it only has a maximum working temperature of around 500 °C before thermal fractures start to form.

To determine if borosilicate was more susceptible to microwave radiation than silica, constant power experiments were performed using 700 mg of SiC as the sample, in the bulb cell and with a constant applied power set to 90 W. The results showed that the borosilicate cell produced a higher sample temperature than the equivalent silica cell under the same conditions (see Graph 11). This increase in sample temperature is due to the combination of borosilicate coupling and the differences in thermal conductivity (Borosilicate = 1.14, silica glass = 1.30 W m^{-1} K^{-1}) having a greater insulating effect.

Borosilicate did couple slightly with microwaves, requiring less power to get to the set point, therefore enabling it to be suitable for qualitative work but not quantitative MWTA experiments, as the extent of this additional heating was dependent on individual cells. The contribution to the overall heating was small so it could be used for the analysis of low temperature transitions.

100% SiC cell011 constant power 30% (90W) (iris 25x15, 138mm from flange, tunning at 90mm)
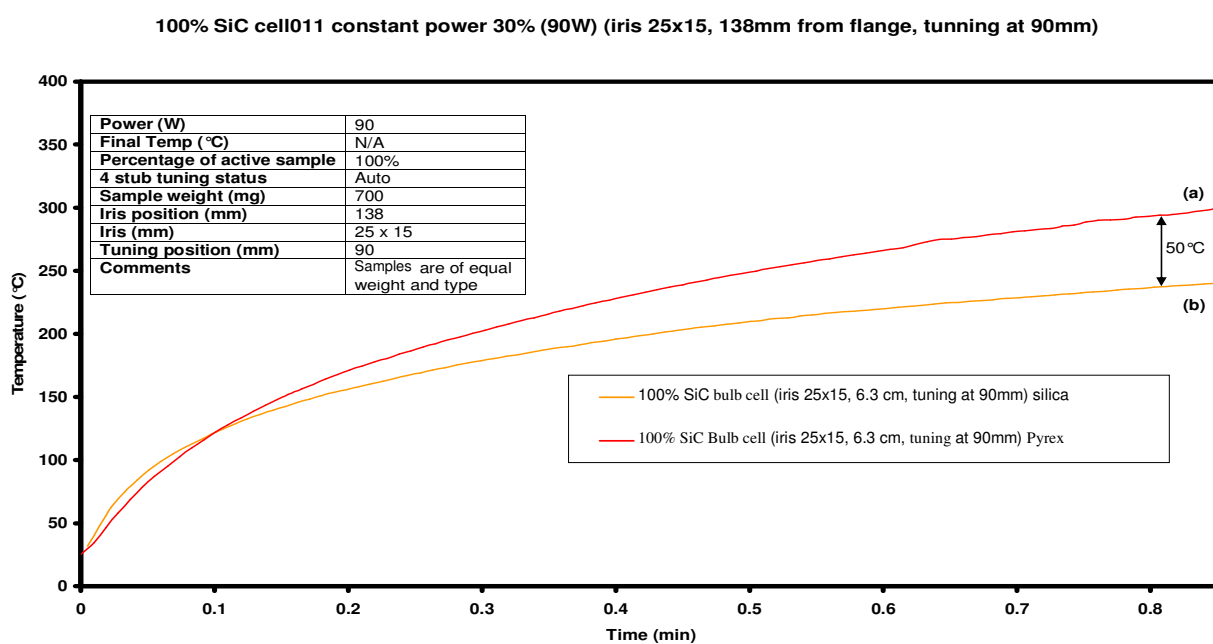
Graph 11: Overlay of the maximum temperature reached by 700 mg of SiC in equivalent conditions in (a) a Borosilicate cell (b) a fused quartz cell

5.1.3 Design of sample cells

A number of cell designs were tested both in the development of the MWTA and the MWDTA cells. Diagrams of a selection are shown below.
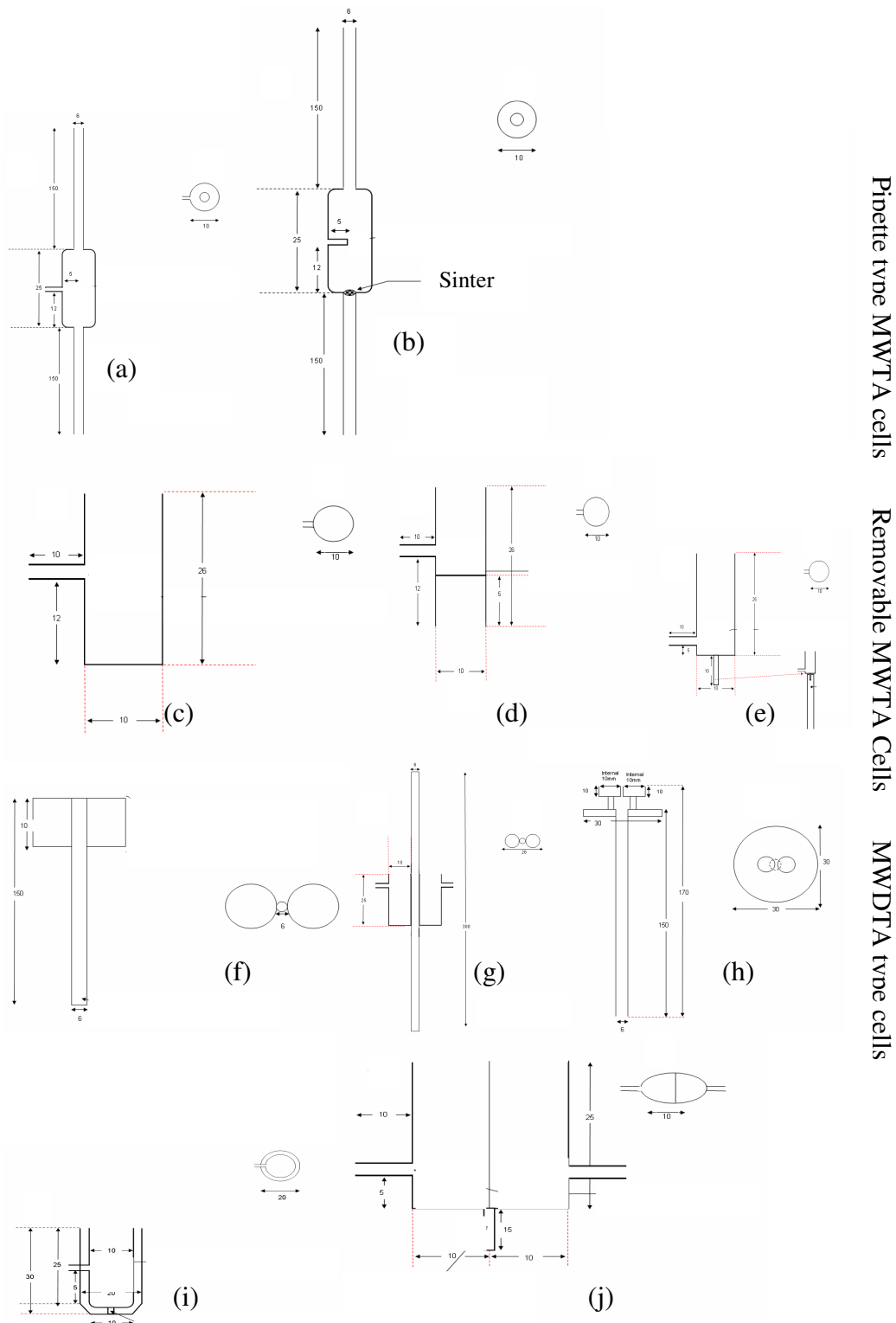
Figure 55: Diagrams of previous cell designs

(a) Pipette type MWTA cell   (b) Flow through pipette cell   (c) Large volume removable cell

(d) Reduced volume removable cell   (e) pin cup cell   (f) Cup type MWDTA cell   (g) trident cell

(h) MWDTA sample pan platform   (i) powder insulated MWDTA cell   (j) thermal contact MWDTA cell

5.2 Development of the microwave thermal analysis cell

Original cell development focussed on modifications of the original bulb designs. A range of designs were produced and tested with the results being used to guide further modifications. The process is shown schematically in Figure 57. The aim was to produce a sample cell that would have a minimum perturbation effect on the cavity and simplify the location and removal of samples.
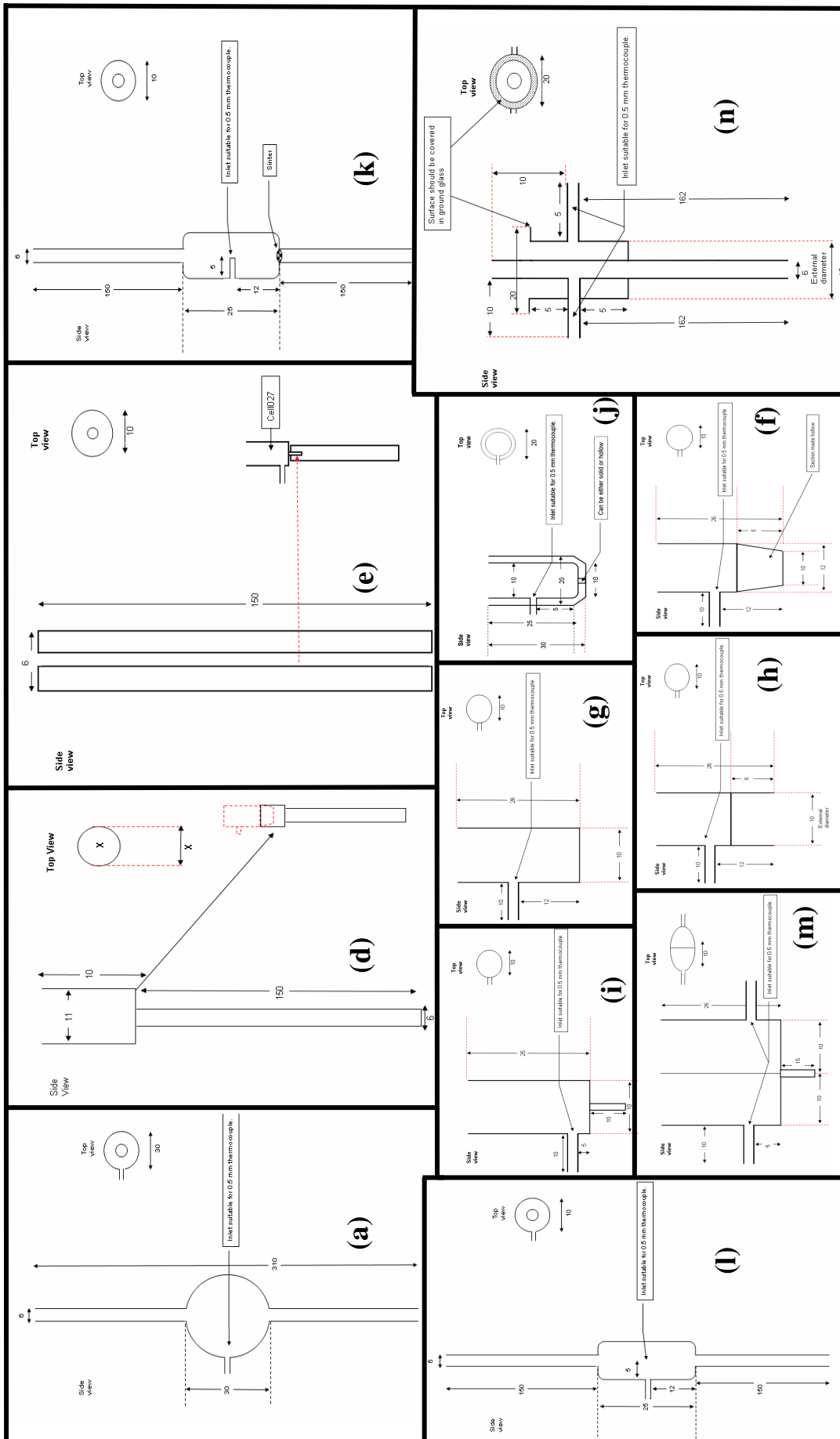
Figure 56: Diagrams of sample cell. Developments route shown in Figure 57
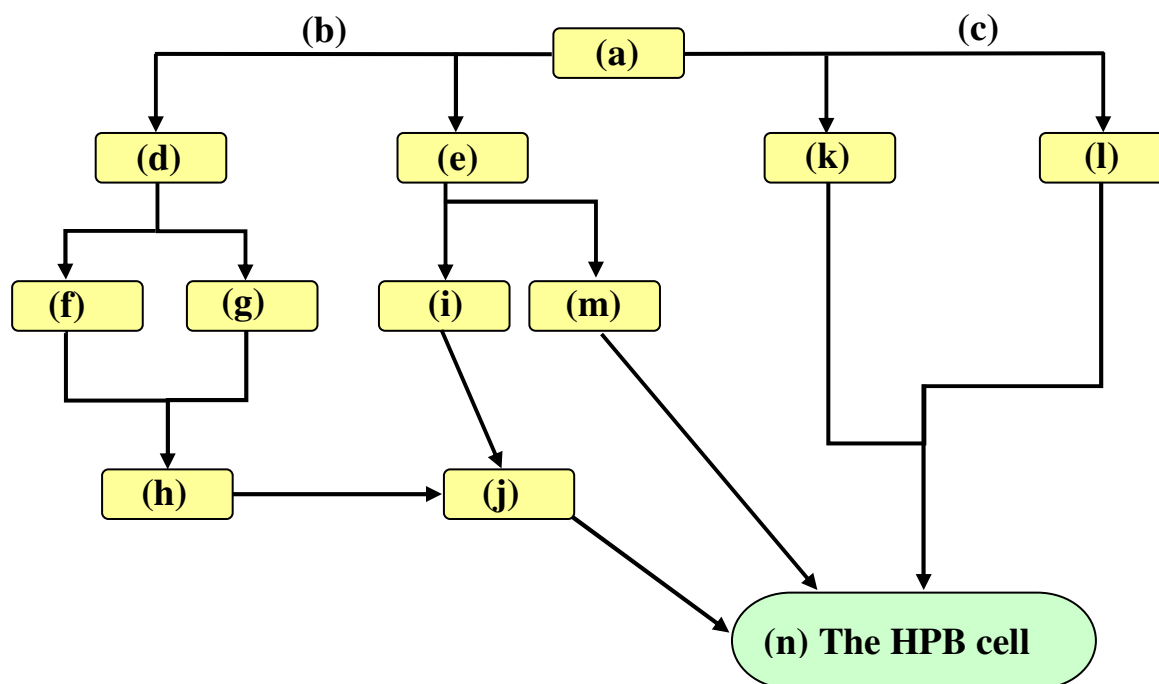
Figure 57: Order of the major developments in the final sample cell designs

(a) Bulb cell (b) Cup type route   (c) Pipette type route   (d) Cup Stalk

(e) Pin stalk   (f) Cone based cup   (g) Large volume removable cell

(h) reduced volume removable cell   (i) Pin cup   (j) powder Insulated MWTA cell

(k) Flow through pipette cell   (l) pipette type MWTA

(m) Thermal contact MWDTA cell   (n) HPB cell

5.2.1 Pipette type

Pipette type MWTA cells showed interesting results, but had several drawbacks. Upon testing thermally decomposing materials the confined opening resulted in pressure releases, e.g. vaporised water forcing the material to move away from good thermal contact with the thermocouple. This caused an increase in the applied power to compensate for a sudden fall in sample temperature. The movement of the sample along the neck of the cell also increased the possibility of the sample being deposited in the waveguide. The water condensing in the upper portion of the cell on occasion was prone to falling back into the sample causing a reflux like effect. Another disadvantage was the physical size of the cells. In order for the cell to be manufactured, the size of the cell was relatively large (cell volume approximately 2 cm^3), with a 12 mm gap from the bottom of the cell to the thermocouple inlet, which set the minimum bed depth of the sample in order to be in thermal contact with the thermocouple. The samples were therefore tested on a semi-preparative scale rather than an analytical one.

5.2.2 Cup type

To replicate the high throughput capability of removable cells used in conventional TA, removable MWTA cells were designed. Each design consisted of a sample cup and a receptacle stalk so that the sample could be placed in the maximum of the field. Two different stalks were designed as shown in Figure 56 (d) and (e). Both showed promising results when relocating the sample within the cavity although the full cup arrangement was more durable. The full cup type stalk also showed an interesting development limitation. It had always been believed that silica glass did not interact with the applied wave making it an idea sample holder material.

During the development of the MWTA cell, transitions were occurred over a greater temperature range than seen in the original bulb cell. In order to determine if this was a fault of the instrument which was affecting resolution, an experiment to observe the decomposition of copper oxalate (detailed further in later sections) and stearic acid was designed.

The experiment simply consisted of placing 500 mg of sample into the cell and heating it past the transition point, for copper oxide (400 °C), for stearic acid (100 °C) at 10 °C/min, then visually studying the residue before any possible reversing of the transition could take place. Copper oxalate (green) decomposes to copper oxide (black) in air.

This abrupt colour change made identification of the residue relatively easy. The residue showed two very definite layers with one black bed and below it a green bed indicating only partial heating of the sample. What was even more interesting was the unreacted bed was the same depth as the cup on the stalk where the sample was located. When the experiment was repeated replacing the cup with a level platform the entire sample was changed to copper oxide and no layers could be identified.

Figure 58: Pictures of the copper oxalate residue observed after heating in the large volume removable cell placed in the cup stalk.

The experiment was repeated using stearic acid to determine if this result was a universal effect or just selective to copper oxalate. In stearic acid the observed transition was a fusion. Stearic acid has the appearance of small white opaque flakes, and upon heating through the melt the sample becomes a transparent colourless liquid. Due to its large enthalpy of fusion stearic acid will remain molten for a period of time which allowed it to be removed from the system and studied without the risk of rapid re-crystallisation. The result showed that once again the lower portion of the sample cell remained unchanged. The experiment was repeated without the sample cup stalk and the results showed complete fusion of the whole sample.
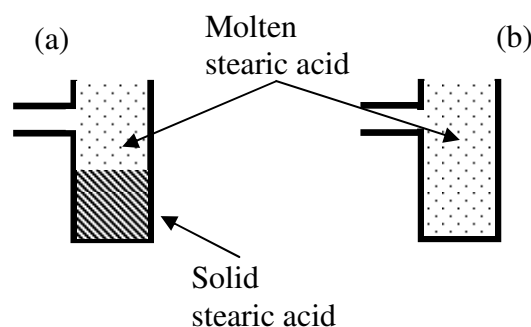
Figure 59: Diagram of stearic acid residue after microwave thermal analysis (a) with sample cup (b) without sample cup

It therefore appeared that the addition of an extra 1 mm wall of silica in close proximity to the sample had a large effect on how the sample interacted with the applied wave. The results from the experiments performed on a level platform showed that the whole of the sample was in the hot zone of the instrument, and other sample cells of different designs but same construction material did not exhibit the same effect, which indicated that the silica glass was not interacting with the wave (in addition if the silica was exhibiting dielectric loss then the extra heating effect would cause the sample to go through the transition) and therefore an unlikely cause of the phenomenon. The exact cause was not determined during this research although it is probable that there was an increase in reflections of the applied wave due to the addition of more material in the sample cell wall.

5.2.3 Powder insulation MWTA cell

The thermal losses from a microwave cell to the surrounding area are substantial. Graph 12 shows an experiment where 992 mg of SiC was placed in a bulb cell, and a constant power of 25 % (75 W) was applied. Once the sample temperature had reached an equilibrium with its surroundings its temperature was recorded, the thermocouple was then moved at 1 mm increments away from the

centre position. Following each increment a steady temperature was obtained and recorded. The experiment was then repeated to obtain an average at each increment. It was also repeated at the higher power of 50 % (150 W). The result indicated the need for insulation.

Graph to show the difference in sample temperature from the centre to the outside edge of the sample a bulb cell (radius 12.5mm) with SiC as the sample material

Heating Rate (℃/min)	N/A
Final Temp (℃)	N/A
Percentage of active sample	100%
4 stub tuning status	Auto
Sample weight (mg)	992.3
Iris position (mm)	138
Iris (mm)	28 x 15
Cell	Bulb cell
mixture material	N/A
Principle T/C	N/A
Tuning position (mm)	96
Comments	Air

Graph 12: Constant power 100% SiC thermal gradient comparison

Although the point of thermal contact would still be in very close proximity to the sample (indicating that accuracy would be conserved) sample at x + 1 mm (x = centre of the hot zone) would give rise to peak broadening due to the temperature gradient.

The powder insulation cell gave the first real indication of the effect of surrounding a sample with another material and the concept of the HPB cell (detailed in later sections). At this time the powder insulation cell was still only used for transitions in microwave absorbent materials and had no differential capabilities, limiting its versatility and sensitivity to non-dielectric transitions. The combination of all the advantages of previous cell designs and the new information obtained from the powder insulation cell led to developing the HPB cell.

5.3 Development of a microwave differential cell

Conventional differential cell designs where there are two separate pans made from silica were tried although they showed poor results, most likely due to the differences in dielectric properties of the sample before and after a transition compared with the reference and indeed the differences in dielectric properties between the sample itself and the reference material.

When the Trident cell [see Figure 56 (f)] was tested at constant power using equal volumes of SiC, it showed promising results with a very level baseline and only a few degrees difference in temperature (-1.7 °C) between the reference and sample temperature (see graph below).

Validation of trident cell (cell003) IH0120

Heating Rate (°C/min)	N/A
Final Temp (°C)	N/A
Percentage of active sample	100%
4 stub tuning status	Auto
Sample weight (mg)	1300
Iris position (mm)	138
Iris (mm)	25 x 15
Tuning position (mm)	91
Comments	
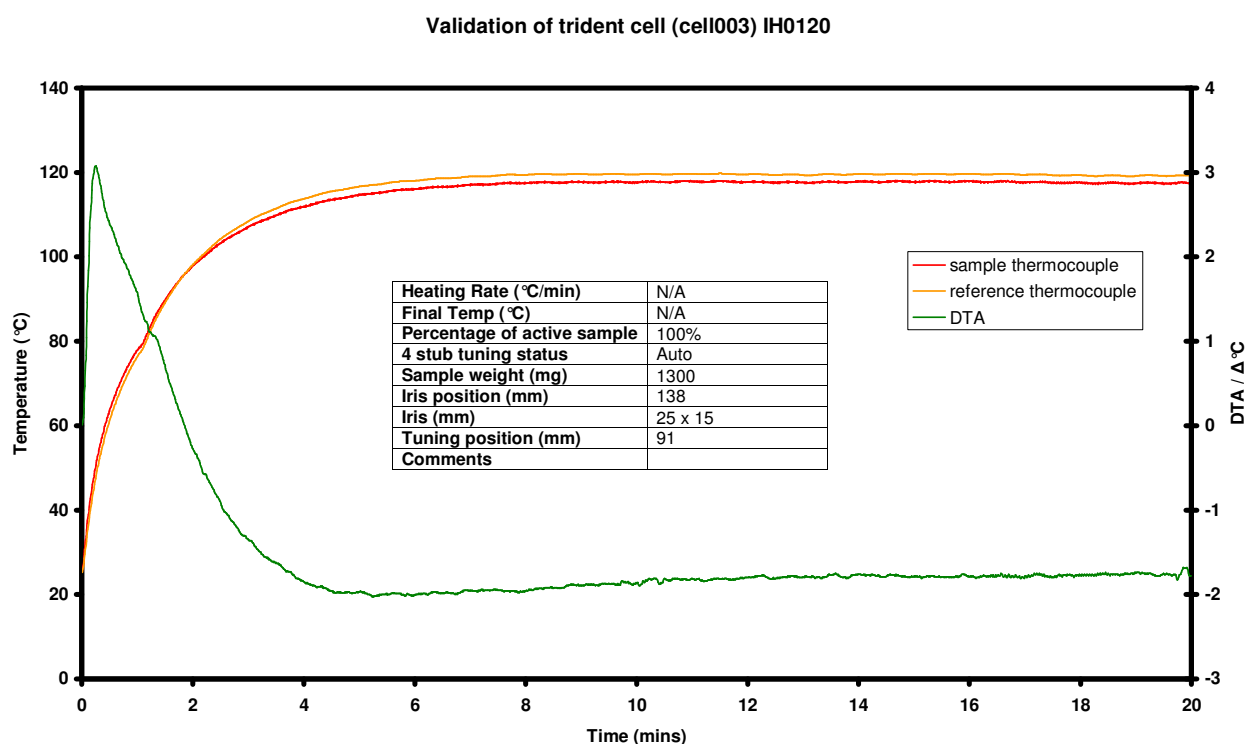
Graph 13: MWDTA of SiC using trident cell

On linear heating with a sample that underwent a thermally induced transition the trace became very noisy and the transition information was lost. The most likely reason was the sample environment. Although the two samples were joined via a centre support they were not equally covered by the hot zone, which had the effect of partially heating the sample and reference. It was decided that in order for good results to be obtained the sample and reference needed to be in very close proximity to each other. The thermal contact cell [Figure 57 (j)] was designed to address this problem. In this design the sample and reference chambers are touching, ensuring that the

temperature difference between sample and reference remains small (as in heat flux DSC) and both chambers are in the middle of the hot zone.

MWDTA SiC (both ref +sample) under Argon IH0373 (all in one cell)

Heating Rate (°C/min)	10
Final Temp (°C)	600 Ref. temp
Percentage of active sample	100%
4 stub tuning status	Auto
Sample weight (mg)	(2500) 2500
Iris position (mm)	138
Iris (mm)	25 x 15
Tuning position (mm)	118
System	5
Comments	Ar 50ml/min. Ref. principle thermocouple Ref SiC
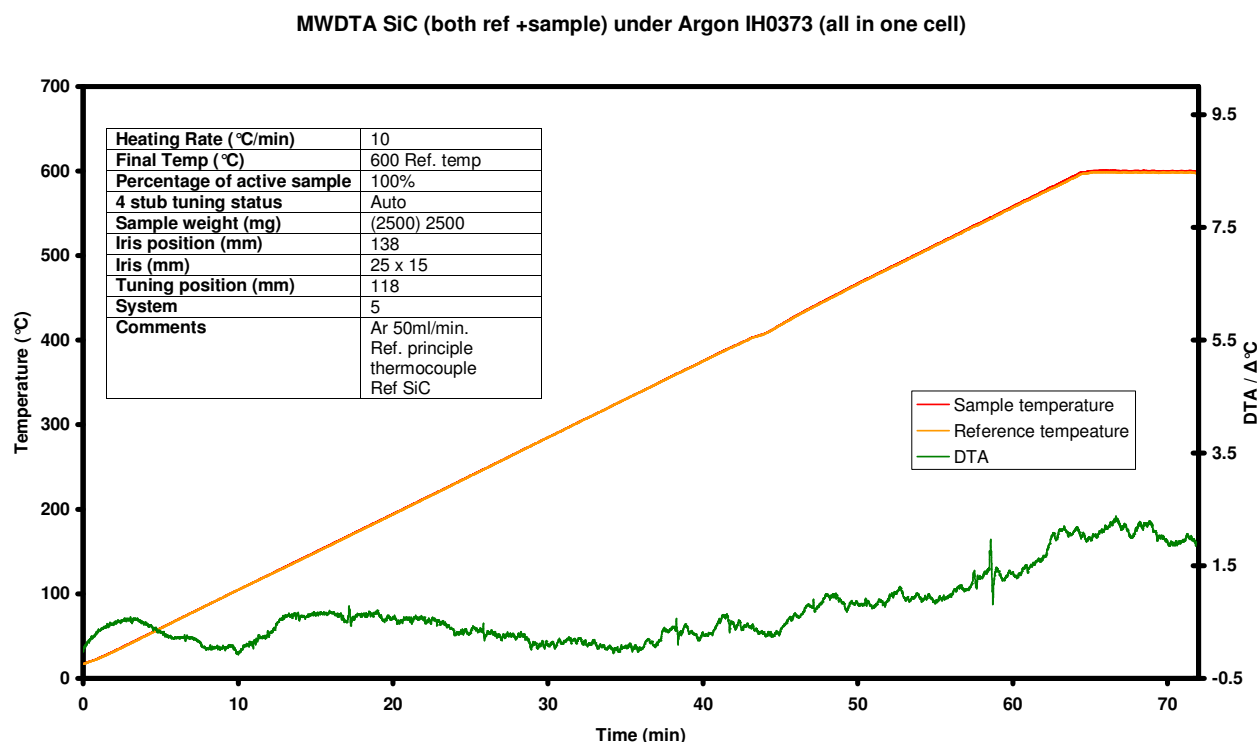
Graph 14: MWDTA of SiC using the thermal contact cell

Linear heating of SiC as both the sample and reference at 10 °C/min showed (see Graph 14) promising results, but when a mixture 50 % stearic acid 50 % SiC was tested the difference in the samples solid and liquid dielectrics caused a very large deviation in the sample and reference temperatures which again caused the transition to become unclear (see Graph 15, page 130). Another source of the possible loss in accuracy can be found in the field of thermodynamics. As the cavity surrounding the cell is more than likely to be much colder then the sample cell (due to volumetric heating) a very large thermal gradient from the susceptor to the surroundings will be set up, whatever the cell's design.

This differential will be far greater than the heat sink between the sample and the reference provided by the adjoining wall, such that the system will favour loss to its surround rather than to the adjacent sample chamber, and in effect contributing no heating to the sample. This coupled with the experiment being controlled on the reference meant the sample did not receive the required power or conductive heat to be able to reach the set point at the same time as the reference resulting in the large baseline drift.

Linear heating 50% stearic acid (DTA type) REF. 100% SiC IH0321

Heating Rate (°C/min)	2
Final Temp (°C)	150
Percentage of active sample	50%
4 stub tuning status	Auto
Sample weight (mg)	1400
Iris position (mm)	138
Iris (mm)	28 x 15
Reference material	SiC
Principle T/C	Reference
Tuning position (mm)	87
Comments	Under argon 80ml/min
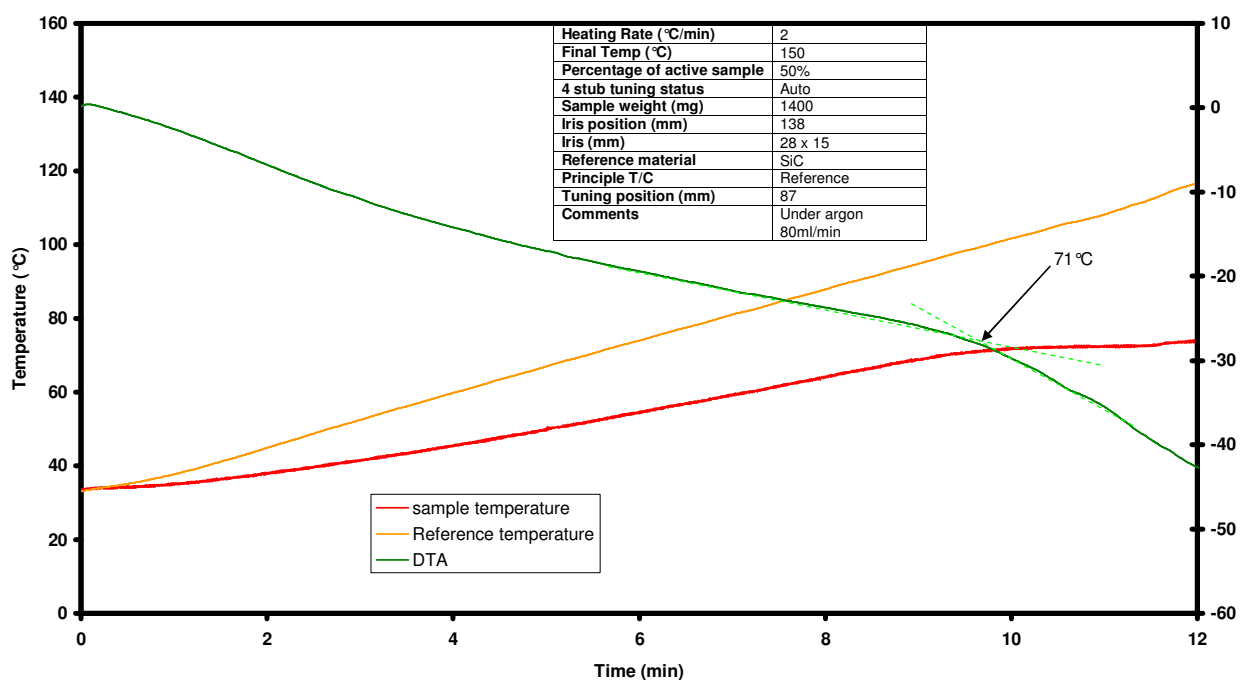
Graph 15: Linear heating of a 50% mixture of stearic acid and SiC using the thermal contact cell

Due to volumetric heating, MWDTA is able to do something which has not been possible previously. The design of the HPB cell allows the sample to be surrounded by the reference at all times, which has the effect that the sample is always in good thermal contact with the reference, providing a very similar heating environment to the sample and giving a near ideal way of ensuring the sample heats at a set rate. In arranging the cell in this way it once again creates a heat flux type environment, making the difference in dielectrics between the sample and reference insignificant until a transition takes place that changes tan δ.

The advantage of this is the sample temperature and the reference temperature remain close, reducing the thermal gradient and also allowing sample sizes to become much smaller. The disadvantage arises from samples with significant enthalpy/dielectric changes, now directly affecting the reference temperature during a transition, causing it to deviate from linearity. During an event of this kind if the sample temperature alters the reference the problem is partially overcome by the differential signal compensating. The difference in the two temperatures will be seen in both traces though more noticeably in the sample, resulting in a deflection in the differential trace but will reduce the quantitative nature of the experiment.

5.3.1 HPB cell

A cell was designed to take advantage of volumetric heating and was given the name the Hamilton-Parkes-Barnes cell (HPB), which was designed to address some of problems observed with the previous cells.
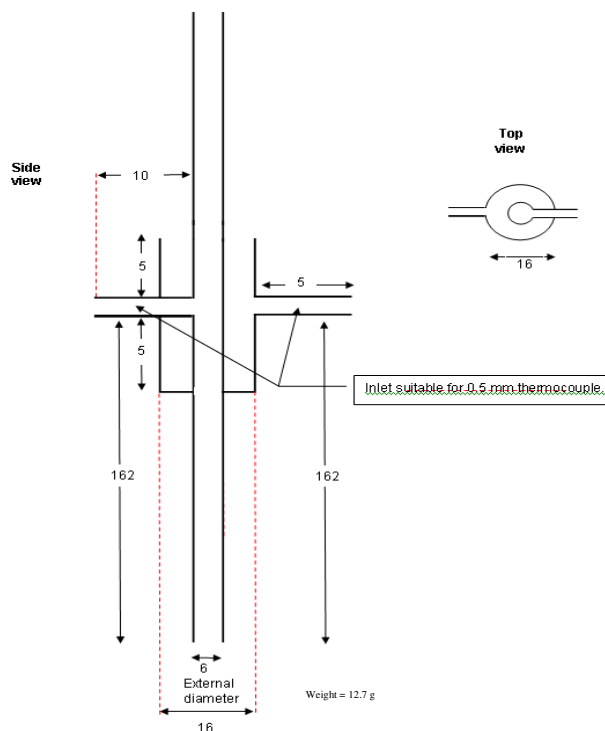
Figure 60: Diagram of new MWDTA cell designed for MWTA

The cell itself consisted of a hollow 6 mm tube running through its centre, with a thermocouple inlet branching from one side. Surrounding the tube a silica cup was moulded with a thermocouple inlet branching from the opposite side. The inner tube formed the sample section of the cell and was capable of containing sample sizes from 1 – 2500 mg. As it was hollow it was able to accommodate carrier gas flow as well as blanket gas. The outer chamber formed the reference portion of the cell.

The sample section was plugged with a small amount of silica wool just below the base of the reference cup (outside the hot zone to reduce the possibly of it coupling at elevated temperatures). Above the wool the tube was filled with alumina (which is referred to in this thesis as the alumina bed) to just below the thermocouple inlet. The sample was then placed level with the thermocouple inlet ensuring that measurements were made in a section of pure analyte. In some cased to increase thermal contact in materials with low density or vigorous fusions, alumina was added above the

sample in order to restrict sample movement during an experiment. If this type of arrangement was used it was referred to as an alumina sandwich (see Figure 61).
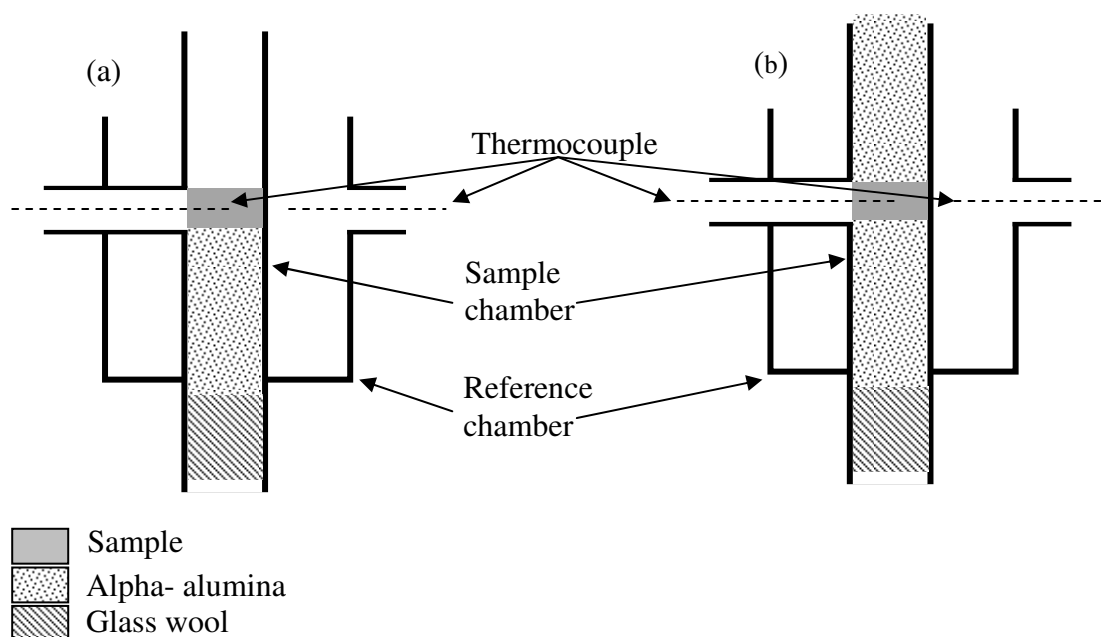
Figure 61: Diagram of the internal packing of the HPB cell (a) alumina bed arrangement (b) alumina sandwich arrangement

The design of a microwave thermal analysis experiments has many obstacles, the first being the material which the cell is made from. In conventional thermal analysis metal pans are used as they provide excellent thermal conductivity and therefore aid the conduction of heat from the furnace walls to the sample reducing thermal gradients. In a microwave cavity, the high electrical conductivity of metals could cause the wave not to propagate and instead be reduced to a skin effect preventing the creation of a standing wave and increasing the risk of forming an electrical arc. The problem is increased by the nature of MWTA. Materials tested in the instrument are subjected to volumetric heating and therefore only materials susceptible to microwaves will heat. Silica glass is highly temperature resistant (continuous working temperature of 1000 °C), chemically resistant and not thermally susceptible to microwave radiation. The combination of these properties makes it an ideal material to manufacture MWTA cells. However, the factor which prevents MWDTA experiments to be directly comparable to heat flux DSC is the low thermal conductivity of silica of around 1.3 W m^{-1} K^{-1} compared to a metal such as aluminium (237 W m^{-1} K^{-1}). This insulation effect is in fact an advantage in MWTA. There is a possibility of a large thermal gradient existing in a microwave experiment due only to the sample heating and its surroundings remaining at ambient temperature, causing a large heat flow away from the sample. Hypothetically volumetric heating has the potential to cause a reversal in the direction of the thermal gradient during an experiment, due to a sample having a low tan δ at low temperatures and therefore behaving as a heat sink (the

conventional heating model). After a positive change in dielectric properties which dramatically increases tan δ the sample no longer acts as a sink but becomes a source, as it now remains constantly hotter than the reference.

(a) (b)
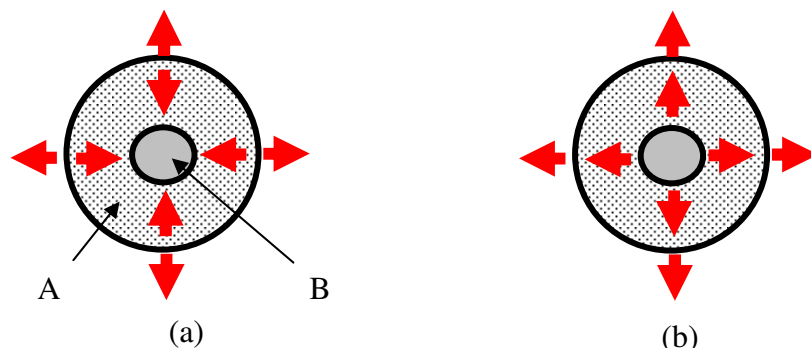
Figure 62: Schematic cross-section of the HPB cell showing heat flows for samples where (a) Reference has a greater tan δ than the sample (b) the sample has a greater tan δ than the reference. A: Reference, B: Sample

This is not usually a problem in a conventional furnace as the area surrounding the sample will be at the same temperature (usually slightly hotter) than the sample being measured. In MWTA the sample needs to be insulated which is a complicated task as most insulation materials are either hard to manufacture e.g. aerogels or are susceptible to microwaves. MWTA has the ability to insulate samples via 'passive or active insulation'. Passive insulation refers to a chemically and thermally inert powder which has no or very little dielectric loss when subjected to microwaves but also high thermal resistance. Active insulation is of great advantage in MWTA experiments. By adding a susceptor to the reference side of the HPB cell it provides the reference temperature for DTA type experiments, allowing the overall heating rate to be linear. It also provides insulation as the sample temperature will not be greater than the reference (until a significant dielectric change in the sample, or if the sample under investigation couples to microwaves as well as or better than the reference) therefore creating an inward thermal gradient towards the sample from all sides. This arrangement in effect never allows the sample to be out of good thermal contact with the reference (an ideal heat-flux arrangement). The problem of the cool exterior wall of the sample is now transferred to the exterior wall of the reference.

This problem can be partially resolved once again by volumetric heating. As long as the reference thermocouple is in the centre of the reference cup and completely surrounded by susceptor then in effect the reference will insulate itself. The whole body of the reference is heated at the same rate, assuming it remains in the 'hot zone' (area of maximum E-field) of the cavity, therefore a relatively large area around the thermocouple will be at the same temperature during heating, and so actively insulating itself. The use of silica glass also helps to reduce the loss from the outside wall due to its

low thermal conductivity, the insulation effect can also be increased by using a carrier gas with a low thermal conductivity such as argon or air. Small volumes of powder can be used to insulate the cell for materials that couple with microwaves by surrounding the sample with a microwave transparent material with a low thermal conductivity such as alumina. In order to determine the effect of powder passive insulation a series of experiments were performed at constant power. The constant power experiment consisted of applying 60 W of power to a known mass of SiC (370 mg) surrounded by different insulation materials for 4 minutes then reducing the power to 0 W and monitoring the cooling curve for a further 16 minutes.

Constant power 20% (60W) 100% SiC insulated with various refractory materials

Heating Rate (°C/min)	N/A
Final Temp (°C)	N/A
Percentage of active sample	100%
4 stub tuning status	Auto
Sample weight (mg)	370
Iris position (mm)	138
Iris (mm)	28 x 15
Cell	029
Reference material	See legend
Principle T/C	Sample
Tuning position (mm)	122.5
Comments	

Legend:
- Sample temperature (Glass spheres)
- Sample temperature (Air)
- Sample temperature (Alumina)
- Sample temperature (Zirconium Oxide)
- Sample temperature (Boron Carbide)
- Sample temperature (Silicon carbide)
- Sample temperature (Zirconium Silicate)

Graph 16: Overlay of cooling curves obtained by different insulation materials

It can be seen from Graph 16 the time taken for the sample to return to 50 °C varies with the different insulation powders, with SiC exhibiting the greatest insulation properties but also the maximum temperature reached. The active insulation nature of SiC means it is not comparable with the other insulation types. The most promising passive insulation was shown to be zirconium silicate. Although it did not reach the elevated temperature of the next best insulator it did show better insulating properties.

In order to determine if the cell is suitable to use as a differential cell, the difference between the sample and reference must be as small as possible during heating until a transition takes place. By filling the sample section with an inert substance with no microwave activity (alumina) and the reference section with a susceptor, the amount the sample temperature lags behind the reference will give an indication of how big the differential signal will be for the extreme of a sample which does not interact with microwave radiation at all. The results of such a test showed that there was minimal difference between the sample and reference (depending on heating rate) until around 500°C.

MWDTA 100% Alumina IH0544

Heating Rate (°C/min)	10
Final Temp (°C)	800
Percentage of active sample	100%
4 stub tuning status	Auto
Sample weight (mg)	n/a
Iris position (mm)	138
Iris (mm)	28 x 15
Reference material	SiC
Principle T/C	Reference
Tuning position (mm)	122
Comments	Alumina sandwich Silica wool base
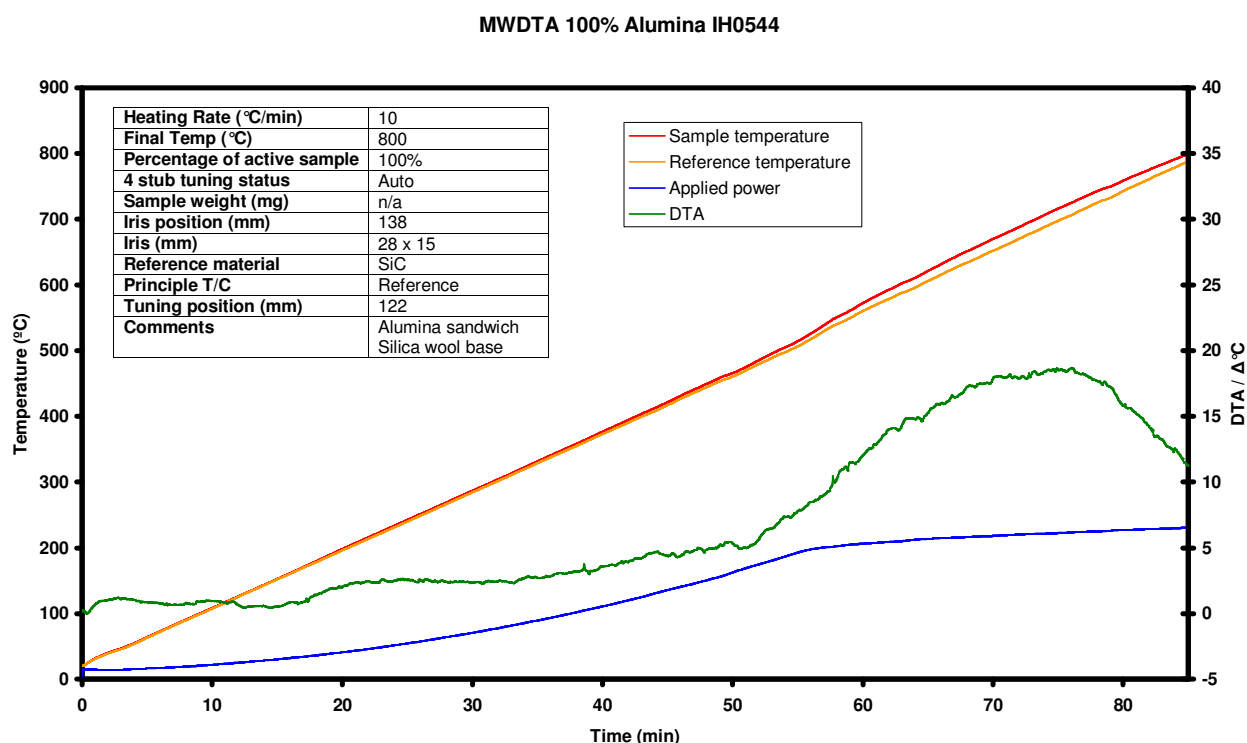
Graph 17: MWDTA with SiC as reference and 100% alumina as sample

To determine what thermal gradient existed between the sample and the reference when using the HPB cell, an experiment was devised to monitor the maximum differential temperature reached at different heating rates. It consisted of using alumina as the sample and SiC as the reference. The samples were then subjected to a linear heating program under different atmospheric conditions to 700 °C. The maximum differential temperature observed over the run was recorded and compared as shown in Table 11 below, (a – sign indicates the reference temperature was hotter than the sample temperature).

Heating rate (°C/min)	Maximum differential temperature in static air (Δ°C)	Maximum differential temperature in Helium (Δ°C)	Maximum differential temperature in Argon (Δ°C)
200	-52	8	12
150	-36	17	26
100	-20	27	44
75	-15	28	48
50	-11.5	24	33
25	-6.5	24	38
20	-7	24	38
15	-6.1	23	40
10	-5.5	-15	38
5	-4.3	-14	34
2	-1.5	6	22

Table 11: Indication of the maximum differential temperature reached for an alumina sample heated in the HPB cell

By utilising volumetric heating the thermal lag experienced by conventional furnaces is dramatically reduced allowing the possibility of enhanced sensitivity due to the similar environment of the sample and the reference. The results also showed in air the heat losses from the sample meant the reference was always hotter than the sample regardless of heating rate. The high thermal conductivity of helium gas had the effect of reducing the thermal gradient between the sample and reference at certain heating rates, with the most obvious advantage being at high heating rates. The use of the insulation properties of argon resulted in the sample always being hotter than the reference, it is thought that the explanation is due to the carrier gas reducing heat losses to the surroundings from the reference.

The question then arises that the instrument no longer heats by microwaves but acts like a conventional furnace and heats by conduction powered by microwaves [18]. In order to address this question a material with a significant dielectric change was placed in the sample section and tested. If there was no microwave interaction with the sample then the results would show a change of enthalpy and the temperature will return to a value close to the reference temperature. If there is an interaction then the change in dielectric properties would cause the sample to heat far better than the reference and remain elevated, unlike in conventional methods. Rubidium nitrate was used as its first transition has a low dielectric change whereas the other two transitions have significant changes in tan δ. To show that this deviation in temperatures is not merely due to changes in heat capacity a DSC experiment was performed on the sample. The results showed that there was no significant change in baseline before and after transitions before the II-I phase change indicating little or no change in heat capacity.

In a conventional system the same mass of sample and reference is needed so that similar heat capacities exist in the sample and reference, although this is an approximation as changes in heat capacity occur when a transition takes place in the sample that will not be mirrored in the reference. The dimensions of the HPB cell mean the reference chamber is 10 times bigger in volume than the sample chamber, as calculated below:

$$\text{Volume contained by outer clinder} = \text{Volume of outer clinder} - (\text{Volume contained by inner clinder} - \text{thinkness of walls})$$

$$\text{Vol} = \pi r^2 h$$

$$h = 10mm \Rightarrow 1cm$$

$$r_1 = 2mm \Rightarrow 0.2cm \ (\text{internal volume})$$

$$r_{1(inc \ wall)} = 3mm \Rightarrow 0.3cm \ (\text{total internal volume})$$

$$r_2 = 7mm \Rightarrow 0.7cm \ (\text{external volume minus outer wall})$$

$$(a) \text{External volume} = \pi 0.7^2 \times 1 = 1.54cm^3$$

$$(b) \text{internal volume inc wall} = \pi 0.3^2 \times 1 = 0.283cm^3$$

$$\text{corrected external volume} = (a) - (b) = 1.257cm^3$$

$$\text{internal volume} = \pi 0.2^2 \times 1 = 0.125cm^3$$

$$\text{Ratio } 10:1, \text{reference}:\text{sample}$$

Equation 28: Calculation of the sample to reference ratio of the HPB cell

The mismatch in heat capacities due to size can be said to be negligible as the instrument primarily monitors the dielectric changes which are significantly greater than heat capacity changes, although enthalpy changes can be monitored. Therefore the relative ratio of sample to reference is not thought to be a disadvantage.

It was finally concluded that the HPB cell outperformed all of the previous cells. Its ability to produce both, enthalpy and dielectric data plus the advantage of close to ideal heat flux arrangement ensured it was both versatile and functional for microwave differential thermal analysis.

5.3.2 Correlation between DSC pan types when using the HPB cell

In order to further understand how the HPB cell behaves in relation to a conventional DSC pan, the dehydration of calcium sulphate dihydrate ($CaSO_4.2H_2O$) was performed using conventional methods in an open pan environment and then repeated in an encapsulated pin-hole pan. Upon heating the decomposition of $CaSO_4.2H_2O$ proceeds via two stages:-

$$CaSO_4.2H_2O \rightarrow CaSO_4.\frac{1}{2}H_2O + 1\frac{1}{2}H_2O$$

$$CaSO_4.\frac{1}{2}H_2O \rightarrow CaSO_4 + \frac{1}{2}H_2O$$
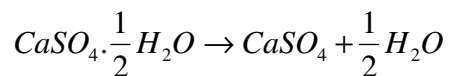
Equation 29: Thermal decomposition of calcium sulphate dihydrate

Experimental data (Graph 18 and Graph 19) shows that in an open pan the dehydration occurs in a single broad step. When the sample is placed in a pin holed pan the increase in water vapour pressure causes the two stages of the dehydration to become more resolved due to the build up of an atmosphere of product gas above the sample, especially in the cases where there is no carrier gas through the cell.

3.62 mg Calcium sulfate dihydrate
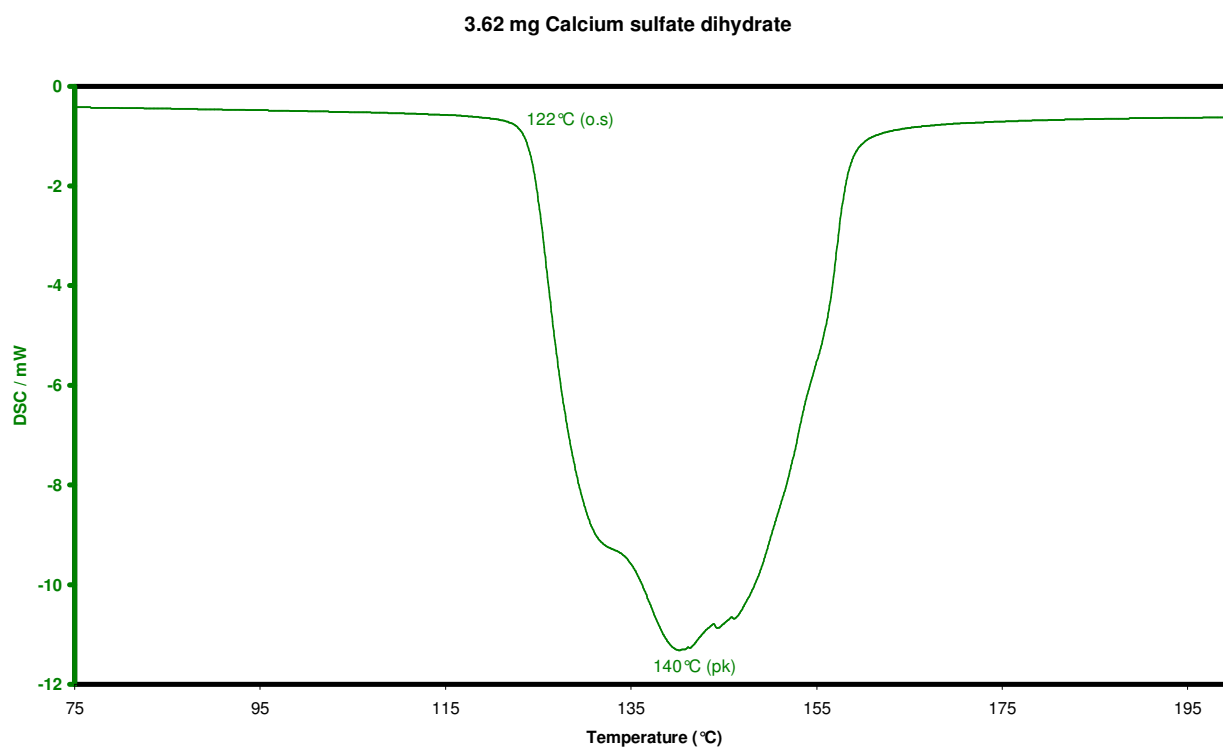
Graph 18: Dehydration of calcium sulphate dihydrate in an open DSC pan

3.62 mg Calcium sulfate dihydrate
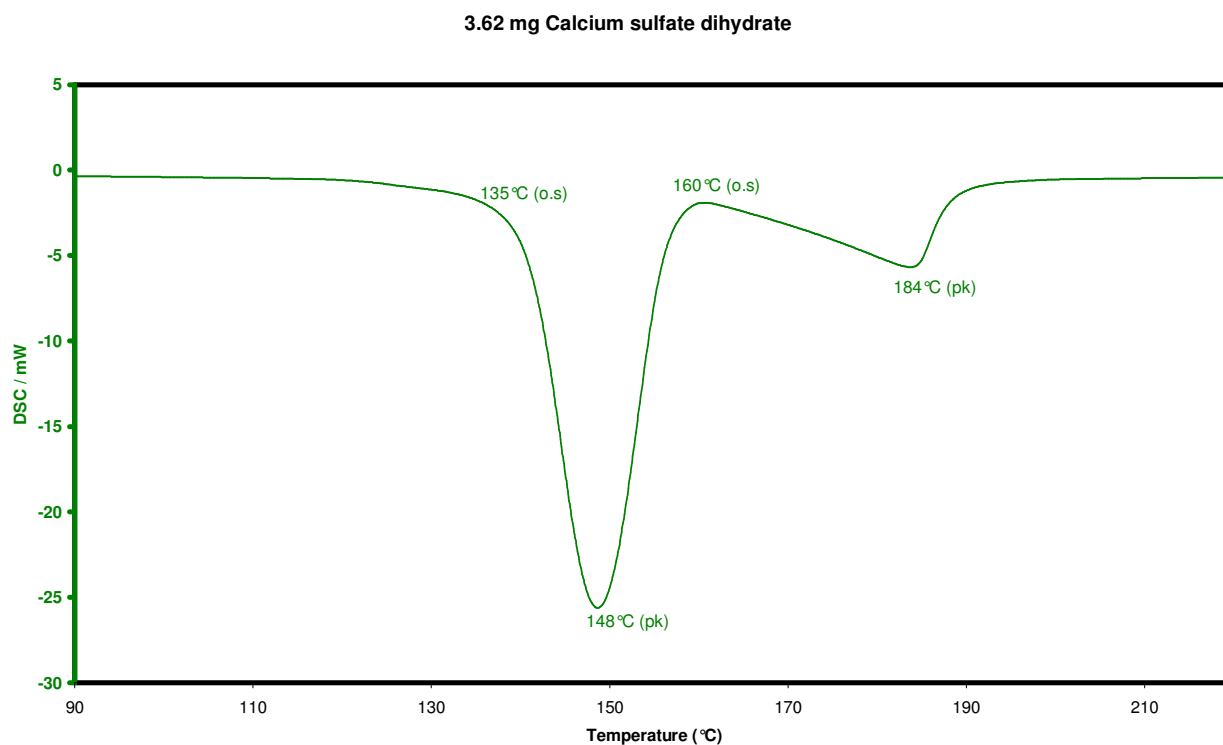
Graph 19: Dehydration of calcium sulphate dihydrate in a pin-hole DSC pan

The DSC experiment shows a distinct difference between the two pan types. The comparable MWDTA experiment consisted of heating 30 mg calcium sulphate dihydrate (Gypsum) at 10 °C/min to 250 °C, in static air. The HPB cell is not encapsulated and was thought to act more like an open pan type arrangement, upon testing the experiment showed that the two events were very well resolved (see Graph 20, page 140).

MWDTA 100% Gypsum IH0848
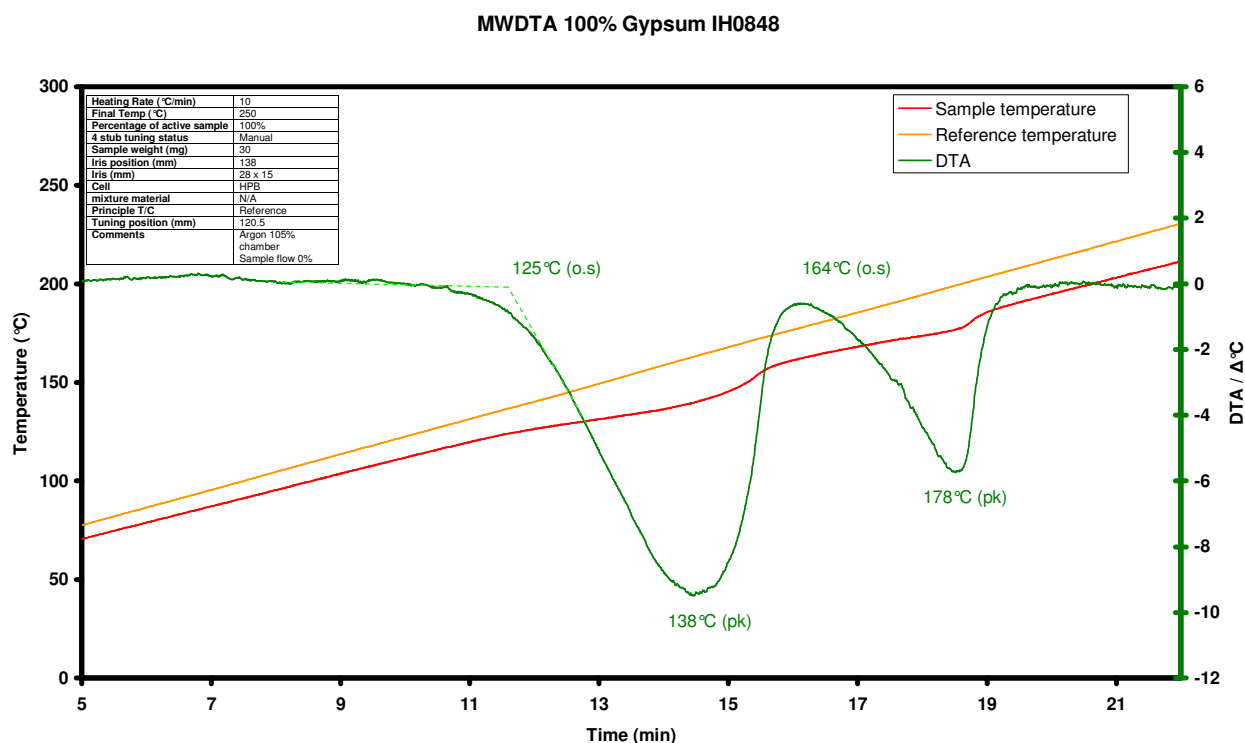
Graph 20: MWDTA dehydration of calcium sulphate dihydrate in a HPB cell with no gases flowing through the sample section.

A further comparison was made using a Stanton-Redcroft high temperature DSC (HDSC) which uses 6 mm diameter, 20 mm height, quartz crucibles without lids and is therefore more comparable in construction with the HPB cell.
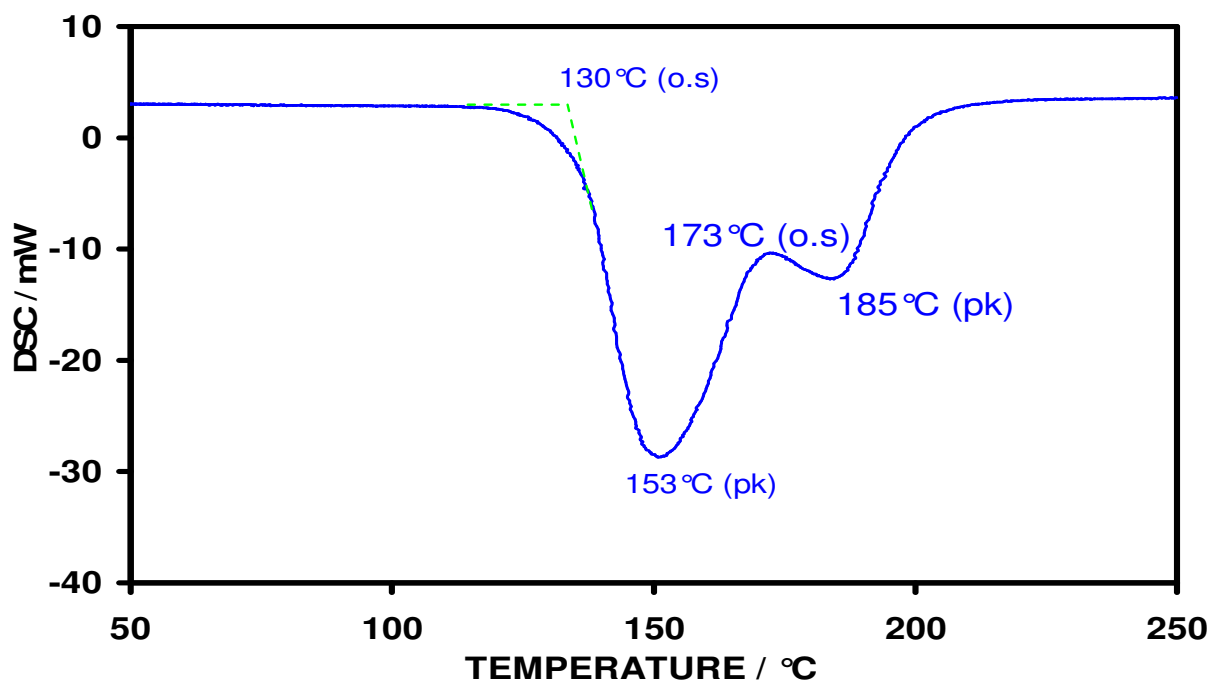
Graph 21: HDSC dehydration of calcium sulphate dihydrate in a 6 mm open quartz crucible under Argon.

Graph 21 shows an experiment using the HDSC on a sample of gypsum but using an atmosphere of argon. The resolution of the two peaks is better than the open DSC pan (Graph 18) but poorer than the pinhole DSC pan experiment (Graph 19). The height of the cell allows formation of a higher partial pressure of product gas, in a similar manner to the HPB cell in the MWTA, which results in the better resolution.

5.4 Design of a sample chamber to allow the use of a blanket gas

The option of being able to operate under an inert atmosphere is a great advantage in thermal analysis, as it reduces unwanted side reactions that could otherwise be observed, e.g. oxidation of the sample at high temperatures. It was therefore decided to develop a cylindrical sample chamber that would fit into the waveguide and surround the HPB and other cells.
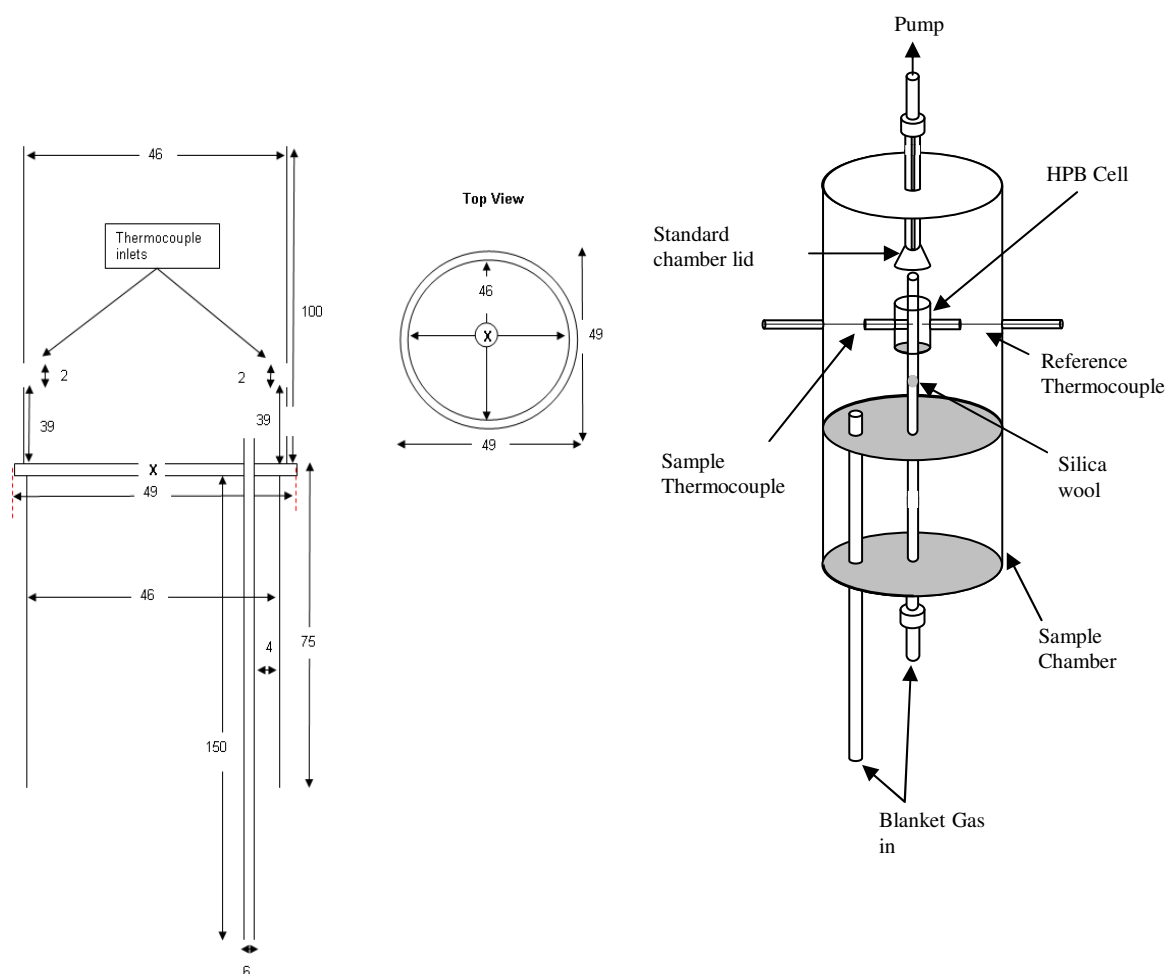
Figure 63: Diagram of MWTA sample chamber

The design of the sample chamber is shown in Figure 63. The chamber is of cylindrical design with an open port at the top for operator interaction. In line with the waveguide thermocouple ports, two 2 mm holes were drilled exactly 180 ° apart. The top of the chamber was sealed with a sampling hood which was used primarily to remove unwanted or possibly toxic generated vapours from the sample section so the chamber was safe after the experiment was completed. It was found to be essential for the chamber itself to be kept clean in order for residues not to affect the tuning of the instrument.

The hood was attached to a vacuum diaphragm pump via two Dreschel bottles containing a base (5 M solution of NaOH) in one and water in the other to trap any noxious/acidic gases evolved.

The base of the upper portion of the chamber was sealed with high vacuum grease to prevent air being drawn into the chamber or gases being lost. The lower portion of the chamber consisted of a cylinder the same dimensions as the upper. 4 mm from the external wall a 6 mm silica tube ran from the upper portion through the length of the lower and additionally 10 mm past the base of chamber. The lower chamber is used for support of the upper chamber and to reduce the dead volume of the sample area.

An additional benefit of using a sample chamber was to provide protection for the waveguide. A number of gaseous products can be evolved during a thermal analysis experiment. Many of these products are (1) corrosive or (2) are likely to condense inside the waveguide. Both situations are undesirable as in the case of:

1. The corrosive material could attack the brass construction of the waveguide giving rise to uneven surfaces and increasing the likelihood of reflections, reducing efficiency.
2. The condensation of any material with a significant tan δ (i.e. water) within the waveguide could cause localise heating, which in turn could damage the waveguide reducing its life and also distort the E-field within the cavity affecting tuning.

The added advantage of creating an enclosed sample area allowed the study of materials under controllable atmospheres. As with the sample cell, the construction material of the chamber needed careful consideration. It was eventually decided that the minimal microwave interaction of silica glass was sufficient to outweigh the additional cost of manufacture compared to borosilicate.

Evaluation experiments demonstrated that, apart from requiring a slight alteration of the adjustable short, the chamber had no other effect on the instrument operation.

To demonstrate the efficiency of the sample chamber in excluding air, a series of experiments were performed using copper oxalate following the methodology of Mullens *et al.* [37]. The experiment consisted of heating a sample of copper oxalate at a rate of 10 ºC/min to 600ºC under an inert gas flowing at 50 ml/min through the sample chamber, and comparing with a similar experiment but using static air.

According to Lamprecht *et al.* [38], copper oxalate (green-blue) decomposes via two different routes, as shown in Equation 30, depending on the presence of oxygen. In the absence of oxygen route (a) is favoured with the formation of copper metal (red). In the presence of oxygen the decomposition results in copper oxide (black).

$$(a)\ CuC_2O_4(s) \xrightarrow{\ inert\ } Cu(s) + 2CO_2(g);$$
$$(b)\ CuC_2O_4(s) \xrightarrow{\ O_2\ } CuO(s) + CO(g) + CO_2(g)$$
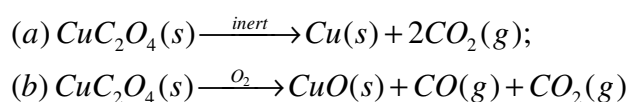
Equation 30: Competitive reactions for the decomposition of copper oxalate

These colour changes were of great advantage in evaluating the sample chamber as they gave a quick indication of which reaction was favoured and additionally if there was any residue of copper oxalate.
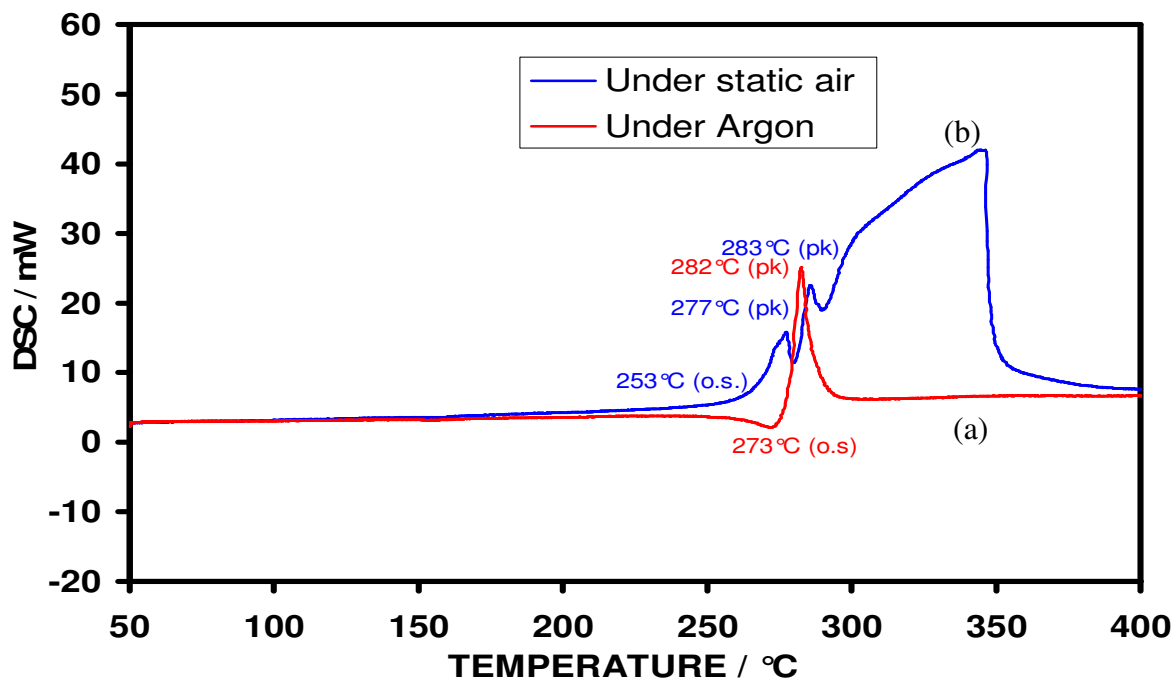
Graph 22: DSC overlays of the decomposition of copper oxalate in (a) Argon atmosphere (b) under air

Graph 22 shows the results of two HDSC experiments on 25 mg samples of copper oxalate in 6 mm quartz crucibles using atmospheres of static air and argon. The complex peak observed for the decomposition under static air arises from the additional exothermic oxidation of copper to copper oxide and CO to CO_2. The decomposition under argon produces a simpler trace as these additional oxidation steps are absent.

MWDTA 100% Copper oxalate overlay
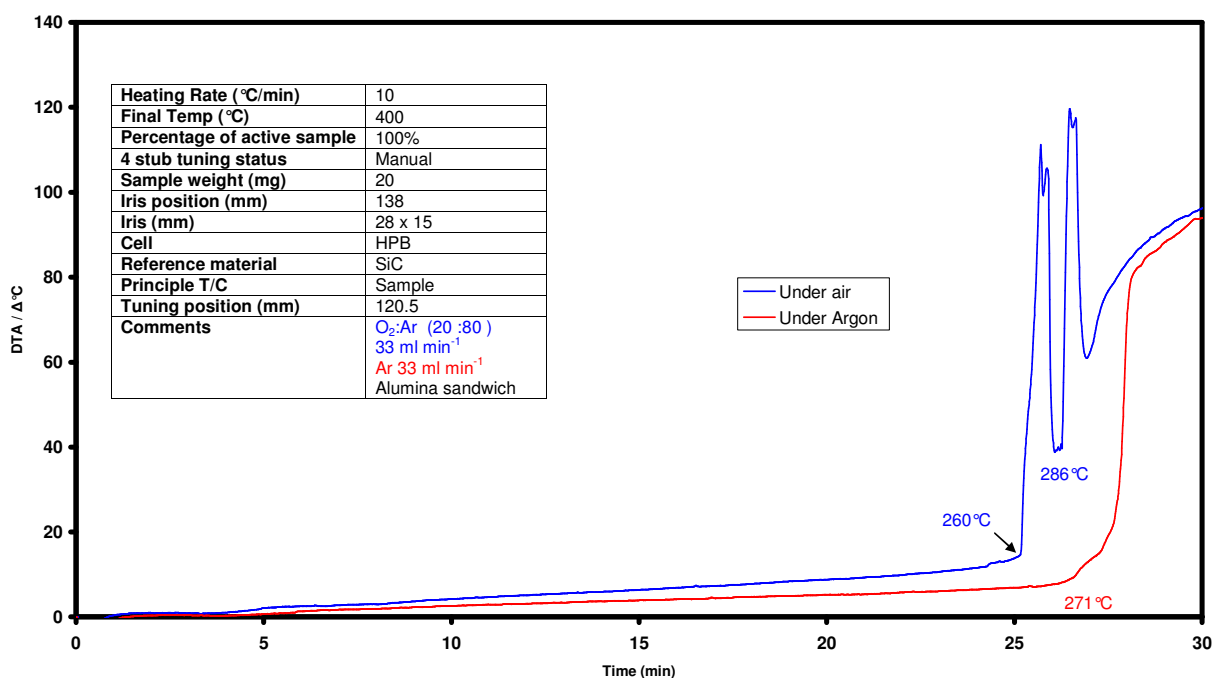
Graph 23: MWDTA overlays of decomposition of Copper oxalate in (a) Argon atmosphere (b) under air

Graph 23 shows the comparable experiments but utilising the HPB cell and sample chamber. Again, the profile for the experiment under air is more complex because of the additional oxidation processes. The results also show a close correlation of the onset temperatures (o.s) with those obtained with the HDSC for both argon and air atmospheres. An examination of the colour of the product suggested that no black CuO was formed when argon was used as a blanket gas in the sample chamber, i.e. it successfully excluded air. To confirm the visual observations, the products were analysed using XRD (see Graph 24 and Graph 25, page 146). Standard samples of the products were used to assign the peaks observed (the present of SiC in the trace is due to unavoidable carryover of the reference material from the HPB cell when the sample was transferred to the XRD sample holder).
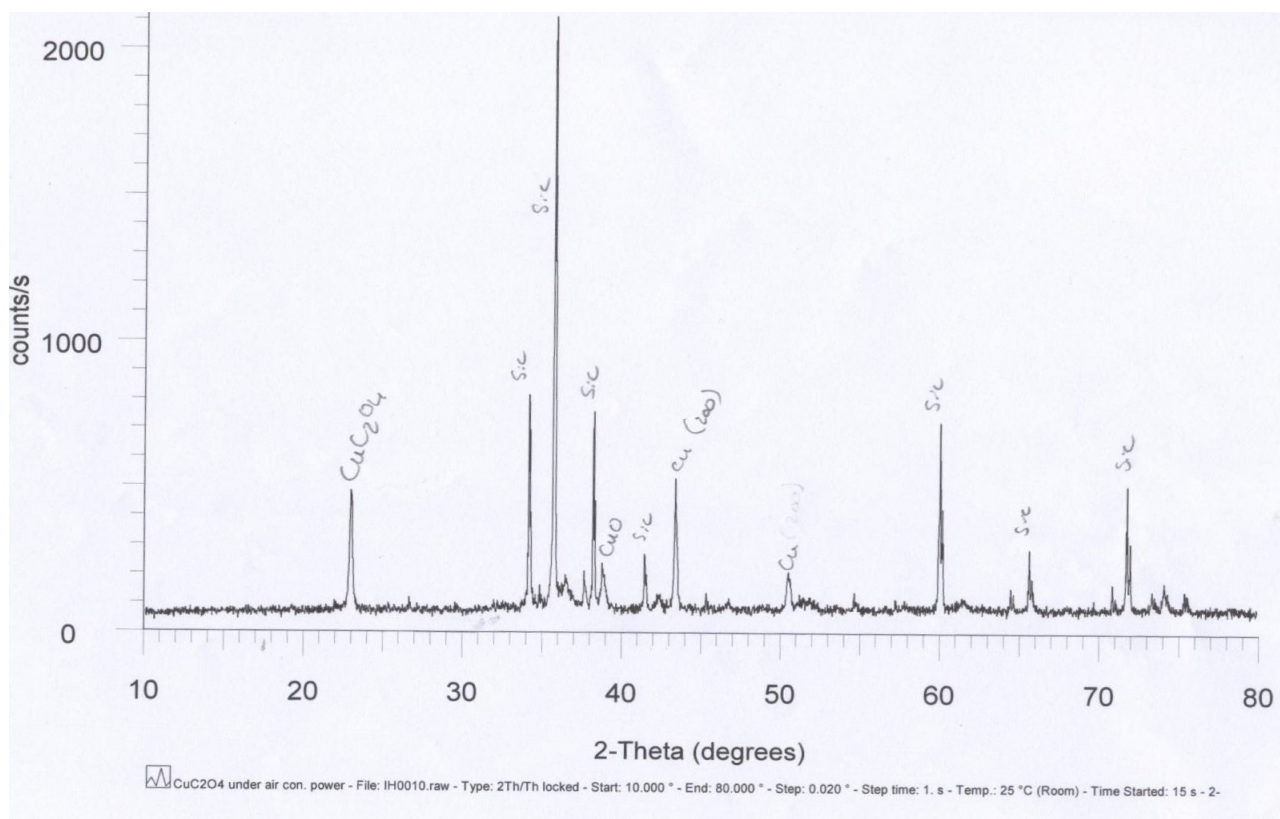
Graph 24: XRD pattern of the copper oxalate residue after decomposition under air
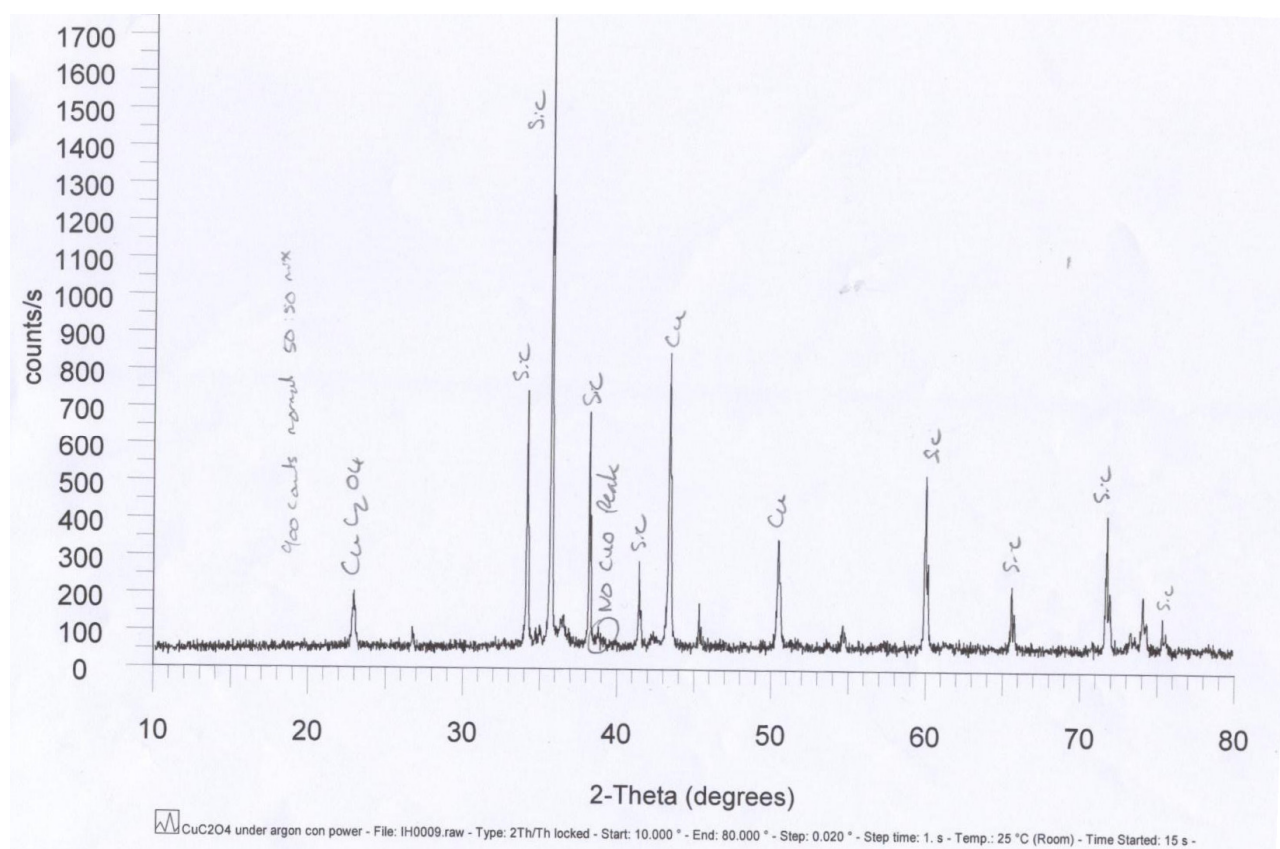
Graph 25: XRD pattern of copper oxalate residue after decomposition under argon

The results showed that in air there was evidence that copper oxide was formed (at 39 ° 2-Theta) and some copper metal (at 43 ° and 50 ° 2-theta). When the sample was heated under argon the copper oxide peaks were absent and the copper metal peaks increased in size in relation to the other peaks present.

The large volume of the sample chamber meant that the there was a purge time for the chamber to become fully saturated with the chosen atmosphere. This time was calculated (assuming no losses and a flow rate of 80 ml/min) using the following equations:-

$$\text{Volume} = \pi r^2 h$$
$$\text{Volume} = \pi (2.3^2)10 = 166 cm^3$$
$$\text{Purge time} = \frac{Chamber\ volume}{Flow\ rate} = \frac{166\ cm^3}{80\ cm^3\ \min^{-1}} = 2.075\ \min.$$

Equation 31: Calculation of the purge time of the MWTA sample chamber

The calculated two minutes became the standard equilibrium time before any experiment using the chamber.

5.4.1 Effect of carrier and blanket gases using the HPB cell and sample chamber

The effect of carrier and blanket gas on the resolution of the dehydration of gypsum observed using the HPB cell with sample chamber was investigated. Two gases were studied: helium which has a density less than air and argon which has a density greater than air. In these experiments the gases were passed through the sample cell (carrier gas) and used as the blanket gas.

Graph 26 and Graph 27 show the dehydration experiments under helium and argon, respectively.

MWDTA 100% Gypsum IH0850
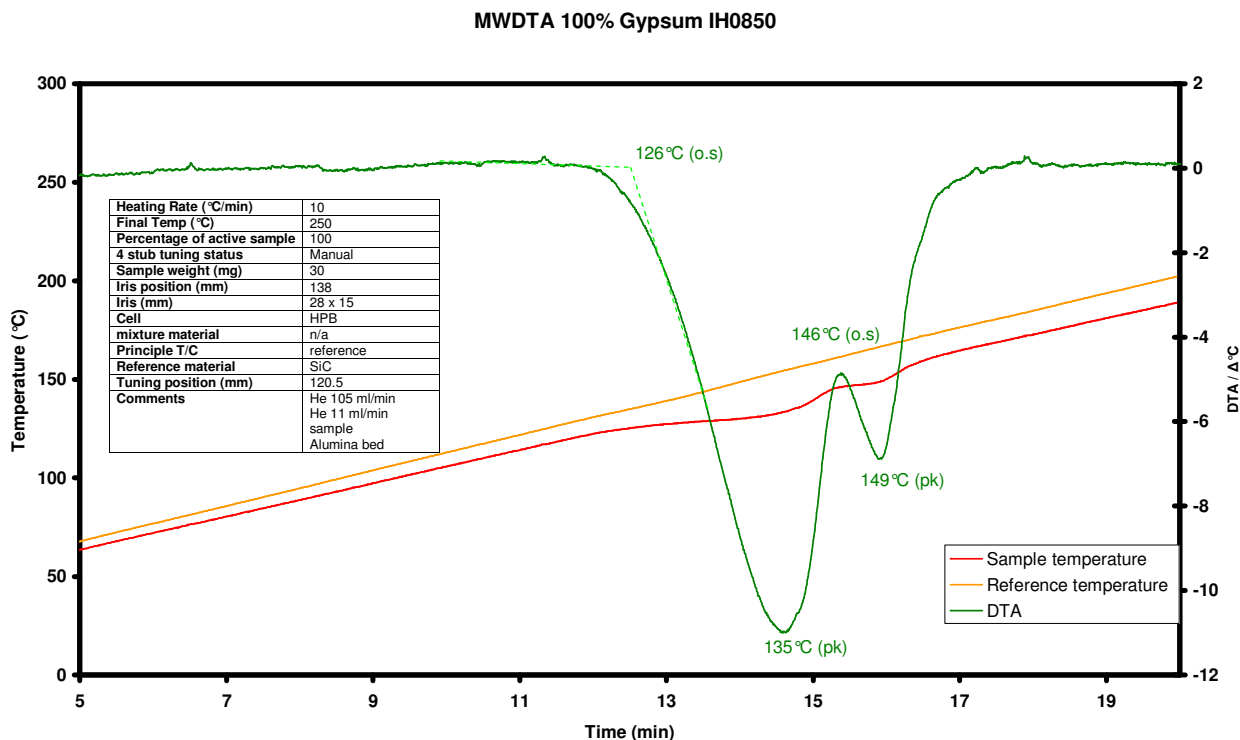
Graph 26: MWDTA dehydration of calcium sulphate dihydrate in a HPB cell under helium (blanket gas flowing through sample section)

MWDTA 100% Gypsum IH0851
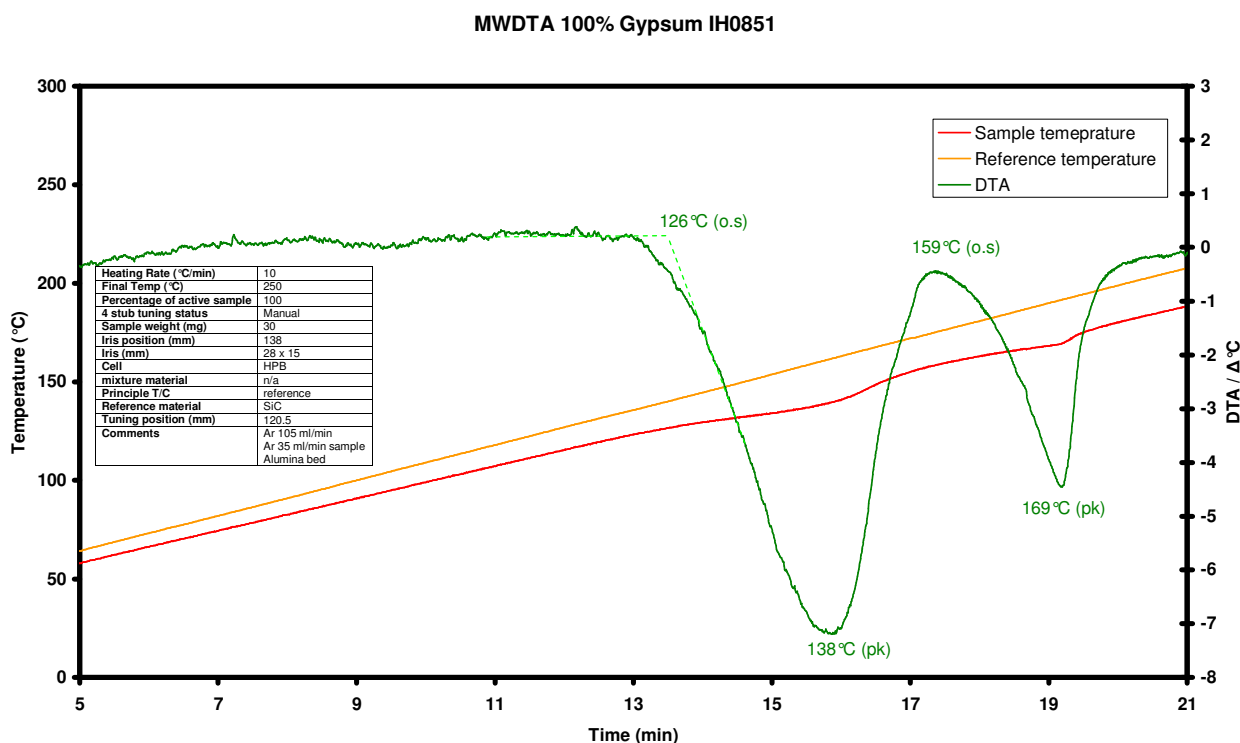
Graph 27: MWDTA dehydration of calcium sulphate dihydrate in a HPB cell under Argon (blanket gas flowing through sample section)

In both these microwave experiments the onset temperatures were in good agreement with each other. However, it can be seen that a greater resolution was obtained with the argon atmosphere.

This probably is due to the greater density of argon making it more efficient in sweeping the evolved water vapour away from the sample than the lighter helium (or static air) thus reducing the partial pressure in the vicinity of the sample.

These results show that by altering the flow of the carrier gas the HPB cell could be made to behave like either an open or pinhole DSC pan.

5.5 The removable crucible HPB cell (RCHPB)

As mentioned in previous sections, locating the thermocouple within the sample causes it to act as a heat source (or sink) and thermal impedance. In the cell designs mentioned in this chapter the sample temperature measurement was recorded using the thermocouple situated within the analyte, as the problem of thermal impedance was thought to be greatly reduced (or eliminated) due to volumetric heating. The sample temperature as a whole is assumed to be uniform. The addition of an indirect measurement arrangement had the advantages that:-

- The sample could be easily placed in a reproducible position,
- The thermocouple was less likely to become contaminated with previous sample residues,
- The reference now remained at a constant mass, therefore reducing the errors from different volumes of susceptor heating to different extents,
- The removable crucibles could accommodate analytical sized samples (1 – 100 mg).

In order to determine if the Boersma indirect type arrangement [5] could be utilised in MWTA an adaptation of the HPB cell was designed and tested.
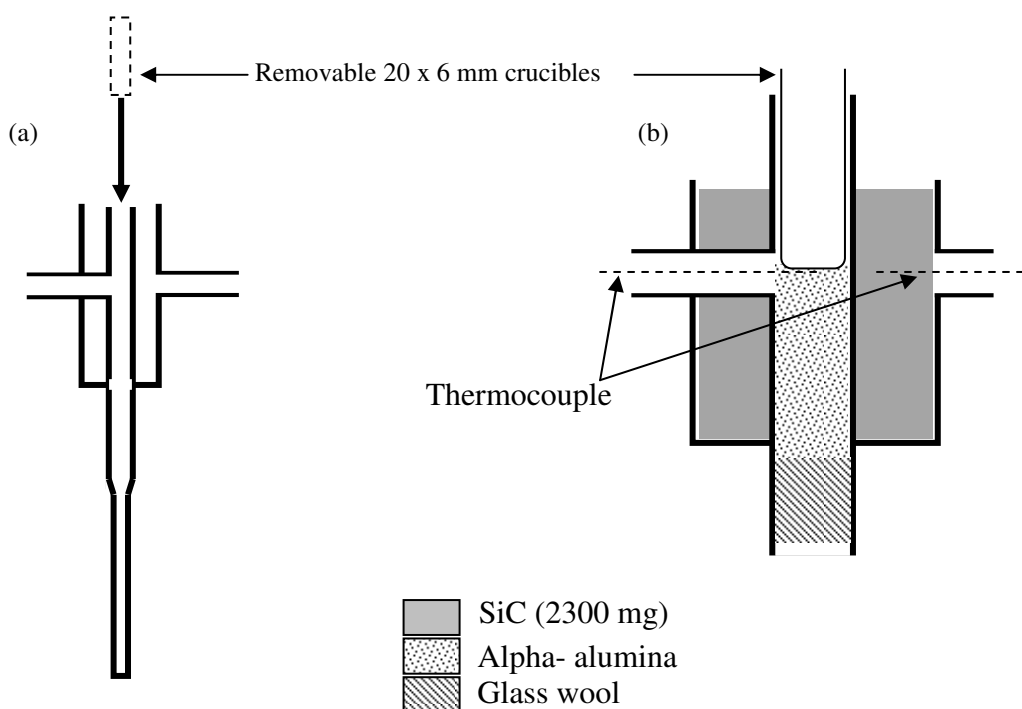
Figure 64: Illustration of (a) the RCHPB cell arrangement (b) enlargement of the cell packing in RCHPB

The main difference from the HPB design was the chambers were 2 mm larger (in diameter) in this design in order to accommodate a 6 mm (external diameter) silica sample cell (shown at the top of the diagram). The inner chamber was filled will α-alumina to the same level as the thermocouple inlet and the outer chamber filled with SiC. The standard MWTA thermocouples were then inserted into the RCHPB and remained in situ throughout all the experiments. The largest drawback of this type of arrangement is the additional wall of silica between the sample and the thermocouple and the possibility of a poor thermal contact between the thermocouple tip and the base of the sample cell. To increase the contact area between the base of the sample cell and thermocouple tip and also to aid thermal conductivity the tip was surrounded by α-alumina (thermal conductivity ~ 30 W $\cdot$ M^{-1} $\cdot$ K^{-1} @ 300 K [33]).

The conventional Boersma DSC instrument has the advantage that the thermocouple junction is attached to a thermally conductive plate which is in contact with a thermally conductive sample pan. MWTA requires the use of a microwave transparent construction material (silica) which unfortunately (in this case) has a low thermal conductivity as described earlier.

Other possible problems faced by this arrangement arose due to the increase in the physical size of the cell as a whole. As microwave penetration depth is constant as the dimensions of sample increases the chance of the wave being able to reach the centre decreases. Therefore the addition of 2 mm to the diameter of the reference chamber has the effect of increasing the chamber volume by

30 %, possibly reducing the penetration depth and resulting in the sample not interacting with sufficient applied power to be able to undergo thermal transitions when microwaves are the main mode of heating (the sample is then more likely to heat via conduction of heat from the reference).

5.5.1 Effect of atmosphere in RCHPB baselines

The importance of the carrier gas has been discussed previously in this thesis. Argon has been the favoured gas for its insulation properties and the reduction in the thermal gradient between the sample cell and walls of the chamber. The additional air gap (thermal conductivity ~ 0.0262 W m^{-1}K^{-1} @ 300 K [39]) between the RCHPB and the internal reference wall introduced another possible point of poor thermal contact. It was believed a highly conductive gas such as helium (thermal conductivity ~ 0.1509 W m^{-1}K^{-1} @ 300 K [39]) would aid the thermal contact between the cell and the internal reference wall/thermocouple tip.

To evaluate the RCHPB cell and effects of blanket and carrier gases on the ΔT baseline a series of experiments was performed using α-alumina. The flow arrangements are shown in Figure 65. 15 mg of the sample was placed in the silica sample cell and heated at a rate of 10 °C/min to 730 °C with either argon or helium flowing into the chamber.

5.5.1.1 Gas flow arrangements for the RCHPB

Arrangement 1   **Arrangement 2**

→ = Gas flow

= Removable crucible
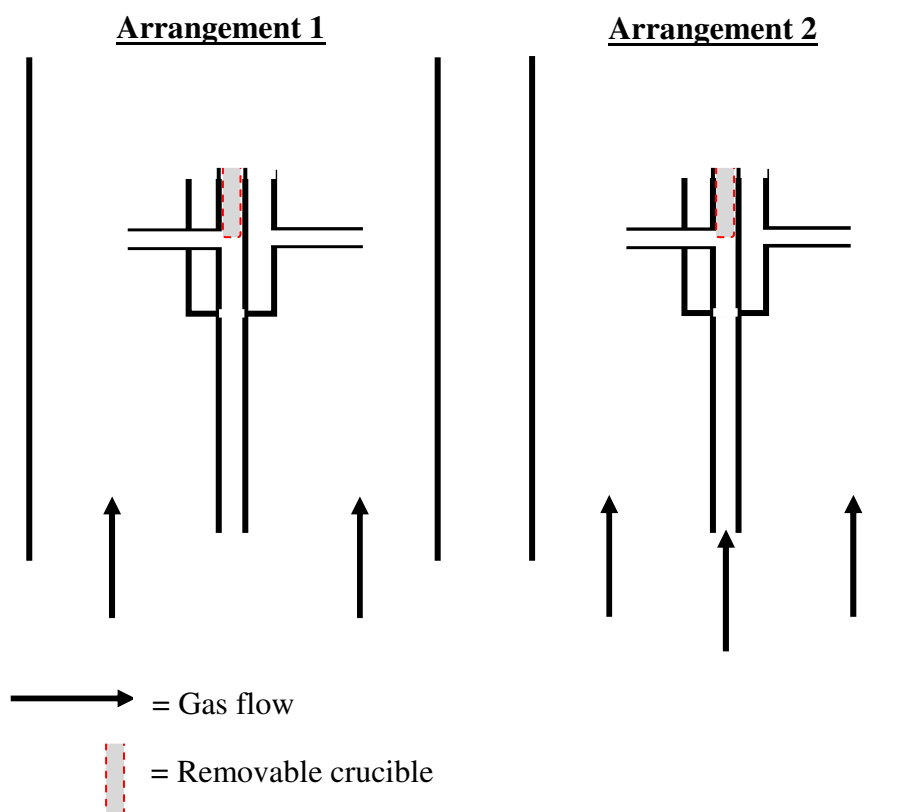
Figure 65: Illustration of the RCHPB arrangement

In arrangement 1 gas was solely supplied to the chamber at a flow rate of 105 cm^3 min^{-1}. In arrangement 2 a controlled flow of the carrier gas was also supplied through the sample section of the cell.

Helium

The baseline was investigated using two gas flow arrangements. The first involved flooding the outer chamber with the carrier gas but not the sample area (arrangement 1).

MWDTA indirect 100% Alumina IH1024

Heating Rate (°C/min)	10
Final Temp (°C)	830
Percentage of active sample	100%
4 stub tuning status	Manual
Sample weight (mg)	15
Iris position (mm)	138
Iris (mm)	28 x 15
Cell	HPB indirect
mixture material	N/A
Principle T/C	Reference
Tuning position (mm)	120.5
Comments	Helium 105% Sample flow 0% Alumina sandwich

Max Δ°C = 96 °C
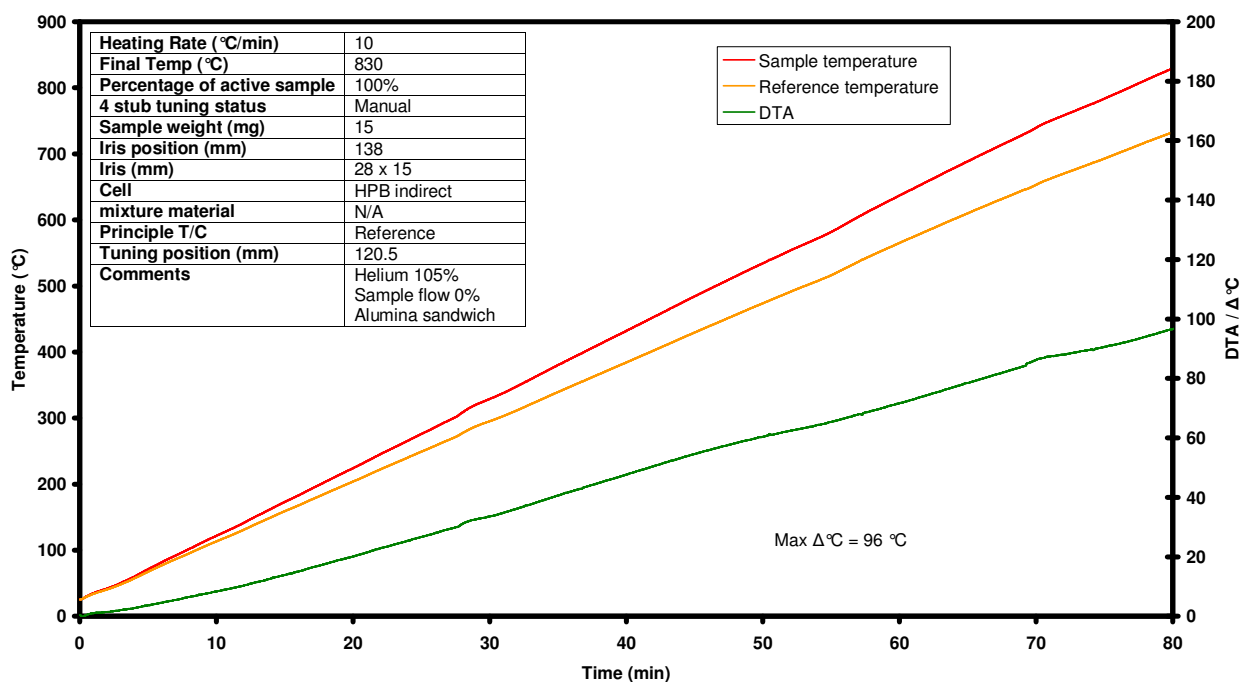
Graph 28: The baseline drift experience with the RCHPB under helium in arrangement 1 (blanket gas)

The results showed a constantly drifting baseline believed to be attributed to the blanket gas facilitating the transfer of heat away from the sample (see Graph 28).
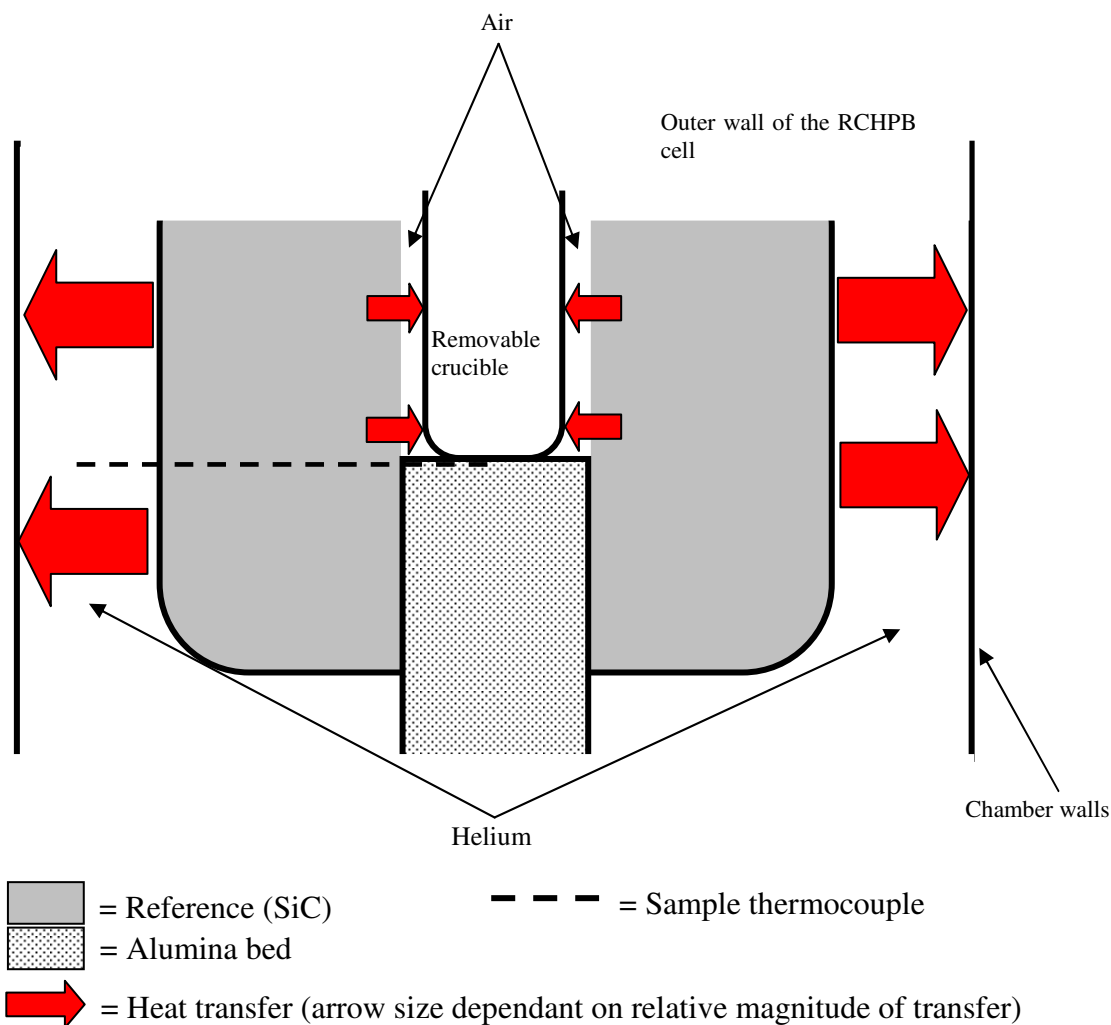
Figure 66: Illustration of the thermal gradient when using a highly conductive blanket gas

Evidence of these findings can be seen by the elevated temperature of the inert sample in respect to the reference, as the centre of the cell (sample area) must be at the internal temperature of the reference (as it is in a near ideal heat-flux environment and the sample could not heat on its own accord). Heat loss must be lost from the reference chambers outer walls and top.

The experiment was repeated using a gas flow arrangement which not only flooded the chamber (blanket gas) but also supplied helium at a rate of 4 ml/min through the sample (carrier gas) section of the RCHPB (arrangement 2) in order to aid the thermal contact between the sample cell and the inner reference wall and have the overall effect of creating a more uniform temperature within the chamber.

MWDTA indirect 100% Alumina IH1026

Heating Rate (°C/min)	10
Final Temp (°C)	800
Percentage of active sample	100%
4 stub tuning status	Manual
Sample weight (mg)	15
Iris position (mm)	138
Iris (mm)	28 x 15
Cell	Boersma type
mixture material	N/A
Principle T/C	Reference
Tuning position (mm)	113
Comments	Helium 105% Sample flow 22% Alumina sandwich

Max Δ°C = 11.42 °C
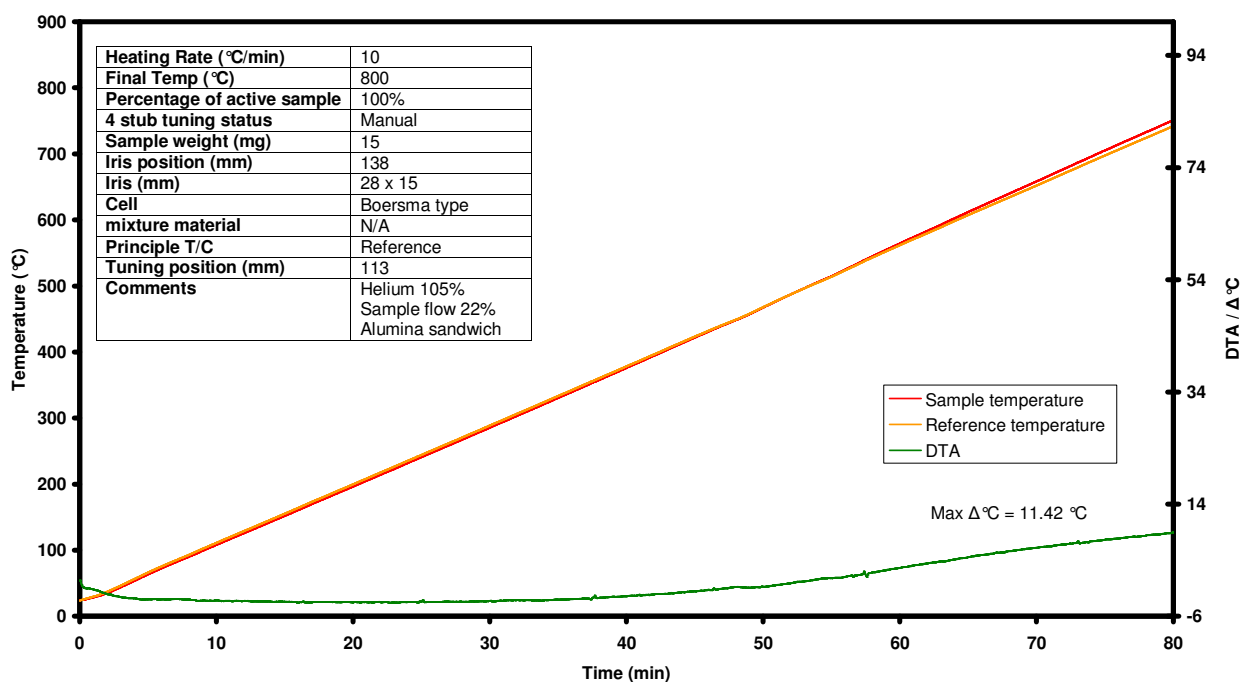
Graph 29: The baseline drift experience with the RCHPB under helium in arrangement 2 (blanket and carrier gas).

The experiment showed a promising baseline with a slight increase in differential temperature at around 500 °C, which could be due to the heat transfer away from the external reference wall being aided by the thermal conductivity of the carrier gas at elevated temperatures as in the previous case. Overall the advantage of flowing helium gas through the inner chamber reduced the differential temperature by around 80 °C giving a flatter baseline).

Under Argon

The insulation properties of argon gas (thermal conductivity ~ 0.01772 W $m^{-1}K^{-1}$ @ 300 K [33]) have been used in this research to prevent thermal gradients from the hot cell body towards the cold chamber wall. To determine the effect it had in reducing the differential temperatures observed in the helium experiments the runs were repeated. In the first instance only the chamber was flooded with argon (arrangement 1).

MWDTA indirect 100% Alumina IH1023

Heating Rate (℃/min)	10
Final Temp (℃)	730
Percentage of active sample	100%
4 stub tuning status	Manual
Sample weight (mg)	15
Iris position (mm)	138
Iris (mm)	28 x 15
Cell	HPB indirect
mixture material	N/A
Principle T/C	Reference
Tuning position (mm)	120.5
Comments	Argon 105% Sample flow 0% Alumina sandwich

Max Δ℃ = 6.22 ℃
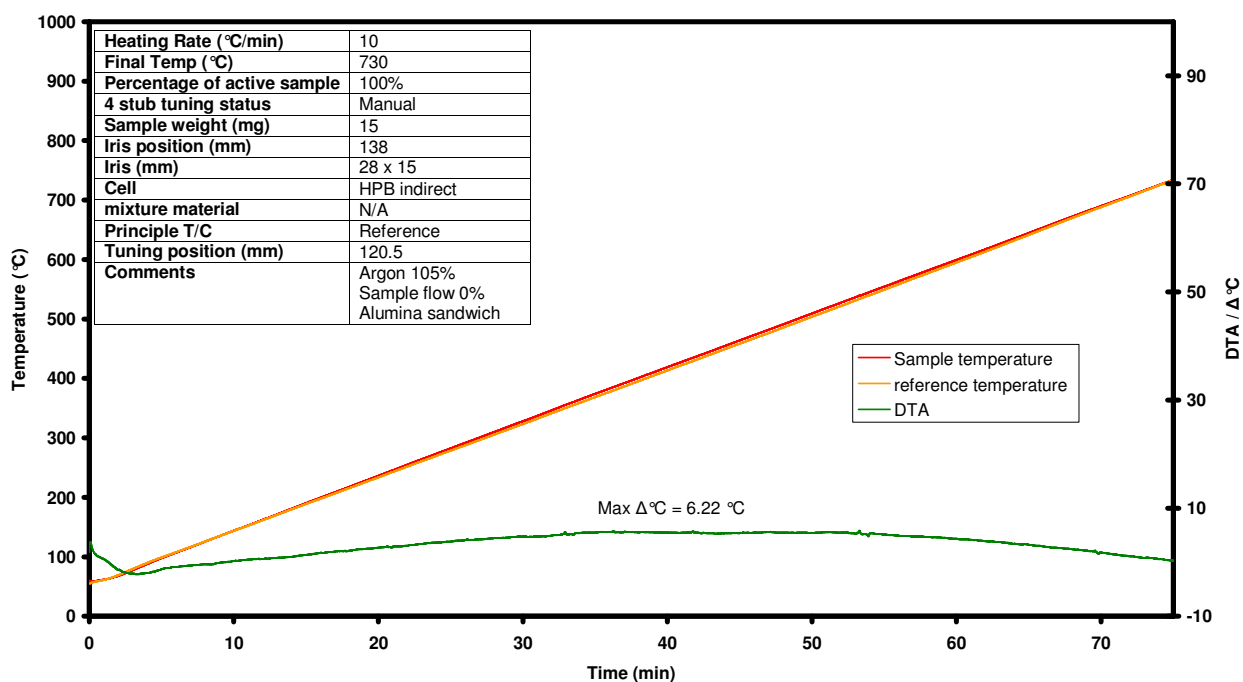
Graph 30: The baseline drift experience with the RCHPB under argon in arrangement 1 (blanket gas only).

The results showed a large improvement on the equivalent helium run with the maximum differential down to around 6 °C, 90 °C lower than the comparable helium experiment. In this arrangement the gap between the cell and chamber walls was thought to have a lower thermal conductivity than the gap from the internal reference wall and sample cell leading to the belief that the thermal gradient tended towards the sample explaining the lowering in differential temperature.

Air

Outer wall of the RCHPB
cell

Removable
crucible

Chamber walls

Argon

= Reference (SiC)   = Sample thermocouple
= Alumina bed

= Heat transfer (arrow size dependant on relative magnitude of transfer)
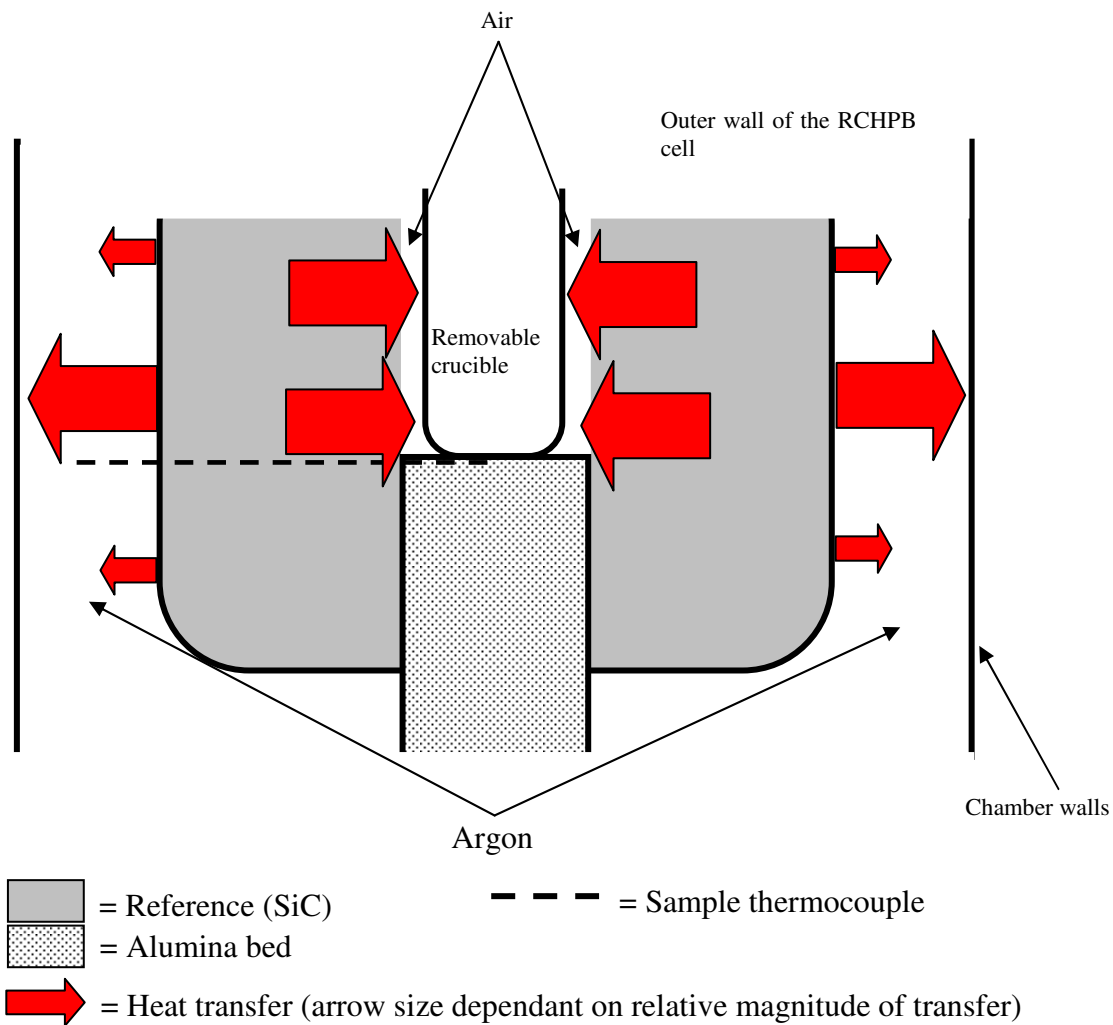
Figure 67: Illustration of the thermal gradient when using a blanket gas with a low thermal conductivity

When the experiment was repeated with the carrier gas flowing through the sample area of the
RCHPB the results (see Graph 31, page 158) showed a reduction in differential temperature in the
lower temperature stages. As expected the differential reading increased during the experiment, the
most likely cause being the reduction in thermal conductivity between the inner wall of the
reference and cell, due to argon diffusing into the gap between the two.

MWDTA indirect 100% Alumina IH1039

Heating Rate (°C/min)	10
Final Temp (°C)	700
Percentage of active sample	100%
4 stub tuning status	Manual
Sample weight (mg)	20
Iris position (mm)	138
Iris (mm)	28 x 15
Cell	Boersma type
mixture material	N/A
Principle T/C	Reference
Tuning position (mm)	113
Comments	Argon 105% Sample flow 22% Alumina sandwich
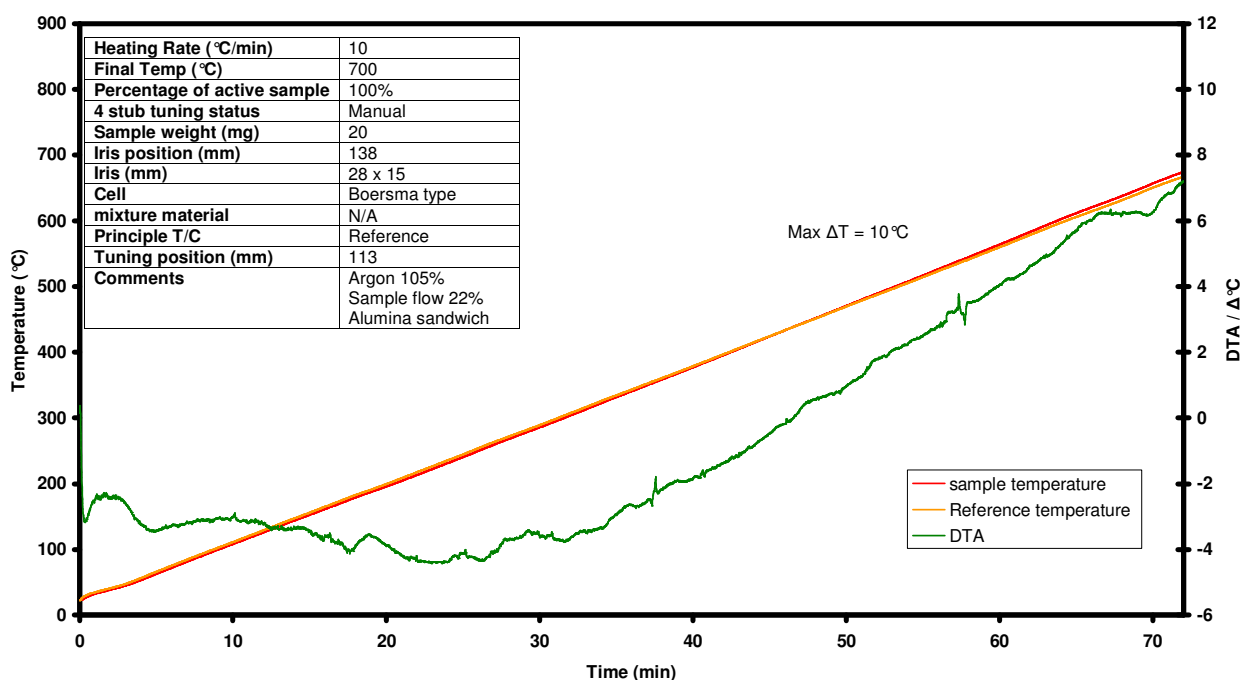
Graph 31: The baseline drift experience with the RCHPB under argon in arrangement 2.

5.5.2 Evaluation of Removable Crucible HPB cell with well characterised materials using different atmospheres

To further evaluate the RCHPB cell a series of experiments were performed using four materials, silver iodide (AgI), sorbitol, indium and a mixture of potassium and sodium hydrogen carbonate.

- Silver iodide has a solid-solid phase change at 147 °C to a fast ion conducting form with a resultant increase in tan δ.

- Sorbitol undergoes fusion at 95 °C also associated with an increase in tan δ.

- Indium is a well known thermal calibration standard which undergoes fusion at 156 °C. Normally, the use of a metal within a microwave cavity can be problematic but the benefit of the RCHPB cell is that the sample is electrically isolated from the earthed thermocouple and so would not be expected to cause arcing.

- Potassium and sodium hydrogen carbonate have broad decomposition steps centred on 156 °C and 206 °C respectively. Neither reactants nor products couple well with microwaves and so would not be expected to produce a significant change in tan δ.

Two sets of experiments were performed (under helium, and under argon) in cell arrangement 2 where both the blanket gas and carrier gas were the same. All experiments used 20 mg samples with control on the reference (SiC).

MWDTA indirect 100% silver iodide IH1027

Heating Rate (℃/min)	10
Final Temp (℃)	170
Percentage of active sample	100%
4 stub tuning status	Manual
Sample weight (mg)	20
Iris position (mm)	138
Iris (mm)	28 x 15
Cell	Boersma type
mixture material	N/A
Principle T/C	Reference
Tuning position (mm)	113
Comments	Helium 105% Sample flow 22% Alumina sandwich
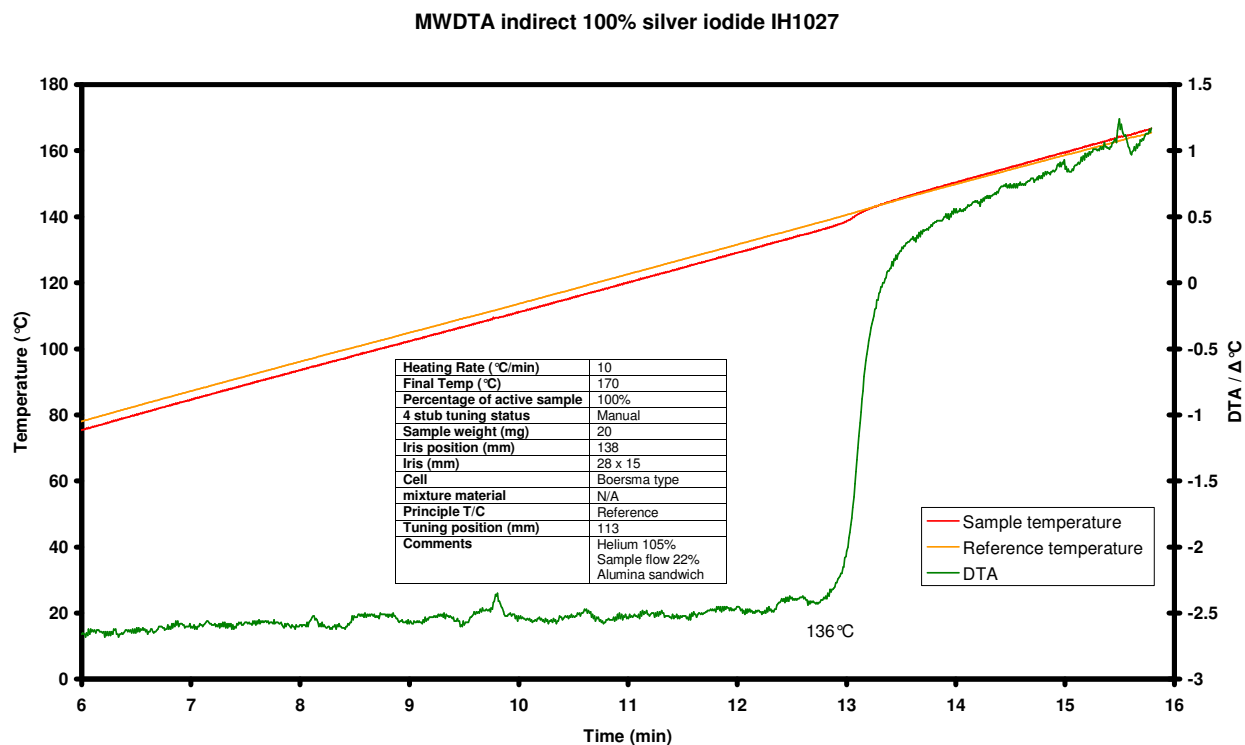
Graph 32: Silver iodide experiment conducted in the RCHPB under helium in arrangement 2.

Graph 32 shows the results of the experiment performed using silver iodide under helium at 10 °C/min. There is a sharp increase in ΔT of about 3 °C at 136 °C which can be attributed to the phase change although it appears 11 °C lower than the literature value. To test whether this difference resulted from the effect of heating rate, two further experiments were done using 5 °C/min and 2 °C/min (Graph 33 and Graph 34 respectively). In both cases the measured transition temperature of the phase change was 136 °C and the magnitude of the increase in ΔT did not change significantly. As a result, all subsequent evaluation experiments were performed using 10 °C/min.

MWDTA indirect 100% Silver iodide IH1037

Heating Rate (℃/min)	5
Final Temp (℃)	170
Percentage of active sample	100%
4 stub tuning status	Manual
Sample weight (mg)	20
Iris position (mm)	138
Iris (mm)	28 x 15
Cell	Boersma type
mixture material	N/A
Principle T/C	Reference
Tuning position (mm)	113
Comments	Helium 105% Sample flow 22% Alumina sandwich
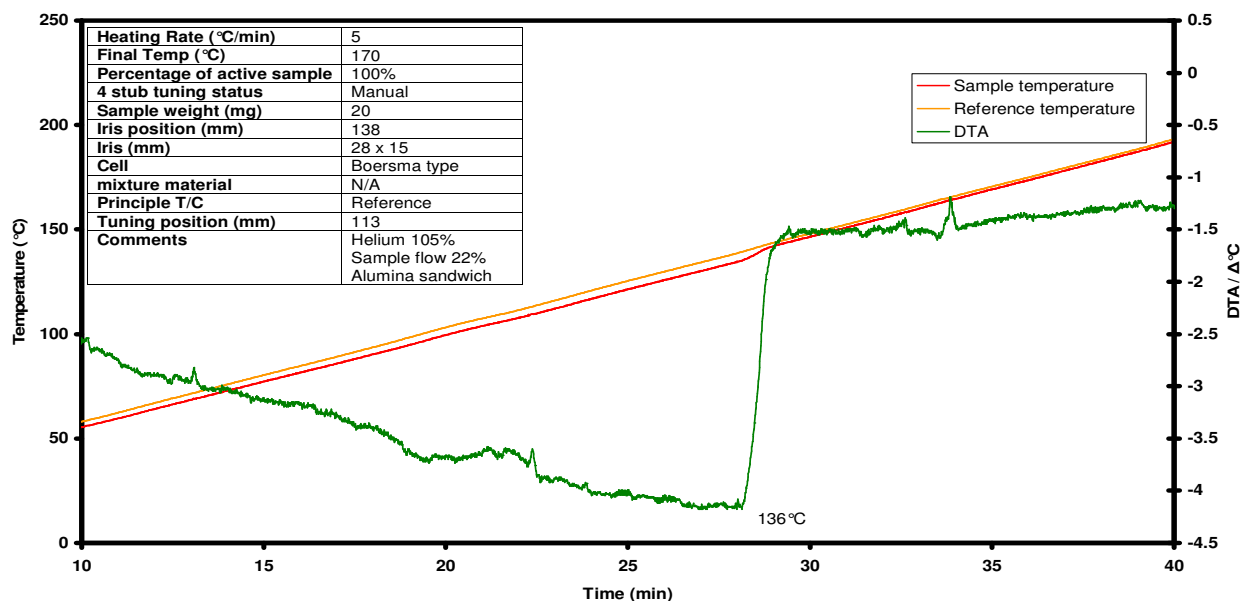
Graph 33: Silver iodide experiment conducted in the RCHPB under helium in arrangement 2 (heating rate changed to 5 °C/min).

MWDTA indirect 100% Silver iodide IH1028

Heating Rate (℃/min)	2
Final Temp (℃)	170
Percentage of active sample	100%
4 stub tuning status	Manual
Sample weight (mg)	20
Iris position (mm)	138
Iris (mm)	28 x 15
Cell	Boersma type
mixture material	N/A
Principle T/C	Reference
Tuning position (mm)	113
Comments	Helium 105% Sample flow 22% Alumina sandwich
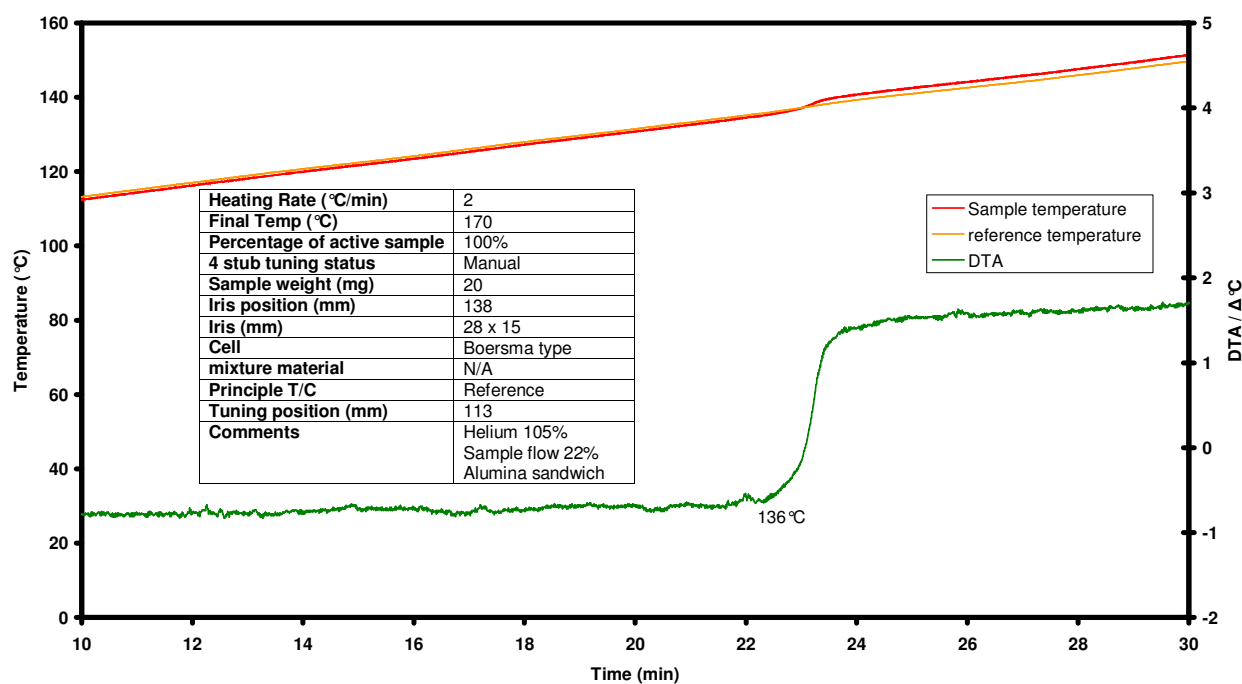
Graph 34: Silver iodide experiment conducted in the RCHPB under helium in arrangement 2 (heating rate changed to 2 °C/min).

Graph 35 shows an equivalent experiment at 10 °C/min under argon. The initial magnitude of ΔT is larger than in the experiment under helium but the onset temperature (135 °C) and size of the ΔT step (2.5 °C) are very similar.

MWDTA indirect Silver iodide IH1040

Heating Rate (°C/min)	10
Final Temp (°C)	170
Percentage of active sample	100%
4 stub tuning status	Manual
Sample weight (mg)	20
Iris position (mm)	138
Iris (mm)	28 x 15
Cell	Boersma type
mixture material	N/A
Principle T/C	Reference
Tuning position (mm)	113
Comments	Argon 105% Sample flow 22% Alumina sandwich
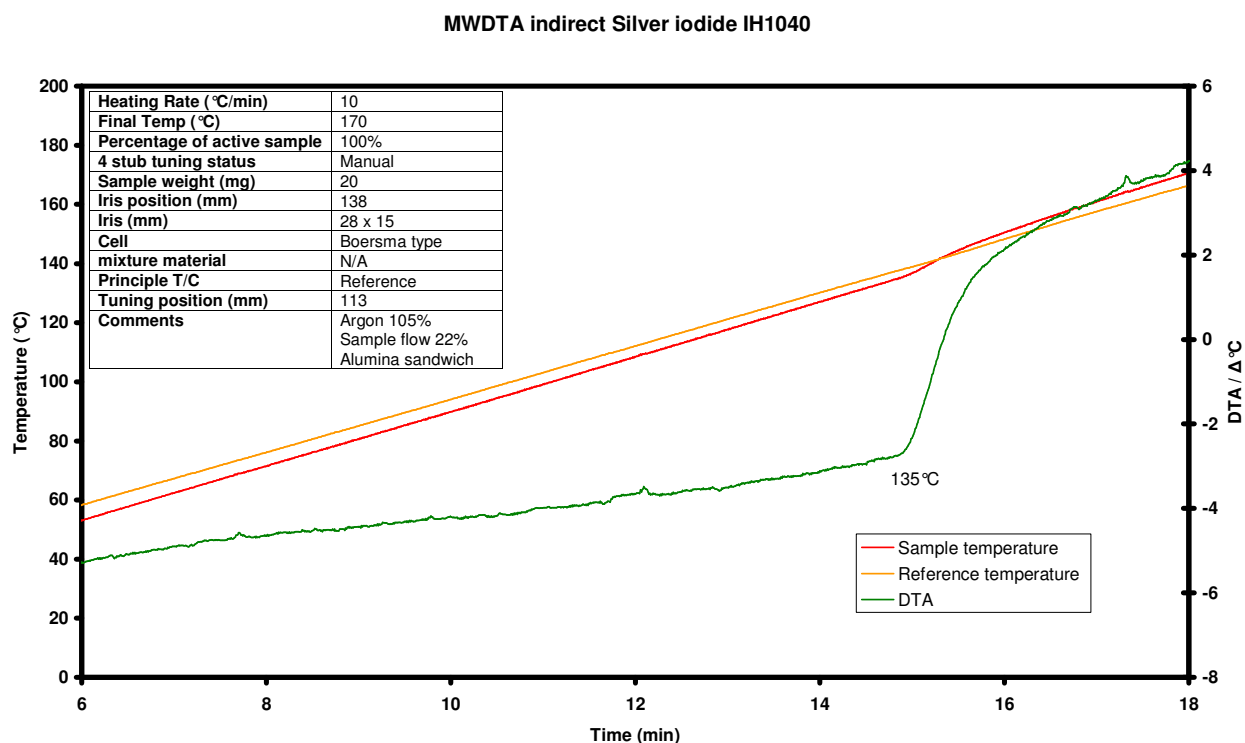
Graph 35: Silver iodide experiment conducted in the RCHPB under argon in arrangement 2

Volumetric heating can result in the sample (possibly) heating under its own accord while the reference is heating at the set rate, resulting in the two different heating rates never really allowing the sample and cell temperature to fully equilibrate. The low thermal conductivity of the silica glass is also likely to insulate the thermocouple from the sample, a problem increased by the thickness of the base of the cell. The combination of these two factors gives the depression of the transition temperature seen in the experiments, as the insulated thermocouple will be reading a lower temperature than the true value while the sample has more than likely reached the true transition temperature, making the transition appear to have occurred early.

Graph 36 shows the result of the experiment with sorbitol under helium. There is an increase in ΔT of about 3 °C at 87 °C which can be attributed to the fusion although, again, it appears considerably lower than the literature value (95 °C).

MWDTA indirect 100% D-Sorbitol IH1032

Heating Rate (℃/min)	10
Final Temp (℃)	120
Percentage of active sample	100%
4 stub tuning status	Manual
Sample weight (mg)	20
Iris position (mm)	138
Iris (mm)	28 x 15
Cell	Boersma type
mixture material	N/A
Principle T/C	Reference
Tuning position (mm)	113
Comments	Helium 105% Sample flow 22% Alumina sandwich
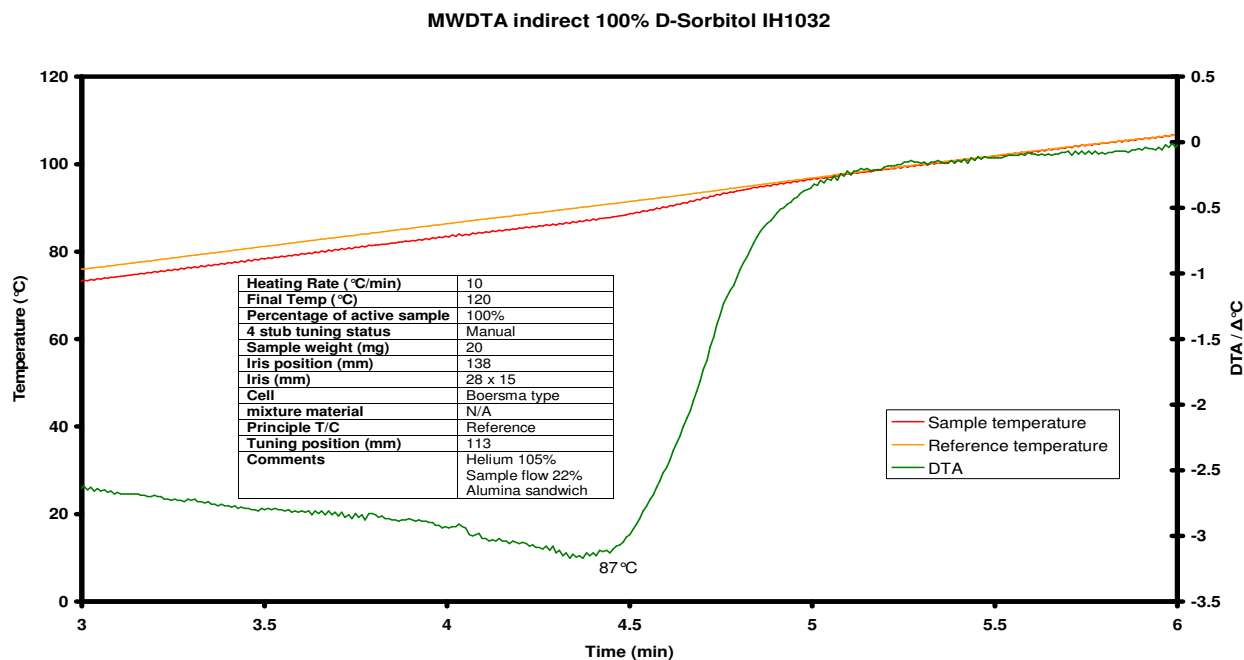
Graph 36: D-sorbitol experiment conducted in the RCHPB under helium in arrangement 2.

Graph 37 shows the comparable experiment under argon. Again, the initial magnitude of ΔT is larger than in the experiment under helium. The onset of the fusion was measured at a slightly higher temperature (89 °C) and the ΔT step is larger at 6 °C.

MWDTA indirect 100% D-sorbitol IH1044

Heating Rate (℃/min)	10
Final Temp (℃)	120
Percentage of active sample	100%
4 stub tuning status	Manual
Sample weight (mg)	20
Iris position (mm)	138
Iris (mm)	28 x 15
Cell	Boersma type
mixture material	N/A
Principle T/C	Reference
Tuning position (mm)	113
Comments	Argon 105% Sample flow 22% Alumina sandwich
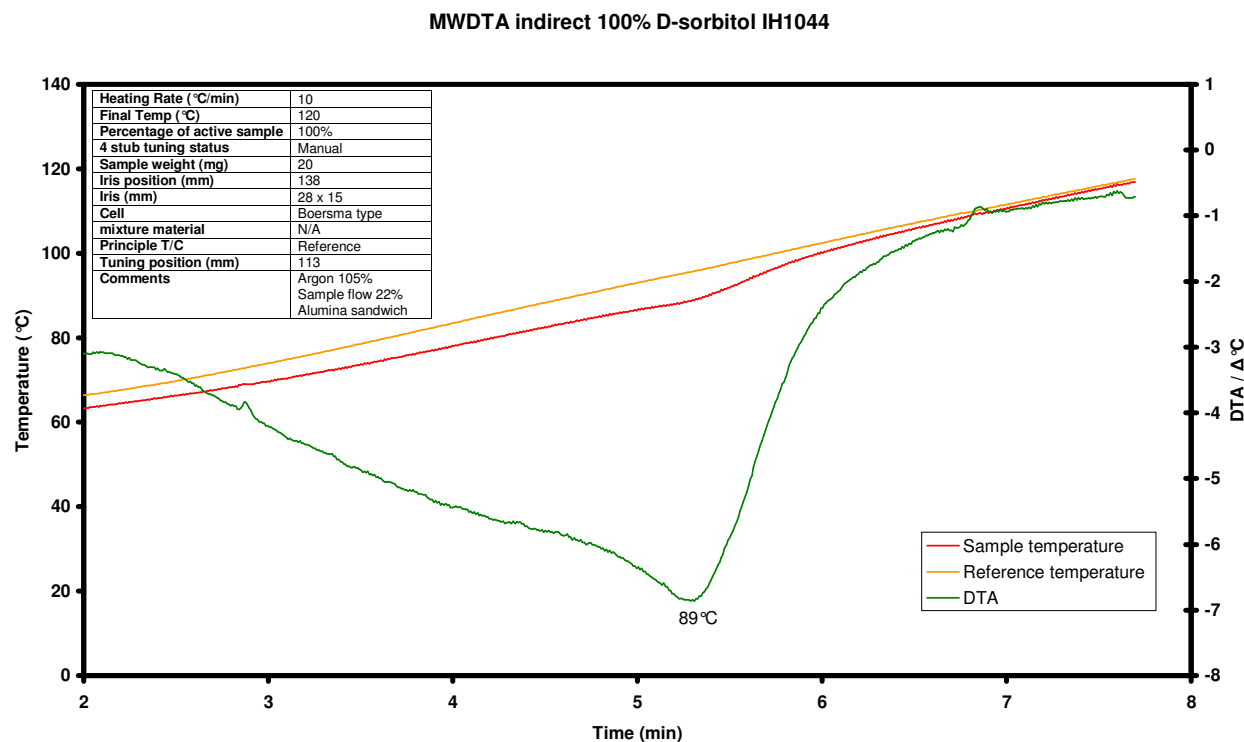
Graph 37: D-sorbitol experiment conducted in the RCHPB under argon in arrangement 2

Graph 38 shows the results of the experiment with Indium under helium. There is an overall increase in ΔT of less than 0.5 °C at 147 °C which can be attributed to the fusion although, again, it appears considerably lower than the literature value. In this experiment the ΔT profile is more comparable to that seen with a conventional DTA with a peak produced by the endothermic enthalpy of fusion. There is a slight indication of a step in ΔT after the peak which may result from a very small difference between how the solid and liquid forms couple with microwaves.

MWDTA indirect 100% indium

Heating Rate (°C/min)	10
Final Temp (°C)	170
Percentage of active sample	100%
4 stub tuning status	Manual
Sample weight (mg)	20
Iris position (mm)	138
Iris (mm)	28 x 15
Cell	Boersma type
mixture material	N/A
Principle T/C	Reference
Tuning position (mm)	113
Comments	Helium 105% Sample flow 22% Alumina sandwich
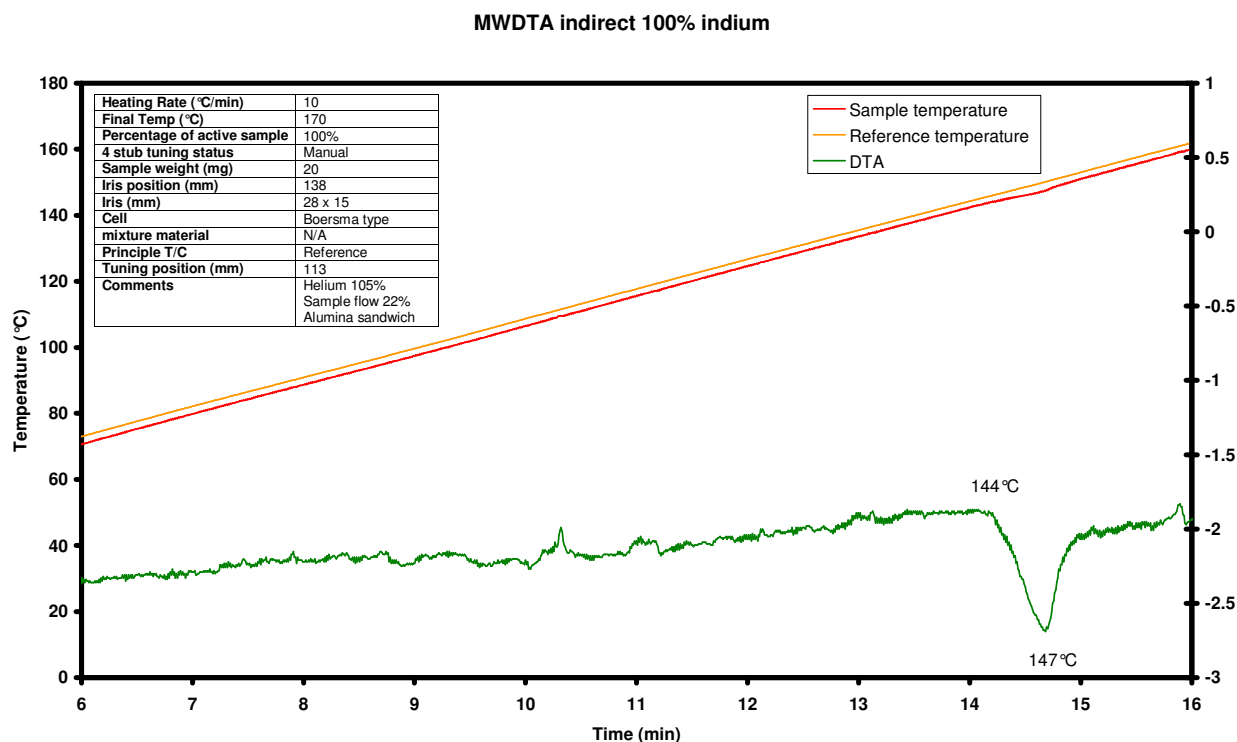
Graph 38: Indium experiment conducted in the RCHPB under helium in arrangement 2.

Graph 39 shows the comparable experiment under argon. In this case, the magnitude of the ΔT step is double that of the experiment under helium while the peak temperature of the fusion was measured 2 °C lower at 145 °C. Again, the initial magnitude of ΔT is greater under argon than helium.

MWDTA indirect indium IH1035

Heating Rate (℃/min)	10
Final Temp (℃)	170
Percentage of active sample	100%
4 stub tuning status	Manual
Sample weight (mg)	20
Iris position (mm)	138
Iris (mm)	28 x 15
Cell	Boersma type
mixture material	N/A
Principle T/C	Reference
Tuning position (mm)	113
Comments	Argon 105% Sample flow 22% Alumina sandwich
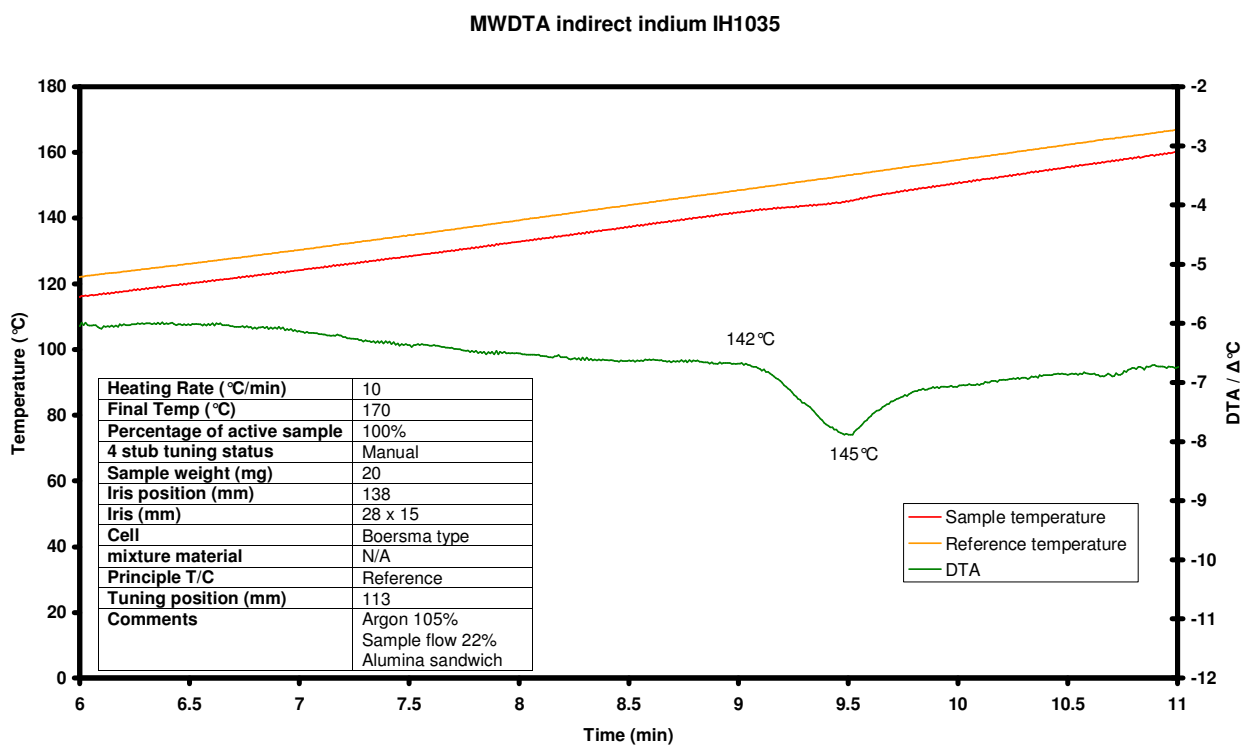
Graph 39: Indium experiment conducted in the RCHPB under argon in arrangement 2

The previous samples studied in the RCHPB method all possessed dielectric changes. To determine the extent of the lag in the recorded temperature readings a sample with no dielectric change was investigated as it removed the variable of conductive heating from the sample to the sample cell. Graph 40 shows the result of an experiment performed using a 50:50 mixture of sodium and potassium hydrogen carbonate under helium. The ΔT profile is again broadly similar to that expected from a conventional DTA with two broad endothermic peaks centred on 149 °C and 191 °C, both approximately 1 to 1.5 °C in size.

MWDTA indirect 50:50 Sodium bicarbonate: Potassium bicarbonate IH1055

Heating Rate (℃/min)	10
Final Temp (℃)	220
Percentage of active sample	100%
4 stub tuning status	Manual
Sample weight (mg)	20
Iris position (mm)	138
Iris (mm)	28 x 15
Cell	Boersma type
mixture material	N/A
Principle T/C	Reference
Tuning position (mm)	113
Comments	Helium 105% Sample flow 22% Alumina sandwich
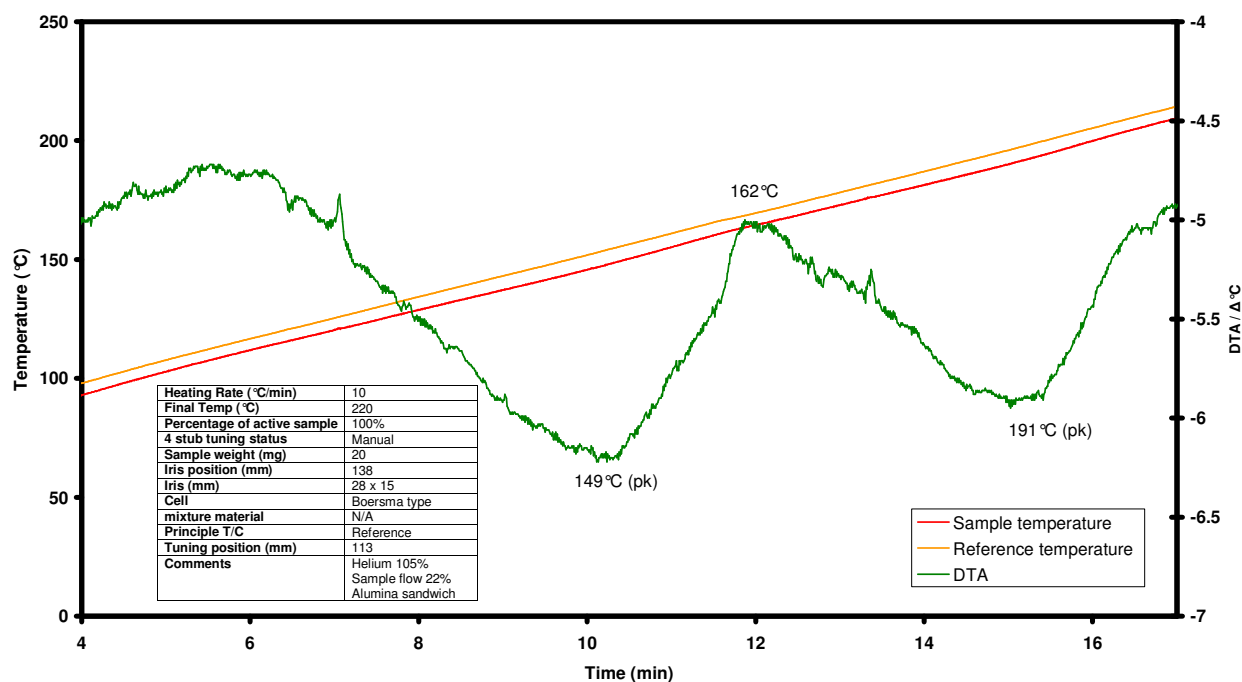
Graph 40: 50:50 mixtures (w/w) of sodium bicarbonate: potassium bicarbonate experiment conducted in the RCHPB under helium in arrangement 2

Graph 41 shows the comparable experiment under argon. The two peaks are centred on 140 °C and 189 °C both approximately 2 °C in size. Again, the peaks appear at a lower temperature but are larger in size than the helium experiment.

MWDTA indirect 100 % sodium bicarbonate:potassium bicarbonate IH1045

Heating Rate (℃/min)	10
Final Temp (℃)	220
Percentage of active sample	100%
4 stub tuning status	Manual
Sample weight (mg)	20
Iris position (mm)	138
Iris (mm)	28 x 15
Cell	Boersma type
mixture material	N/A
Principle T/C	Reference
Tuning position (mm)	113
Comments	Argon 105% Sample flow 22% Alumina sandwich
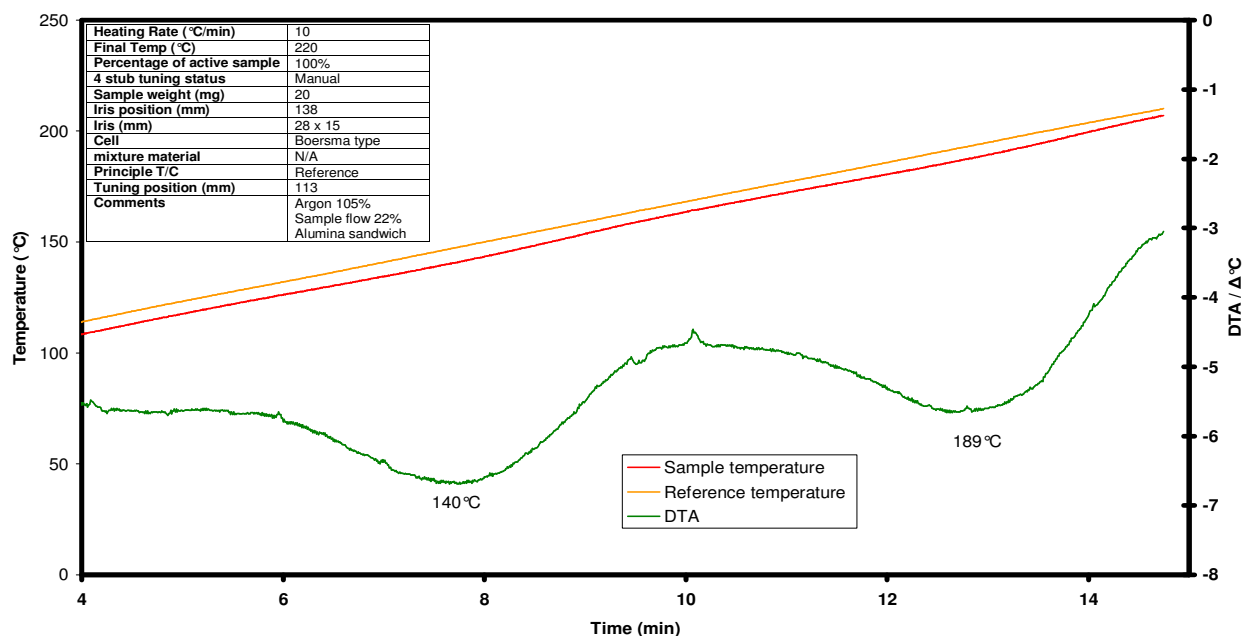
Graph 41: 50:50 mixtures (w/w) of sodium bicarbonate: potassium bicarbonate experiment conducted in the RCHPB under argon in arrangement 2

5.5.3 Optimisation of the indirect microwave method

Although the RCHPB cell proved the concept that measurements could be obtained in a non-contact environment, the errors in the transition temperatures compared to the conventional instrument temperatures were too erratic for the method to be accurate. In order to resolve this problem, arrangement 1 was investigated, where argon was only used to flood the chamber outside of the RCHPB (blanket gas only). The baseline run showed the most promising reduction in maximum differential temperature.

Silver iodide

The extrapolated onset of the AgI transition was recorded to be 1 °C lower than equivalent onset in conventional methods. The results tended to show that the instrument was behaving like DTA even though the permanent changes in differential temperature seen in microwave thermal analysis were still observed.

MWDTA indirect 100% Silver iodide IH1053

Heating Rate (°C/min)	10
Final Temp (°C)	170
Percentage of active sample	100%
4 stub tuning status	Manual
Sample weight (mg)	20
Iris position (mm)	138
Iris (mm)	28 x 15
Cell	Boersma type
mixture material	N/A
Principle T/C	Reference
Tuning position (mm)	113
Comments	Argon 105% Sample flow 0% Alumina sandwich
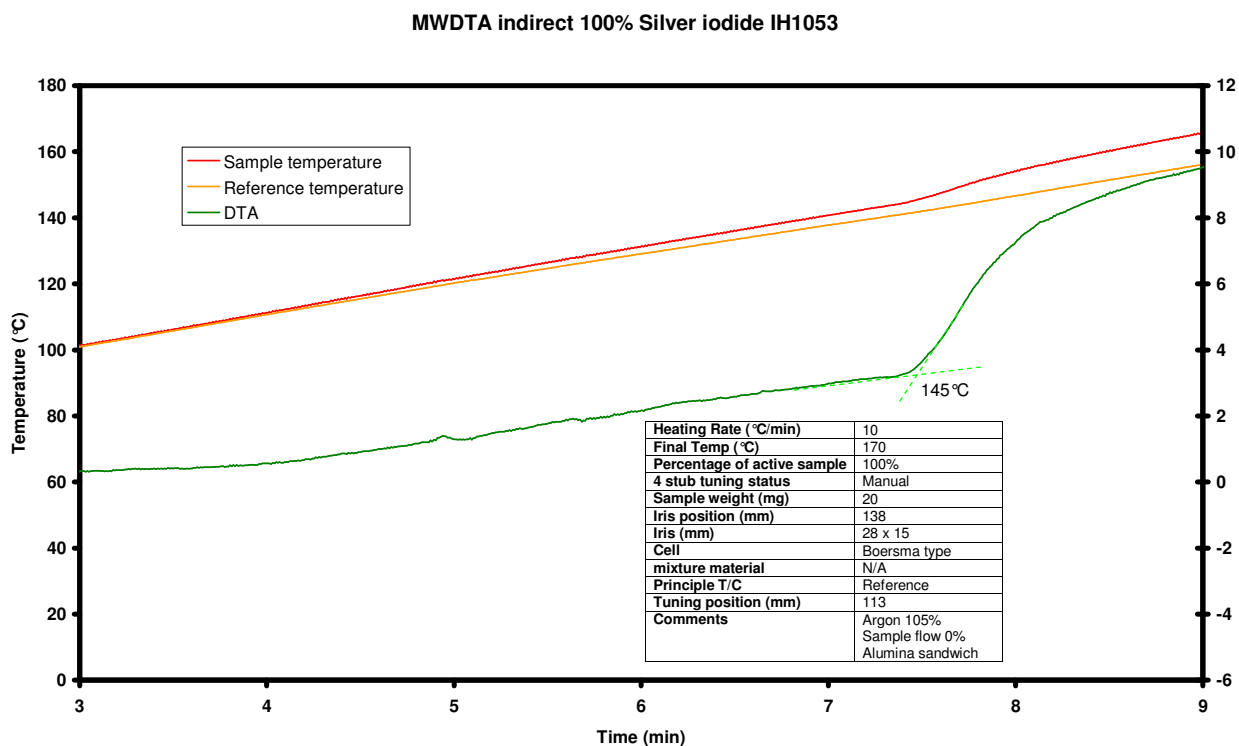
Graph 42: Silver iodide experiment conducted in the RCHPB under argon in arrangement 1.

Indium

The measurement obtained from the indium experiment showed the peak of the transition temperature to occur very close to the DSC measurement. The peak did show a shoulder as it

returned to the baseline, this shoulder occurred at the literature and DSC temperature (156 °C) slowing the return to linearity.
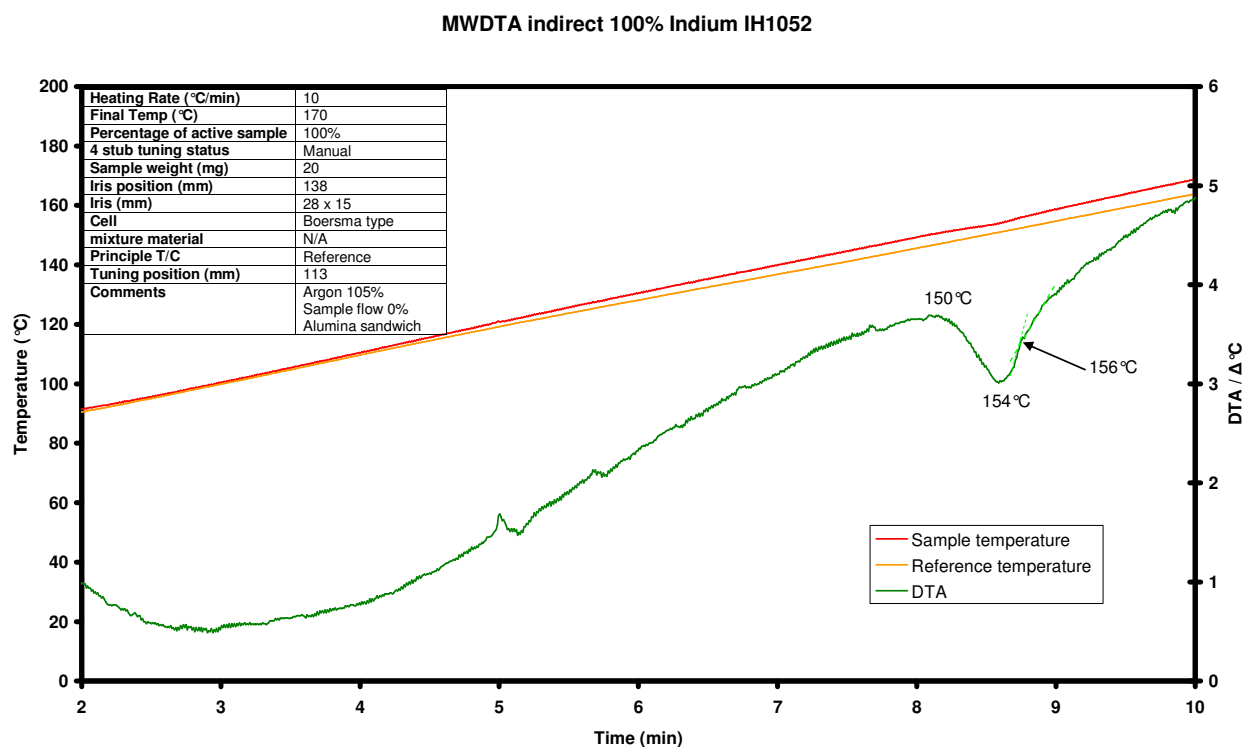
Graph 43: Indium experiment conducted in the RCHPB under argon in arrangement 1.

Bicarbonate mixture

The results (see Graph 44, page 168) showed a ~ 5 °C depression in transition temperature with this material which would not supply additional heat to the sample cell due to changes in coupling. The results showed gas arrangement 1 did bring the temperature closer to the MWDTA results and in certain cases (rubidium nitrate, and bicarbonate mixtures) to the DSC results. The discrepancy with dielectric materials is likely to be due to the rapid self induced heating rate of the sample during a dielectric change. The magnitude of this heating rate affected the amount the transition temperature lagged behind the conventional measurement.

MWDTA indirect 100% 50:50 Sodium bicarbonate:Potassium bicarbonate IH1054
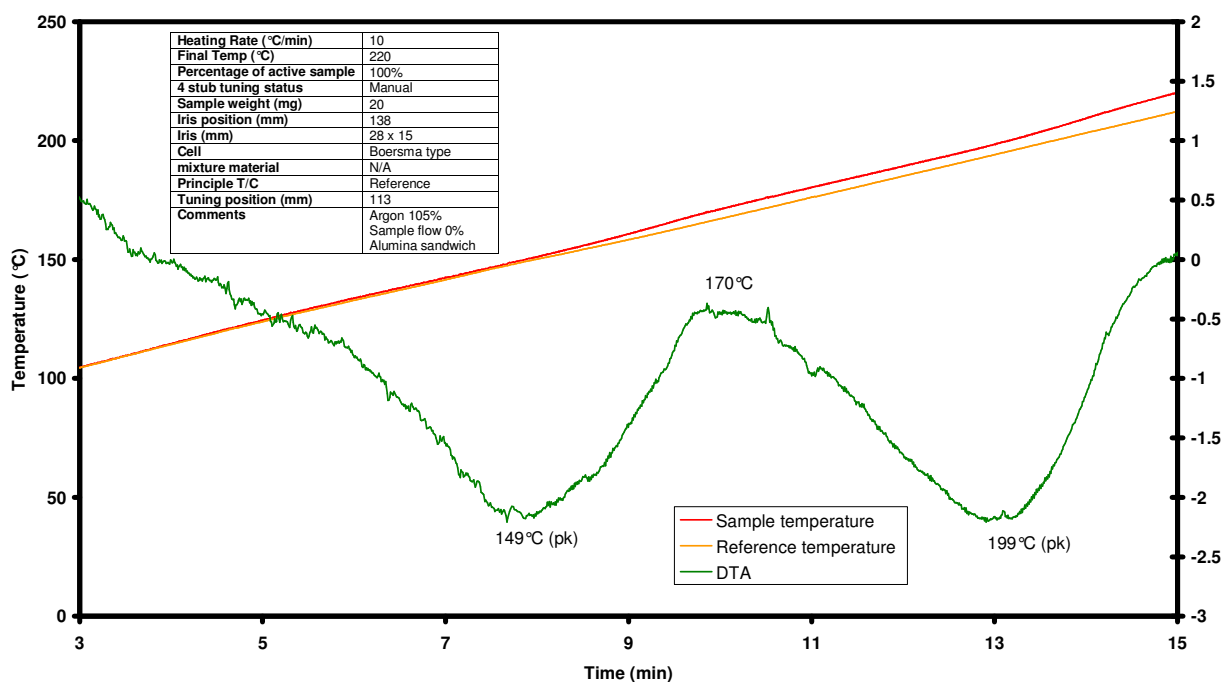
Graph 44: 50:50 mixtures (w/w) of sodium bicarbonate: potassium bicarbonate experiment conducted in the RCHPB under argon in arrangement 1.

5.5.4 Summary of the RCHPB technique

The results for all these evaluation experiments show a similar trend and are summarised in the following table (Table 12) showing the average transition temperatures of the different samples, the difference in temperature between DSC measurements and measurement made in the RCHPB, and finally the differences in temperature between the HPB and the RCHPB measurements.

Sample	DSC onset temperatures (less otherwise stated)	HPB measurements	Indirect under argon (outside only)	Indirect under argon	Indirect under helium
Materials with changes in tan δ					
Silver iodide	146	149	145	135	136
Sorbitol	89	95	89	89	87
Indium	154	144	150	142	144
Materials with no changes in tan δ					
NaHCO₃ : K₂HCO₃ (50:50 mix)	158 (pk), 206 (pk)	158, 205	149, 199	140, 189	149, 191
(pk) = peak temperature					
* = Seen in the DSC as a small signal					
Temperature differences between HPB and RCHPB techniques and DSC					
Materials with changes in tan δ					
Silver iodide	-	3	-1	-11	-10
Sorbitol	-	6	0	0	-2
Indium	-	-10	-4	-12	-10
Materials with no changes in tan δ					
NaHCO₃ : K₂HCO₃ (50:50 mix)	-	0, -1	-9, -7	-18, -17	-9, -15
Temperature differences between RCHPB and the HPB techniques					
Materials with changes in tan δ					
Silver iodide	-	-	-4	-14	-13
Sorbitol	-	-	-6	-6	-2
Indium	-	-	6	-2	0
Materials with no changes in tan δ					
NaHCO₃ : K₂HCO₃ (50:50 mix)	-	-	-9, -6	-18, -16	-9, -14

Table 12: Initial results obtained from the indirect MWDTA method.

Under helium, changes in ΔT are smaller and events appear at a lower temperature. In addition, the initial magnitude of ΔT is greater under argon than helium. These results can be explained in terms of the different thermal conductivity of the gases. With helium as a carrier gas there is better thermal contact between sample and thermocouple so processes appear closer to the literature values. The changes in ΔT are smaller because heat is more effectively transported away from the sample by the blanket gas of helium surrounding the cell. The initial magnitude of ΔT (i.e. the difference in temperature between sample and surrounding reference) is smaller for the same reason. With argon as the carrier and blanket gas the reverse is observed. Changes in ΔT are larger because the sample is more insulated but the poorer heat transfer between sample and thermocouple make the apparent temperature of events seem lower. Experiments performed under argon required slightly less microwave power for similar reasons.

One possible improvement considered was to have argon as the blanket gas and helium as the carrier gas to give the benefits of larger ΔT changes (greater sensitivity) with more accurate temperatures. However, the cost and complexity of having two simultaneous gas streams meant this idea was not pursued further.

Generally the cell was operated under a blanket of argon with no carrier gas. To increase the reliability of temperature measurement, particularly for quantitative work, two modifications were made to the cell and crucible. Firstly, the alumina bed was replaced with powdered mono-crystalline synthetic diamond which has a much higher thermal conductivity (900 – 2300 W m^{-1} K^{-1}) but is microwave transparent. In addition, the diamond bed increased the area of thermal contact between crucible and the thin thermocouple tip thus emulating the plate thermocouples of conventional DTAs. Secondly, the base of the crucible was ground to 0.5 mm thickness. Both these changes aided transfer of heat from sample to thermocouple without the loss of the benefit of having a removable crucible.

The only other cell modification was to permit evolved gas analysis.

It was thought that MWTA (in MWDTA mode) for possibly the first time had the ability to be coupled to an EGA apparatus, giving not only important information about transitions seen in the observed trace, but also making the instrument more comparable to modern advances in thermal analysis.

To couple the MWTA to MS, only minor additions had to be made. The HPB cell lends itself to the EGA work very readily as it already has a gas flow-through arrangement. The only additions that had to be made were a sampling hood and the ability to close off the sample chamber. These problems were addressed with the following designs:-
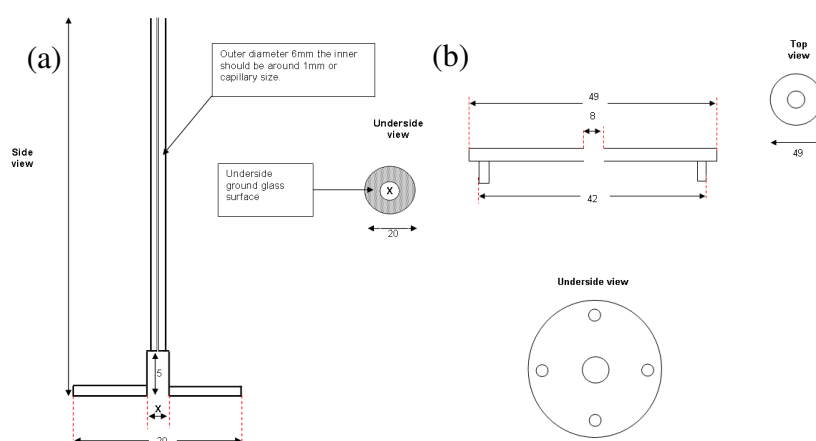
Figure 68: (a) EGA sampling Hood (b) Sample chamber lid

Figure 68 (a) shows the sampling hood which was designed so that the lower plate sat over the reference portion of the HPB cell. The long tubular upper portion of the sampling hood had a reduced internal diameter (around capillary size, <1 mm) so as not to draw too much gas into the

mass spectrometer. The hood was made so as to fit through the 8 mm gap shown in sample chamber lid Figure 68 (b).

5.6 Summary of the sample cell design

The development of the sample chamber and its cells improved the versatility of the MWTA technique. The low volume MWTA cell allowed purely dielectric changes to be monitored, although compared to many other thermal analysis techniques the sample size was very large.

The HPB cell was a novel advancement which allowed microwave thermal analysis equipment to become a comparative differential thermal instrument. For the first time it allowed the problem of differences in dielectric properties between the reference and sample to be solved and as an additional bonus allowed all types of samples to be tested without the need for diluent mixtures. This was the case even for those that were not susceptible to microwave radiation at an analytical scale.

The design of the HPB cell formed the basis for the RCHPB cell, which although it slowed the high through-put nature of MWTA, showed promising results. Three main problems faced the RCHPB:

- The gaps between the sample and the cell wall, and the internal reference wall and sample cell reduced thermal conductivity giving rise to a thermal lag.
- The construction of the sample cell out of silica had the adverse effect of insulating the thermocouple tip from the sample resulting in inaccurate transition temperatures. Ideally the base of the sample cell would be constructed from a cheap, high temperature resistant, thermally and chemically inert substance with a high thermal conductivity and low thermal expansion.
- Poor thermal contact, as point rather than plate thermocouples were used to reduce microwave leakage, although this problem was greatly reduced by using a diamond bed.

The design of the RCHPB showed promising results, and proof of concept, although it was evident that improvements needed to be made before it could be used as a standard method. These improvements are discussed in Chapter 8.

The implementation of a sample chamber was of great advantage as for the first time MWTA experiments could be performed under controlled atmospheres. The secondary effect of reducing the temperature gradient from the sample cell to the waveguide to the sample cells and the chamber was also of great advantage.

Chapter 6

Qualitative MWTA

The following chapter details the scope of MWTA using a range of samples exhibiting a number of transition types (solid to liquid and solid to solid phase changes, dehydration and decomposition processes).

The resultant response curves (temperature and applied microwave power) are used to demonstrate the potential advantages and disadvantages of MWTA as a qualitative thermal analysis technique.

6.1 Solid to liquid phase transition in stearic acid

These initial experiments were undertaken to

a) Provide familiarisation of the MWTA instrument and software, particularly the control parameters required to obtain linear heating.

b) Observe the response of the instrument when heating samples which undergo a significant change in dielectric properties (common for many materials changing from a solid to a liquid phase).

6.1.1 Stearic acid

Stearic acid $C_{18}H_{36}O_2$ is a fatty acid and has a fusion point of 71 ℃. Recently it has found applications in the phase change material (PCM) industry. PCM materials are those which have low temperature but highly endothermic phase changes. This combination of factors means that they are used to remove heat from environments such as waste disposal process or hot office environments without the need for electronic devices such as air conditioning.

6.1.2 Melting of stearic acid using constant power

Constant power is the simplest form of MWTA experiment. In the example given a 700 mg sample of stearic acid was subjected to a constant power of 45 W (15 %) until the sample temperature reached 110 °C when the applied power was reduced to 0 W and the cooling curve was monitored. The experiment used the large volume removable cell with an atmosphere of static air.

The resulting temperature and power profiles are shown in Graph 45. When the microwave power is initially applied the sample temperature rises at approximately 20 ℃/min until it reaches 71 ℃. The enthalpy of fusion holds the temperature constant for about a minute until the temperature rises again. This second temperature rise is much more rapid (approximately 40 ℃/min) as a result of the greater tan δ of stearic acid in its liquid form where the effects of dipolar polarization dominant. When the microwave power is switched off the temperature falls in the expected cooling curve. At 71 ℃ the temperature levels off again as heat is released on recrystallisation and only commences the fall again at the end of the experiment.

Constant power 100% Stearic acid IH0263

Heating Rate (°C/min)	N/A
Final Temp (°C)	110
Percentage of active sample	100%
4 stub tuning status	Manual
Sample weight (mg)	700
Iris position (mm)	138
Iris (mm)	25 x 15
Tuning position (mm)	91
Comments	15% power to 110°C then 0% power till ambient 0.5mm grounded thermocouple
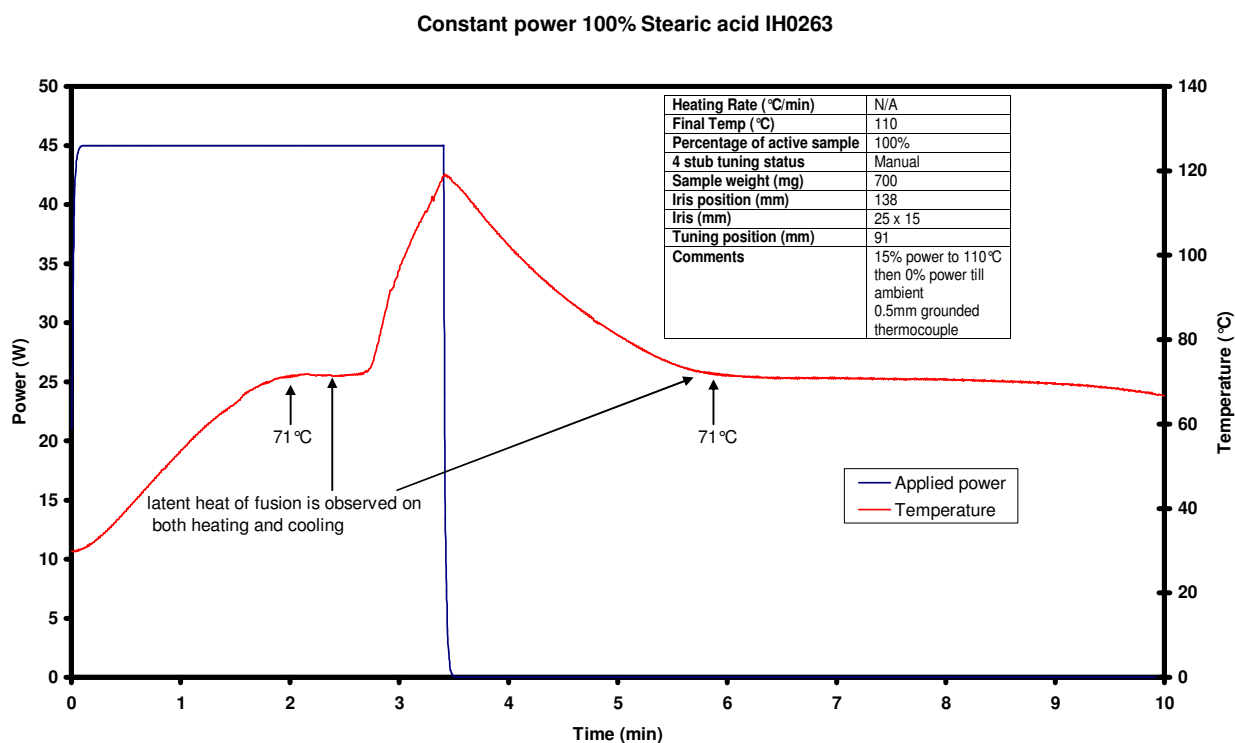
Graph 45: Constant power (15 %) MWTA experiment of stearic acid conducted in the large volume removable MWTA cell.

6.1.3 Melting of stearic acid using linear heating

Typically, thermal analysis experiments are performed using linearly increasing temperature ramps (linear heating). In the majority of cases, it is the furnace that is linearly heated with the sample temperature following. In MWTA using linear heating, an attempt is made to the make sample temperature increase linearly using a PID control algorithm (3.2.10 PID control algorithm for linear heating, page 72). This is a far more demanding situation as the sample's ability to couple with microwave energy can change extremely rapidly making temperature control difficult.

A typical run on the melting of stearic acid using MWTA and linear heating is shown in Graph 46. This experiment used the large volume removable cell with a 700 mg sample under an atmosphere of static air. The set heating rate was 2 °C/min to 90 °C (controlling on the sample temperature).

At the start of the experiment it can be seen that temperature control is good with a slow, smooth rise in microwave power sufficient to maintain the set heating rate. However, at around 63 °C the power needs to increase more to maintain the heating rate, possibly because fusion is starting to occur and more energy is required to counteract the enthalpy of the process. At 73 °C the melting is complete and the temperature rises sharply as a result of the increase in tan δ. The power falls

rapidly as the PID algorithm attempts to bring the temperature under control. Initially, the applied microwave power falls by 20 W and then needs to rise again by approximately 3 W until the sample temperature returns to its set heating rate. The difference in tan δ between the solid and liquid forms of stearic acid is clearly shown by less power being required to maintain the heating rate *after* the sample becomes molten than before.

MWTA Linear heating 100% Stearic acid IH0277

Heating Rate (°C/min)	2
Final Temp (°C)	90
Percentage of active sample	100%
4 stub tuning status	Manual
Sample weight (mg)	700
Iris position (mm)	138
Iris (mm)	25 x 15
Tuning position (mm)	91
Comments	
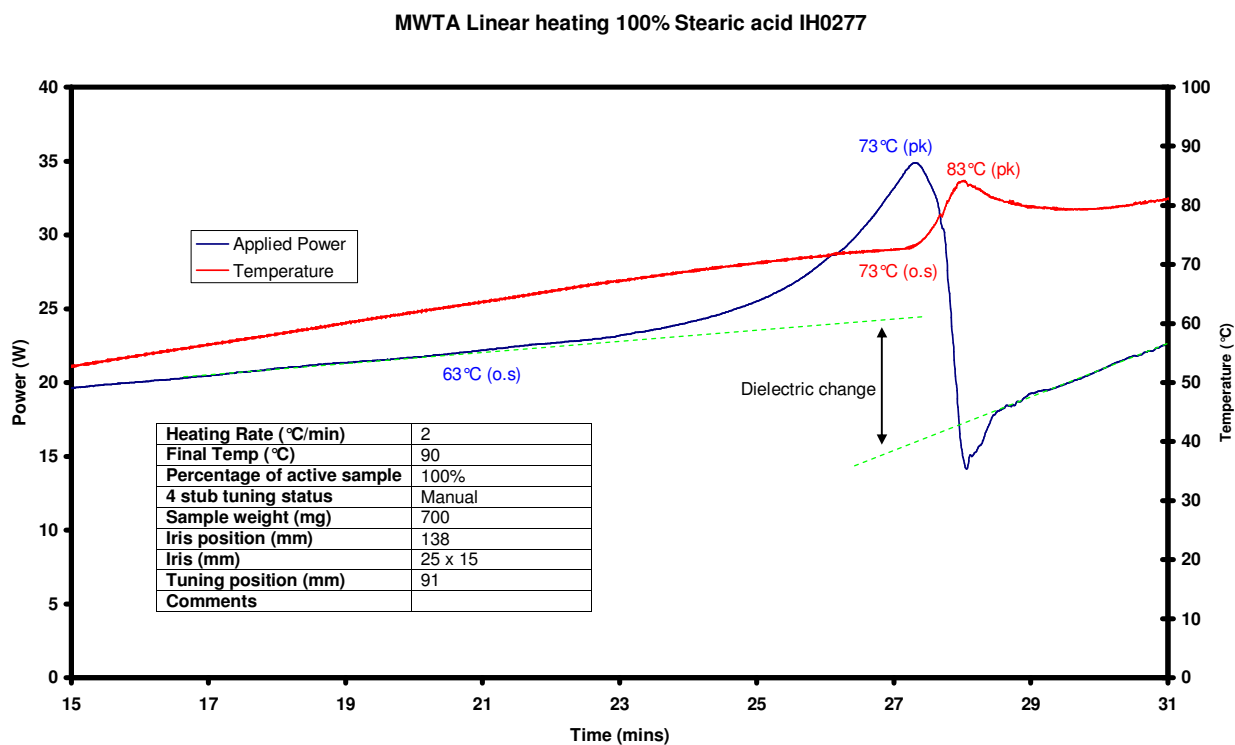
Graph 46: MWTA experiment of stearic acid conducted in the large volume removable MWTA cell.

6.2 MWTA of nitrates

Three nitrates (potassium nitrate, rubidium nitrate and caesium nitrate) were selected for analysis because all have at least one temperature induced solid-solid phase change.

6.2.1 Potassium nitrate

The solid-solid phase change in potassium nitrate has been of interest to microwave chemists as the dielectric change is easy to control. The polymorphism occurs at an onset temperature of 128 °C, peaking at 130 °C. MWTA experiments were performed in the large volume MWTA cell under argon. The sample masses were typically around 740 mg, and the heating rate was set to 10 °C/min (controlling on the sample temperature).

MWTA Potassium nitrate IH0457

Heating Rate (℃/min)	10
Final Temp (℃)	350
Percentage of active sample	100
4 stub tuning status	Auto
Sample weight (mg)	740
Iris position (mm)	138
Iris (mm)	25 x 15
System	5
Tuning position (mm)	125.5
Comments	Argon 80ml/min Gas chamber in place
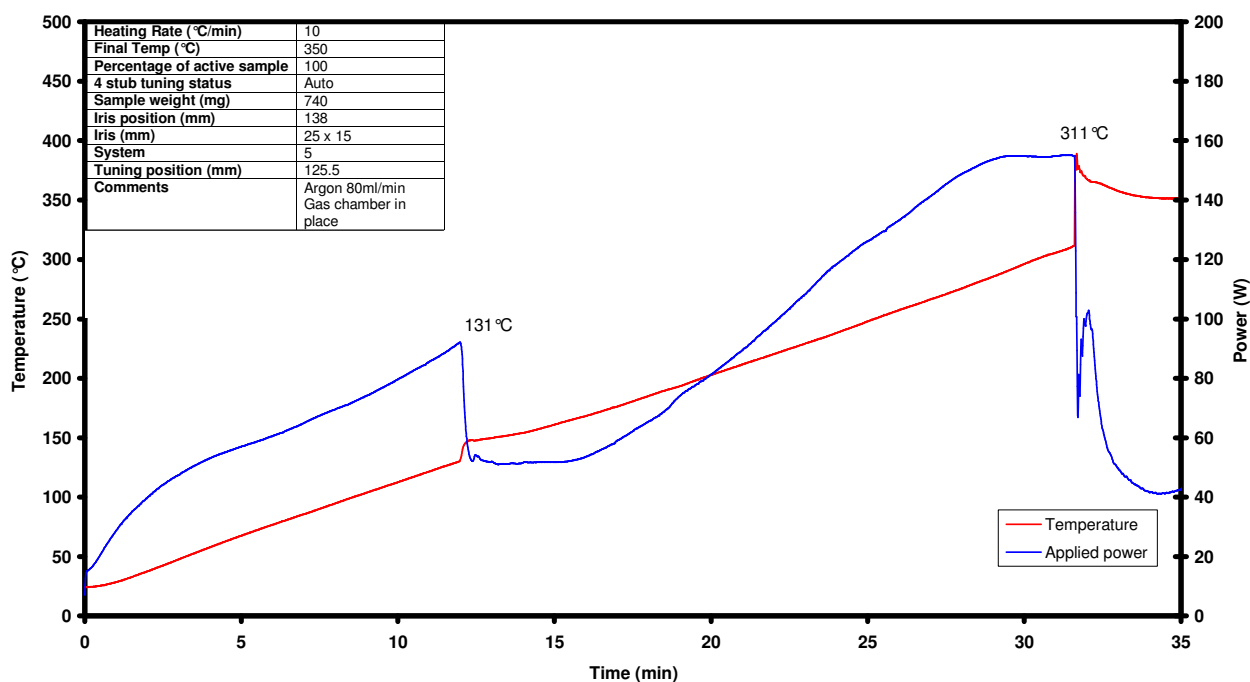
Graph 47: MWTA experiment of potassium nitrate conducted in the large volume removable MWTA cell.

The results illustrated in the graph above show the power steadily rising until the transition temperature where there appears to be a clear drop in applied power indicating that once the sample had gone through the phase change at 131 °C it coupled better with microwave radiation. The same is also seen after the melt. The rise in the power profile is possibly due to the instrument compensating for heat losses to the surroundings or the possibility that the high temperature phase has a tan δ that decreased with temperature.

The MWTA(MWDTA) method, where the HPB cell is used while still controlling on the reference temperature has the advantage of smoothing the trace, and proving additional information in the form of the differential curve. The experiments were performed under an argon blanket gas, and subjected to a linear heating programme of 20 °C/min (controlling on the sample temperature). A sample mass of around 10 mg was used in these experiments, the results of which are shown in

MWTA (MWDTA) 100% Potassium nitrate IH0720

Heating Rate (°C/min)	20
Final Temp (°C)	200
Percentage of active sample	100%
4 stub tuning status	Manual
Sample weight (mg)	10
Iris position (mm)	138
Iris (mm)	28 x 15
Cell	HPB
Reference material	SiC
Principle T/C	Sample
Tuning position (mm)	120.5
Comments	Argon 80 ml/min
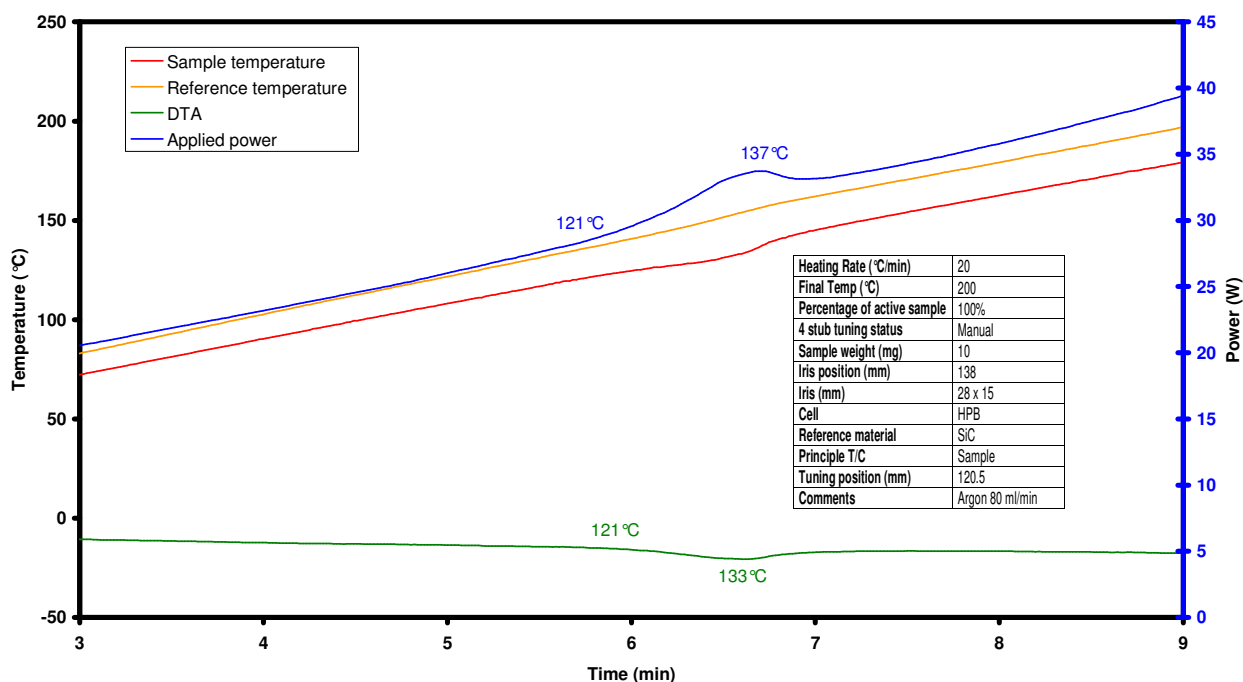
Graph 48: MWTA (MWDTA) experiment of potassium nitrate conducted in the HPB cell. (Power trace shown on the second axis)

The advantage of MWTA using the HPB cell as shown in Graph 49 is that either the power profile or the differential profile can be used to record the transition, depending on which provides more useful information.

MWTA (MWDTA) 100% Potassium nitrate IH0720

Heating Rate (°C/min)	20
Final Temp (°C)	200
Percentage of active sample	100%
4 stub tuning status	Manual
Sample weight (mg)	10
Iris position (mm)	138
Iris (mm)	28 x 15
Cell	HPB
Reference material	SiC
Principle T/C	Sample
Tuning position (mm)	120.5
Comments	Argon 80ml/min Vac off
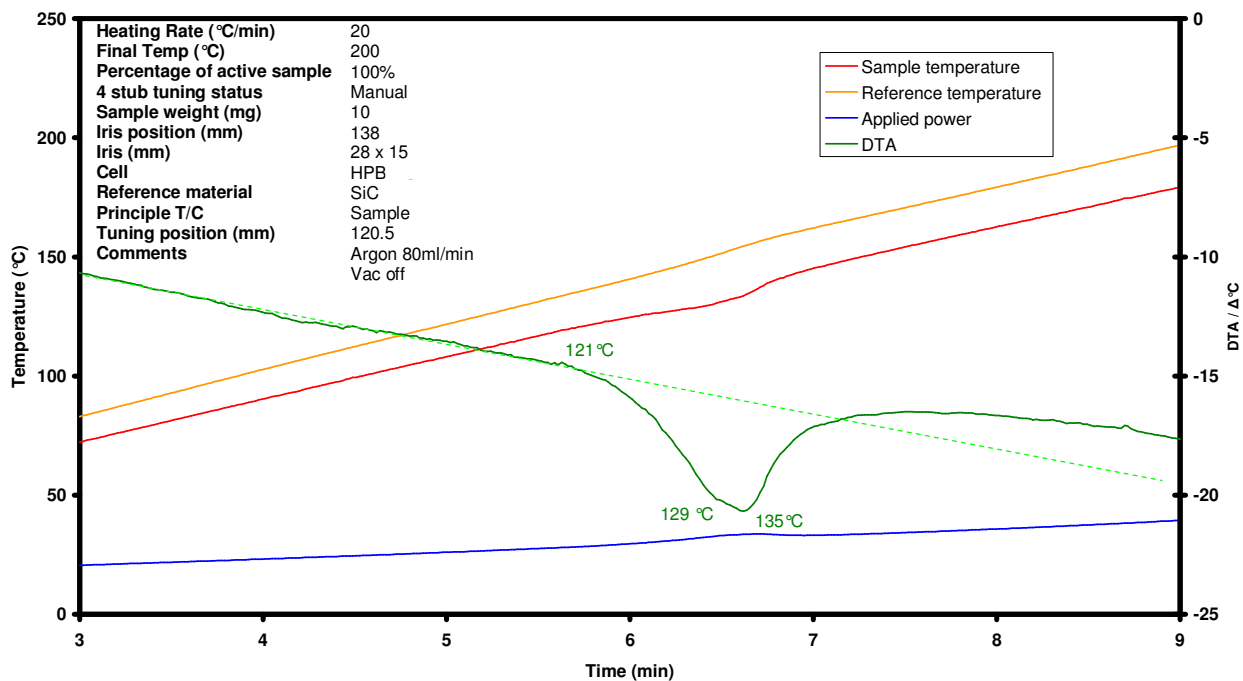
Graph 49: MWTA (MWDTA) experiment of potassium nitrate conducted in the HPB cell. (Differential trace shown on the second axis)

177

The results showed a steady gain in applied power until 121 °C where the rate increases as the sample temperature beings to drop. The transition appears to peak at 135 °C in the power trace and 133 °C in the differential. The origin of the discrepancy is due to the timing cycle in PID algorithm.

A clear transition was seen with a peak temperature close to literature and a change in baseline after the transition. This gave the indication there is a change in dielectric so the sample is heating better than before the transition, at the same relative power.

6.2.2 Caesium Nitrate

Caesium nitrate contains one solid-solid transition at 154 °C peaking at around 155 °C which can be seen clearly using conventional TA methods such as DSC. Microwave experiments (shown in Graph 50) were performed using 600 mg of sample, under argon at a heating rate of 5 °C/min (controlling on the sample temperature), in the low volume removable cell.

MWTA Cesium nitrate 99.999% IH0486

Heating Rate (°C/min)	5
Final Temp (°C)	450
Percentage of active sample	100
4 stub tuning status	Auto
Sample weight (mg)	600
Iris position (mm)	138
Iris (mm)	25 x 15
System	5
Tuning position (mm)	125.5
Comments	Argon 80ml/min Gas chamber in place
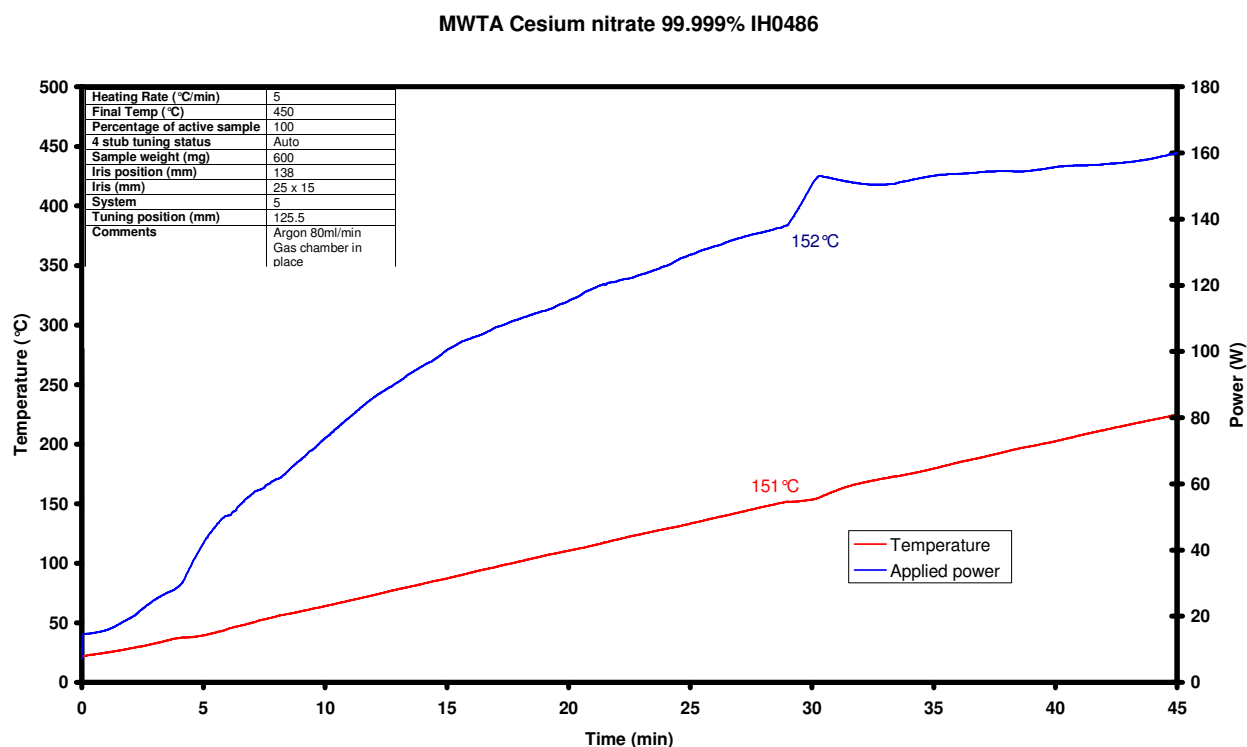
Graph 50: MWTA experiment of caesium nitrate conducted in the large volume removable MWTA cell.

The experiments showed only a small change in tan δ at 151 °C (possibly the first point of change of the sample). This caused a problem as without sufficient change in tan δ the rate of increase of applied power will not change and the transition will be lost when using this method of MWTA technique. The advantage of using MWDTA (see Chapter 7) is it allows transitions to be monitored

using its enthalpy in addition to its changes in tan δ. Meaning that if a transition has a low change in its value of tan δ but a recordable change in enthalpy (like in caesium nitrate) a transition can still be recorded even though it would have been missed using purely the MWTA technique. This method also gives the added data that there is only a very small dielectric change during the transition.

6.2.3 Rubidium nitrate

Rubidium nitrate undergoes three solid-solid phase transitions (trigonal-cubic, cubic- rhombohedral, rhombohedral-cubic) [40, 41] occurring at an onset temperature around 161 °C, 221°C, and 283 °C respectively. At 305 °C the sample undergoes fusion.

These transitions are all very different in terms of their changes in tan δ, which results in them being very hard to control during a MWTA run, although some promising results were obtained. Another factor also complicated the results, which can be explained by referring to the equation for the total loss factor and tan δ (see Equation 7 and Equation 8, page 39 and 40 respectively). The equations show that the value of effective loss factor (ε''_{eff}) and therefore tan δ is also dependant on electrical conductivity of the sample as well as the loss factor (ε''). As a result, the extent to which the sample heats and therefore the amount of power required to meet the set-point will be directly affected by the change in electrical conductance.

Several literature sources mentioned changes in electrical conductance [40-41] in rubidium nitrate crystals as it is heated. This would produce an additional signal on a MWTA run as it would directly affect the applied power profile.

The publication by Brown *et al*. [41] details that on measuring the conductance of rubidium nitrate as function of temperature several changes occurred.

- IV-III transition took place at 164 ºC conductance increases by a factor of 100.
- III-IV transition took place at 161 ºC with a corresponding decrease in conductance.
- III-II transition took place at 230 ºC where conductance decreases by a factor of 3.
- On cooling transformation took place at 218 ºC and conductance increased by a factor of 30.

Other sources such as Chary *et al*. [40] mention:

- A zone between 145 °C and 178 °C during which time the conductivity increases rapidly.

- At 222 °C there is a steep fall in conductivity which corresponds to the III-II transition.

- IV-III and II-I transitions are associated with an increase in conductivity

- III-II transition is associated with a decrease.

- The fall in conduction can be attributed to the inhibition of the mobility of the defects in the crystal.

Experiments consisted of heating the sample at a rate of 5 °C/min (controlling on the sample temperature) under argon in the large volume removable cell. The sample mass was typically around 560 mg.

MWTA Rubidium nitrate IH0415
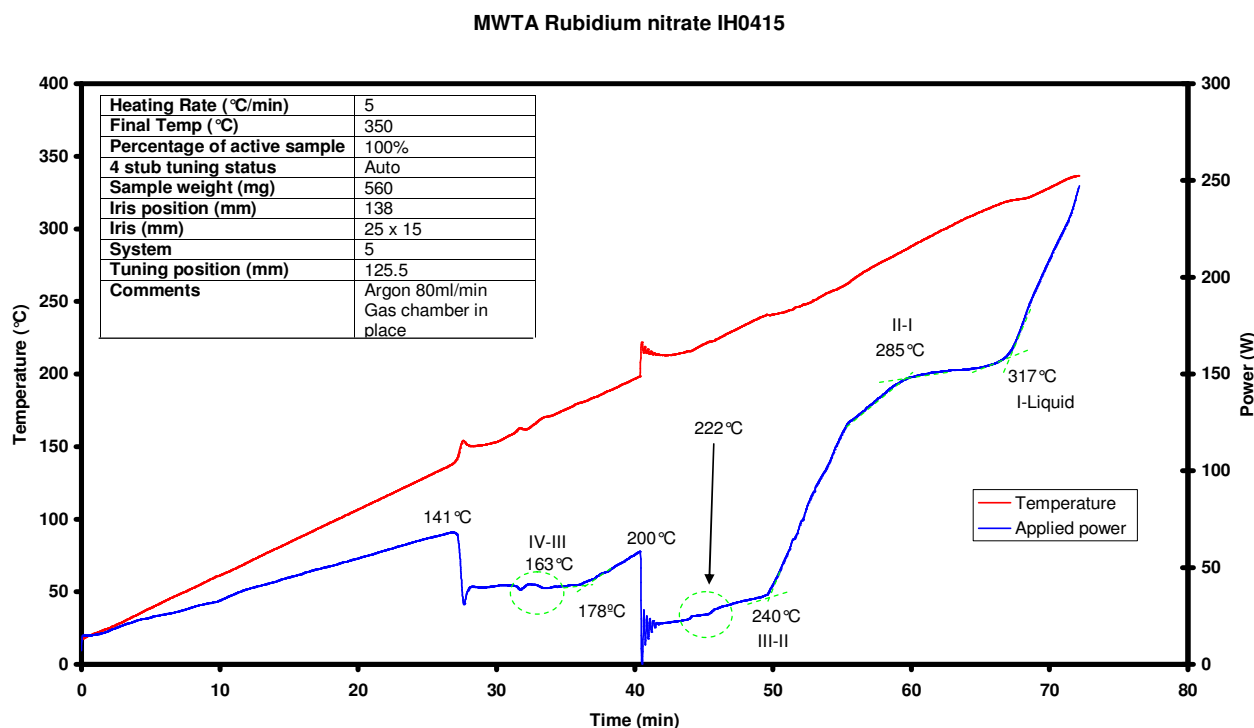
Graph 51: MWTA experiment of rubidium nitrate conducted in the large volume removable MWTA cell.

The results shown in Graph 51 indicated that the III-II, II-I and I-Liquid changes can be clearly seen using this technique. The IV-III is not clearly seen in the power trace indicating little dielectric change. The sharp rise in power at the III-II transition indicates the loss of the samples ability to couple in this phase. The II-I shows an increase in the ability to couple. Strangely the I-Liquid transition shows a decrease in coupling ability the opposite to the expected result. This could be attributed to other effects such as sample loss in the molten state, changes in volume and/or heat capacity or thermal conductivity. Regardless of this, the transition can still clearly be seen. The additional responses seen in the trace could be explained by conductivity changes.

If the unexplained responses in the trace are not artefacts then the trends seen in conductivity experiment would correspond to the undesignated transitions. The first unexplained result occurs at 141 °C and indicates a large drop in applied power. Literature talks of an increase in conductivity in this temperature region. There appears to be a large change in the coupling at 200 °C which is not explained by either morphology or conductance unless it is related to the earlier conductance change. At the III-II transition there is an increase in power possibly indicating a fall in conductance as Brown *et al.* and Chary *et al.* indicate. The change in gradient of the power profile before the II-I transition could indicate a small increase in conductivity.

The relationship of microwave heating and conductivity is interesting but it is not believed to be a reliable method to make conclusions on a systems properties, as many factors will dramatically affect the results such as sample packing, impurities, electrical contact with the thermocouple, thermocouple interaction etc.

6.2.4 Magnesium nitrate hexahydrate

Magnesium nitrate hexahydrate is one of many phase change materials (PCM) which have become of greater interest over the last 30 years as a possible heat storage device. The anhydrous form like many of its group I nitrate counterparts is a polymorphic material. When in the hydrated form it undergoes a highly endothermic dissolution (making it of interest in the field of PCMs). The phase change has an onset temperature around 73 °C, which quickly runs into the dissolution which peaks around 92 °C.

Experiments were performed in the large volume removable cell under argon and the results are shown in Graph 52. The slower heating rate of 5 °C/min (controlling on the sample temperature) was set in order to retain resolution of the two closely occurring transitions. Typical sample sizes were around 680 mg.

MWTA 100% Magnesium nitrate hexahydrate IH0589
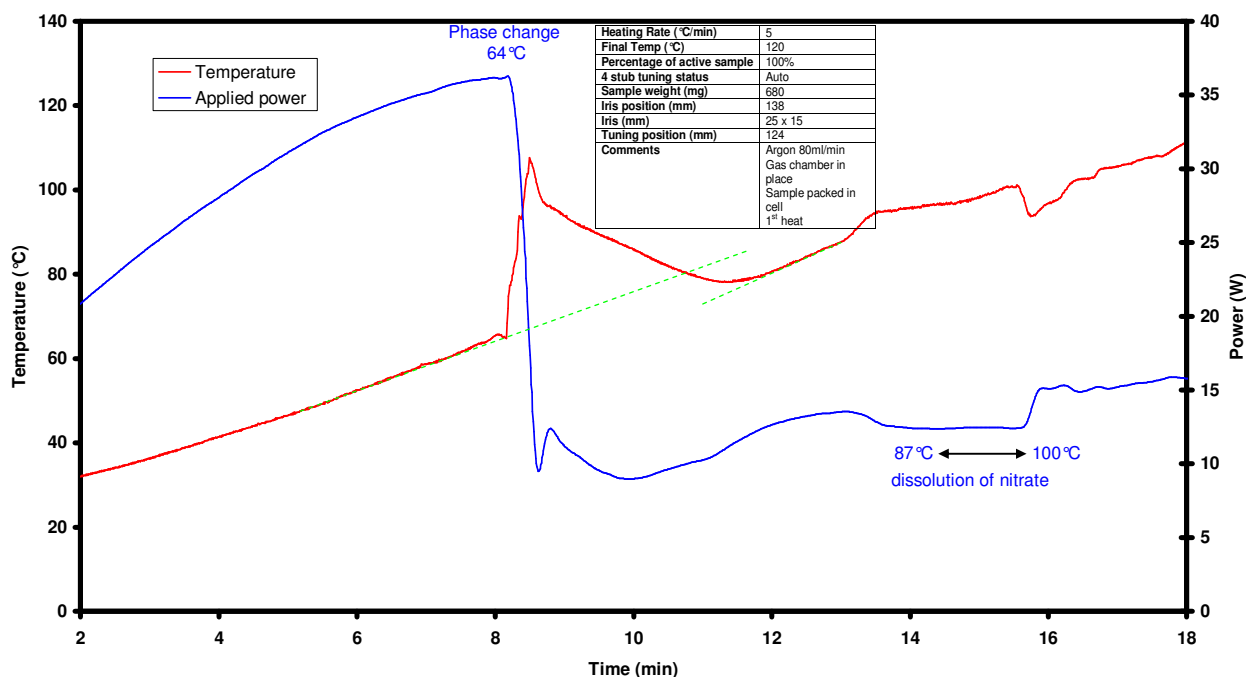
Graph 52: MWTA experiment of magnesium nitrate hexahydrate conducted in the large volume removable MWTA cell.

MWTA shows the solid-solid phase change to have a large change in the samples dielectric properties at 67 °C, indicated by the large drop in power and lower power required after the transition. The transition which can be seen at 87 °C occurs at the temperature of the dissolution of the nitrate in its own water of crystallization. The increase in coupling ability at the start of transition requires less power as the sample becomes more fluid. The end of dissolution is shown by the increase in power at 100 °C most likely due the evaporation of the water.

Unfortunately the resolution of the experiment was greatly reduced due to the large change in tan δ at the phase change. The change caused a very large overshoot of the set point that resulted in the sample temperature exceeding the transition temperature of the later events. At the time, these problems in resolution were due to the large volume, removable cell requiring a large sample mass for good thermal contact. This large volume meant the changes were too fast for the PID settings to control, a problem which was resolved by the use of the HPB cell.

6.2.5 Sodium nitrate

Sodium nitrate is a group I nitrate and following the trend, undergoes a polymorph at an extrapolated onset temperature of around 269 °C (see Graph 116) closely followed by an isotropic melt at around 303 °C. The polymorph is shown as weak transition in DSC methods. The

experiments were performed in the HPB cell under a blanket gas of argon the results are shown in Graph 53. The heating rate was set to 10 °C/min (controlling on the sample temperature) and a 20 mg sample was used. In this case both the large volume and reduced MWTA cells could not be used as the final transition became uncontrollable for using large sample masses.

MWTA (MWDTA) 100% Sodium nitrate IH0942

Heating Rate (°C/min)	10
Final Temp (°C)	350
Percentage of active sample	100%
4 stub tuning status	Manual
Sample weight (mg)	20
Iris position (mm)	138
Iris (mm)	28 x 15
Cell	HPB
mixture material	N/A
Principle T/C	Sample
Tuning position (mm)	120.5
Comments	Argon 105% Sample flow 0% Alumina sandwich
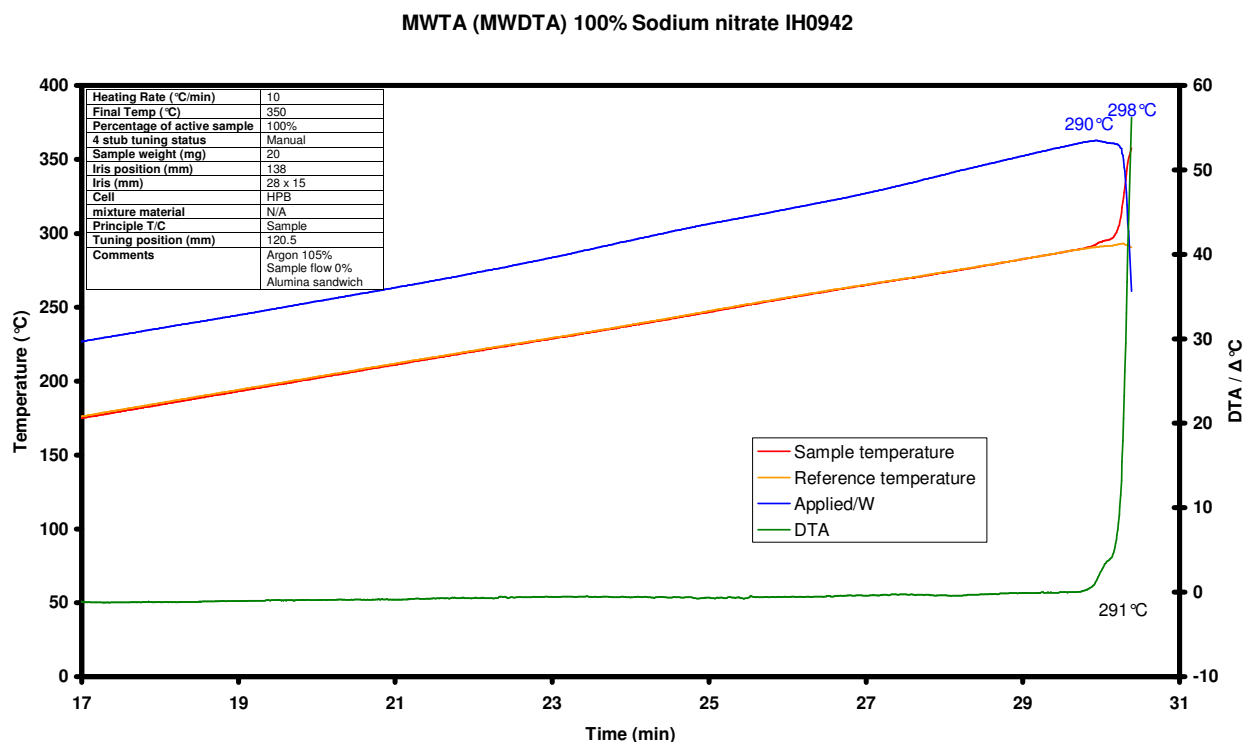
Graph 53: MWTA experiment of sodium nitrate conducted in the HPB cell.

Using MWTA methods the phase transition (usually seen at 269 °C) is not evident suggesting it has little or no dielectric change. At 290 °C the sample temperature rapidly deviates from the reference temperature, showing a swift change in the material's ability to couple, attributed to the additional heating via dipolar polarization when the sample is molten. The magnitude of the T_m response is so great when using 20 mg of sample that the instrument is unable to bring the sample temperature back under control before the experimentally set upper temperature limit is reached, indicating the level of sensitivity the technique has towards certain melting transitions.

6.3 MWTA of organic materials

6.3.1 Benzil

Benzil is a diketone with the chemical formula $(C_6H_5CO)_2$ it is often used as an organic synthesis intermediate and a photo initiator in free radical polymer curing, and is a thermal analysis temperature standard. The fusion of benzil at an onset temperature of 92 °C has been of interest in the development of microwave heating analysis techniques [16, 42] due to a large change in tan δ

on melting. The experiments were performed in the HPB cell to reduce the sample size under a blanket gas of argon. The heating rate was set to 10 °C/min (controlling on the sample temperature) and a 20 mg sample was used.

MWTA (MWDTA) 100% Benzil IH0929
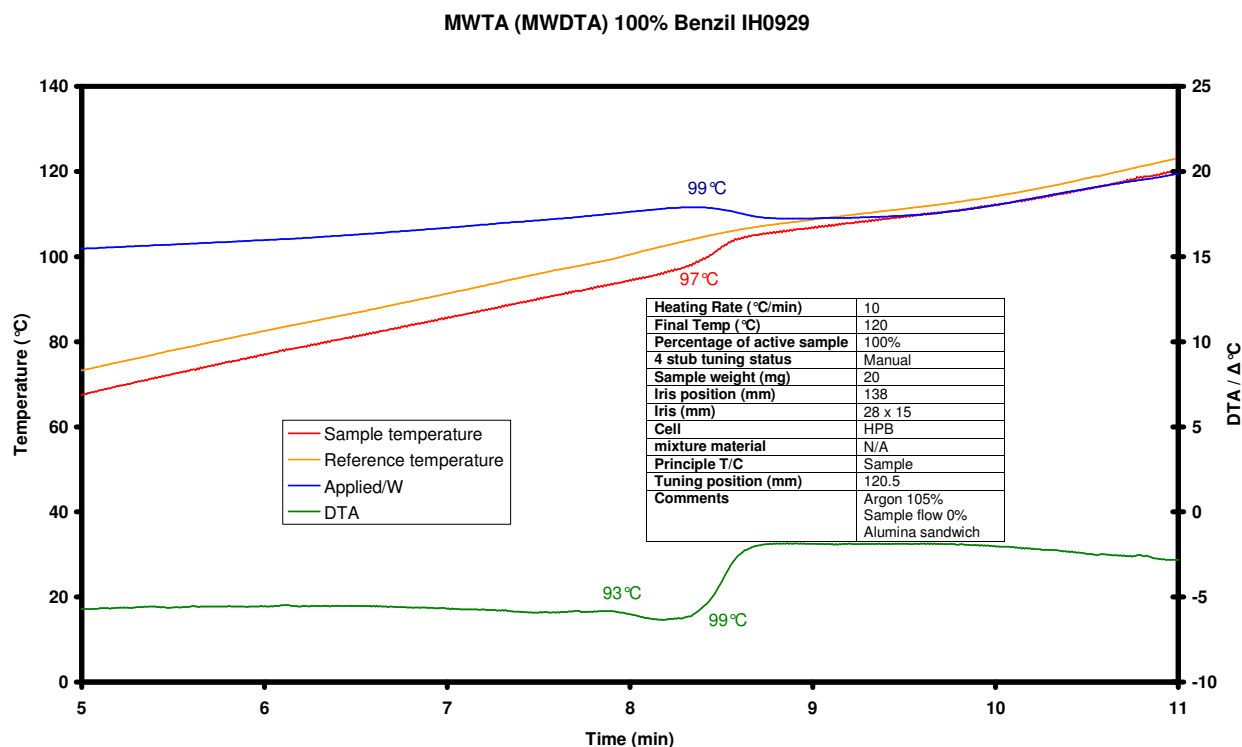
Graph 54: MWTA(MWDTA) experiment of benzil conducted in the HPB cell.

Both the sample temperature and reference temperature rose smoothly till the transition temperature, as did the applied power profile. The result showed a decrease in the required applied power, although its extrapolated onset occurred at the step of the differential trace, and several degrees later than the expected transition temperature. The reason is due to the timing cycle in the PID controller not being able to respond fast enough. Of greater importance is the DTA trace (shown in green). With the added sensitivity that differential techniques provide, the small drop in sample temperature (at 93 °C) prior to the transition, where the endothermic nature of the transition is stronger than the increased coupling of the molten state is more evident, information which was missed when using the large or reduced volume removable cells. This extrapolated onset temperature is in good agreement with DSC measurements. The point at which dipolar polarisation becomes dominant can also be clearly seen in the differential trace as the step occurring at 99 °C (close to the peak temperature of DSC measurements).

The experiment showed that in the molten state the sample coupled better to microwaves.

6.3.2 Sorbitol

Sorbitol is a substitute for sugar often used in cough medicines and food stuffs for healthy eating products. It has the chemical formula $C_6H_{14}O_6$ and is known as a sugar alcohol due to the hydroxyl groups at either end of the molecule. The material has a broad extrapolated onset to the large endothermic melting point occurring at 89 °C which peaks near to 99 °C. Experiments were performed in the HPB cell with the sample thermocouple used to control the PID under argon. The heating rate was set to 10 °C/min and sample sizes were kept to 20 mg.

MWTA (MWDTA) 100% D-Sorbitol IH0777

Heating Rate (°C/min)	10
Final Temp (°C)	150
Percentage of active sample	100%
4 stub tuning status	Manual
Sample weight (mg)	20
Iris position (mm)	138
Iris (mm)	28 x 15
Cell	HPB
Reference material	SiC
Principle T/C	Sample
Tuning position (mm)	120.5
Comments	Argon 105 % Sample flow 0 % Alumina sandwich
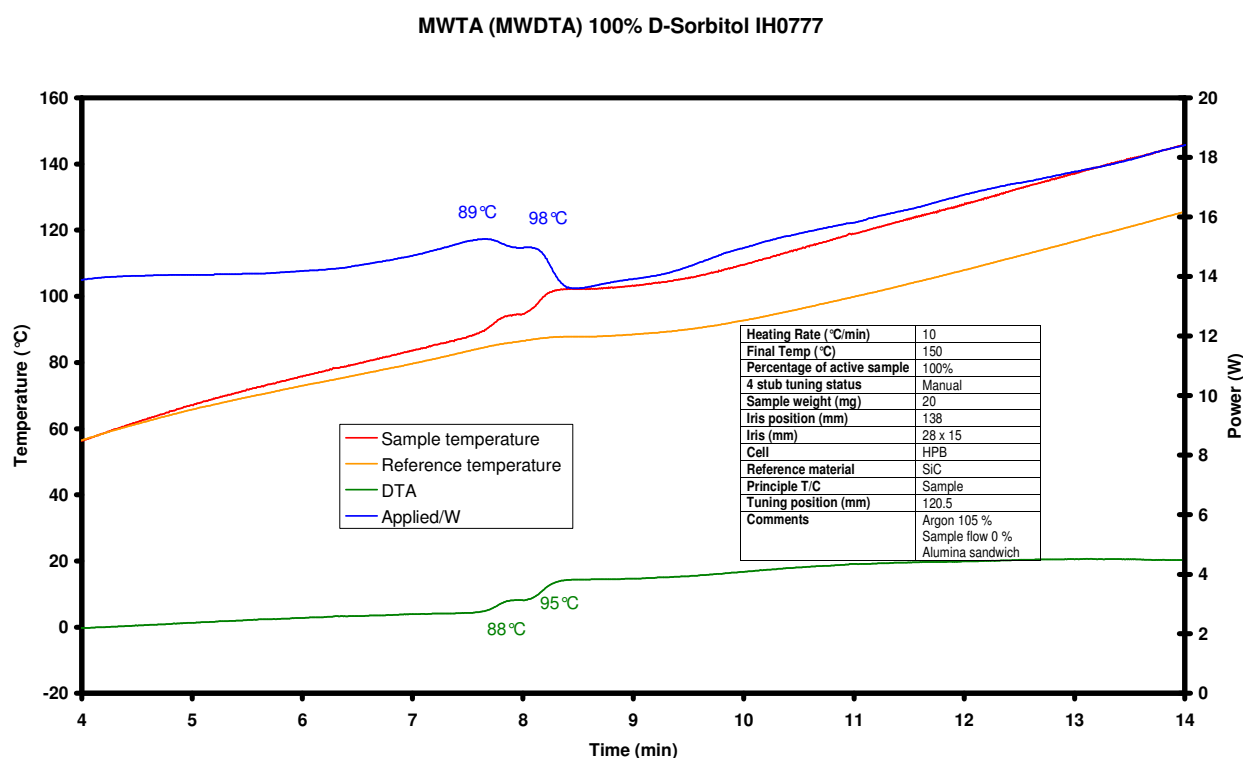
Graph 55: MWTA(MWDTA) experiment of D-sorbitol conducted in the HPB cell.

The trace showed a relatively constant applied power level before the transition, with the sample coupling well, shown by the low required applied power and the elevated sample temperature (red line) compared to the reference temperature. Once the transition temperature (89 °C) was reached the molten sample coupled better to microwaves as expected, (shown by the increased positive value of the differential signal) resulting in a drop in the applied power. The differential trace (green line) shows two rises in temperature. This is not believed to be due to two separate transitions or instrumental artefact, but may result from the endothermic nature of the fusion opposing the temperature rise from the increased coupling. At 95 °C (the peak temperature on an equivalent heating performed on a DSC, see Graph 135, page 278) the two are in equilibrium resulting in a plateau in the temperature and power profile. The second fall in power indicates the completion of enthalpy effect from the fusion, and the domination of the dielectric effect.

6.3.3 Acetaminophen

Acetaminophen (more commonly known as paracetamol) is an analgesic and a common replacement for aspirin in pharmaceutical formulations. It processes the chemical formula $C_8H_9NO_2$. The extrapolated onset temperature of the fusion of acetaminophen occurs at 168 °C, peaking at 171 °C. As in previous MWTA (MWDTA) testing, experiments were performed in the HPB cell with the sample thermocouple used to control the heating rate under argon. The heating rate was set to 10 °C/min and sample sizes were kept to 20 mg.

MWTA (MWDTA) 100% Acetaminophen IH0946

Heating Rate (°C/min)	10
Final Temp (°C)	210
Percentage of active sample	100%
4 stub tuning status	Manual
Sample weight (mg)	20
Iris position (mm)	138
Iris (mm)	28 x 15
Cell	HPB
mixture material	N/A
Principle T/C	Sample
Tuning position (mm)	120.5
Comments	Argon 105%
	Sample flow 0%
	Alumina sandwich

Legend: Sample temperature; Reference temperature; Applied/W; DTA

Graph 56: MWTA(MWDTA) experiment of acetaminophen conducted in the HPB cell.

The acetaminophen did not couple to microwaves strongly prior to the transition temperature resulting in a negatively sloping differential trace (green line). As with sorbitol the transition appeared to be separated into two events relating to the enthalpy change masking the dielectric change, then being overcome at the point of maximum change. The transition recorded on the power profile (blue line) was in good agreement with the expected results. The differential trace on the other hand appears to show two transitions earlier than the T_m (152 °C and 157 °C) that do not appear in the power trace or DSC traces. The difference between the power profile and the differential profile is due to the lag in the PID response. Prior to the fusion the sample temperature lags behind the reference (SiC) but as the sample couples better after the transition the two temperatures converge. This effect would only be possible if there was a change in tan δ for the sample.

6.3.4 Aspirin

Aspirin or acetylsalicylic acid is often used as an anti-inflammatory and analgesic drug. It has a formula $C_9H_8O_4$ and is a member of the salicylic drug family. The fusion of aspirin occurs at an extrapolated onset temperature of 131 °C, peaking at 140 °C. Experiments were performed in the HPB cell with the sample thermocouple used to control the PID under argon. The heating rate was set to 10 °C/min and sample sizes were kept to 20 mg.

MWTA (MWDTA) 100% Asprin IH0934

Heating Rate (°C/min)	10
Final Temp (°C)	170
Percentage of active sample	100%
4 stub tuning status	Manual
Sample weight (mg)	20
Iris position (mm)	138
Iris (mm)	28 x 15
Cell	HPB
mixture material	N/A
Principle T/C	Sample
Tuning position (mm)	120.5
Comments	Argon 105% Sample flow 0% Alumina sandwich
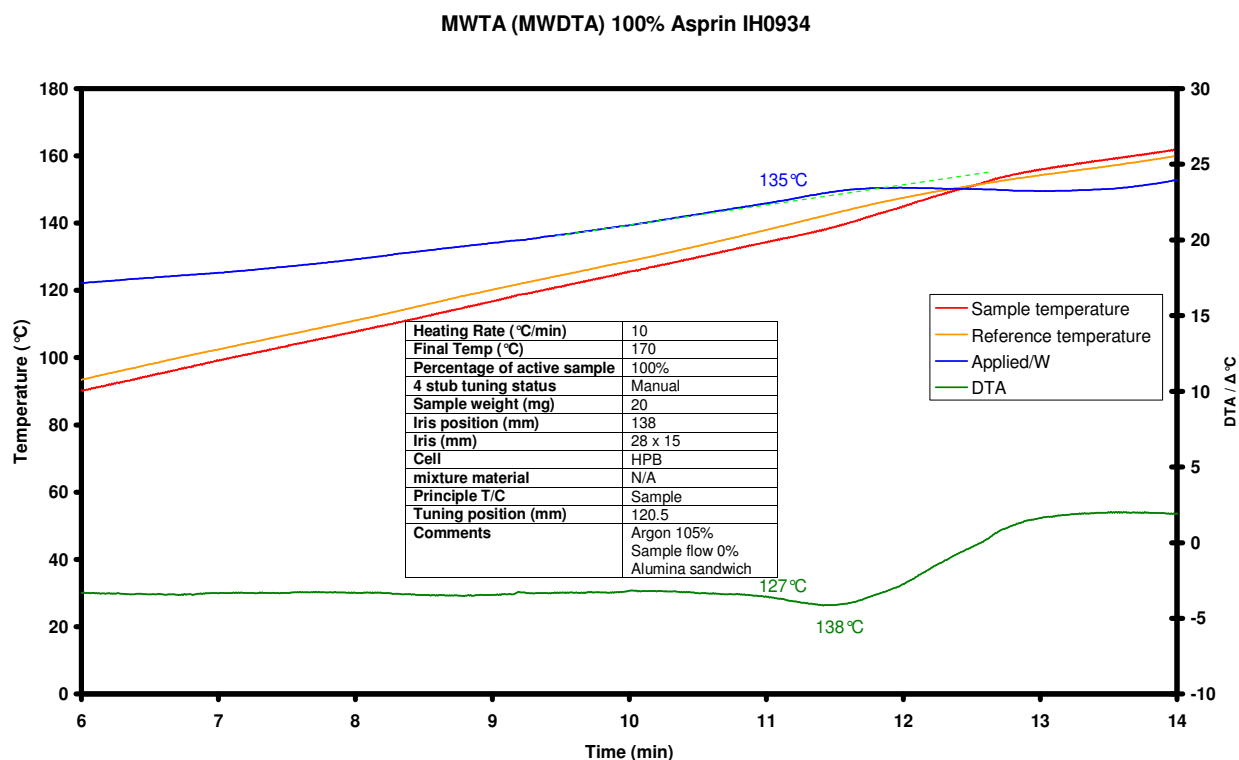
Graph 57: MWTA(MWDTA) experiment of aspirin conducted in the HPB cell.

The experiment shows the sample to heat better than a reference material after the T_m, a phenomenon not seen in conductive heating where heat is supplied to sample, from the furnace which is always hotter than the sample. It is also worth noting the sustained elevated temperature. Even with a strong endothermic event the sample temperature usually returns to near the reference over time under conventional heating, making this change in the hotter body another way of determining dielectric changes.

6.3.5 Ascorbic acid

Ascorbic acid or vitamin C is an antioxidant organic acid with the formula $C_6H_8O_6$. Experiments were performed in the HPB cell using the sample thermocouple to control the linear heating conditions under argon. The heating rate was set to 10 °C/min and sample sizes were kept to 20 mg.

MWTA (MWDTA) 100% Ascorbic acid IH0939

Heating Rate (℃/min)	10
Final Temp (℃)	250
Percentage of active sample	100%
4 stub tuning status	Manual
Sample weight (mg)	20
Iris position (mm)	138
Iris (mm)	28 x 15
Cell	HPB
mixture material	N/A
Principle T/C	Sample
Tuning position (mm)	120.5
Comments	Argon 105% Sample flow 0% Diamond bed
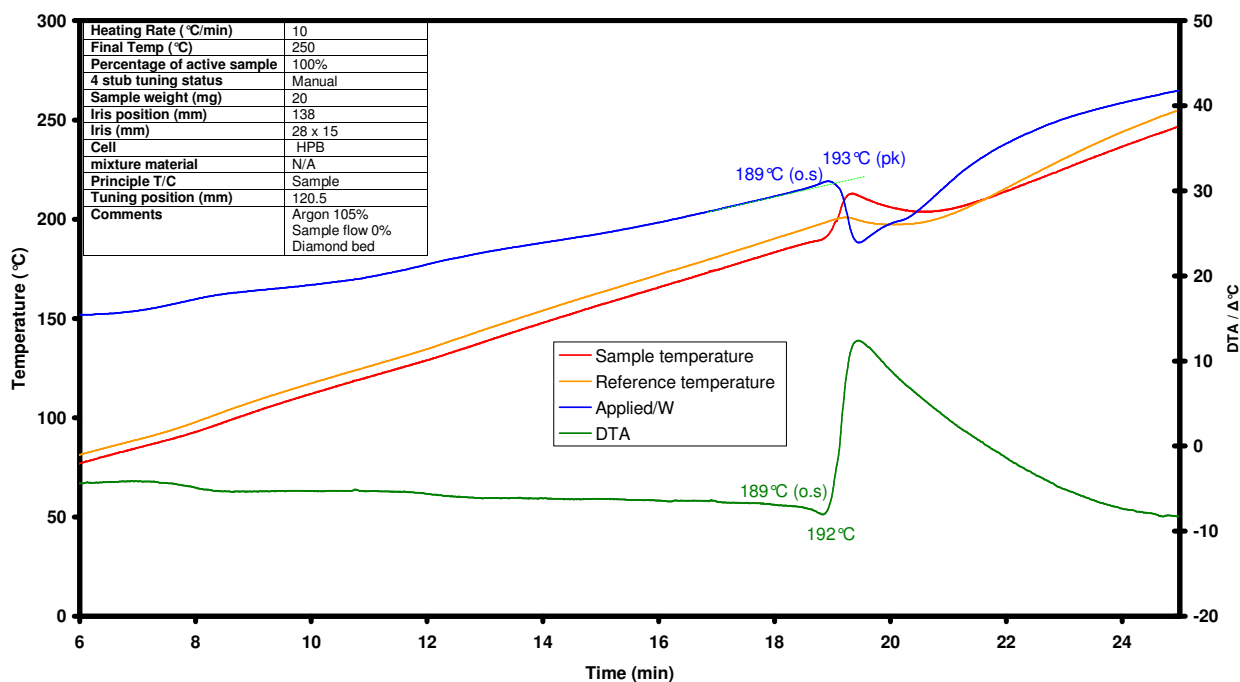
Graph 58: MWTA(MWDTA) experiment of ascorbic acid conducted in the HPB cell.

The applied power trace rose steadily until near the transition where there was an increase in the applied power prior to the transition. This is an example where the initial effect of the endothermic nature of the event (onset 189 °C in the green trace, Graph 58) is greater than the change in tan δ for a short period of time. This effect is useful as the separate parts of the fusion can be defined in microwave work. The differential (green line) and the applied power traces (blue line) return to near their original values after the transition, indicating the molten sample has the same dielectric properties as the room temperature state, although the process of changing physical form has a large change in tan δ.

6.4 MWTA of inorganic materials

6.4.1 Copper oxalate hemihydrate

The oxysalt copper oxalate hemihydrate (formula $CuC_2O_4.\frac{1}{2}H_2O$) decomposes to the oxide at high temperatures under oxidising atmospheres (see Equation 30, page 143. The decomposition is known to produce it's own inert atmosphere (CO_2) which prevents oxidation for a time, producing the metal at 263 °C (or a lower valency oxide). Once oxygen has diffused back to the sample the common oxide is formed (CuO) at 280°C [43].

The experiment was performed in the large volume removable cell with a blanket gas of air. The heating rate was set to 10 °C/min. Copper oxalate does not couple to microwave radiation therefore in order to reach the transition temperature with the applied power available (300 W) the sample had to be mixed with a standard susceptor (SiC) at a ratio 1:1 by weight. Therefore the active sample mass was 500 mg. The diluent mixture did not affect the ability to monitor the transition in this case as the sample went from a material that did not couple at all (copper oxalate) to a good coupling material (copper oxide).

linear heating 50:50 SiC: Copper oxalate under flowing Air IH0350

Heating Rate (°C/min)	10
Final Temp (°C)	600
Percentage of active sample	50%
4 stub tuning status	Auto
Sample weight (mg)	1000
Iris position (mm)	138
Iris (mm)	25 x 15
System	5
Tuning position (mm)	124
Comments	Flowing air Gas chamber in place Vacuum on
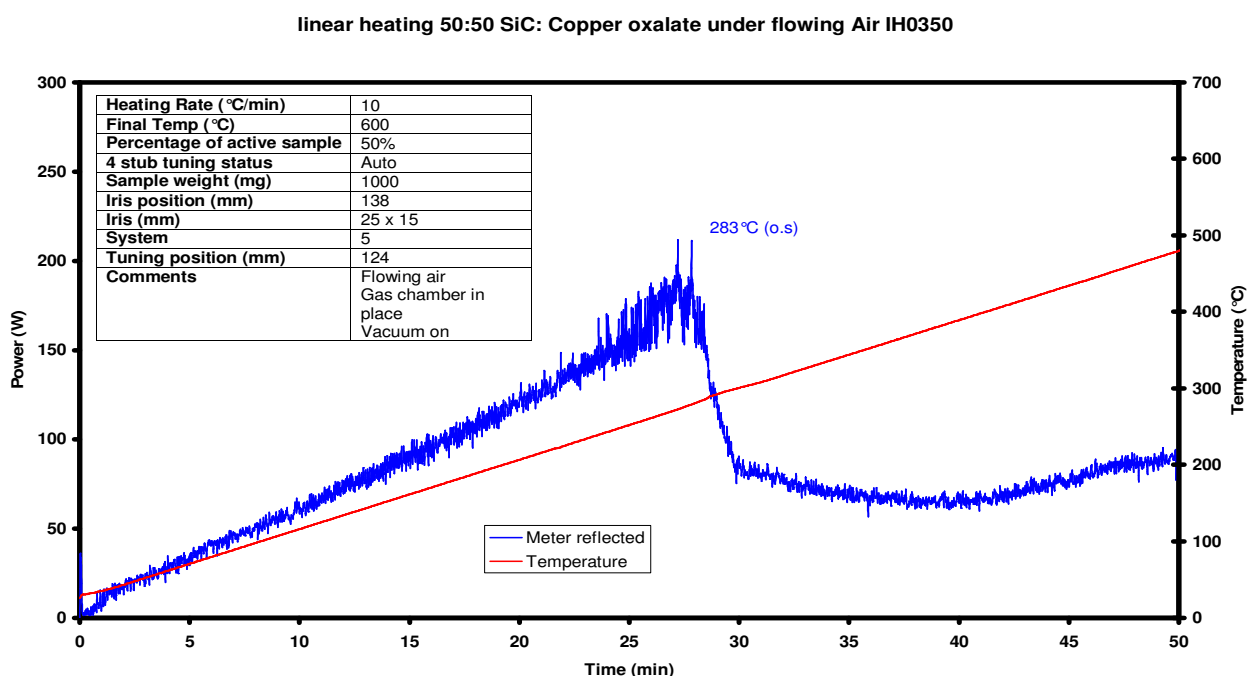
Graph 59: MWTA experiment of copper oxalate hemihydrate conducted in the large volume removable MWTA cell.

The meter reflected trace illustrated in Graph 59 followed the applied power trace in this experiment in all aspects except the magnitude of the reading. Using the meter reflected trace shows

the effect the sample had on the noise seen in the wave after the sample section during a transition, indicating how the newly formed material interacts with the wave. The trace shows steady noise in the meter reflected profile (blue line) as it approaches the transition temperature of the metal formation (263 °C). There is a noticeable increase in noise as the metal is formed indicating that the formation of copper metal has a large effect on the applied wave (information not seen when the applied power trace is used). The noise reduces as copper oxide is formed at 283 °C, as does the reflected power.

The experiment was repeated under a blanket gas of flowing air. The HPB cell with the sample thermocouple used to control the heating rate allowed the use of a 100 % copper oxalate sample.

MWDTA (MWTA) 100% Copper oxalate IH0673

Heating Rate (°C/min)	10
Final Temp (°C)	150
Percentage of active sample	100%
4 stub tuning status	Manual
Sample weight (mg)	20
Iris position (mm)	138
Iris (mm)	28 x 15
Cell	HPB
Reference material	SiC
Principle T/C	Sample
Tuning position (mm)	120.5
Comments	Argon 105 % Sample flow 0 % Alumina sandwich
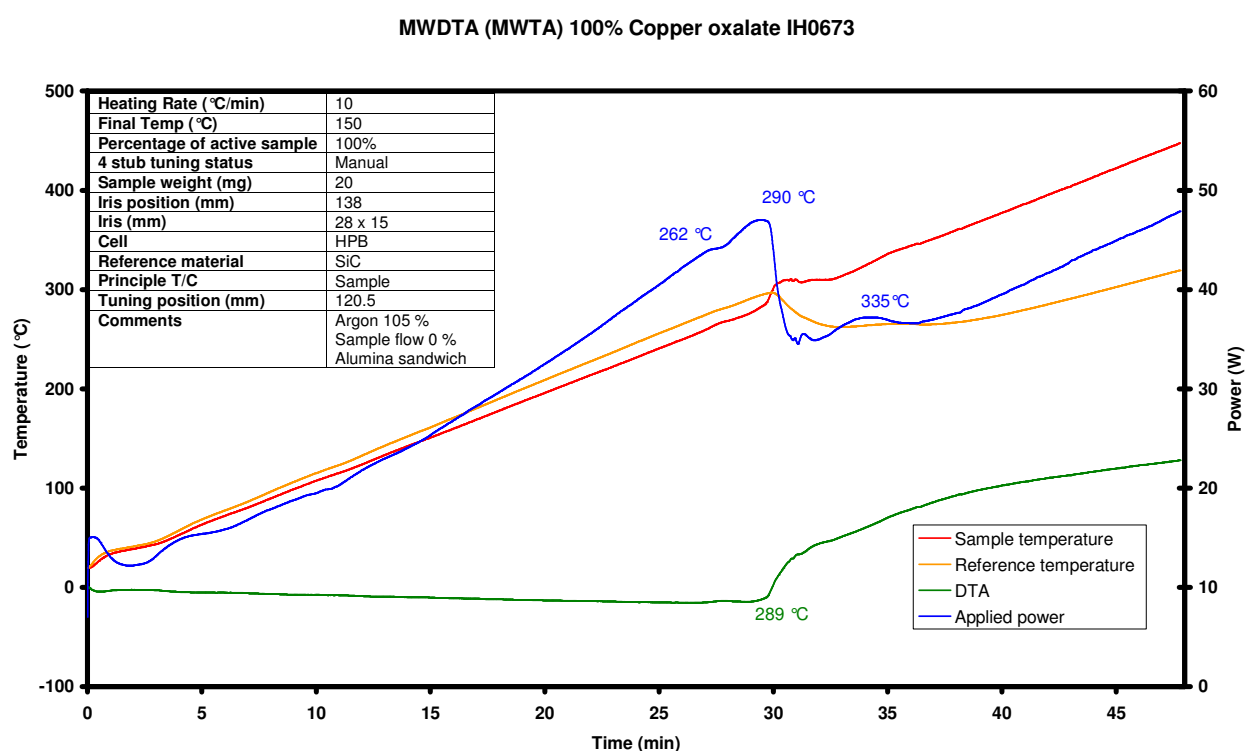
Graph 60: MWTA(MWDTA) experiment of copper oxalate hemihydrate conducted in the HPB cell.

The heating rate was set to 10 °C/min and sample sizes were kept to 20 mg. The same trends were seen in both methods with a large dielectric change seen between 283–290 °C, and a slightly smaller dielectric change at 262 °C. The event seen at 335 °C is a result of PID recovery and is not thought to be a true transition.

6.4.2 Copper sulphate pentahydrate

The dehydration of copper sulphate pentahydrate ($CuSO_4.5H_2O$) is well documented in thermal analysis. The dehydration proceeds via a loss of two water molecules at around 70-90 °C then the subsequent loss of two more water molecules around 115-120 °C. The final one is lost in the temperature range of 200-250 °C. It was expected that with each subsequent loss of water the power required to maintain the heating rate would increase (due to coupling species being lost). Experiments were performed in the large volume removable cell under argon, where the heating rate was set to 10 °C/min. The anhydrous form of copper sulphate does not couple well to microwaves therefore a 75:25 (copper sulphate pentahydrate: SiC) mixture was used. The active sample mass was therefore 817.5 mg.

MWTA 75:25 Copper sulphate.5H$_2$0: SiC IH0346

Heating Rate (°C/min)	10
Final Temp (°C)	600
Percentage of active sample	75%
4 stub tuning status	Auto
Sample weight (mg)	1090
Iris position (mm)	138
Iris (mm)	25 x 15
System	5
Tuning position (mm)	129
Comments	Argon 50ml/min Gas chamber in place Vacuum on
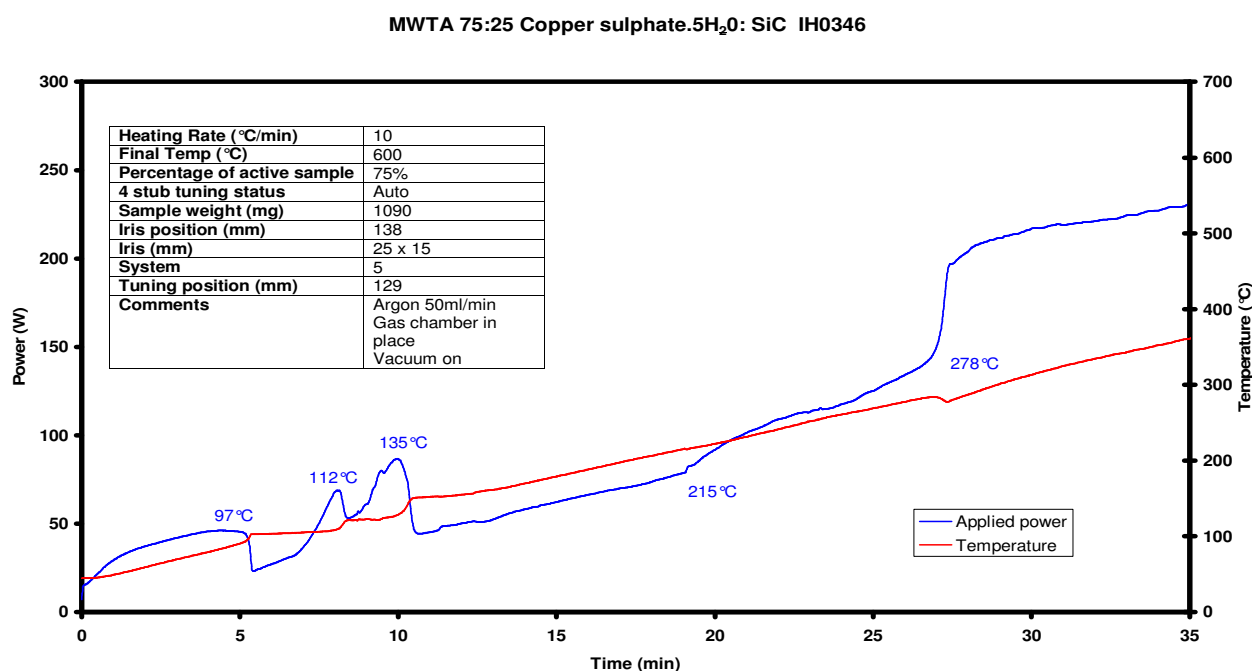
Graph 61: MWTA experiment of a mixture 75:25 (w/w) copper sulphate pentahydrate: SiC conducted in the large volume removable MWTA cell.

The results indicated several possible changes in enthalpy superimposed on changes in tan δ. These changes have been explained below:

- 97 °C-Loss of two waters (an endothermic transition)
    - Temperature rises due to the evolution of free water coupling to the applied power.
    - When the free water is lost from the measurement area more power is required to keep to set point shown by the increase in applied power.
- 112 °C-Loss of two waters
    - Same trend is observed as with the first transition.
- 135 °C-peak temperature shown by DSC for the first 2 transitions.
    - As with the organic melting experiments, the end of the endothermic process allows the full dielectric effect to take place, resulting in a reduction in the applied power.
- 215 °C–Start of the loss of 5th and final water
    - The final loss of water does not follow the trend of the first four as at this temperature the water is released as vapour rather than free water.
    - Power rise due to the endothermic transition damping out the dielectric effect.
    - Slight fall in power as enthalpy is overshadowed by changes in coupling (260 °C peak temperature of the 3rd transition shown by DSC).
- 278 °C–End of event
    - Anhydrous $CuSO_4$ formed which appears to have little coupling.

It appears that from the power profile $CuSO_4.H_2O$ had a greater ability to coupling than $CuSO_4.5H_2O$ which had a greater ability than the anhydrous copper sulphate.

6.4.3 Sodium tungstate dihydrate

Alkali tungstates are crystalline hydrates that are known to undergo solid-solid phase changes at high temperatures. Although Sodium tungstate dihydrate ($Na_2WO_4.2H_2O$) does not have many uses in a chemistry lab, it is useful source of tungsten and a strong oxidizing agent. Sodium tungstate dihydrate undergoes several thermal transitions on heating, the first occurring at an onset temperature of 81 °C, peaking at 122 °C. At an onset temperature of 560 °C the sample undergoes a solid-solid phase change peaking at 594 °C, which is closely followed by the melt at an onset of 689 °C, peaking at 696 °C.

Experiments were performed in the HPB cell with the sample thermocouple used to control the PID under argon. The heating rate was set to 10 °C/min and sample sizes were kept to 40 mg.

MWTA (MWDTA) 100% Sodium Tugstate IH0757
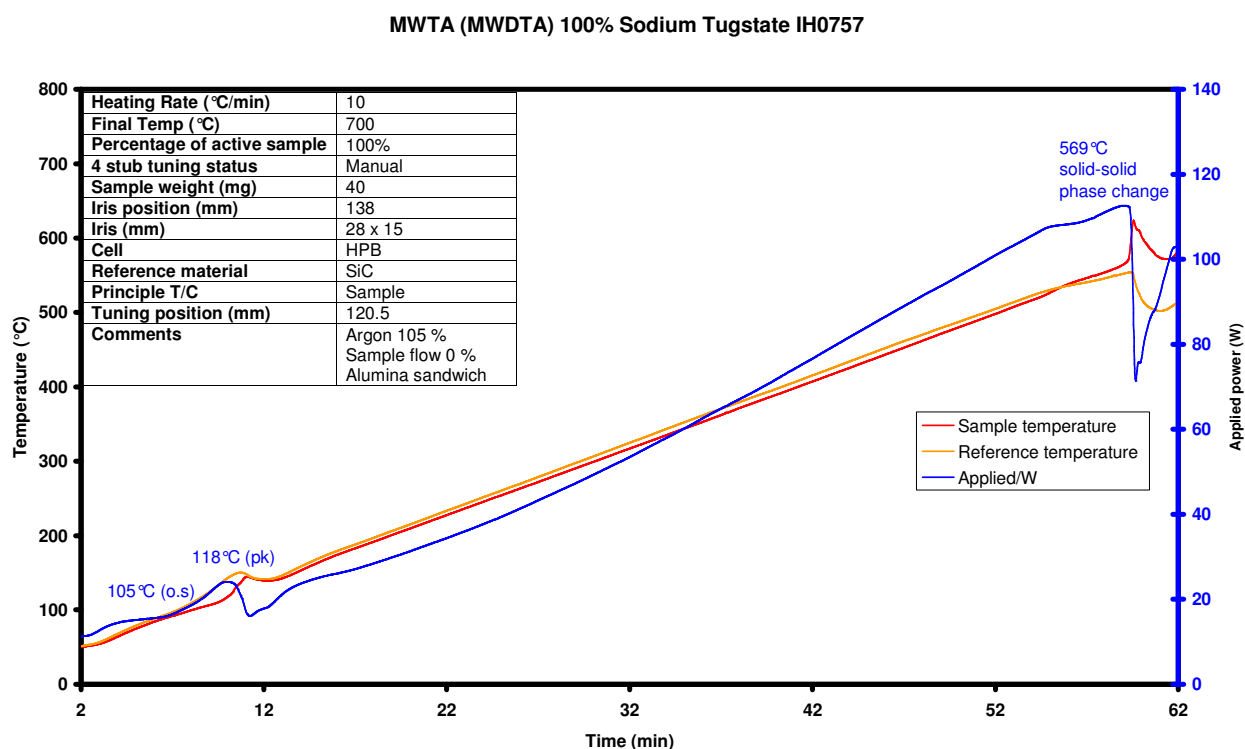
Graph 62: MWTA(MWDTA) experiment of sodium tungstate conducted in the HPB cell.

As observed in previous results the first transition (dehydration) requires an input of applied power (blue line) at 105 °C to overcome the enthalpy change, the power then drops as the dielectric effect takes over at 118 °C. At around 525 °C there is a levelling of the applied power as the sample temperature rises. DSC shows no transition at this temperature, TGA also confirms the lack of a transition, showing no mass losses, indicating this is a purely dielectric effect (see 7.4.4.2 Sodium tungstate dihydrate page 233).

The solid-solid phase change again has a rise in power to overcome the enthalpy then a lowering of the applied power indicating the increase in coupling. The extrapolated onset temperature at the solid-solid phase change appears to occur at a lower temperature than observed in conventional thermal analysis. Although this could be put down to a microwave effect it is believed more likely that the instrument is responding to the first point of change of the sample. If the area around the onset in a DSC trace is expanded then the first point of deviation occurs around 560-570 °C. For a microwave instrument to respond at this point is feasible. Assuming that all the sample is heated to the same temperature at the same time (unlike a conventional experiment where heating is via conduction so time dependent) then the time dependent factor is removed, so the point at which the first crystal changes would be the point at which all of the crystals change. By conducting DSC

experiments at very slow heating rates (1 °C/min) it is believed that the transition temperature would tend towards the transition temperature seen in MWTA.

6.4.4 Silver iodide

Silver iodide (AgI) is used in processes such as photography, rain making and antiseptic medicines. It exists in three crystal structures. At temperatures below 147 °C it exists in the β-phase and the γ-phase can also be present which is reported to be seen on cooling at 143.5 °C [44]. Above this temperature the α-phase is dominant. Experiments were performed in the HPB cell with the sample thermocouple as the input to the PID controller under argon. The heating rate was set to 10 °C/min and sample sizes were kept to 20 mg.
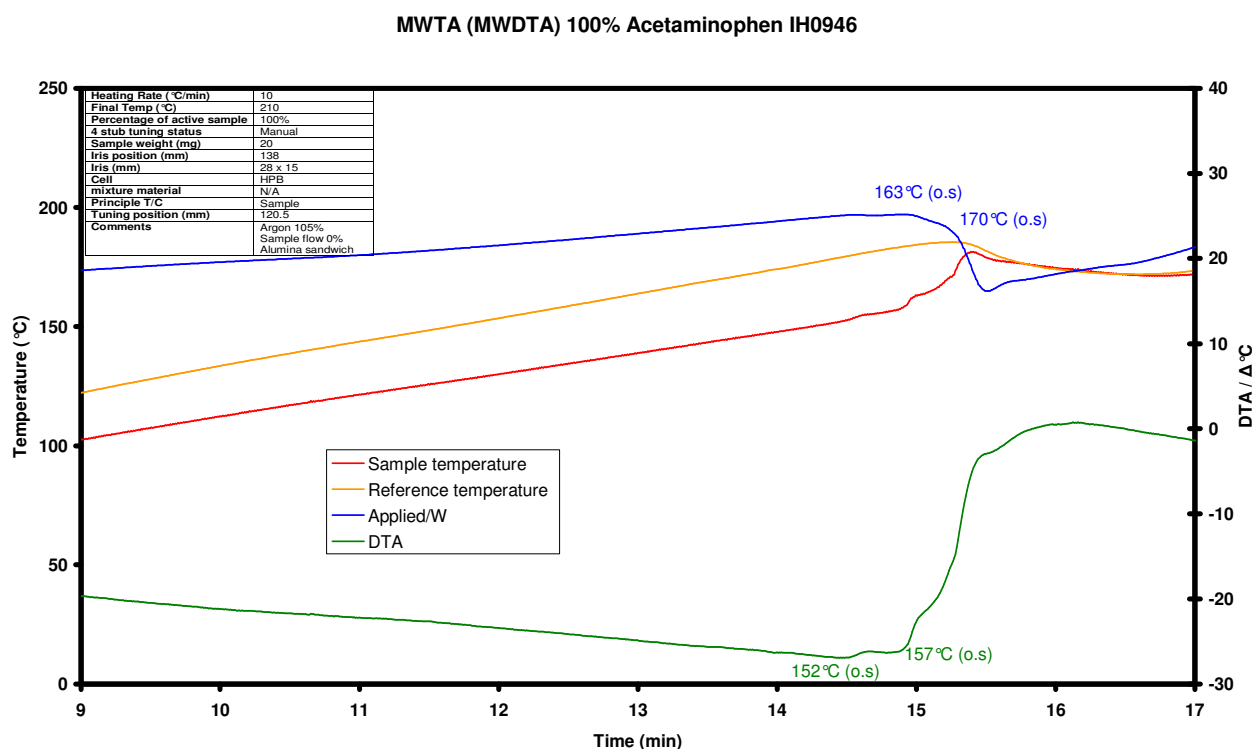
MWTA (MWDTA) 100% Silver iodide IH0910

Heating Rate (°C/min)	10
Final Temp (°C)	175
Percentage of active sample	100%
4 stub tuning status	Manual
Sample weight (mg)	20
Iris position (mm)	138
Iris (mm)	28 x 15
Cell	HPB
mixture material	N/A
Principle T/C	Sample
Tuning position (mm)	120.5
Comments	Argon 105% Sample flow 0% Alumina sandwich
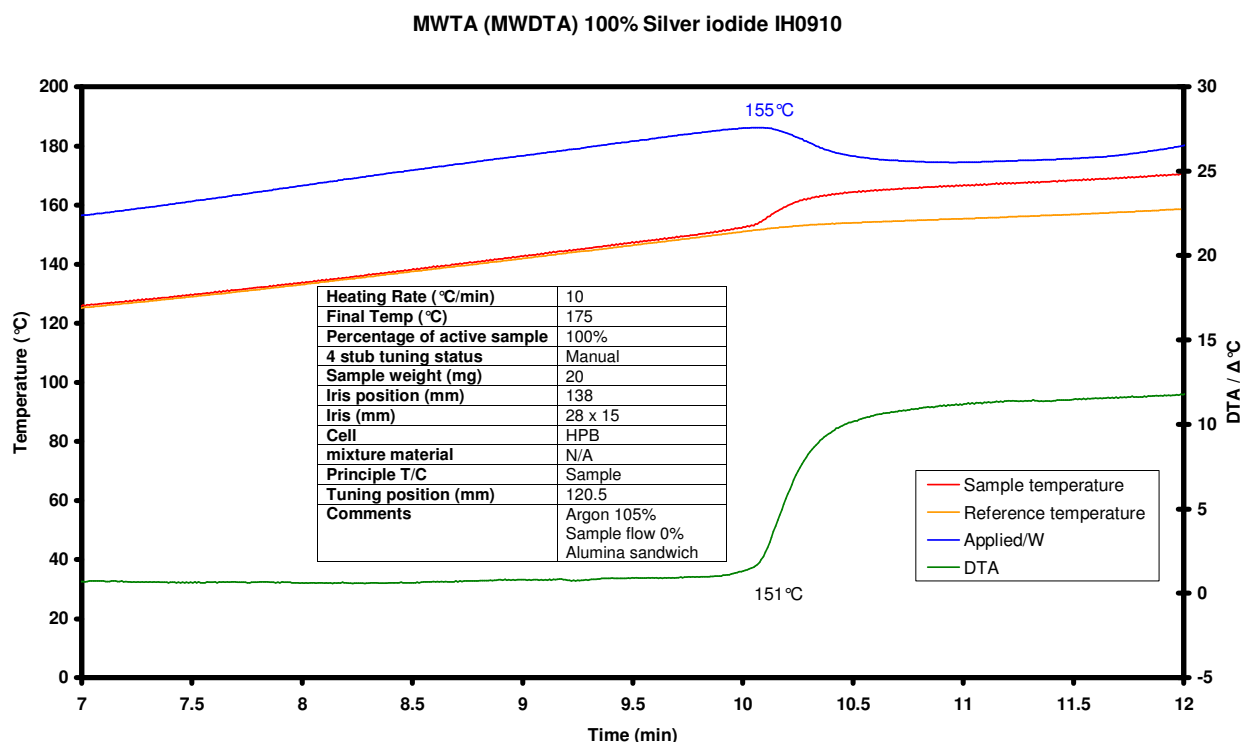
Graph 63: MWTA (MWDTA) experiment of silver iodide conducted in the HPB cell.

The results showed a change in the material's ability to couple to the applied wave which remained till the end of the experiment, indicated by the constant elevated differential value after the transition. The transition temperature is higher than found in DSC, and is most likely due to the PID controller. As the heating rate changed so dramatically in such a short period of time, by the time the controller had responded to the error signal the sample temperature had risen by several degrees showing the extrapolated onset to be higher than expected. This is a possible disadvantage of controlling on the sample temperature.

6.5 Summary of the MWTA technique

MWTA is has proven to be exceptional in identifying melting processes, dielectric changes, points of thermal runaway under microwave radiation and in a number of cases polymorphs in inorganic materials. The technique has also shown its inability to record enthalpy-only changes within a system.

The advantage of being able to see the equilibrium of enthalpy verses dielectric change during highly endothermic events, allows the user to determine the maximum point of enthalpy change as well as the extent of changes to microwave interaction in one experiment.

Transition temperatures appear higher than expected in some cases where there is a dramatic change in heating rate, which is believed to be due to the PID controller. The sampling interval of 250 ms may not be sufficient to be able to instantly respond to a dramatic change in heating rate and by the time the controller has reacted and altered the applied power, the sample temperature had risen by several degrees. The results obtained which showed this alteration in the transition temperature indicated a limitation of the PID controller in the MWTA instrument when controlling solely on the sample. With modern controllers (utilised by the latest thermal instruments) it is possible that the level of control could be increased.

Chapter 7

Qualitative MWDTA

The development of the novel HPB cell allowed for possibly the first time repeatable differential results to be obtained from MWTA.

This chapter details the results and problems gained from the validation of the MWDTA technique.

The chapter also describes a wide range of thermal transition types and therefore what can be expected from different materials under MWDTA experimentation.

7.1 Comparison of differential techniques

As described in previous chapters, the ability to monitor the differential signal during an experiment adds increased sensitivity. The development of the HPB cell and control on a reference, gave a new and more stable baseline and heat flux environment not seen before in other cell designs. With the reduced sample size the instrument could now be directly compared to conventional DTA experiments.

To show the versatility of microwave thermal analysis, samples that undergo well characterised types of thermal transitions were tested with both conventional thermal methods and microwave differential methods and the results compared. These transition types included organic fusions, glass transition of polymers, decompositions, dehydration of bound species, dehydration of water of crystallisation, solid-solid phase changes, liquid crystal fusions, pharmaceutical fusions, and changes to fast ion conductor states. The effect of heating metals in microwaves was also briefly studied.

7.1.1 Experimental conditions

7.1.1.1 MWDTA performed in the HPB cell

All microwave differential experiments (unless stated otherwise) are performed using the HPB cell. The heating rate was kept at 10 °C/min and the susceptor was 200-450 mesh SiC. Argon was used as the blanket gas unless oxygen was required, in which case compressed air was supplied to the test chamber. Although it is common in thermal analysis to use nitrogen (for economic reasons) or helium (for the heat conductivity) argon was chosen as a blanket gas to avoid the possible interaction with oxygen at high temperatures which nitrogen can undergo to form N_2O, resulting in phantom exothermic temperature changes. The disadvantage of using helium in microwave thermal analysis is down to volumetric heating. As the sample is the only part of the chamber which heats, the thermal gradients that exist between the sample itself and the outer walls of the chamber are large. The use of a highly thermally conductive blanket gas only increased the size of this gradient increasing the differential between the sample and the reference. Air and argon have low thermal conductivities and hence aid the reduction of the thermal gradient.

7.1.1.2 Differential thermal measurements

Conventional experiments were performed on a TA Instruments MDSC 2900, MettlerToledo TGA/SDTA851e or a Stanton Redcroft DSC1500 calibrated for temperature with the T_m of indium and lead standards.

Unless otherwise stated all conventional experiments detailed in this chapter were performed using air and argon as the blanket gas, and a dynamic heating rate of 10 °C/min was utilised.

In the MDSC 2900 (TA Instruments) samples were encapsulated in pin holed aluminium pans. Therefore the samples sizes are much smaller than those in the microwave experiments. HDSC experiments were performed using sample pans which were of cylindrical design and were constructed of quartz. The pans measured 20 mm by 6 mm therefore the sample sizes are directly comparable with those of the HPB cell. TGA runs utilised alumina crucibles.

When modulated experiments where performed to increase sensitivity, a heating rate of 3 ºC/min was used with a modulation amplitude of 0.5 ºC and a period of 60 seconds.

7.1.2 Instrumental resolution of non-dielectric events in MWDTA

The resolution of events that occur at temperatures in close proximity to each other is an important ability in thermal analysis. Traditionally, increased resolution is obtained via very slow heating rates (typically 1 °C/min), resulting in very long and impractical experimental times. The decompositions of potassium and sodium bicarbonate occur in the region of 110 °C to 210 °C. When a equal mixture of the two are heated the two events are almost fully resolved at a rate of 1 °C/min [43]. It can be seen from the conventional DTA trace below, that sensitive apparatus can show partial resolution between the two events at faster dynamic heating rates (10 °C/min).
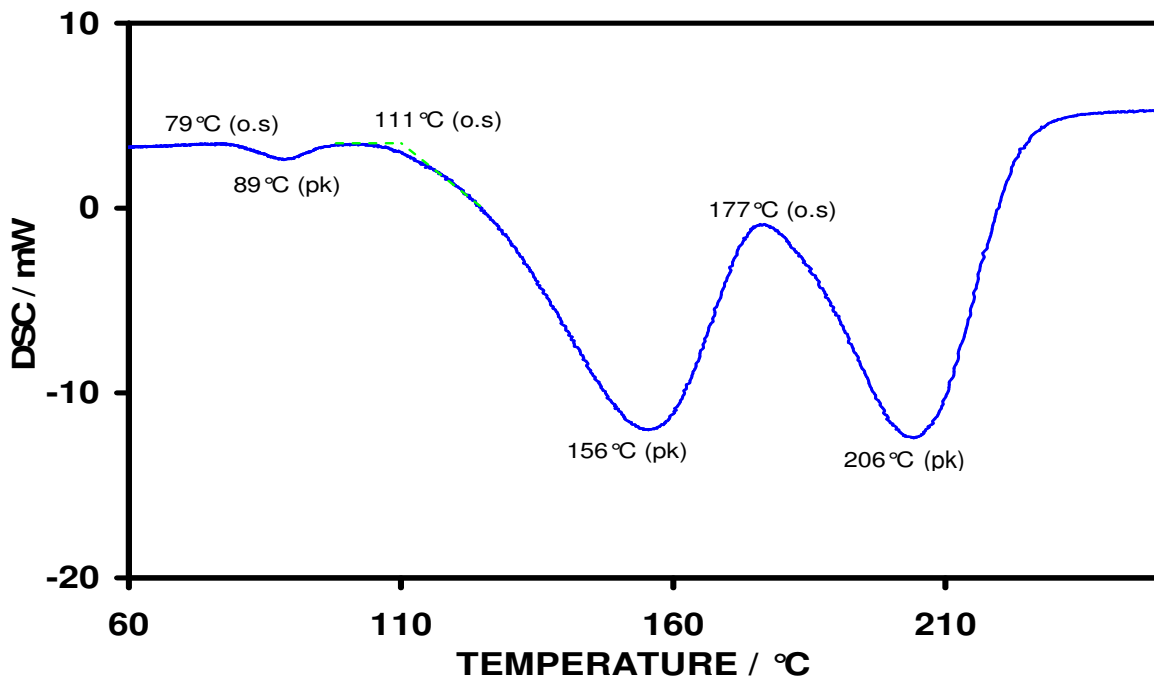
Graph 64: HDSC experiment of a mixture of 50:50 sodium bicarbonate: potassium bicarbonate performed under argon.

In order to determine if the same resolution could be achieved in MWDTA the experiment was repeated in the HPB cell at the same heating rate using 40 mg of the sample mixture.
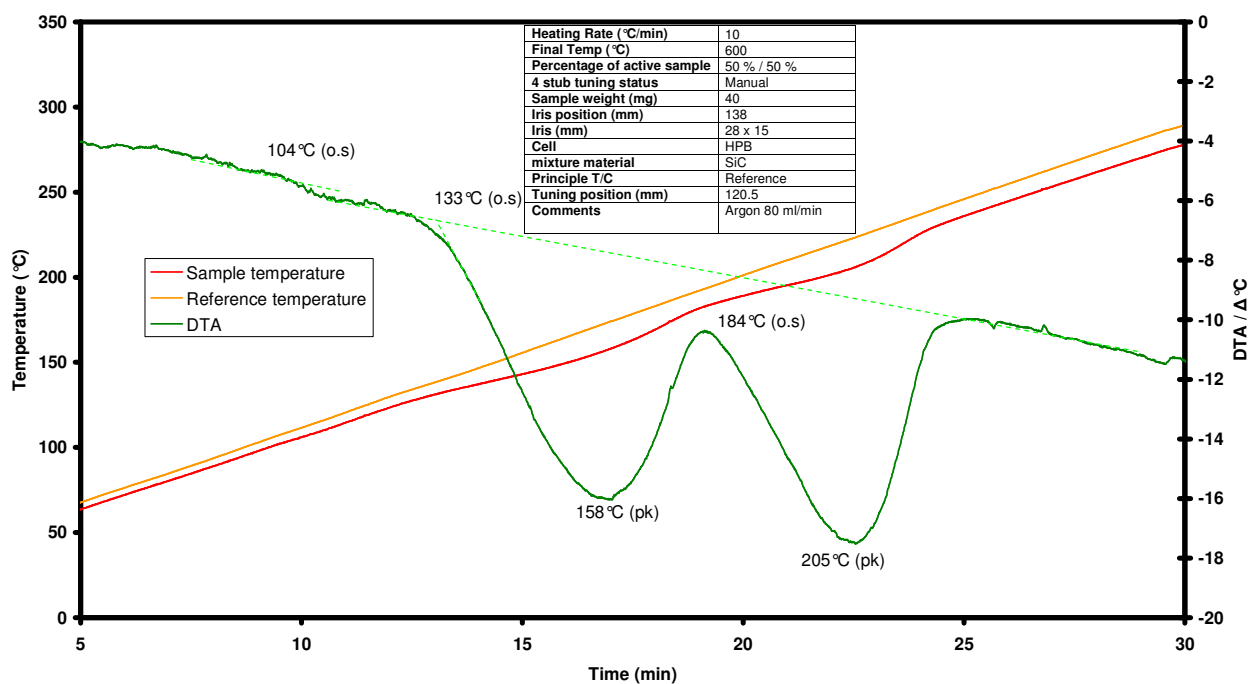
Graph 65: MWDTA experiment of a mixture of 50:50 sodium bicarbonate: potassium bicarbonate performed under argon.

The experiment showed good resolution between the two events with good agreement of peak temperatures obtained from the HDSC.

With the ability to monitor both dielectric and enthalpy only transitions (with good resolution between events) MWDTA looked to be a promising advancement to the field of microwave thermal analysis.

7.2 Study of organic fusions using MWDTA

The melting point of organic materials is a useful property for organic and pharmaceutical chemists, as it can be used to characterise compounds and determine purity. The usefulness of thermal analysis in determining melting temperatures is well established, and is the sole application for industries where highly accurate measurements need to be obtained. The melting process involves a material transforming from a solid state to a liquid state. The energetics required for this transformation results in a lag in the sample temperature during a dynamic experiment. Therefore a sample requiring a relatively large input of energy (endothermic melt) will result in a relatively large negative peak in the DSC/DTA trace (assuming exothermic processes are positive). Microwave experiments differ from conventional experiments since the energetics of a process can be overshadowed by the changes in tan δ as a sample's main mode of heating changes from Ohmic to dipolar polarization (usually a large effect and not thought to be dependent on the energy required to reorder bonds). However, the nature of the fusion transition opposes the changes in coupling ability.

In this section a range of standard organic materials were subjected to a dynamic heating rate of 10 °C/min under argon in both microwave and conventional experiments.

7.2.1 Benzoic acid
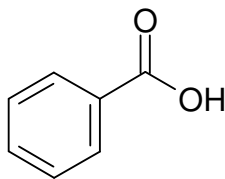
Benzoic acid has been recommended as a calibration material by IUPAC [45] as it exhibits "ideal" behaviour. Ideal behaviour refers to a sample which has well defined and repeatable points of melting and evaporation. Benzoic acid is also of interest to the microwave chemist as the melting is accompanied by a notable dielectric change [17].
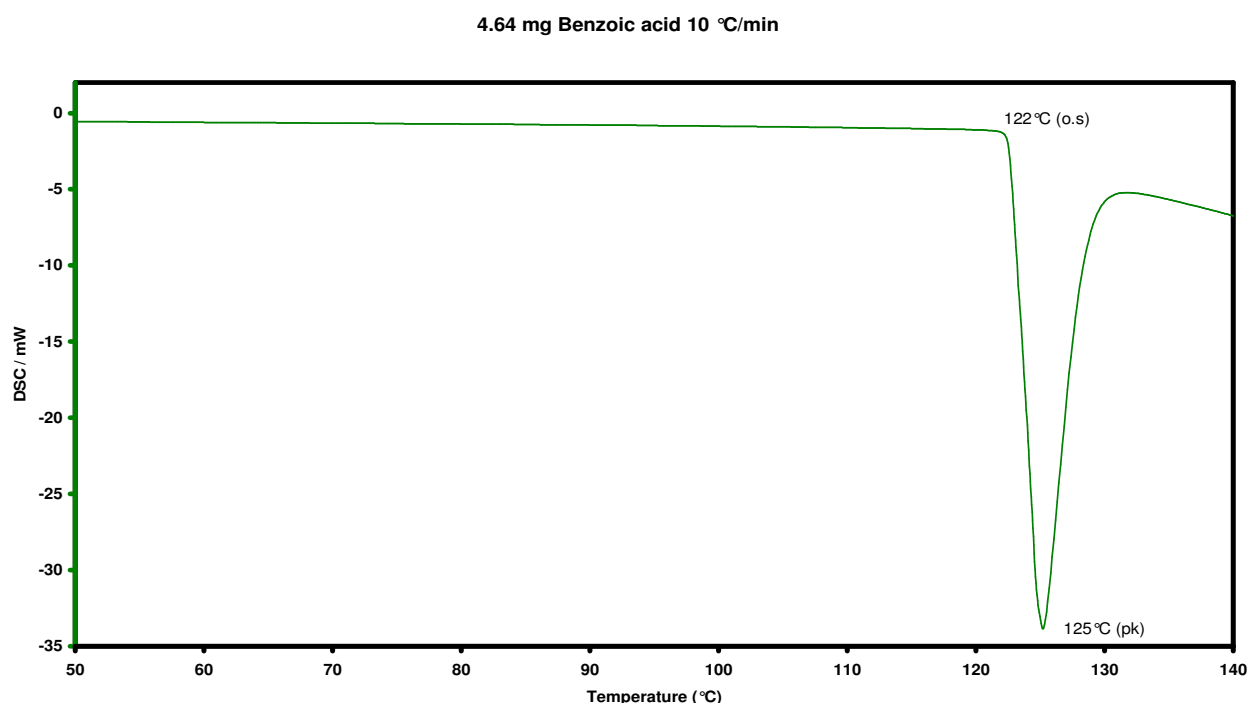
Graph 66: MDSC experiment of benzoic acid performed under argon.

Graph 66 shows the DSC measurement of benzoic acid. An extrapolated onset at a temperature of 122 °C with a peak temperature of 125 °C was recorded.

MWDTA 100% Benzonic acid IH0970

Heating Rate (℃/min)	10
Final Temp (℃)	150
Percentage of active sample	100%
4 stub tuning status	Manual
Sample weight (mg)	20
Iris position (mm)	138
Iris (mm)	28 x 15
Cell	HPB
mixture material	N/A
Principle T/C	Reference
Tuning position (mm)	120.5
Comments	Argon 105% Sample flow 0% Alumina sandwich

Graph 67: MWDTA experiment of benzoic acid performed under argon.

The MWDTA (Graph 67) run showed a close correlation to these transition temperatures. The microwave experiment also recorded a repeatable transition at 118 °C which was not clearly seen in the DSC experiments. This transition temperature appears to be correlate with the partial sublimation of the sample prior to the melt [45]. Sublimation or the conversion from a solid to a gas requires at some point increased mobility of the molecule therefore making the sample more likely to be more susceptible to dipolar polarization resulting in an increase in coupling (which is quickly lost as the sample becomes gaseous. In a microwave experiment there is an increased possibility this event is more noticeable, as unlike conventional experiments it is no longer solely a surface effect as the bulk of the material will have obtained the same energy as the surface.

The second recorded transition in the microwave experiment occurred at 122 °C, the onset temperature observed in the DSC trace. At this point the endothermic nature of the samples fusion is evident by the lag in the sample temperature and the resultant negative peak in the MWDTA trace. Near the peak temperature seen in the DSC trace (125 °C) the microwave trace starts to return to the baseline as expected but as dipolar polarization had become the main mode of heating there is a increase in the baseline value (a microwave effect). This increase in the baseline is the opposite of DSC profiles where a negative sloping baseline is usually observed.

To further investigate the transition seen at 118 °C prior to the melting of the sample in microwave experiments, a series of linear power experiments were performed. In these, the power is programmed to increase independent of either the reference or sample temperature, which means that the sample's response to the applied wave at the applied power (although heating is still aided by the reference) can be studied. The instrument was set to increase the applied power by 0.5 %/min (1.5 W/min) to a final power of 45 W. Atmospheric conditions remained the same.

MWDTA Linear power Benzoic acid (BZ3) ACS grade IH0619

Power Rate (%/min)	0.5
Final power (W)	45
Percentage of active sample	100%
4 stub tuning status	Auto
Sample weight (mg)	50
Sample cell	HPB
Iris position (mm)	138
Iris (mm)	28 x 15
Reference material	SiC
Principle T/C	N/A
Tuning position (mm)	124
Comments	Argon 105% Alumina sandwich
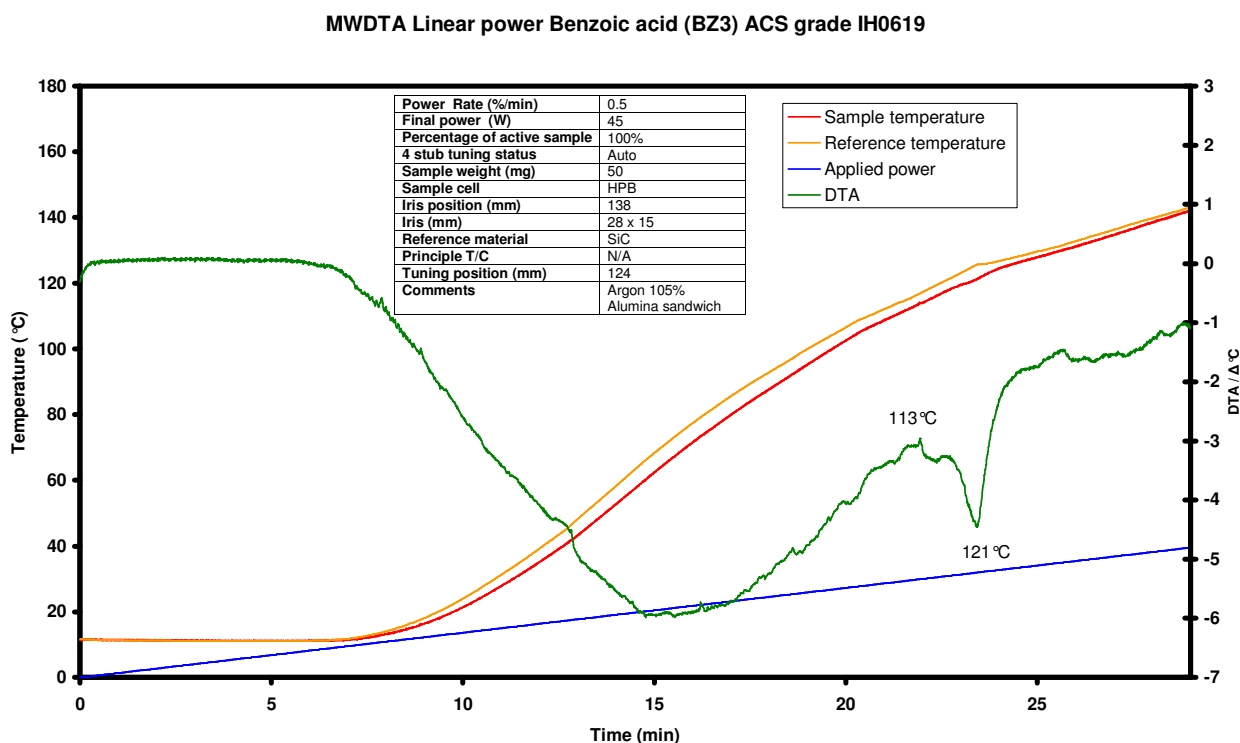
Graph 68: Example of a typical linear power MWDTA experiment of benzoic acid under argon.

The results showed the same pre-step to the melt observed in both MWTA and MWDTA occurred 5 °C earlier. This depression of the transition temperature is probably attributed to several factors, including the elevated power level at the point of the transition and the temperature range of the unknown transition. The slope of the differential trace also changed after the transition, indicating the molten sample couples to microwaves better then the pre-transition sample. Another feature which was shown by the linear power experiment was the proportion of the applied power which the post transition sample takes in relation to the pre-transition sample. Comparing the reference trace (orange line) and sample trace (red line) after the differential peak temperature (121 ºC), it can be seen the reference temperature falls while simultaneously the sample temperature increases, indicating the sample is using a higher portion of the applied power than before.

The experiments also showed an interesting instrument feature. The heating program in all temperature rate controlled experiments is set to "soft start", meaning a power of 5 % (15 W) is applied at the start of the run. The linear heating experiment showed that below 3.333 % (10 W) no heating occurred in the sample or the reference, showing heating for this susceptor required at least 10 W of applied power to cause interaction or even satisfy boundary conditions.

7.2.2 Stearic acid

$$CH_3(CH_2)_{15}CH_2 - \overset{O}{\underset{\|}{C}} - OH$$
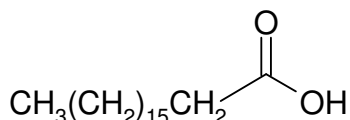
Stearic acid (also known as octadecanoic acid) is a useful fatty acid obtained from animal or, vegetable oils and fats which have found many commercial uses. Great interest has been given to stearic acid in the field of PCM materials for heat storage. As with benzoic acid the fusion of the compound is accompanied with a change in the material's dielectric properties and as such has made it a well used material in the development of thermal microwave techniques [18].
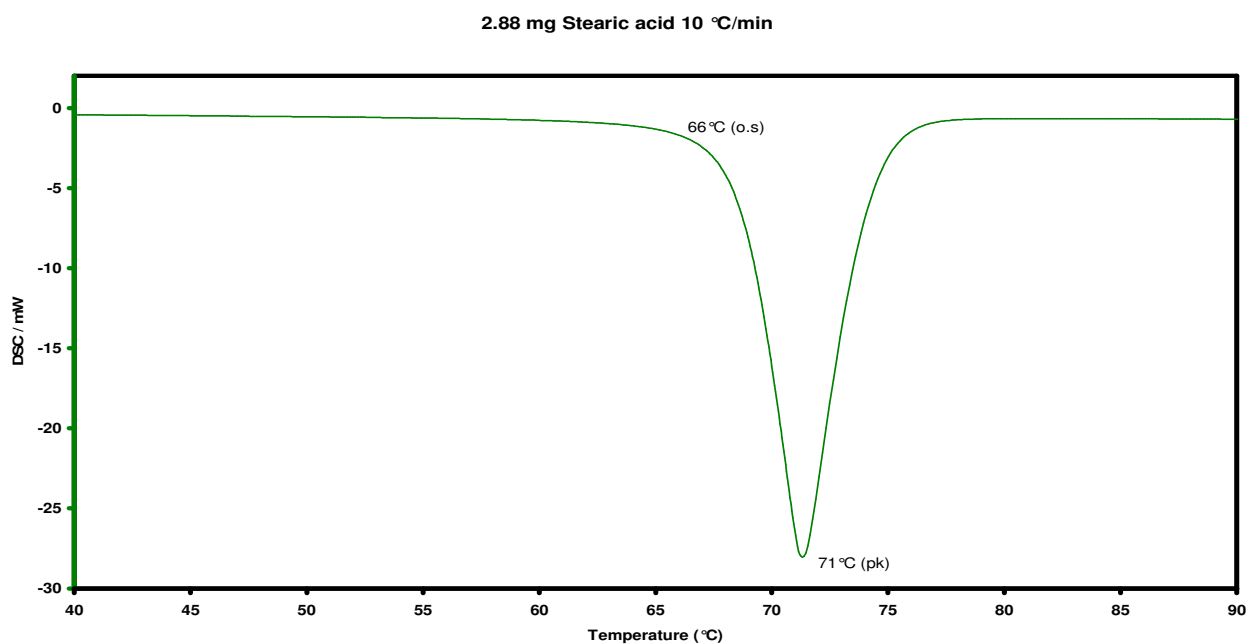
Graph 69: MDSC experiment of stearic acid performed under argon.

Graph 69 shows the extrapolated onset seen in the DSC profile (66 °C) indicating close correlation with the MWDTA experiment, the same was also found in the peak temperature (71 °C).

MWDTA 100% Stearic acid IH0572

Heating Rate (°C/min)	10
Final Temp (°C)	90
Percentage of active sample	100%
4 stub tuning status	Auto
Sample weight (mg)	40
Iris position (mm)	138
Iris (mm)	28 x 15
Reference material	SiC
Principle T/C	Reference
Tuning position (mm)	122
Comments	Silica wool base Alumina sandwich
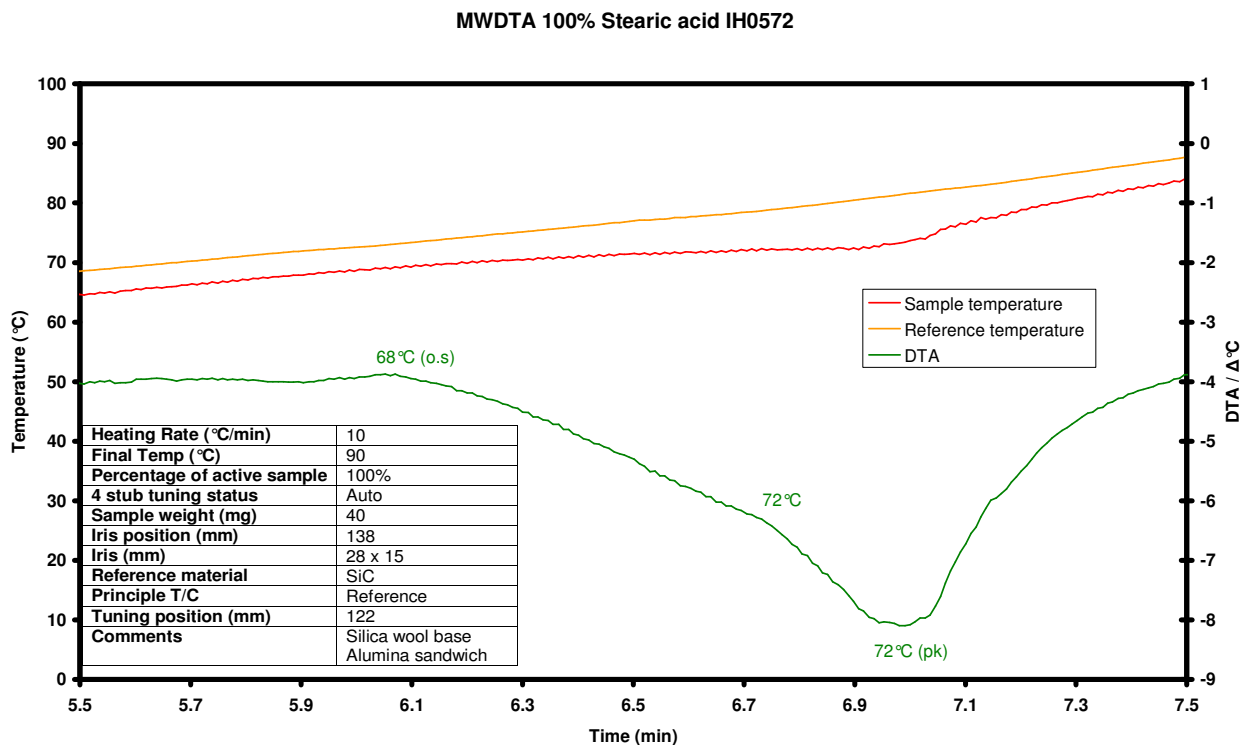
Graph 70: MWTA experiment of stearic acid performed under argon.

On closer examination of the microwave differential profile (Graph 70) of the peak there appeared to be a shoulder in the lead into the peak minimum. This was believed to be due to the highly endothermic nature of the fusion just prior to the maximum rate of change, forcing the sample temperature further behind the reference (72 °C) causing an increase in the differential signal. A large change in coupling was not observed in this series of experiments due to the formation of a dimer which has no overall dipole.

7.2.3 Benzil
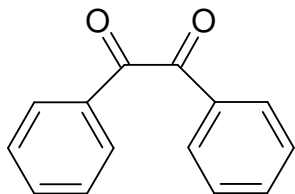
The melting of benzil has a strong and well documented dielectric change [16, 42] at 96 ℃.

2.84 mg Benzil 10 ℃/min
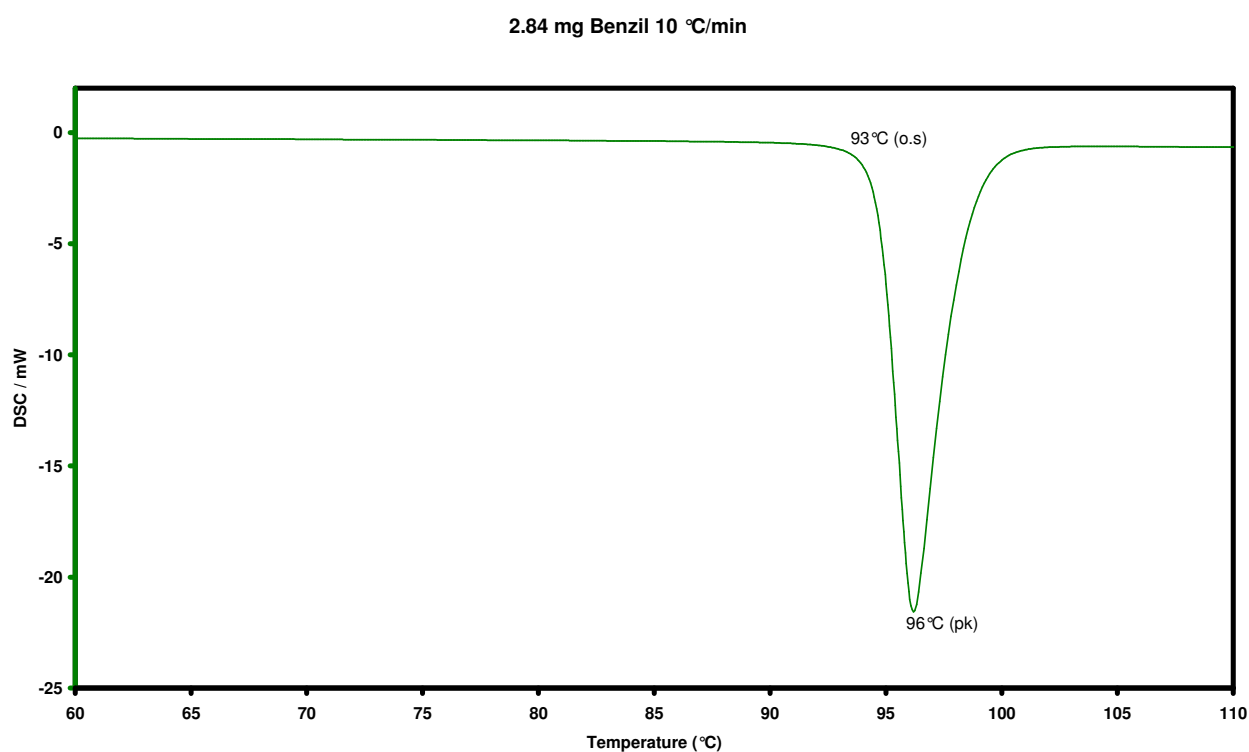
Graph 71: MDSC experiment of benzil performed under argon.

The extrapolated onset can be seen in the DSC profile above to occur at 93 °C. The peak temperature was found to be 96 °C.

MWDTA 100% Benzil IH0928

Heating Rate (℃/min)	10
Final Temp (℃)	120
Percentage of active sample	100%
4 stub tuning status	Manual
Sample weight (mg)	20
Iris position (mm)	138
Iris (mm)	28 x 15
Cell	HPB
mixture material	N/A
Principle T/C	Reference
Tuning position (mm)	120.5
Comments	Argon 105% Sample flow 0% Alumina sandwich
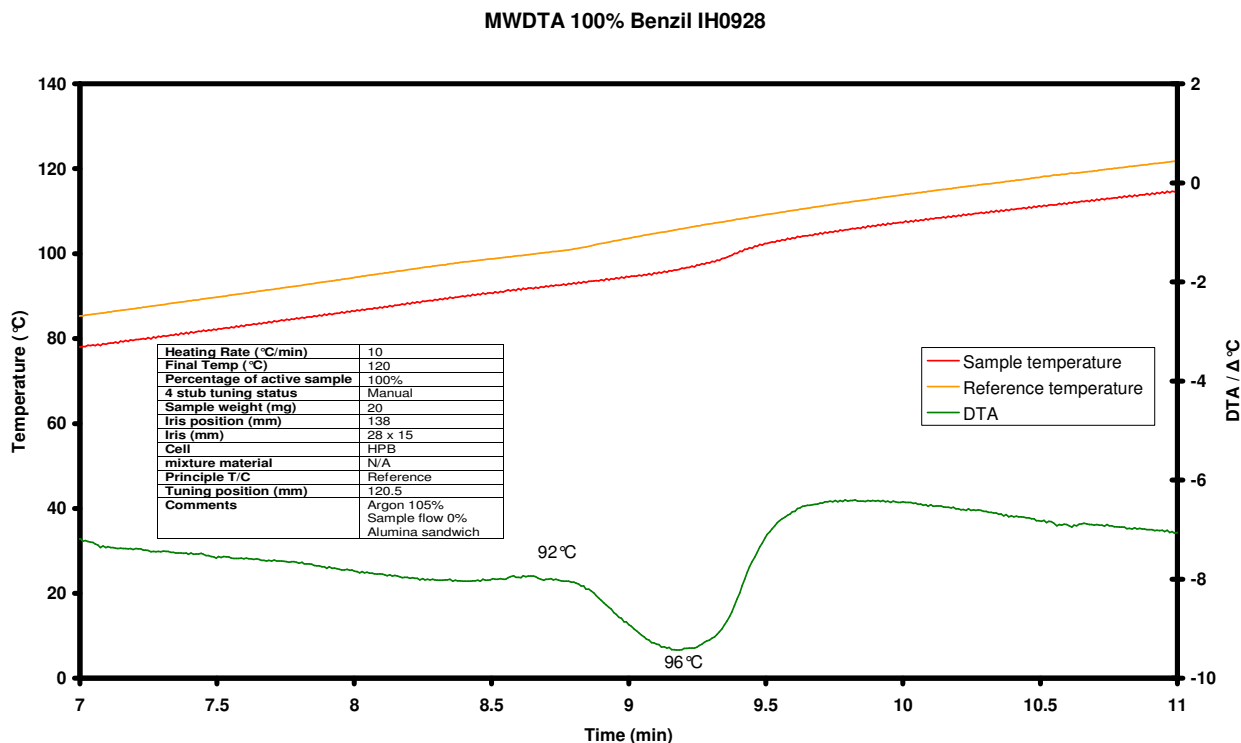
Graph 72: MWDTA experiment of benzil performed under argon.

As with the other simple organic materials detailed, the transition in the microwave experiments occurred within close correlation to the DSC measurements. The change in value of the baseline, after the transition had occurred made this material of interest in MWDTA. It can be seen from the DSC trace that there was no change in baseline due to heat capacity, whereas in the microwave experiment there is a significant constant elevation of the differential signal due to the increase in coupling ability as the sample becomes molten. The experiment gave an indication of the expected profile of a fusion process accompanied by a large dielectric change.

7.3 Glass transition of polymers

In the manufacturing of synthetic polymers the glass transition temperature (T_g) is of great interest. The glass transition temperature can be described, as the temperature at which the structure of an amorphous polymer goes from inelastic to elastic or vice versa. This does not affect the physical properties of the material, but changes the heat capacity, thermal expansion coefficient, and free volume. As there is no change in the latent heat of the material these transitions are deemed to be second order.

DSC/DTA has been used for many years to identify this phase change. In order to determine if MWDTA can be applied in this field, two of the most common amorphous polymers were tested:

- polymethyl methacrylate
- polystryrene.

The low energy of the transition meant it was unlikely that the transitions would be clear on an instrument that was not designed to monitor energetics, although it was not known if the transition had an accompanied dielectric change.

To gain further information (and because a T_g is a reversible transition) modulated DSC was used. Experiments were performed under nitrogen. The modulated heating rate was set to 3 °C/min the modulation amplitude was set to 0.5 °C per 60 s.

7.3.1 Poly (methyl methacrylate)
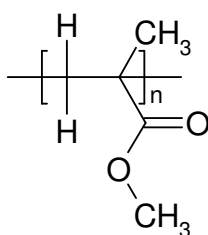
Poly (methyl methacrylate) or PMMA has found many uses in industry from thin film production to a freezing point depressant of machine oils for sub-ambient work. The use of thermal analysis to determine the glass transition of the polymer has become a useful characterization technique. The different forms of the polymer affect the transition temperature seen in TA. Isotactic, syndiotactic, and atactic (60-61 °C, 105-111 °C, and 100-105 °C respectively [46]). For these experiments the syndiotactic form was used.

5.47 mg Methyl Methacrylate mod
(amp.: 0.5℃ per.: 60 s)
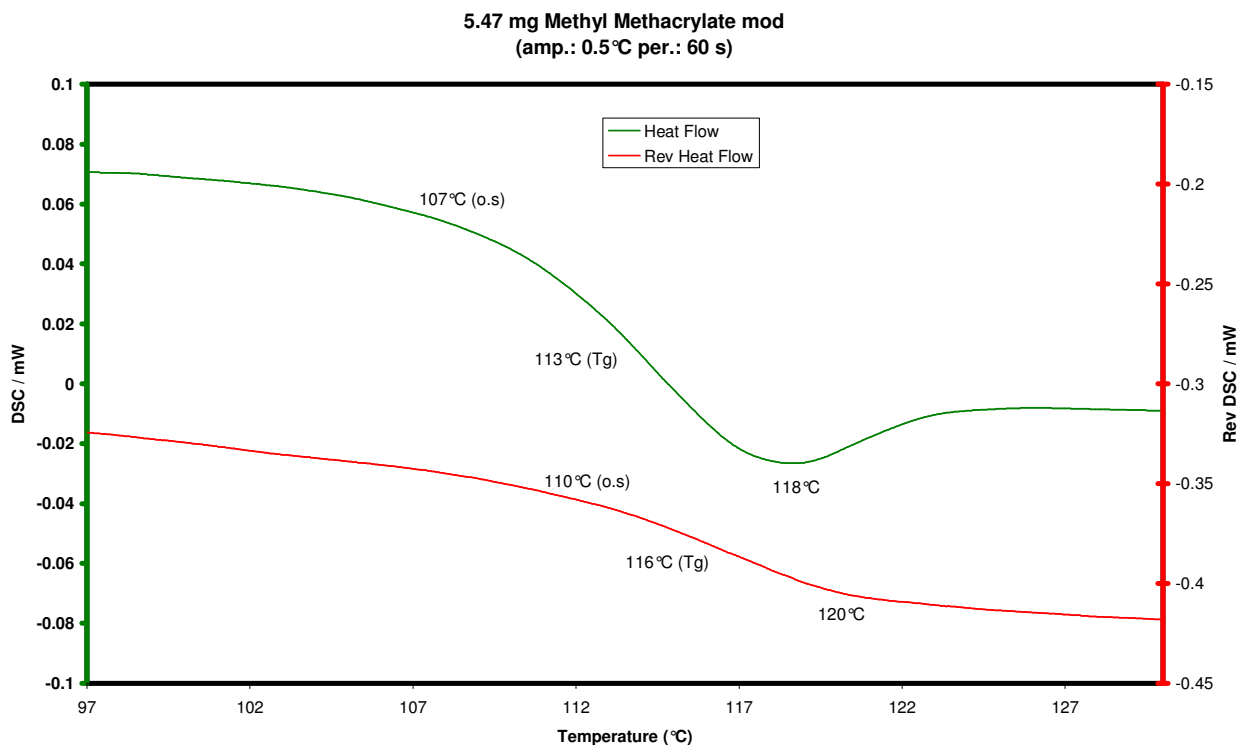
Graph 73: MDSC experiment of poly (methyl methacrylate) performed under argon.

Modulated DSC data showed the transition to occur at 113 °C in the forward direction and 116 °C in the reversing signal.

MWDTA 100% Atactic poly(methyl methacrylate) IH0961

Heating Rate (℃/min)	10
Final Temp (℃)	120
Percentage of active sample	100%
4 stub tuning status	Manual
Sample weight (mg)	70
Iris position (mm)	138
Iris (mm)	28 x 15
Cell	HPB
mixture material	N/A
Principle T/C	Reference
Tuning position (mm)	120.5
Comments	Argon 105% Sample flow 0% Alumina sandwich
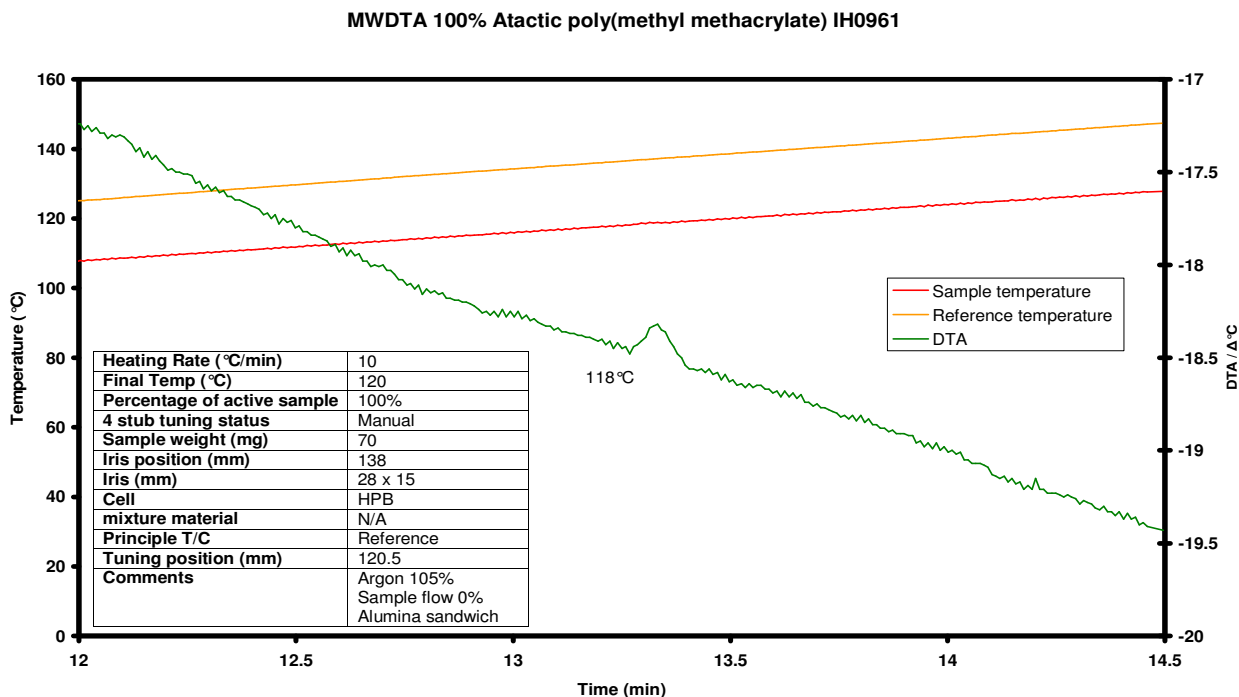
Graph 74: MWDTA experiment of poly (methyl methacrylate) performed under argon.

The microwave experiment showed no distinct change in the MWDTA trace at first glance, when the trace was expanded around the expected transition temperature it could be seen that there was a small deviation in the trace, which possessed no overall dielectric change (no alteration of the slope of the baseline). The magnitude of this response was only ~ 0.2 °C only twice that of the minimum temperature difference the thermocouple could record. As the sample size (70 mg) was three and a half times more than a normal MWDTA experiment and the response were so low it was agreed that MWDTA was not a suitable technique for investigating the T_g of PMMA unless a more sensitive temperature recorder could be used.

7.3.2 Polystyrene
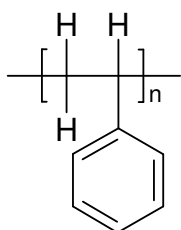
Polystyrene is among the most popular and widely used polymers in modern times. It finds uses in objects from plastic cups to thin film coatings. The glass transition temperature of polystyrene has been stated as being 95 °C although upon testing on DSC the mid-point of the transition indicates a T_g at around 105 °C. The change in heat capacity in polystyrene during the glass transition is usually easily seen in thermal analysis. It was thought this energy change may be recorded on the MWDTA not as a dielectric change but as an enthalpy change.

9.98 mg Polystrene 3 ℃/min
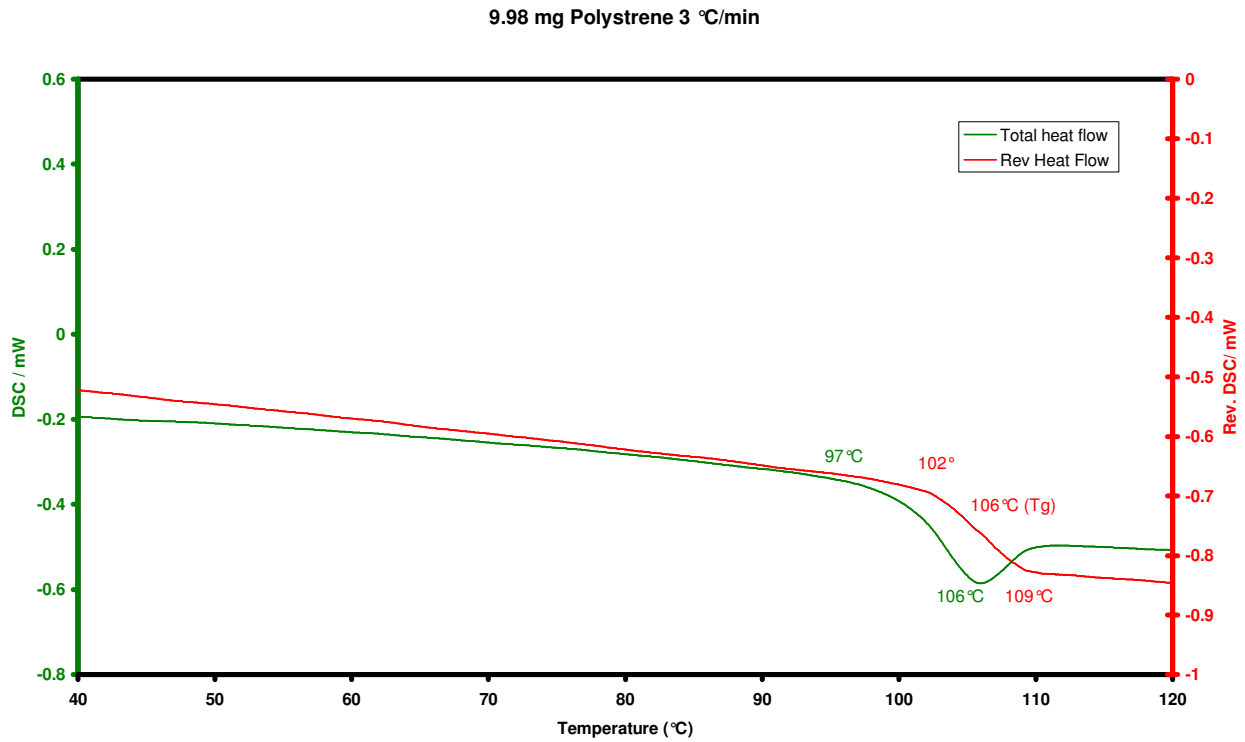
Graph 75: MDSC experiment of polystyrene performed under argon.

MWDTA 100% Polystyrene IH0957

Heating Rate (℃/min)	10
Final Temp (℃)	120
Percentage of active sample	100%
4 stub tuning status	Manual
Sample weight (mg)	70
Iris position (mm)	138
Iris (mm)	28 x 15
Cell	HPB
mixture material	N/A
Principle T/C	Reference
Tuning position (mm)	120.5
Comments	Argon 105% Sample flow 0% Alumina sandwich
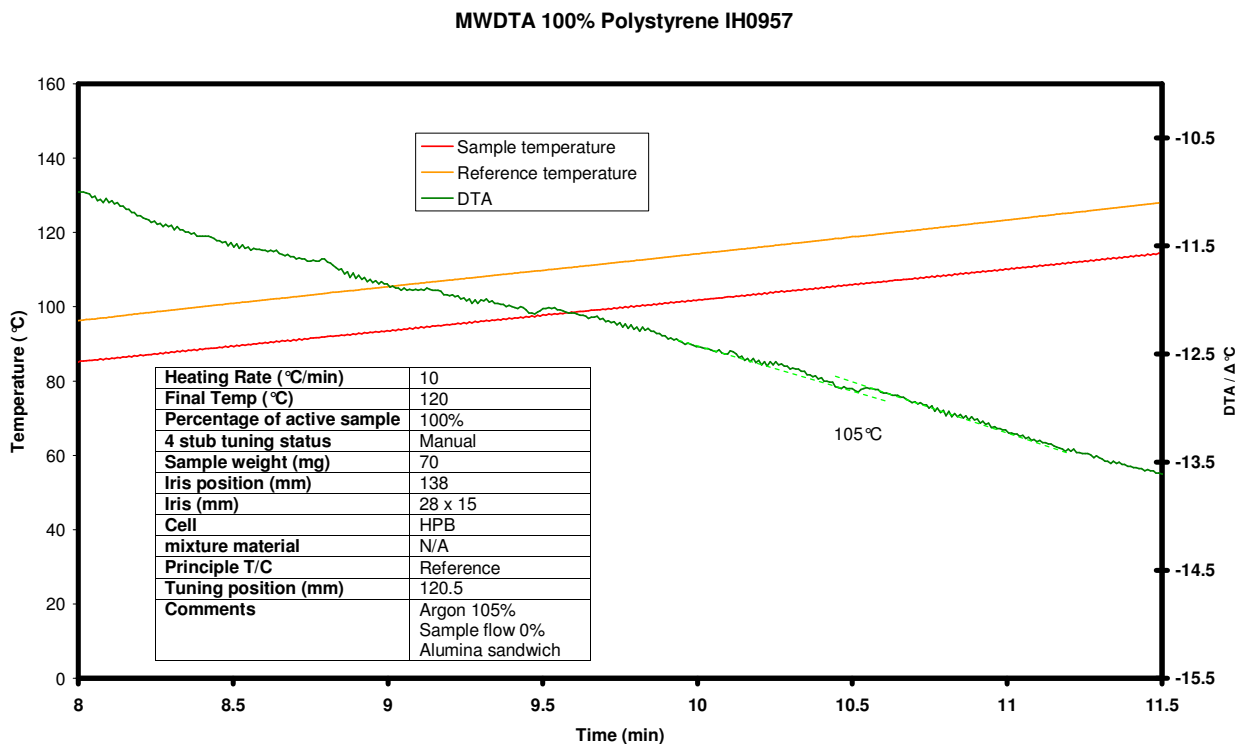
Graph 76: MWDTA experiment of polystyrene performed under argon.

As a glass transition is a very low energy change (second order) with apparently very little dielectric change, the response seen in MWDTA is likely to be due to changes in heat capacity (Cp). This

211

assumption was further investigated using MWTA but the sample did not show any ability to heat purely by dielectric losses and mixing it with a susceptor masked the changes that were observed in the MWDTA trace. Once again the size of the transition is too small to make a definitive definition as the T_g, owing to the response having the same magnitude as possible instrumental noise, although there is a permanent change in the microwave differential baseline at 105 °C.

The determination of glass transition temperatures showed the limits of the instrumental temperature measurement capabilities, as a typical polystyrene transition is around 0.1-0.2 Δ°C [47] and the lower limit of the thermocouple is 0.1 °C. MWDTA did not seem to be successful in identifying glass transition temperatures, therefore for MWTA to be used to determine these types of transitions a more modern and sensitive thermocouple arrangement would need to be adopted.

7.4 Inorganic phase changes and decompositions

A number of inorganic materials are known to undergo changes in their crystal structure (polymorphs) prior to fusion or before they decompose, this process of re-ordering is usually accompanied by a change in energy and is shown in thermal analysis as a sharp endothermic peak as energy is consumed.

The thermal decomposition of samples also is accompanied by a change in energy, which are usually exothermic (oxidation). These decompositions also are associated with changes in mass or more relevantly volume. A reduction in volume in a microwave experiment is believed to have a large effect in the sample's ability to heat under microwaves. Under volumetric heating the combination of both enthalpy and volumetric responses was thought would give clear transitions in the microwave differential trace.

7.4.1 Calcium oxalate monohydrate

The thermal decomposition of calcium oxalate monohydrate ($Ca(COO)_2 \cdot 1H_2O$) has been well studied in the field of thermal analysis as it possesses three distinct and well defined decompositions, which are commonly used to calibrate mass measurements in TGA [48].

As expected the three stages are accompanied with changes in enthalpy. The first, the dehydration takes place in the temperature range of 100–200 °C and gives rise to an endothermic peak on the DTA trace.

The anhydrous material is subjected to another step around 400 °C which is attributed to the formation of an intermediate carbonate before the stable oxide formation. The response seen in this step is dependent on the carrier gas, as the anhydrous oxysalt decomposes to the carbonate via the loss of carbon monoxide. In an oxidising environment the carbon monoxide can disproportionate to carbon dioxide, the formation of which is shown to be exothermic as energy is realised during the formation.

In an inert atmosphere the disproportionation does not occur and so the step is seen as an endothermic peak. The final step to the commonest oxide occurs at high temperatures (around 600 °C) where the carbonate loses carbon dioxide in an endothermic process.

$$CaC_2O_4.H_2O \xrightarrow{\sim 200°C} CaC_2O_4 + H_2O$$
$$CaC_2O_4 \xrightarrow{\sim 400°C} CaCO_3 + CO$$
$$\left(2CO + O_2 \rightarrow 2CO_2\right)$$
$$CaCO_3 \xrightarrow{\sim 600°C} CaO + CO_2$$
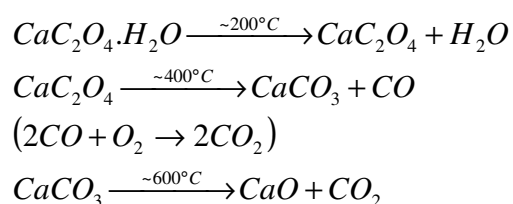
The details of the conventional experiment consisted of testing 25 mg of calcium oxalate monohydrate at a rate of 10 °C/min to 650 °C under flowing argon, then in static air. The decomposition was not taken to the formation of the oxide as the equivalent microwave run had complications reaching the upper temperature at slower heating rates (this was overcome in subsequent experiments detailed later in this section). It was thought that the dehydration step would be accompanied with a small dielectric change. The formation of the carbonate in the second step was not believed to have a noticeable dielectric change as the product formed or released was

not one that was thought to couple to microwaves, although the loss in mass may affect the extent of volumetric heating causing the sample temperature to lag further behind the reference than before the transition.
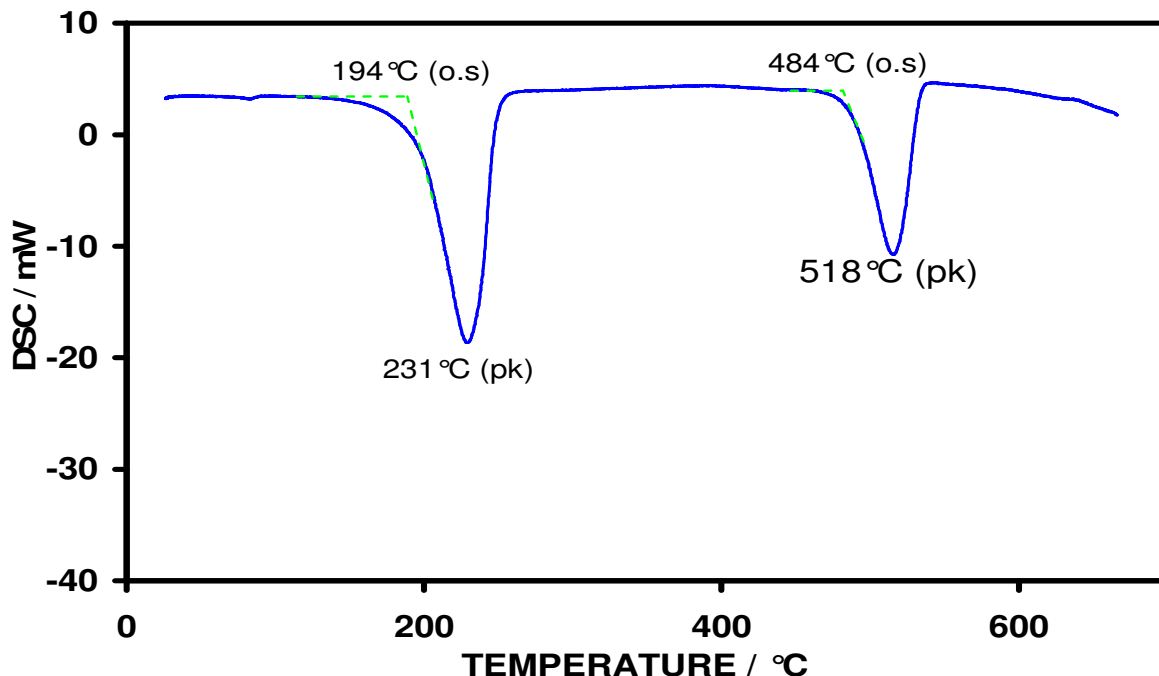
Graph 77: HDSC experiment of calcium oxalate monohydrate performed under argon.

The HDSC showed the dehydration to occur at an extrapolated onset of 194 °C peaking at 231 °C. The carbonate formation appeared to have an onset temperature of 484 °C peaking at 518 °C.
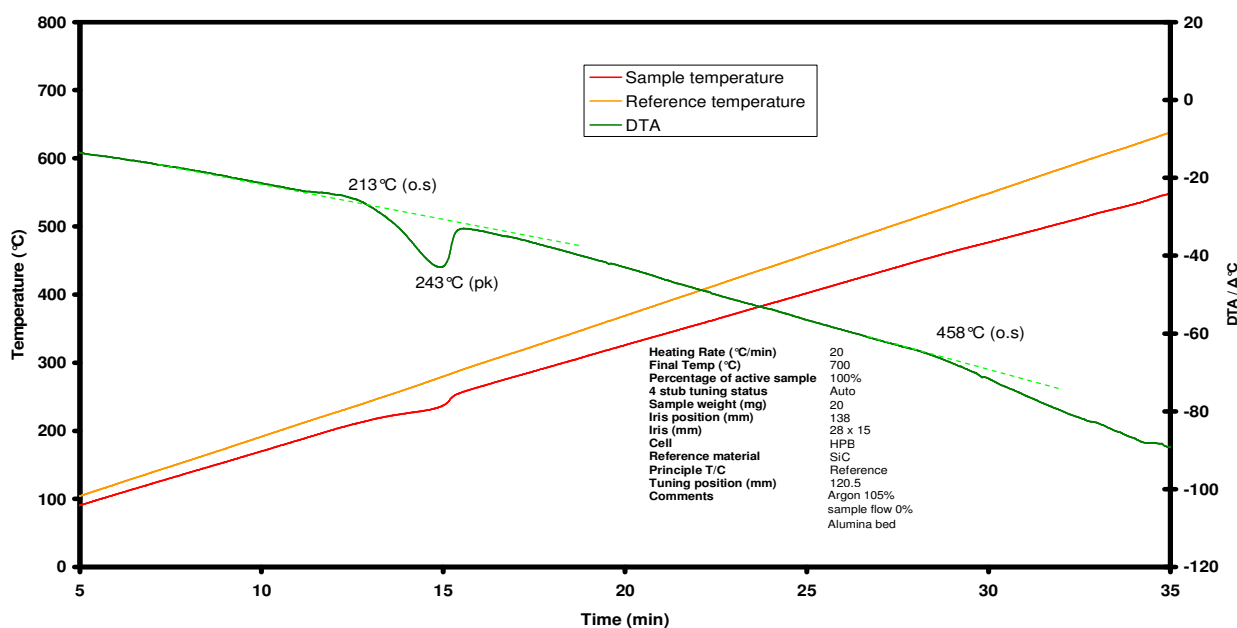
Graph 78: MWDTA experiment of calcium oxalate monohydrate performed under argon.

From the results of the two techniques (Graph 77 and Graph 78) it appeared the dehydration did not occur at the same temperature, with the extrapolated onset occurring around 19 °C later (213 °C) in the microwave experiment. On closer examination of the microwave runs it can be seen the first point of deviation from the baseline is in fact a rise in the differential signal before the onset of the peak. This rise occurs at a temperature of 190 °C, 4 °C earlier than the conventional run, an acceptable variation for a dehydration transition as the temperature of such an event relies greatly on sample preparation.

The rise in the MWDTA trace is attributed to the water of crystallisation being evolved and briefly coupling to applied power, thus increasing the sample temperature before the endothermic nature of the dehydration, accompanied with the loss of the water from the measurement area, overcame the additional heating effect caused by the temporary increase in tan δ.

By extrapolating the pre-transition baseline it can also be seen that the post transition baseline is lower than the before. This indicated the sample is no longer heating as well as it did when it was a hydrate. The DSC trace shows no such change in baseline so it was assumed this was not a change in heat capacity but rather a change in tan δ caused by the loss of a coupling group (water) or volume of the sample.

The second step appears to have much more of a dielectric change which again can be seen by the change in baseline after the transition. The MWDTA shows a fall in the differential signal which never recovers and stays linear until the end of the experiment.

This is believed to be a dielectric change caused by the loss of volume aided by the endothermic nature of the transition. Again the microwave and conventional transition temperatures did not appear to be in good agreement with each other although when the onset in the conventional trace was expanded it showed the first point of deviation from the baseline to occur at around 460 °C, a close correlation with the microwave experiment.

This finding showed that the changes in transition temperatures seen between the conventional and microwave techniques may not always be attributive to the so called "microwave effect", seen in materials such as water but instead the possibility of microwave thermal analysis detecting

transitions by the first point of change from the baseline. Conventional thermal analysis tends to use the extrapolated onset to record transitions as it gives a more repeatable result but the true onset can take place several degrees before the extrapolated point. The true onset is dependent on several factors such as thermal conductivity of the sample, the cell and the scale of the transition curve before taking the reading. This allows the proposal that microwave thermal analysis transitions occur at the first point of change (explained by the reduction of the time needed for the whole of the sample to reach the transition temperature) to be more feasible.

As described earlier, in the microwave experiment, difficulties were encountered in reaching the third transition in MWDTA mode at a heating rate of 10 °C/min. This was a problem seen in the development of the instrument during experiments where the sample has a low tan δ. In situations of this type, the combination of heat losses from the outer wall of the cell and the heat sink created by the sample temperature, lowering the reference temperature (due to the inward thermal gradient) resulting in increasing the applied power required for the reference temperature to reach the set-point. This causes the instrument to reach its upper applied power limit before the completion of the run. It was thought that if the time factor was removed from the run set-up then heat losses would be greatly reduced and the experiment would be able to reach the upper temperature.

The experiments consisted of testing 40 mg of the sample in the HPB cell under argon and applying a constant power of 165 W (55 %) then monitoring the differential, sample, and reference temperatures over time till the sample temperature reached 650 °C.

Constant power 165 W (55%) Calcium oxalate IH0977

Heating Rate (°C/min)	Sample dependant
Final Temp (°C)	Sample dependant
Percentage of active sample	100%
4 stub tuning status	Manual
Sample weight (mg)	40
Iris position (mm)	138
Iris (mm)	28 x 15
Tuning position (mm)	120.5
Comments	Argon 105%
	Sample flow 0%
	Alumina sandwich
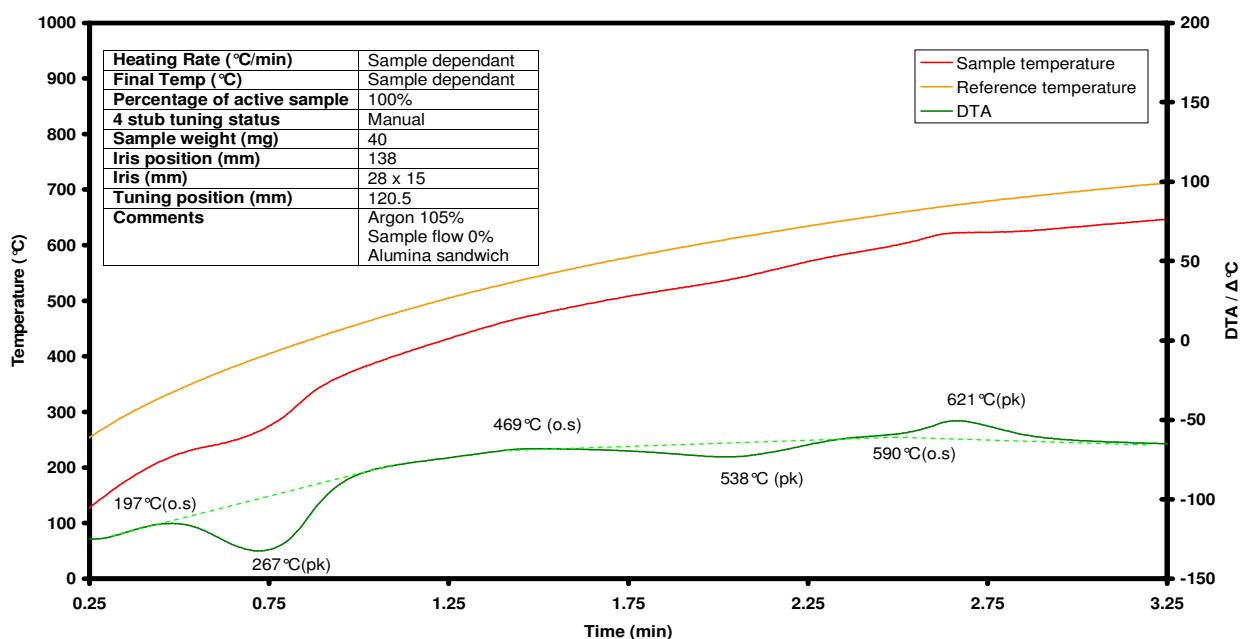
Graph 79: constant power (55 %) MWDTA experiment of calcium oxalate monohydrate performed under argon.

Unfortunately as there is no linear control over the experiment it meant that fitting an underlying baseline was difficult as the rate of heating changes as the heat losses become more evident as temperature increases. The advantage of this technique is the final temperature (not previously obtainable when testing this material), could be reached using only 58 % of the power need in the dynamic experiments. The experiment also showed an overall heat rate of 153 °C/min meaning the experiment took just under 3 ½ minutes, nearly 60 minutes less than the linear run.

The transition temperatures seen in both the linear heating and constant power microwave experiments showed a correlation with each other, the discrepancies most likely originating from the differences in heating rates. The broadness of the second transition was also of interest. In the linear heating run it seemed that there was a dielectric change as it appeared that the MWDTA trace did not return to the pre-transition value, the constant power run showed there was a recovery although it was very broad (for this assumption to be true a linear baseline had to be fitted to a non-linear trace). The broadness of the carbonate decomposition is characteristic of carbonate decompositions [28] and so showed a good example of problems that could be faced in MWDTA experiments. The constant power experiment also supported the theory that carbonate decomposition would have little or no dielectric change.

Both the conventional and microwave experiments were repeated under static air to determine if when disproportionation occurred, it could be monitored by MWDTA.
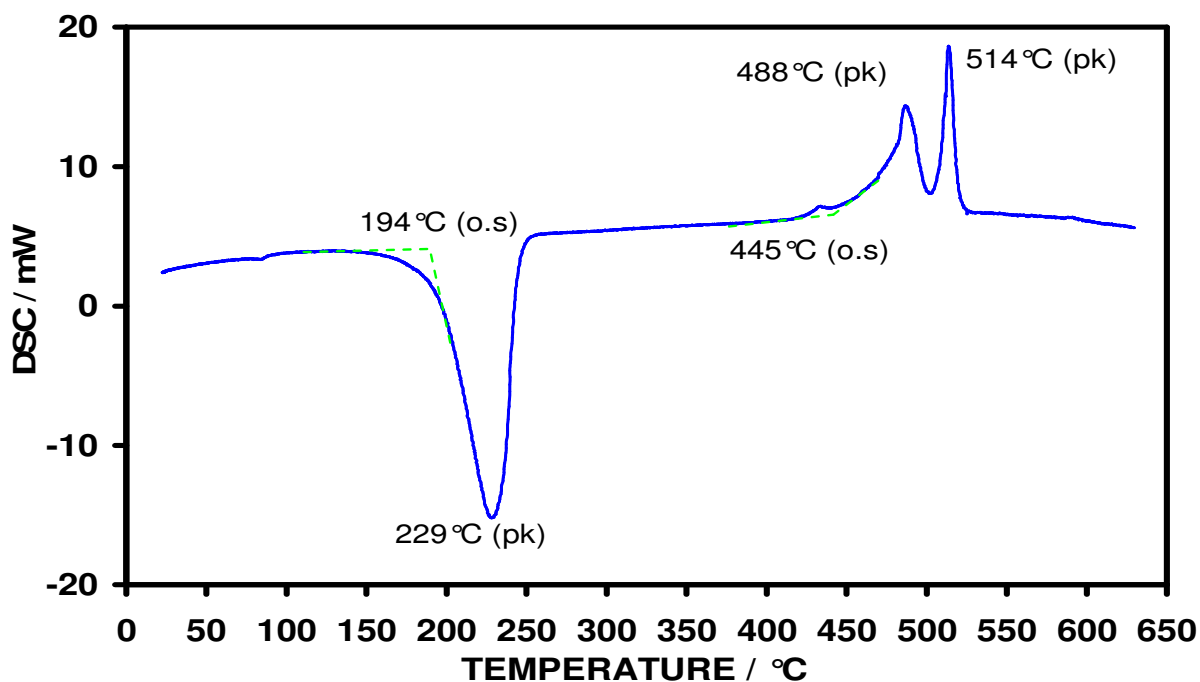
Graph 80: HDSC experiment of calcium oxalate monohydrate performed under static air.

Again there appeared to be a correlation between the two techniques and as before even though the extrapolated onset temperatures were different. The first point of deviation from the baseline was shown to be at 420 °C in the conventional experiment and 414 °C in the microwave run.

MWDTA 100% calcium oxalate IH0818
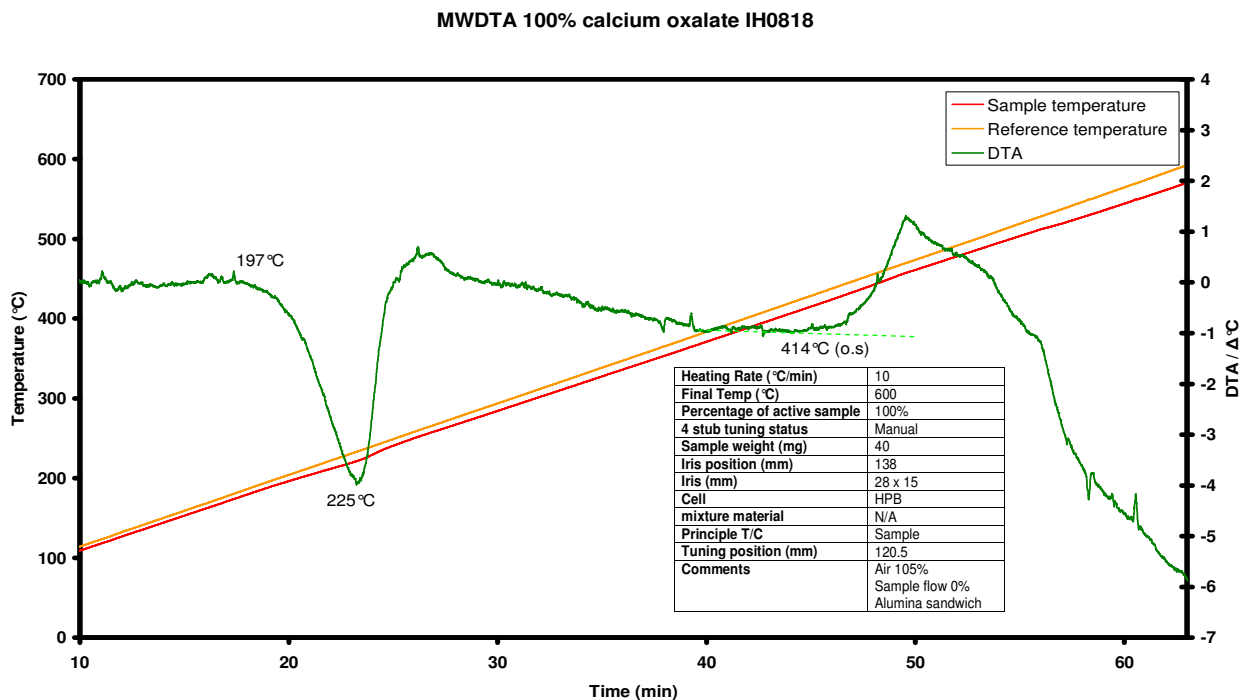
Graph 81: MWDTA experiment of calcium oxalate monohydrate performed under static air.

The results above from this set of experiments again showed MWDTA monitoring the first point of change to be a probable assumption.

The decomposition of the carbonate and subsequent disproportionation was shown in both the constant power and linear heating techniques to have a positive response in the DTA trace. The negative change in baseline in the MWDTA trace is probably due to the loss of sample from the measurement area caused by the evolution of hot gases during exothermic transition.

The experiment also showed that the sample chamber designed for MWDTA was sufficient to exclude air from the sample when required.

Con. power 55% (165 W) Calcium oxalate IH1002

Heating Rate (°C/min)	Sample dependant
Final Temp (°C)	Sample dependant
Percentage of active sample	100%
4 stub tuning status	Manual
Sample weight (mg)	20
Iris position (mm)	138
Iris (mm)	28 x 15
Tuning position (mm)	120.5
Comments	Air 105% Sample flow 0% Alumina sandwich
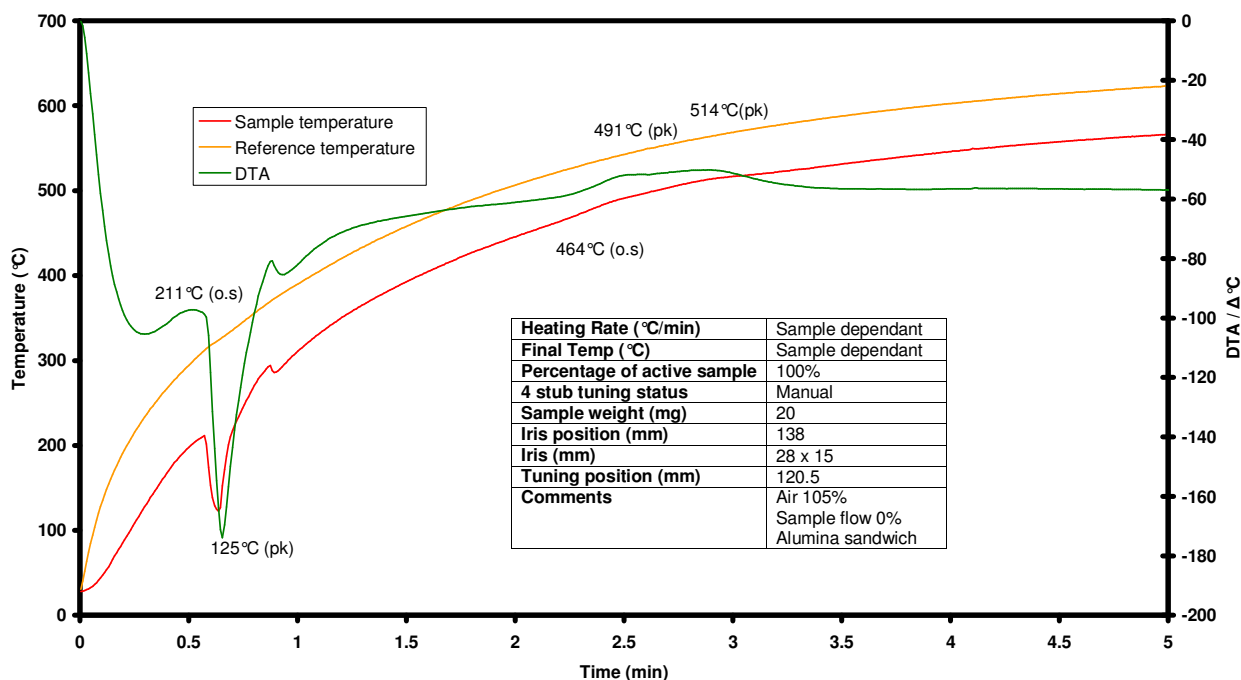
Graph 82: constant power (55 %) MWDTA experiment of calcium oxalate monohydrate performed under static air.

During the constant power runs (Graph 82) a slight problem with the loss of sample during decomposition using this material was observed, meaning it could not reach the final transition temperature under the same experimental conditions as the inert run, although the same problem was not observed in most other exothermic transitions, arising from increased coupling.

7.4.2 Copper oxalate hemihydrate

The thermal decomposition of copper oxalate hemihydrate has been thoroughly discussed in previous chapters owing to its varying decomposition routes under different atmospheric conditions. It is well known that the residue will either mainly be composed of powdered copper metal or copper oxide (both materials which couple strongly with microwaves).

Conventional measurements were taken using two instruments, the Stanton Redcroft DSC1500 and MettlerToledo TGA/SDTA851e, in quartz and alumina crucibles respectively. Again the heating rate was set to 10 °C/min. In the first instance the experiments were performed in an inert atmosphere (argon).
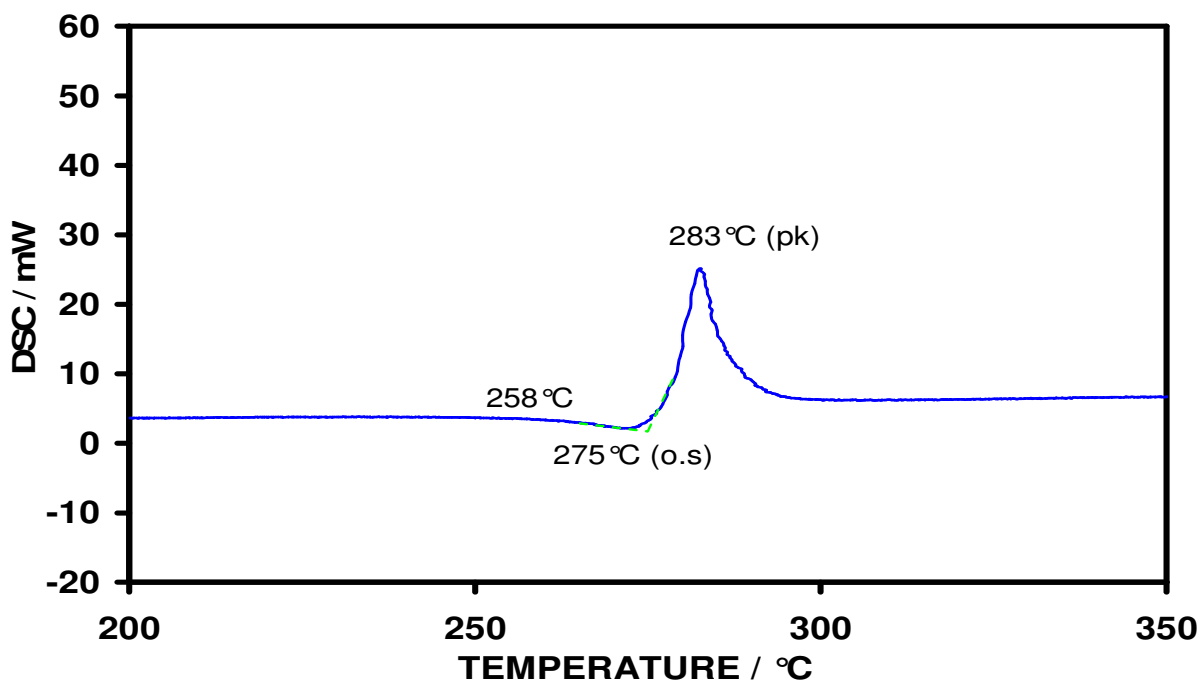
Graph 83: HDSC experiment of copper oxalate hemihydrate performed under argon.

DTA-TGA 17.8331 mg Copper oxalate
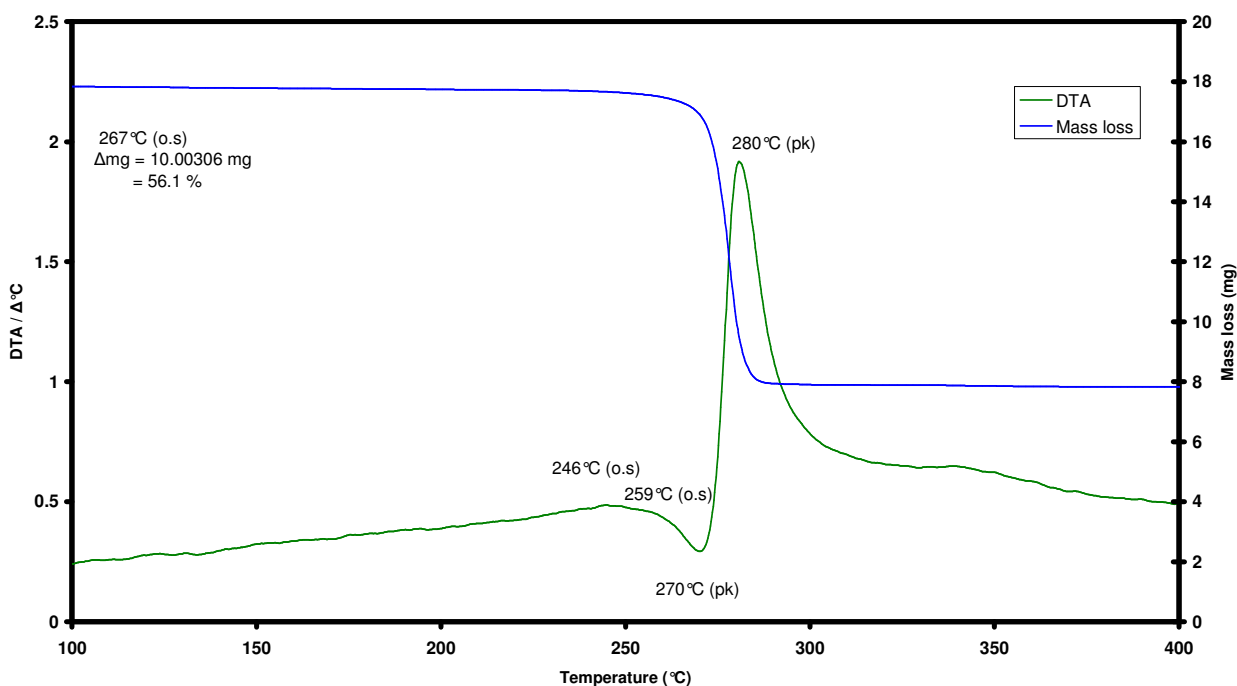
Graph 84: DTA-TGA experiment of copper oxalate hemihydrate performed under argon.

The results showed a correlation between instruments with the onset of the exotherm (loss of carbon dioxide) occurring between 270–275 °C. The variation of pre-transition endothermic response is

thought to be due to differences in the sensitivity of the instruments, although there was a correlation between the endothermic onset seen in the TGA and the HDSC trace between 258–259 °C.

The added information of the TGA curve strongly indicated that under inert conditions the product librated from the sample was carbon dioxide ($2CO_2 = 54.8\%$) and therefore the residue was thought to be Cu metal powder.

The microwave experiments were performed using 20 mg of sample under Argon at a heating rate of 10 °C/min also.

MWDTA 100% copper oxalate IH0836

Heating Rate (°C/min)	10
Final Temp (°C)	400
Percentage of active sample	100%
4 stub tuning status	Manual
Sample weight (mg)	20
Iris position (mm)	138
Iris (mm)	28 x 15
Cell	HPB hood
Reference material	SiC
Principle T/C	Reference
Tuning position (mm)	120.5
Comments	100% Argon 105 ml/min 33ml/min
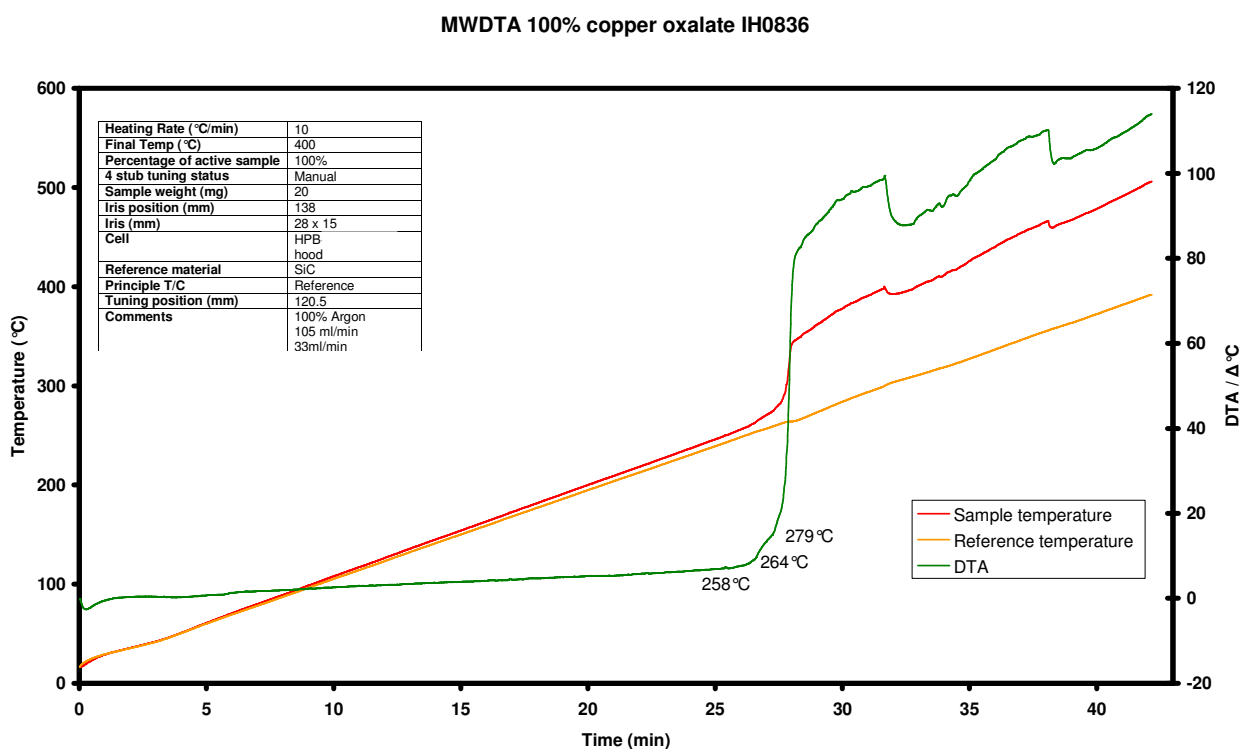
Graph 85: MWDTA experiment of copper oxalate hemihydrate performed under argon.

The results showed the first deviation from the differential baseline to occur at 258 °C and the extrapolated onset at 271 °C. The temperature rise attributed to the change in dielectric loss was not smooth, shown in the green trace as shoulders in the transition step at the temperatures 264 °C and 279°C. It is not known what occurs at 264 °C and is possibly an artefact. The 279 °C transition occurs at the same temperature as the peak maximum of the copper metal powder formation, the point at which the main enthalpy effect had ended. It is at this point the full dielectric change could

be witnessed as in previous experiments. The experiment showed copper metal particulates had an increase in tan δ upon formation which caused the differential temperature to rise sharply by 60 °C the experiment was also an example of a system that had an exothermic transition and also dielectric change, not seen in previous experiments. The system indicated that the full effect of changes in the materials ability to couple with microwave energy did not occur until all enthalpy effects had ceased regardless of whether they were exothermic or endothermic.

The experiment was repeated under an oxidising atmosphere. As before the same instruments were used and the heating rate was set to 10 °C/min. Several literature sources show the decomposition to take place via different routes under static air [49, 50]. The literature indicated the residue would mainly consist of a mixture of copper oxides (a known microwave susceptor). The HDSC trace showed the decomposition did not occur in a single stage and was at a slightly elevated temperature than the equivalent experiment under inert conditions.
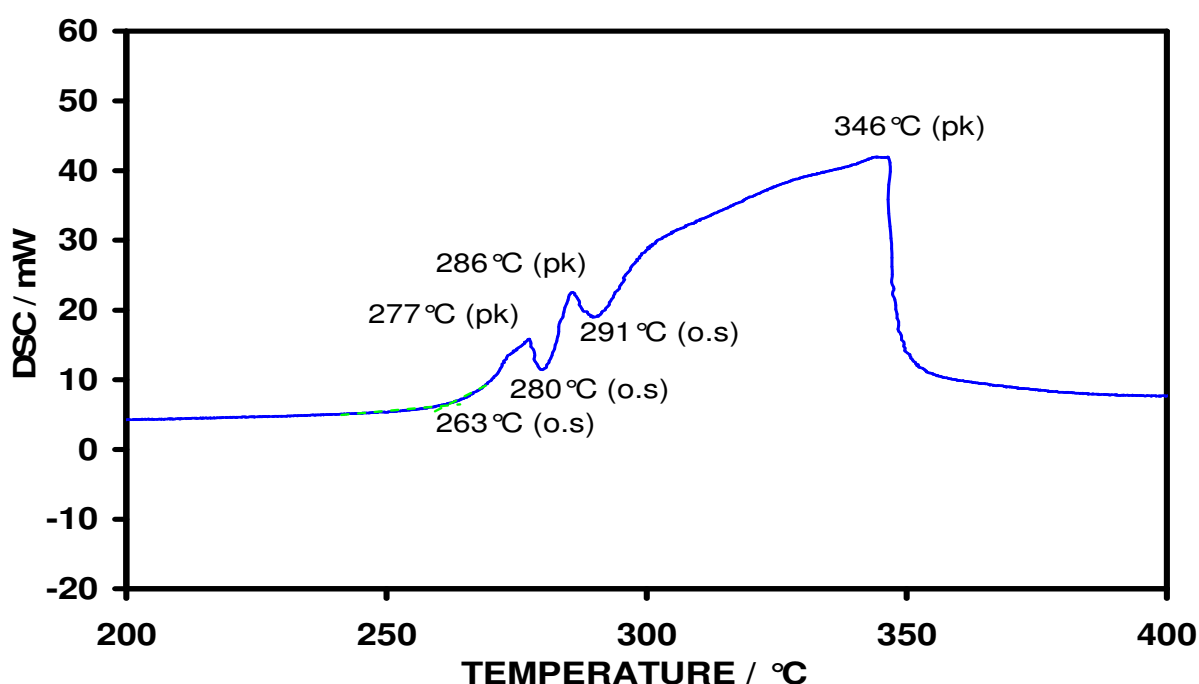
Graph 86: MWDTA experiment of copper oxalate hemihydrate performed under air.

From the HDSC trace it was concluded that the self generated inert atmosphere facilitated the formation of copper metal in the first instance by driving oxygen out until the carrier gas diffused back giving rise to the oxide formation. Evidence of this mechanism can be found in literature [28] and also the mass gain seen in the TGA traces soon after the decomposition.

DTA-TGA 19.0365 mg Copper oxalate under air
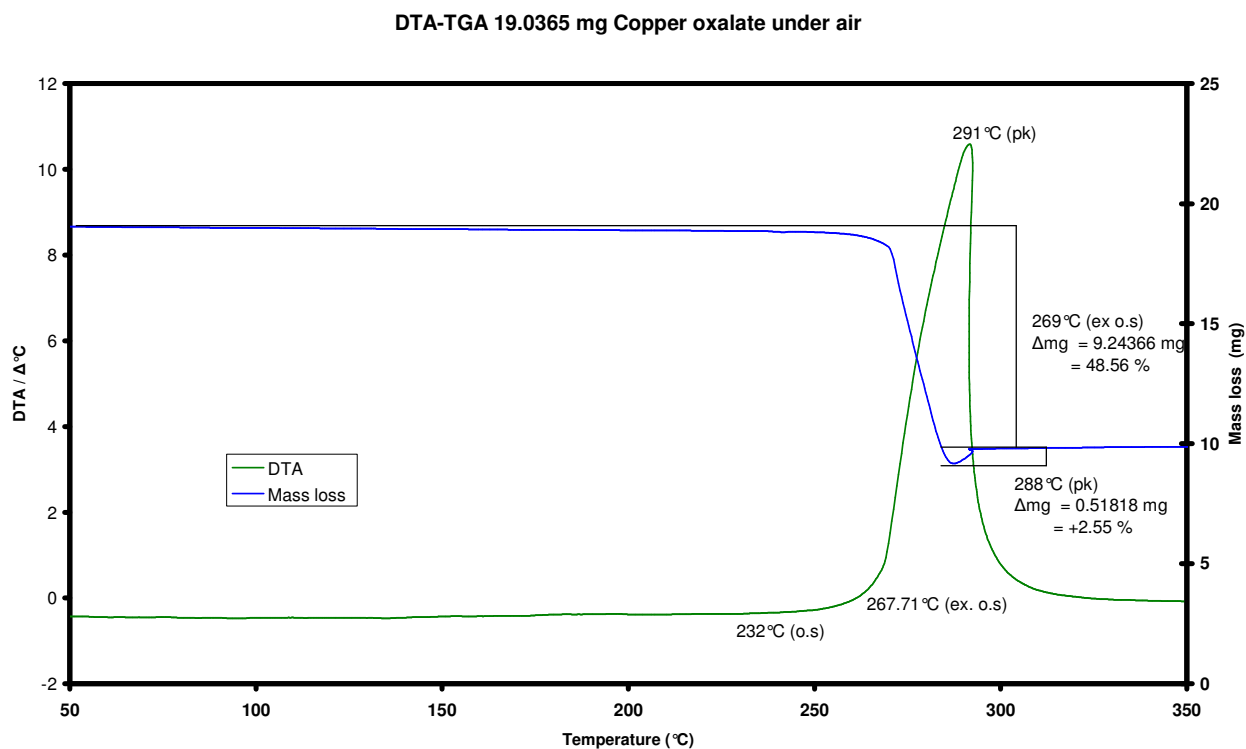
Graph 87: MWDTA experiment of copper oxalate hemihydrate performed under air.

The changes in coupling attributed to the copper metal powder (around 263 °C) and copper oxide (around 280-290 °C) formation should be illustrated in the MWDTA experiment as two distinct steps in the differential trace. As in previous experiments 20 mg of sample was tested at 10 °C/min. A mixed gas consisting of 20 % oxygen 80 % argon was used in order to try and retain some insulation properties of the chamber and reduce thermal gradients to the outer walls.

MWDTA 100% Copper oxalate IH0832
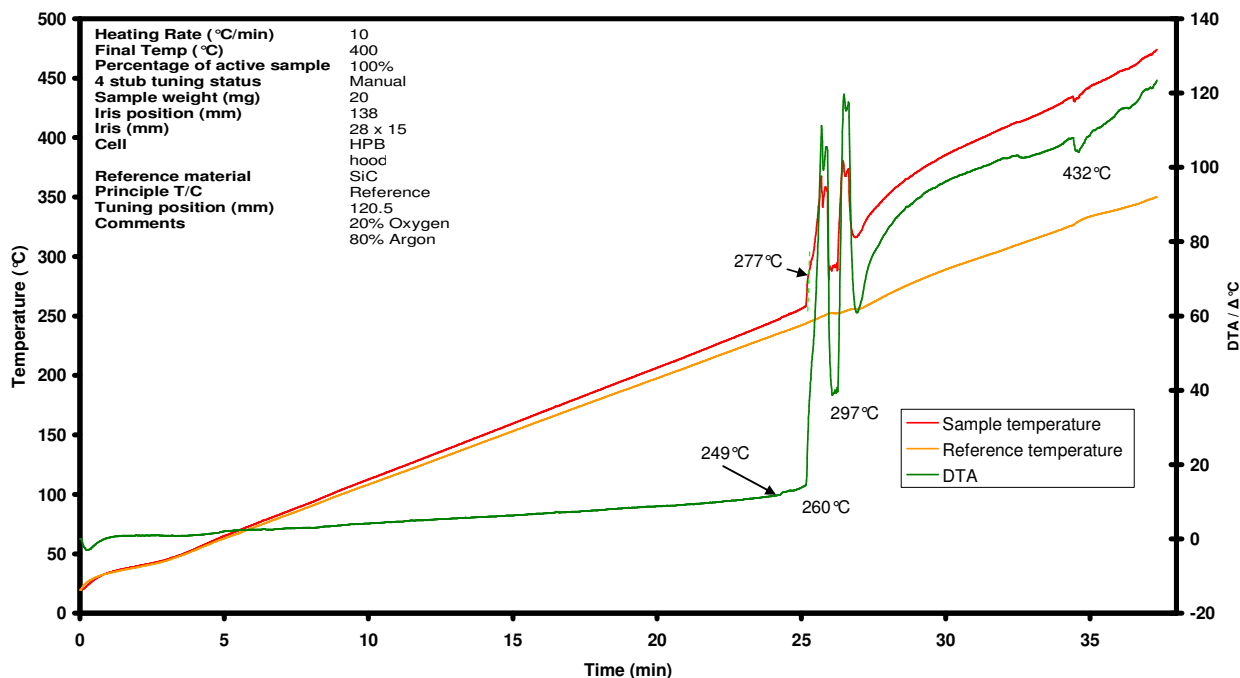
Graph 88: MWDTA experiment of copper oxalate hemihydrate performed under a mixed gas of 20 % oxygen: 80 % argon.

On analysis of the trace it could be seen that there were two distinct steps as expected, the onset of the first transition occurred at 249 °C, correlating to the first deviation from the baseline in conventional experiments. The extrapolated onset of the transition occurs at 260 °C correlating to the HDSC experiments. Once again the enthalpy of the transition can be seen by the change in slope at 277 °C (the peak temperature of the copper metal powder formation). Unfortunately the response and resultant increased heating rate caused the instrument to overshoot the set-point and therefore the full extent of second transition was masked, indicated by the fall in reference temperature (orange trace) and therefore applied power (not shown), as control was attempted to be restored. The MWDTA experiments showed the second transition to be several degrees later than the conventional experiments, but it did show the increase in heating which arose from the greater coupling of copper oxide to the applied power.

The reason for the sharp falls in differential temperature could not be fully explained, although it was thought that is was due to either heat losses to the surroundings superimposed on temperature alteration from PID control, or the formation of a strongly coupling species (CuO, copper metal powder) which altered the optimum tuning of the instrument. Copper oxide absorbs microwave radiation as well as (or possibly better than) SiC. In MWDTA the formation of a new coupling

species which was not turned in the initial instrument set-up has the potential of increasing the reflections and/or having a greater affinity for the applied wave then the reference therefore causing the reference temperature to fall resulting in a drop in the differential temperature.

7.4.3. Potassium methyl sulphate

The thermal decomposition of potassium methyl sulphate is not well documented in literature. It is thought the compound undergoes a phase change, a fusion then a closely followed decomposition. Conventional measurements were again taken on both the HDSC 1500 and the TGA/SDTA851e. In order to see all the transitions clearly the sample mass was increased to 30 mg in the HDSC experiment, but to avoid contamination of the TGA head (due to the sample creeping) the sample remained at the routine 20 mg and a 50 mg lid was put in place. Again the heating rate remained at 10 °C/min and all experiments were performed under inert atmospheres (argon).
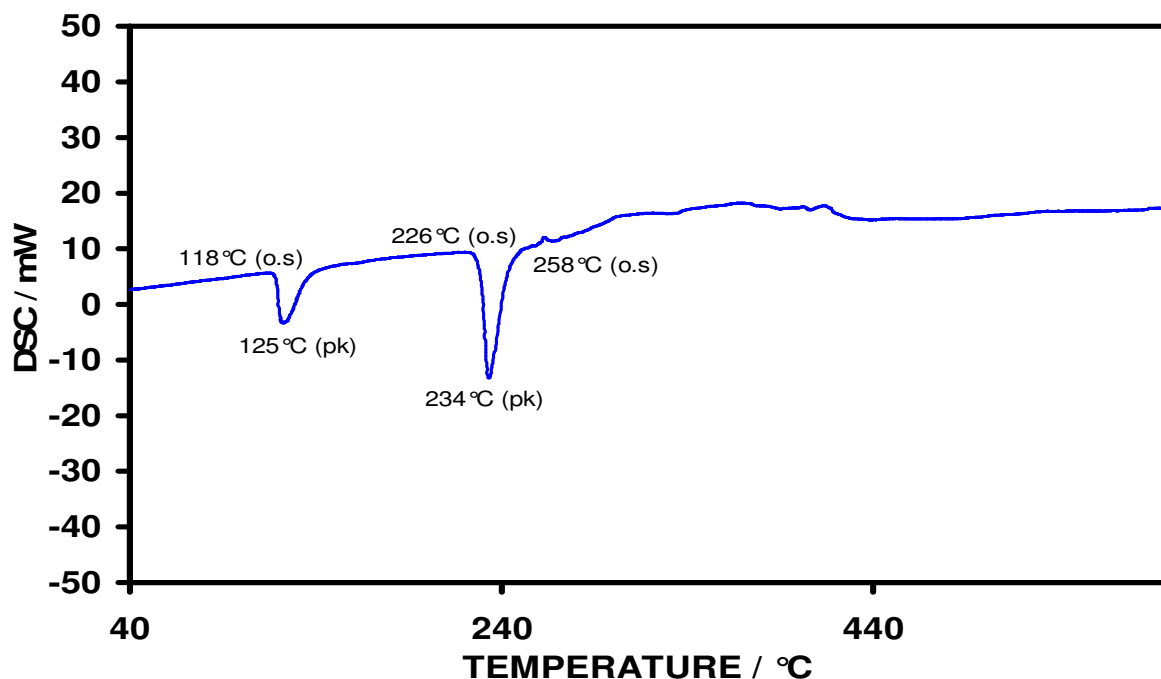
Graph 89: HDSC experiment of potassium methyl sulphate performed under argon.

The HDSC trace showed three transitions, and in order to further understand the processes, the TGA trace was also studied.

DTA-TGA 19.02 mg Potassium methyl sulphate
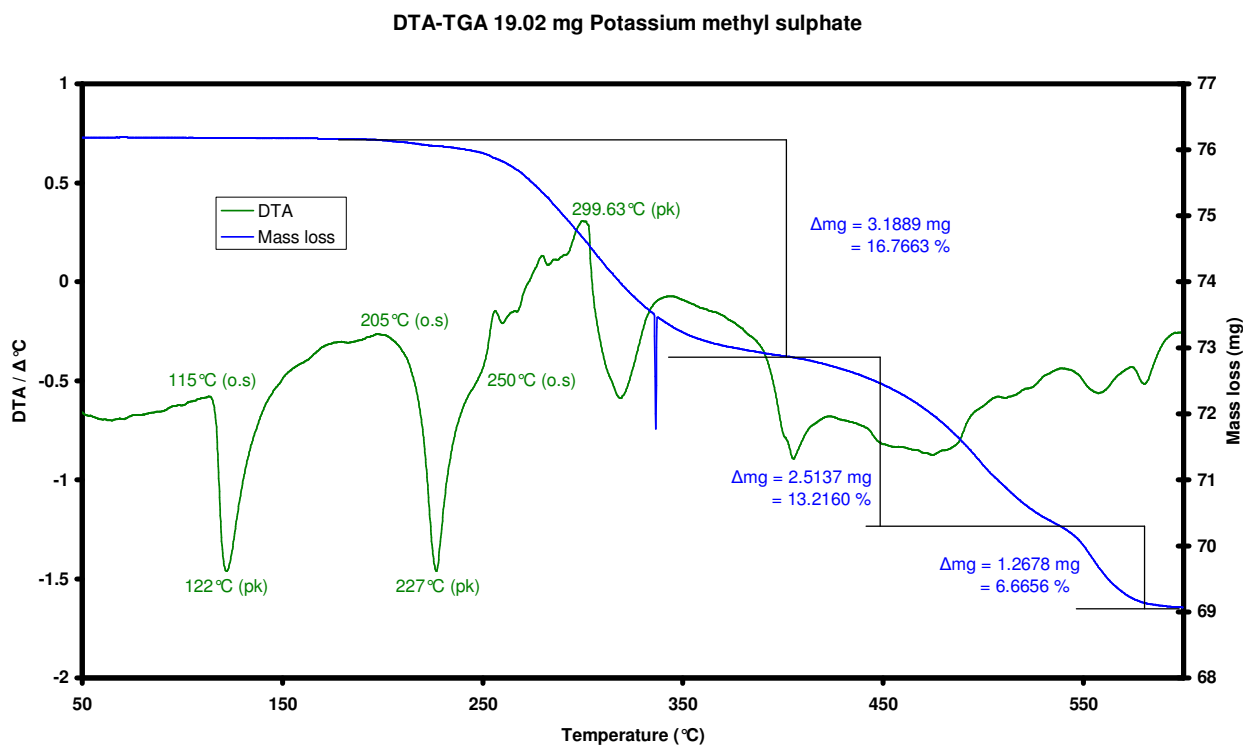
Graph 90: DTA-TGA experiment of potassium methyl sulphate performed under argon.

In the TGA experiment (Graph 90) no weight loss was apparent during the first transition indicating that it was likely to be a solid-solid phase change or a fusion. The transition temperature was in the region of a possible dehydration but the lack of weight loss supported the theory of the phase change. The mass losses appeared to occur close to/during the second transition were suspected to be the fusion of the material. It was believed that during the fusion the sample also begins to decompose. The decomposition appeared to be exothermic in both the HDSC and the TGA trace and quite vigorous. The correlation between the two conventional techniques was generally good with the extrapolated onset of the solid-solid phase change occurring between 115-118°C, and the fusion between 205–226 °C. The onset of the exothermic decomposition appeared to occur between 250–258 °C.

MWDTA   100% potassium methyl sulfate IH0797

Heating Rate (°C/min)	10
Final Temp (°C)	420
Percentage of active sample	100%
4 stub tuning status	Manual
Sample weight (mg)	40
Iris position (mm)	138
Iris (mm)	28 x 15
Cell	HPB-EGA with EGA hood
Reference material	SiC
Principle T/C	Reference
Tuning position (mm)	120.5
Comments	Argon 105 ml/min M/S Torr
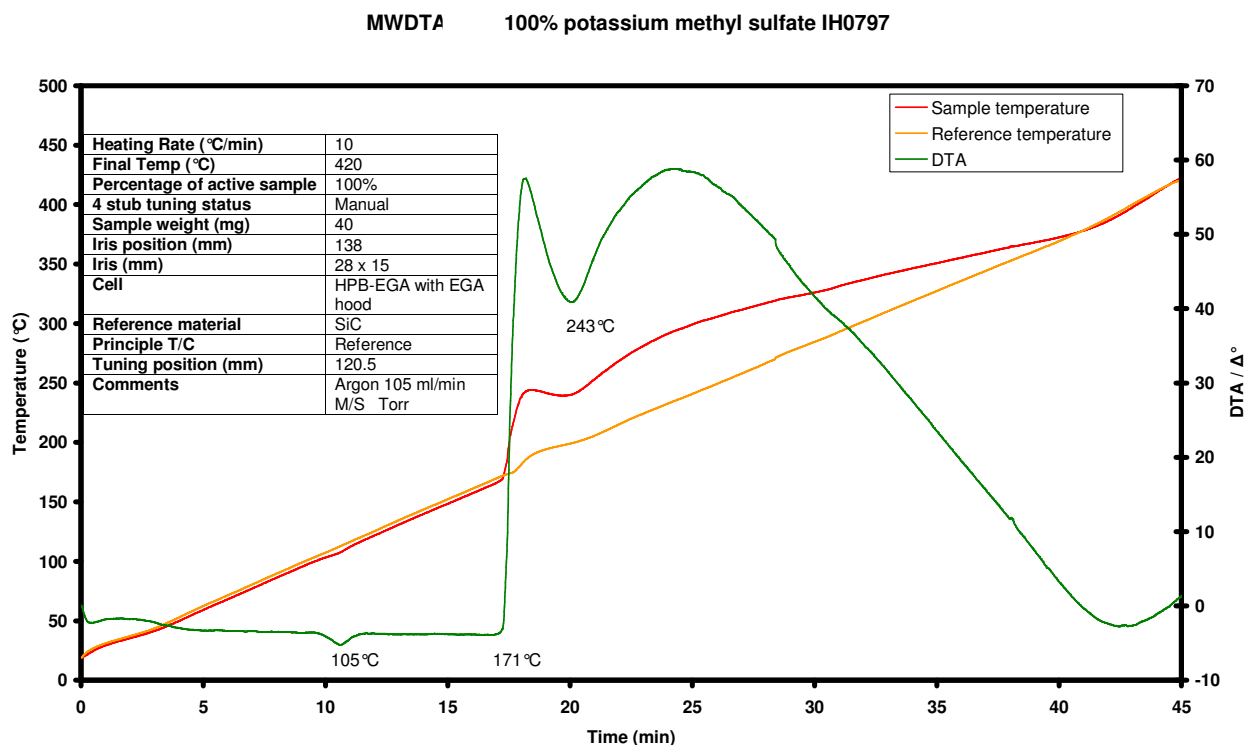
Graph 91: MWDTA experiment of potassium methyl sulphate performed under argon.

There appeared to be poor correlation between transition temperatures in the conventional runs when compared to the microwave experiments. The MWDTA traces showed the phase changes to occur several degrees earlier than the conventional traces. Although this lowering of transition temperature is seen in many MWDTA experiments, it can usually be related to a feature in a conventional experiment. This was not easily the case with potassium methyl sulphate.

The first transition seen in the microwave experiment (Graph 91) shows no dielectric change indicating an enthalpy only transition not usually seen for a solid-solid phase transition in MWDTA experiments, although any changes in the baseline could have been overshadowed by the magnitude of the following transition. The second transition is seen around 171 °C and is shown as a large rise in differential temperature due to a change in tan δ and is believed to be attributed to the fusion of the material. The discrepancy in the transition temperature is again believed to be due to the microwave responding to the first point of change of the material.

Unfortunately the magnitude of the response reduced the resolution of the experiment. At the maximum of the 171 °C transition the sample temperature reached 239 °C (the peak temperature of the HDSC experiments), at this point the differential temperature appears to dramatically fall

indicating that the phase change has an associated change in tan δ but the product has possibly a low dielectric loss, although as the next transition is quickly reached the overall effect could not be observed. It is believed the analyte has changed from the starting material to a species with less dielectric loss. The final transition observed in the MWDTA trace is the temperature rise at around 243 °C thought to be a result of the exothermic decomposition of the material, closely followed by a dramatic fall in the differential temperature resulting from the loss of material from the sample section, producing a residue which heated purely by conduction from the reference.

A reheat of the residue showed no transitions as expected for a decomposed material as the material had fundamentally changed.

MWDTA 100% Potassium methyl sulfate 2nd Heat

Heating Rate (°C/min)	10
Final Temp (°C)	550
Percentage of active sample	100%
4 stub tuning status	Manual
Sample weight (mg)	40
Iris position (mm)	138
Iris (mm)	28 x 15
Cell	HPB-EGA
Reference material	SiC
Principle T/C	Reference
Tuning position (mm)	120.5
Comments	Argon 80 ml/min
	Vac on
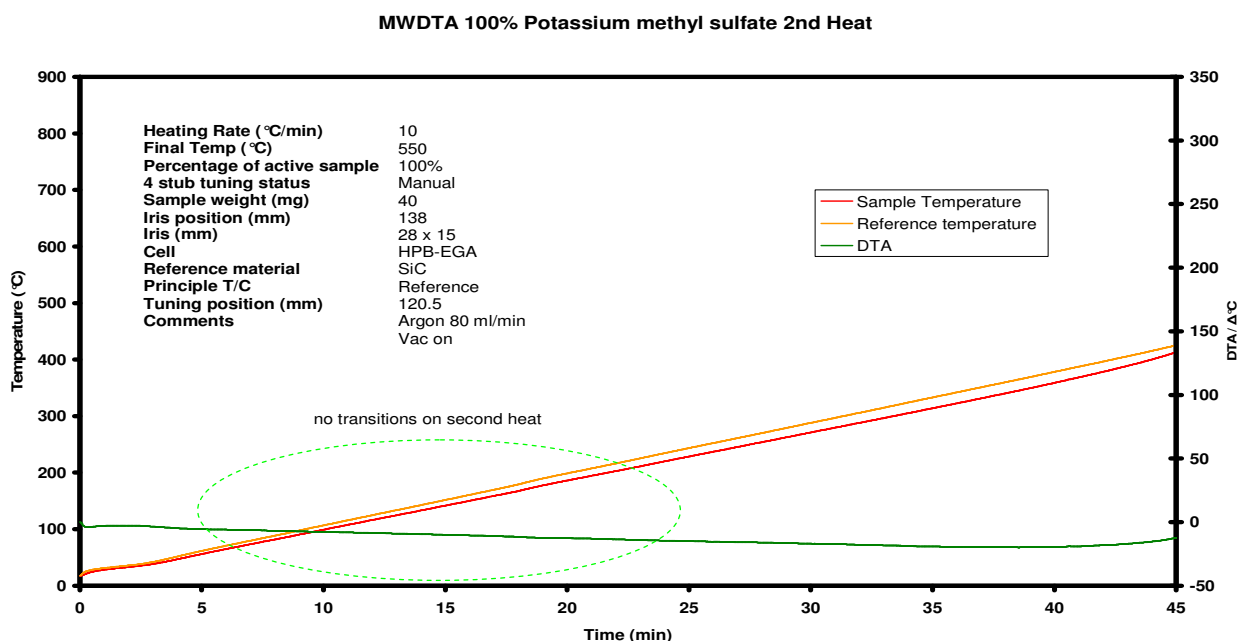
Graph 92: MWDTA experiment of potassium methyl sulphate second heat performed under argon.

To further understand the decomposition of the material and in order to understand the causes of the responses seen in the MWDTA trace the weight losses obtained in TGA experiments were studied.

The decomposition appeared to take place over 3 stages:

1. 16.77 %   @ 201 °C
2. 13.22 %   @ 403 °C
3. 6.67 %   @ 539 °C

$$2KCH_3S0_{4(S)} \rightarrow K_2SO_{4(S)} + (C_2H_6 + H_2O)_{(V)} \qquad = 16.77\ \%$$
$$2K_2SO_{4(S)} \rightarrow 2K_2O_{2(S)} + (2SO_2)_{(V)} \qquad = 19.89\ \%$$
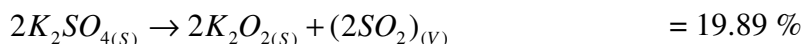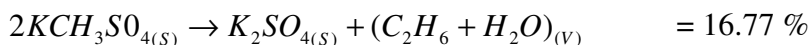
From the mass losses it was believed that the decomposition evolved ethane (which disproportionated to methane in some cases) and water from the material leaving a residue of potassium sulphate. The second higher temperature decomposition evolved sulphur dioxide leaving potassium peroxide. The similarity of peroxides and oxides may have explained the loss of coupling as previous experiments have shown some metal oxides (calcium oxide) tend to have poor dielectric losses.

7.4.4 Tungstates

It was believed the study of alkali tungstates had the potential of giving a further insight into the possible trends that may be exhibited when using MWDTA. A selection of mono tungstates were chosen with varying cation sizes. From the literature [51] it can be seen that as the cation changed the lattice structure also changed. Lithium, sodium and potassium tungstates were chosen, with rhombohedral, cubic, and monoclinic structures respectively.

All of the starting materials conformed to the same formula of X_2WO_4. It was therefore thought that if microwave heating was dependent on the lattice then the differences in coupling ability would be expressed by changes in the magnitude of the response observed at solid-solid transitions.

Tungstates were chosen since their crystalline structure is always imperfect. Materials which contain impurities such as vacant lattice sites, interstitial atoms or exhibit dislocations can directly affect the microwave heating rate. Even though the number of these defects is small they can decrease the energy gap between conduction bands and valence bands and increase electrical conductivity [52].

7.4.4.1 Lithium tungstate

Lithium tungstate has the smallest cation of the tested tungstates. It was reported to be a poor ionic conductor [53] which was thought would affect the extent to which microwaves would heat the material and in turn the response of the transition to the applied power.

It is discussed in literature that lithium tungstate undergoes a solid-solid phase change prior to the melt. Unfortunately the literature did not agree on the melting temperature, therefore the melting point could lie between 730 °C [53] and 1128 °C [51]. The transition temperatures of this specific

material were obtained by testing 25.49 mg of the sample on the HDSC at a rate of 10 °C/min under argon.
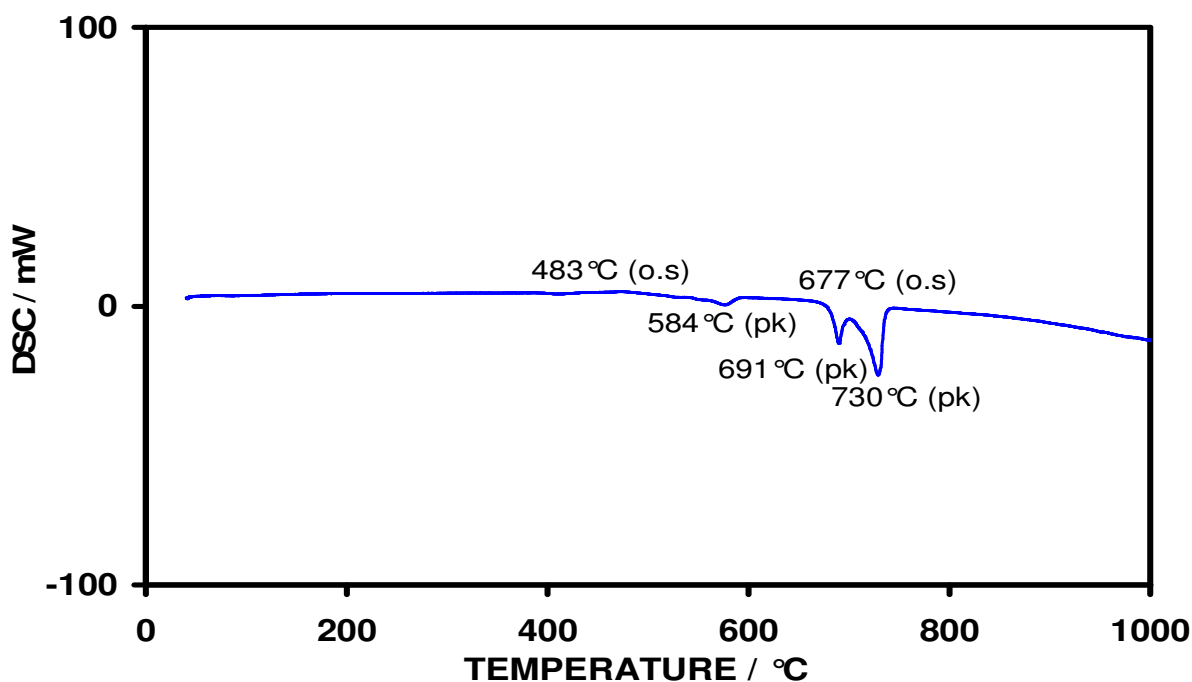
Graph 93: HDSC experiment of lithium tungstate performed under argon.

The result showed three transitions. The first transition at around 483 °C (extrapolated onset) was very weak and is thought to be due to possible dehydration of the sample. Although the sample is stated as being in the anhydrous form, lithium compounds are known to be hygroscopic in nature therefore may have become hydrated to some extent during storage. Yahaya *et al.* [54] discusses the same situation and proposed (using evidence from XRD patterns and TGA measurements) the anhydrous form was a product of the dehydration of the hydrated form at high temperatures (above 470 °C) and therefore the experiment proceeded by:-

$$7Li_2WO_4.4H_2O \rightarrow 5Li_2WO_4 + Li_2W_2O_7 + 2LiOH.H_2O + H_2O$$
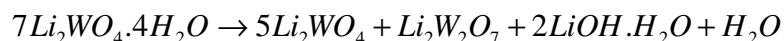
It has also been discussed in Nagasaki *et al.* [55] that after a detailed XRD study pure Li_2WO_4 has no phase transition before the melt, and the phase transitions seen in thermal studies arise from a eutectic being formed between Li_2WO_4 and $Li_2W_2O_7$ further strengthening the route posed by Yahaya *et al.*[54]. Nagaski *et al.* also state that a phase change from Li_2WO_4 (I) to Li_2WO_4 (II) does exist although it is thought to be very slow.

The second transition at around 677 °C (extrapolated onset) is believed to be a solid–solid phase transition closely followed by the onset of the melt at 730 °C (peak minimum).

The MWDTA experiment experienced several problems with resolution at the standard sample size (20 mg) therefore the sample size was reduced to 5 mg. Experimental conditions were the same with the heating rate remaining at 10 °C/min under argon.

MWDTA 100% Lithium Tungstate IH1019

Heating Rate (°C/min)	10
Final Temp (°C)	900
Percentage of active sample	100%
4 stub tuning status	Manual
Sample weight (mg)	5
Iris position (mm)	138
Iris (mm)	28 x 15
Cell	HPB
mixture material	N/A
Principle T/C	Reference
Tuning position (mm)	120.5
Comments	Argon 105%
	Sample flow 0%
	Alumina sandwich
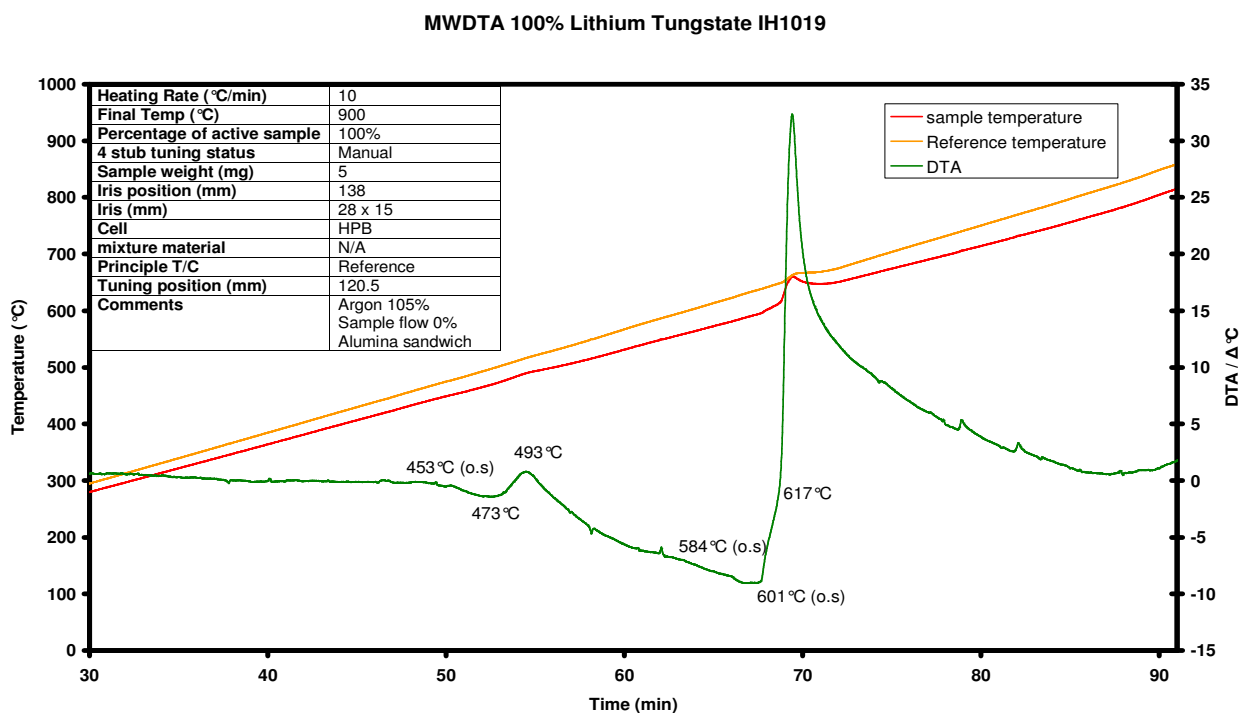
Graph 94: MWDTA experiment of lithium tungstate performed under argon.

The results showed the dehydration of the sample at around 453 °C (extrapolated onset) as in the conventional run. It can be seen the endothermic nature of the transition counteracts the dielectric change until the expulsion of water vapour increases the coupling for a short time. Following the loss of water from the sample area the overall coupling of the sample is reduced as expected from the low conductivity of material discussed previously. At this point the sample was expected to be a mixture of Li_2WO_4 and $Li_2W_2O_7$ (the expected starting material). As the sample temperature approaches 600 °C there is a sharp increase in the material's dielectric losses due to the phase change and the temperature rise is around 40 °C from a 5 mg sample. Unfortunately even at these low masses the adjacent transition was lost and therefore the fusion endotherm was not observed in this mode of microwave analysis.

In a bid to combat the problem of resolution the experiment was repeated in MWDTA (MWTA) mode in the HPB cell, where the temperature was controlled by the sample temperature not the reference, in theory allowing for faster responses to larger changes in coupling.

MWDTA(MWTA) 100% Lithium tungstate IH1017

Heating Rate (°C/min)	10
Final Temp (°C)	900
Percentage of active sample	100%
4 stub tuning status	Manual
Sample weight (mg)	5
Iris position (mm)	138
Iris (mm)	28 x 15
Cell	HPB
mixture material	N/A
Principle T/C	Sample
Tuning position (mm)	120.5
Comments	Argon 105% Sample flow 0% Alumina sandwich
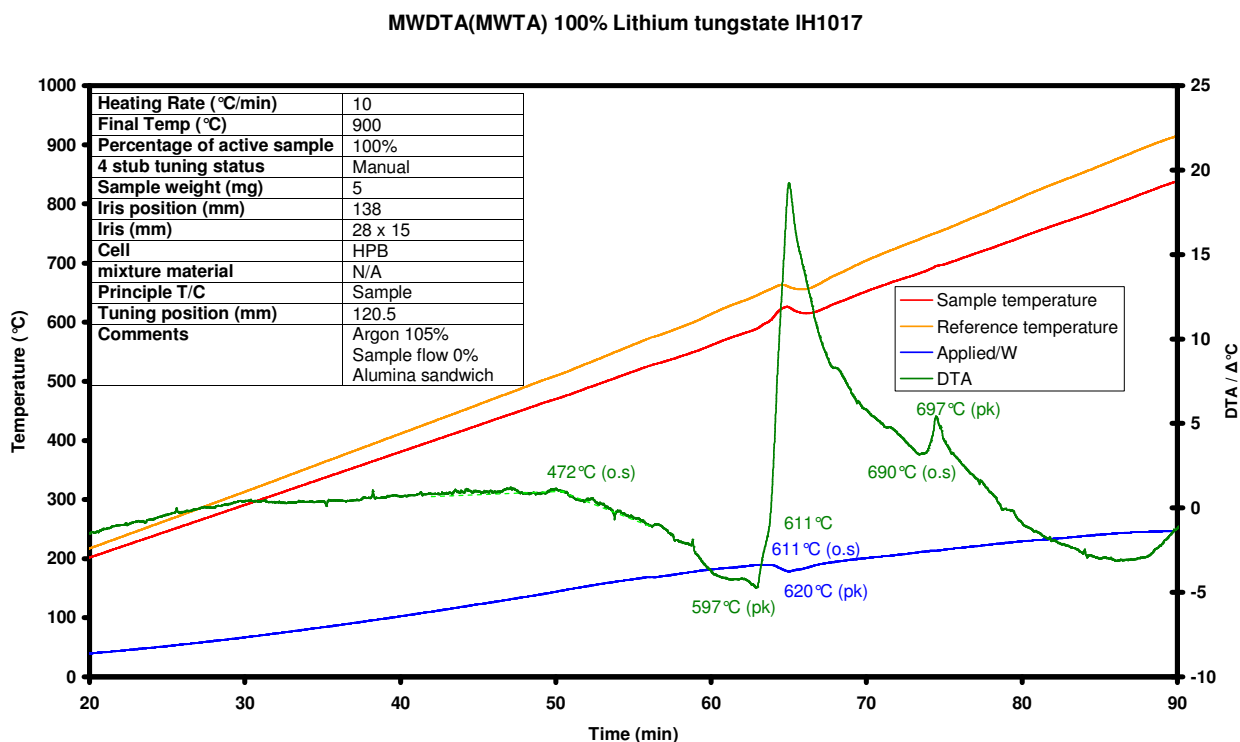
Graph 95: MWTA(MWDTA) experiment of lithium tungstate under argon.

Again the experiment showed a drop in coupling at around 472 °C associated with the dehydration. Both the applied power trace and the differential showed a transition occurring between 600 °C and 612 °C associated with the phase change. The change in mode allowed the melt to observed around 700 °C, although the true magnitude of the transitions was dramatically reduced.

7.4.4.2 Sodium tungstate dihydrate

Sodium tungstate has many uses such as the preparation of coated electrodes and fire retardants [56]. The response to heating is known to proceed via the loss of the two water molecules in a single step, then a solid-solid phase change, closely followed by the melt. The phase change is known not to be a single transition but two closely occurring ones:

$$\gamma \leftrightarrow \beta \ \ 580 \text{ °C}$$
$$\beta \leftrightarrow \alpha \ \ 620 \text{ °C [57]}$$
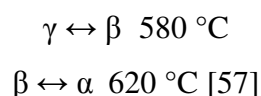
HDSC experiments were performed using 25.49 mg of the sample (as with lithium tungstate) on the HDSC at a rate of 10 °C/min under argon.
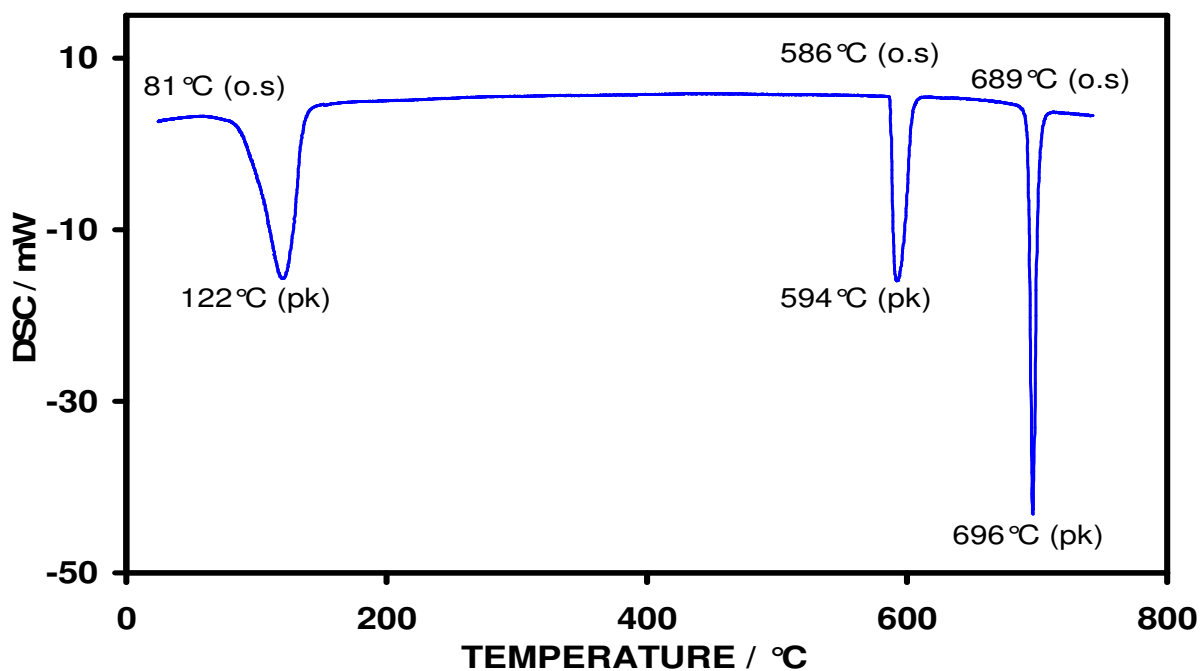
Graph 96: HDSC experiment of sodium tungstate dihydrate under argon.
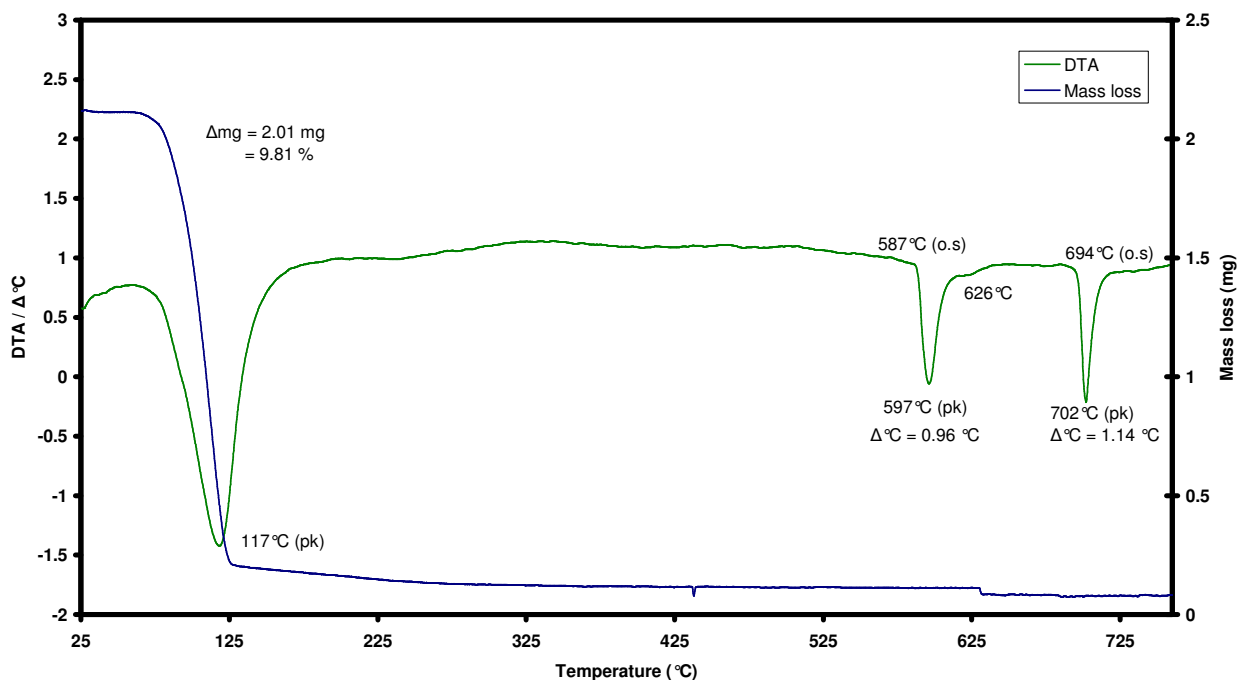
Graph 97: DTA-TGA experiment of sodium tungstate dihydrate under argon.

The traces clearly showed the dehydration with an onset temperature of around 81 °C. The HDSC (unlike the TGA) did not show any evidence of two phase changes occurring. It is possible the instrument was not sensitive enough to be able to record the β to α transition. The melt was clearly recorded at an extrapolated onset of around 689 °C.

MWDTA 100% Sodium tungstate IH0765

Heating Rate (°C/min)	10
Final Temp (°C)	800
Percentage of active sample	100%
4 stub tuning status	Manual
Sample weight (mg)	15
Iris position (mm)	138
Iris (mm)	28 x 15
Cell	HPB-EGA
Reference material	SiC
Principle T/C	Reference
Tuning position (mm)	120.5
Comments	Argon 80 ml/min Vac on
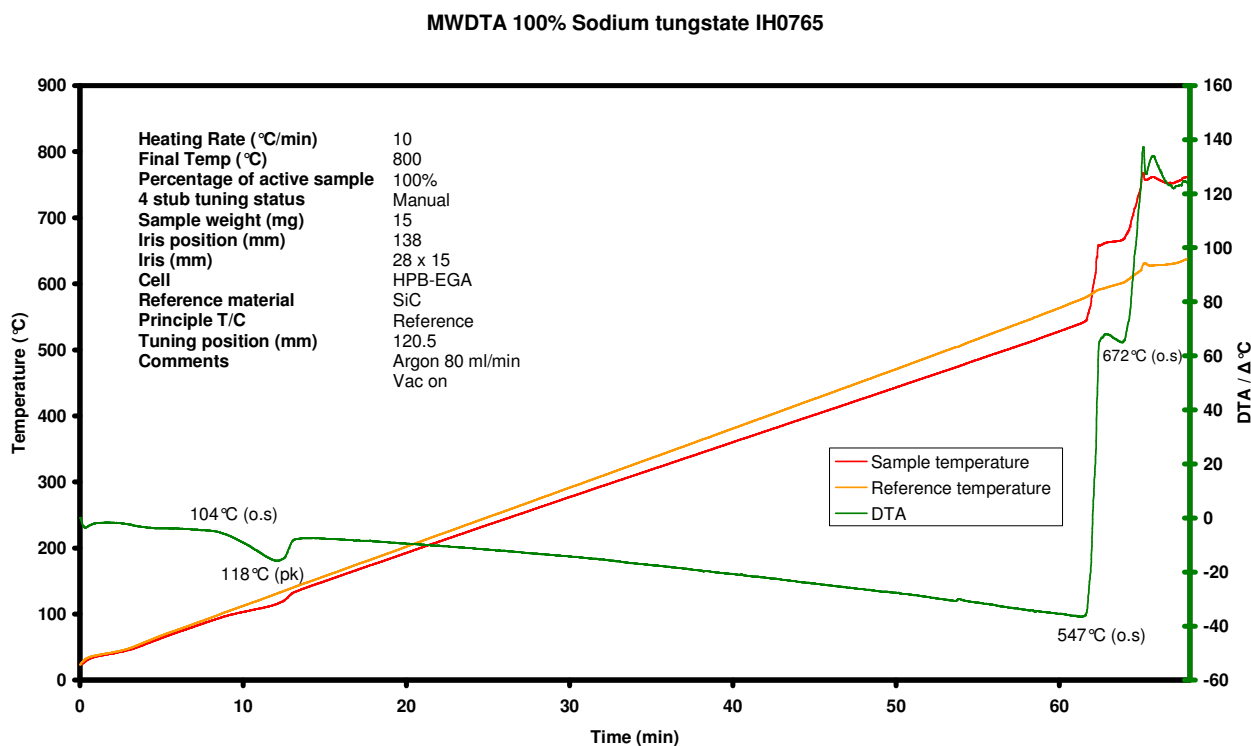
Graph 98: MWDTA experiment of sodium tungstate dihydrate under argon.

The sample size was reduced to 15 mg for the MWDTA experiment to increase resolution, once again the heating rate remaining at 10 °C/min under argon. The microwave induced dehydration continued over a shorter range then the conventional experiments. The onset of the transition was recorded around 104 °C, approximately 23 °C later than conventional heating. The recorded peak temperatures of the first transition from the different techniques were within several degrees of each other giving a good indication that there was still acceptable temperature calibration.

The second transition possessed a large response to the applied microwave power resulting in a 100 °C rise in temperature (compared to a 0.96 °C rise seen in conventional experiments with larger masses), although the onset temperatures did not correlate with conventional experiments. At first glance it appeared the transition was around 40 °C early under microwave radiation. It was not believed this was a so called "microwave effect" therefore the HDSC trace was expanded around the transition temperature seen in the MWDTA trace.

235

It was observed in the HDSC run that there is a slight deviation in the baseline leading into the main onset of the transition, indicating the first point of change in the sample. At this temperature it is likely that the parts of the sample closest to the furnace walls, and therefore possessing the most energy were changing, the response getting bigger as the bulk of the sample receives enough energy to transform (thermal mass) shown as the main onset recorded, usually later than the first change in a dynamic run. As the sample is heated volumetrically in MWDTA the first point of change is the same as the change of the bulk material, removing the dependence of the onset temperature on thermal mass. The experiment further supported the idea of MWDTA being sensitive to the first point of change of solid materials (giving rise to lower than expected transition temperatures). The fusion also appears to occur slightly early (around 17 °C) than conventional methods again the temperature correlated with the first point of change on the expanded HDSC trace. The sodium tungstate experiment was another good example of how the enthalpy opposes dielectric change during endothermic transitions. The latent heat of fusion of the transition (672 °C) was so strong that it halted the temperature rise caused by the phase change (allowing resolution to be conserved) before the full microwave response could be observed.

7.4.4.3 Potassium tungstate

Potassium tungstate has the largest cation of the alkali tungstates tested in this research. Literature states that upon heating, the sample undergoes two phase changes, the first occurring at 367 °C ± 5 the second at 461 °C ± 5 [58]. Conventional experiments were performed on the HDSC 1500 utilizing 24.95 mg of sample heated at 10 °C/min under argon.
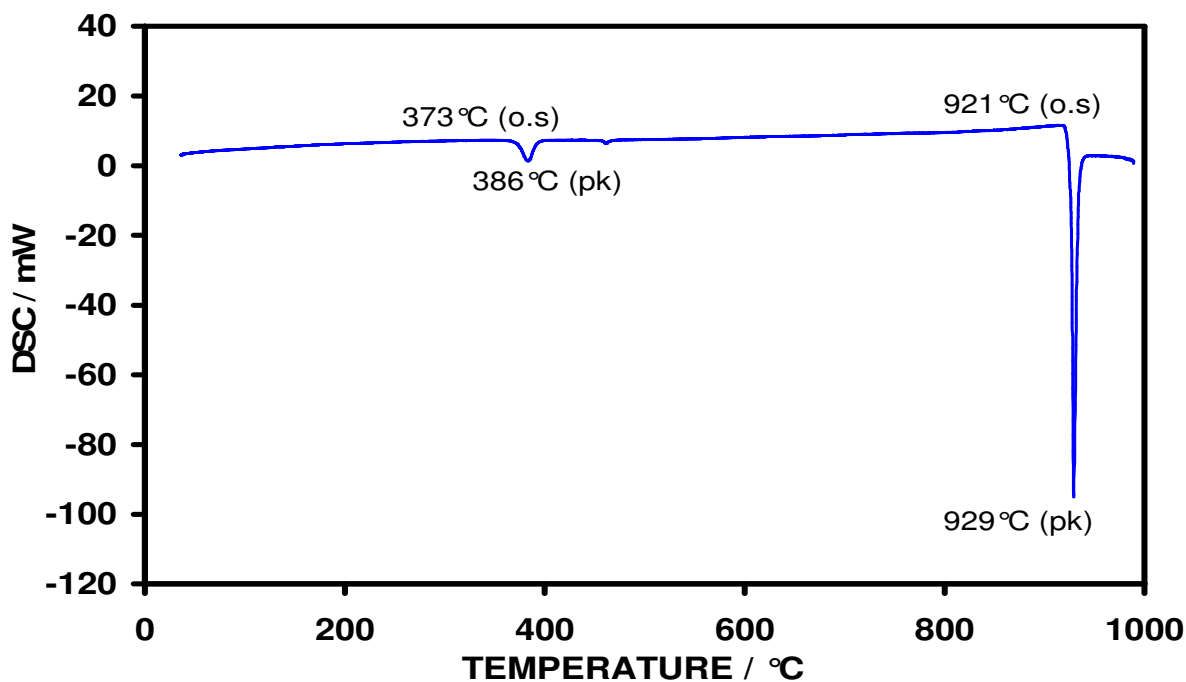
Graph 99: HDSC experiment of potassium tungstate under argon.

The results showed the first transition clearly at 373 °C (extrapolated onset) which agreed with the literature. The second expected transition (461 °C) was not clearly seen although around the expected temperature there was a slight change in the baseline which could possibly be a very weak transition. The final recorded transition was the fusion at 921 °C (extrapolated onset) curiously the slope of the baseline changes leading into this final transition, noticeably around 600 °C.

In order to record the polymorphic phase changes in the MWDTA experiment the sample size had to be increased to 100 mg, five times the normal sample size for a MWDTA experiment. The samples were tested at 10 °C/min under argon.

MWDTA 100% Potassium tungstate IH1022
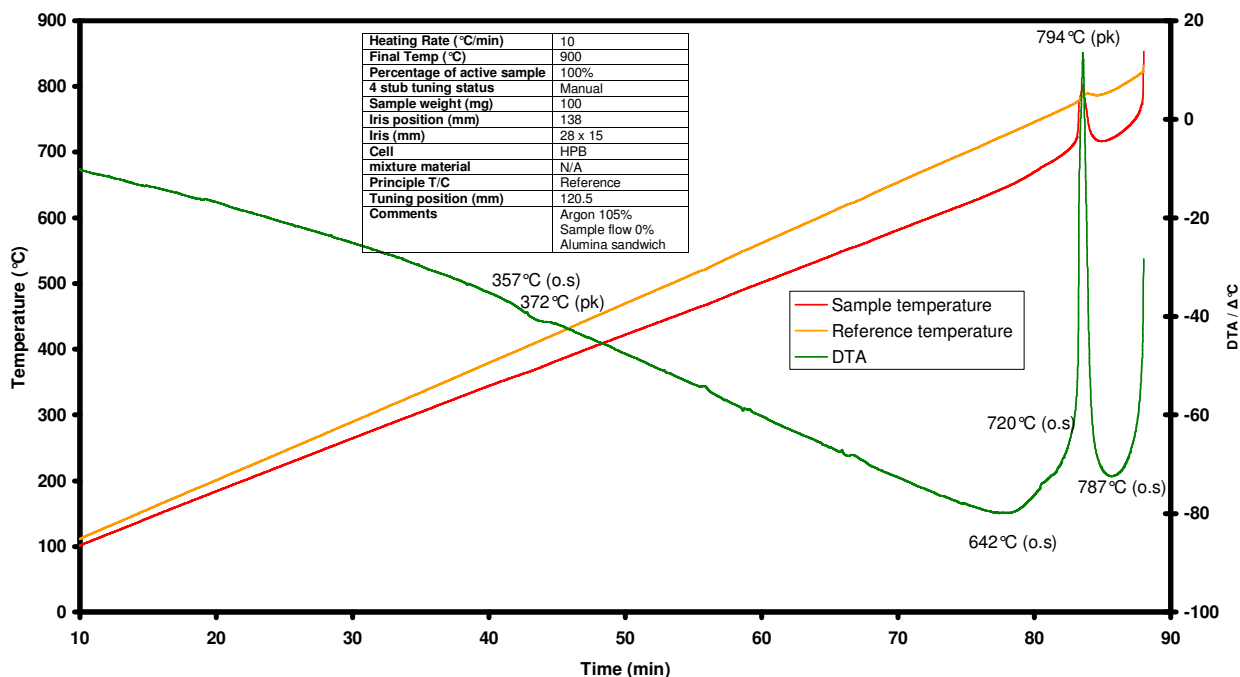
Graph 100: MWDTA experiment of potassium tungstate under argon.

The results showed poor response to the phase change even at the increased sample size, with the first transition weakly recorded (taking into account the magnitude of the following transitions). The MWDTA experiment showed the first transitions to occur around 16 °C earlier than the extrapolated onset seen in the HDSC. The shift in transition temperature could not be explained as it did not correlate to any significant change on the conventional curves. Overall the transition appeared to have no dielectric change and a weak change in enthalpy. The second transition recorded on the HDSC (475 °C) seemed to have a minimal change in enthalpy which was below the sensitivity of the MWDTA and not a dielectric change. Therefore it was unable to be recorded in a microwave experiment. Strangely the MWDTA recorded a significant change in coupling at 642 °C, a transition not recorded in HDSC experiments. The experiment showed how microwave thermal analysis was able to clearly show transition which may be important in processes involving microwaves, the extent of which would be missed in conventional experiments. The transition at 642 °C in the microwave trace correlated to a change in slope of the baseline leading into the melt around 300 °C later in the HDSC trace. The MWDTA was not recording the melt at this temperature but rather responding to the cause of the change in heat capacity that gave rise to the increase in the slope observed in the HDSC experiments (Graph 99). The reason for the extent of the rise still remains unknown. It is not thought that the discrepancies were due to impurities as the

same sample source tested in the HDSC was used in the MWDTA experiments. It is possible the final transitions recorded (at 720 °C and 787 °C) could be a result of the fusion although it occurred 200 °C earlier than expected, but the response of the previous transition meant the sample temperature overshoot the consecutive transition which was too close to the upper temperature limit of the instrument so the run was automatically terminated.

7.5 Dehydration of bound species

The dehydration of inorganic compounds which do not melt before they reach their decomposition temperatures was investigated. Comparing decomposition temperatures in different instruments is not generally advised as many factors such as atmosphere, heating rate, changes in impurities between samples, orientation of crystals, lattice strain, packing density, shape of the sample cell and possibly the catalytic nature of the sample pan [47], can cause discontinuities between techniques. The carrier gases in both the microwave and conventional techniques were argon. Conventional measurements were made using a HDSC 1500 which could accommodate 20mm x 6 mm quartz sample cells with the same internal bore and material as the HPB cell. The heating rate was also kept to a standard rate of 10 °C/min. The biggest disadvantage of using differential techniques to monitor decompositions is that the technique cannot give information of the decomposition product. Therefore certain responses cannot be explained as they may arise from secondary reactions such as disproportionation.

The literature discusses the possibility that certain oxide types would not heat well under microwave radiation [52] due to their positive nuclei being effectively shielded, as the metal radii are small, resulting in small polarisability. Previous MWDTA experiments have found difficulties in maintaining heating when group II oxides have been formed as the result of decompositions from carbonates. It was believed that forming oxides from hydroxides might give an insight into whether the problems faced were due to oxides having adverse effects in the cavity or if it was the method of the formation which caused the complications.

7.5.1 Magnesium hydroxide

Magnesium hydroxide has many industrial uses which include flame retardants in polymers, as the expulsion of water effectively dilutes the volatile species released on polymer degradation [59]. The sample (25 mg) was tested using the HDSC at a heating rate of 10 °C/min under argon.
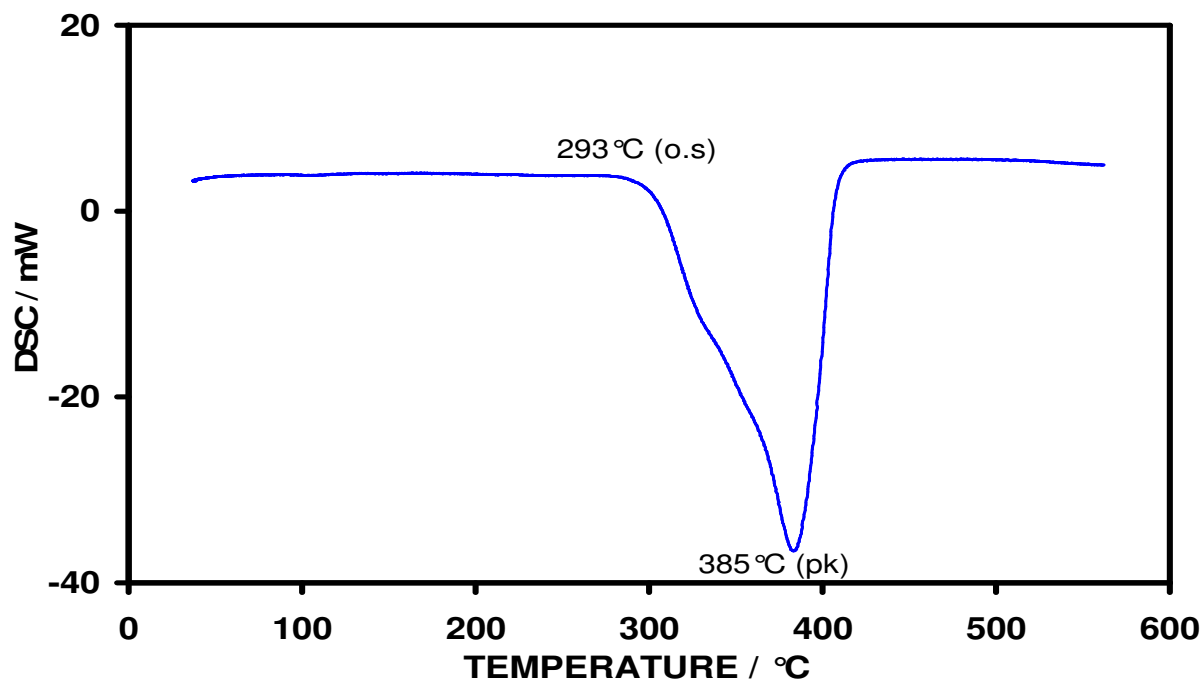
Graph 101: HDSC experiment of magnesium hydroxide under argon.

The results showed an onset temperature of around 293 °C. The run also showed a shoulder prior to the peak minimum beginning at 328 °C and leading into the peak at 385 °C. A slight increase in the heat capacity was also noticed after the transition once the oxide had been formed.

The MWDTA experiment required a relatively large sample size (40 mg) in order to obtain clear results. The sample was heated at 10 °C/min under argon.

MWDTA 100% Magnesium hydroxide IH0867
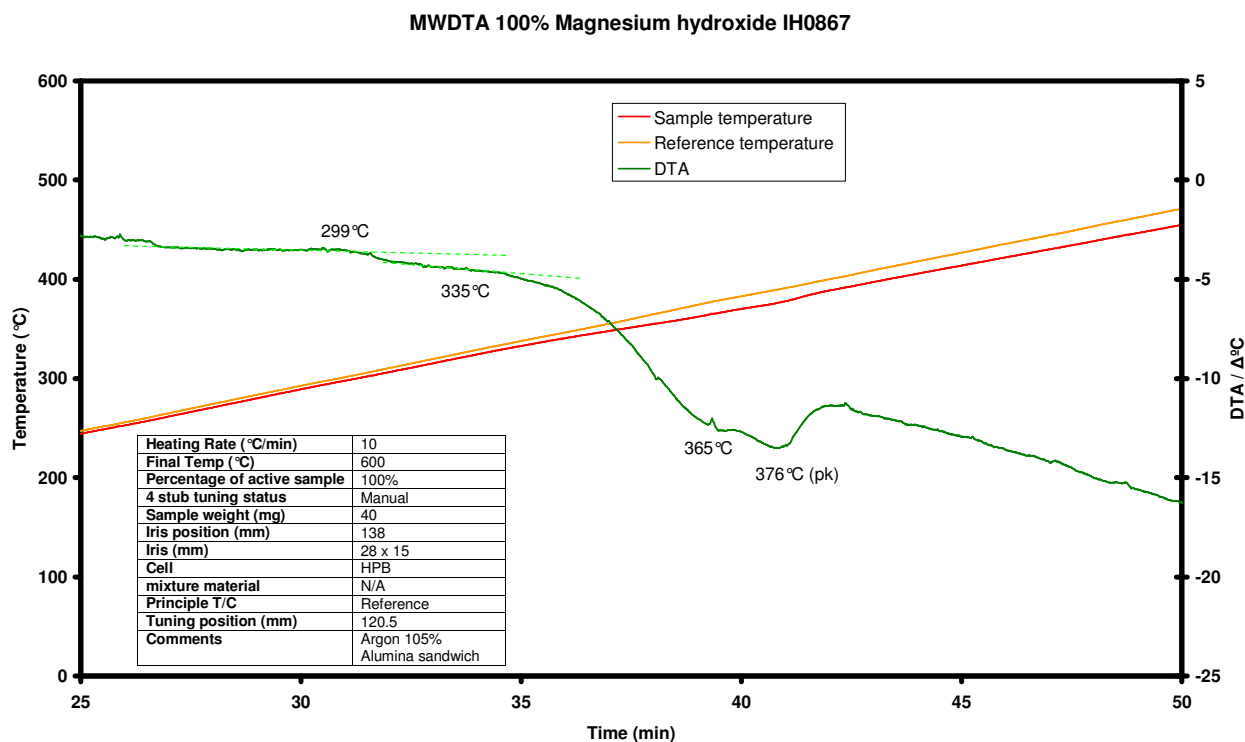
Graph 102: MWDTA experiment of magnesium hydroxide under argon.

The onset temperatures from the MWDTA did not closely correlate with the main onset recorded by the HDSC (293 °C) and only a small deviation (ΔT = 1.2 °C) was seen in the microwave differential trace around this temperature (299 °C). There was a close correlation with the onset of the shoulder discussed earlier (328 °C) and with the main onset of the MWDTA trace at 333 °C. It was thought this was due to the increasing rate of water lost from the sample at this point of the decomposition. In many of the other dehydration experiments detailed in other sections water was lost as free liquid, increasing the coupling ability, resulting in an increase in the differential temperature, then quickly vaporising, resulting in the temperature falling. With the decomposition of hydroxides the water is removed in the form of a vapour, as the high temperature means that it could not exist in the liquid form at atmospheric pressure. This vapour has no effect on the dielectric loss of the sample as it is removed from the measurement area too quickly. It appeared that the main change in coupling of the sample did not become evident until a large portion of the water had left the material and therefore altered its structure. The shoulder in the MWDTA trace occurred at around 365 °C close to the end of the shoulder seen in the HDSC. At this point it was believed that the enthalpy of the transition had opposed any dielectric change. The peak temperature recorded in the MWDTA experiment was several degrees lower than the HDSC trace, possibly due to differences in the instruments, or due to volumetric heating. Water is removed from the sample far more efficiently in a microwave experiment than conductive heating resulting in a more rapid

decomposition. The rise in differential temperature at 376 °C (green trace) was not thought to be due to an increase in tan δ but rather recovery from the enthalpy effect. The lower value of tan δ can be seen by the -5 °C difference in the pre-transition baseline and the value of the resultant oxide baseline (between 42.2–50 minutes in the microwave trace). The sample continually lost heat in the oxide form suggesting it was now solely heating via conduction and possibly storing more of the applied wave (increasing the value of the lower portion of the tan δ term).

7.5.2 Calcium hydroxide

Calcium oxide proved very hard to heat when it was formed from the decomposition of calcium oxalate monohydrate. In order to determine if the problem was caused by the formation of the oxide via a carbonate or if as mentioned previously certain oxides are just not suited to microwave heating, the decomposition of calcium hydroxide was studied. Again the samples were tested on the HDSC at a rate of 10 °C/min under argon.
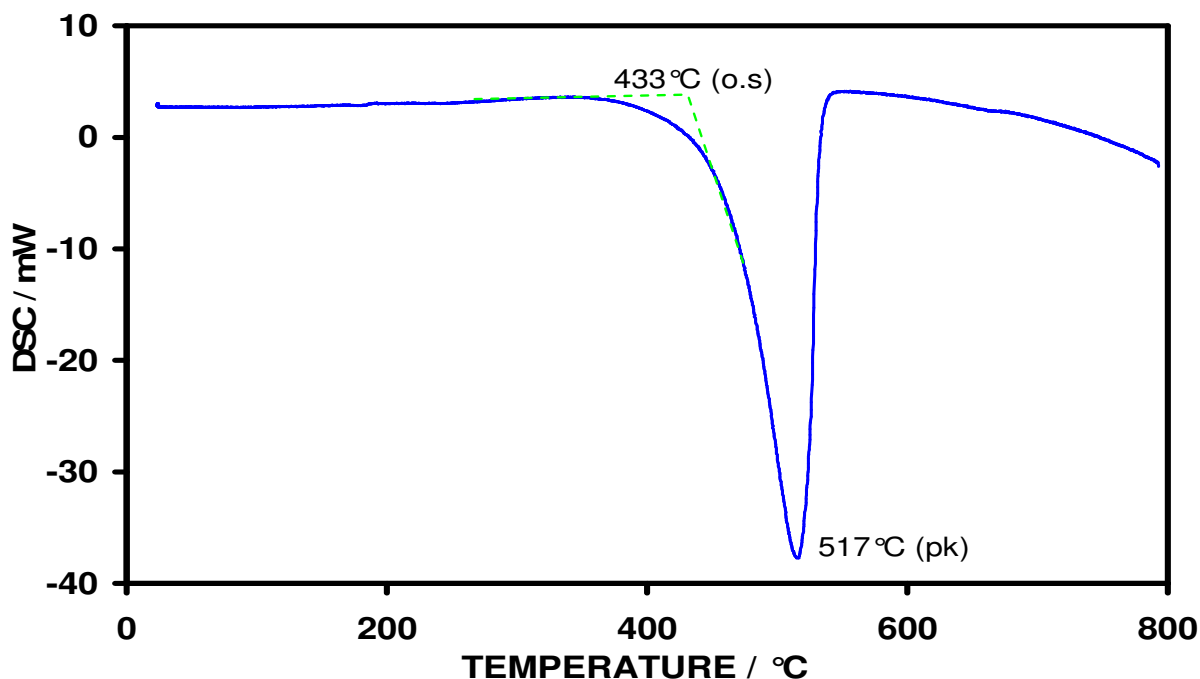
Graph 103: HDSC experiment of calcium hydroxide under argon.

The result showed the extrapolated onset to occur at around 433 °C, it could also be seen after the transition there was a distinctive change in the baseline possibly indicating a fall in heat capacity.

The MWDTA experiments consisted of using a larger sample size of 40 mg to account for the loss of volume during the decomposition and the usual heating rate of 10 °C/min.

MWDTA 100% Calcium hydroxide IH0864
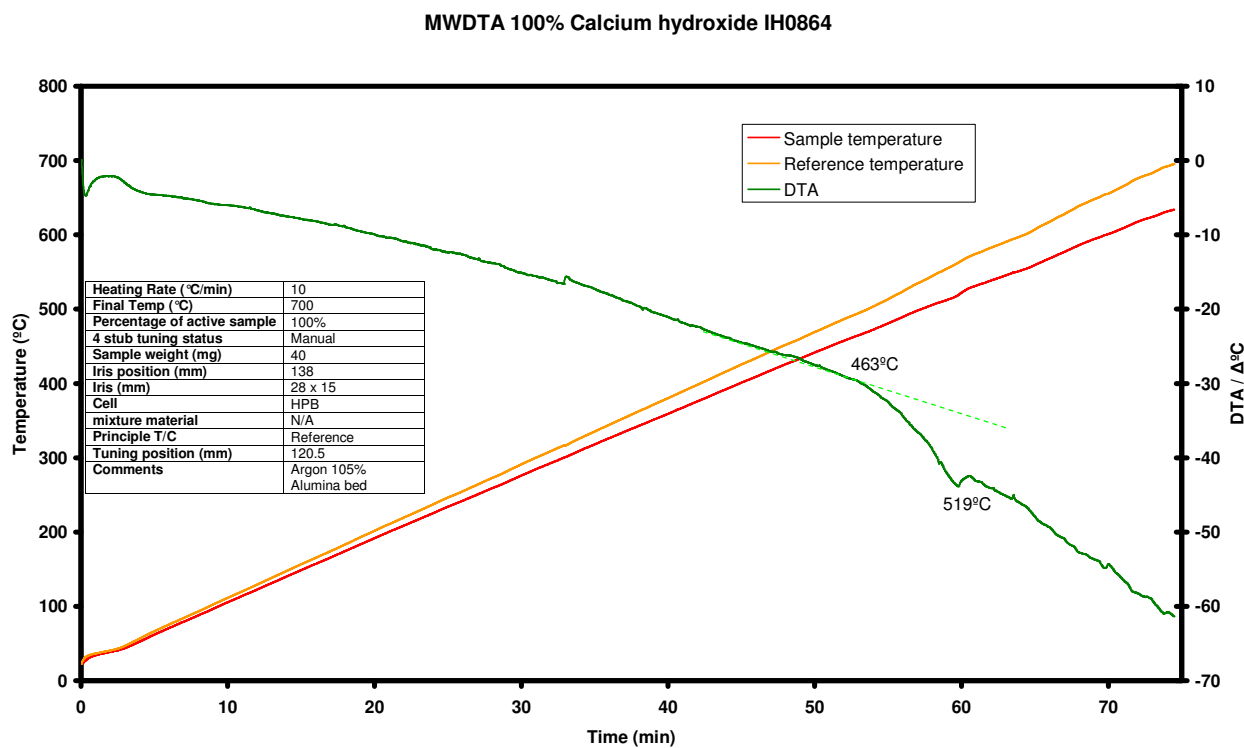
Graph 104: MWDTA experiment of calcium hydroxide under argon.

It appeared that the lack of coupling from the sample resulted in a negatively sloping baseline as the heating of the material arose solely from conduction, therefore allowing the reference and sample temperatures to diverge. Unfortunately the HPB cell is not ideally suited for this type of heating and therefore the negative sloping baseline was unavoidable. The peak temperatures of the two techniques were within 2 °C of each other although their onsets occurred 30 °C apart. After the completion of the decomposition it can be seen that there was some recovery in the differential temperature (the end of the endothermic transition as in the case of magnesium hydroxide). The post transition baseline showed the newly formed material to couple far less than the original starting material (the difference in ΔT = -13.7 °C). During the transition the reference temperature deviated slightly from linearity possibly due to increased conduction from the sample or the newly formed material reflecting rather than absorbing the applied wave.

The combination of the loss of coupling from the formation of the oxide, and the heat losses from the elevated temperatures in the calcium oxalate experiment was thought to be a large contributing factor to the loss of control seen in previous experiments where calcium oxide was formed.

7.5.3 Strontium hydroxide

Strontium hydroxide is the third of the group II hydroxides studied and has many uses including the refining of beet sugars and stabilizers in plastics. The samples were tested in the same manner as the previous hydroxides where 26 mg of the material was subjected to a heating rate of 10 °C/min under argon in the HDSC.
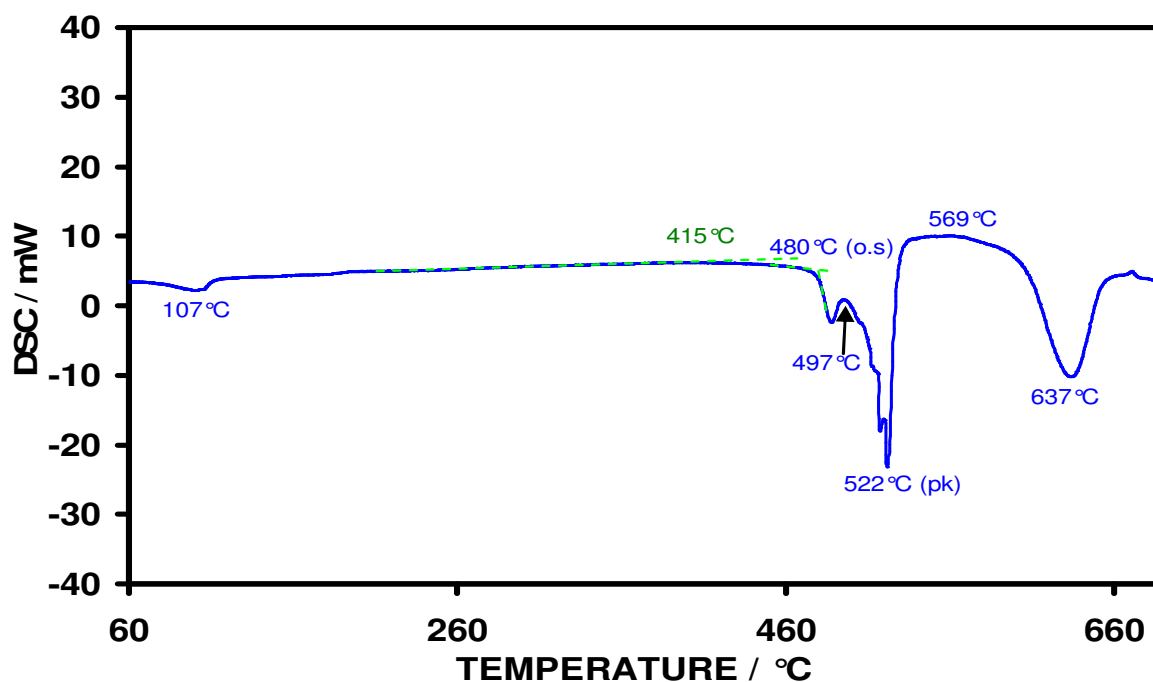
Graph 105: HDSC experiment of strontium hydroxide under argon.

The results showed the first transition occurring at a peak temperature of 107 °C owing to the loss water of crystallisation. The next transition occurring around 415 °C showed as a slight deviation of the baseline leading into the main extrapolated onset shown around 480 °C (polymorph). Some recovery can be seen which then runs into another onset of around 497 °C (T_m). The decomposition temperatures appeared to fit with those suggested by Dinescu *et al.* [60] which also suggested the possibility of a polymorph around 480 °C. The onset of the fusion transition appeared to be a very noisy transition until around 522 °C. The reason for this noise was not given in this publication

although it did mention that the transition led into the decomposition spanning three stages, finally forming the amorphous strontium oxide by 700 °C. The work of Makurin *et al.* [61] gives the possible explanation of the three stage decomposition being due to the rate of temperature diffusion from the surface to the bulk which slowed due to the creation of a surface oxide layer, which remained until the bulk of the material reached the temperature at which it could convert to the oxide.

MWDTA 100% Strontium hydroxide IH0857

Heating Rate (°C/min)	10
Final Temp (°C)	700
Percentage of active sample	100%
4 stub tuning status	Manual
Sample weight (mg)	40
Iris position (mm)	138
Iris (mm)	28 x 15
Cell	HPB
mixture material	none
Principle T/C	Reference
Tuning position (mm)	120.5
Comments	Air 105% Alumina bed
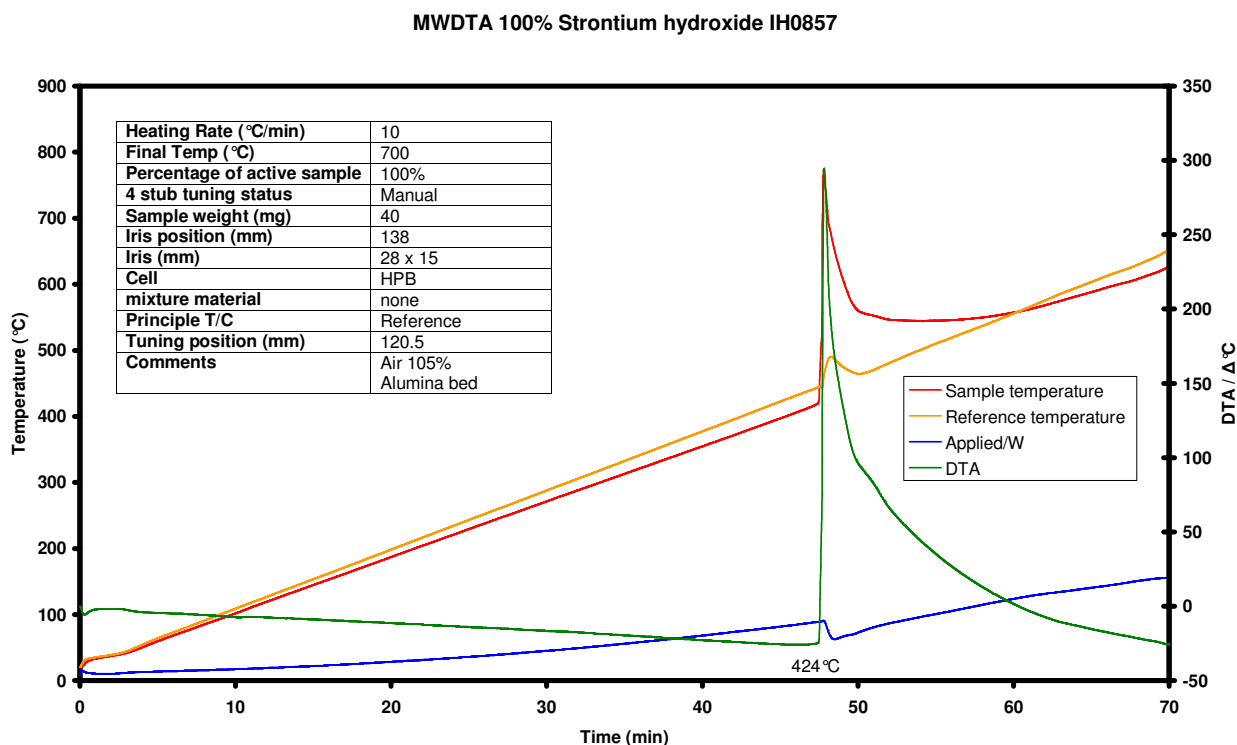
Graph 106: MWDTA experiment of strontium hydroxide under argon.

The MWDTA experiment showed unexpected results. Firstly the sample appeared to heat relatively well before the transition compared to similar hydroxides under microwave radiation. Secondly the transition had a very large dielectric response unlike any of the other group II hydroxides. The response can be seen to be over 300 °C (the exact magnitude was not obtained as the heat evolved from the sample altered the reference temperature). The explanation of the magnitude of this response is thought to be due to a combination of factors:-

- The increased coupling owing to the phase change combined with dielectric change.

- The partial sample melt

- The larger electron cloud in the strontium ion being more polarisable than the other group II metal hydroxides studied.

The other transitions seen in the conventional experiments were thought to be lost in the temperature rise seen in the MWDTA experiment which caused formation of the oxide in a far shorter time period than a conductive furnace, therefore removing the problem of the bulk heating slower than the surface.

The response, it seemed, was not a permanent change in tan δ as seen by the differential temperature returning to a pre-transition value after the transition. It is thought this response arose from the possible polymorph discussed by Dinescu *et al*. [60]. The reason for its non-permanent nature was the additional heating from the change in tan δ, causing the sample temperature to exceed the decomposition temperature, forming a new material (strontium oxide) which was thought to have similar ability to couple to microwave energy as the other oxides in group II and also a loss of volume during the transition. The transition temperature in the MWDTA experiments showed no obvious correlation with the HDSC trace, although it did appear to occur during the deviation of the baseline mentioned earlier in the HDSC experiments. It was believed that like most other MWDTA experiments the instrument was responding to the first point of change as the sample started to undergo the solid-solid phase change.

7.5.4 Sodium bicarbonate
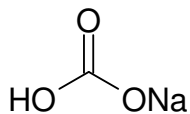
The thermal decomposition of sodium bicarbonate is well characterised [62, 63] and documented and its characteristic behaviour means that it is a standard calibration material used in TGA mass calibration. Although the transition is not believed to have any dielectric change it was thought that the experiment would provide information on the validation of the instrument sensitivity in respect to purely enthalpy transitions. The conventional experiments were performed on the HDSC 1500 where 25.41 mg of sample was investigated at a heating rate of 10 °C/min under argon.
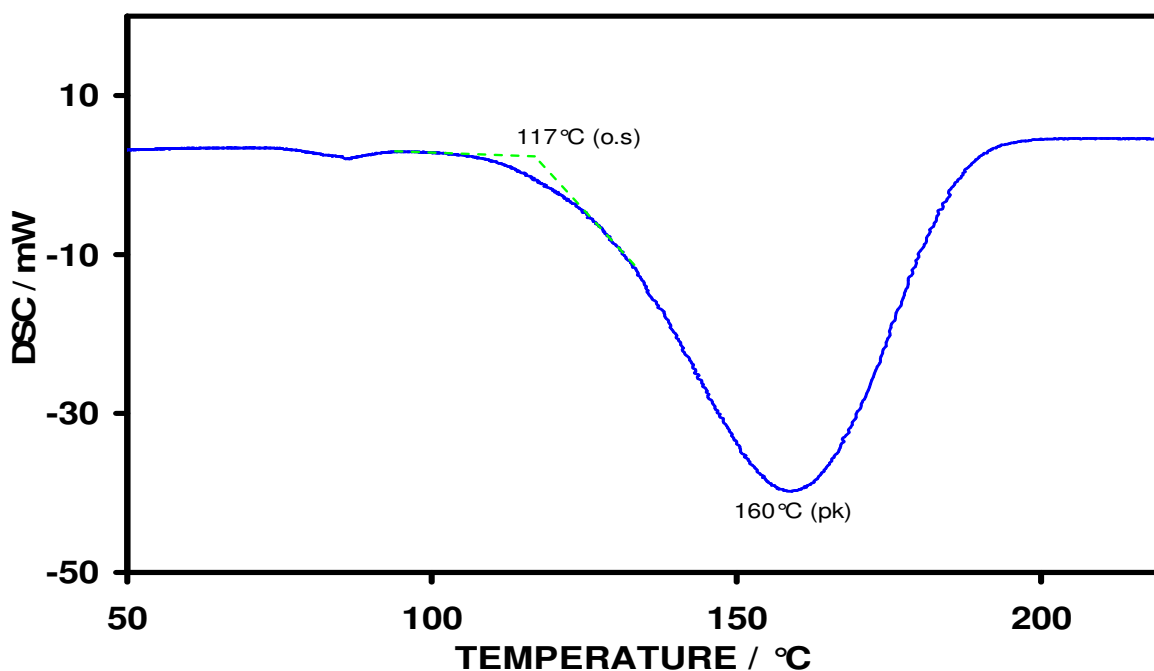
Graph 107: HDSC experiment of sodium bicarbonate under argon.

The results showed the main extrapolated onset to occur at around 117 °C and a slight increase in heat capacity following the transition (indicated by the increased value of the baseline).

MWDTA 100% Sodium bicarbonate IH0728

Heating Rate (℃/min)	10
Final Temp (℃)	600
Percentage of active sample	100%
4 stub tuning status	Manual
Sample weight (mg)	30
Iris position (mm)	138
Iris (mm)	28 x 15
Cell	HPB-EGA
Reference material	SiC
Principle T/C	Reference
Tuning position (mm)	120.5
Comments	Argon 80ml/min Vac on
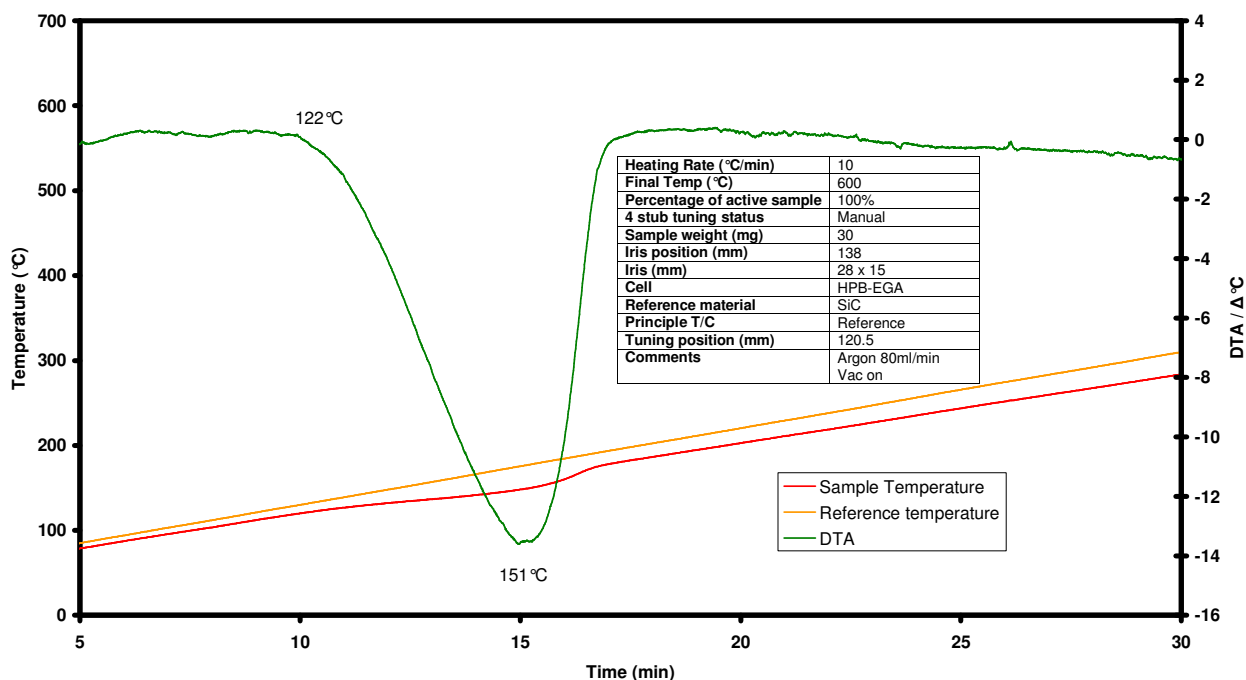
Graph 108: MWDTA experiment of sodium bicarbonate under argon.

The MWDTA experiments were also performed under argon at a rate of 10 °C/min, the sample size was increased to 30 mg to account for volume losses as the sample decomposed. The MWDTA trace showed a slight increase in the value of the differential trace, and as with other hydrated species the range over which the transition took place was smaller (possibly an indication of increased resolution of transitions of this type when using MWDTA methods). The extrapolated onset occurred around 122 °C, 5 °C later than the conventional method. The peak temperature also appeared to be premature by around 9 °C. The experiment showed the instrument was capable of providing not only dielectric data but also enthalpy specific information with confidence.

7.5.5 Potassium bicarbonate
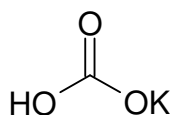
As with sodium bicarbonate, potassium bicarbonate is widely used as a calibration material in thermal analysis. Again the decomposition occurs in a broad single step and results in a slight change in heat capacity after completion of the event. Like the sodium bicarbonate experiment the

conventional experiments were performed on the HDSC 1500 where 25 mg of sample was investigated at a heating rate of 10 °C/min under argon.
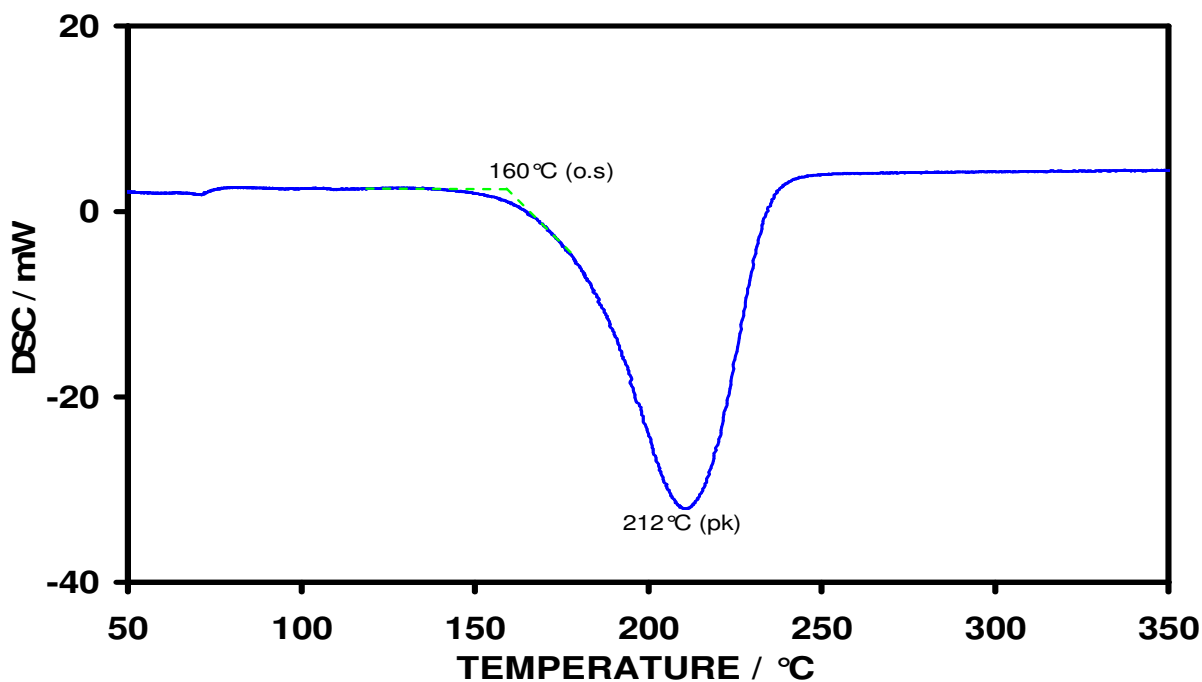
Graph 109: HDSC experiment of potassium bicarbonate under argon.

The trace showed an onset temperature (extrapolated) of 160 °C and a peak temperature of around 212 °C.

The MWDTA experiments were again performed under argon at a rate of 10 °C/min, the sample size was increased to 30 mg.

The MWDTA experiment again showed a change in baseline after the transition. Curiously in this case the baseline change was far more dramatic. It is possible that the slight increase in the rate of the decomposition due to water being lost at higher temperatures (shown by the slope of the conventional trace compared to the sodium bicarbonate run) may expel more of the material from the sampling area, reducing the volume and in turn affecting volumetric heating and the sample's ability to heat. Once more the transition occurred over a smaller temperature range then seen in the HDSC experiment strengthening the possibility of greater resolution when using microwave methods.

MWDTA 100% Potassium bicarbonate IH0800

Heating Rate (℃/min)	10
Final Temp (℃)	300
Percentage of active sample	100%
4 stub tuning status	Manual
Sample weight (mg)	40
Iris position (mm)	138
Iris (mm)	28 x 15
Cell	HPB
mixture material	N/A
Principle T/C	Reference
Tuning position (mm)	120.5
Comments	Argon 105% Sample flow 0% Alumina bed

152 ℃ (o.s)

199 ℃

Sample temperature
Reference Temperature
DTA
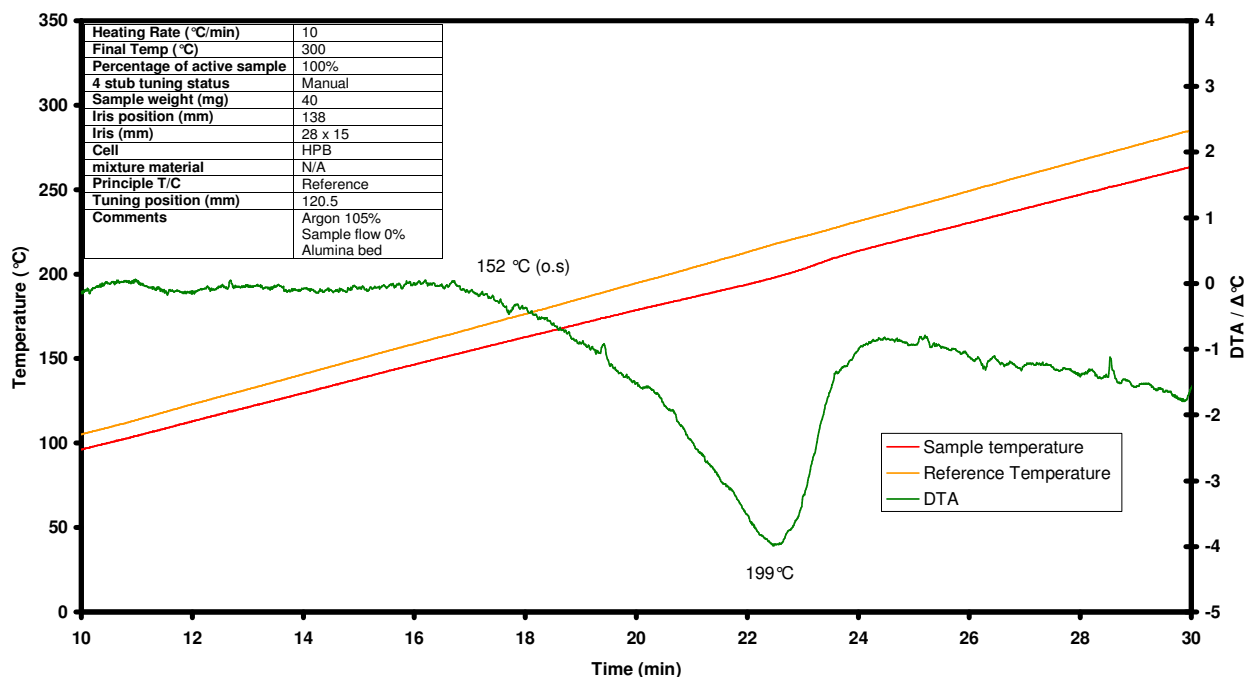
Graph 110: MWDTA experiment of potassium bicarbonate under argon.

7.6 Dehydration of water of crystallisation

The thermal decomposition of salt hydrates has been well studied for a number of years. Recently these types of transitions have been used to demonstrate the sensitivity of instruments and the resolution of techniques. The problems associated with the thermal dehydration of salt hydrates are that the results are not always consistent and are affected by many experimental parameters. The main cause of these discrepancies is that the reaction is reversible (depending on the vapour concentration of the water in the surrounding atmosphere) due to the dehydration in a closed environment. Regardless of the problems these types of samples were of great use to show the resolution which was obtainable when testing samples that evolve strongly coupling species, such as water, in close succession to each other.

The crystalline lattice of hydrates characteristically collapses when water is removed from the system. Therefore the anhydrous form shows no simple relationship with the hydrate [64] which was thought may have a possible effect on the material's conductivity and consequently its susceptibility to Ohmic heating.

7.6.1 Copper sulphate pentahydrate

The dehydration of copper sulphate pentahydrate is well known to proceed via the following route:-

$$CuSO_4.5H_2O \xrightarrow{-2H_2O} CuSO_4.3H_2O$$
$$2H_2O_{(l)} \rightarrow 2H_2O_{(g)}$$
$$CuSO_4.3H_2O \xrightarrow{-2H_2O} CuSO_4.H_2O$$
$$CuSO_4.H_2O \xrightarrow{-H_2O} CuSO_4$$
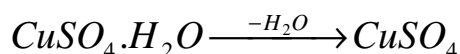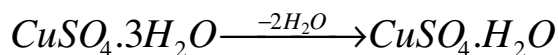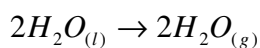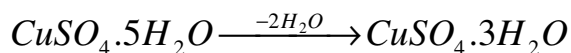
The first two events are usually not fully resolved when using a dynamic heating rate of 10 °C/min and the vaporisation of water can be seen at slower heating rates such as 2 °C/min [43].

Both microwave and conventional methods consisted of heating at 10 °C/min to 340 °C under argon.
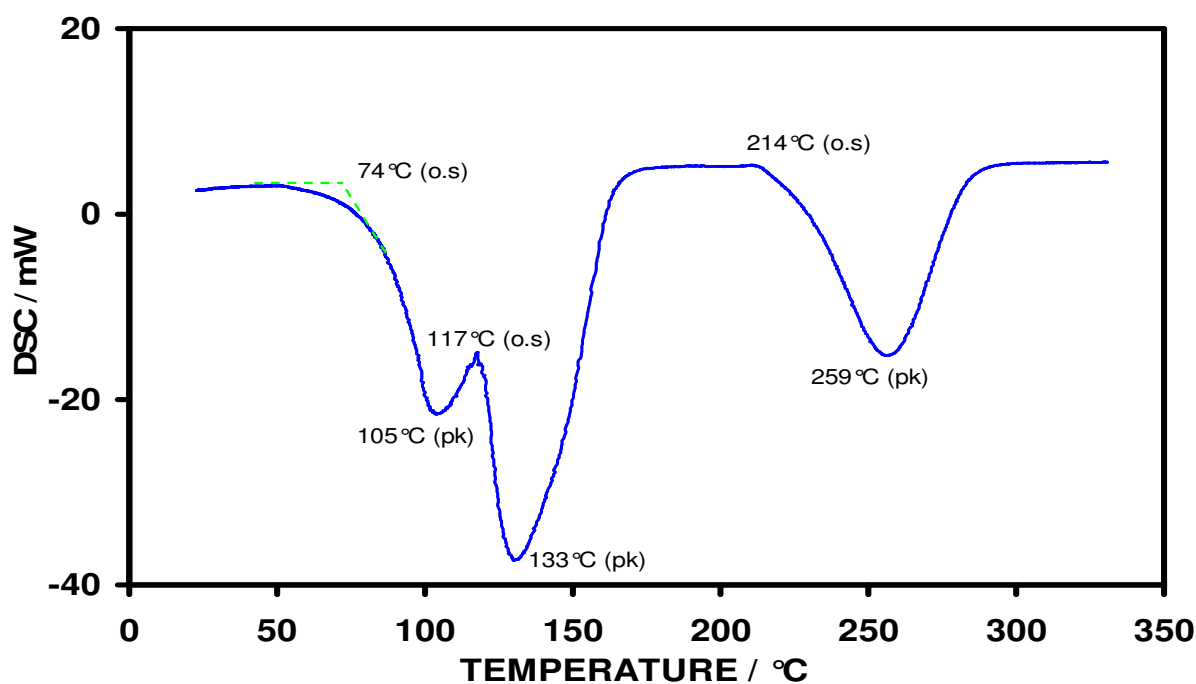
Graph 111: HDSC experiment of copper sulphate pentahydrate under argon.

The HDSC trace showed all three transitions clearly at the standard heating rate. Although as suggested in literature the first two transitions were not fully resolved, the experiments were unable to illustrate the vaporisation of free water expelled from the first transition.

MWDTA 100% Copper Sulphate pentahydrate IH0706
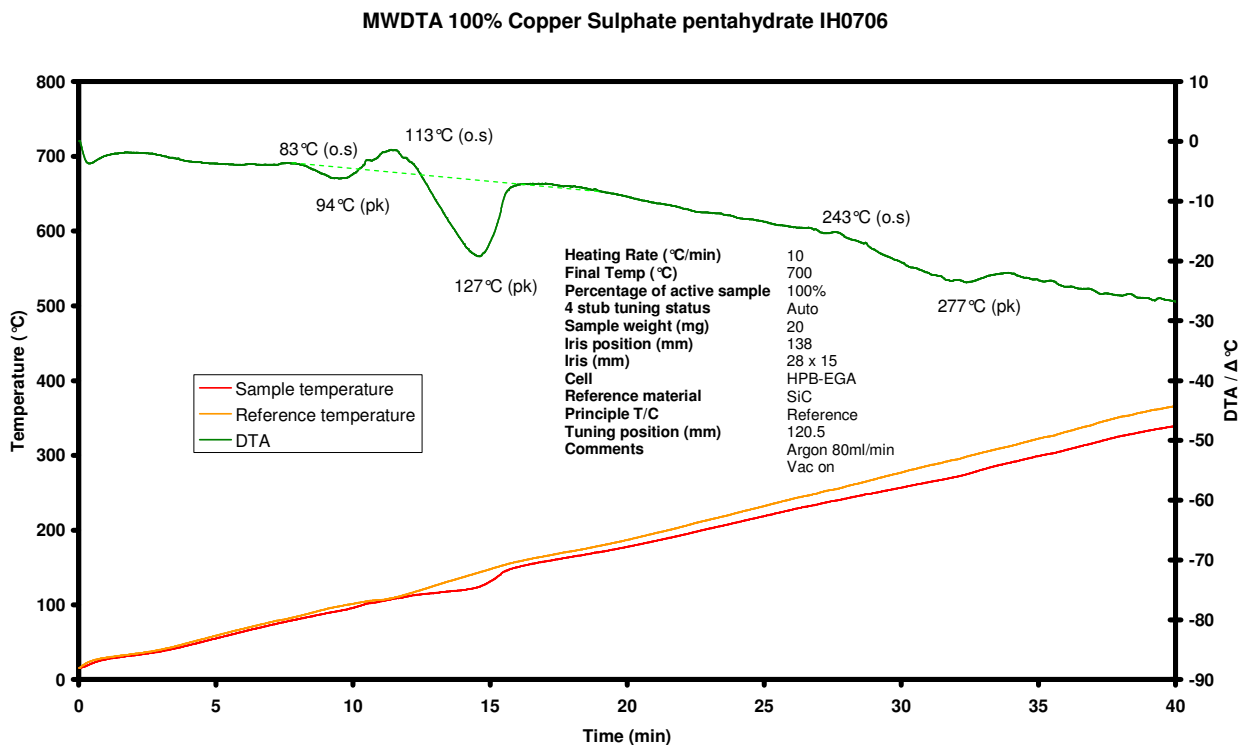
Graph 112: MWDTA experiment of copper sulphate pentahydrate under argon.

Inspection of the microwave experiment showed that the transition temperatures were different, the onset of the first dehydration taking place several degrees later than the DSC experiment. It is believed this is again a result of volumetric heating. Water is a well known coupler to microwave radiation and the subject of discussion about the so called "microwave effect" owing to its elevated boiling point under microwave conditions.

The cause of the discrepancies in transition temperatures is more likely associated with the transfer of energy. The heat capacity of water results in it requiring a relatively large amount of energy to induce a temperature rise, which consequently increasing the thermal lag exhibited by the system. In theory in a MWDTA experiment the bulk of the material is at the same temperature, therefore overcoming the problem of thermal lag and reducing the lead into the transition and hence the span of the peak.

It is suspected that the transition is not shown as a step because the evolved material is lost from the sample area and therefore does not remain to add to the overall heating of the material. Evidence of the sample being lost can be seen in the MWDTA trace (105 °C) by the differential temperature rising above the baseline then promptly falling as the onset of the second transition is reached. The rise in temperature is a result of the free water coupling to the applied power then boiling away, a

transition not always seen in conventional experiments at this heating rate. This material showed an example of the increased sensitivity of MWDTA for the detection of certain transitions.

By the second transition's peak temperature the MWDTA experiment showed a return to baseline with a peak temperature occurring within 6 °C of the conventional measurements. The onset of the third transition (243 °C) again took place at an elevated temperature and appeared to have little or no change overall in tan δ.

The magnitude of the response is believed lesser than expected due to the vaporised water not remaining in the sample area for a measurable length of time, therefore leaving only the enthalpy of the transition being illustrated. This hypothesis could be tested if a pressurised MWDTA cell could be developed.

7.6.2 Calcium sulphate dihydrate

The use of gypsum (calcium sulphate dihydrate) has been used previously in this research in order to determine how the newly designed HPB cell behaved in relation to a DSC sample pan. The decomposition of the material can either be in a single step (when in an open pan) or it two resolved steps when the vapour pressure is increased (as in a pin holed pan). The two transitions types are shown below. The experiments were performed on the MDSC and consisted of testing 3.62 mg in both an open pan and the pin holed pan. All experiments were conducted under argon at a dynamic heating rate of 10 °C/min.
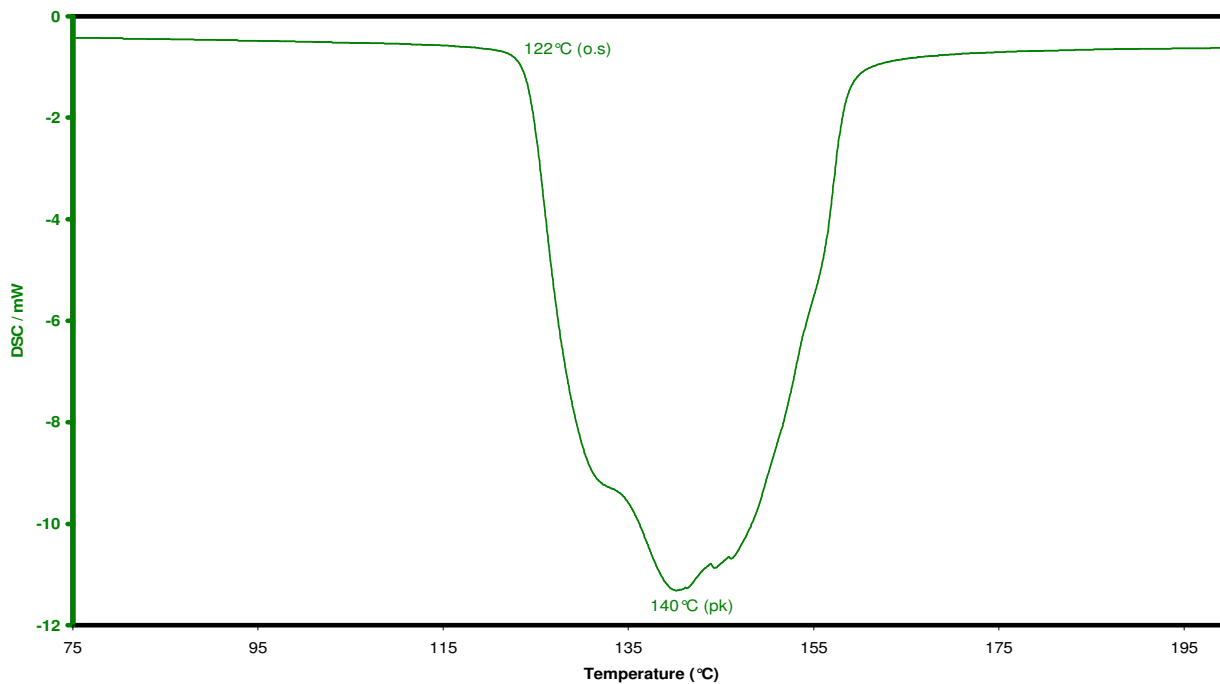
Graph 113: MDSC experiment (open pan) of calcium sulphate dihydrate under argon.
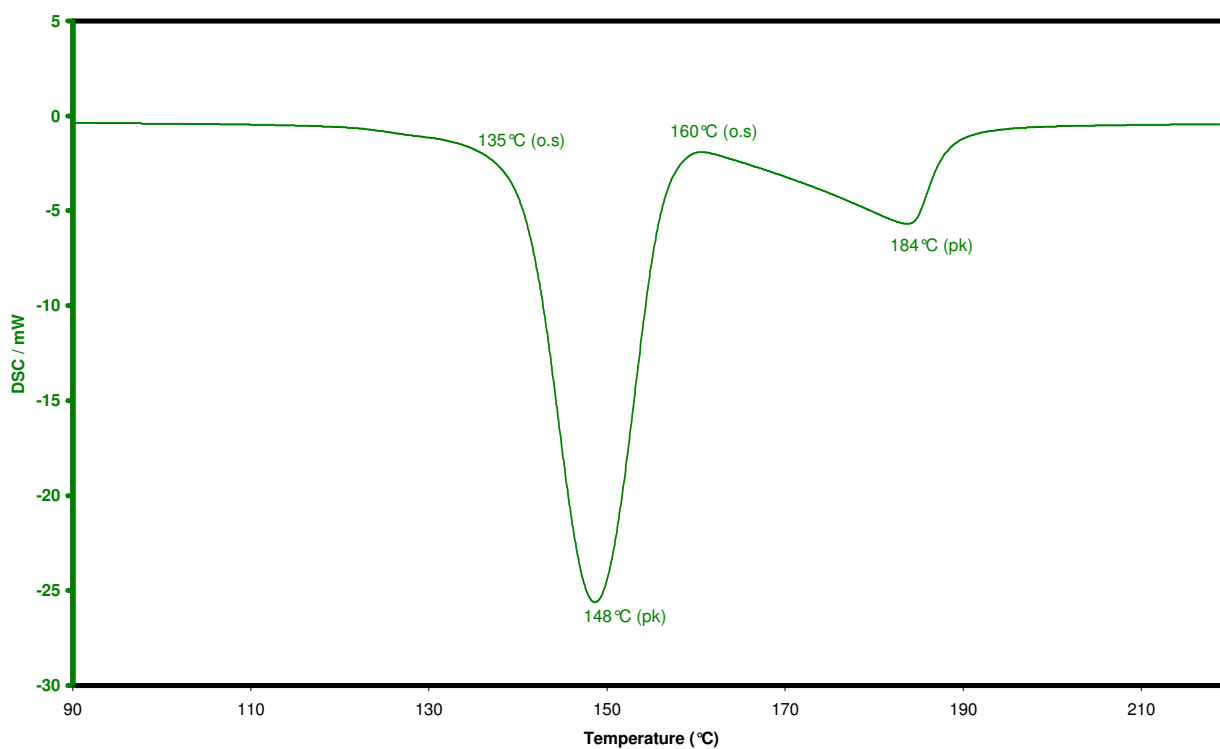
Graph 114: MDSC experiment (pin hole pan) of calcium sulphate dihydrate under argon.

MWDTA experiments were performed under argon at a heating rate of 10 °C/min. Sample sizes were typically 30 mg.

MWDTA 100% Gypsum IH0848

Heating Rate (°C/min)	10
Final Temp (°C)	250
Percentage of active sample	100%
4 stub tuning status	Manual
Sample weight (mg)	30
Iris position (mm)	138
Iris (mm)	28 x 15
Cell	HPB
mixture material	N/A
Principle T/C	Reference
Tuning position (mm)	120.5
Comments	Argon 105% chamber Sample flow 0%

Graph 115: MWDTA experiment of calcium sulphate dihydrate under argon.

The MWDTA showed resolution between the two events as in the pin hole type arrangement. It is not believed this is a "microwave effect" but more likely a result from of the sample pan type. The HPB cell is fundamentally a long sided quartz crucible, and therefore more susceptible to retaining sample induced atmospheres and increasing the likelihood of the portions outside the hot zone condensing the evolved vapour. The induced atmosphere has the effect of increasing the vapour pressure like the pin holed type arrangement and can be removed by increasing the flow rate of the carrier gas if required.

Comparison between microwave and conventional techniques again showed the transition to occur at dissimilar temperatures, the first transition appearing to start at a lower temperature. Again this is thought to be due to the reduction in thermal mass. The second transition appeared to start within 4 °C of the HDSC measurement but the peak minimum temperature was reduced by around 10 °C possibly due to more of the sample being at a uniform temperature in a microwave run, compared to the time dependence of a conventional system. Overall there seemed to be no change in how well the material coupled between the hydrated species and the anhydrous form possibility indicating the sample only showed enthalpy transitions.

7.7 Solid-solid phase changes

The transitions observed in the thermal studies of polymorphic materials fundamentally can be put into two categories:-

- Where the transition is accompanied by a change in energy, either an evolution or absorption.
- The transition has a change in heat capacity but little or no overall change in latent heat between the two phases.

The latter of the two was discussed in section 7.3 Glass transition of polymers.

Some materials exhibit changes in crystal structure when subjected to a heating program. This change in structure requires the input of energy, usually in the form of heat. This effect can be monitored using TA.

In this thesis, group I and II nitrates were studied as it was believed they might produce a trend in their ability to heat/response to applied microwaves as the cation is increased in size.

7.7.1 Sodium nitrate

Sodium nitrate ($NaNO_3$) has the second smallest cation of the group I nitrates. As with the other nitrates in the group it is known to undergo a solid-solid phase change prior to the fusion. DSC studies showed the response from the phase change was relatively small compared to the fusion and also possessed a broad onset to the transition. The experiment consisted of testing around 4 mg in a pin-holed pan under argon in the MDSC in the dynamic mode. Once again the heating rate was set to 10 °C/min.
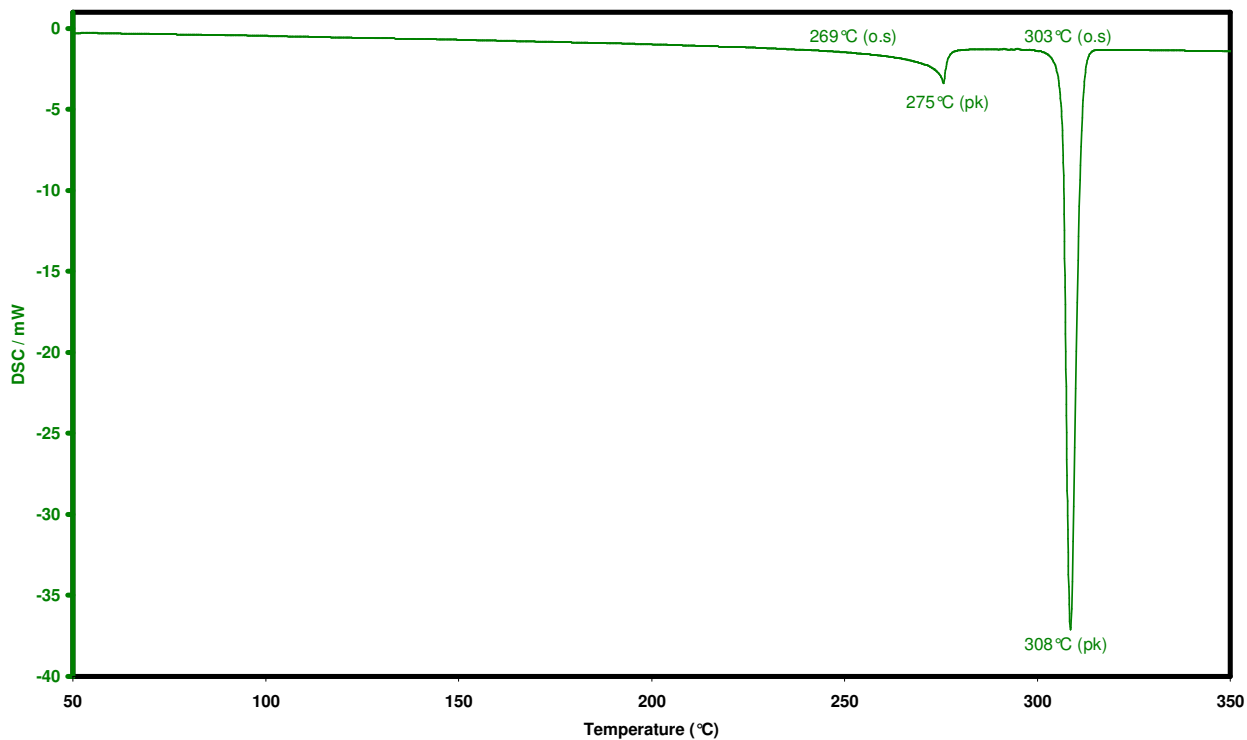
Graph 116: MDSC experiment (pin hole pan) of sodium nitrate under argon.

The results showed a broad transition with an onset at around 269 °C, followed by a melt at an extrapolated onset temperature of 303 °C.

The MWDTA experiments consisted of testing 20 mg of sample under argon at a heating rate of 10 °C/min.

MWDTA 100% Sodium nitrate IH0938

Heating Rate (℃/min)	10
Final Temp (℃)	350
Percentage of active sample	100%
4 stub tuning status	Manual
Sample weight (mg)	20
Iris position (mm)	138
Iris (mm)	28 x 15
Cell	HPB
mixture material	N/A
Principle T/C	Reference
Tuning position (mm)	120.5
Comments	Argon 105% Sample flow 0% Alumina sandwich
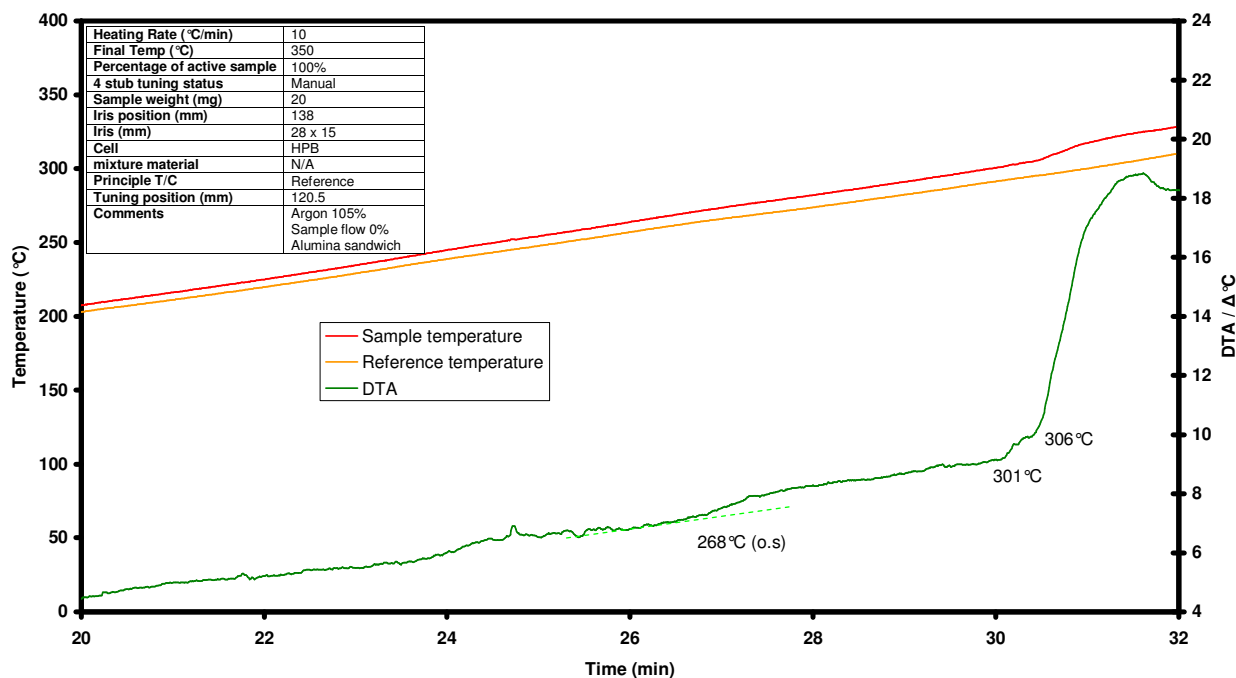
Graph 117: MWDTA experiment of sodium nitrate under argon.

The results did not show a clear transition at the phase change only a slight (but continuous) deviation in the baseline most likely due to a slight increase in coupling after the polymorph is formed. The second recorded transition was characteristic of a strongly endothermic transition with a dielectric change where the MWDTA responds to the first point of change seen in the MDSC (301 °C) as the temperature approaches the peak maximum (308 °C) seen in the MDSC (the maximum rate of change). The temperature rise due to changes in coupling is balanced by the full endothermic nature of the melting process, but eventually dominates.

7.7.2 Potassium nitrate

The phase transition in potassium nitrate is not as straightforward as it would appear. Potassium nitrate has two closely occurring phase changes both in the region of 128–134 °C. On heating there is a transformation from form II to form I at 128 °C (extrapolated onset). On cooling a form III is evident. At low temperatures the transformation from form III to form II is slow therefore reheating the sample soon after the first heat resolves the transition to a form III to form I transition peaking at 130 °C.

In a DSC experiment the first heat usually shows both phases which can be seen as a double headed unresolved peak. On the second heat only the III-I phase change is evident.

Conventional experiments were performed on the MDSC and consisted of testing around 5.03 mg in a pin-hole pan under argon in the dynamic mode. Once again the heating rate was set to 10 °C/min.
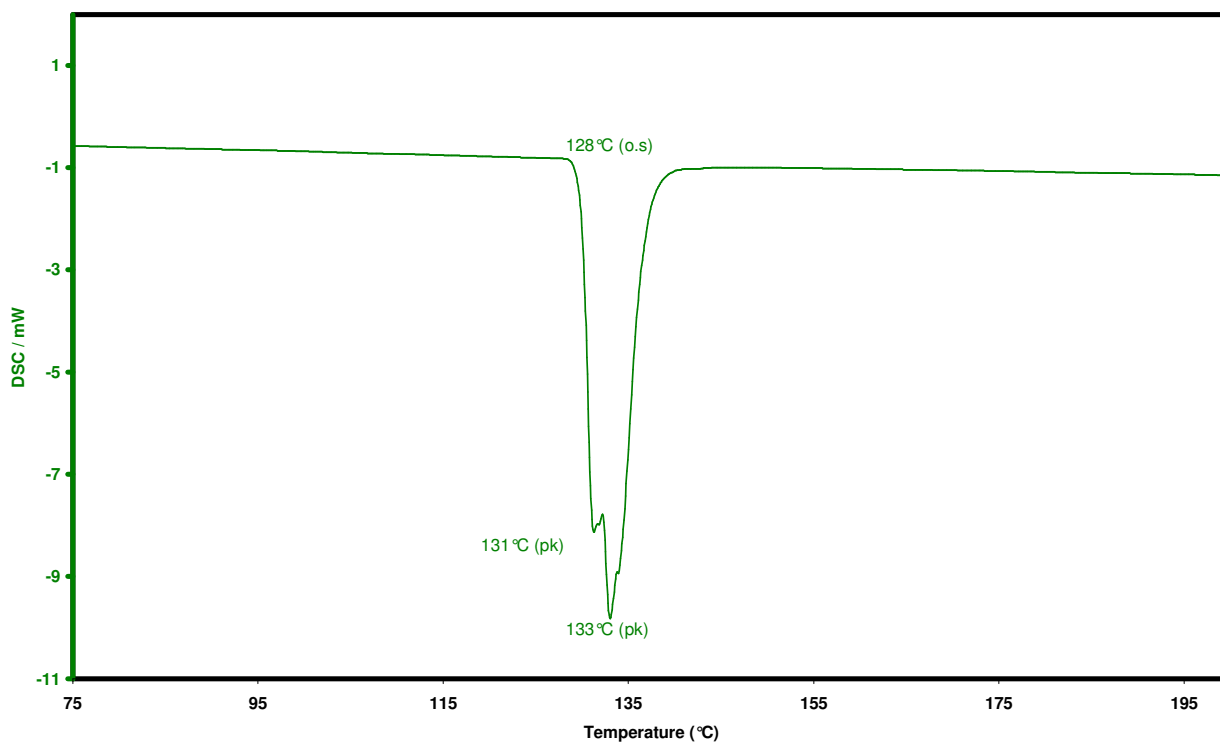
Graph 118: MDSC experiment (pin hole pan) of potassium nitrate under argon.

On the first heat the sample showed an extrapolated onset of 128 °C. The peak temperature was shown to be 131 °C. This was thought to be the transition from form III-II. A second peak temperature was also seen at 133 °C, due to the residual material in form II going through the phase change to form I.

The second heat of the material showed only the III-I transition as the sample was not left long enough to revert to the II form.

Potassium nitrate 2nd heat
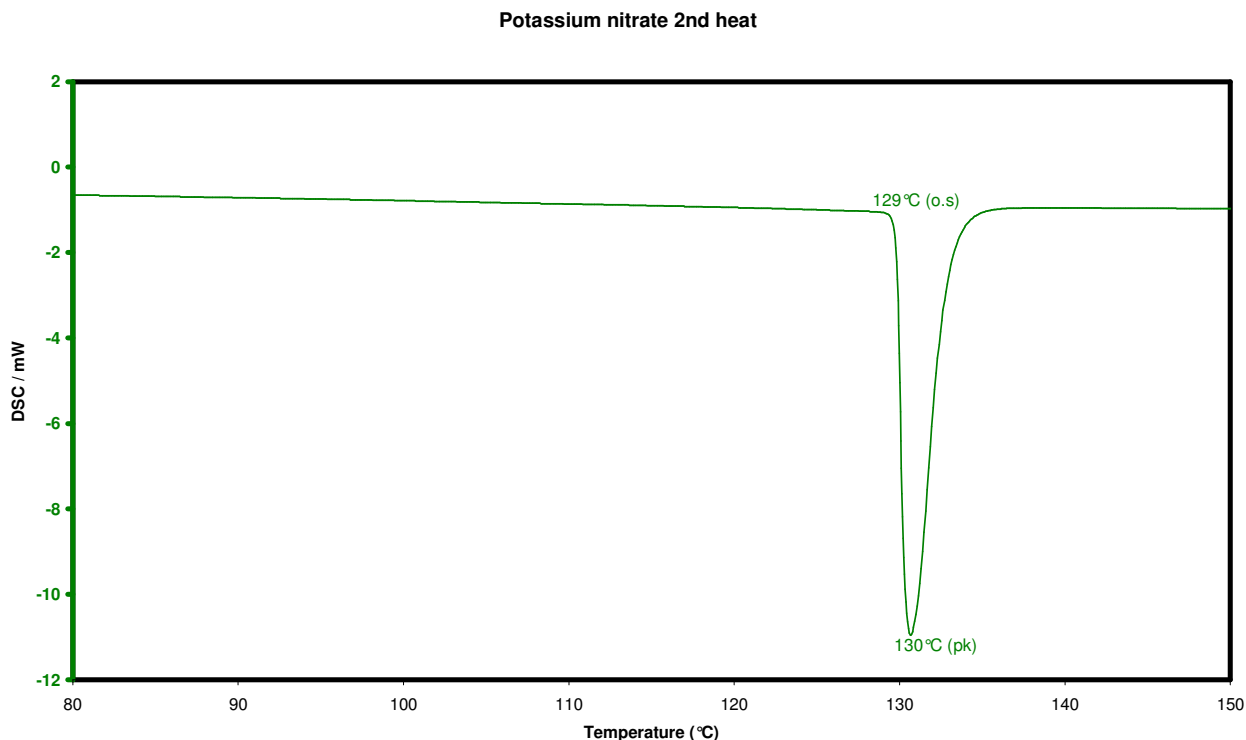
Graph 119: MDSC experiment (pin hole pan) of potassium nitrate (second heat) under argon.

The MWDTA experiments did not show the same trends in heating as conventional methods. The experiments consisted of 40 mg sample being tested under argon at a heating rate of 10 °C/min.

MWDTA 100% Potassium nitrate IH0565
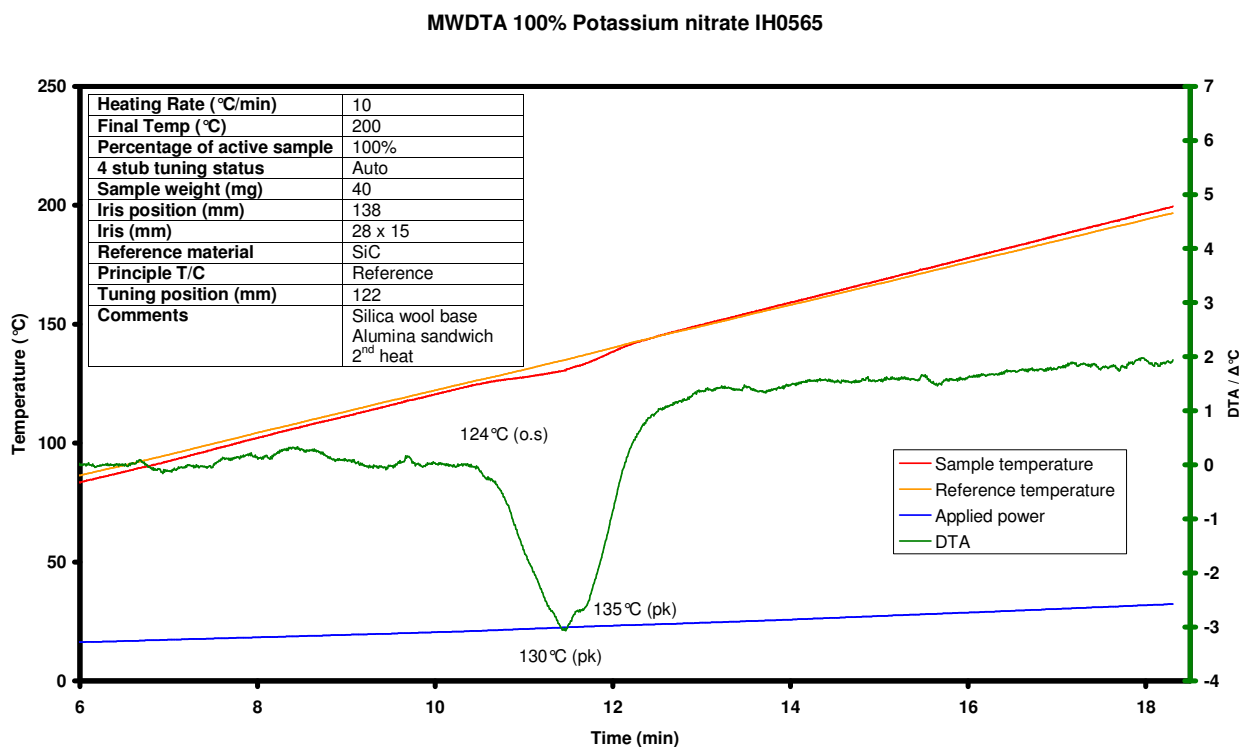
Graph 120: MWDTA experiment of potassium nitrate (second heat) under argon.

The results showed that both phases could be seen even in the second heat. This is because the magnitude of a response from even very low amounts of materials is so large that it can influence the differential trace, illustrating an example of the increased sensitivity seen in MWDTA experiments. A change in baseline was also evident after the transition due to the increase in coupling ability of the I form of the material compared to the III and II forms.

7.7.3 Rubidium nitrate

Rubidium nitrate is well known to have three solid-solid transitions where the $RbNO_3$ crystal changes shape before the melt. The changes between IV, III, and II are reported in literature to involve changes in the position of the rubidium ions [41]. At the final transition temperature the sample goes through a melt. Literature reports the transition temperatures as being:

$$IV \xrightarrow{\ 164°C\ } III \xrightarrow{\ 219°C\ } II \xrightarrow{\ 291°C\ } I \xrightarrow{\ 315°C\ } liquid$$

$$\text{trigonal} \rightarrow \text{cubic} \rightarrow \text{rhombohedral} \rightarrow \text{cubic}\ \ [65]$$
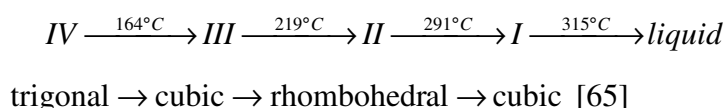
Conventional experiments were performed on the MDSC and consisted of testing around 5.13 mg in a pin-holed pan under argon in the dynamic mode. Once again the heating rate was set to 10 °C/min.
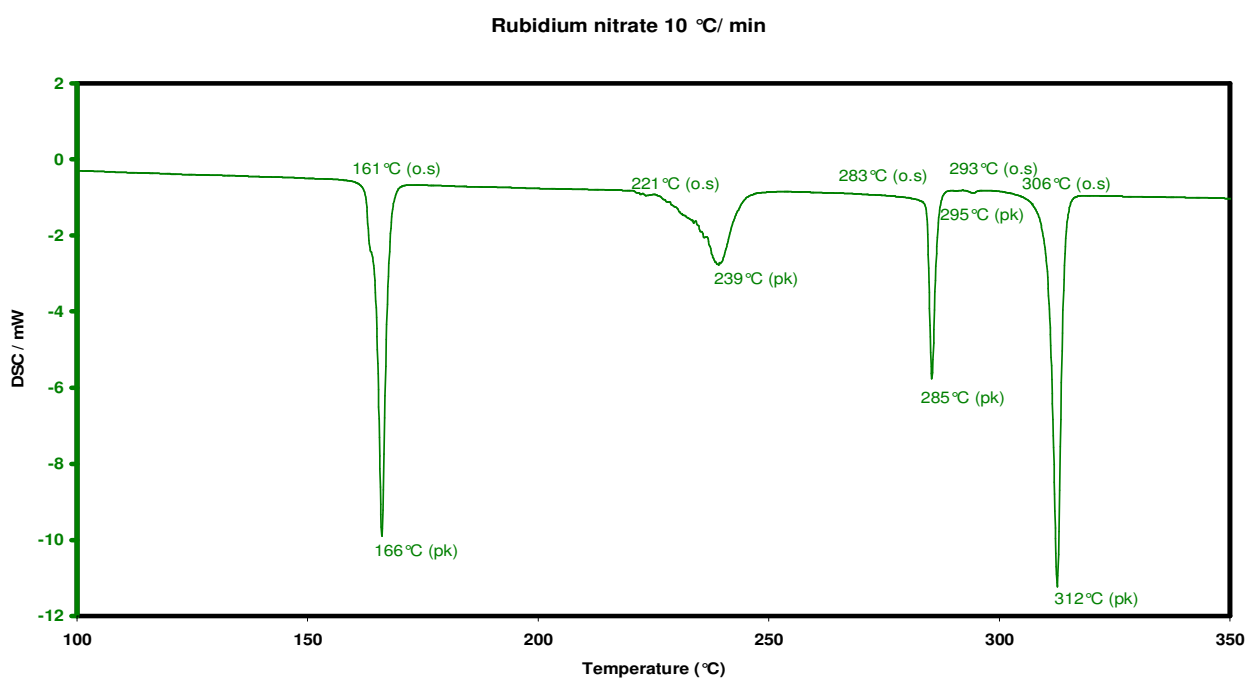
Graph 121: MDSC experiment (pin hole pan) of rubidium nitrate under argon.

The experiment showed the four transitions clearly and in good agreement with literature. The second transition recorded at the III-II temperature transition appeared to be noisy on the first heat, but reheating of the sample appeared to greatly resolve this (see Graph 122, page 262).

Rubidium nitrate 2nd heat 10 ℃/ min
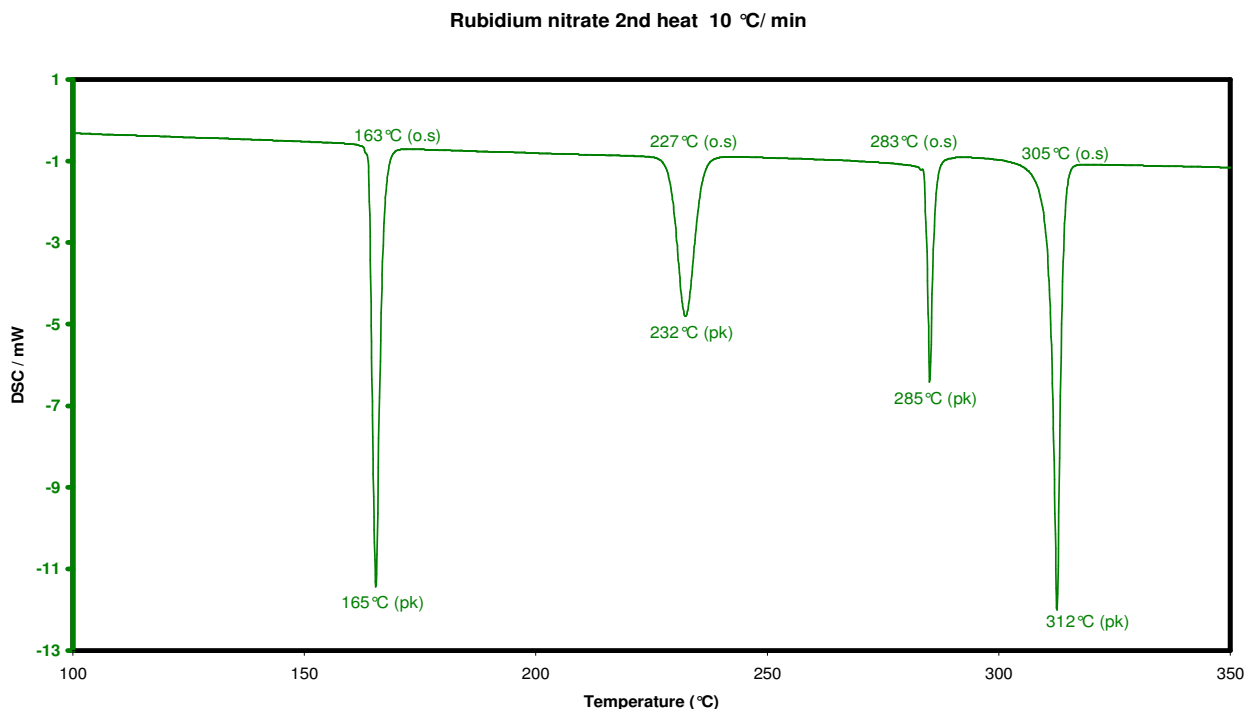
Graph 122: MDSC experiment (pin holed pan) of rubidium nitrate (second heat) under argon.

The MWDTA experiments consisted of 6 mg sample being tested under argon at a heating rate of 10 °C/min. The sample size was reduced as it was found several of the dielectric changes observed during heating were uncontrollable at higher masses. It should also be noted in order to gain control over the stronger transitions, the instrument was operated in MWTA (MWDTA) mode where the heating rate was controlled on the sample temperature and not the reference. In this mode a decrease in tan δ is illustrated in the trace as an increase in the differential temperature as the power will fall to keep the sample temperature linear resulting in a fall in the reference temperature.

MWDTA 100% Rubidium nitrate IH0539
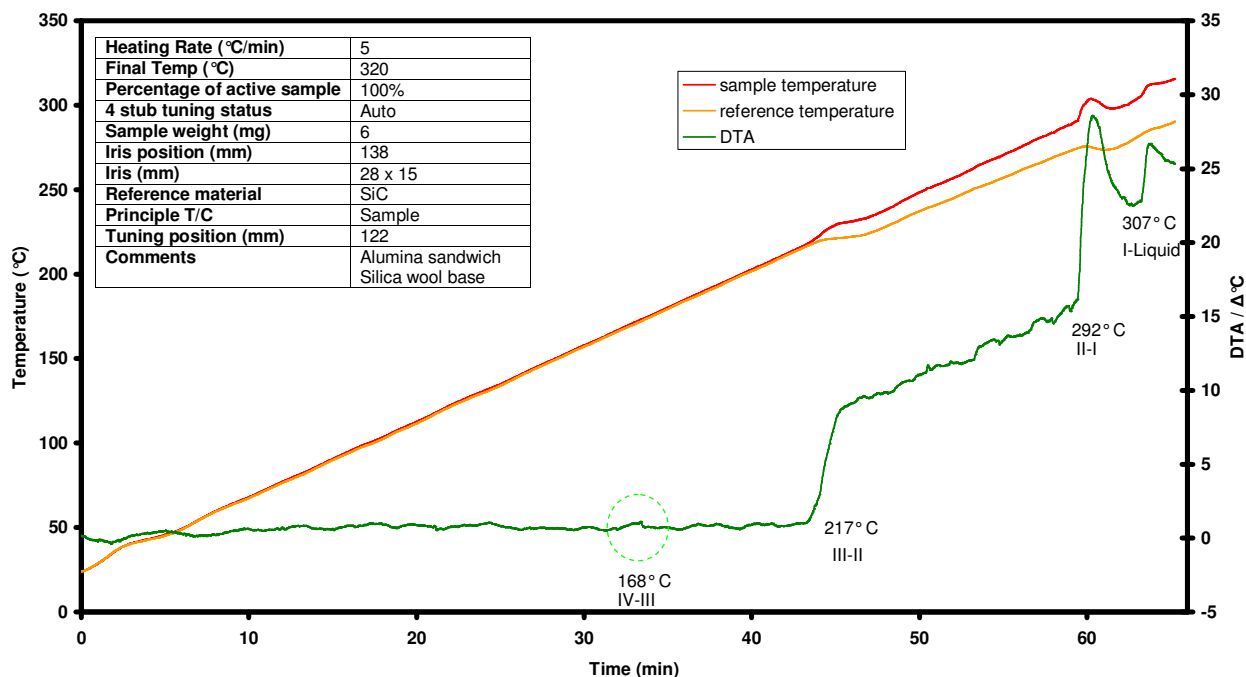
Graph 123: Representative MWTA (MWDTA) trace of Rubidium nitrate.

The first transition (IV-III) does not appear to have a very noticeable change in dielectric, and as a result of the reduced sample size the enthalpy change was small also. Graph 123 highlights how the temperature where the IV-III should be observed is featureless.

The other two transitions have a large change in coupling which causes the temperatures to deviate from one another. All the structural changes could be seen to be in close correlation with literature [65] although the II-I, and the I-Liquid change occur slightly earlier than expected. This is again believed to be the instrument responding to the first point of change seen in the DSC.

MWDTA 100% Rubidium nitrate IH0559
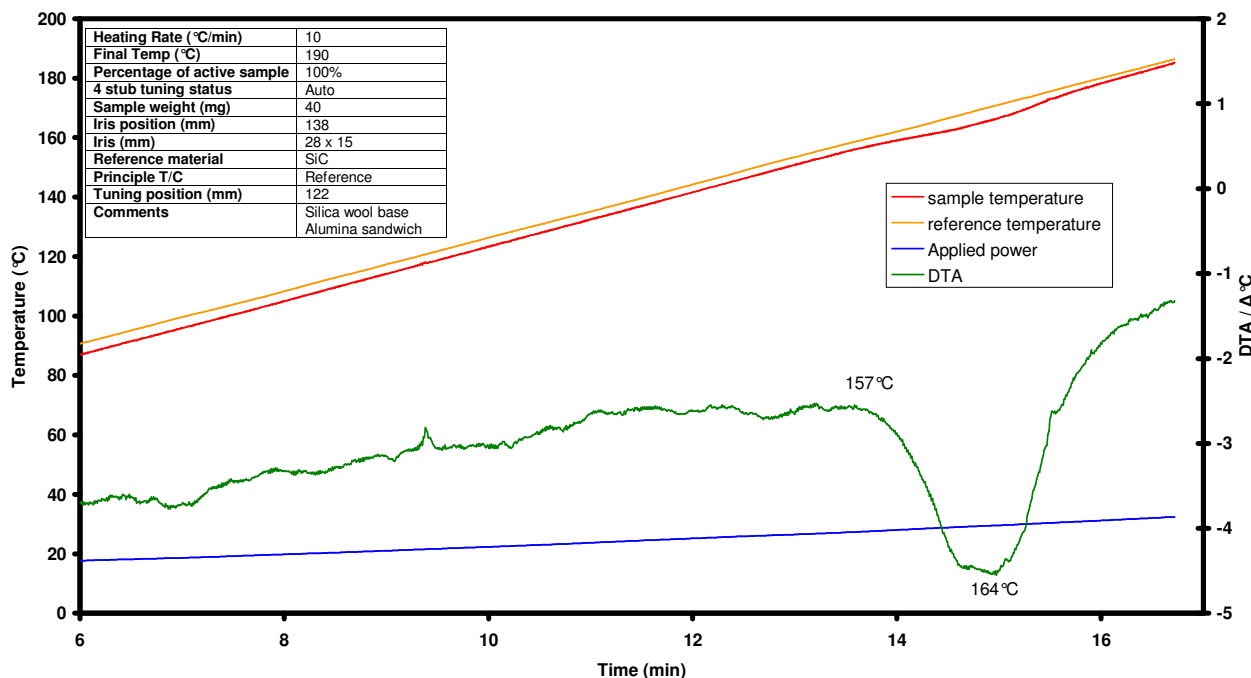
Graph 124: Representative MWDTA trace of Rubidium nitrate up to the completion of the first transition

In order to show the first transition was recordable another experiment was performed with a larger sample mass under the same conditions. The sample was taken to just past the first transition temperature. The result showed the transition exhibits very little dielectric change (~ 1 °C when using a large sample for this cell type) but significant enthalpy change.

The rubidium nitrate experiments showed for the first time a material which exhibited a number of different responses in MWDTA in a single experiment.

1. The IV-III transition appeared to show purely enthalpy responses in a microwave experiment,
2. A solid-solid phase change that appeared to show a reduction in tan δ (the first solid-solid transition which showed this response during this research)
3. The expected rises in coupling attributed to phase changes.

7.7.4 Caesium nitrate

The polymorph of caesium nitrate proved problematic when tested in MWTA mode as it appeared to have little or no dielectric change. The power of differential techniques is the increased sensitivity in regards to weak transitions. Conventional experiments were performed on the MDSC and consisted of testing around 5.3 mg in a pin-hole pan under argon in the dynamic mode. Once again the heating rate was set to 10 °C/min.
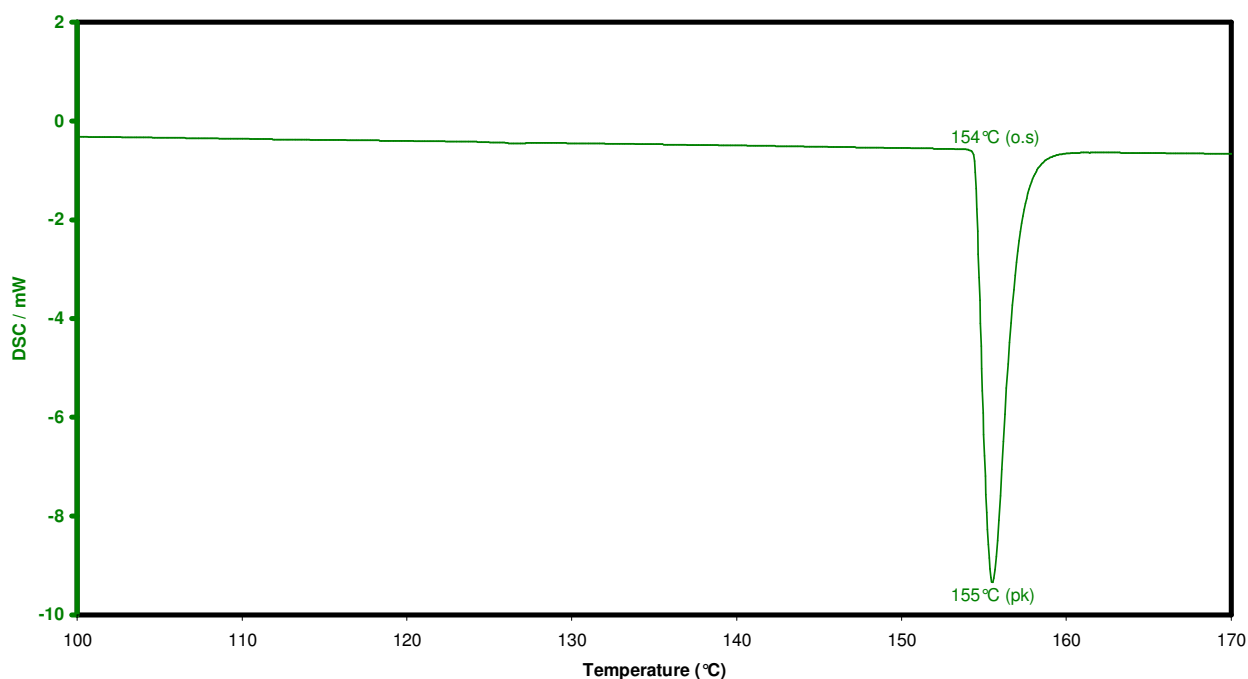
Graph 125: MDSC experiment (pin hole pan) of caesium nitrate under argon.

The results showed the transition could be clearly seen on the MDSC, with an extrapolated onset at around 154 °C.

The MWDTA experiment consisted of a 40 mg sample being tested under argon at a heating rate of 10 °C/min.

MWDTA 100% Cesium nitrate 99.999% IH0553
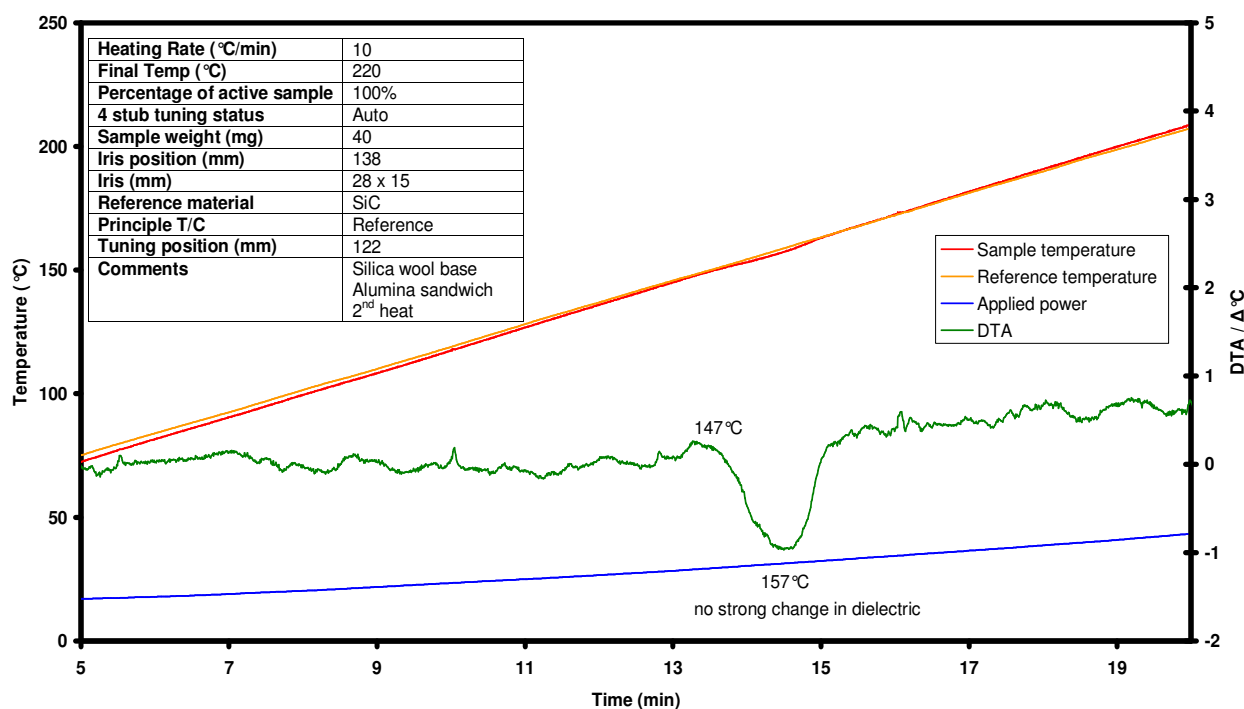
Graph 126: MWDTA experiment of caesium nitrate under argon.

The sample size was increased in order to observe the phase change as it is an enthalpy only transition, the lack of any abrupt changes in the applied power trace (blue line) is shown in Graph 126 to illustrate that sample did not directly interact with the applied wave. The results showed an onset temperature of 147 °C, slightly lower than the conventional experiments. In general the transition appeared to occur over a larger area. It is believed as the instrument is not designed to monitor enthalpy changes, and functioned (at best) as an entry level DTA, this peak broadening was a result of the difference in instrumentation. The baseline showed little change from the pre-transition value, indicating no significant dielectric change as the material was heated. The MWDTA run of caesium nitrate showed again that enthalpy only or weakly dielectric events can be seen in a microwave experiment even though the instrument was not designed for such transitions the implementation of the HPB cell made it possible.

7.7.5 Magnesium nitrate hexahydrate

The industrial application of magnesium nitrate hexahydrate has been discussed in previous chapters. The material is known to undergo a polymorphic change (like group I nitrates) followed by a dehydration. Conventional experiments were performed on the MDSC and consisted of testing

around 4.46 mg in a pin-hole pan under argon in the dynamic mode. Once again the heating rate was set to 10 °C/min.
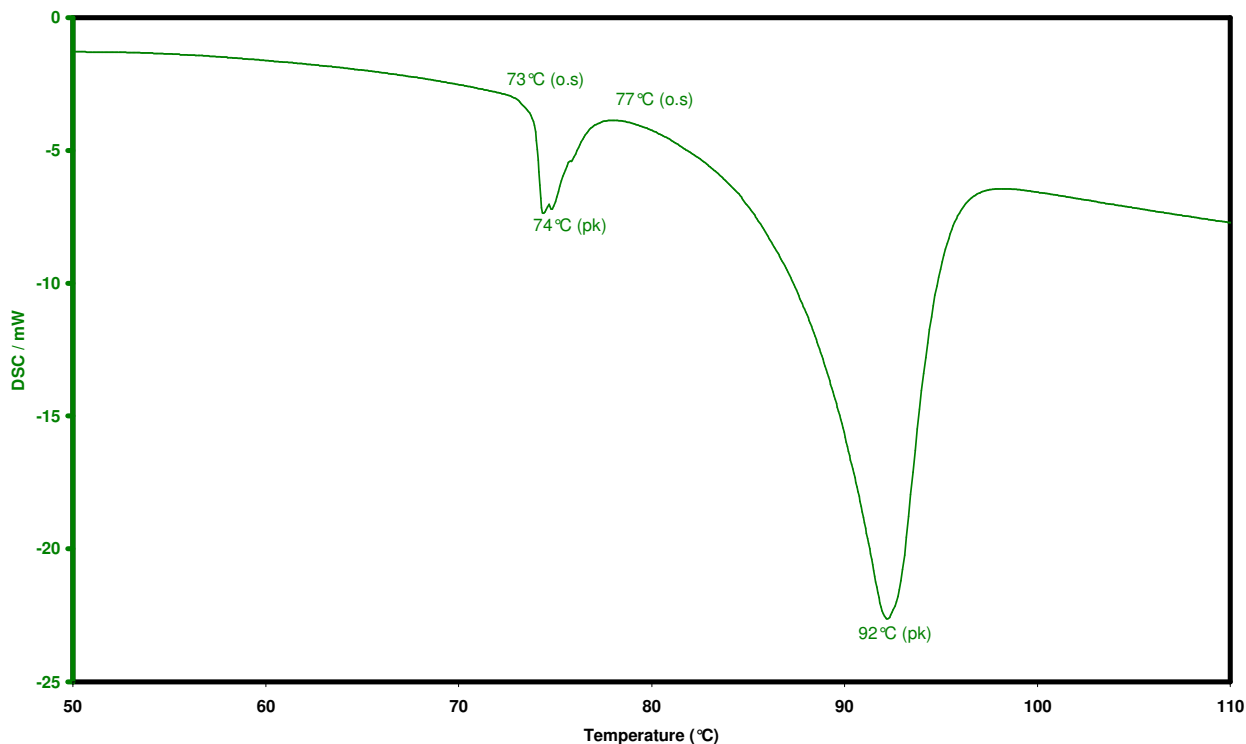
Graph 127: MDSC experiment (pin hole pan) of magnesium nitrate hexahydrate under argon.

The results showed both transitions in close succession to each other, the first transition (polymorph) showed an onset temperature of around 73 °C. The dehydration onset temperature was around 4 °C later. The broadness of the peak is thought to be due to the nitrate dissolving in its own water of crystallisation.

The MWDTA experiment consisted of 40 mg sample being tested under argon at heating rate of 10 °C/min.

MWDTA 100% magnesium nitrate hexahydrate IH0585
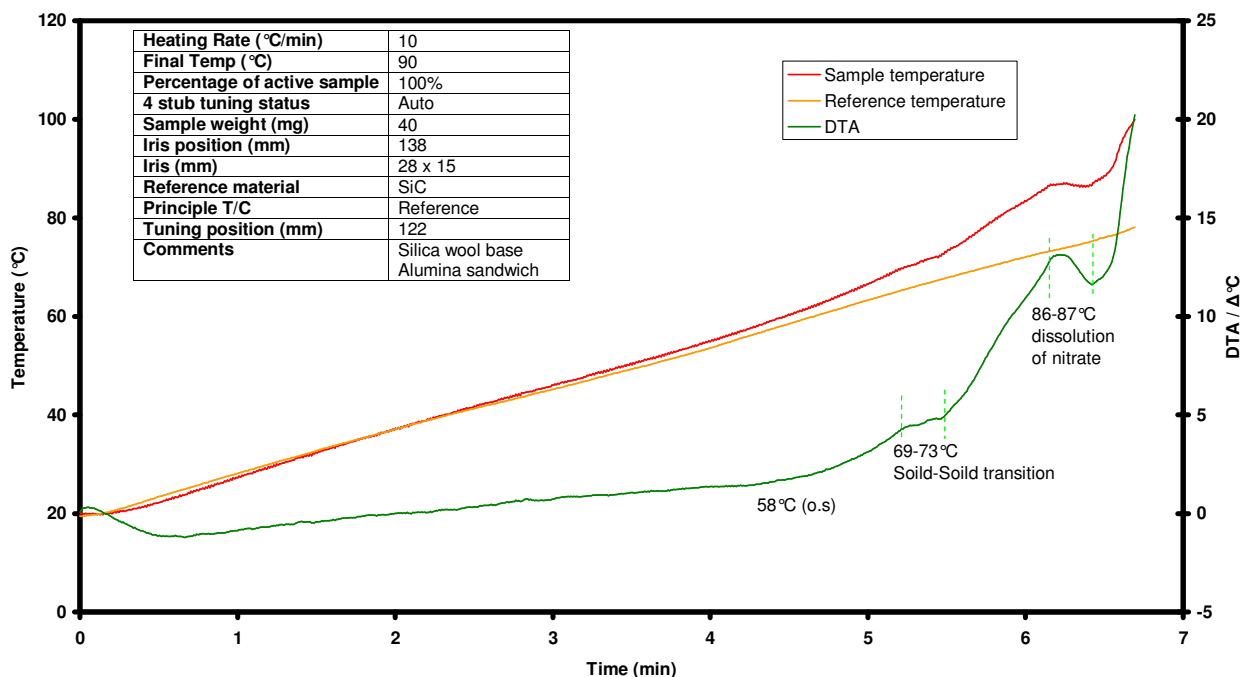
Graph 128: MWDTA experiment of magnesium nitrate hexahydrate under argon.

The results showed a deviation of the differential trace at a 58 °C which did not correlate with any transition seen in the MDSC experiment. It did however occur at the point where the DSC trace started to deviate from linearity. It was possible this was a result of the sample starting to liberate free water, resulting in the increase in the coupling recorded, and the endothermic trend seen in the MDSC.

The next event is seen as a levelling off of the temperature rise. It corresponded to the solid-solid phase change possibly indicating that the endothermic nature of the transition was balanced by the change in tan δ. The change in morphology had the effect of increasing the temperature rise seen by the change in gradient of the MWDTA trace (73 °C). The temperature rise is again opposed by the endothermic nature of the dissolution of the nitrate (86-87 °C). The dissolution is closely followed by a sharp increase in the sample temperature probably resulting from the molten sample (now an aqueous ionic nitrate solution) coupling well with the applied microwave radiation.

7.8 Liquid crystal fusions

In the 1800's an Austrian botanist, Fredrich Reinitzer was researching the role of cholesterol in plants. Near the end of the century he was starting to measure the melting point of cholesteryl benzoate when he noticed the sample appeared to have two melting points. Reinitzer sought the help of a German physical chemist, Otto Lehmann who at the time was developing a method of studying melting and re-crystallization processes, using polarized light microscopy. His studies found that a turbid, brightly coloured liquid existed between the liquid phase and the crystal phase. This property was usually found with birefringent materials and was associated with amorphous samples, although these samples also had the ability to flow (a liquid property). The combination of both of these properties led them to propose the existence of a so called "liquid crystal".

Liquid crystals can undergo several phases changes before forming the isotropic liquid, the most common of which is the nematic phase, in this form the centres of the molecules are arranged randomly but in general all the molecules point in the same direction. Another common phase is the smectic phase where the arrangement of the molecules in adjacent layers shows no correlation with each other although the principle axis of the layers all point in the same direction.
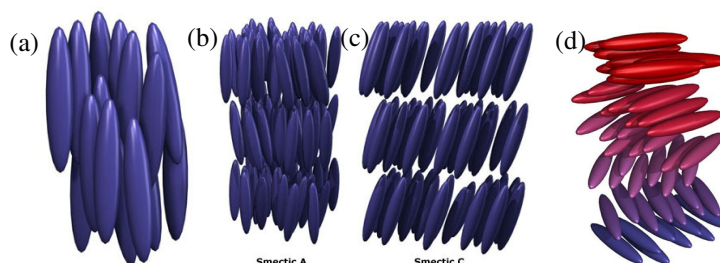
Figure 69: Different liquid crystal forms (a) nematic (b) smectic A (c) smectic C (d) cholesteric [66]

At the isotropic liquid phase change or "clearing temperature" the molecular arrangement is lost and the liquid acts as a normal liquid. Recently, liquid crystals have been of interest to thermal analysts as calibration standards [67] as a test of sensitivity.

It was thought that the changes in structure would affect how the material interacted with microwave power, as the extent of dipolar polarisation would change as the material became more fluid. As it was unsure how well events would be illustrated in non-modulated DSC traces and to confirm that each event recorded was a fusion, the following group of experiments where performed using a modulated method. The experimental conditions, as detailed previously (see 7.1.1.2 Differential thermal measurements, page 198). Both the forward and reversing traces are

included in the following graphs to aid in confirming that all the transitions seen in the DSC traces where fusions and not a fusion flowed by a different transition type.

For the first time the heating rates of the conventional and microwave experiments were not identical. The reason for this change was because for clear modulated results a slower heating rate is required (~3 °C/min), whereas slower heating rates in the MWDTA showed a large increase in instrumental noise which had the potential to eclipse the smaller liquid crystal fusions. With a heating rate three times faster than the conventional method it was expected that the resolution of the MWDTA would be worse than the modulated method, therefore if resolution could be achieved at this heating rate it would be beneficial.

If resolution could not be achieved it may be due to the heating rate and not just the technique, unfortunately time did not allow for improvements to be made to the noise reduction at slower heating rates during this research.

7.8.1 Azoxyanisole
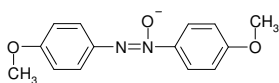
Azoxyanisole has been used by many manufactures to demonstrate instrumental sensitivity for observing consecutive transitions over small temperature ranges. Azoxyanisole undergoes several changes before the isotropic liquid. Firstly the sample goes from crystalline to a nematic then into the isotropic liquid. The semi-liquid states of the nematic phases and the isotropic liquid stage were thought would have a large change in dielectric owing to the increase in dipolar polarisation associated with each phase change in a microwave experiment.

The conventional experiment consisted of analysing around 5 mg of sample in an encapsulated pin hole aluminium pan under argon.
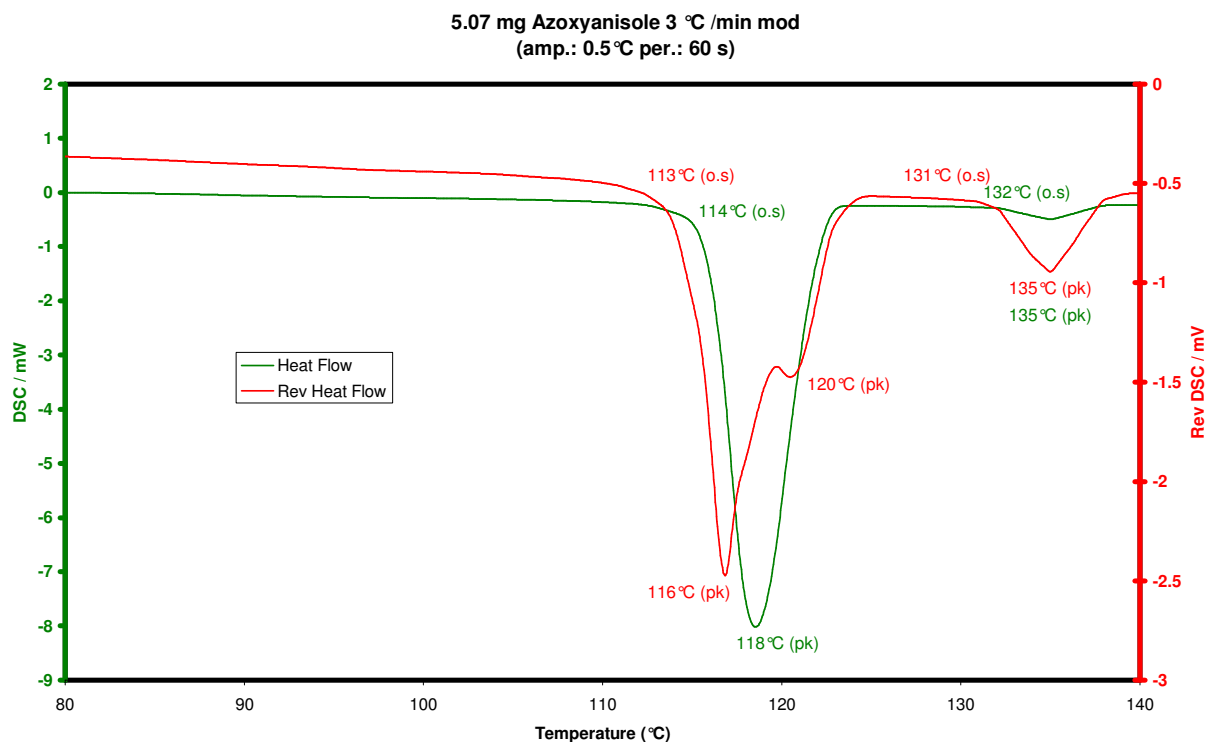
Graph 129: MDSC experiment (pin hole pan) of azoxyanisole under argon.

The results (shown in Graph 129, where the green trace shows the heat flow in the forward direction and the red trace show the reversing heat flow) from the forward heat flow trace indicate a strong transition with an onset of around 114 °C while the second transition gives an onset temperature of around 132 °C. The reversing heat flow showed that both transitions were reversible and therefore probable they were melts.

The equivalent MWDTA experiment consisted of 20 mg of sample being tested in the HPB cell under argon at a heating rate of 10 °C/min.

MWDTA 100% Azoxyanisole IH0738
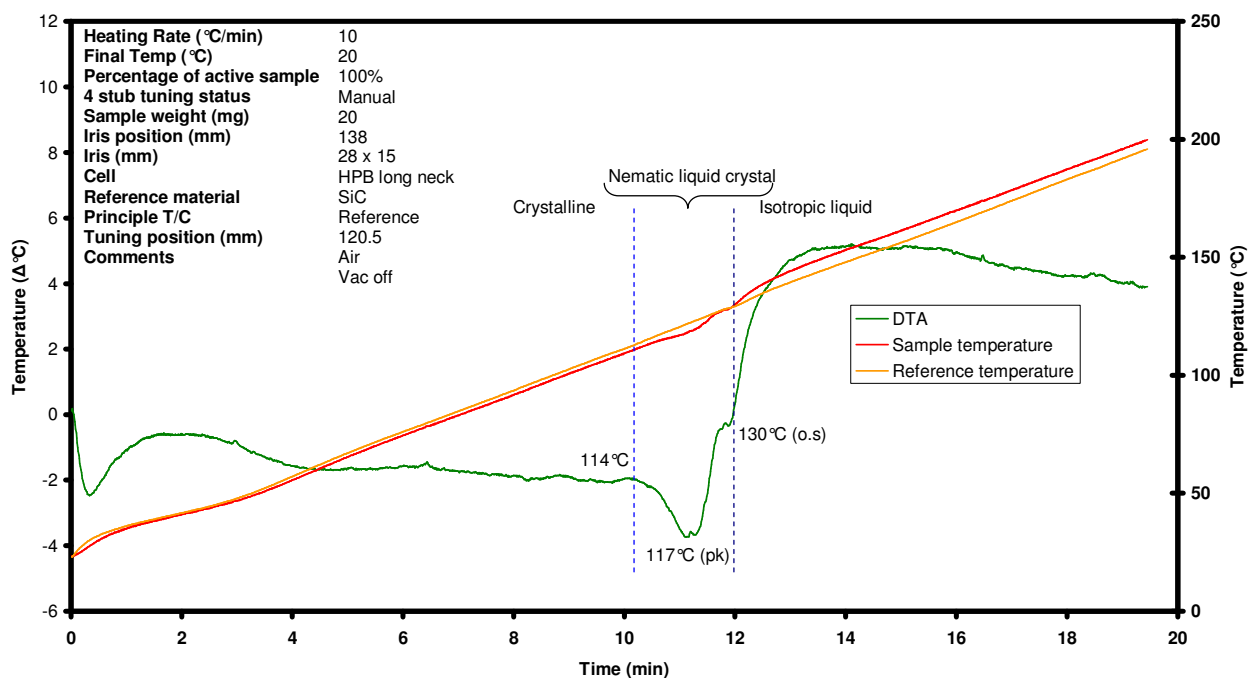
Graph 130: MWDTA experiment of azoxyanisole under argon.

The MWDTA experiment shown in Graph 130 showed interesting results, it was expected that the two stages would be shown as two steps in close succession to each other. It appeared the MWDTA did not record the change from crystalline to nematic as a change in coupling with an increase in the differential temperature but only the enthalpy of the transition was observed. The explanation is thought to be due to the large enthalpy of the liquid crystal formation overshadowing any small change in tan δ. The transition temperature for both techniques appeared to occur within close proximity of each other. The sample showed a short recovery (where the differential baseline returned to linearity) before the second change where the weak enthalpy of the second transition (nematic to isotropic liquid) was strongly overshadowed by the change in coupling resulting in a positive step in the differential trace at 130 °C. The experiment showed that the MWDTA has the potential to resolve the transitions clearly as two different steps. This is an advantage as in a conventional experiment the second transition is very weak in terms of enthalpy and has the potential to be easily missed.

7.8.2 Cholesteryl benzoate
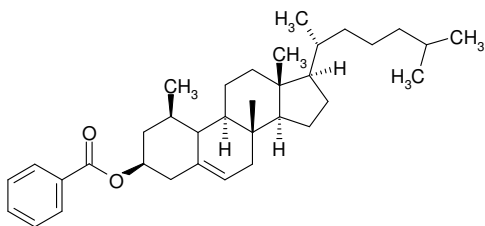
Cholesteryl benzoate was the first liquid crystal to be discovered [66]. Its thermal characteristics are similar to that of azoxyanisole with a change from the crystalline to nematic form then into an isotropic liquid. Graph 131 shows the results of an MDSC experiment on a 4.22 mg sample of cholesteryl benzoate. The change from crystalline to nematic can be seen as a strong endotherm at 144 ºC. The change to an isotropic liquid appears as a much weaker event at 178 ºC.
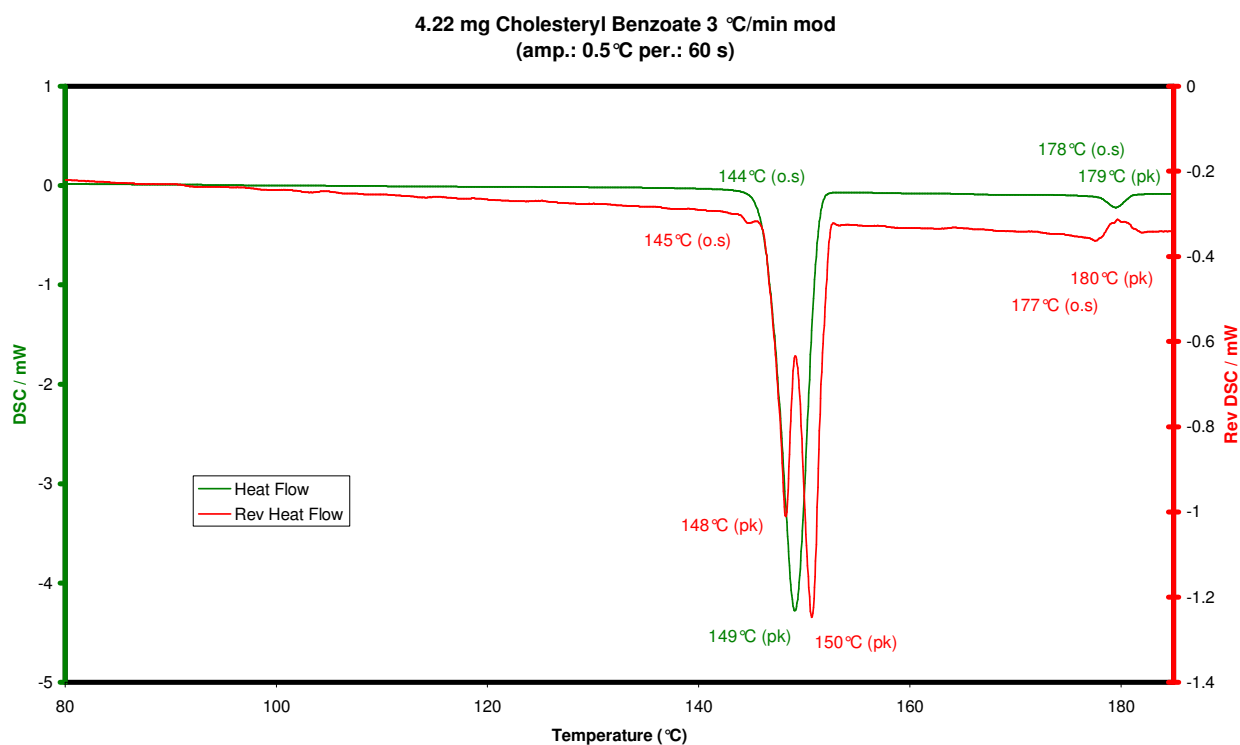
Graph 131: MDSC experiment (pin hole pan) of cholesteryl benzoate under argon.

The MWDTA experiment used a 40 mg sample with a 10 ºC/min heating rate. The results are shown in Graph 132.

MWDTA 100% Cholesteryl benzoate IH0751
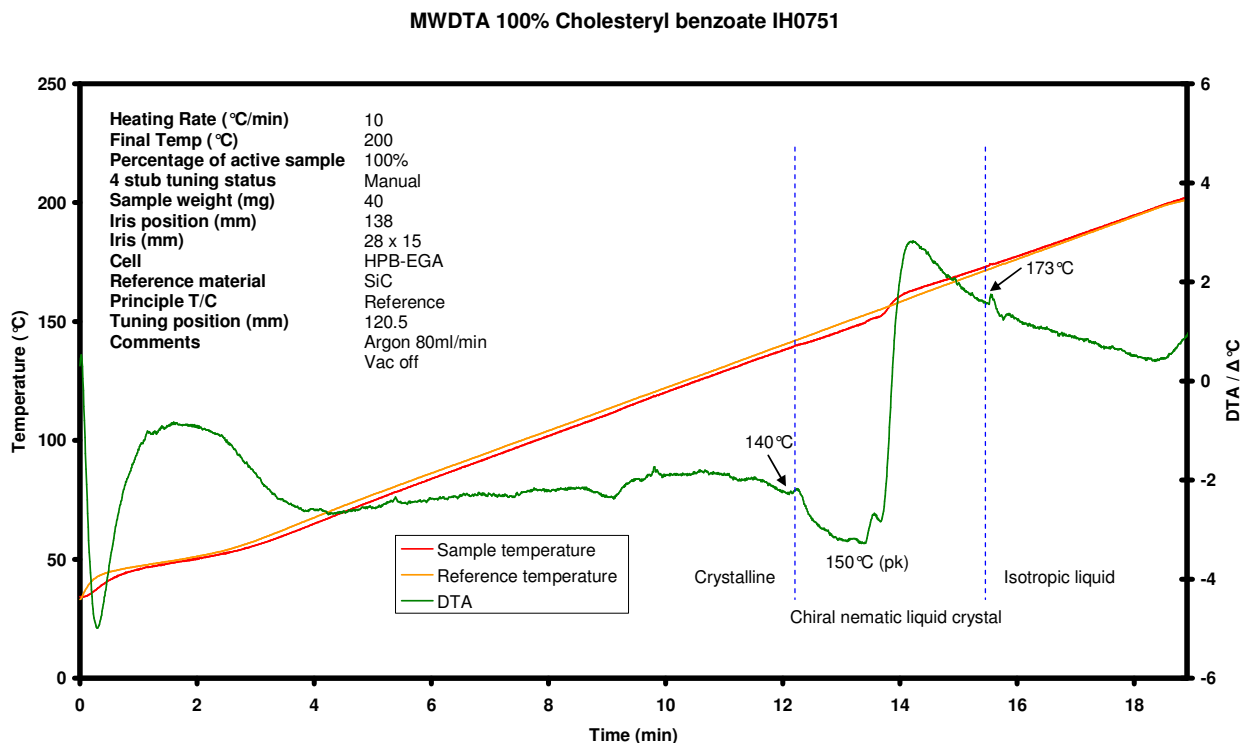
Graph 132: MWDTA experiment of cholesteryl benzoate under argon.

The differential temperature profile shows less resolution between the various transitions than observed with the azoxyanisole sample. There is an indication of the change from crystalline to nematic liquid crystal at around 140 ºC and also a significant step change at around 150 ºC. However, the transition to isotropic liquid at 173 ºC is very small and not large enough to be distinguishable from instrumental noise.

The shape of the differential profile around 150 ºC may again be due to the competition between the enthalpy of the process (ΔT goes negative) and a slight increase in tan δ (ΔT goes positive).

7.8.3 Cholesteryl myristate
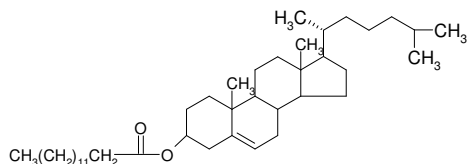
Cholesteryl myristate undergoes several liquid crystal forms before it becomes an isotropic liquid [66] over a narrow temperature range of 72 ºC – 85 ºC.

$$Crystal \xrightarrow{72°C} Smectic \xrightarrow{80°C} Cholesteric \xrightarrow{85°C} Isotropic$$
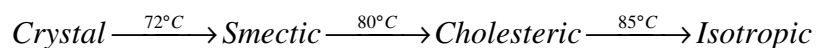
Theses structural changes are not always observed by even sensitive forms of thermal analysis equipment and are usually only monitored by polarised optical methods.

MWDTA did not show clear cut results with previous liquid crystal experiments, although it was thought possible that these different molecular arrangements (smectic, cholesteric) could have clearer responses then the nematic experiments.

5.45 mg Cholesteryl Myristate 3 ℃/ min mod
(amp.: 0.5 ℃ per.: 60 sec)
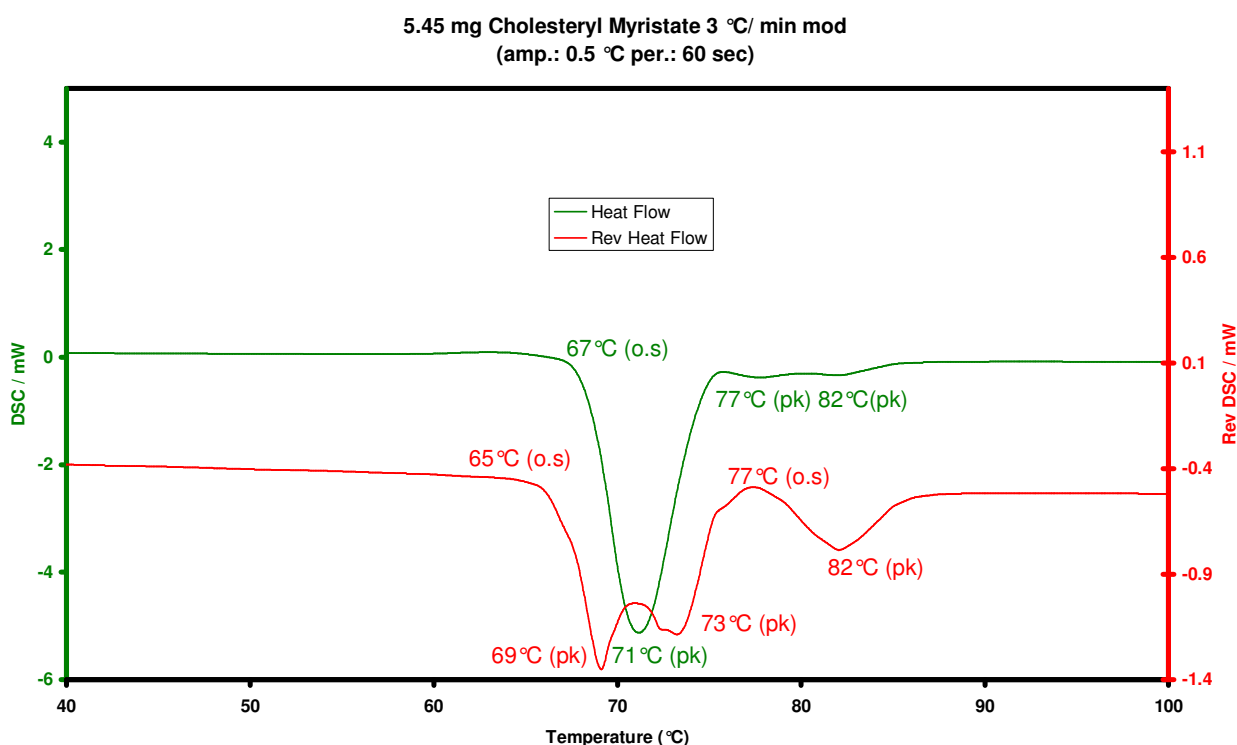
Graph 133: MDSC experiment (pin holed pan) of cholesteryl myristate under argon.

The results of testing 5.45 mg of sample are given in Graph 133 where the crystalline to smectic change is clearly seen at 71 ℃. Very weak transitions were also observed in the forward direction at the peak temperatures of 77 °C and 82 °C which are believed to be the changes to from smectic to cholesteric and cholesteric to isotropic liquid respectively.

The MWDTA experiment consisted of a sample weight of 20 mg.

MWDTA 100% Cholestryl Myristate IH0922

Heating Rate (℃/min)	10
Final Temp (℃)	100
Percentage of active sample	100%
4 stub tuning status	Manual
Sample weight (mg)	20
Iris position (mm)	138
Iris (mm)	28 x 15
Cell	HPB
mixture material	N/A
Principle T/C	Reference
Tuning position (mm)	120.5
Comments	Argon 105% Sample flow 0% Alumina sandwich
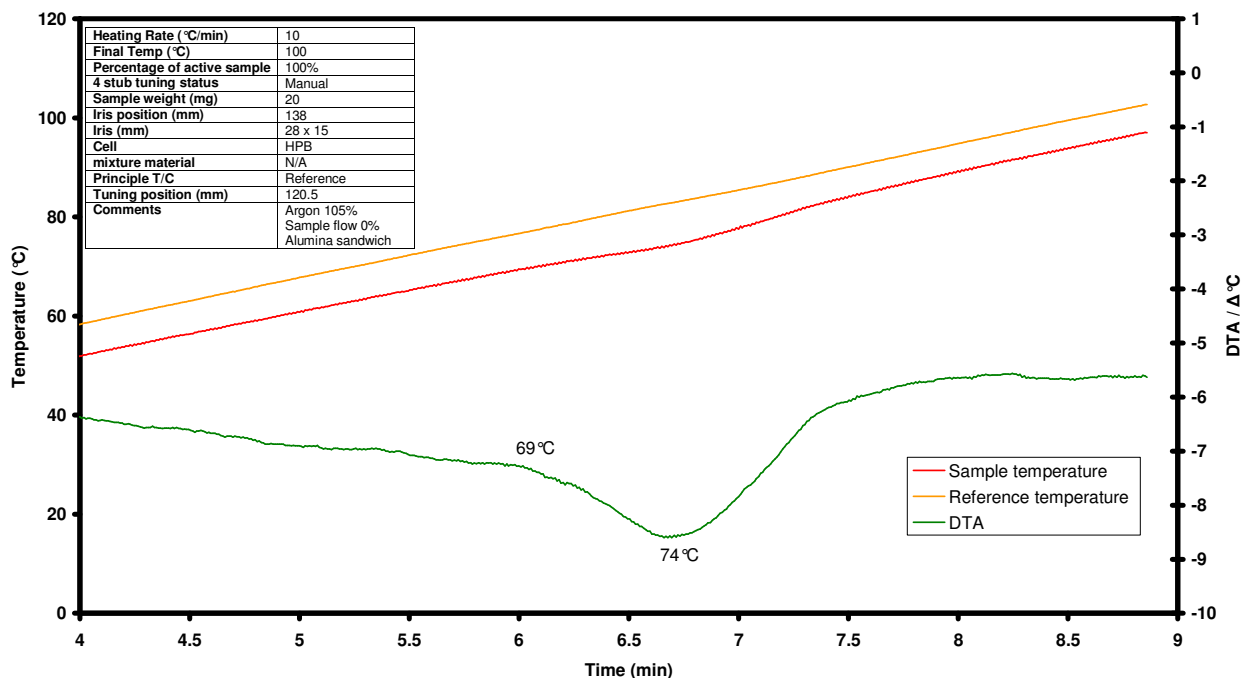
Graph 134: MWDTA experiment of cholesteryl myristate under argon.

The MWDTA experiment (Graph 134) showed poor resolution compared to the MDSC experiment. The recorded onset temperature was observed at around 69 °C, the peak temperature showed a close correlation to the maximum point of change seen in the MDSC signal, after which the full change in coupling was evident. The trace showed no other clear transition, although when the trace was expanded a slight fall in the differential temperature could be seen at around 80 °C coinciding with the transition temperature of the cholesteric to isotropic liquid phase change.

7.9 Pharmaceuticals

Information on the how pharmaceuticals couple to microwaves has become of greater interest recently owing to companies looking at microwave radiation as an alternative form of drying [68]. During the manufacturing process the products have to be dried several times, a problematic and time consuming practice.

Problems arise due to the characteristics of pharmaceuticals such as polymorphism, solvent content, and temperature stability. The thermal drying of pharmaceuticals and other powders in conventional process is dependent on evaporation of surface moisture via energy transfer from the surrounding,

and then the internal moisture moving from the bulk of the material to the surface were it is evaporated.

The thermal sensitivity of large number of pharmaceuticals mean they have to be dried at low temperatures under high vacuum resulting in long drying times or added expense. Microwaves offer an alternative, rapid, and cost-effective solution. The interaction of microwave energy with drugs, excipients or drug/excipient mixtures has not been studied in detail during this research.

MWDTA could be a useful method to investigate the effectiveness, and possible problems, which could arise in the microwave processing of different systems.

As detailed previously, in these experiments, conventional DSC was performed using the MDSC in non-modulated mode with a heating rate of 10 ºC/min. Samples were encapsulated aluminium pin holed pans and heated under argon.

The MWDTA experiments used the 20 mg of sample (unless otherwise stated) and a heating rate of 10 ºC/min. All tests were performed in the HPB cell and used argon as a blanket gas.

7.9.1 Sorbitol
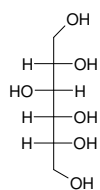
Sorbitol is commonly used as an excipient in many medicines as a sweetener or a thickening agent. The results of heating a 4.14 mg sample in the MDSC are shown in Graph 135.
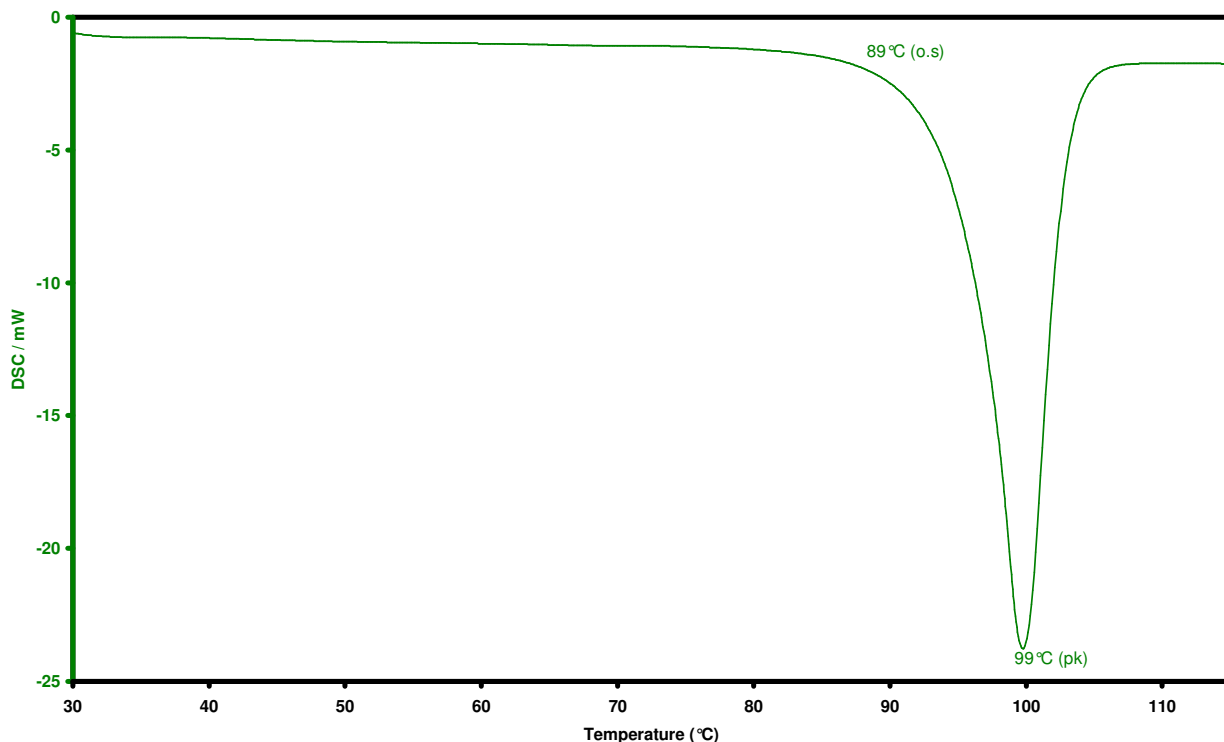
Graph 135: MDSC experiment (pin hole pan) of D-sorbitol under argon.

The results show a large, broad, endothermic transition (fusion) with an extrapolated onset at around 89 °C and a peak temperature of 99 °C.

MWDTA 100% Sorbitol IH0947

Heating Rate (°C/min)	10
Final Temp (°C)	120
Percentage of active sample	100%
4 stub tuning status	Manual
Sample weight (mg)	20
Iris position (mm)	138
Iris (mm)	28 x 15
Cell	HPB
mixture material	N/A
Principle T/C	Reference
Tuning position (mm)	120.5
Comments	Argon 105% Sample flow 0% Alumina sandwich
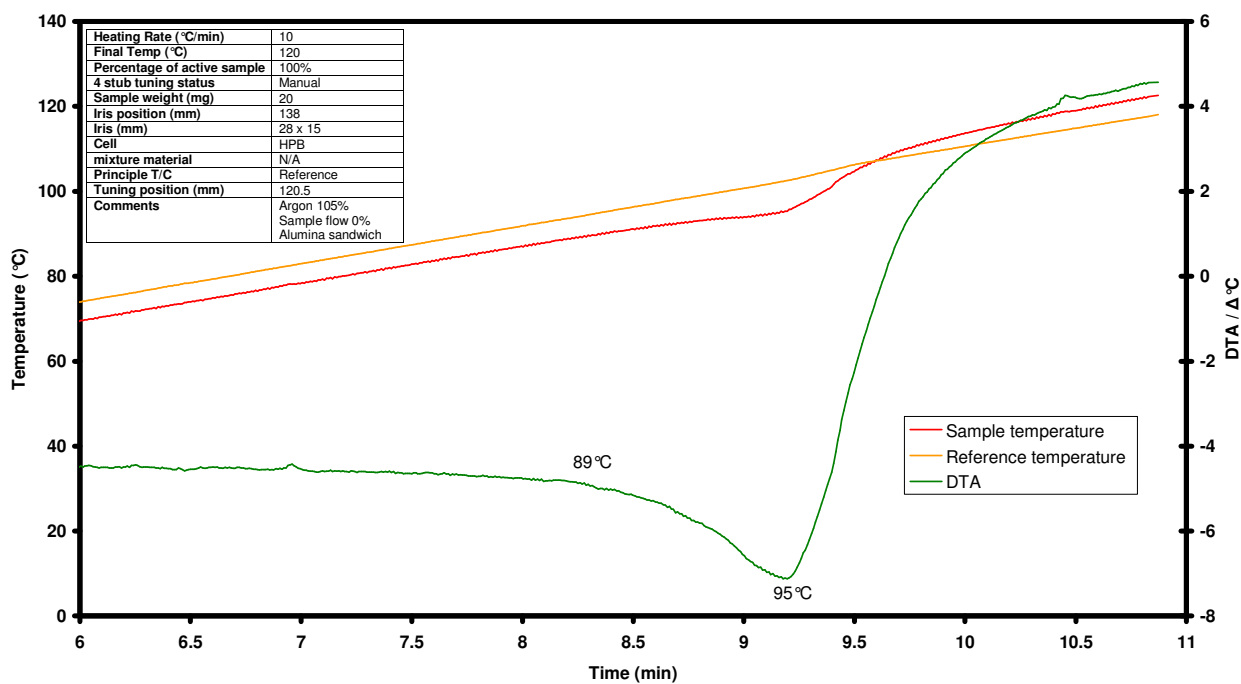
Graph 136: MWDTA experiment of D-sorbitol under argon.

The results from the MWDTA experiment on a 20 mg sample are shown in Graph 136. The differential temperature profile is fairly characteristic for many systems involving melting where the competition between the enthalpy of the process and an increase in tan δ as the contribution from dipolar heating becomes more significant as the sample becomes liquid.

7.9.2 α-D-Lactose
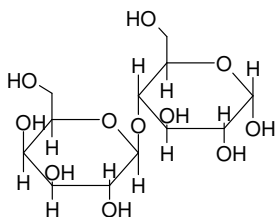
Lactose is a popular excipient used in many formulations as a binder to hold the ingredients of a tablet together. Binders are used to achieve a required mechanical strength and volume to low active dose drugs.
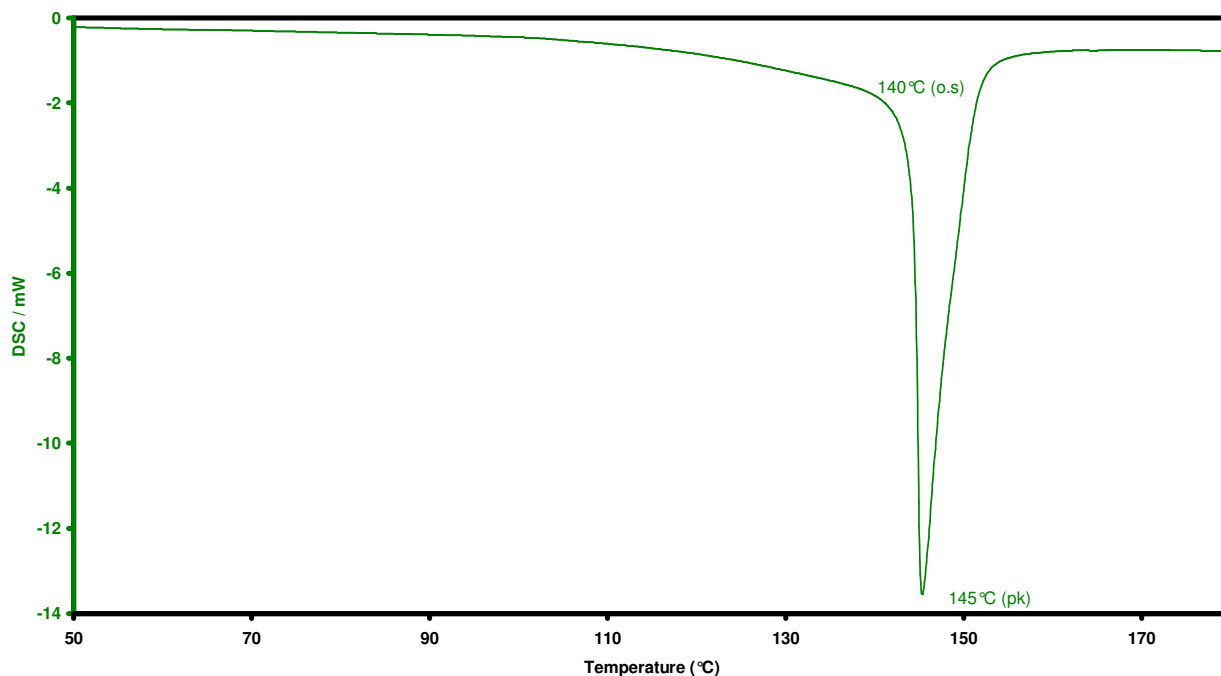
Graph 137: MDSC experiment (pin hole pan) of α-D- lactose under argon.

The results of the DSC experiment using a 3 mg sample are shown in Graph 137. A broad onset with an extrapolated temperature of around 140 °C, attributed to the endothermic melting of the

sample, can be seen. A slight change in the baseline was also recorded probably due to a change in heat capacity.

MWDTA 100% Alpha-D-Lactose IH0786

Heating Rate (°C/min)	10
Final Temp (°C)	180
Percentage of active sample	100%
4 stub tuning status	Manual
Sample weight (mg)	20
Iris position (mm)	138
Iris (mm)	28 x 15
Cell	HPB-EGA
Reference material	SiC
Principle T/C	Reference
Tuning position (mm)	120.5
Comments	Argon 80 ml/min Vac off
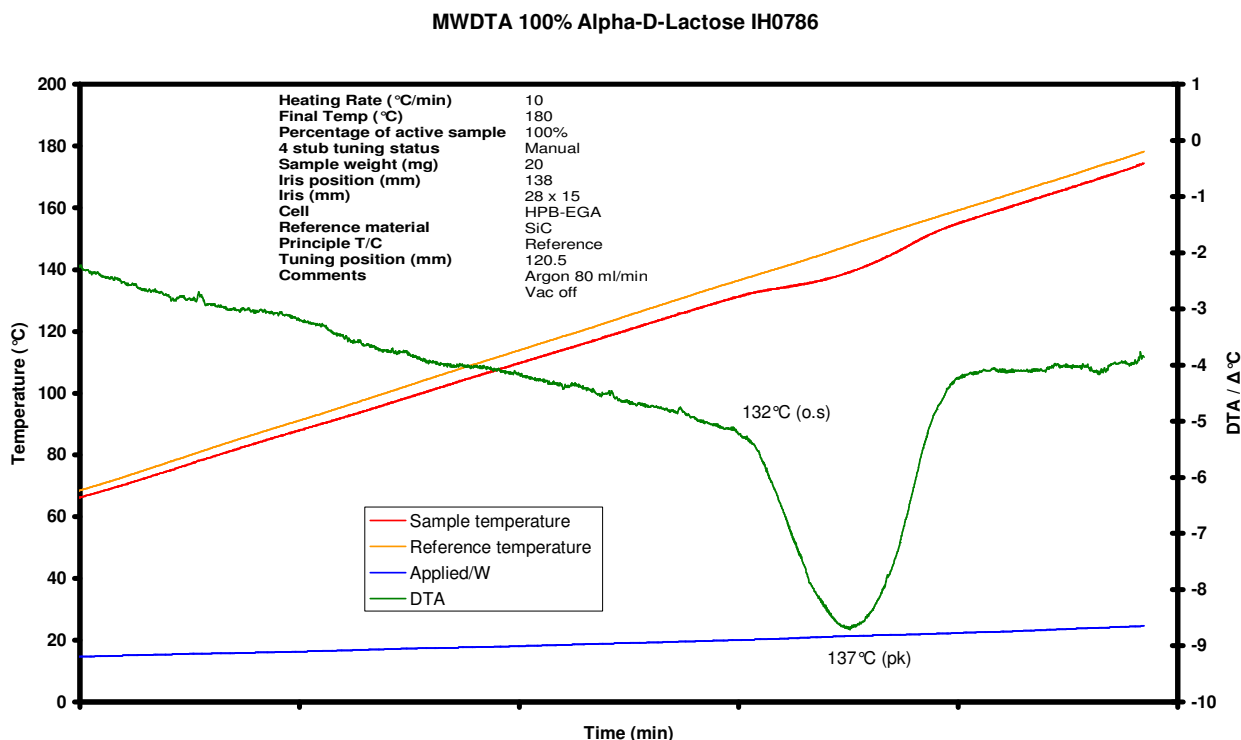
Graph 138: MWDTA experiment of α-D- lactose under argon.

The differential temperature trace for the MWDTA using a 20 mg sample is shown in Graph 138. The profile suggests that the enthalpy of the process predominates and the only suggestion of a change in tan δ is the difference in baseline before and after the event although heat capacity may also have an effect. The onset temperature observed with MWDTA is lower than that seen with MDSC although the peak maximum (137 °C) is comparable.

7.9.3 Aspirin
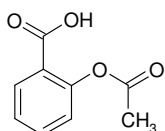
Aspirin is an anti-inflammatory and analgesic drug commonly used as an active ingredient in many pharmaceutical formulations. MDSC experiments (shown in Graph 139) were performed on 2.78 mg of sample.
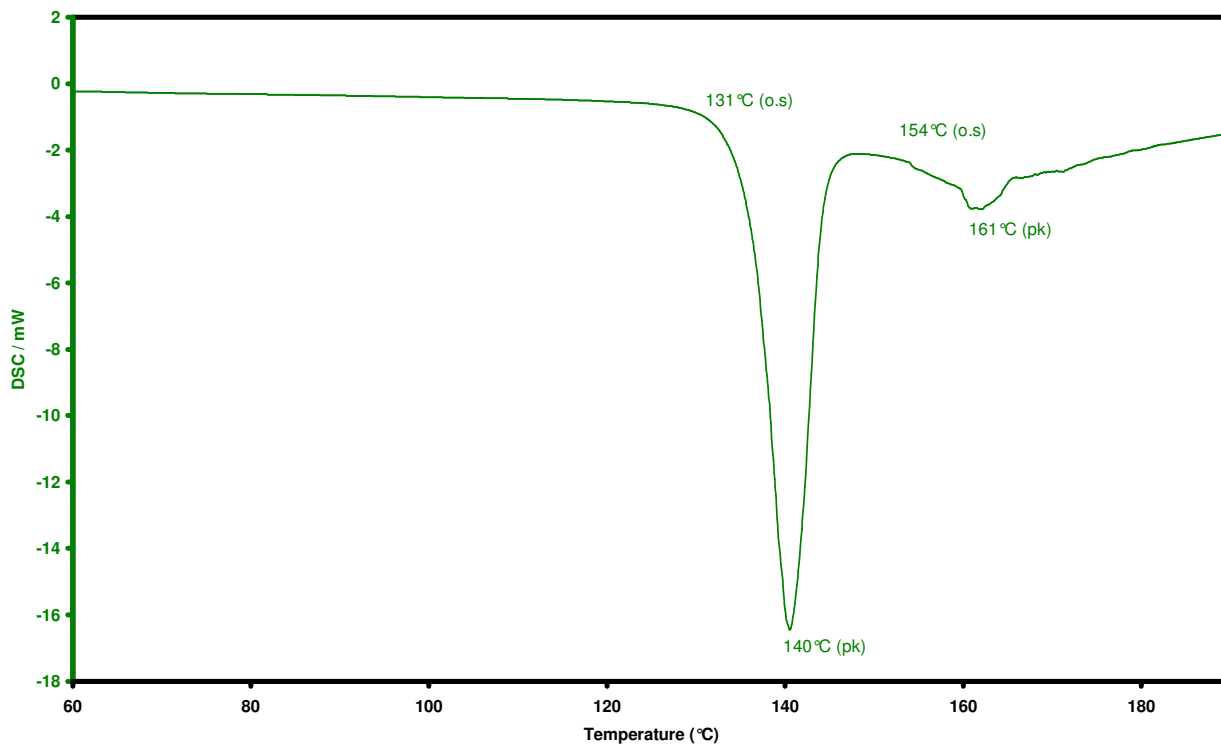
Graph 139: MDSC experiment (pin holed pan) of aspirin under argon.

The results showed the extrapolated onset of the melting process is observed at around 131 °C, post melt the sample showed a secondary transition which was believed to be the decomposition of the material at a peak temperature of 161 °C.

MWDTA 100% Asprin IH0932
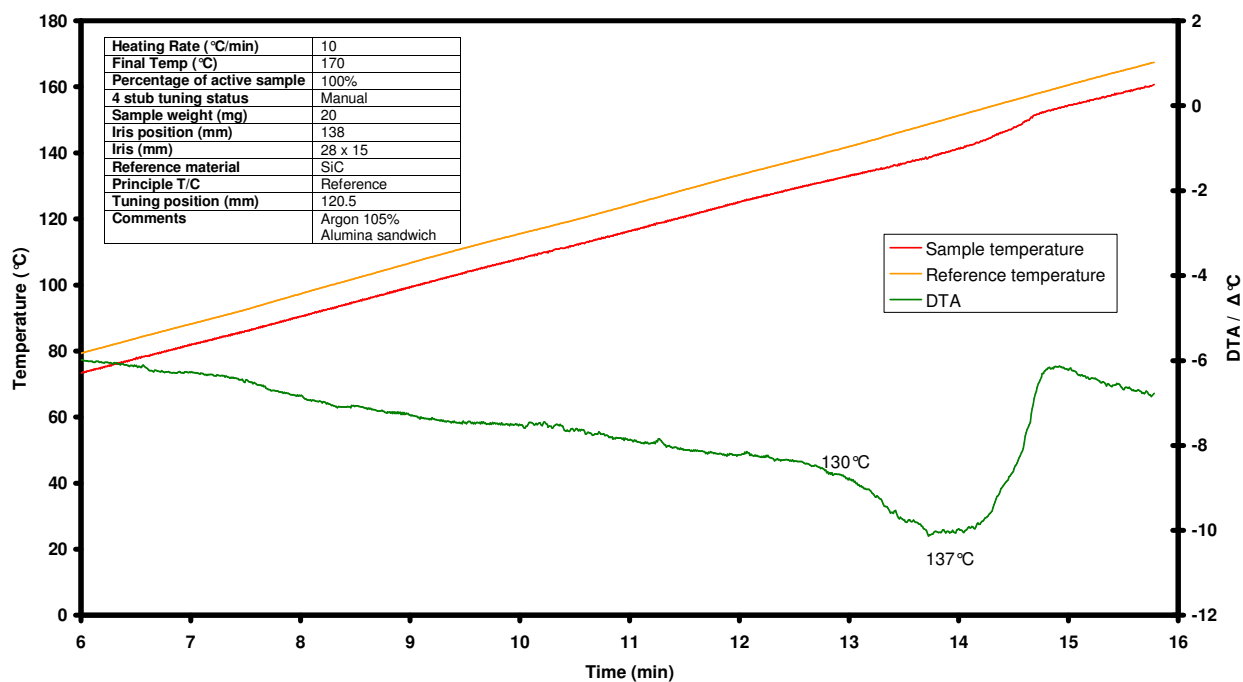
Graph 140: MWDTA experiment of aspirin under argon.

The results of the MWDTA experiment using a 20 mg sample are shown in Graph 140. Again, the ΔT profile is consistent with a process with an enthalpy change and a slight increase in tan δ.

7.9.4 Acetaminophen
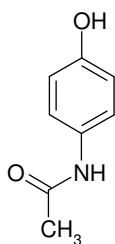
Acetaminophen (more commonly known as Paracetamol) is a widely used over the counter analgesic and antipyretic (fever reducer). It is a major ingredient of cold and flu remedies.
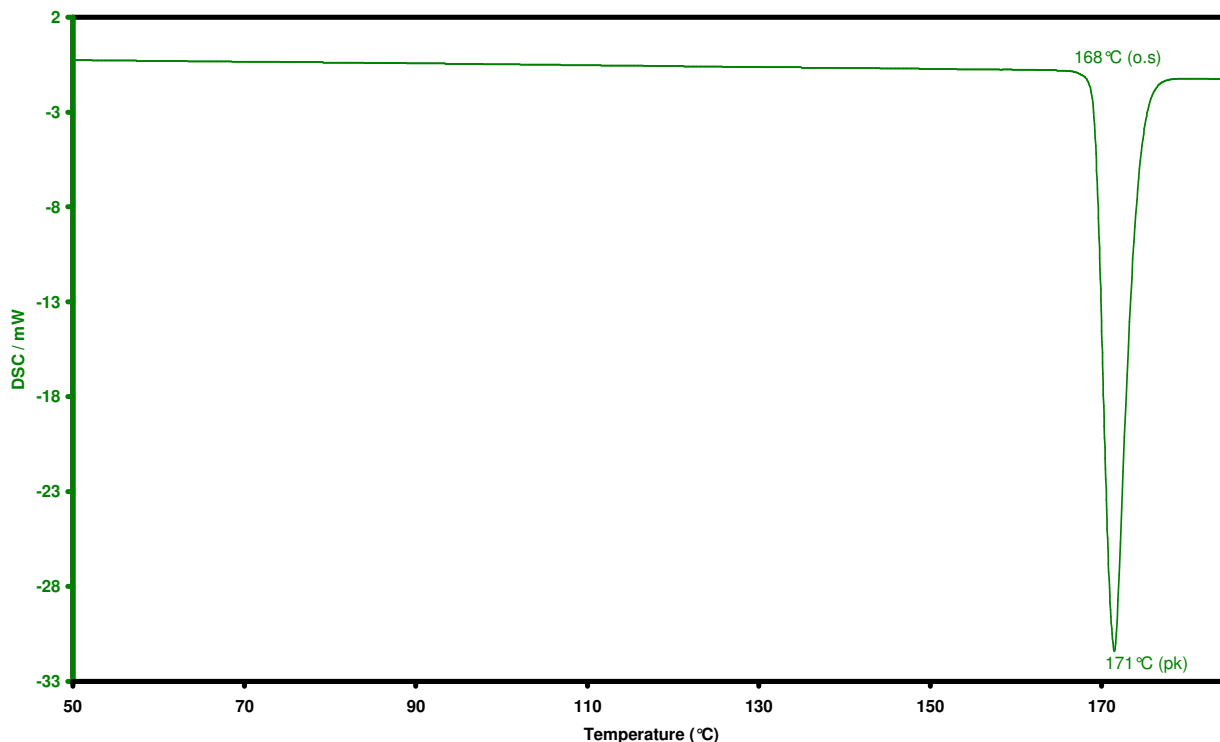
Graph 141: MDSC experiment (pin hole pan) of acetaminophen under argon.

The DSC trace for a 3.36 mg sample (Graph 141) shows a clear endothermic transition with an extrapolated onset around 168 °C and a peak temperature of around 171 °C.

MWDTA 100% Acetaminophen IH0944

Heating Rate (℃/min)	10
Final Temp (℃)	210
Percentage of active sample	100%
4 stub tuning status	Manual
Sample weight (mg)	20
Iris position (mm)	138
Iris (mm)	28 x 15
Cell	HPB
mixture material	N/A
Principle T/C	Reference
Tuning position (mm)	120.5
Comments	Argon 105% Sample flow 0% Alumina sandwich
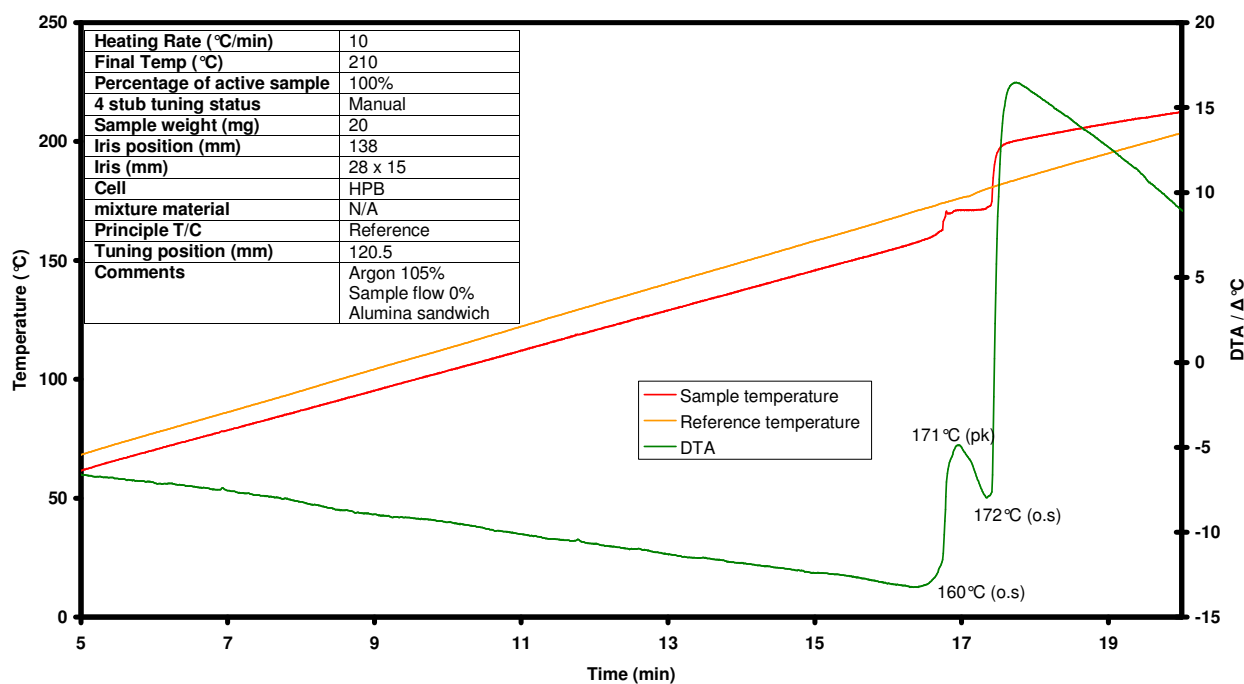
Graph 142: MWDTA experiment of acetaminophen under argon.

The results for the MWDTA experiment using a 20 mg sample are shown in Graph 142. The differential temperature profile shows slight differences to those seen previously although it is believed that the underlying causes are the same. Here the change in tan δ appears greater and the ΔT profile rises immediately as melting commences at 160 ºC. As the process continues the enthalpy of the melting temporarily counteracts the effect of increased coupling with microwaves energy to produce the small peak at 172 ºC. As the cooling effect of the enthalpy fades the increased heating arising from the change in tan δ again becomes dominant and ΔT rises until it is approximately 30 ºC greater than before the melt. The subsequent fall in the baseline may be due to decomposition of the sample.

7.9.5 L-Ascorbic acid
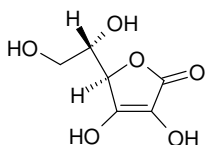
Ascorbic acid (more commonly known as vitamin C) is another popular drug used in many pharmaceutical formulations.
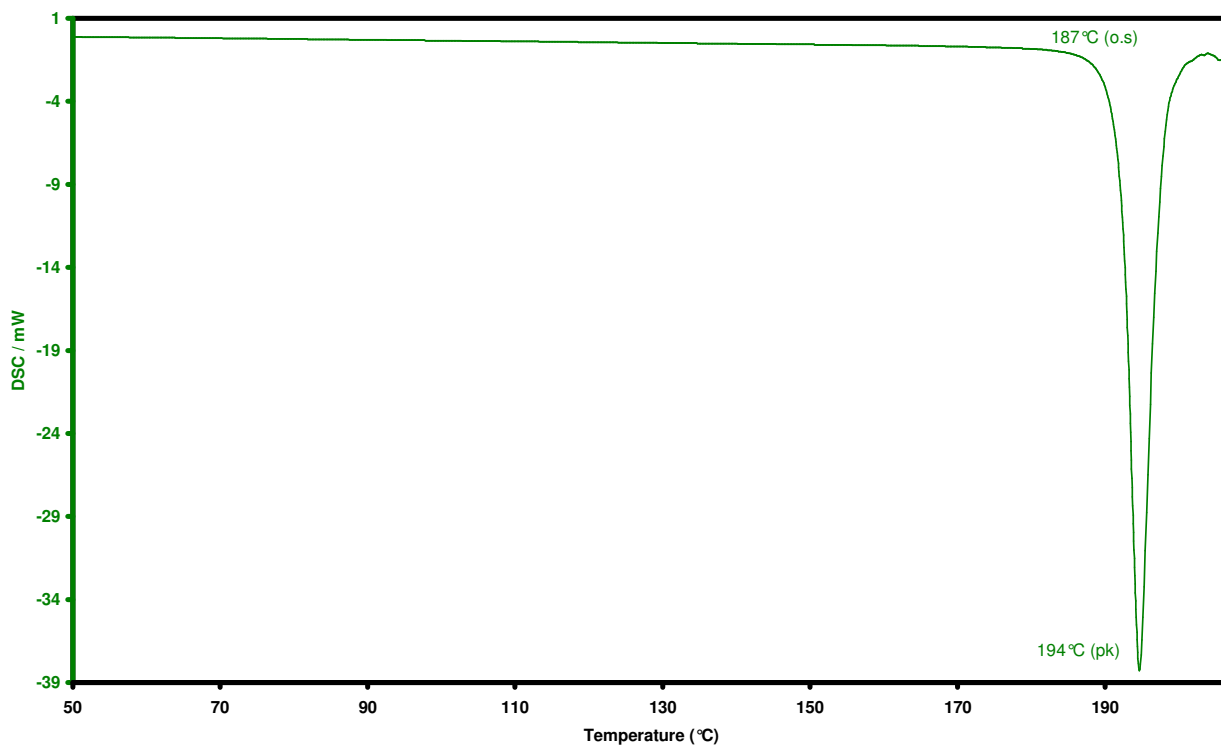
Graph 143: MDSC experiment (pin hole pan) of L-ascorbic acid under argon.

The results of a MDSC experiment using 3.62 mg sample are shown in Graph 143. An endothermic transition attributed to the melt with an onset temperature of around 187 °C and a peak temperature of around 194 °C can be seen. The trace also shows a deviation in the baseline after the transition possibly due to decomposition or evaporation of the sample.

MWDTA 100% Asorbic acid IH0937

Heating Rate (°C/min)	10
Final Temp (°C)	250
Percentage of active sample	100%
4 stub tuning status	Manual
Sample weight (mg)	20
Iris position (mm)	138
Iris (mm)	28 x 15
Cell	HPB
mixture material	N/A
Principle T/C	Reference
Tuning position (mm)	120.5
Comments	Argon 105% Sample flow 0% Alumina sandwich
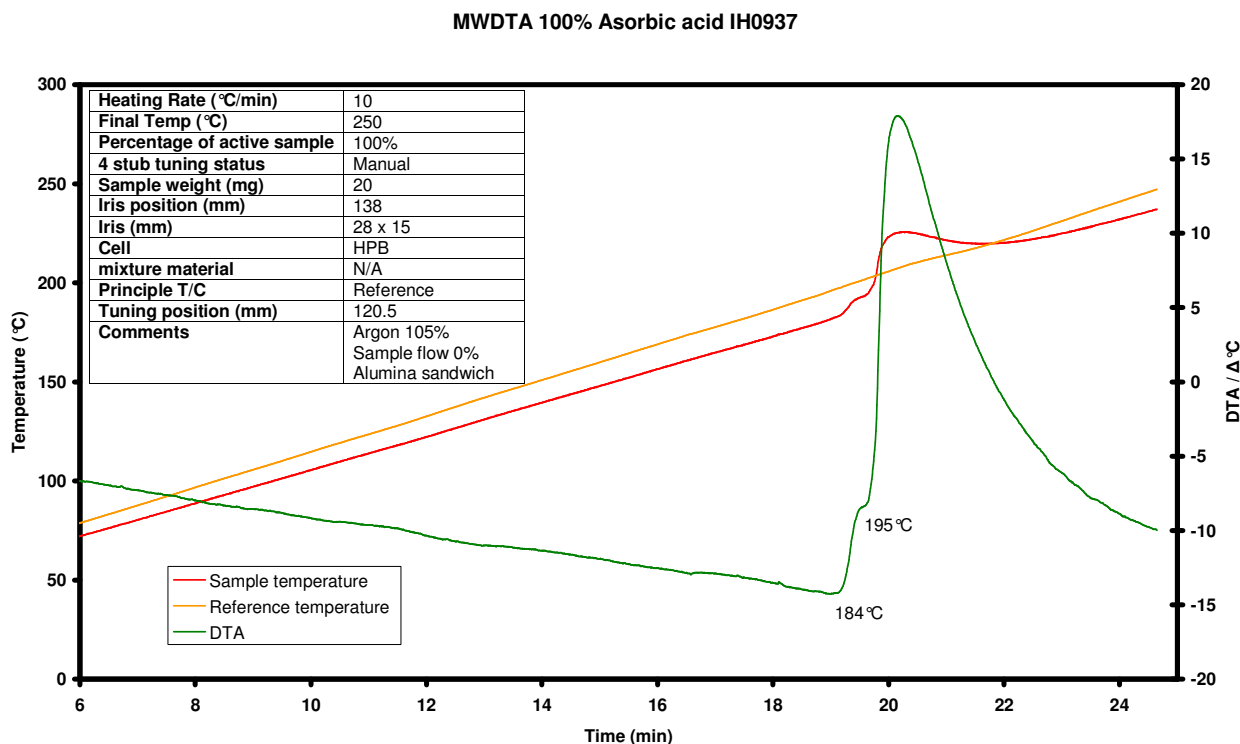
Graph 144: MWDTA experiment (pin holed pan) of L-ascorbic acid under argon.

Graph 144 shows the results of a MWDTA experiment using a 20.9 mg sample. The ΔT profile is similar to that observed with acetaminophen with an underlying increase in tan δ causing an overall increase of 30 °C with a smaller effect from enthalpy producing a step at 195 °C. The decline in ΔT after the transition almost certainly arises from the loss of the sample through decomposition or evaporation.

7.10 Fast ion conductors

Several ionic solids have been found to have higher electrical conductivities then expected for compounds of their type. These compounds are termed 'fast ion conductors' and their behaviour can be explained by point defects in the structures allowing the possibility of atoms or ions to move through the lattice; a process impossible in a near perfect crystal. The movement of ions through the lattice can occur via two standard 'hopping' mechanisms:-

- **The vacancy mechanism** – Where an atom size hole (defect) is present in the lattice and atoms move into the hole under ion transport influenced by an external electrical field.
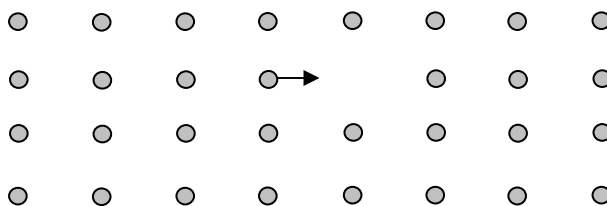
- **The interstitial mechanism** – Where interstitial ions jump into adjacent equivalent sites.
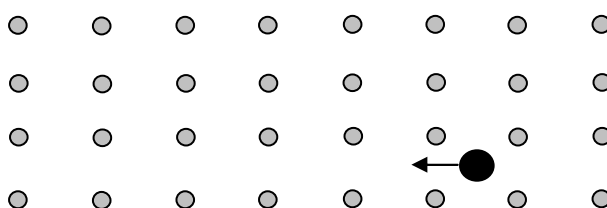
The structure of the fast ion conductors usually allow for the ion to be surrounded by several equivalent interstice sites in which the ion can hop to, far more then found in regular ionic solids. One of the earliest found was the high temperature phase of silver iodide in 1913.

7.10.1 Silver iodide

The solid-solid phase change of silver iodide has been of interest to microwave thermal analysis chemists for a number of years [42]. The β to the high temperature α phase recorded at 147 °C is known to give rise to an ionicially conductive species, the result of which is a vast increase in the ability of the material to couple with microwaves. Two papers [69, 70] cite silver iodide as a good example of the so called 'microwave effect' where thermal transitions appear to occur at lower temperatures than seen in conventional heating experiments. These papers give the transition temperatures as 126 °C, 20 °C earlier than the literature value. However, microwave energy was not the only source of heating used in this work and the applied power used was far greater than the current research (75 W compared to 25 W in MWDTA experiments). Both factors could affect the transition temperature of the sample, as premature melting of the surface can occur, due to localised thermal runaway with high power levels and masses.

Graph 145 shows the results of a conventional DSC experiment using 26.8 mg of sample, quartz crucibles, an argon atmosphere and a heating rate of 10 °C/min. the profile clearly shows the transition at 147 ℃ and the melt at around 560 ℃.
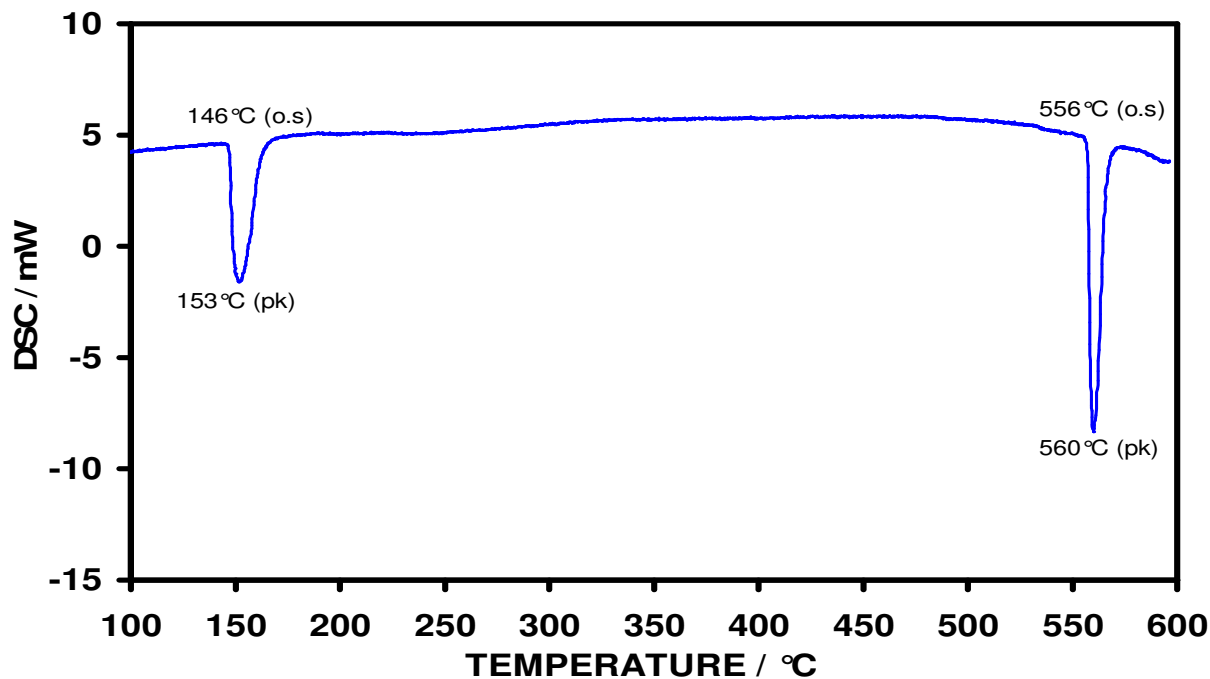
Graph 145: HDSC experiment of silver iodide under argon.

Graph 146 shows the result of an MWDTA experiment on 20 mg of silver iodide using an argon atmosphere and a heating rate of 10 ℃/min.

MWDTA 100% Silver iodide IH0909
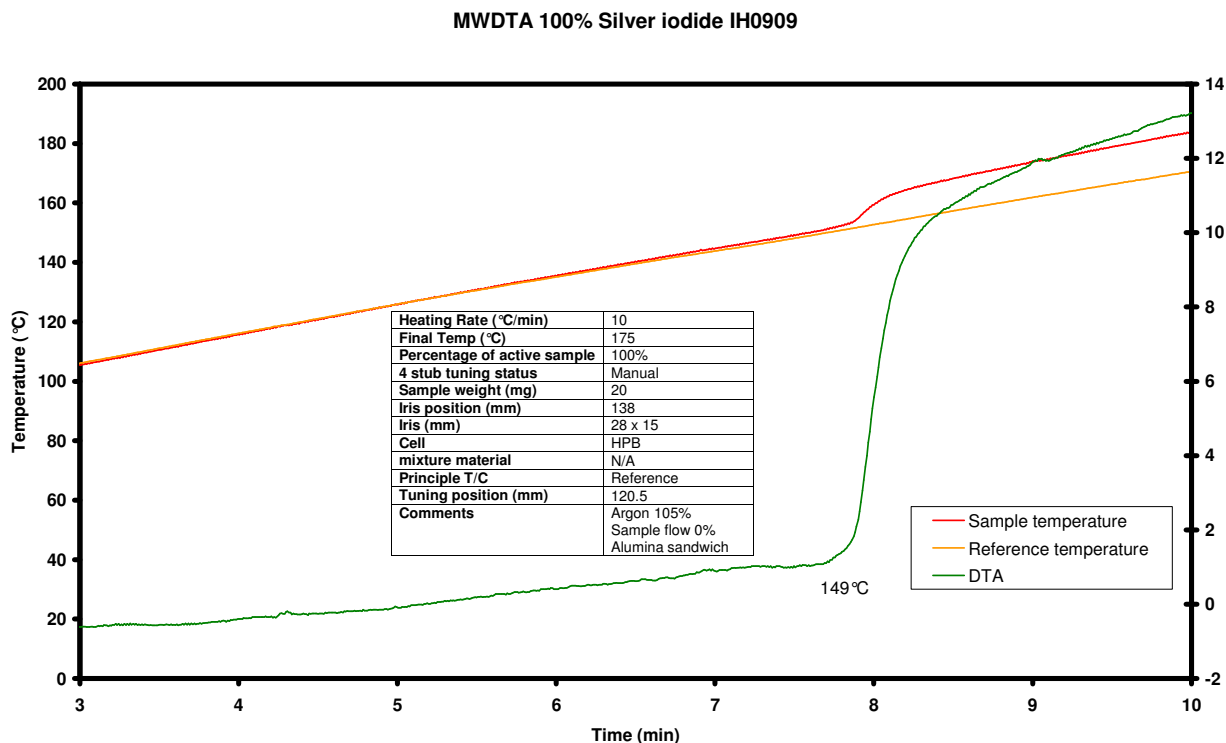
Graph 146: MWDTA experiment of silver iodide under argon.

The MWDTA profile clearly shows the transition which, interestingly, was in close correlation with the HDSC experiment rather than that reported by other workers using microwave heating [69, 70]. It is thought this possibly was due to the differences in sample size and conditions. Although the MWDTA step was significant at 10 ºC there was no indication of the expected thermal runaway.

7.11 Using MWDTA to study metal powders

Several metals (e.g. Indium, Lead and Tin) are used as temperature calibration standards in thermal analysis as they have sharp melting points and large associated enthalpies readily detectable with DTA or DSC. It was, therefore, considered important to investigate selected metals using MWDTA.

Generally, it is considered undesirable to place ungrounded metal objects in a microwave cavity as the E-field can cause a large build-up of charge on the surface of the metal (the 'skin effect') resulting in arcing [6]. This phenomenon does not arise with the thermocouples used in the system to measure temperature as they are thin and at 90° to the E-field so the interaction is negligible. Despite the potential problems, a series of MWDTA experiments were performed on Indium and Nickel.

7.11.1 Fusion point of Indium

Indium is one of the most commonly used thermal calibration standards with a sharp melting point at 156 °C [28]. Graph 147 shows the results obtained using DSC with a 5.1 mg sample encapsulated in an aluminium pinhole pan with a heating rate of 10 °C/min and an argon atmosphere. A single peak at 156 °C is clearly apparent.
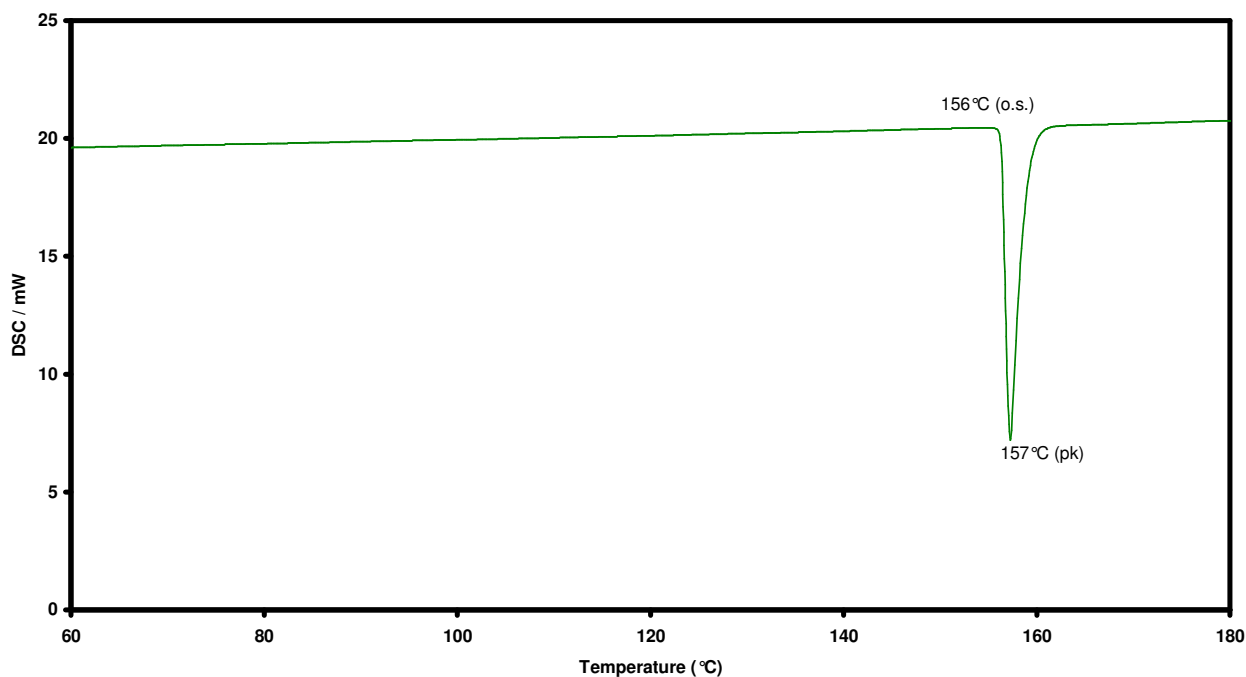
Graph 147: MDSC experiment of indium under argon.

Graph 148 shows the result of a comparable experiment using MWDTA. Again, the heating rate was 10 °C/min with an argon atmosphere but because of the cell characteristics a larger sample of 40 mg was used.

MWDTA 100% Indium powder IH0594

Heating Rate (°C/min)	10
Final Temp (°C)	200
Percentage of active sample	100%
4 stub tuning status	Auto
Sample weight (mg)	40
Iris position (mm)	138
Iris (mm)	28 x 15
Reference material	SiC
Principle T/C	Reference
Tuning position (mm)	122
Comments	Silica wool base Alumina sandwich 2nd heat
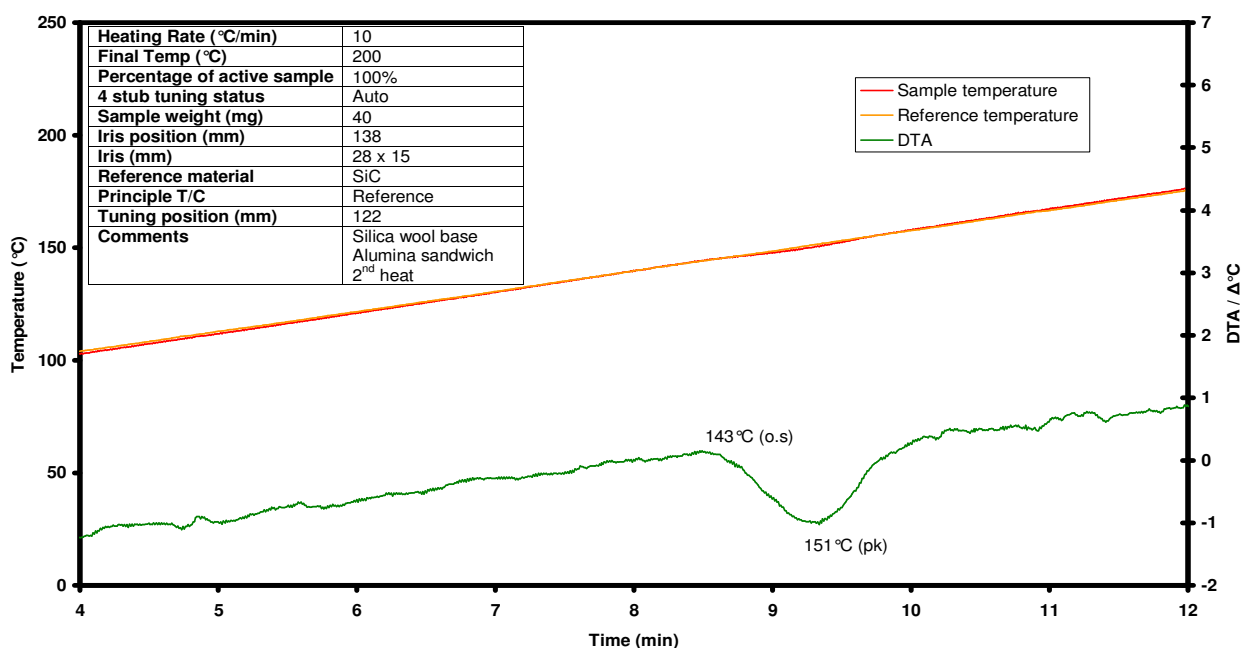
Graph 148: MWDTA experiment of indium (second heat) under argon.

The ΔT profile shows a peak similar to that expected for an endothermic transition with no significant change in tan δ. However, the temperature of melting is considerably lower than expected with an onset at 143 °C. The reason for this apparent lowering of the melting point is uncertain but it is possible that there was some interaction between the metal and the grounded thermocouple with which it was in direct contact. However, measurement of the leakage at the base of the thermocouple inlet using a microwave monitor (Apollo Scientific) gave a near zero value. Another possibility was the formation of localised hot-spots caused by 'micro arcing' between some of the metal powder granules although no indications of larger scale arcing were observed.

7.11.2 Curie point transition in Nickel

Nickel is also used as a thermal calibration standard, particularly for thermobalances [28]. Here the transition of interest is not the melting point but a Curie point transition at 356 °C [28] where the metal goes from ferromagnetic (attracted to magnets) to paramagnetic. It was thought that presence of a Curie point would make nickel an interesting material to study by MWDTA as it could reveal whether magnetic heating, where the alternating magnetic field interacts with a magnetic material, occurs in addition to the more common interaction with the E-field.
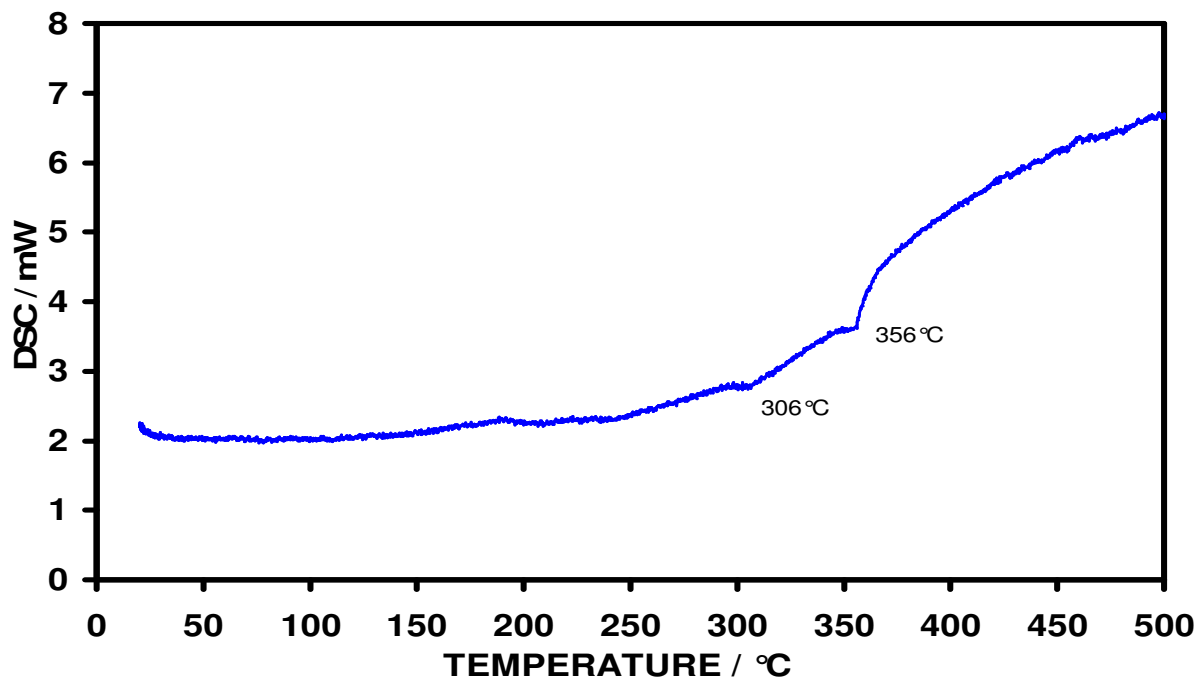
Graph 149: HDSC experiment of nickel under argon.

Graph 149 shows the results of a conventional DSC experiment using a 25.8 mg sample of nickel heated at 10 °C/min under argon. The profile is fairly featureless apart from a general baseline drift which increases with temperature although there is a very small event at 356 °C which can be attributed to the (low enthalpy) Curie point.

MWDTA 100% Nickel IH0761
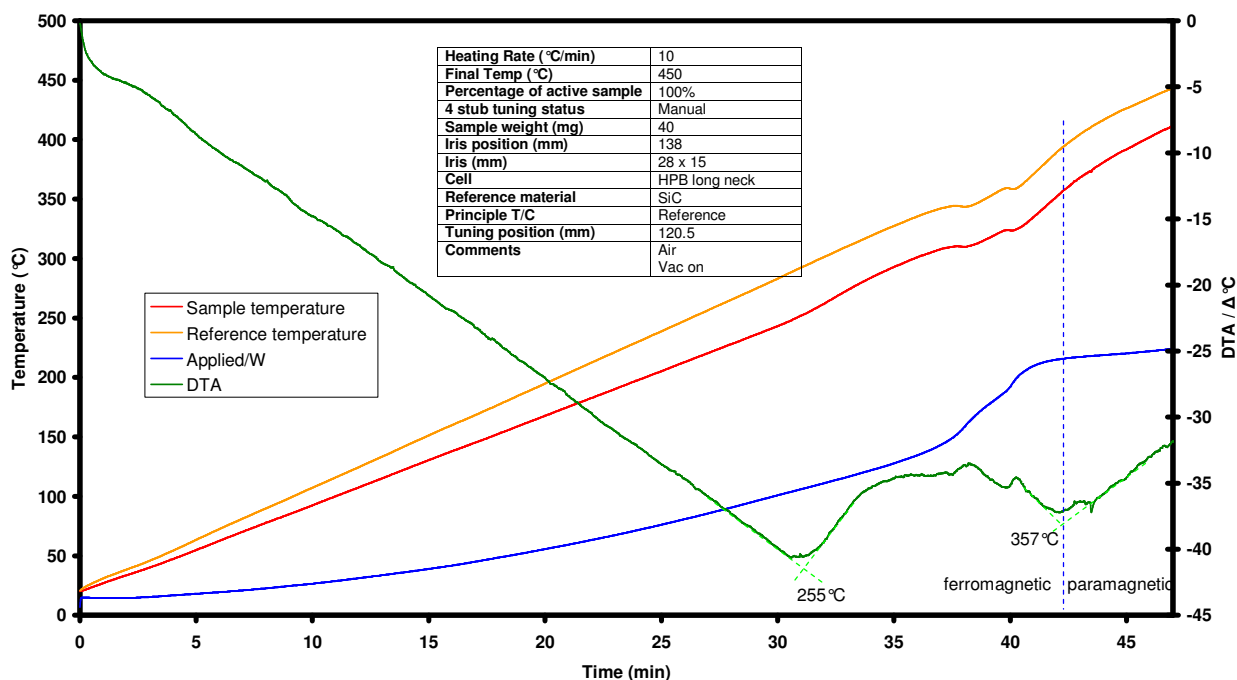
Graph 150: MWDTA experiment of nickel under air.

Graph 150 shows the result of an MWDTA experiment using a 40 mg sample and a heating rate of 10 °C/min with an argon atmosphere. The ΔT profile is complex. Initially, there is a constant fall in ΔT which could be attributed to the metal powder coupling less well than the reference. However, at 255 °C there is a sharp change in direction of the profile. The reasons for this are unknown as it does not correspond to any known transition in nickel. There are some small features on the profile around 280 to 320 °C but as these occur on both the sample and reference temperatures their significance is suspect and they are probably instrumental artefacts. There is a detectable change in the profile at 357 °C which is presumably a result of the Curie point but the effect is small and does not suggest that magnetic heating played a significant role.

Unfortunately, there was insufficient time to repeat the experiment or investigate other materials with Curie point transitions although this would be an interesting area of future research.

7.12 Summary of the MWDTA technique

The addition of the HPB cell to MWTA produced a DTA –like technique called MWDTA. Changes in tan δ in relatively small samples could be detected through the temperature difference between the sample and the surrounding susceptor jacket which acts as a reference and insulation. By removing the sample temperature from the control loop in MWDTA experiments, problems with heating control were largely eliminated.

Using MWDTA, the temperature of transitions could be measured with accuracy. In many cases, the transition appeared to occur at lower temperatures than obtained with conventional experiments or from the literature. It appears that microwave heating is very sensitive to the initial onset of the transition (when the effect of enthalpy will be small and so not detectable by DSC). It is also possible that the small samples usable in MWDTA will be heated with greater uniformity by microwave heating than in DSC where heat has to be transported from the surface of the sample to the centre by conduction – a process that would raise the apparent temperature at which a transition would occur.

Overall MWDTA proved to be a very powerful and sensitive qualitative technique which is amenable to a vast range of sample types including metallic compounds and also poorly coupling materials with low tan δ values. Some problems found in the study of metal oxides were overcome by the versatility of the technique and improvements detailed in previous chapters.

Chapter 8

Quantitative MWDTA and induced heating rates

The previous chapters have demonstrated that MWTA can be used to detect physiochemical changes through associated changes in tan δ.

This chapter describes the experiments performed to determine whether MWDTA could provide quantitative as well as qualitative information.

8.1 Quantitative Measurements

The earliest TA experiments were too crude for quantitative studies. The work of Norton *et al.* [4] in the late 1930's was the first to indicate that the technique was capable of reproducible, quantitative measurements. Their work, using a DTA, demonstrated that the height of a DTA peak was directly related to the heating rate and that the peak area was a reliable measure of the magnitude of the enthalpy of the process under study.

As equipment improved, the relationship between the heat of reactions (Q) and ΔT became more apparent.

$$Q = m.\Delta H = \int K.\Delta T.dt$$

Equation 32: Calculation of the reaction heat change with respect to time.

Where: K   = proportionality factor dependent on the geometry and thermal conductivity of the sample.

ΔH   = specific heat of the reaction

Q   = reaction heat

ΔH   = specific heat of the reaction

m   = mass

t   = time

In effect, if a series of DTA experiments were performed using a given sample and a range of masses, then a calibration curve of peak area against mass can be constructed, from which the mass of an unknown quantity of the sample can be determined. Great care has to be taken with experimental conditions, as thermal conductivity and temperature gradients affect the reliability of the results.

It is not directly possible to relate the quantitative aspect of conventional DTA with MWDTA as the former is dependent upon the enthalpy of the thermal process being studied, while in the latter the effect of dielectric changes upon the sample often predominate. Regardless of the difference in techniques it was thought that the standard methods of calculating quantitative thermal measurements could be tested so the extent of dielectric changes on peak areas could be seen and the relationship to sample mass investigated.

Another factor is the nature of the ΔT response signal. In DTA sigmoidal peaks are common, which generally return to a flat baseline (assuming factors such as changes in heat capacity before and

after the transition being recorded are not significant). Obtaining the height or area of such a peak is relatively straightforward.

In MWDTA however, the ΔT signal is often in the form of a step caused by the change in tan δ before and after the event. In addition the gradient of the ΔT baseline either side of the step may be different. This means determining the magnitude of the ΔT step is more complex and several approaches are possible.

8.2 Initial quantitative studies using AgI

Initially measurements were made on the fast ion conductor phase change in silver iodide (7.10.1 Silver iodide, page 286).

The dielectric change in silver iodide is recorded as a permanent step in the MWDTA trace which does not have a parallel post-transition baseline making the end of the transition difficult to determine. In the first instance, three methods were used to determine the range over which to take a quantitative measurement.

- The triangle method – the baseline was extrapolated beyond the deviation from the initial baseline (1) next a tangent was drawn over the error signal (2). A second tangent was also drawn to the post transition baseline (3) and where the two tangents intersected a line was drawn to the extrapolated pre-transition baseline (4). The area of this square based triangle was then calculated (5) using the equation:

$$Area = \frac{1}{2}ab$$

Where: a = (1)

b = (4)
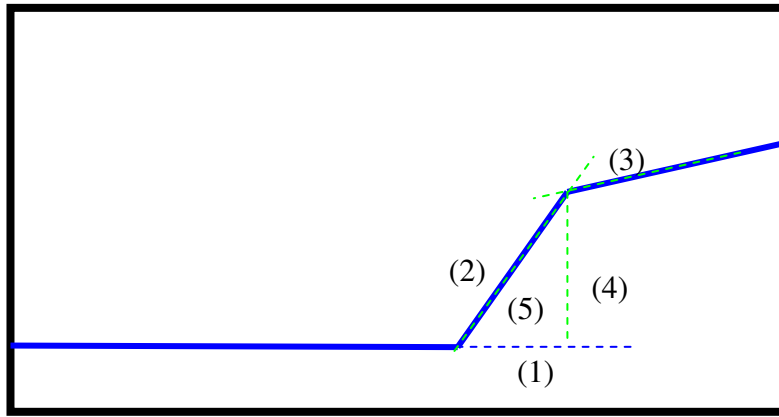
Figure 70: Schematic of an MWDTA profile showing construction for the triangle method

- Deviation method – The pre-transition baseline was extrapolated (1), the post-transition baseline was extrapolated back towards zero (2) the differential temperatures between the two baselines were taken (3).
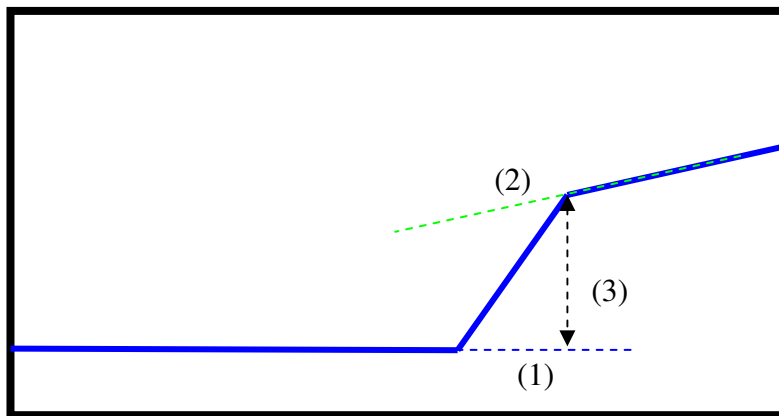
Figure 71: Schematic of an MWDTA profile showing construction of the deviation method

- The area method – As with the triangle method the end point of the transition was determined by extrapolation then the area under the curve was calculated using trapezium rule (3) much like conventional methods.
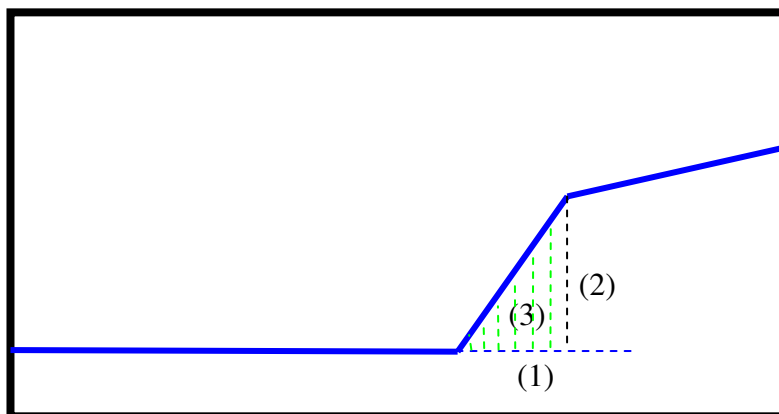
Figure 72: Schematic of an MWDTA profile showing construction of the area method

8.2.1 Experimental

Experiments were performed in the RCHPB as described in chapter 5. The samples themselves were tested as received and all mass measurements were taken using a five figure balance. The materials were subjected to a heating rate of 10 °C/min under argon and the resultant differential temperature signal plotted against time.

Three repeats for each mass were taken except for 20 mg where five repeats were needed as there appeared to be a large variation between results.

8.2.2. Results

The results for the experiments on different masses of AgI using all three measurement methods are shown in the table below.

	Mass (mg)	Triangle method ($\Delta T/dt$)	Mean	SD	Deviations method (ΔT)	mean	SD	Area method ($\Delta T/dt$)	mean	SD
Phase change occurring at 136 °C	1	0.2 0.2	0.2	0.0	0.2 0.2	0.2	0.00	0.12 0.13	0.13	0.0
	5	0.8 0.9 0.8	0.8	0.1	1.3 1.4 1.3	1.3	0.06	0.27 0.47 0.29	0.35	0.1
	10	4.6 3.9 4.3	4.3	0.4	6.9 6.3 6.6	6.6	0.30	1.78 1.54 1.84	1.72	0.2
	20	26.6 17.74 11.47 6.59 5.45 5.62	12.2	8.5	29.9 24.55 15.02 10.89 10.37 9.79	16.8	8.49	3.55 2.44 3.46 1.58 1.31 1.53	2.32	1.0
	25	7.66 8.4 9.02	8.4	0.7	10.28 10.36 13.46	11.4	1.81	2.25 1.89 2.73	2.29	0.4

Table 13: Results of the initial quantitative MWDTA results of silver iodide

The experiments also indicated several potential problems:

- The temperature of the phase change appeared lower (by -10 °C) than obtained with either conventional DTA/DSC or using MWDTA with the HPB cell.
- The methods for calculating the magnitude of the step all required a subjective human interaction which gave rise to errors.
- There was a lot of variation in the results particularly for the 20 mg sample.

The discrepancy in transition temperature was suspected to be a result of the removable crucible used. Repeat experiments were performed using a modified removable crucible which has a thin ground silica base and was situated on a bed of highly thermally conductive diamond (900-2320 $Wm^{-1}K^{-1}$) where the sample thermocouple was embedded. In a conventional instrument the sample cell sits on a conductive metal plate, in a microwave this is not possible as it can led to an electrical discharge. The results from testing showed that the diamond bed had no adverse effect on the experiments. With the modifications to the cell a much closer match between the microwave transition temperature and that of the HDSC was observed (see graph below), although there is a slight loss in sensitivity as measured by the size of the ΔT step compared unmodified RCHPB cell.
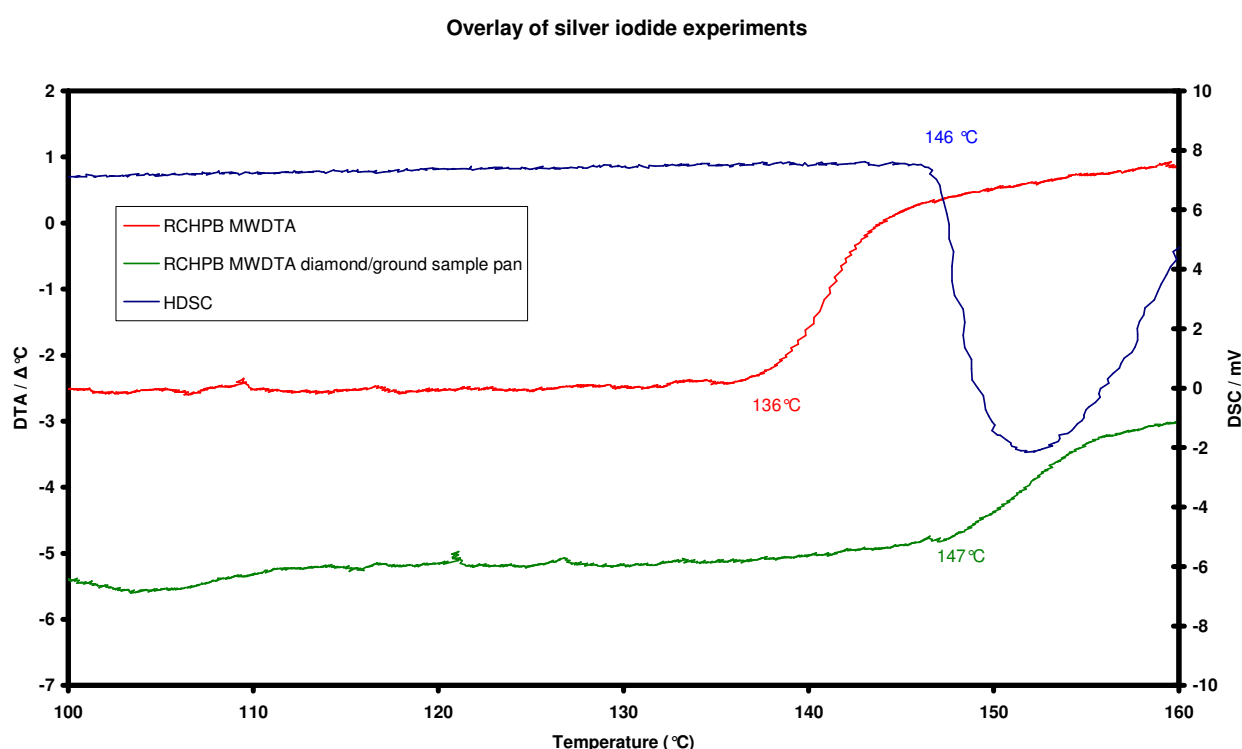
Graph 151: Comparison of the transition temperatures of 15 mg silver iodide illustrating the improvements made to the RCHPB cell, HDSC trace (blue line), RCHPB MWDTA measurement as detailed in chapter 5 (red line), RCHPB MWDTA after further development (green line).

In order to eliminate heating rates as the cause of discrepancies, equivalent masses were tested at the different heating rates of 2, 5 and 10 ℃. The results of these experiments (shown in Graph 152, page 301) showed that the transition temperature was largely independent of changing the heating rate over the range used.

MWDTA 100% Silver iodide
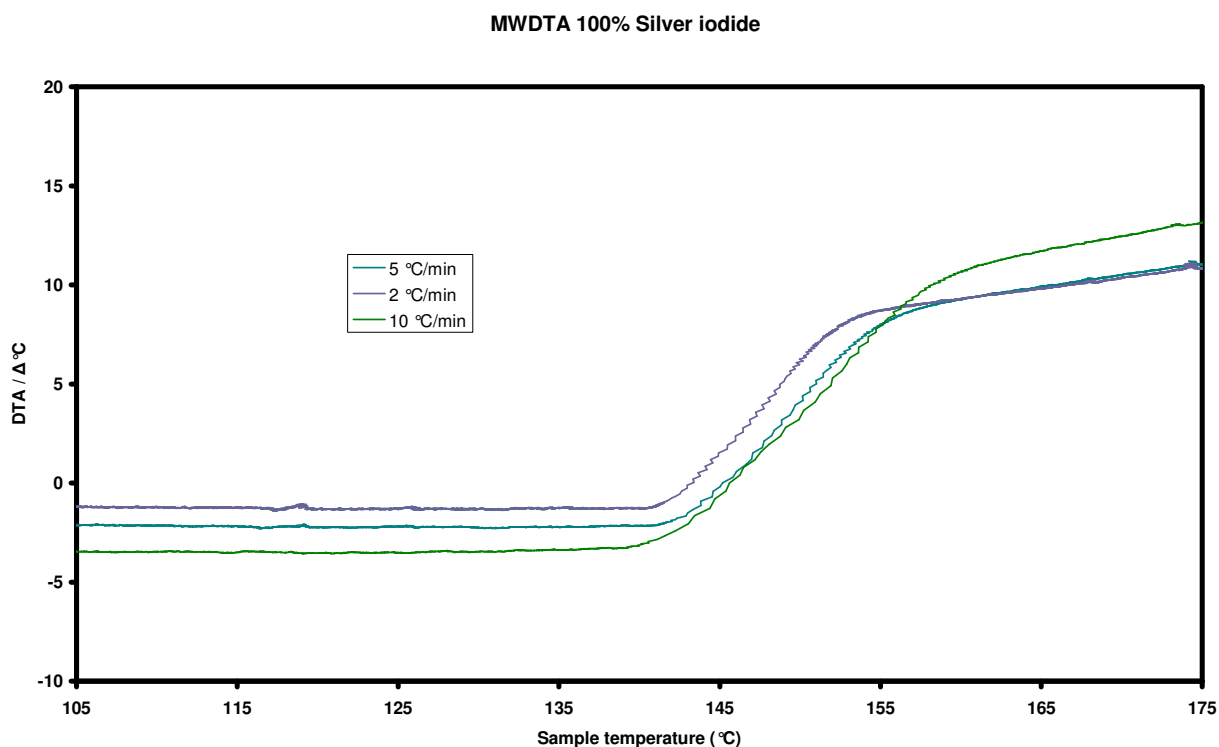
Graph 152: Comparison of heating rates for a 20 mg sample of Silver iodide in the RCHPB cell.

One of the problems found in the initial experiments using AgI was the determination of the range over which the integration of the step should occur, i.e. such as between given power limits.

However analysis of the repeat experiments on the 20 mg AgI sample (which gave the most variation in area) showed that there were slight differences in the applied power even though the temperature of the transition was constant in each case.

The difference in power was only of the order of 0.5 W and would probably be within the variability of the microwave generator itself.

MWDTA 100% Silver iodide overlay

Heating Rate (°C/min)	10
Final Temp (°C)	200
Percentage of active sample	100%
4 stub tuning status	Manual
Sample weight (mg)	20 mg
Iris position (mm)	138
Iris (mm)	28 x 15
Cell	Indirect HPB
mixture material	n/a
Principle T/C	Reference
Tuning position (mm)	114
Comments	Argon 105% Sample flow 0%
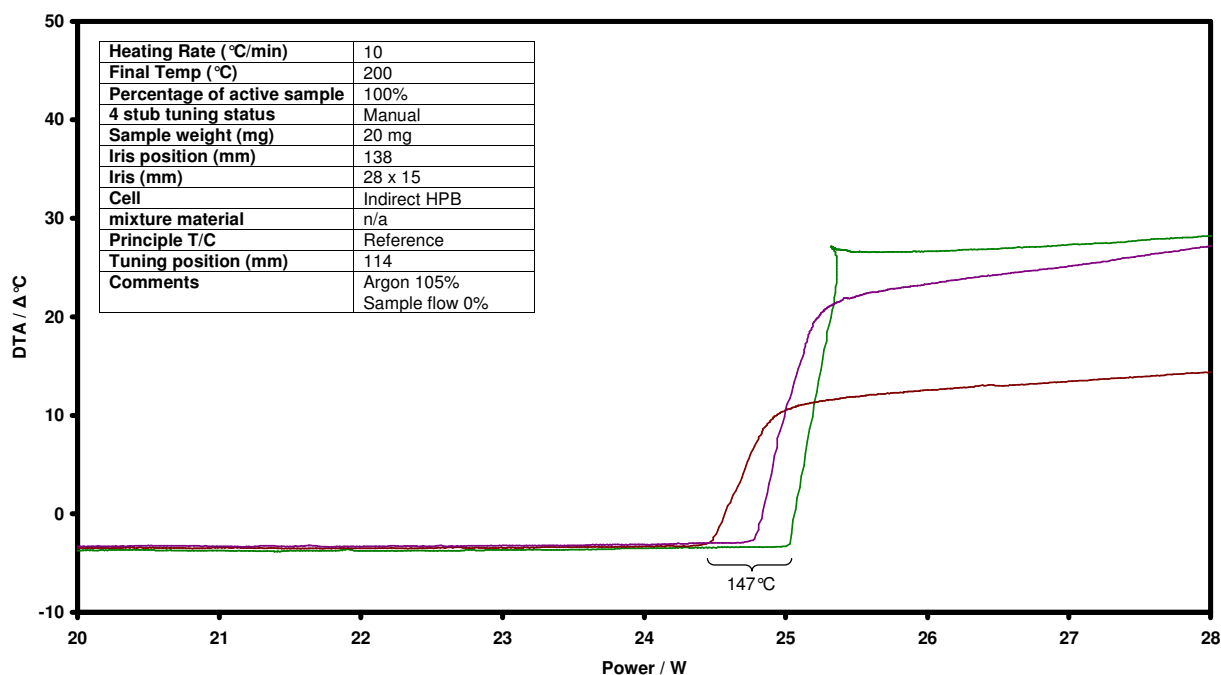
Graph 153: Comparison of the variation of the required applied power to reach the transition temperature of 20 mg of silver iodide in equivalent runs.

The ΔT response of the transition does appear linked to the power at which it occurred, with the highest power giving the largest ΔT response and this may be the cause of the quantification errors observed.

Although no ideal solution presented itself, it was decided that subsequent quantitative measurements involving a step in the ΔT would be based on an integration between two set points of power (clearly before and after the transition) of a plot of the ΔT signal against the applied power, also integration by hand was replaced by a more accurate computer integration program (Orginlabs - Origin version 7).

With the new methods and instrumental improvements in place, measurements on silver iodide were repeated. Once again the samples were subjected to a heating rate of 10 °C/min under argon. 15, 25, 30 and 50 mg samples were weighed accurately to four significant figures. The remaining samples tested (around 4.84 and 43 mg) were used to see if non-standard samples masses fitted the calibration curve, therefore the sample was added to the crucible then accurately weighed (to ensure it was near the desired value), recorded then tested unaltered. In order to maintain a constant volume samples were made up to 50 mg with α-alumina (the sample itself was not mixed with the alumina) as shown in Figure 73. Each run was repeated in triplicate.
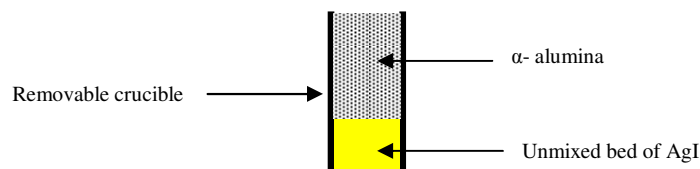
Figure 73: Diagram of the sample packing for quantitative RCHPB experiments

Analysis was performed in Origin 7, and the transition area was integrated between the operator defined, first point of deviation to the applied power of 25 W.

The results of these experiments are shown in Table 14 and also as a plot of $\Delta T/\Delta W^{-1}$ verses sample mass in Graph 154.

Constant mass to 25 W. (50 mg) AgI indirect Diamond		
Average mass (mg)	Average area ($\Delta T/\Delta W^{-1}$)	SD
4.84	1.56	0.56
15	4.36	1.56
25	5.63	1.12
30	8.62	1.72
43	30.82	6.17
50	40.28	11.02

Table 14: Results of quantitative silver iodide experiments made after the improvements to the sample cell. (Standard error = ± 3.69 $\Delta T/\Delta W^{-1}$)
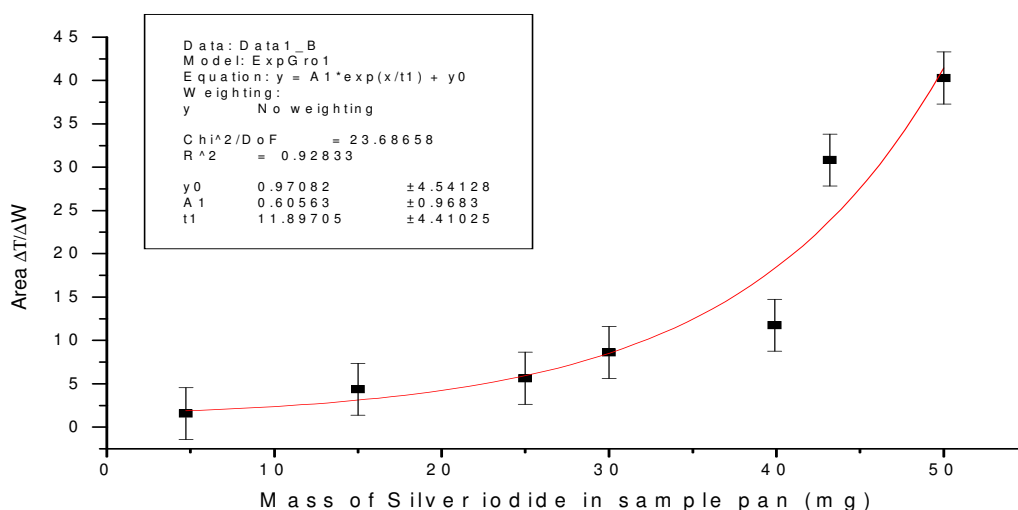
Graph 154: Average integration areas of the MWDTA results for the solid-solid transition in silver iodide (error bars based on standard error).

The plot shows a possible exponential relationship between the calculated area and the mass of the sample with an R^2 value 0.93.

8.3 Quantitative Potassium bicarbonate measurements

To evaluate the reliability of the MWDTA for quantitative work without the complexity caused by dielectric changes simpler systems were investigated. The decomposition of sodium bicarbonate was shown previously to produce very little change in tan δ (Chapter 7) and the enthalpy of the process is reasonably large making the measurement of the conventional peak in the MWDTA trace possible even with relatively small mass samples.

Experiments were performed using masses from 5 mg to 50 mg in the RCHPB cell under an atmosphere of argon and at a 10 °C/min heating rate. Areas were calculated from plots of ΔT verses W, where transitions that resulted in heat being lost from the sample or the baseline to go below 0 (as in endothermic processes or a reduction in coupling) are given as negative areas by the software and transition where the opposite was the case had positive values. The results of these experiments are given in Table 15 below.

Mass (mg)	Area (ΔT/ΔW)	Mean	SD
5	-2.32 -4.33	-3.32	1.43
10	-5.31 -4.43	-4.87	0.62
15	-10.63 -8	-9.31	1.86
20	-9.01 -13.13	-11.07	2.91
25	-11.3 -18.3	-14.78	4.98
50	-32.85 -30.26	-31.55	1.83

Table 15: Results of quantitative calibration made on potassium bicarbonate in MWDTA

The results were plotted as $\Delta°C/\Delta W^{-1}$ ($\Delta T/\Delta W^{-1}$) verses mass as given in Graph 155. The end point was determined as the return to linearity as in conventional thermal analysis (as the results of a non-dielectric event produce a peak), and integration was performed by the software.

$y = -0.6125x$
$R^2 = 0.992$
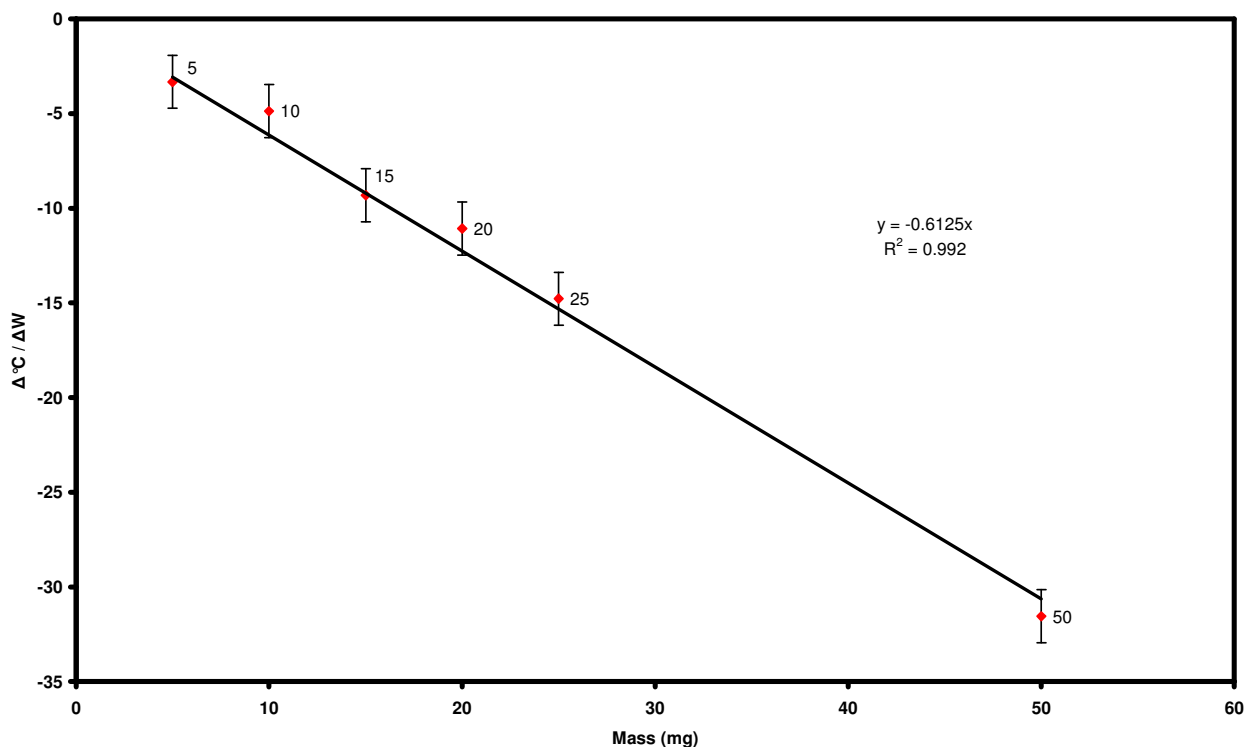
Graph 155: Average integration areas of the MWDTA results for potassium bicarbonate (error bars based on standard error)

The graph shows a very good linear correlation ($R^2 = 0.992$) and demonstrates that the equipment and measurement approach was sufficient to determine if a quantitative response existed with transitions where there was little or no change in tan δ.

8.4 Quantitative Rubidium nitrate measurements

Rubidium nitrate has three solid-solid phase changes, all of which were detectable using MWDTA (see Chapter 6 and Chapter 7). Of these three transitions the first (IV-III) appeared to produce little change in tan δ, the second showed a decrease in tan δ, while the third showed a strong increase in tan δ.

The material was considered interesting for quantitative work as it had the potential to show the effect of a largely 'enthalpy only' event (similar to potassium bicarbonate experiments) and a step change tan δ (similar to the silver iodide experiments) in a single experiment.

8.4.1 IV-III transition in Rubidium nitrate

If the assumption was true that a non-dielectric event would have a linear quantitative relationship, then the expected results were thought would lie on a linear slope like the bicarbonate work. The

conditions of these experiments remained the same as other quantitative MDWTA work where, the heating rate remained at 10 ºC/min and argon was used as a blanket gas.
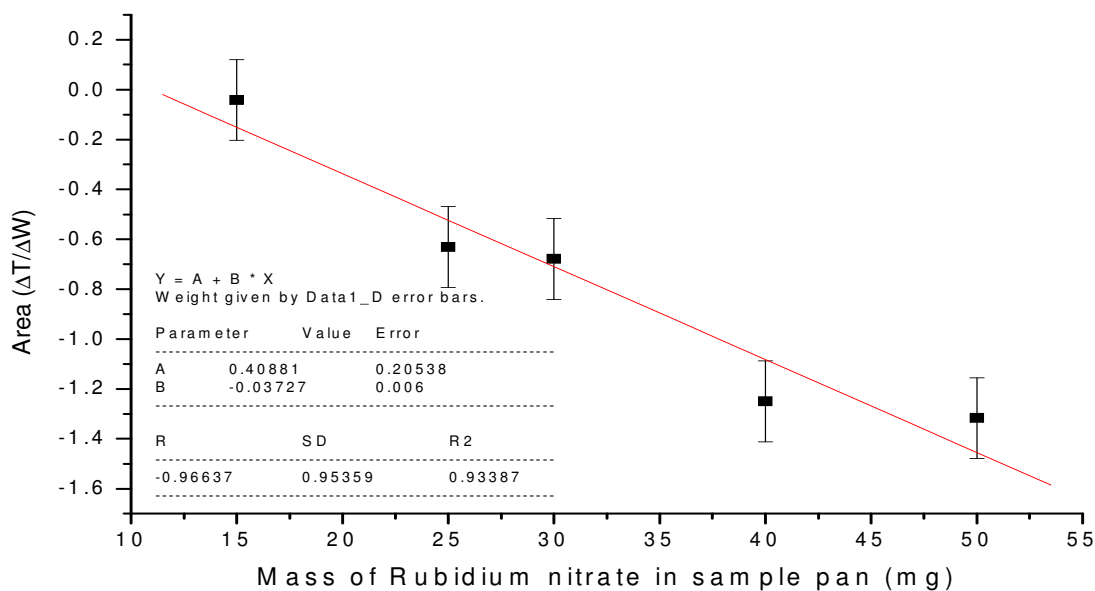
Graph 156: Average integration areas of the MWDTA results for the IV-III transition in rubidium nitrate (error bars based on standard error)

The results shown in Graph 156 agreed with this hypothesis, although the R^2 value was only 0.934. A possible source of error was that the IV-III transition did have a small associated change in tan δ and so an experiment was performed to investigate this.

8.4.1.1 Dielectric change in the IV-III transition of Rubidium nitrate

A simple experiment was set-up where the sample temperature was raised to 150 °C held isothermal for 10 minutes, then raised at 10 °C/min to 200 °C, then again kept isothermal for a further 10 minutes. If the transition involved a change in tan δ then the DTA signal would show a change in value after the transition compared to the pre-transition value. To rule out heat capacity effects the baseline in the DSC trace was also studied and showed a slight reduction in value.

Indirect MWDTA 100% Rubidium nitrate IH1140

The following settings are shown in the embedded table:

Parameter	Value
Heating Rate (°C/min)	Isothermal, 10, Isothermal
Final Temp (°C)	Hold 150, ramp 200, hold 200
Percentage of active sample	100%
4 stub tuning status	Manual
Sample weight (mg)	50 mg
Iris position (mm)	138
Iris (mm)	28 x 15
Cell	Indirect HPB
mixture material	n/a
Principle T/C	Reference
Tuning position (mm)	114
Comments	Argon 105% Sample flow 0%

Graph 157: MWDTA curve of the IV-III transition of rubidium nitrate under argon.

The results shown in Graph 157 from the MWDTA experiment showed a slight increase in the value ($\sim 1\ °C$) of the differential trace indicating a small change in tan δ. It was believed this could be the cause of the slight deviation from linearity seen in the quantitative measurements.

8.4.2 III-II transition in Rubidium nitrate

The results obtained from the step change in ΔT for the III-II transition are shown in Graph 158.
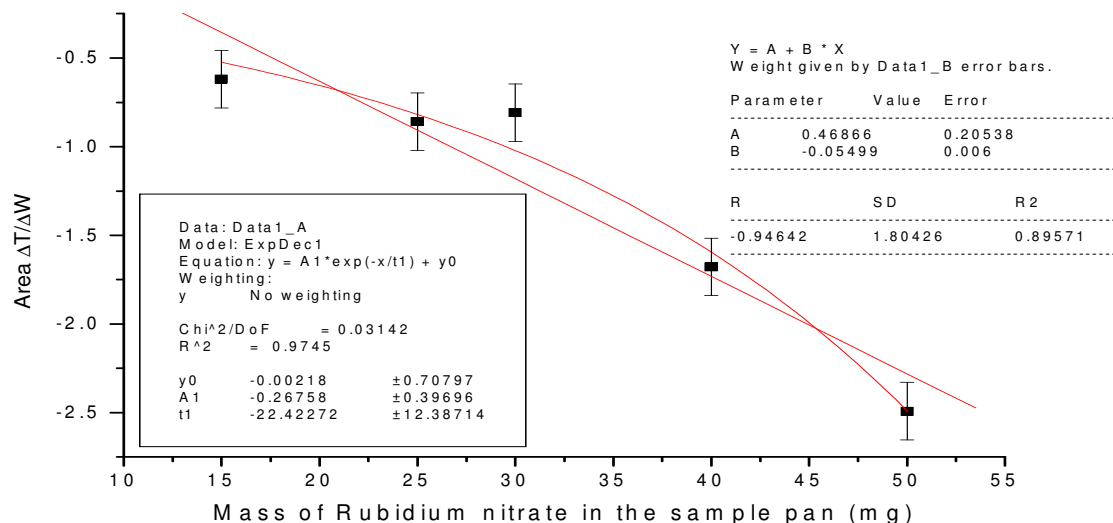
Graph 158: Average integration areas of the MWDTA results for the III-II transition in rubidium nitrate (error bars based on standard error)

The areas were measured using the area method described in previous sections.

The points showed considerably more deviation from linearity than the IV-III transition, particularly the apparent discrepancy with the results for 15, 30 and 50 mg. The data can be better fitted by an exponential decay ($R^2 = 0.97$) rather than a straight line ($R^2 = 0.89$), however, the reason for this needed explanation.

8.5 Possible explanations of trends in quantitative MWDTA

The research into quantitative MWDTA yielded interesting results, although it appeared that a linear relationship between mass and transition area was not obtained with microwave experiments, possibly because of the results in many cases being a mixture of enthalpy and heat capacity effects combined with changes in tan δ. Closer examination of the low mass results appeared to show a linear relationship, it is possible the explanation of the response produced by the larger masses is linked to thermal runaway.

Thermal runaway, as mentioned in previous chapters, occurs when a positive change in tan δ arises as a result of some transition in a material. This change in tan δ can cause a rapid rise in the sample temperature (an increase in the 'induced' heating rate) which is only prevented if the microwave

power is decreased or limited by the effects of cooling to the surroundings. This increase in the rate of ΔT, which would also be mass dependent, could cause the non-linear behaviour observed in the quantitative experiments.

8.6 Microwave induced heating rates

The temperature rise produced by a material subjected to microwaves heating is given in Equation 14, (page 44) assuming there are no heat losses. From Equation 14 it can be seen that for a given sample and a constant microwave power the rise in temperature is directly related to ε''_{eff}. However, this term can itself vary non-linearly with temperature in a number of cases [6],[71].

If a small sample is heated through a transition over a narrow temperature range using MWDTA then the change in ΔT will be sufficiently small enough to have no effect on ε''_{eff}. However, a larger sample may produce a change in ΔT sufficient to have a measurable effect on ε''_{eff} increasing ΔT further through positive feedback. Only the countering effect of cooling between the sample and the colder (and much larger thermal mass) of the reference prevents complete thermal runaway.

Metaxas *et al*. [6] describes a method to show that the critical volume of a sample can be identified, it was thought the same methods could be used to determine the critical mass. The critical mass that can produce thermal runaway was calculated by drawing a tangent to the steepest rise of the curve and extrapolating it back to the x axis. This process was applied to the data obtained with AgI as shown in Graph 159.

The data can be viewed as being in two regions. Up to 40 mg, the change in ΔT is less than 10 °C and the relationship between response and mass is reasonably linear. Above 40 mg, the response exceeds 25 °C. A line extrapolated through the last three points intersect the x axis between 35 and 40 mg, a good estimation of the critical mass leading to thermal runaway under the experimental conditions used.
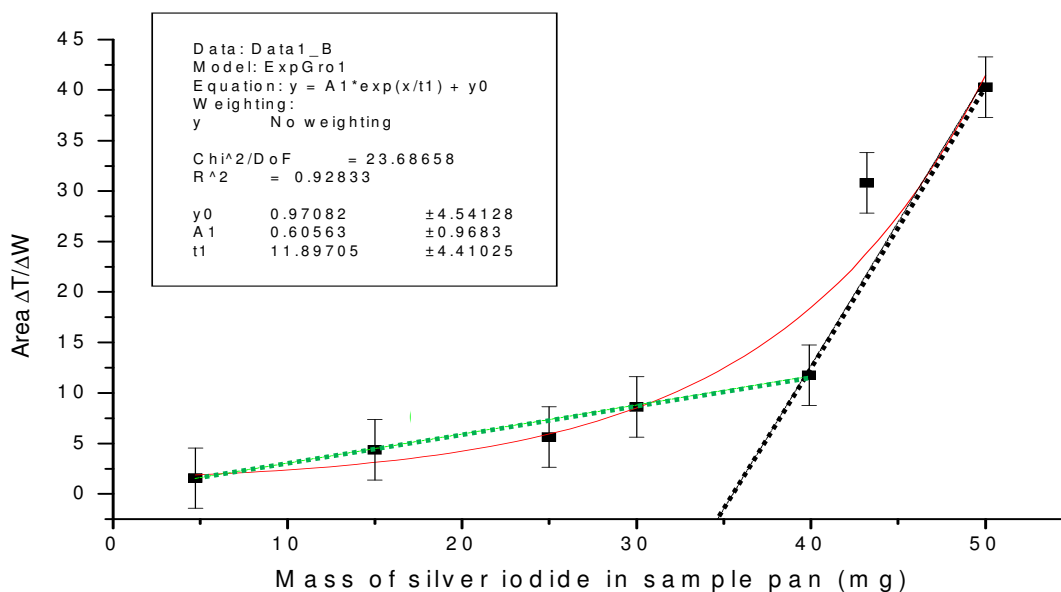
Graph 159: Example of a critical mass calculation for the solid-solid transition in silver iodide (error bars based on standard error) using MWDTA.

8.7 Summary of Quantitative MWDTA and induced heating rates

The results of this chapter indicated that quantitative information can be obtained with MWDTA using materials that have thermal transitions that are primarily 'enthalpic' and also ones where there is a significant change in tan δ. In these latter cases, the work with AgI suggested that the linearity of the response as a function of mass applies only up to a critical mass. Above this mass, the effect of the exponential relationship between $\varepsilon"_{eff}$ and temperature appears to be predominate.

It is possible that if the sample temperature was controlled, rather than the reference as in all the MWDTA results reported here, then a linear response would be obtained over a larger mass range. However, as discussed earlier, the current MWTA software has insufficient a response time to effectively control the temperature of a material undergoing a transition with a significant change in tan δ.

Restrictions on time prevented a more detailed study of the quantitative potential of MWDTA although future work could include testing whether the 'critical mass' effect applied to other materials and also the response of a material with a decrease in tan δ after a transition.

Chapter 9

Development of Microwave differential thermal analysis coupled with evolved gas analysis (MWDTA-EGA)

One drawback with MWDTA (like conventional DTA and DSC) is that there is no means of identifying the reactions that correspond to the changes in ΔT observed. To overcome this limitation it is possible to couple a secondary technique, such as evolved gas analysis (EGA). Careful design is necessary when developing this combined form of thermal analysis to ensure that the requirements for one have minimal impact on the performance of the other.

This chapter describes the background to the use of EGA in thermal analysis and the adaptations made to MWDTA to allow it to be connected to a mass spectrometer.

9.1 Microwave DTA coupled with evolved gas analysis (EGA)

Classic thermal analysis techniques are generally non-specific and only indicate underlying chemical processes indirectly though mass or enthalpy changes. EGA allows the monitoring of thermally induced processes that produce (or consume) a vapour and can be extremely useful in the study of complex systems.

Early EGA systems involved the collection or trapping of evolved species which is analysed later using a technique such as gas chromatography. However, coupled systems, where the evolved species are continuously monitored throughout the thermal analysis experiment have become more common. Coupled arrangements are usually favoured for many reasons including reduction of experimental time, and elimination of number of variables.

A variety of EGA detectors, both specific and non-specific have been used [27, 39, 43], but mass spectrometry has many advantages, not least that it can be possible to record several different species at once. Combined TA-EGA systems using MS have been applied to systems as diverse as heterogeneous catalysts, pyrotechnics and absorbents [72, 73].

For reliable results the time between the evolution of gas and detection must be minimised, this involves using short heated capillary connecting tubes (to avoid condensation), constructed from an inert material to prevent catalytic decomposition of the gas-phase material and high flow rates. Glass-lined metal capillary or metal-sheathed silica tubes are often used.

9.2 MWDTA-EGA instrumentation

This section describes the instrumentation and experimental conditions used to couple MWTA with EGA using a mass spectrometer.

9.2.1. MWTA-EGA cell design
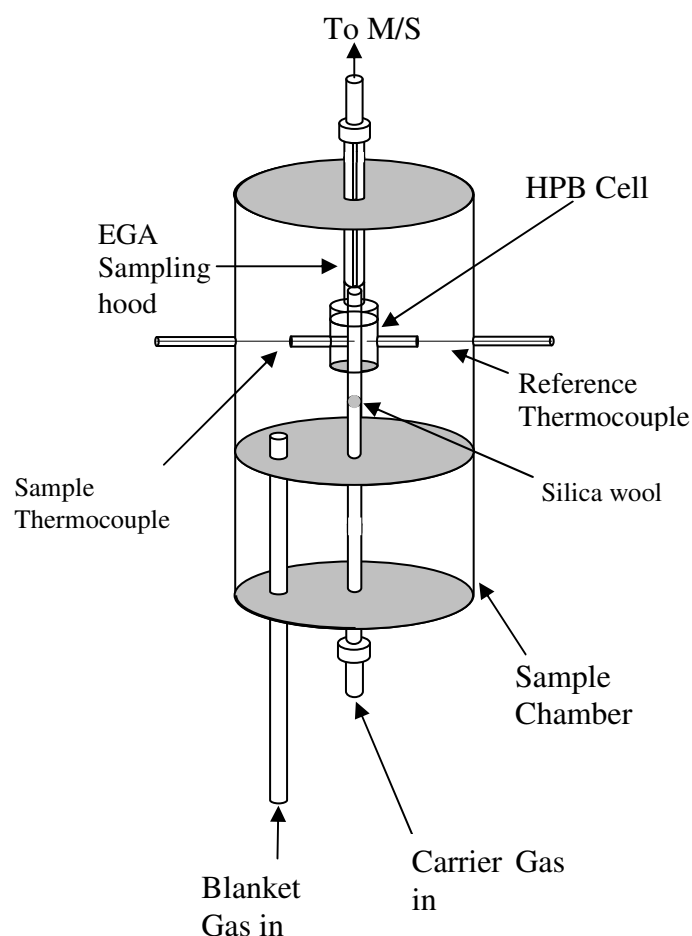
Figure 74: Diagram of MWDTA-EGA set up

The cell used for the MWDTA-EGA work is shown in Figure 74. It was based upon the HPB DTA cell design with the addition of a silica 'sampling hood', positioned directly above the sample to collect any evolved gases, and an outer sample chamber to provide atmospheric containment. The sample chamber had two drilled holes to allow access for the sample and reference thermocouples and a removable lid to allow access to the sample.

The sample hood was heated by a 0.25 mm nichrome wire wrapped around the exposed points of the sampling hood outside the cavity and heating to ~150 °C using a 20 V DC supply. Two gas inlets were used. One provided a blanket gas for the chamber while a carrier gas passed through the sample in the inner cell and helped transport evolved gases to the sampling hood. Typically, the carrier gas used was helium with a flow rate of 20 to 40 ml/min while three different blanket gases

(helium, argon and nitrogen) were used with flow rates of 80 to 100 ml/min. The higher flow rate for the blanket gas was to ensure that air was swept from the chamber which could not be made completely air tight. Gas control was provided by two mass flow controllers (Brookes).

9.2.2 Mass spectrometer

A HPR-20 (Hiden Analytical) quadrupole mass spectrometer was used for this work. The instrument is specifically designed for low mass evolved gas work and has a range of 1-300 amu. The MS has a heated capillary inlet held at 150 °C and with a sampling flow rate variable between 10 and 20 ml/min dependent on the setting of a needle valve which restricts the flow into the inlet. This was interfaced to the MWDTA-EGA cell using a 6 mm Ultra-Torr fitting (Swagelok).

The Hiden software allows the partial pressure of selected m/z values to be monitored as a function of time although it cannot distinguish between species that have the same integer m/z value (e.g. CO and N_2 both have principal fragments wit h m/z = 28). Data collected with the Hiden software was exported to Excel and merged with the MWTA data after each experiment.

9.2.3 Conventional EGA instrument set up
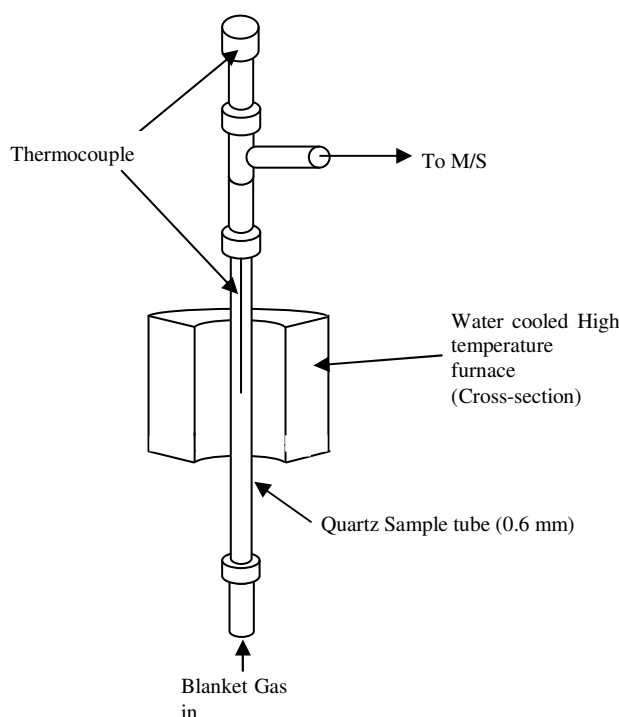
Figure 75: Cross section of the conventional EGA setup

For comparative experiments a conventional EGA system was developed as shown in Figure 75. The system comprises a 6 mm silica tube where the sample was situated and a water-cooled furnace controlled by an E818P temperature programmer (Eurotherm). A thermocouple was situated down the tube directly into the sample and a crude ΔT signal obtained from the difference between the sample and furnace temperatures. Helium with a flow rate of 30 ml/min was used as a carrier gas and coupling to the MS was done using a 6 mm Ultra-Torr fitting (Swagelok) as with the MWDTA-EGA arrangement. Data acquisition used software developed within the research group for conventional EGA studies.

9.3 Initial evaluation of the MWDTA-EGA system using calcium oxalate monohydrate

The MWDTA-EGA was initially evaluated using the decomposition of calcium oxalate monohydrate. This material was chosen as it has three distinct decomposition steps (see Equation 33) up to 600 °C. The second step in an inert atmosphere is the endothermic evolution of CO but if sufficient oxygen is present all the CO is converted to CO_2 and the process becomes overall exothermic. As such, it provides a useful measure of the quality of the atmosphere control around the sample.

$$(a)\ CaC_2O_4.H_2O \xrightarrow{\sim 200°C} CaC_2O_4 + H_2O \text{ (endothermic)}$$
$$(b)\ CaC_2O_4 \xrightarrow{\sim 400°C} CaCO_3 + CO \text{ (endothermic)}$$
$$2CO + O_2 \rightarrow 2CO_2 \text{ (exothermic)}$$
$$(c)\ CaCO_3 \xrightarrow{\sim 600°C} CaO + CO_2 \text{ (endothermic)}$$
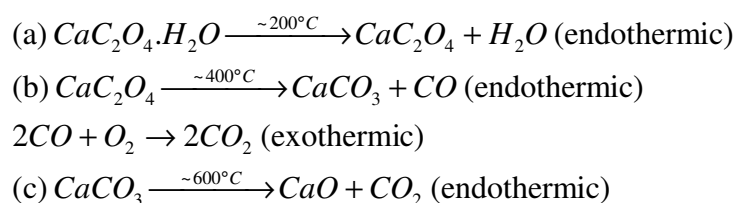
Equation 33: The thermal decomposition of copper oxalate monohydrate

A conventional EGA experiment was performed using a 20 mg sample of $CaC_2O_4.H_2O$ heated at 10 °C/min to 600 °C with helium as the carrier gas and with two m/z fragments monitored: 18 (H_2O) and 44 (CO_2). The results of this experiment are shown in Graph 160, which shows the relative concentrations of the two fragments and the DTA signal as a function of sample temperature. The DTA signal mainly shows the underlying lag between the sample and furnace temperatures although there is a suggestion of an endothermic peak during the initial loss of water step. Some CO_2 is produced during the second decomposition step possibly indicating a very small air leak in the system.

Linear heating-EGA Calcium oxalate IH0002
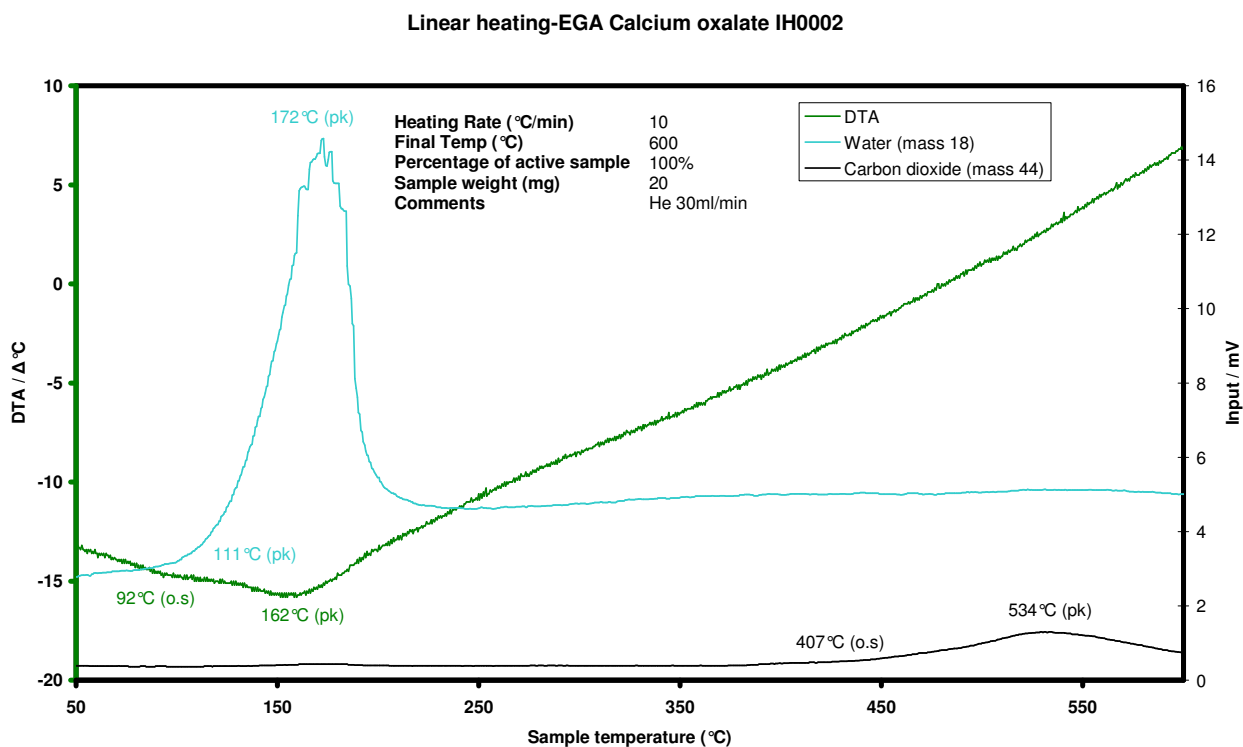
Graph 160: Conventional linear heating experiment of calcium oxalate performed under helium.

Graph 161 shows the results from the matching MWDTA-EGA experiment with helium used as both the carrier and blanket gas. The partial pressures of the two fragments and the DTA signal are plotted as a function of time.

It is apparent that the signal-to-noise ratios for the evolved gas profiles are much worse than with the conventional EGA. This is a result of the much larger overall volume of the system where diffusion of some of the evolved gases into the outer chamber cause peak broadening and reduction in signal intensity.

The evolution of water during the first decomposition step is clearly evident although the peak shape is distorted. This almost certainly arises from condensation on the cold surfaces within the MWDTA-EGA cell (much larger in area than in the conventional EGA system); a problem never satisfactorily resolved.

Some CO_2 is seen during the second decomposition step which suggests that the blanket gas did not completely exclude all the air. The DTA trace is largely uninformative with a large drift although there is a suggestion of the expected endothermic event during the water loss.

MWDTA-EGA 100% Calcium oxalate IH0817
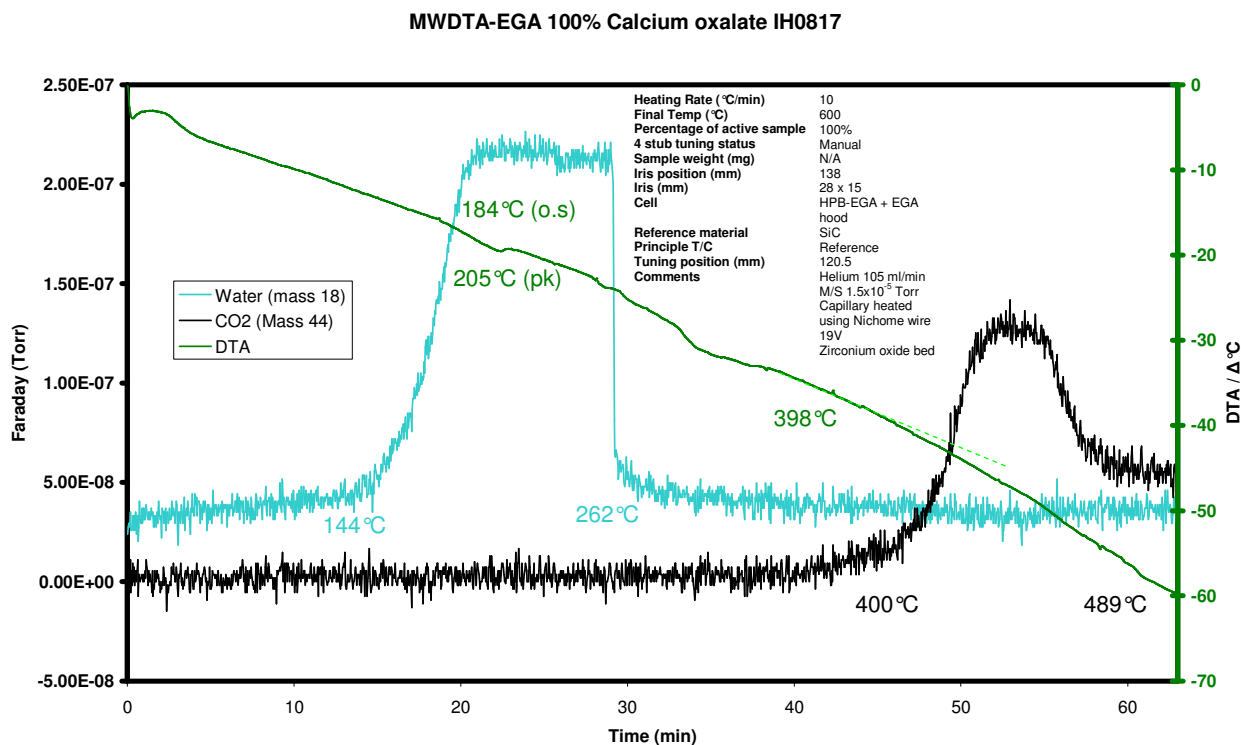
Graph 161: MWDTA-EGA experiment of calcium oxalate performed under helium.

The conventional and MWDTA EGA experiments were repeated by using air as the carrier/blanket gas. Graph 162 shows the results from the conventional EGA experiment and the much larger CO_2 peak and exothermic DTA peak is clearly apparent for the second decomposition step. A similar result is seen with the MWDTA-EGA experiment (Graph 163) although the data quality and peak shapes are worse, again particularly for the water.

Linear heating-EGA Calcium oxalate IH0001
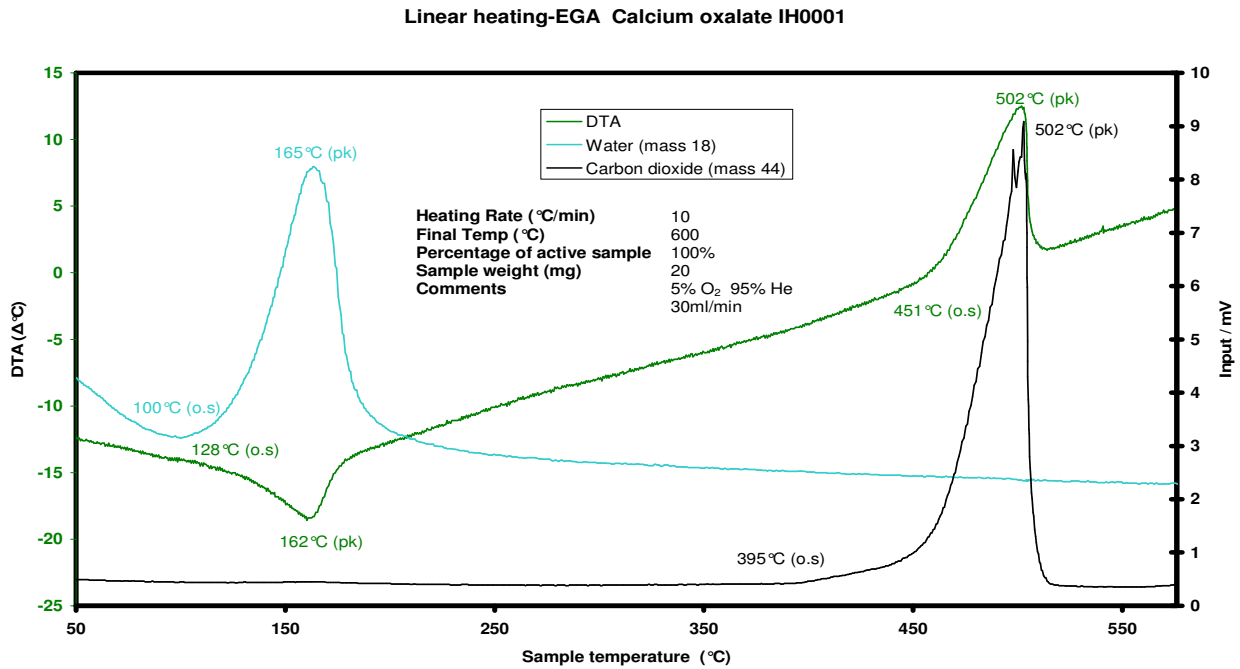
Graph 162: The conventional linear heating experiment of calcium oxalate performed under a mixed gas of 5 % O₂: 95 % He.

MWDTA-EGA 100% calcium oxalate monohydrate IH0818
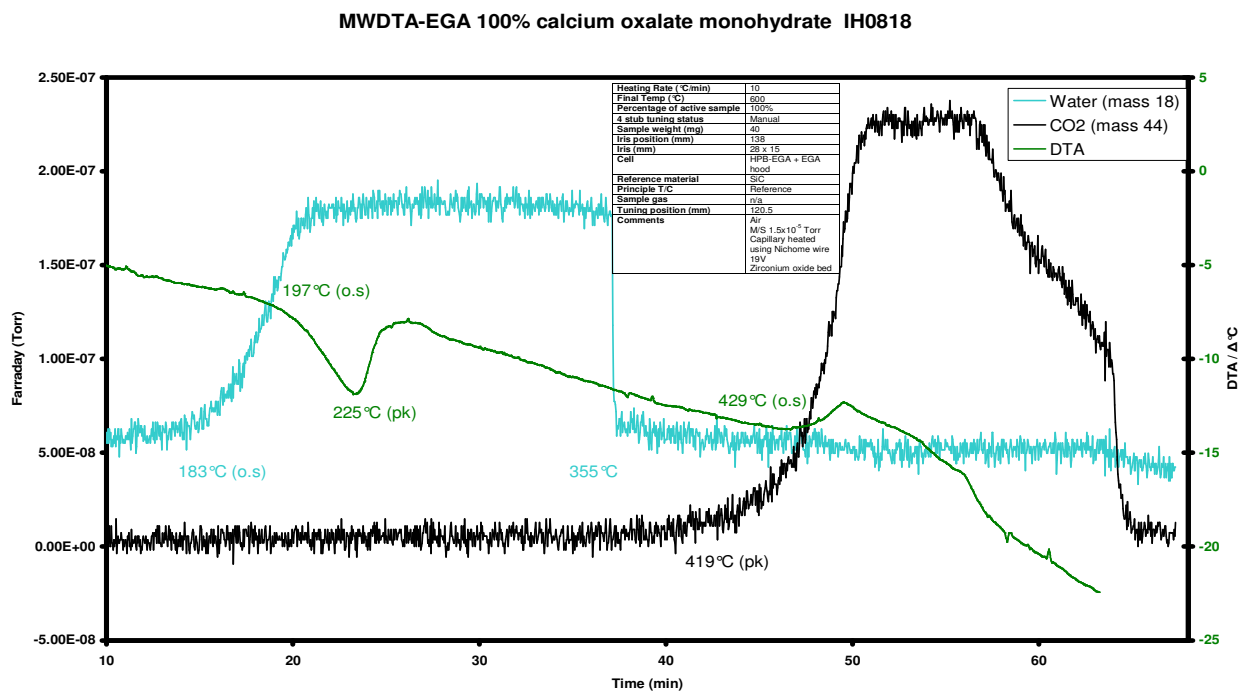
Graph 163: The MWDTA-EGA experiment of calcium oxalate monohydrate performed under flowing air.

As a result of these experiments the flow rates of both the carrier and blanket gas were adjusted to optimise the MWDTA-EGA as far as possible with flows of 35 ml/min and 100 ml/min, respectively, being adopted.

9.4 MWDTA-EGA experiments

After the initial tests with calcium oxalate a series of experiments were performed to further investigate the scope and limitations of MWDTA-EGA using a range of standard materials with decomposition steps evolving simple gases.

9.4.1 Decomposition of sodium bicarbonate

The decomposition of sodium bicarbonate (sodium hydrogen carbonate) occurs in one stage, with the simultaneous release of water and carbon dioxide to form sodium carbonate (Equation 34).

$$2NaHCO_3 \rightarrow Na_2CO_3 + H_2O + CO_2$$

Equation 34: Thermal decomposition of sodium bicarbonate

Conventional and MWDTA-EGA experiments were performed using 20 mg of sodium bicarbonate and a heating rate of 10 °C/min to 250 °C with helium as a carrier and carrier/blanket gas. Two m/z fragments were monitored: 18 (H_2O) and 44 (CO_2).

Linear heating-EGA 100% sodium bicarbonate IH0003
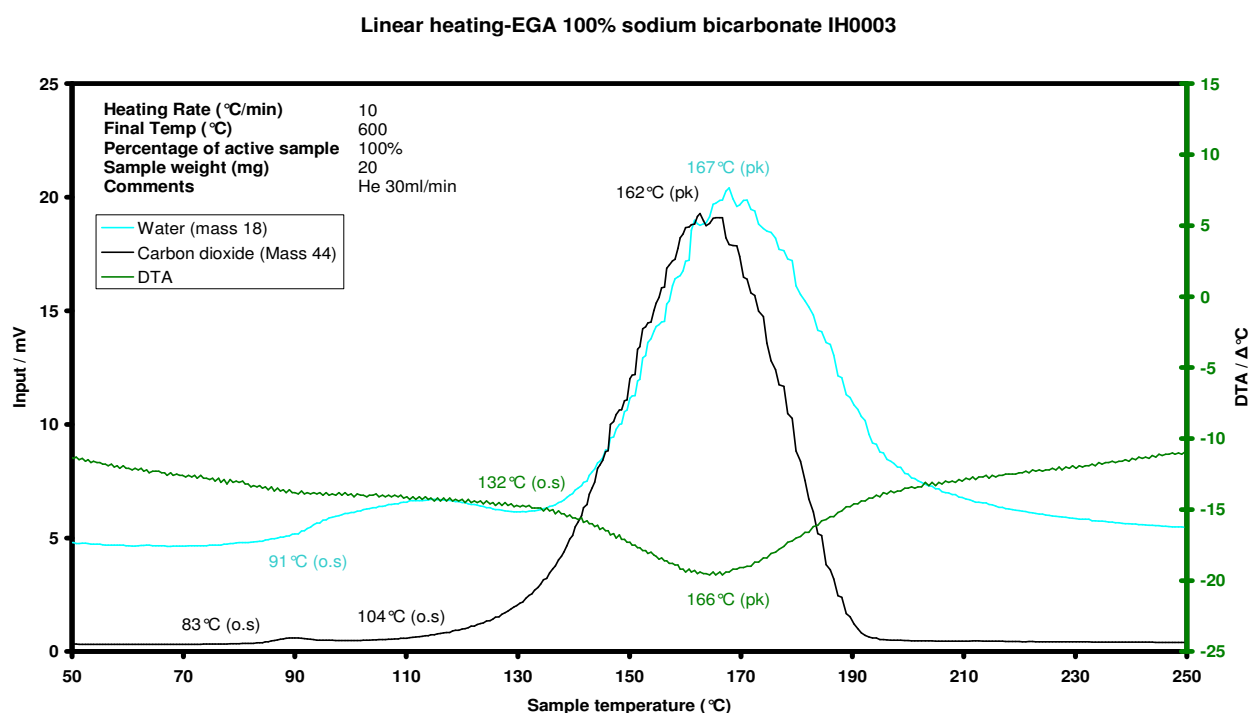
Graph 164: Conventional linear heating experiment of sodium bicarbonate performed under helium.

Development of Microwave differential thermal analysis coupled with evolved gas analysis

Graph 164 shows the results of the conventional EGA experiment as a function of temperature. The DTA clearly shows the endothermic nature of the process with the simultaneous evolution of the H_2O and CO_2, although the peak for the former is slightly broader than the latter, probably due to partial condensation on a cold spot.

MWDTA-EGA 100% sodium bicarbonate IH0808

Heating Rate (°C/min)	10
Final Temp (°C)	200
Percentage of active sample	100%
4 stub tuning status	Manual
Sample weight (mg)	40
Iris position (mm)	138
Iris (mm)	28 x 15
Cell	HPB-EGA + EGA hood
Reference material	SiC
Principle T/C	Reference
Tuning position (mm)	120.5
Comments	He 105 ml/min Samp: 33ml/min M/S 2.0x10⁻⁶ Torr Capillary heated using Nichome wire 19V Alumina bed

Graph 165: MWDTA-EGA experiment of sodium bicarbonate performed under helium.

The MWDTA-EGA results (Graph 165) are very similar to those of the conventional EGA with the exception of the evolved water profile where condensation has completely distorted the peak.

9.4.2 Decomposition of potassium bicarbonate

The decomposition of potassium bicarbonate (potassium hydrogen carbonate) is very similar to that of sodium with a single decomposition step with the simultaneous release of water and carbon dioxide to form potassium carbonate (Equation 35).

$$2KHCO_3 \rightarrow K_2CO_3 + H_2O + CO_2$$

Equation 35: the thermal decomposition of potassium bicarbonate

Conventional and MWDTA-EGA experiments were performed using 20 mg of potassium bicarbonate and a heating rate of 10 °C/min to 250 °C with helium as a carrier and with two m/z

320

Development of Microwave differential thermal analysis coupled with evolved gas analysis

fragments monitored: 18 (H_2O) and 44 (CO_2). In this instance however, the MWDTA-EGA experiment used N_2 as a blanket gas (to see if any undesirable effects were recorded from the change in gases).

Linear heating - EGA 100% Potassium bicarbonate IH0007
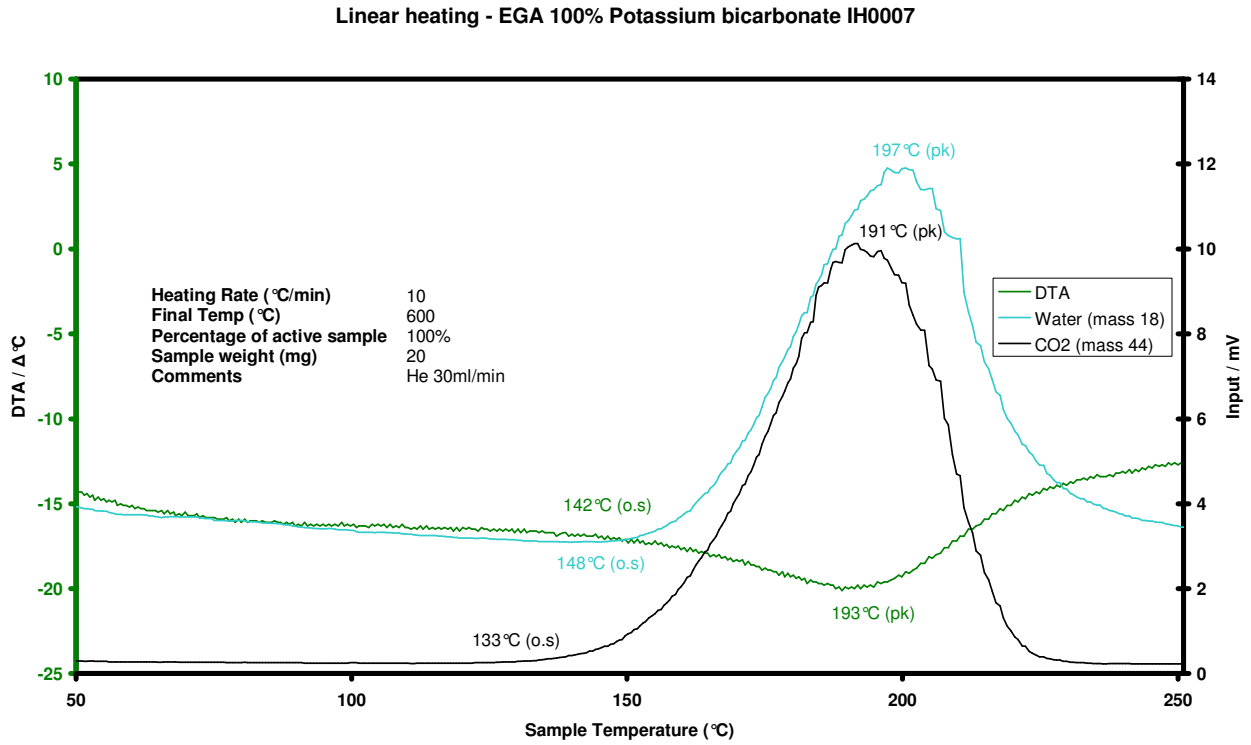
Graph 166: Conventional linear heating experiment of potassium bicarbonate performed under helium.

MWDTA 100% Potassium bicarbonate IH0803
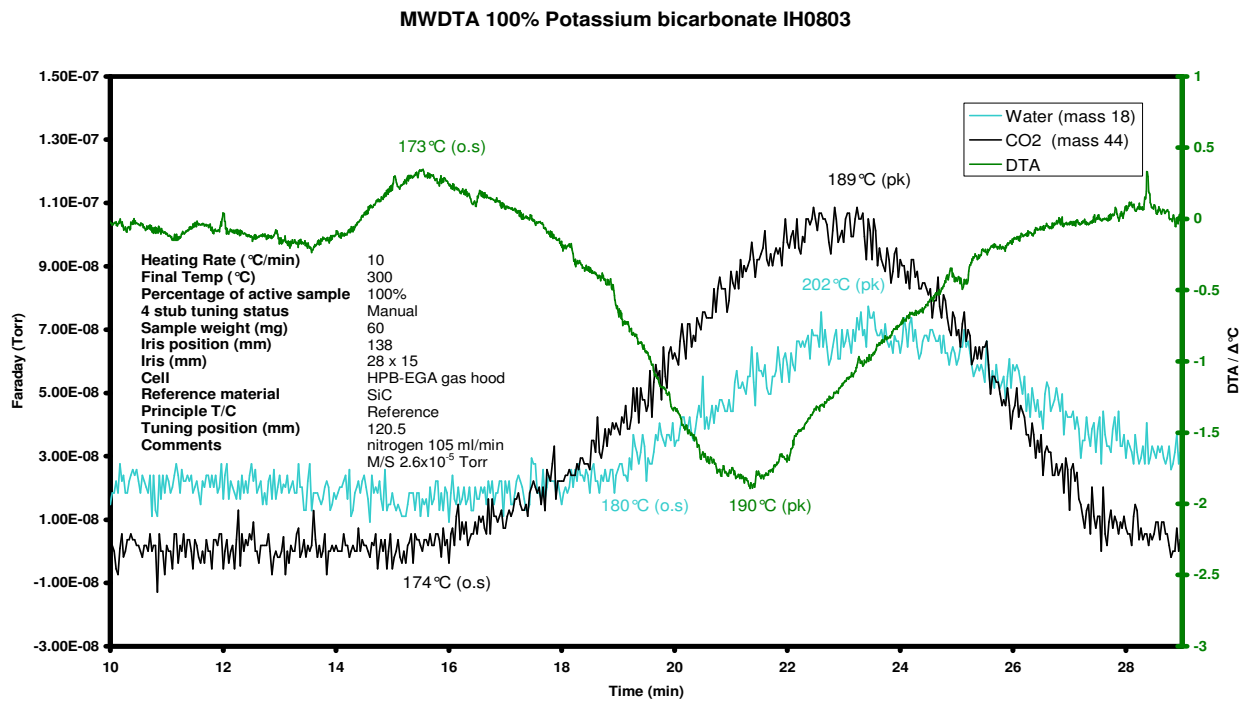
Graph 167: MWDTA-EGA experiment of potassium bicarbonate performed under nitrogen.

Graph 166 and Graph 167 show the results of the conventional EGA and MWDTA-EGA experiments, respectively. Both the DTA and evolved gas profiles are comparable between the two although, again, the signal-to-noise ratio for the MWDTA-EGA experiment is much worse possible due to the use of nitrogen carrier gas.

9.4.3 Dehydration of copper sulphate pentahydrate

Copper sulphate pentahydrate loses water in 3 steps as shown in Equation 36 [1].

$$(a)\ CuSO_4 \cdot 5H_2O \xrightarrow{85°C} CuSO_4 \cdot 3H_2O + 2H_2O$$
$$(b)\ CuSO_4 \cdot 3H_2O \xrightarrow{115°C} CuSO_4 \cdot 1H_2O + 2H_2O$$
$$(c)\ CuSO_4 \cdot 1H_2O \xrightarrow{230°C} CuSO_4 + H_2O$$
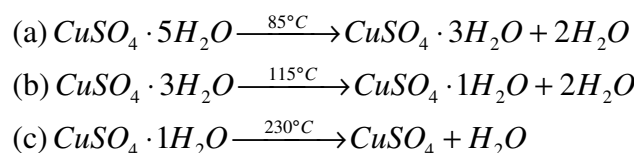
Equation 36: The thermal decomposition of copper sulphate pentahydrate

Conventional and MWDTA-EGA experiments were performed using 20 mg of copper sulphate pentahydrate and a heating rate of 10 °C/min to 250 °C with helium as a carrier gas. A single m/z fragment was monitored: 18 (H_2O). For the MWDTA-EGA experiment N_2 was used as blanket gas (to reduce the large thermal gradient seen when using helium).

Linear heating - EGA 100% Copper sulphate IH0011

Heating Rate (°C/min)	10
Final Temp (°C)	700
Percentage of active sample	100%
Sample weight (mg)	20
Comments	He 30 ml/min
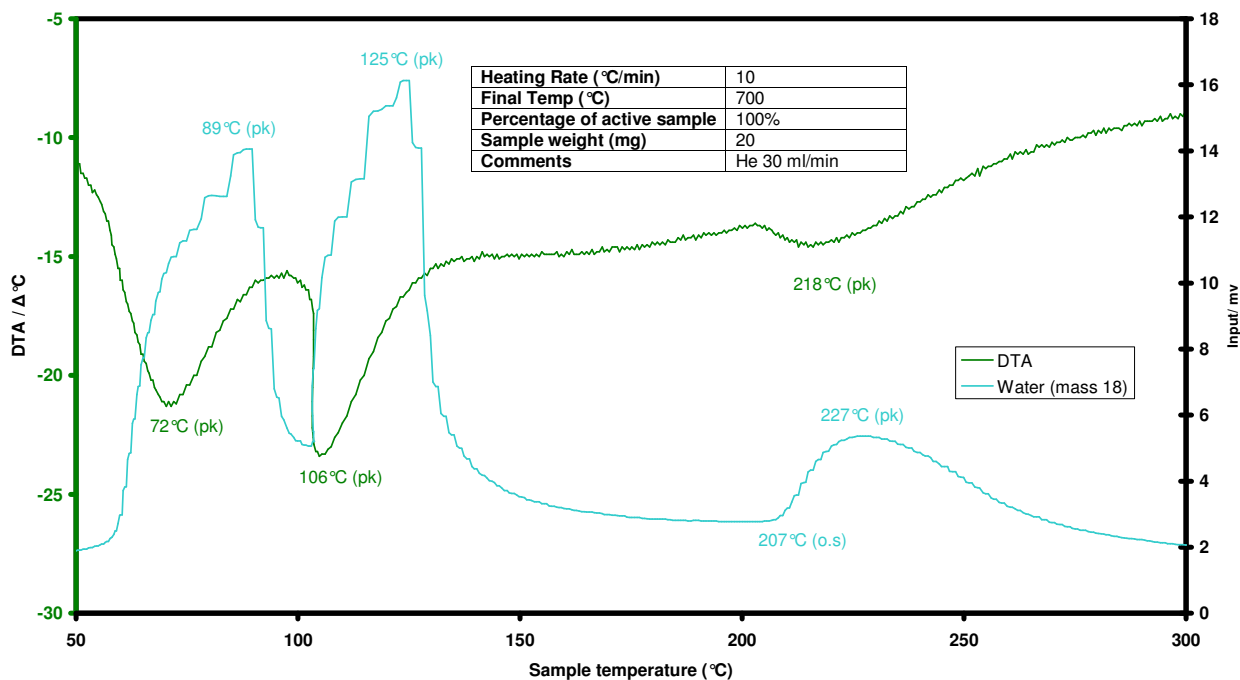
Graph 168: conventional linear heating experiment of copper sulphate pentahydrate performed under helium.

MWDTA-EGA 100% Copper sulphate pentahydrate IH0813
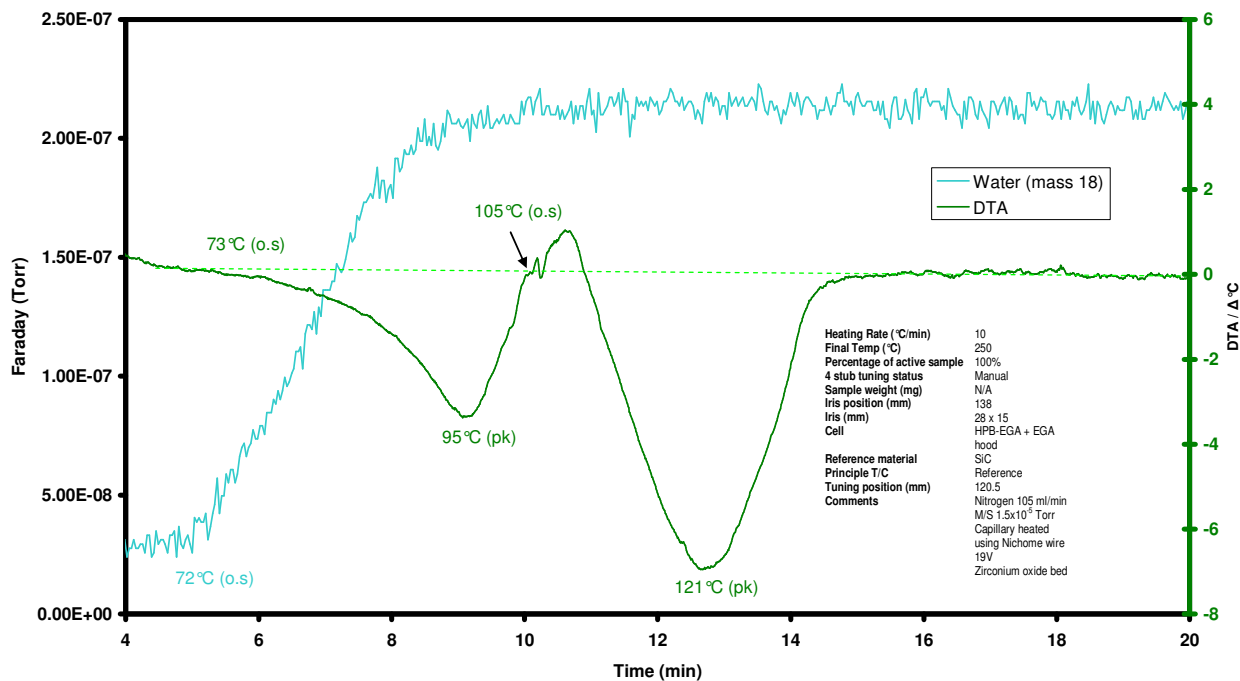
Graph 169: MWDTA-EGA experiment of copper sulphate pentahydrate performed under helium.

Graph 168 and Graph 169 show the results of the conventional EGA and MWDTA-EGA experiments, respectively. While the conventional EGA profile shows two distinct water evolution

peaks, again, condensation in the MWDTA-EGA cell (made worse by the relatively large amount of water evolved from this system) means that all information (other than water is evolved at all) is lost.

9.5 Summary of MWDTA-EGA

The results of the MWDTA-EGA work indicate that it is possible to combine MWDTA and mass spectrometry to produce a genuine couple technique. However, considerable problems were experienced with systems evolving water and the current cell design where the relatively large area of unheated glassware made condensation a significant problem. With volatile gases, such as CO_2, the results obtained were comparable to those seen with a conventional EGA system.

Improvements to the design of MWDTA-EGA cell could include:
- (a) Decreasing the size of the outer chamber to minimise the diffusion volume and aid the efficiency with which the blanket gas swept the chamber.
- (b) Currently, the cell design means that the blanket gas escapes through the thermocouple inlets and, to some extent, up the sampling hood which dilutes the evolved gases being monitored. Incorporation of a proper blanket gas vent combined with efforts to improve the gas tightness of other parts of the cell (possibly using suitable grease) might also be beneficial.
- (c) Coating the sampling hood with a susceptor so that it would heat and help to reduce the effects of condensation.

Discussion

Chapter 10

Trends and patterns in microwave thermal analysis

This section covers some of the trends identified from the results obtained using MWTA to see whether it would be possible to predict the thermal behaviour (in terms of the extent of heating) of a previously untested material.

Trends and perditions in microwave thermal analysis

The work in this thesis has concentrated on how materials heat under microwaves as they go through thermal transitions such as fusions, dehydrations, curie points and decompositions.

Although definitive trends are hard to determine certain trends have been observed which may help to predict how untested material will behave.

10.1 Ohmic heating in MWTA

Ohmic heating is only effective with semi-conductors. Above a certain point, increasing the electrical conductivity actually decreases the effectiveness of Ohmic heating to the extent that a material (such as a metal) may not heat at all. However, the use of cells where heating is assisted by the presence of a susceptor (where the reference is surrounding the sample i.e. as in MWDTA, see 5.3.1 HPB cell, page 131) means that even these materials can be studied.

10.1.1 Effect of different modes of carbon activation on microwave heating

Different forms of activated carbon were analysed used MWTA to see the extent which they would heat at a set applied power (section 4.1 Initial familiarisation with MWTA using carbons, Page 89). It was observed that when physically activated carbons (typically produced at temperatures in excess of 700 °C) were compared to low-temperature chemically activated carbons made from the same precursor, that the former were more effectively heated using microwave energy. In addition, if a poor coupling carbon was heated to a high temperature it subsequently coupled more effectively. It is thought that this effect arises from an increase in the short range order within the carbon at high temperature enhancing the numbers conductive pathways within the sample and hence the effectiveness of Ohmic heating. These results show that the thermal history of a sample could be important in microwave thermal analysis.

10.1.2 Effects of electrical conductivity on Ohmic heating

The changes in electrical conductivity are also important in the extent that a solid heats under applied microwave heating. Material defects (interstitial or vacancy) can help to facilitate the movement of charge throughout the sample, therefore increasing its ability to couple to the applied wave (increasing heating), an example of which is in the fast ion conductor silver iodide (7.10 Fast ion conductors, page 285) were the sample shows a sustained rise in differential temperature after it has gone through the fast ion conductor transition. Creating defects by methods such as fine grinding of large crystals is expected to aid in heating. Additional evidence to support this finding can be seen in the study of susceptors (4.2.1 Susceptor 1: Silicon carbide, page 96) where it was shown that finer ground SiC (200-450 mesh) heated between 72 to 100 °C degrees higher than the larger sized (-400 mesh) material.

While an extensive study was not performed on the effects of defects in microwave heating, the processes of grinding sample is expected to increase the extent to which a material will heat during a MWTA/MWDTA experiment.

10.2 Dipolar polarisation in MWTA

Dipolar polarisation is the main mode of heating in liquids and semi molten samples. It arises from the material's ability to track the changes in the applied wave and subsequently lagging behind the changes in the poles. The inability to completely track the wave results in dielectric losses, where the energy from the change in movement is turned to heat (molecular friction).

The work presented in this thesis has shown many cases of the effects of dipolar polarisation as the microwave heating of a material moves from reliance on Ohmic heating (solid) to dipolar polarisation (liquid) during transitions such as fusion.

10.2.1 Fusion of Materials

The previous chapters (Chapter 5, page 117, Chapter 6, page 172) have shown examples of how the fusions of different materials behave under microwave heating. Therefore it is now possible to predict the type of trace that is likely to be seen if there is little information available.

10.2.1.1 Fusion of a material with significant changes in tan δ.

Experiments of this type, such as the heating of polar organic compounds, have shown to occur at lower temperatures than the equivalent DSC values. This is due to large rises in temperature occurring at the first point of charge of transition. [The point in DSC profiles where the baseline first deviates from linearity see Figure 76(a)]. Reaction at first point of change is possible due to the volumetric heating, where the bulk and surface heating in unison, rather than the conventional conduction model were the surface heats from the walls of the furnace and the bulk is heated via conduction through the sample. This conduction model gives rise to thermal mass and therefore longer ranges of the onset temperatures to transitions.
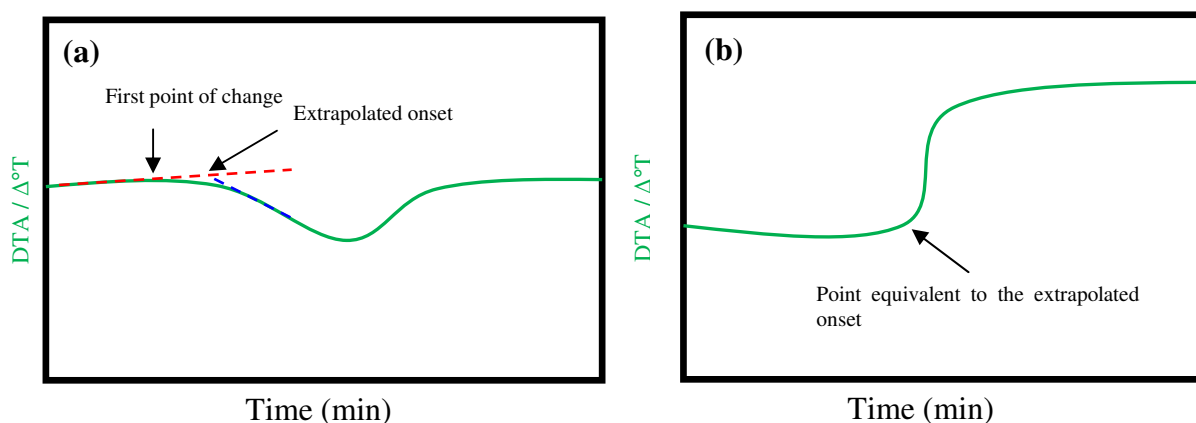
Figure 76: Illustration of (a) where the first point of change occurs in a DSC profile (b) the equivalent point on a MWDTA profile

Reaction to the first point of change of a transition therefore makes it difficult to forecast the transition temperature that will be recorded in MWDTA using data from conductive heating methods or when heating materials for the first time. It can however be expected that in many cases the transition is likely to occur at a lower temperature than expected.

In some materials the temperature rise can be hundreds of degrees earlier (i.e. 7.4.4.2 Sodium tungstate dihydrate, page 233). The cause for this phenomenon was not obtained from this research,

although there is the possibility that electrical conductivity discontinuities (which were not seen in DSC experiments) maybe involved. MDTA could be used to prove/disprove this proposal.

10.2.1.2 Transition with little or no changes in tan δ

Prior to the current research, the MWTA was largely restricted to monitoring transitions that had a change in tan δ significant enough to necessitate an alteration of the applied microwave power level required to maintain linear heating. The HPB cell, (page 131) allowed for a reference measurement, which was not dramatically altered by the mismatches in tan δ compared to the sample, to be obtained. This meant that not only the changes in tan δ could be recorded but also 'enthalpy only' transitions from the differential signal. A good example of such a transition is the solid-solid phase change of caesium nitrate shown in Sections 6.2.2 Caesium Nitrate, page 178 and 7.7.4 Caesium nitrate, page 265), where the MWTA experiment showed that only a small change in tan δ was detectable on the MWTA applied power profile, but when studied using the HPB cell the transition could be clearly seen from the differential profile using only 6 % of the sample weight (40 mg) required for the MWTA experiment (600 mg) .
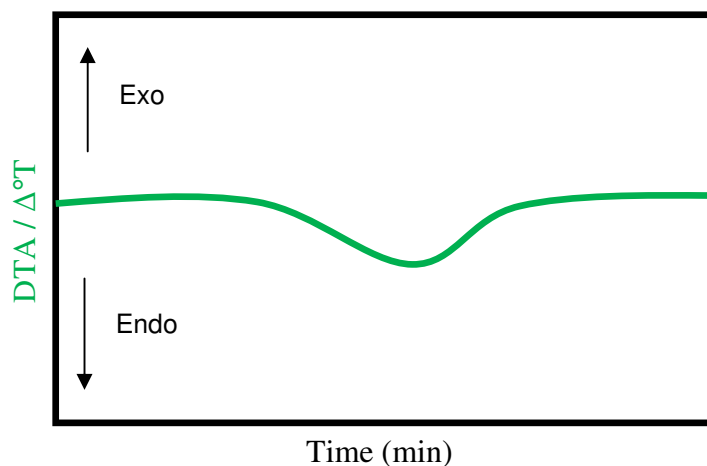
Figure 77: Illustration of the expected profile of a material with an endothermic transition which has little or no change in tan δ

When using MWDTA to monitor 'enthalpy only' transition the resultant profile is expected to (in many cases) be very similar to that of a DSC profile.

Although the HPB cell proved a valuable addition to the MWTA instrument it was found to be insufficiently sensitive enough to detect very weak enthalpy only transitions or 2nd order phase such as glass transition temperatures.

10.2.1.3 Transition with little or no changes in enthalpy

The case of a 'tan δ only' change (i.e. one where the enthalpy change appears negligible) is possible although only one instance was observed during this research; the conductivity changes in the microwave heating of rubidium nitrate. During this experiment a change in electrical conductivity of the sample resulted in the MWTA altering the applied power levels to maintain linear heating. A schematic of the response from a change in electrical conductivity is shown in Figure 78. It is possible if all electrical conductivity changes behave in a similar manner to rubidium nitrate then a fall in applied power will be observed when conductivity rises and vice versa.
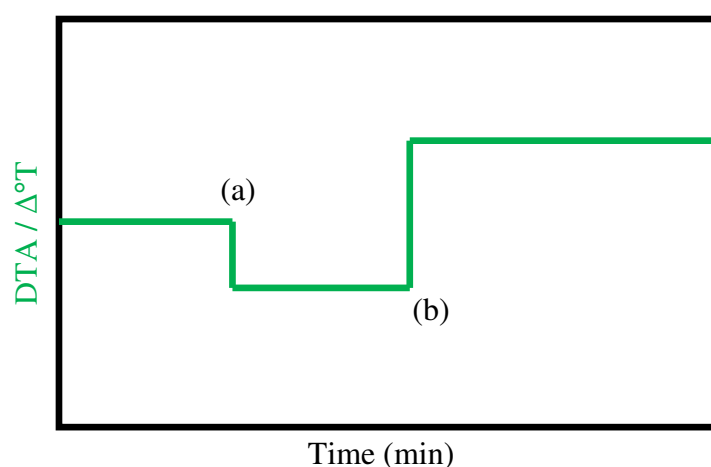
Figure 78: Illustration of the DTA profile expected from a change in electrical conductivity of a sample during an MWDTA experiment (a) response from a rise in electrical conductivity (b) a fall in electrical conductivity.

Unfortunately, as this was the only example of this kind of transition encountered during this research a reliable prediction of how materials of this type would behave in the MWTA is not possible without further investigation of similar materials.

10.2.1.4 Fusion of strongly endothermic materials

The fusions of several organic polar materials have been studied during this research. The results have consistently shown that MWTA is sensitive to fusions that have a large change in tan δ. The technique has also shown that there are competitive processes occurring during these transitions, where the latent heat of fusion of strongly endothermic materials such as acetaminophen and sorbitol temporarily suppress the temperature rises due to the increased coupling via dipolar polar polarisation.

The predicted MWDTA trace profiles of materials where the endothermic fusion of materials alter the change in coupling are shown in Figure 79.
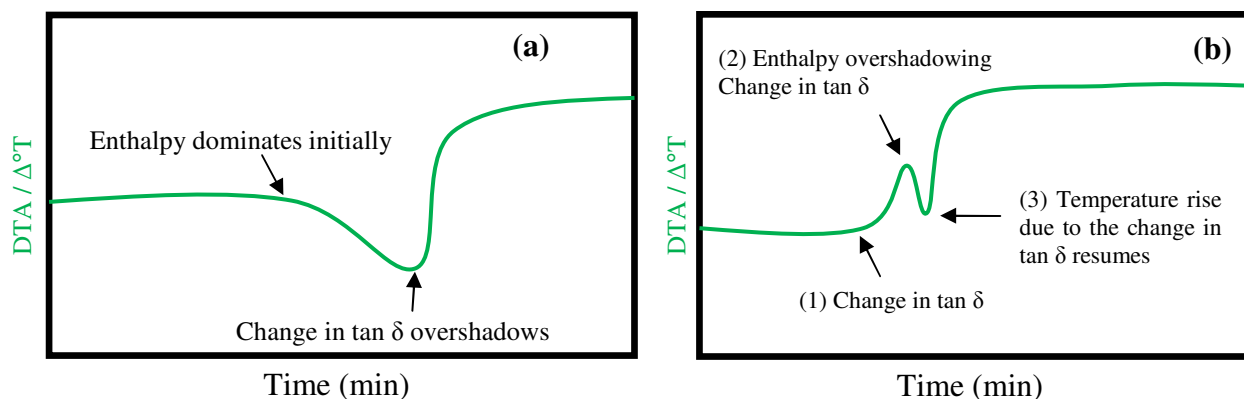
Figure 79: Predicted MWDTA profiles for (a) a material undergoing fusion where enthalpy briefly overshadows changes in tan δ (b) a material undergoing fusison where enthalpy occurs earlier than the change in tan δ

The shape of the profile is dependent on both the magnitude and rapidity of the endothermic transition. For those materials whose enthalpy effects occur immediately after the onset of the transition [Figure 79(a)] a reduction of the differential temperature will be seen leading into step rise due to the change in tan δ. For those materials where the endothermic nature of the fusion occurs sometime after the onset of the transition [see Figure 79(b)] a more complex profile is seen.

Initially, there is a partial step rise in the differential temperature before the enthalpy of the material temporarily overshadows the change in tan δ causing a fall in the differential temperature. Eventually, sufficient energy is supplied to the material to satisfy the latent heat of fusion, and the step change completes. Note that both these examples assume a positive change in tan δ after the fusion.

The two profiles exemplified in Figure 79 (a) and Figure 79 (b) are probably not truly distinct types and variations in-between will be possible depending on the relative magnitude of the enthalpy and change in tan δ. The heating rate will also have an effect. Rapid heating rates will tend to increase the magnitude of the peak produced by the enthalpy while decreasing the time over which it occurs (as in conventional DSC or DTA) and this may favour the formation of a Figure 79 (b) profile. Very slow heating rates will mean that the fall in the differential temperature due to enthalpy is smaller (but longer in duration) and this may favour formation of a Figure 79 (a) profile.

Although, there is a possibility that the increase in power levels due to the increased heating rate may make the change in tan δ uncontrollable and result thermal runaway.

10.2.1.5 Dehydrations transitions in MWDTA

The dehydration of materials is one of the few transition were a drop in the differential profile can be expected in MWDTA heating. This reduction in coupling can be seen in sections 7.6 Dehydration of water of crystallisation (page 250) and 7.5 Dehydration of bound species, (page 239) and is shown by the decrease in the value of the differential signal. The origin of the negative value is due to the loss of a coupling species from the sample area (in the examples described it was water) which prior to the transition aiding in the heating of the material. The extent the residual material can heat depends on how well the anhydrous/dehydrated form of the material couples to microwaves. The HPB cell was well suited to monitor these types of transitions as the heat supplied by the reference allowed the sample to continue to heat even after the loss of the coupling material, while at the same time showing the information that there was a reduction in coupling.

10.3 Magnitude of MWDTA responses during transitions

In DSC or DTA heating, the samples profile returns to (or near to) its pre-transition baseline value after the event, depending on changes in heat capacity. This is not normally the case in MWDTA experiments when heating a material which exhibits a change in tan δ during a transition.

The response for a positive change in tan δ during MWDTA has been shown in previous sections to be a sustained step to a higher differential temperature as the sample couples more effectively to the applied power. The applied power in an MWDTA remain fairly constant during a transition as it is being used to control the heating of the inert reference susceptor (except in case where the temperature rise is great enough to alter the reference temperature due to reverse thermal gradients, see 5.3.1 HPB cell, page 131), leaving the temperature rise of the material to be fairly uncontrolled. This sample dependent temperature rise can reach high values (in the order of 10's-100's ºC, or even more) rather than the 0.01-1's ºC seen in conventional DSC or DTA experiments. This increase in sensitivity compared to DSC can be useful when performing qualitative measurements with small samples (for materials which have tan δ discontinuities). For materials that exhibit very large positive change in tan δ there is a risk of thermal runaway, however the extent of the temperature rise can be controlled by reducing sample size or by using a highly thermally conductive carrier gas (see section 10.3.2 Methods of controlling thermal runaway).

10.3.1 Effects of sample size on MWDTA responses

Chapter 8 describes how the selected sample size is critical to the response seen in a MWDTA experiment. It was found that by testing a range of samples masses (under the same conditions), a point where the response is no longer linear can be found by drawing a tangent to the curve and finding the point where the tangent intersects the x axis of a plot of area ($\Delta T/\Delta W$) verse mass. This point was called the critical mass.

The reason for this response is partly due to the limitations of the current PID routine used in the software being unable to control the thermal runaway triggered by tan δ changes when larger samples are used. The critical mass of sample can only be determined by creating a calibration curve for the material of interest as differences in tan δ between materials are so varied.

10.3.2 Methods of controlling thermal runaway

The previous section discusses that when using large masses the MWDTA could not control thermal runaway, it is possible that the extent of the uncontrolled heating can be reduced using highly thermally conductive carrier gases such as helium.

The HPB cell is prone to a phenomenon called 'reverse thermal gradients' (5.5.1.1 Gas flow arrangements for the RCHPB, page 152) where, after a positive change in tan δ, the sample becomes hotter than the reference. By surrounding the sample cell with a highly thermally conductive blanket gas such helium, heat is conducted towards the cold outer walls of the sample chamber and away from the sample. It is thought by using this method to remove heat better control of thermal runaway can be achieved.

10.4 Instrument conditions

During this research it was found that certain conditions have to meet for the instrument to work effectively. Some examples are described in the following sections.

10.4.1 Limitations of the generator

The microwave generator did not produce any power until the control signal from the DAC exceeded approximately 0.5V (equivalent to 15 W or 5 % of the maximum output). This 'boundary condition' meant that no control of the heating was possible below this level.

10.4.2 Effect of the iris on efficient heating

The experiments described in section 4.4.1.1 Discovery of the size of the 'hot zone', (page 107) demonstrated the importance of positioning the sample in the maximum of the applied wave and how careful positioning of tuning components within the instrument is required for efficient heating. The extensive study of the impact on the position of the moveable iris within the waveguide (4.4.1 Investigation into the effect of iris size and position, page 105) on the temperature achieved by a sample heated using a constant power showed that only positions where the distance from the iris can be calculated to place a maximum of the wave over the sample (taking the iris as the position of a node) were fully effective heating positions. The size of the iris was also found to be important in how easy the instrument was to tune, as a small iris only allowed for a very small variance in tuning (which was usually lost during a transition), and a large iris had only a small impact on improving heating.

10.5 Predictions of suitable material types to heat in MWTA

MWDTA/MWTA has been shown to be very sensitive in detecting thermal transition in many materials. However the analysis of solid samples with poor Ohmic heating or liquid samples with little dipolar polarisation is difficult. Use of the HPB cell, with its susceptor reference jacket around the sample has allowed both strong and weakly coupling materials to be successfully heated.

However, the ability to predict beforehand which materials will heat would be useful in indicating how the sample will behave and which sample cell will be most appropriate for the analysis.

Generally, samples which are likely will heat are:
- Through dipolar polarisation:
    - Liquid materials which have polar groups (e.g. Water).
- Through Ohmic heating:

   o Semi-conducting materials

   o Non-uniform materials with conductive pathways (i.e. carbons, especially those prepared at high temperatures).

   o Materials which exhibit charge delocalisation or where conjugation increases electrical conductivity

   o Doped materials, such as samples mixed with an electron donor (such as an alkali metal)

Materials which would not generally be expected to heat well include:

- Insulating materials such a polymers and silicates
- Perfect crystals
- Straight chained unconjugated organic compounds lacking polar groups
- Highly electrically conductive materials (metals)

However, many other factors can have a significant effect including the particle size of the material, its thermal history, how densely it is packed.

Chapter 11

Discussion and further work

The chapter gives a summary of interesting points found during the research of microwave thermal analysis, and the addition work which could be performed.

11.1 Conclusion

The scope of this current research has shown that MWTA (in its many modes) is a novel and powerful new addition to the family of thermal analysis techniques.

Discussed results have shown that the instrumental data can be directly compared with convention DTA when studying strong enthalpy transitions with little or no change in tan δ. The development of the new MWDTA cell has allowed the analysis of samples regardless of if their innate ability to couple with microwaves energy and with the added advantage of identifying even small changes in tan δ through the differential temperature profile.

This current research has also highlighted many interesting observation about the MWTA technique:

- Increased sensitivity to certain transitions, for instance in the phase change in sodium tungstate (see Graph 97, Graph 98), where DSC measurements using 20 mg of sample only recorded a 0.96 °C rise, while MWDTA produced a rise of 96 °C with a smaller sample. This indicates the possibly of applying the technique as a trace detection method.

- MWTA/MWDTA often appears very sensitive to the initial start of a transition. This is often observed at a temperature several degrees lower than the *extrapolated* onset given in DSC where no deviation in the signal is possible until the enthalpy of the process is significant. MWTA may therefore give a better indication of the lowest temperature at which an event will occur.

- MWDTA profiles for the fusion of highly endothermic polar organic materials showed the competition for dominance of enthalpy over changes in tan δ, resulting in the maximum rate of change (peak minimum/maximum) being seen as a shoulder (or negative peak) in the differential temperature profile, a useful addition to the instrument which was not designed to monitor enthalpy changes.

This new form of thermal analysis maybe of great interest to industry and research as microwave processes becomes more widely used.

11.2 Further work

Unfortunately, due to time constraints, several interesting aspects of microwave thermal analysis could not be explored in this project. Further work in these areas could develop the scope of the technique.

The MCRC has developed another microwave technique (Microwave Dielectric Thermal Analysis [MDTA]) where ε" and ε' of a sample can be measured directly (using a cavity perturbation technique) as a function of temperature. Although, instrumental problems (namely the contradiction in the relatively large sample size needed for effective microwave heating and the small sample size needed for the measurements) have limited the application of this particular technique, it would be interesting to link results obtained with MWTA to fundamental dielectric measurements.

An area where the MWTA instrument itself could be developed is through the addition of a cooling system. The addition of cooling in thermal analysis provides several advantages, such as allowing the operator to perform experiments at sub ambient temperatures and the ability to increase the baseline leading into a low-temperature transition. An additional benefit of cooling would be that better temperature control could be achieved, particularly with samples tending to thermal runaway.

Using Curie points to determine the possibility of magnetic heating was discussed in section 7.11.2 Curie point transition in Nickel. Further investigations into this phenomenon could involve the study of other ICTAC certified Curie point standards such as Permanorm 3, Mumetal, Permanorm 5 and Trafoperm to see if the trends match, and whether the response seen is a true result for this type of transition under microwave thermal analysis.

The ability to be able to directly compare MWDTA responses with DSC calculation of the energy of transitions should be investigated, along with profiles of transitions types. Chapter 8 showed strong evidence that the area under a power versus differential temperature graph was related to the mass, it would be of further interest if it could be determined that the calculated area was also related to the reaction heat as seen in DSC.

Microwave assisted organic synthesis (MAOS) has become widely utilised. During the development of the sample cells detailed in Chapter 5 a cell was produced which was able to monitor differential and non-differential temperature responses of liquids under microwave conditions. It was believed this cell could provide information on the dissolution of solids in polar

solvents and the microwave energy required to perform certain reactions, possibly information of great use in the scale up of MAOS experiments. The cell would also allowed the study of ionic liquids; materials which have generated a lot of interest recently. Unfortunately, time only allowed the use of a few samples to validate the cell but its potential was apparent.

To truly test the instrument it needs to be used in conjunction with real world samples from many areas such as domestic, scientific, medical and pharmaceutical samples although for this to be truly beneficial collaboration with companies and/or other institution would be of advantage.

Rubidium nitrate appeared to show dramatic changes in coupling depending on what phase it was in and a link between electrical conductance and the response from the instrument. It would therefore be of interest to see if the extent of heating was linked to the crystal structures and to compare electrical conductivity changes with changes in heating. To perform a full study would require the use of hot stage XRD and a conductance meter both of which were unavailable at the time of this research.

In conventional DTA and DSC experiments increasing the heating rate often results in sharper peaks and it would be interesting to see whether the same trend is observable using MWTA. Rapid heating rates were generally avoided during the current work as they adversely affected temperature control.

It may also be of interest to study the steps in differential temperature to see how they alter with heating rate. In DSC experiments increasing the heating rate results in shaper more resolved transitions. It is not known if the same trend will be observed in MWTA or whether the increased power (required to maintain the faster heating rate) will cause thermal runaway.

References

[1]   Wendlandt WW. Thermal methods of analysis. Texas: interscience publishers 1964.

[2]   T.Meisel. To what extent is thermal analysis an analytical method? Journal of thermal analysis 1984;29:1379-92.

[3]   Roberts-Austen WC. Fifth report to the alloys research committee: Steel. Proc Inst Mech Engrs. 1899;1:35.

[4]   Norton FH. Critical study of the differential thermal method for the identification of the clay minerals American ceramic society 1939;22:54.

[5]   Boersma SL. A theory of differential thermal analysis and new method of measurement and interpretation J Amer Ceram Soc. 1955;38:281.

[6]   A.C. Metaxas RJM. Industrial microwave Heating London Peter Peregrinus 1983.

[7]   Hippel ARV. Dielectric material and their applications MIT press 1954.

[8]   J.P Tierney PL. Microwave Assisted Organic Synthesis Blackwell publishing 2005.

[9]   Gedye R, Smith F, Westaway K, Ali H, Baldisera L, Laberge L, et al. The Use of Microwave-Ovens for Rapid Organic-Synthesis. Tetrahedron Letters. 1986;27(3):279-82.

[10]   Gedye R, Smith F, Westaway K. Microwaves in Organic and Organometallic Synthesis. Journal of Microwave Power and Electromagnetic Energy. 1991;26(1):3-17.

[11]   Karmazsin E, Barhoumi R, Satre P, Gaillard F. Use of Microwaves in Thermal-Analysis. Journal of Thermal Analysis. 1985;30(1):43-7.

[12]   Karmazsin E, Barhoumi R, Satre P. Thermal-Analysis with Microwaves - Temperature and Power-Control. Journal of Thermal Analysis. 1984;29(6):1269-77.

[13]   Karmazsin E. Use of Low-Power and High-Power Microwave-Energy for Thermal-Analysis. Thermochimica Acta. 1987 Feb 1;110:289-95.

[14]   Parkes GMB, Bond G, Barnes PA, Charsley EL. Development of a new instrument for performing microwave thermal analysis. Review of Scientific Instruments. 2000 Jan;71(1):168-75.

[15]   Parkes GMB, Barnes PA, Charsley EL, Bond G. Microwave differential thermal analysis in the investigation of thermal transitions in materials. Analytical Chemistry. 1999 Nov 15;71(22):5026-32.

[16]   Parkes GMB, Barnes PA, Charsley EL, Bond G. Microwave thermal analysis - A new approach to the study of the thermal and dielectric properties of materials. Journal of Thermal Analysis and Calorimetry. 1999;56(2):723-31.

[17]   Parkes GMB, Barnes PA, Bond G, Charsley EL. Qualitative and quantitative aspects of microwave thermal analysis. Thermochimica Acta. 2000 Aug 7;356(1-2):85-96.

[18]   Nesbitt A, Navabpour P, Degamber B, Nightingale C, Mann T, Fernando G, et al. Development of a microwave calorimeter for simultaneous thermal analysis, infrared spectroscopy and dielectric measurements. Measurement Science & Technology. 2004 Nov;15(11):2313-24.

[19]   Nair BKS, Parkes GMB, Barnes PA, Sibley MJN, Bond G. Development of a novel instrument for microwave dielectric thermal analysis. Review of Scientific Instruments. 2006 Apr;77(4):-.

[20]   Thuery J. Microwaves: Industrial, Scientific and Medical Applications London: Artech House publisher 1992.

[21]   Wei JB, Shidaker T, Hawley MC. Recent progress in microwave processing of polymers and composites. Trends in Polymer Science. 1996 Jan;4(1):18-24.

[22]   Sairem. Sairem Data Sheet

[23]   Kawashima R, Uchiumi T. Temperature and Frequency-Dependence of Electric-Conductivity near the Successive Phase-Transition Points of Rubidium Nitrate Crystal. Solid State Commun. 1986 Jun;58(9):625-7.

[24]   Johnson MA, Moradi MH. PID control – new identification and design methods Springer-Verlag London Limited 2005.

[25]   Skoog H, Nieman. Principles of instrumental analysis. 5 ed. Saunders golden sunburst series: Saunders college pulishing 1998.

[26]   Charsley EL. Recent advances in thermal analysis techniques. Chemistry in Australia. 1994:188-92.

[27]   Barnes PA. Evolved Gas Analysis Analytical proceedings 1990;27:150.

[28]   Haines PJ. Principles of thermal analysis and calorimetry. Cambridge: The Royal Society of Chemistry 2002.

[29]   Carrott PJM, Nabais JMV, Carrott MMLR, Menendez JA. Thermal treatments of activated carbon fibres using a microwave furnace. Microporous and Mesoporous Materials. 2001 Oct;47(2-3):243-52.

[30]   Hanks KS. Microwave assisted removal of organic pollutants from aqueous effluent streams. Lancashire University of Lancashire

[31]   J. Muntasell JN. A study of the polymorphism of potassium nitrate starting from room temperature and at atmospheric pressure Thermochimica Acta. 1984 1985;83:173-9.

[32]   Jakobsen BVSaHJ. Phase transitions in KNO3 studied by variable-temperature 15N Majic-angle NMR spectroscopy Journal of solid state chemistry 1998 1999(145):10-4.

[33]   Lide DR. Handbook of Chemistry and Physics: CRC; 72 edition (June 10, 1991) 1991.

[34]   Nagano K, Mochida T, Takeda S, Domanski R, Rebow M. Thermal characteristics of manganese (II) nitrate hexahydrate as a phase change material for cooling systems. Applied Thermal Engineering. 2003 Feb;23(2):229-41.

[35]   S.M. Pourmortazavi MF, S.S. Hajimirsadeghi, S.G. Hosseini. Thermal behavior of aluminum powder and potassium perchlorate mixtures by DTA and TG. Thermochimica Acta. 2006(443):129-31.

[36]   Quélais V. untitled   Huddersfield University of Huddersfield 2003.

[37]   Mullens J, Vos A, Carleer R, Yperman J, Vanpoucke LC. The Decomposition of Copper Oxalate to Metallic Copper Is Well Suited for Checking the Inert Working-Conditions of Thermal-Analysis Equipment. Thermochimica Acta. 1992 Oct 1;207:337-9.

[38]   Lamprecht E, Watkins GM, Brown ME. The thermal decomposition of copper(II) oxalate revisited. Thermochimica Acta. 2006 Jul 1;446(1-2):91-100.

[39]   Brown ME. Introduction to thermal analysis : Techniques and applications Chapman and Hall Ltd 1988.

[40]   Chary AS, Reddy SN. Effect of structural changes on DC ionic conductivity of rubidium nitrate single crystals. Phys Status Solidi B. 1998 Aug;208(2):349-52.

[41]   R.N.Brown, A.C.McLaren. The Thermal transformations in solid Rubidium nitrate. Acta Cryst. 1961;15:974 - 6.

[42]   Binner JGP, Price DM, Reading M, Vaidhyanathan B. Hybrid microwave/conventionally heated calorimeter. Review of Scientific Instruments. 2005 Jun;76(6):-.

[43]   P.J.Haines. Principles of Thermal analysis and calorimetry: RSC paperbacks 2002.

[44]   J. G. P. Binner GD, D. M. Price, M Reading and B. Vaidhyanathan Hysteresis in the β-α phase transition in silver iodide Journal of thermal analysis and calorimetry 2006;84(2):409-12.

[45]   S. F. Wright PP, D. Dollimore, K. S. Alexander. An overview of calibration materials used in thermal analysis-benzoic acid. Thermochimica acta. 2002;392-393 251 – 7.

[46]   Hyeon Suk Shin YMJ, Taoe Young Oh, Taihyun Chang, Seung Bin Kim, Do Hyung Lee, Isao Noda Glass transtion temperature and conformational changes of poly(methyl methacrylate) thin films determined by two-dimensional map representation of temperature-dependance reflection-absorption FTIR spectra American chemical society 2002;18:5953-8.

[47]   M.I. Pope MDJ. Differential thermal analysis - A guide to the technique and its applications: Heyden & Son Ltd 1977.

[48]   Kutaish N, Aggarwal P, Dollimore D. Thermal analysis of calcium oxalate samples obtained by various preparative routes. Thermochimica Acta. 1997 Aug 25;297(1-2):131-7.

[49]   Mohamed A. Mohamed AKG, Samih A. Halawy. A comparative study of the thermal reactivities of some transition metal oxalates in selected atmospheres. Thermochimica Acta 2005;429:57-72.

[50]   Emmanual Lamprecht GMW, Michael E Brown The thermal decomposition of copper(II) oxalate revisted Thermochimica Acta.

[51]   Rieck GD. Tungsten and its compounds: Pergamon press oxford 1967.

[52]   Hua Yixin LC. Heating rate of minerals and componds in microwave field Transactions of NFsoc. 1996;6(1).

[53]   A.H. Yahaya ZAI, A.K. Arof. Thermal, electrical and structural properties of Li2WO4 Journal of alloys and compounds 1996;241:148 - 52.

[54]   A.H. Yahaya AKA. X-Ray and thermogravimetric studies of hydrated Li2WO4. materials science and engineering 1995;B34:7 -11.

[55]   Takanori Nagasaki KK, Abdul Hamid Yahaya, Naoki Igawa, Kenji Noda, Hideo Ohno Phase identification and electrical conductivity of Li2WO4 Solid state ionics 1997;96:61-74.

[56]   Giulio G.T Guarini LD. The thermal dehydration of Na2WO4.2H2O Thermochimica acta 1995;250:85-96.

[57]   L.Erdey JS, S. Gal and G. Liptay Thermoanalytical properties of analytical – grade Reagents – IVA sodium salts. Talanta. 1966;13:67-80.

[58]   A.A Guarnieri AMM, C.B Pinheiro, N.L. Speziali Structural and calorimetric studies of mixed K2MoxW(1-x)O4 (0≤x≤1) compounds Physica B. 2003;334:303-9.

[59]   Antonietta Genovese RAS. Structure and thermal interpretation of the synergy and interactions between the fire retardants magnesium hydroxide and zinc borate Polymer Degradation and stability 2007;92:2-13.

[60]   Preda RDaM. Thermal decomposition of strontium hydroxide Journal of Thermal Analysis and Calorimetry. 1973;5(4):465-73.

[61]   Yu. N. Makurin YMP, N. A. Zhelonkin, G.G. Kasimov, and V.G. Teplov Thermal and emission processes in the thermal decomposition of strontium hydroxide in vacuum Inorganic materials 1986;22(4):614.

[62]   Pavan K Heda DD, Kenneth S. Alexander, Dun Chen, Emmeline Law, Paul Bicknell A method of assessing solid state reactivity illustrated by thermal decomposition experiments on sodium bicarbonate Thermochimica Acta 1995;255:255-72.

[63]   Pavan K. Heda KSA. An assessment of the solid state reactivity of sodium bicarbonate in the presence of solid dental excipients using thermal analysis. Thermochimica Acta 1999;340-341:165-85.

[64]   Magdalena olszak-humienik jm. Eyring parameters of dehydration proceses. thermochimica acta 2003;405:171-81.

[65]   Fujimoto S, Yasuda N, Shimizu H, Tsuboi S, Kawabe K, Takagi Y, et al. Dielectric Properties of Rubidium Nitrate under Hydrostatic-Pressure. J Phys Soc Jpn. 1977;42(3):911-5.

[66]   Barrett: C. Barrett Lab.   [cited 2008; Available from: http://barrett-group.mcgill.ca/contact/index.htm

[67]   Heiko K. Cammenga KG, Stefan M. Sarge. 4,4'- Azoxyanisole for temperature calibration of differential scanning calorimeters in the cooling mode- yes or no? . Thermochimica Acta. 2006;446:36-40.

[68]   C.M. McLoughlin WAMM, T.R.A. Magee. Physical and dielectric properties of pharmaceutical powders Powder technology 2003;134:40-51.

[69]   Biju Kumar S. Nair GMBP Barnes PA. Development of a novel instrument for Microwave Dielectric Thermal Analysis (MDTA). University of Huddersfield.

[70]   J.G.P. Binner DMP, M. Reading, B. Vaidhyanathan. Modulated temperature calorimetry of silver iodide in the presence of microwave radiation. Thermochimica Acta.46.

[71]   C.A. Vriezinga SS-P, J Grasman. Thermal runaway in microwave heating: A mathematical analysis Applied mathematical modelling. 2002;26:1029-38.

[72]   D.Dollimore GAG, and T.J.Taylor. Mass spectrometric evolved gas analysis-an overview. Thermochimica Acta. 1984;75:59-69.

[73]   Charsley EL, Walker C, Warrington SB. Applications of a New Quadrupole Mass-Spectrometer System for Simultaneous Thermal-Analysis - Evolved Gas-Analysis. Journal of Thermal Analysis. 1993;40(3):983-91.

[74]   analytical H. HPR-20 QIC System operation manual.

Publications

Investigation of the microwave dielectric heating characteristics of various carbon adsorbents

GMB Parkes, EA Dawson, PA Barnes, I Hamilton, HM Williams and *G Bond
Centre for Applied Catalysis, University of Huddersfield, UK
*University of Central Lancashire, Preston, UK

Regeneration of carbon adsorbent beds by microwave heating to induce desorption has previously been the subject of limited investigation (1-15). In this study, several types of activated carbon (from different precursors, either chemically or physically activated, having different pore size distributions and physical form) were chosen to give a representative cross-section of typical carbon adsorbents. Their microwave dielectric properties (the real and imaginary components of the dielectric constant, tan δ and the effective conductivity) were measured using a network analyser (Hewlett Packard, HP 8720 ET) and the cavity perturbation method, giving numerical data related to the extent to which the carbons couple with, and heat in a microwave electric field. A custom-built microwave thermobalance (MWTB) was used to study the mass loss characteristics during microwave heating and the temperatures reached at various power levels were monitored using microwave thermal analysis (MWTA). This was carried out in equipment designed and built in our laboratory (16,17). Data from MWTA and MWTB experiments were compared with conventional simultaneous TG-DSC measurements. From these studies, a detailed picture of the thermal behaviour of different carbons subjected to microwave heating was developed, which can usefully inform the choice of carbon and method of regeneration for a particular application.

(For oral presentation)

Induction programmes / seminars / workshops / conferences attended:

Lab demonstrating:

- 1st year Physical chemistry
- 1st year Organic chemistry
- Science foundation physiology taster class
- 1st and 2nd year Inorganic chemistry
- 2nd year Analytical chemistry
- Science foundation Health and the Environment
- Science foundation Physics
- Science week

1. Department of chemical and biological sciences research seminars
2. Seminar with Prof. J. Booske-What's Hot and What's Not: How microwave fields transfer energy to materials for heating and even stranger effects
3. An induction program looking at the effect of microwave heating on activated carbons was set up, results were submitted for oral presentation by Dr E. Dawson at the Carbon Conference in Aberdeen, July 2006
4. Master module SMA001 Fundamentals of Analytical Science (Huddersfield)
5. RSC TMG-The science and application of thermal analysis
   - Thermogravimetric analysis and combination techniques
   - Practical demonstration analysis

6. Seminars:

Mechanistic aspects of Co substituted metallo-beta lactamase from Bacilus cereus
Adriana Badarau

Ammonia Adsorption Microcalorimetry Study of Supported Heteropoly Acids
Claire Savill Jowitt

Safety Matters
Gary Wood, University of Huddersfield

Susceptibility to adult diseases is programmed in fetal life by maternal nutrition
Dr Shamus Burns, University of Huddersfield

Mass Spectrometry in the Detection of Horse Doping (Chaos before Chemistry) Royal Society of Chemistry Lecture
Prof J Monaghan, University of Edinburgh

Nanoman IV: The Quest for Peace and the Fabrication of Nanostructured Materials
Dr Tim Gabriel, University of Huddersfield

Fiddling with Phosphorus
Royal Society of Chemistry Lecture
Dr Simon Jones, University of Sheffield

Catalysis - Can life as we know it exist without it?
Professorial Lecture
Professor Phil Barnes, University of Huddersfield

7. Conferences

Royal Society of Chemistry Thermal methods group meeting 2007

Glasgow: 3rd-4th April 2007

PerkinElmer–Pharmaceutical characterisation seminar

Beaconsfield: May 2007

TA Instruments pharmaceutical seminar 2007
Derby: 21st–22nd June 2007

Royal Society of chemistry Thermal methods group meeting 2008

Teddington: 1st-4th April 2008

i. The author of this thesis (including any appendices and/or schedules to this thesis) owns any copyright in it (the "Copyright") and s/he has given The University of Huddersfield the right to use such Copyright for any administrative, promotional, educational and/or teaching purposes.

ii. Copies of this thesis, either in full or in extracts, may be made only in accordance with the regulations of the University Library. Details of these regulations may be obtained from the Librarian. This page must form part of any such copies made.

iii. The ownership of any patents, designs, trade marks and any and all other intellectual property rights except for the Copyright (the "Intellectual Property Rights") and any reproductions of copyright works, for example graphs and tables ("Reproductions"), which may be described in this thesis, may not be owned by the author and may be owned by third parties. Such Intellectual Property Rights and Reproductions cannot and must not be made available for use without the prior written permission of the owner(s) of the relevant Intellectual Property Rights and/or Reproductions.